

Seismic Behavior and Retrofitting of RC Frame Structures with Emphasis on Beam-Column Joints – Experiments and Numerical Modeling

Von der Fakultät Bau- und Umweltingenieurwissenschaften
der Universität Stuttgart zur Erlangung der Würde
eines Doktor-Ingenieurs (Dr.-Ing.)
genehmigte Abhandlung

Vorgelegt von
Akanshu Sharma
aus Mumbai, Indien

Hauptberichter: Prof. Dr.-Ing. Rolf Eligehausen
Mitberichter: Prof. Dr.-Ing. habil Manfred Bischoff
Prof. Dr.-Ing. Jan Hofmann

Tag der mündlichen Prüfung: 25.07.2013

Institut für Werkstoffe im Bauwesen der Universität Stuttgart
2013

To My Wife and Daughter

ABSTRACT

The vulnerability and poor seismic performance of the beam-column joints of old non-seismically designed reinforced concrete (RC) frame structures has been proven time and again, both at laboratory level as well as by natural disasters in real life situations. However, replacing a vast majority of existing structures designed with non-seismic considerations is not economically and practically viable. Such structures need to be correctly assessed to predict their seismic performance and retrofitted, if required. In order to realistically predict the seismic performance of such structures, practical and accurate models for simulating the inelastic joint behavior at structural level, are of utmost importance. Equally important is to associate realistic and practical hysteretic rules to capture the inelastic dynamic behavior of the structures. Assessment of existing structures using such tools can predict the seismic performance of the structures with high degree of confidence. Based on such assessment, a cost-effective and efficient retrofit solution can be designed and developed. Often, the retrofitting of such structures revolves around retrofitting of the beam-column joints. Thus, a need of practically viable retrofit solution for joints cannot be denied. This work is aimed at providing the practical solutions to the above-mentioned problems, through experimental and numerical modeling approach.

Experiments have been performed first at the joint sub-assembly level to understand the behavior of poorly detailed joints with different anchorage details. To study the interaction of the various failure modes likely to occur in a non-seismically designed structure, experiment on a full-scale structure has been performed under pushover loads. Further, shake table tests were carried out on a 2D structure to verify the performance of joints at structural level under real life type seismic loads. These tests provided large database and helped in improving the overall understanding of the joint behavior under seismic loads.

Fully fastened haunch retrofit solution (FFHRS) have been investigated as a viable retrofit option for poorly detailed joints. The solution has been tested through tests at sub-assembly level under cyclic loads as well as at structural level under dynamic loads. The results clearly displayed the efficacy of the FFHRS in safeguarding the joints thereby improving the global seismic behavior of structures. However, it is very important to confirm that the structural members shall not become shear critical due to the retrofit. It is also essential that the anchorage system used for fastening the haunch elements to frame members serve their purpose well. It was observed that the performance of the FFHRS in experiment on structure under dynamic loads is better than that in experiment on beam-column joints under cyclic loads. This is attributed partially to the phase difference between the force in anchor and crack opening and partially to instantaneous loading.

To assess the seismic performance of structures giving due consideration to joint distortion, a new joint model has been presented. The model is based on realistic deformation of the joint sub-assembly and excellent agreement with the experimental results at sub-assembly as well as structural proves the efficacy and suitability of the model. To model the hysteretic behavior of the structure, an extension to pivot hysteretic model is presented. The model parameters are derived in a more rational way and can be applied at a wide range of structures. Further, a model is presented to simulate seismic behavior of joints retrofitted with FFHRS considering inelastic behavior of anchorage. The models were implemented in commercial software SAP2000. All the models have been vastly validated against experiments conducted by author as well as those available in the literature. In the end, the application of the models to assess and retrofit structures has been demonstrated by a real life case study.

KURZFASSUNG

Ein ungünstiges Verhalten von alten nicht-seismisch bemessenen Stahlbetonrahmenknoten unter seismischen Lasten wurde unter Laborbedingungen mehrfach nachgewiesen und hat sich auch in der Realität bei Naturkatastrophen gezeigt. Ein Neubau aller betroffenen existierenden Bauwerke ist jedoch aus Kostengründen nicht realisierbar. Diese Bauwerke sollten zuerst untersucht werden, um das Verhalten unter seismischen Beanspruchungen beurteilen zu können, und sollten bei Bedarf nachgerüstet werden. Praktische und genaue Modelle für die Simulation des unelastischen Knotenverhaltens in Rahmenkonstruktionen sind für eine realistische Vorhersage des Tragverhaltens des Bauwerks bei einem Erdbeben unverzichtbar. Genauso wichtig ist es, das unelastische, dynamische Verhalten der Baukonstruktion mit Hilfe einer realistischen und praktischen Hysterese-Kurve zu beschreiben. Solche Modelle ermöglichen eine sehr zuverlässige Vorhersage des Verhaltens des Bauwerks unter seismischen Beanspruchungen. Aufgrund einer derartigen Bewertung kann eine effiziente und wirtschaftliche Nachrüstung entwickelt werden. In vielen Fällen besteht die Nachrüstung dieser Bauwerke aus der Ertüchtigung der Rahmenknoten. Es besteht daher ein Bedarf an einer praktikablen Methode um diese Rahmenknoten nachzurüsten. Das Ziel dieser Arbeit ist es durch numerische und experimentelle Methoden eine pragmatische Lösung für die oben genannten Problemstellungen zu finden.

Es wurden Versuche zur Untersuchung des Rahmenknotenverhaltens durchgeführt, um das Verhalten der schlecht bemessenen Rahmenknoten mit unterschiedlichen Befestigungen beurteilen zu können. Die „Pushover“-Versuche an maßstäblichen Rahmenkonstruktionen dienen zur Untersuchung der Interaktion der möglichen Versagensarten in schlecht bemessenen Rahmenkonstruktionen. Es wurden auch „Shake-Table“-Versuche mit einer 2-dimensionalen Rahmenkonstruktion durchgeführt um das Verhalten der Rahmenknoten unter realistischen, seismischen Beanspruchungen zu verifizieren. Aus den Ergebnissen der Versuche wurde eine Datenbank erstellt, die zum verbesserten Verständnis des Rahmenknotenverhaltens beigetragen hat.

Eine Ertüchtigungslösung mit nachträglich befestigten Stahldiagonalen (Fully fastened haunch retrofit solution (FFHRS)) wurde als eine wirtschaftliche Nachrüstung der schlecht bemessenen Rahmenknoten untersucht. Zu diesem Zweck wurden Versuche sowohl an Rahmenknoten unter zyklischen Lasten als auch an Rahmenkonstruktionen unter dynamischen Lasten durchgeführt. Aus diesen Versuchen hat sich ergeben, dass die FFHRS eine sehr effiziente Nachrüstung für Rahmenknoten darstellt und damit das Verhalten der Rahmenkonstruktion positiv beeinflusst. Allerdings ist es sehr wichtig nachzuweisen, dass die nachgerüstete Konstruktion auf Abscheren nicht anfällig ist. Weiter muss sichergestellt werden, dass die Befestigungselemente zwischen FFHRS und Rahmenelementen ihren Zweck erfüllen. Es wurde festgestellt, dass das FFHRS Verhalten in Rahmenkonstruktion besser ist als das FFHRS Verhalten in den einzelnen Rahmenknoten, was auf die Phasendifferenz zwischen der Befestigung und der Rissöffnung als auch auf die unmittelbare Belastung zurückgeführt wurde.

Um das seismische Rahmenkonstruktionsverhalten unter Berücksichtigung der Rahmenknotendistorsion beurteilen zu können, es wurde ein neues Rahmenknotenmodell entwickelt. Das auf der realistischen Verformung des Rahmenknotens basierte Modell weist eine sehr gute Übereinstimmung mit den experimentellen Ergebnissen sowohl für die einzelnen Rahmenknoten als auch auf die gesamte Rahmenknotenkonstruktion auf, wodurch sich das Modell als effizient und geeignet bewiesen hat. Weiter wurde eine Erweiterung des Pivot-Modells entwickelt, die zur Erfassung der Hysterese dient. Die Modellparameter wurden

verbessert und dadurch eine breitgefächerte Anwendung auf Baukonstruktionen ermöglicht. Des Weiteren wurde ein Modell zur Analyse des Rahmenknotenverhaltens nach der Nachrüstung unter Berücksichtigung des unelastischen Befestigungsverhaltens vorgestellt. Die Modelle wurden in kommerzielle Software SAP2000 implementiert. Alle Modelle wurden ausführlich mit eigenen und in der Literatur vorhandenen Versuchsergebnissen verifiziert. Abschließend wurde die Anwendbarkeit des Modells durch ein reales Fallbeispiel demonstriert.

ACKNOWLEDGEMENTS

As per Indian culture, the place of a Guru comes first. Therefore, to begin with I would like to pay my sincerest gratitude towards my guide Prof. Rolf Eligehausen for not only being my mentor but also for allowing me to have the much required freedom of thought and work. Every single meeting with him has been technically very fruitful, encouraging and enjoyable. His appreciation for the work was one of the biggest motivation for me to try and do various things. The practical approach he uses in his work and the high reputation he commands in the global civil engineering community has always fascinated me. On personal front, the time spent with him in Germany as well as in India has left several good memories to cherish.

I sincerely thank Prof. Manfred Bischoff for his kind acceptance to be a co-guide for my thesis and for his very nice and useful comments and suggestions.

I greatly thank Prof. Hofmann for agreeing to be the co-reporter of my thesis and very fruitful technical discussions held with him. Furthermore, I would like to thank him for supporting me in every possible way to continue my work under the Indo-German cooperation.

It has been great to work with Prof. Ožbolt. His vast knowledge and command on the subject forces one to think and learn more. To work with him on various topics, even those not directly related to this thesis, was highly productive and a great learning experience.

I would also like to thank Dr. Werner Fuchs for his support and encouragement towards the collaborative research and my thesis.

I owe a very high gratitude towards my seniors at BARC for supporting and allowing me to work on my thesis under the Indo-German cooperation. Without the kind and large hearted support of Dr. G.R. Reddy, Mr. K.K. Vaze, Dr. A.K. Ghosh and Mr. H.S. Kushwaha, the work could not have been completed. It was also great to have colleagues and friends like Vinay Mahadik, Tarvinder Singh and Hitesh Lakhani at BARC.

The support of the secretarial staff especially Mrs. Silvia Choynecki, Mrs. Regina Jaeger, Mrs. Gisela Baur and Mrs. Simone Stumpp at IWB is highly acknowledged. The efforts put by them to fulfill the official formalities and make my and my family's stays in Stuttgart comfortable are highly appreciated. General discussions from time to time with Mrs. Silvia about several things were very enjoyable and enriching.

Special thanks are due for Mrs. Monika Werner for finding almost every paper or report I requested, for translating the abstract (Kurzfassung) and German summary (Zusammenfassung) from English to German. Also, normal day to day advices from her were very fruitful.

To come from a totally different culture and to stay away from my wife and daughter for months together has been the biggest challenge for me during the thesis and it would not be possible to endure it if it was not for some very good friends I could make here.

The friendship of Josipa Bošnjak needs a special mention. Both she and her husband, Mario have been very good friends with me and my family. It has always been a great learning experience to work with her, both on experimental and numerical front. The help and support she extended in day to day life during my stays in Stuttgart has been very generous.

The moments spent with Christoph and Philipp Mahrenholtz had been filled with great fun and I learnt a lot of general things from them. They helped me in several respects during my stays in Stuttgart, including picking up at airport to showing several places around and many more. All kinds of technical and general discussions with them were very enjoyable. The time spent with them also with our respective families has been wonderful.

It was wonderful to be friends with Filip Oršanić and Khalil Jebara and some very enjoyable moments were spent with them. Filip's out of the way efforts to help will always be remembered.

I would also like to thank Dr. Goran Periškić for introducing me to MASA and helping me learn to work with Femap and MASA.

Working with Giovacchino Genesio on experiments in India was a very good learning experience in many ways.

It was great to have nice colleagues such as (in alphabetical order) Alexander Assmann, Baris Irhan, Carolin Schmidt, Christian Fischer, Christian Kontzi, Daniela Ruta, Emiliano Sola, Eugen Lindenmaier, Georg Welz, Kaipei Tian, Marina Stipetić, Natalija Bede, Martin Herzog, Paul Schmieder, Philipp Grosser and Zlatko Biočić.

Ever since I met my wife, Swati, in 1997, my biggest motivation to do anything is to impress her and this thesis is no different. It is not only because of the fact that she wants me to do better but also because she believes in me much more than I believe in myself. Without her unconditional love, support, encouragement and motivation, I would not have even tried for this work. To have a daughter like Suteeksha is a blessing. Coming back fully exhausted and stressed out from the work at BARC accompanied by pressure of thesis, one smile and hug from her would make all the stress go away. During the course of my thesis, I spent several days away from my wife and daughter. It is impossible to compensate for both the time I spent away from them and the fact that I was very much pre-occupied by the stress of work even when I was with them. I know that they have suffered much more than me for this thesis and that they are happier than me that it is over. I dedicate this thesis to my wife and daughter.

TABLE OF CONTENTS

Abstract	iv
Kurzfassung (Abstract in German)	v
Acknowledgements	vii
Table of Contents	ix
Notation	xviii
1. INTRODUCTION	1
1.1 Motivation and Problem Statement	1
1.2 Context for the Research	3
1.3 Organization of Work	7
2. SEISMIC BEHAVIOR OF BEAM-COLUMN JOINTS IN REINFORCED CONCRETE FRAME STRUCTURES	8
2.1 Classification of RC Beam-Column Joints	8
2.1.1 Classification based on geometric configuration	8
2.1.2 Classification based on structural behavior	9
2.1.3 Classification based on detailing aspects	10
2.2 Failure modes of a beam-column joint	11
2.3 Mechanics of beam-column joints	12
2.3.1 Exterior Joints	12
2.3.2 Interior Joints	14
2.3.3 Mechanism of Resistance	15
2.4 Problem of bond in beam-column joints	16
3. LITERATURE REVIEW	18
3.1 Review of Existing Shear Strength Models	18
3.1.1 Empirical models	18
3.1.2 Strut and Tie Models	22
3.1.3 Models based on average plane stress plane strain approach	25
3.2 Review of Joint Element Models	28
3.2.1 Models based on experiments	29
3.2.2 Models based on analytical or numerical studies	29
3.2.2.1 Rotational Hinge Models	29
3.2.2.2 Multiple Spring Models	33
3.2.3 Summary of Existing Models	38

4. THE PROPOSED JOINT MODEL	40
4.1 Need for the joint model	40
4.2 Basis for the model	41
4.2.1 Contribution of Joint Shear Deformation to Storey Drift	41
4.2.2 Modelling the Contribution of Joint Shear Deformation to Storey Drift	42
4.3 Characterization of springs for joint model	43
4.3.1 Obtaining spring characteristics using experimental results	44
4.3.2 Obtaining spring characteristics using results of detailed FE analysis	46
4.3.3 Analytical computation of characteristics from mechanics of the joints	48
4.3.3.1 Joints without axial load on column	50
4.3.3.2 Joints with axial load on column	52
4.4 Recommended principal tensile stress v/s shear deformation relations	56
4.4.1 Exterior Joints	56
4.4.1.1 Exterior Joints with beam bars bent in	56
4.4.1.2 Exterior Joints with beam bars bent out	56
4.4.1.3 Exterior joints with straight bottom beam bars with full development length embedment	59
4.4.1.4 Exterior joints with bottom beam bars straight with 150mm embedment	59
4.4.2 Interior Joints	60
4.4.3 Considerations of joint aspect ratio	61
4.4.4 Considerations of eccentricity in joints	62
4.5 Summary	63
5. PIVOT HYSTERESIS MODEL PARAMETERS FOR MEMBERS AND JOINTS	67
5.1 Pivot Hysteresis Model by Dowell et al (1998)	68
5.1.1 Assumptions of pivot hysteresis model (Dowell et al, 1998)	68
5.1.2 Hysteretic Rules	69
5.1.3 Parameters controlling hysteretic response	70
5.1.4 Need for new parameters to control hysteretic response of non-seismically detailed frame structures	71
5.1.5 Methodology to develop parameters for frame structures	72
5.2 Determination of parameters for rectangular sections beams/columns	73
5.3 Determination of parameters for non-seismically detailed beam-column joints	78
6. ASSESSMENT MODEL FOR FULLY FASTENED HAUNCH RETROFIT SOLUTION	81
6.1 Background and motivation	81
6.2 Mechanics of joints retrofitted with HRS	83

6.3 Assessment model for fully fastened haunch retrofit solution	85
6.3.1 Basic modelling philosophy	85
6.3.2 Assumptions behind the model	86
6.3.3 Characteristics for spring to model anchorage system behaviour	90
7. EXPERIMENTAL PROGRAM ON AS BUILT BEAM-COLUMN JOINTS	94
7.1 Experimental Program	94
7.2 Description of Joints	94
7.2.1 Geometry	94
7.2.2 Material Properties	95
7.3 Test Setup	96
7.3.1 Loading and Reaction Frame	96
7.3.2 Test Facility	97
7.3.3 Instrumentation	97
7.3.4 Loading Pattern	99
7.4 Experimental Results	99
7.4.1 JT1-1	99
7.4.2 JT2-1	101
7.4.3 JT3-1	102
7.4.4 JT4-1	104
7.4.5 JT5-1	105
7.5 Summary	107
8. EXPERIMENTAL INVESTIGATION ON INELASTIC SEISMIC BEHAVIOR OF RC FRAME STRUCTURES	108
8.1 Description of the structure	108
8.1.1 Geometry	108
8.1.2 Material Properties	114
8.2 Construction of the frame	115
8.2.1 Construction of Raft foundation	115
8.2.2 Construction of super-structure	115
8.2.3 Loading arrangement	117
8.3 Experimental Setup	119
8.3.1 Test facility	119
8.3.2 Instrumentation	120
8.3.3 Loading sequence	120
8.4 Experimental results	120
8.4.1 Failure patterns	122
8.4.2 Inter-storey drifts	126
8.4.3 Strain data	128

8.4.4 Rotations	129
8.5 Summary of the experiment	131
9. EXPERIMENTAL PROGRAM ON AS-BUILT RC FRAMES UNDER DYNAMIC LOADING (SHAKE TABLE TESTS)	132
9.1 Description of Test Structure	132
9.1.1 Geometry	132
9.1.2 Material Properties	134
9.2 Scaling Philosophy	134
9.2.1 Linear Dimension Scaling	135
9.2.2 Material Scaling	135
9.2.3 Reinforcement Area Scaling	135
9.2.4 Mass Scaling	136
9.3 Test Setup	136
9.3.1 Test Facility	136
9.3.2 Support Structure	136
9.3.3 Added Mass on the structure	137
9.3.4 Layout on shake table	138
9.4 Instrumentation	139
9.5 Loading Pattern and test matrix	141
9.6 Experimental Results	142
9.6.1 Natural time periods of the structure	142
9.6.2 Simulated seismic test with PGA = 0.1g	143
9.6.3 Simulated seismic test with PGA = 0.2g	144
9.6.4 Simulated seismic test with PGA = 0.3g	145
9.6.5 Simulated seismic test with PGA = 0.4g	147
9.6.6 Simulated seismic test with PGA = 0.5g	149
9.6.7 Simulated seismic test with PGA = 0.6g	151
9.6.8 Simulated seismic test with PGA = 0.7g	151
9.6.9 Simulated seismic test with PGA = 0.8g	153
9.6.10 Simulated seismic test with PGA = 0.9g	155
9.6.11 Simulated seismic test with PGA = 1.0g	156
9.7 Summary of Experimental Results	157
10. EXPERIMENTAL PROGRAM ON BEAM-COLUMN JOINTS RETROFITTED WITH FULLY FASTENED HAUNCH RETROFIT SOLUTION	162
10.1 Experimental Program	162
10.2 Description of Joints	163
10.2.1 Geometry	163
10.2.2 Material Properties	163

10.3 Description of Fully Fastened Haunch Retrofit Solution (FFHRS)	164
10.3.1 Haunch Elements	164
10.3.2 Anchorage System	164
10.3.2.1 Bonded Anchors	165
10.3.2.2 Concrete Screws	166
10.3.2.3 Expansion Anchors	166
10.3.2.4 Anchor Installation Parameters	167
10.4 Test Setup	167
10.5 Experimental Results	168
10.5.1 JT1-3	168
10.5.2 JT1-4	170
10.5.3 JT1-5	172
10.5.4 JT1-6	174
10.6 Summary	176
11. EXPERIMENTS ON RC FRAMES RETROFITTED WITH FULLY FASTENED HAUNCH RETROFIT SOLUTION UNDER DYNAMIC LOADING	177
11.1 Description of Test Structure	177
11.1.1 Geometry	177
11.1.2 Material Properties	177
11.1.3 Fully Fastened Haunch Retrofit Solution (FFHRS)	178
11.2 Test Setup	179
11.3 Experimental Results	180
11.3.1 Natural time periods of the structure	180
11.3.2 Simulated seismic test on retrofitted structure with PGA = 0.1g	180
11.3.3 Simulated seismic test on retrofitted structure with PGA = 0.2g	181
11.3.4 Simulated seismic test on retrofitted structure with PGA = 0.3g	182
11.3.5 Simulated seismic test on retrofitted structure with PGA = 0.4g	184
11.3.6 Simulated seismic test on retrofitted structure with PGA = 0.5g	186
11.3.7 Simulated seismic test on retrofitted structure with PGA = 0.6g	188
11.3.8 Simulated seismic test on retrofitted structure with PGA = 0.7g	189
11.3.9 Simulated seismic test on retrofitted structure with PGA = 0.8g	190
11.3.10 Simulated seismic test on retrofitted structure with PGA = 0.9g	192
11.3.11 Simulated seismic test on retrofitted structure with PGA = 1.0g	193
11.4 Summary of Experimental Results	195
12. VALIDATION OF PROPOSED JOINT MODEL AGAINST EXPERIMENTS	200
12.1 Validation of model against experiments at sub-assembly level	200
12.1.1 Exterior Joints	200
12.1.1.1 Tests by Clyde et al (2000)	201

12.1.1.1.1 Test #2 (10% axial load)	202
12.1.1.1.2 Test #6 (10% axial load)	205
12.1.1.1.3 Test #4 (25% axial load)	206
12.1.1.1.4 Test #5 (25% axial load)	206
12.1.1.2 Tests by Pantelides et al (2002)	207
12.1.1.2.1 Test unit 1	209
12.1.1.2.2 Test unit 2	210
12.1.1.2.3 Test unit 5	211
12.1.1.2.4 Test unit 6	211
12.1.1.3 Tests by El-Amoury and Ghobarah (2002)	212
12.1.1.4 Test by Murty et al (2003)	213
12.1.1.5 Test by Hwang et al (2005)	215
12.1.1.6 Tests by Wong and Kuang (2008)	216
12.1.1.6.1 Test BS-L-300	217
12.1.1.6.2 Test BS-L-450	217
12.1.1.6.3 Test BS-L-600	218
12.1.1.7 Tests by Genesio and Sharma (2010)	219
12.1.1.7.1 Joint JT1-1	220
12.1.1.7.2 Joint JT2-1	221
12.1.1.7.3 Joint JT3-1	222
12.1.1.7.4 Joint JT4-1	222
12.1.1.7.5 Joint JT5-1	223
12.1.2 Interior Joints	224
12.1.2.1 Tests by Dhakal et al (2005)	224
12.1.2.1.1 Joint C1	225
12.1.2.1.2 Joint C4	225
12.2 Validation of model against experiment at structural level	227
12.2.1 Modeling aspects	227
12.2.2 Numerical results	228
12.2.2.1 Pushover curves	228
12.2.2.2 Deflection profile	229
12.2.2.3 Failure patterns	230
13. VALIDATION OF PIVOT HYSTERETIC MODEL PARAMETERS FOR MEMBERS AND JOINTS AGAINST EXPERIMENTS	232
13.1 Validation of parameters for rectangular sections at member level	232
13.1.1 Tests by Gill et al (1979)	232
13.1.1.1 Specimen Details	232
13.1.1.2 Experimental and numerical results	233
13.1.1.2.1 Unit 2	234
13.1.1.2.2 Unit 3	234

13.1.1.2.3 Unit 4	235
13.1.2 Tests by Ohno and Nishioka (1984)	235
13.1.2.1 Specimen details	236
13.1.2.2 Experimental and numerical results	236
13.1.2.2.1 Unit L1	237
13.1.2.2.2 Unit L2	237
13.1.3 Tests by Atalay and Penzien (1975)	237
13.1.3.1 Specimen Details	238
13.1.3.2 Experimental and Numerical results	239
13.1.3.2.1 Unit 1S1	239
13.1.3.2.2 Unit 2S1	239
13.1.3.2.3 Unit 5S1	240
13.1.3.2.4 Unit 6S1	241
13.1.4 Summary of analysis at member level	241
13.2 Cyclic Analysis of RC Beam-Column Joints	242
13.2.1 Analysis of tests by Clyde et al (2000)	242
13.2.1.1 Analysis of tests with 10% axial load	242
13.2.1.2 Analysis of tests with 25% axial load	244
13.2.2 Analysis of tests by Pantelides et al (2002)	245
13.3 Validation of parameters against quasi-static-cyclic analysis of RC structures	246
13.3.1 Description of frame structure	247
13.3.2 Experimental and numerical results	248
13.4 Validation of parameters and numerical modelling for dynamic analysis of non-seismically designed RC structures	249
13.4.1 Description of Test Structure	250
13.4.2 Experimental Program	253
13.4.3 Experimental and numerical results	254
13.4.3.1 Static characteristics of the structure	254
13.4.3.2 Dynamic characteristics of the structure	255
13.4.3.3 Simulated earthquake tests and analysis	256
13.5 Nonlinear dynamic analysis of as built 2D RC frame structure	260
13.5.1 Modal analysis	260
13.5.2 Nonlinear dynamic analysis	260
13.5.2.1 Analysis for the loading wave corresponding to PGA = 0.3g	260
13.5.2.2 Analysis for the loading wave corresponding to PGA = 0.5g	262
13.5.2.3 Analysis for the loading wave corresponding to PGA = 1.0g	263
13.5.2.4 Summary of nonlinear dynamic analysis	263
13.5.2.5 Estimating damage in the structure from numerical analysis	263
13.5.2.6 Numerical analysis results beyond experimental range	267
14. VALIDATION OF ASSESSMENT MODEL FOR FULLY FASTENED HAUNCH RETROFIT SOLUTION AGAINST EXPERIMENTS	268

14.1	Validation of model against experiments at joint level	268
14.1.1	Validation against joint JT1-3	268
14.1.2	Validation against joint JT1-4	271
14.1.3	Validation against joint JT1-5	272
14.2	Nonlinear dynamic analysis of retrofitted 2D RC frame structure	272
14.2.1	Modal analysis	273
14.2.2	Nonlinear dynamic analysis	273
14.2.2.1	Analysis for the loading wave corresponding to PGA = 0.3g	274
14.2.2.2	Analysis for the loading wave corresponding to PGA = 0.5g	275
14.2.2.3	Analysis for the loading wave corresponding to PGA = 1.0g	275
14.2.2.4	Summary of Nonlinear Analysis	278
14.2.2.5	Estimating damage in the structure from numerical analysis	278
14.2.2.6	Numerical analysis results beyond experimental range	281
15.	SEISMIC ASSESSMENT AND RETROFITTING OF A REAL LIFE RC FRAME STRUCTURE – A CASE STUDY	283
15.1	Description of the structure	283
15.1.1	Geometry	283
15.1.2	Section properties	284
15.1.3	Material properties	288
15.2	Loads on the structure	288
15.2.1	Dead Loads	288
15.2.2	Live loads	289
15.2.3	Seismic loads	289
15.3	Results of seismic assessment of as-built structure	291
15.3.1	Results of seismic assessment of as-built structure along X-direction	291
15.3.2	Results of seismic assessment of as-built structure along Y-direction	295
15.4	Design of retrofitting	299
15.4.1	Design of FFHRS	299
15.4.2	Sample calculation for design of FFHRS	299
15.5	Results of seismic assessment of retrofitted structure	301
15.5.1	Results of seismic assessment of retrofitted structure along X-direction	301
15.5.2	Results of seismic assessment of retrofitted structure along Y-direction	305
15.6	Analysis under higher level of earthquake	308
15.7	Summary	311
16.	CONCLUSIONS AND RECOMMENDATIONS	313
	Zusammenfassung (German Summary)	319

References	323
APPENDIX-A: GENERATION OF HINGE PROPERTIES FOR FRAME MEMBERS	336
A.1 Determination of Moment-Rotation Characteristics	336
A.1.1 Stress Equilibrium and Strain Compatibility	336
A.1.2 Constitutive laws	338
A.1.2.1 Stress-Strain models for unconfined concrete	338
A.1.2.2 Stress-Strain models for concrete confined by rectangular hoops	340
A.1.2.3 Kent and Park Model	342
A.1.2.4 Modified Kent and Park Model	344
A.1.3 Evaluation of stress block parameters	345
A.1.4 Algorithm for moment-curvature determination	347
A.1.5 Determination of moment-rotation from moment-curvature characteristics	348
A.1.5.1 Relationship between curvature and rotation	348
A.1.5.2 Plastic hinge length formulations	351
A.2 Determination of Shear Force-Deformation Characteristics	352
A.2.1 Formulations for prediction of shear force-deformation characteristics	352
A.2.2 Equilibrium condition of stresses (Watanabe and Lee, 1998)	354
A.2.3 Compatibility condition of strains	355
A.2.4 Constitutive laws	357
A.2.5 Algorithm for prediction of shear characteristics	359
A.3 Determination of Torsional Moment-Rotation Characteristics	360
APPENDIX-B PROCEDURE TO PERFORM INELASTIC STATIC ANALYSIS	362
B.1 General Procedure	362
B.2 Nonlinear static pushover analysis of a portal frame (Example)	363
APPENDIX-C 3D FE ANALYSIS OF BEAM-COLUMN JOINTS UNDER CYCLIC LOADS	371
C.1 Microplane model with relaxed kinematic constraint (Ožbolt et. al, 2001)	371
C.2 Overview of MASA	373
C.3 Constitutive law for reinforcement steel	374
C.4 Discrete Bond Model	375
C.5 Numerical modeling of beam-column joints in MASA	378
C.6 Results of numerical analyses	378
Curriculum Vitae	381

Notation

a	=	Average spacing of diagonal cracks measured perpendicular to the cracks
A_c	=	Gross Area of concrete section in mm^2
$A_{c,N}$	=	Projected area of the group
$A_{c,N}^0$	=	$9h_{ef}^2$
A_f	=	area under the uniaxial tensile stress-strain curve
A_g	=	Gross area of column/ joint cross section
ALR	=	Axial load ratio
A_m	=	Area of reinforcement in model (frame structure)
A_o	=	gross area enclosed by shear flow path
A_p	=	Area of reinforcement in prototype (in this case joint)
A_s	=	Cross-sectional area of the stirrup reinforcement
a_s	=	Shear span
A_{sb}	=	total area of beam reinforcement in tension
A_{si}	=	Area of i^{th} bar
A_{sv}	=	Area of one leg of transverse reinforcement
A_v	=	cross-section of longitudinal column reinforcement
b	=	vertical distance between the end points of the LVDTs
b''	=	Width of confined core measured to outside of hoops
b_b	=	width of beam
b_c	=	width of the column
$b_{j,eq}$	=	equivalent joint width
B_o	=	Shorter dimension of transverse reinforcement
c	=	minimum edge distance
C	=	Flexural compressive force at the beam end sections
[C]	=	damping matrix of the structure
C_b	=	compressive force in beam reinforcement
C_{cb}	=	compressive force in concrete in beam at critical section
C_{con}	=	compressive force in concrete
c_{cr}	=	critical edge distance
C_{sb}	=	compressive force in steel in beam at critical section
d	=	displacement of spring modelling anchor group corresponding to load, N
d	=	Effective depth of the section
D	=	Total depth of section
d''	=	Depth of confined core measured to outside of hoops
d_b	=	diameter of main reinforcing bars
d'_b	=	Effective cover to compression reinforcement
d_b	=	effective depth of beam
d_b	=	Effective depth of the beam
d_i	=	depth of i^{th} bar from extreme compression fiber

D_o	=	Longer dimension of transverse reinforcement
d_s	=	diameter of shear reinforcement
e	=	Eccentricity (Distance between centre lines of beam and column)
E	=	modulus of elasticity
E_0	=	Initial Young's modulus
E_c	=	modulus of elasticity of concrete
E_h	=	Hardening modulus
E_s	=	modulus of elasticity of steel
f_c'	=	Cylindrical compressive strength of concrete
f_c	=	axial stress on the column
f_{ck}	=	characteristic cube strength of concrete
f_{ct}	=	tensile strength of concrete
f_{cu}	=	cubic compressive strength of concrete, MPa
f_{dc}	=	stress of shear reinforcement corresponding to diagonal cracking
FFHRS	=	Fully fastened haunch retrofit solution
f_s	=	stress in reinforcing bar
f_{sh}	=	stress in joint transverse reinforcement at failure
f_{si}	=	Stress in the i^{th} bar
f_{sv}	=	Yield/Ultimate stress of transverse reinforcement
f_t	=	tensile strength of concrete
f_{ws}	=	stress in shear reinforcement
f_y	=	yield strength of reinforcement bars
f_{yv}	=	yield strength of longitudinal column reinforcement
$\{F(t)\}$	=	force vector as a function of time, t
g	=	acceleration due to gravity
G_F	=	fracture energy of concrete
G_s	=	shear modulus
h	=	average element size (width of the crack band)
h_b	=	depth of the beam
h_c	=	depth of the column
h_{ef}	=	effective embedment depth of the anchors
I	=	moment of inertia of the section
j_t	=	Distance between upper and lower stringers
K	=	modification factor to account for confinement in Modified Kent and Park model
$[K]$	=	stiffness matrix of the structure
$K_{0.5N_u}$	=	Secant stiffness of the anchor group corresponding to 50% of N_u
k_1	=	factor to consider influence of type of reinforcement on l_p
k_2	=	factor to consider influence of axial load on plastic hinge length
k_3	=	factor to consider influence of concrete compressive strength on l_p
k_d	=	neutral axis depth

k_{group}	=	stiffness of anchor group
$k_{individual}$	=	stiffness of individual anchor
k_{Nu}	=	Secant stiffness of the anchor group corresponding to N_u
$k_{Nu,cr}$	=	Secant stiffness of anchor group at N_u considering cracked concrete
$k_{Nu,uncr}$	=	Secant stiffness of anchor group at N_u considering uncracked concrete
K_s	=	secant compressive modulus
$K_{t,cr}$	=	cracked stiffness of the section
k_v	=	numerical coefficient
k_α	=	function controlling ‘ α ’ parameter
k_β	=	function controlling ‘ β ’ parameter
l	=	Clear span length
L	=	length of the member
L_b	=	half of the bay width
L_c	=	the storey height
l_j	=	undeformed length of potentiometer
lp	=	plastic hinge length,
M	=	Moment of resistance of the section corresponding to curvature ϕ
$[M]$	=	mass matrix of the structure
M_b	=	moment in beam at the face of column
M_{bh}	=	bending moment in beam at the point of connectivity of haunch
M_{cr}	=	Moment at the critical section for shear
M_t	=	Ratio of yield stress of transverse reinforcement and longitudinal reinforcement
N	=	tension load on anchor group
n	=	number of anchors in anchor group
N_u	=	Ultimate load for the group calculated using CC method
N_u^0	=	failure load of a single anchor in tension
$N_{u,cracked}$	=	peak load carrying capacity of the anchorage system in cracked concrete
$N_{u,uncracked}$	=	peak load carrying capacity of the anchorage system in uncracked concrete
P	=	axial load on the column
P	=	Axial load on column
P_0	=	axial compressive strength of member without bending moment.
P_c	=	Perimeter of concrete section in mm
p_c	=	principal compressive stress
PFA	=	Peak floor acceleration
PGA	=	Peak ground acceleration
p_{sh}	=	percentage volumetric shear reinforcement
p_t	=	principal tensile stress
P_{ult}	=	axial load capacity of the columns
Q_s	=	shear force at diagonal cracking
$s(x)$	=	displacement field
Sa	=	spectral acceleration
Sd	=	spectral displacement

S_{FS}	=	Strength scaling factor for steel
s_h	=	Spacing of hoops
S_L	=	linear scale factor
s_v	=	centre to centre spacing of transverse reinforcement
T	=	Flexural tensile force at the beam end sections
T_b	=	tensile force in beam reinforcement
T_{cr}	=	cracking torsional moment
T_s	=	tensile force in reinforcing bar
V	=	Shear force
v	=	crack shear displacement
V_b	=	shear force in the beam
v_c	=	shear strength of the concrete without shear reinforcement
V_c	=	shear force in column
V_{jh}	=	horizontal joint shear force
V_{jv}	=	Vertical joint shear force
w	=	crack opening displacement
$\{\ddot{x}(t)\}$	=	acceleration vector as a function of time, t
$\{x(t)\}$	=	displacement vector as a function of time, t
$\{\dot{x}(t)\}$	=	velocity vector as a function of time, t
z	=	Distance of critical section from point of contra-flexure
Z_b	=	lever arm of internal forces in beam at column face
z_c	=	lever arm of internal forces in column at joint face
α	=	joint aspect ratio
α parameter	=	parameter controlling unloading in pivot hysteretic model
α_j	=	angle of potentiometer with the horizontal
β parameter	=	parameter controlling pinching in pivot hysteretic model
γ	=	neutral axis depth factor
γ_j	=	joint shear deformation
δ	=	Angle between φ and θ
Δ_c	=	column shear deformation
δd_1	=	change in length measured by LVDT, d_1
δd_2	=	change in length measured by LVDT, d_2
ΔM_i	=	additional inertial mass on the i^{th} floor level in the model structure, for a unit mass in prototype
ε	=	smeared strain of cracked concrete
ε_c	=	strain in concrete in compression
ε_{cm}	=	strain at the extreme compression fiber
ε_{dc}	=	strain of shear reinforcement corresponding to diagonal cracking
ε_s	=	strain in reinforcing bar
ε_v	=	smeared strains due to crack shear displacement
ε_w	=	smeared strains due to crack opening

ε_{xv}	=	shear strain of cracked concrete in x direction
ε_{yv}	=	shear strain of cracked concrete in y direction
θ	=	rotation of the member
θ_p	=	plastic rotation of the member
θ_u	=	ultimate rotation of the member
θ_y	=	yield rotation of the member
$v f_c'$	=	effective compressive strength of cracked concrete
ρ_c	=	ratio of area of longitudinal steel in column to gross column area
ρ_{col}	=	ratio of longitudinal column reinforcement in tension
ρ_s	=	is the ratio of joint reinforcement to joint area
ρ_w	=	ratio of shear reinforcement
σ	=	vertical joint shear stress
σ_1, σ_2	=	Principal stresses in the concrete element
σ_a	=	Mean axial compressive stress on column
σ_c	=	normal stress due to aggregate interlock at cracked surface
σ_c	=	Normal stress at cracked surface due to aggregate interlock
σ_d	=	Normal stress in concrete parallel to crack inclination
σ_{xf}	=	axial stress at the centroidal axis due to load effect just before diagonal cracking
σ_y	=	Vertical compressive stress of the concrete element induced from shear reinforcement.
τ	=	horizontal joint shear stress
τ_0	=	octahedral stress
τ_c	=	nominal shear strength of a column without stirrups
τ_c	=	shear stress due to aggregate interlock at cracked surface
τ_c	=	Shear stress at cracked surface due to aggregate interlock
τ_{cr}	=	stress corresponding to joint cracking
τ_f	=	frictional component in bond strength
τ_f	=	shear stress at the centroidal axis due to load effect just before diagonal cracking
τ_m	=	mechanical interaction component in bond strength
φ	=	curvature
φ_u	=	ultimate curvature
φ_y	=	yield curvature

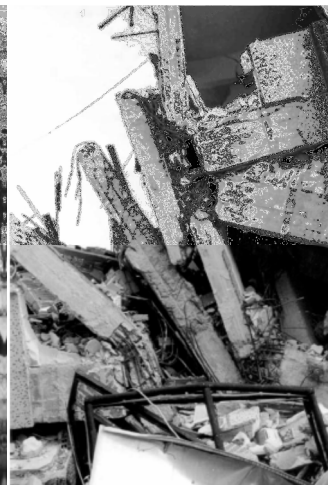
1. INTRODUCTION

1.1 Motivation and Problem Statement

Reinforced concrete (RC) framed structural configuration is probably the most popular construction type throughout the world owing mainly to reasons such as ease of construction, relatively low cost, good thermal insulation etc. This type of construction generally serves its purpose well under normal loads. However, the performance of such structures under seismic loads has exposed the vulnerability of this construction type. One of the most severe deficiencies in RC frame structures which make it vulnerable against earthquakes is the inadequate shear resistance of beam-column joints. A typical example of the failure of beam-column joints in RC frame structure during the 1999 Kocaeli (Turkey) earthquake is shown in Figure 1.1(a) (Ghobarah and Said, 2002) and Figure 1.1(b) shows the failure of beam-column joint during 2008 Wenchuan earthquake (Zhao et al., 2009). Similar failures have been observed elsewhere as well which led to partial/complete collapse of buildings (Figure 1.2).



(a) 1999 Kocaeli, Turkey
(Ghobarah and Said, 2002)



(b) 2008 Wenchuan China
(Zhao et al., 2009)

Figure 1.1 Failure of beam-column joints in RC frame structures

By design, the members, namely beams and columns are designed to undergo ductile failure. This is done by proportioning the section in such a way that the tension reinforcement yields before the concrete in compression reaches its limiting strain under applied bending moments, the so-called under-reinforced section design. Further, shear failure of such sections is avoided by design.

However, traditionally, beam-column joints were considered rigid, which was credited to the confining action of the members framing into the joint core. This approach works well under gravity loads since the joint panel is not subjected to large forces in such cases. However, under the action of seismic forces, beam-column joints are subjected to large shear stresses

in the core. These shear stresses in the joint are a result of moments of opposite signs on the member ends on either side of the joint core. Typically, high bond stress requirements are also imposed on reinforcement bars of beams framing into the joint. The axial and joint shear stresses result in principal tension and compression that leads to diagonal cracking and/or crushing of concrete in the joint core. These stresses in the joint core are resisted by the so-called strut and tie mechanism (Paulay and Priestley, 1992).



(a) 2004 Sumatra Earthquake
(Saatcioglu et al, 2004)



(b) 2011 Christchurch Earthquake

Figure 1.2 Collapse of RC frame structures due to joint failures

To prevent the shear failure of the joint core by diagonal tension, joint shear reinforcement is needed, which is therefore prescribed by the newer design codes e.g. ACI 318 (2011), NZS 3101 (2006), EC8 (2004), IS 13920 (2002) and similar other codes. Moreover, these codes prescribe a large anchorage length of the bars terminating in case of exterior joints, so that a bond failure may be avoided. It is now generally accepted that the design and detailing requirements laid by new codes ensure a better seismic performance as compared to those designed as per old codes. This is especially true for the performance of beam-column joints of structures. However, a majority of the structures around the world were constructed before such codes came into force. The number of such non-seismically designed structures is even larger in case of developing countries where the seismic designs are still not mandatory. In order to ensure the seismic safety of such structures, it is of utmost importance to (i) assess the seismic behavior of such structures realistically, and (ii) design a practical and effective retrofit solution to improve their seismic performance.

Keeping the above-mentioned points in mind, the problem being addressed in this work is a combination of:

1. Understanding the behavior of the non-seismically designed structures with emphasis on beam-column joints, through experiments at sub-assembly level as well as structural level.

2. Development of models for realistic assessment of seismic behavior of non-seismically detailed RC frame structures considering joint distortion and hysteretic behavior.
3. Studying the efficacy and suitability of the fully fastened haunch retrofit solution to improve the seismic performance of beam-column joints and in turn structures.
4. Development of an assessment method for the structures with joints retrofitted with the fully fastened haunch retrofit solution.

1.2 Context for the Research

Although under earthquakes, RC structures invariably go in the nonlinear (inelastic) range, still the analysis and designs till date are mostly based on linear elastic procedures giving an indirect consideration to the nonlinearity by means of reduction factors. Such approaches may not be sufficient for assessment of structures depending on various aspects such as time period of structure, predominant failure modes, sizing and reinforcement detailing aspects etc. Especially for non-seismically designed (or gravity load designed) structures, such approaches can be significantly un-conservative due to the formation of undesirable failure modes that may not be accounted for by such simplistic analysis. Further, this approach does not provide insight on weak links, failure modes, deformation limits etc., the aspects that are essential in assessment and suitable design of retrofitting for the structure.

Based on discussions and arguments similar to the one above, it is well recognized that performance based approach is a more rational and accurate approach for assessment and design of structures. The analysis is aimed at obtaining the actual performance, in terms of damage, expected during a given earthquake. The location, mode and extent of failures, ductility demand, inter-storey and global drifts etc. can be reasonably assessed by this approach. The performance assessment of structure requires determination of inelastic force-deformation curves or hysteretic behavior for the structure. This simplifies the structural model and provides useful information about the likely inelastic behavior of the structure. To capture the complete and realistic picture of the nonlinear behavior of the frame structure, modeling of various nonlinearities expected in the structure is required. Typically, the nonlinearities in an RC frame structure include flexural, shear, axial and torsional behavior for beams and columns as well as more complex behavior at the connections, e.g., joint shear failure, bond failure, etc.

Though it is well-accepted that the beam-column joints, especially of non-seismically designed structures, behave inelastically during the earthquakes, still the analysis approach mainly revolves around considering concentrated plasticity at the member ends and assuming the joint core as rigid. This is not due to negligence of the designers or analysts but is attributed to the fact that the models available in literature generally are not simple enough to be used in commercial programs being at the same time able to predict the shear behavior of the joints reasonably. Moreover, the models either require large computational efforts so that they are not practically useful for analyzing the global structural behavior or they need a

special element with various nodes and springs or a special purpose program to implement the joint nonlinearity. This makes it difficult for the designers and analysts to follow the recommended approaches using the commercial programs.

In this work, a new model for predicting the inelastic shear behavior of beam-column joints is developed that can realistically capture the shear behavior of the joints and also is practical enough to be used with existing commercial software programs available. The model is based on practical deformational behavior of the joint sub-assembly in a structure and follows the principal stress failure criteria so that due consideration may be given to the axial load acting on the column.

Nonlinear dynamic analysis of RC frame structures is currently considered to be complex and time consuming. Nevertheless, it is the most accurate form of seismic analysis for such structures. In order to perform nonlinear dynamic analysis, it is required to develop hysteretic rules that are efficient and easy to implement while being accurate enough to sufficiently capture the hysteretic behavior of the structures. In case of non-seismically designed RC structures, it is important to have models to capture the hysteretic behavior of beams, columns as well as of the joints. In this work, one such model has been presented, which is based on the pivot hysteresis rule (Dowell et al, 1998). The model was originally developed for performing nonlinear dynamic analysis of circular bridge columns. Keeping the basic framework of the model same, parameters were developed to extend the applicability of the model to rectangular sections (beams and columns) as well as to beam-column joints. Certain limitations of the original model that were inherent due to its intended use were also improved upon in the process.

In order to understand the behavior of the beam-column joints and to validate the model, in this work, experiments were conducted on beam-column joints under quasi-static cyclic loads. Further to understand the behavior of joints and their influence on the overall structural behavior, experiments were conducted on RC frame structures under lateral monotonic loads at full-scale level. Further experiments were carried out on scaled down structures under dynamic loads on shake table. Both the models have been validated against experimental results at sub-assembly level as well as structural level. Also the tests in the literature were included for validation of the models.

Using the above mentioned practically implementable and efficient models, an existing structure can be assessed to verify its performance against a given earthquake with high confidence. Such an analysis can provide information on the state of the structure under a given earthquake; while at the same time also point out the deficiencies and weak links in the structure. Following the information provided by numerical analysis, the locations needing the retrofit against various failure modes can be identified. It is very likely that analysis of non-seismically designed structures highlight beam-column joints as one of the most vulnerable zones of the structure. To improve the performance of the structure under seismic loads,

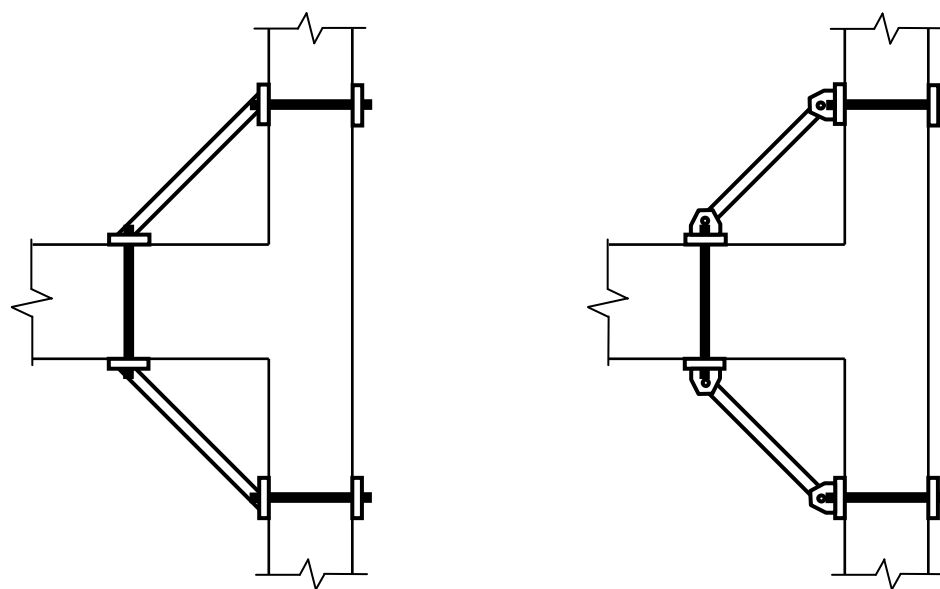
improving the performance of beam-column joints of the same is therefore essential. This calls for the need to develop a retrofit solution for joints of the structure.

A good retrofit solution is the one which is less invasive, easy and fast to implement, reliable and efficient in improving joint behavior. Though various methods of retrofitting the members and joints have been tried by various researchers, most of the methods do not qualify for one or more of the above-mentioned requirements. Further, certain methods that look relatively easy to implement at laboratory level tests have proved to be extremely difficult for implementation in practice. One of the major reasons for that is the restricted approach to the joint core/panel.

Relatively recently, Pampanin et al. (2006) developed and validated haunch retrofit solution (HRS) for RC beam-column joints. The underlying principle of the HRS was to relocate the plastic hinge away from the vulnerable joint panel/core while enhancing the global response of non-seismically designed RC joint sub-assembly by altering the hierarchy of strength suitably. In order to connect the haunch element, which basically consisted of an axial element in the form of a machined bar connected to plates at both ends, two types of connections between axial element and plates namely, hinged and welded were studied. In one specimen, a yielding type fuse element was used as axial element. In order to connect the haunch element with beams and columns, two partially prestressed external rods along with two anchors directly fastened to both beam and column were used. Figure 1.3 shows the schematic of the HRS used by Pampanin et al. (2006).

The tests clearly displayed that the HRS can be very effective in improving the behavior of beam-column joints of non-conforming RC structures. However, one prohibitive requirement of the connection proposed by them was to use external partially prestressed rods to connect the haunch to the frame. To eliminate this limitation, further tests were carried out with the haunch elements connected to the frame members by using post-installed mechanical anchors.

Genesio (2012) investigated the feasibility, strengths, limitations etc of this fully fastened HRS by means of experiments carried out first in University of Canterbury (Genesio and Akgüzel, 2009) and later at BARC, Mumbai (Genesio and Sharma, 2010). The tests were carried out on exterior beam-column joints under quasi-static-cyclic loads. These tests clearly proved the efficacy of the retrofit solution to alter the hierarchy of strength in a beam-column joint sub-assembly in order to prevent brittle joint shear failure and inducing ductile beam failure at much higher loads. However, to establish the suitability of the retrofit solution for seismic performance assessment of structures, experiments were needed to be conducted at structural level under dynamic loads.



(a) Hinged HRS (THR1)

(b) Welded HRS (THR 3)

Figure 1.3 Schematic of haunch retrofit solutions tested and validated by Pampanin et al (2006)

In this work, shake table experiments were carried out on 2D RC frame structures without and with fully fastened HRS. The basic design of the frames was performed so that the exterior joints of the frames are 2/3rd scale replica of the joints tested earlier by Genesio and Sharma (2010) in BARC. The experiments were conducted by subjecting the structures to uniaxial dynamic earthquake loading with the level of loading increased incrementally in steps of 0.1g till failure or till the capacity of shake table (1.0g) was reached. These tests clearly displayed the efficacy of the fully fastened HRS in safeguarding the joints at structural level under seismic loads.

Certain guidelines to design the retrofit solution, using external rods, for a beam-column joint sub-assembly were provided by Pampanin et al (2006). Genesio (2012) extended the same for the HRS using post-installed anchors. However, in order to assess the complete performance of the solution in structure till failure, it is required to have a model that can give due consideration to nonlinear behavior of anchors and can be implemented on practical structural models using frame elements. In this work, one such model is developed that can realistically assess the complete behavior of beam-column joints retrofitted with fully fastened haunch retrofit solution. The model was validated against the experimental results obtained at the joint level as well as at structural level under dynamic loads.

In order to demonstrate the applicability of the models for seismic performance assessment of as-built and retrofitted RC frame structures, a case study was performed on a real-life structure existing in New Delhi, India. The structure was first assessed against seismic loads using the models developed in this work. The weak zones in the structure were established by the performance analysis and based on the results, an optimum retrofit scheme using

HRS was designed. The performance of the retrofitted structure was again assessed using the models developed and it was shown that the suggested retrofitting is capable of improving the seismic performance of the structure significantly.

1.3 Organization of Work

The work carried out within the framework of the thesis is organized as follows:

- a. Development of numerical models
 1. Development of joint model for performance assessment of joints and structures
 2. Development of parameters for extension of pivot hysteresis model
 3. Development of assessment model for joints retrofitted with fully fastened haunch retrofit solution
- b. Experimental Work
 1. Experiments on as-built and retrofitted beam-column joints under cyclic loads
 2. Experiments on a full scale non-seismically designed RC frame structure under lateral monotonic loads
 3. Shake table experiments on as built and retrofitted 2D RC frames under dynamic loads
- c. Validation of models
 1. Validation of joint model against experiments at sub-assembly and structural level
 2. Validation of extended pivot hysteretic model parameters against experiments at member, sub-assembly and structural level subjected to cyclic and dynamic loads
 3. Validation of assessment model for joints retrofitted with fully fastened haunch retrofit solution at sub-assembly and structural level
- d. Case Study
 1. Case study on seismic performance assessment of as built and retrofitted real life existing structure in New Delhi, India

2. SEISMIC BEHAVIOR OF BEAM-COLUMN JOINTS IN REINFORCED CONCRETE FRAME STRUCTURES

A joint is defined as the portion of the column within the depth of the deepest beam that frames into the column (ACI 352 R, 2002). The ideal functional requirement of a joint is to enable the adjoining members to develop and sustain their ultimate capacity. However, for the joints of non-seismically designed structures, this requirement is in most cases not fulfilled, when subjected to seismic forces. This is attributed to the geometrical configuration, reinforcement detailing and mechanics of the joint under seismic forces. This chapter focuses on the behavior of RC beam-column joints under seismic loads.

2.1 Classification of RC Beam-Column Joints

The reinforced concrete beam-column joints used in frames may be classified in terms of geometric configuration (exterior and interior joints), structural behavior (elastic and inelastic joints) or detailing aspects (joints of non-seismically detailed and seismically detailed structures).

2.1.1 Classification based on geometric configuration

Based on the fundamental differences in the mechanisms of beam bar anchorages, it is customary to differentiate between interior and exterior joints.

a. Exterior beam-column joints

Different types of exterior joints present in a building are shown in Figure 2.1. In a plane frame, the corner joints at roof (Figure 2.1(a)) and at intermediate floor (Figure 2.1(d)) fall under the category of exterior beam-column joints. In case of a space frame, the roof corner joint (Figure 2.1(b)), the roof edge joint (Figure 2.1(c)), the intermediate floor corner joint (Figure 2.1(e)) and the intermediate floor edge joint (Figure 2.1(f)) are categorized as exterior beam-column joints.

b. Interior beam-column joints

Different types of interior joints present in a building are shown in Figure 2.2. In a plane frame, the middle joints at roof (Figure 2.2 (a)) and at intermediate floor (Figure 2.2 (b)) fall under the category of interior beam-column joints. In case of a space frame, the roof middle joint (Figure 2.2 (c)) and the intermediate floor middle joint (Figure 2.2 (d)) are categorized as interior beam-column joints.

2.1.2 Classification based on structural behavior

Based on the crack propagation in the joint region and failure mechanism under loading, the joints can be classified as elastic or inelastic (Paulay and Priestley, 1992).

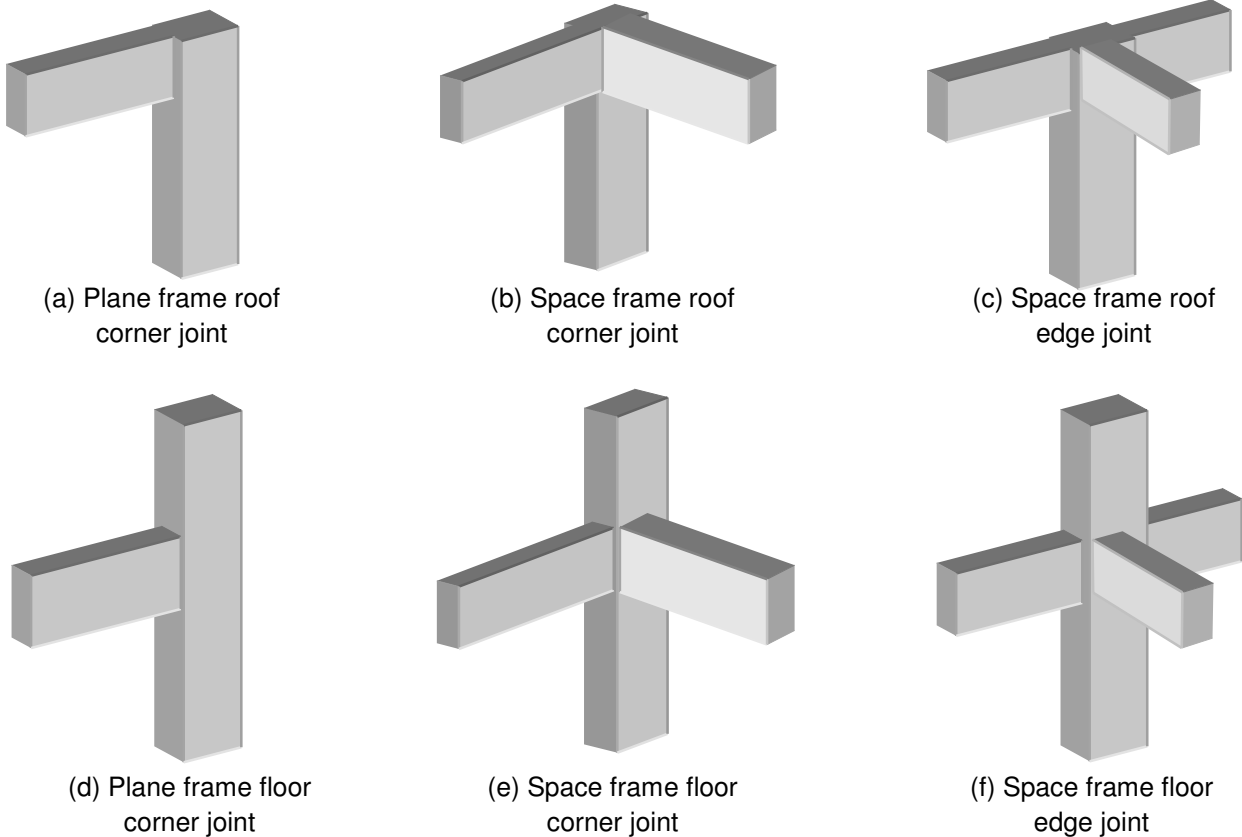


Figure 2.1 Exterior beam-column joints in plane and space frames

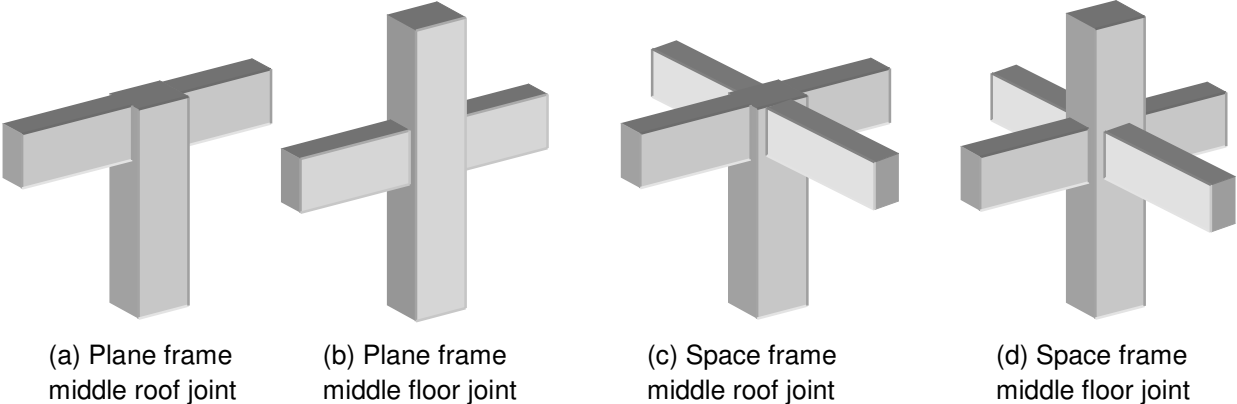


Figure 2.2 Interior beam-column joints in plane and space frames

a. *Elastic beam-column joints*

The most preferable structural behavior for a joint is such that joint remain essentially elastic throughout the response of the structure. Such joints are classified as elastic joints. However, they seldom occur in practice.

b. *Inelastic beam-column joints*

Under seismic loads, the joint generally goes beyond elastic range and there is certain inelastic deformation and cracking of the joint core. This may be due to insufficient shear capacity of the joint or due to the penetration of inelastic strains along the reinforcing bars of the beams framing into the joint. Such joints are classified as inelastic joints.

2.1.3 Classification based on detailing aspects

The reinforcement detailing of beam-column joints form a major part of the ductile detailing norms prescribed by newer seismic design codes ACI 318 (2011), NZS 3101 (2006), EC8 (2004), IS 13920 (2002). The parameters that are controlled by these codes include shear reinforcement in joint core, larger anchorage length, long lap splice, closely spaced ties for better confinement etc. Whether a joint of the structure will behave in a brittle or ductile manner depends largely on its reinforcement details. Based on their behavior under loading, the joints can be classified as

a. *Joints of non-seismically detailed structures*

Joints of non-seismically detailed structures or non-ductile joints are those, are not expected to undergo large deformations before failure. Such joints are characterized typically by insufficient development lengths, short lap splices, discontinuous reinforcements, larger stirrup spacing, and no reinforcement in the joint core. Figure 2.3 (a) shows detailing of beam-column joints of a non-seismically detailed reinforced concrete frame structure (ATC-40:1996).

b. *Joints of seismically detailed structures*

Joints of seismically detailed structures or ductile joints have an ability to undergo large deformations without failure. Such joints absorb large amount of energy through the hysteretic behavior under a severe earthquake. Large anchorage lengths, long lap splices, continuous reinforcements, closer stirrup spacing, and shear reinforcement in the joint core characterize such joints. Figure 2.3 (b) shows typical ductile type reinforcement detailing prescribed by new codes of practice (IS 13920, 2002) for beam-column joints of a frame.

2.2 Failure modes of a beam-column joint

A beam-column joint primarily consists of three elements viz. beam, column and the joint core, generally considered as a part of column (ACI 352R-02). Each of the three elements can undergo failure under different modes as enlisted below

- a. Flexural failure of beam
- b. Flexural failure of column
- c. Shear failure of beam
- d. Shear failure of column
- e. Torsional failure of beam
- f. Torsional failure of column
- g. Shear failure of joint core
- h. Bond failure of reinforcement
- i. Combinations of various modes listed above

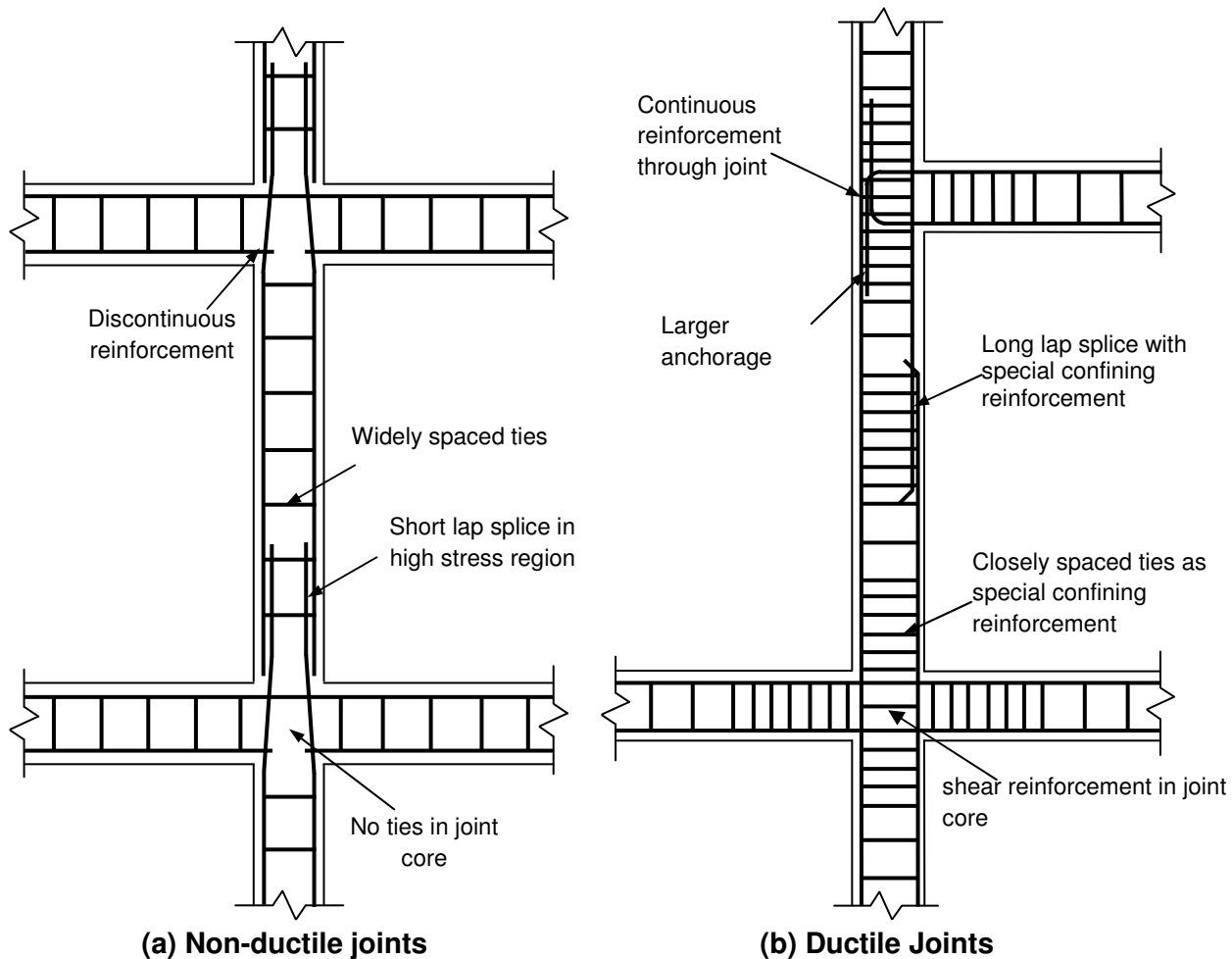


Figure 2.3 Reinforcement detailing of joints prescribed by (a) older and (b) new codes of practice

The most favorable condition from seismic design point of view is to have joint core essentially in the elastic range and formation of plastic hinges shall occur in beams, since it is ductile in nature and would also not lead to formation of global or partial mechanism. However, when the plastic hinges are developed at the ends of the beams immediately adjacent to a joint, it is not possible to prevent inelastic excursion in the joint. Therefore, the ideal situation is to have plastic hinge formation in beams at some distance away from the face of the joint. But it is not possible to achieve this condition unless certain special measures are taken. One such measure is the use of haunch elements, which will be further addressed in detail later in this work.

The torsional failure modes are possible only in case of structures where torsional loads may be transferred to beams due to slabs and to columns due to eccentricity. Since the joint sub-assembly can fail in various modes, a good model for the same shall be able to capture and predict all possible failure modes.

2.3 Mechanics of beam-column joints

The behaviour of a joint is characterized by a complex interaction of shear, bond and confinement mechanisms taking place in a quite limited area (Costa, 2003). Under the action of seismic forces, beam-column joints are subjected to large shear stresses in the core. These shear stresses in the joint are a result of moments of opposite signs on the member ends on either side of the joint core. Typically, high bond stress requirements are also imposed on reinforcement bars entering into the joint. The axial and joint shear stresses result in principal tension and compression that leads to diagonal cracking and/or crushing of concrete in the joint core.

2.3.1 Exterior Joints

When RC moment frames are subjected to lateral seismic loading, high shear forces are generated in the joint core. Figure 2.4 shows the mechanics of exterior joint when subjected to seismic forces. The lateral seismic loading on a frame leads to bending moments and shear forces that can be simulated in the joint as shown in Figure 2.4 (a). Here the length of the beam L_b is half of the bay width and L_c is the storey height (assuming that point of inflexion lies at mid span of beam and mid height of column). Figure 2.4 (b) shows the joint shear forces generated due to these external actions. From equilibrium of the joint, as shown in Figure 2.4 (b), we get,

$$V_{jh} = T_b - V_c \quad (2.1)$$

Now, we have

$$T_b = M_b/Z_b = V_b L_b/Z_b \quad (2.2)$$

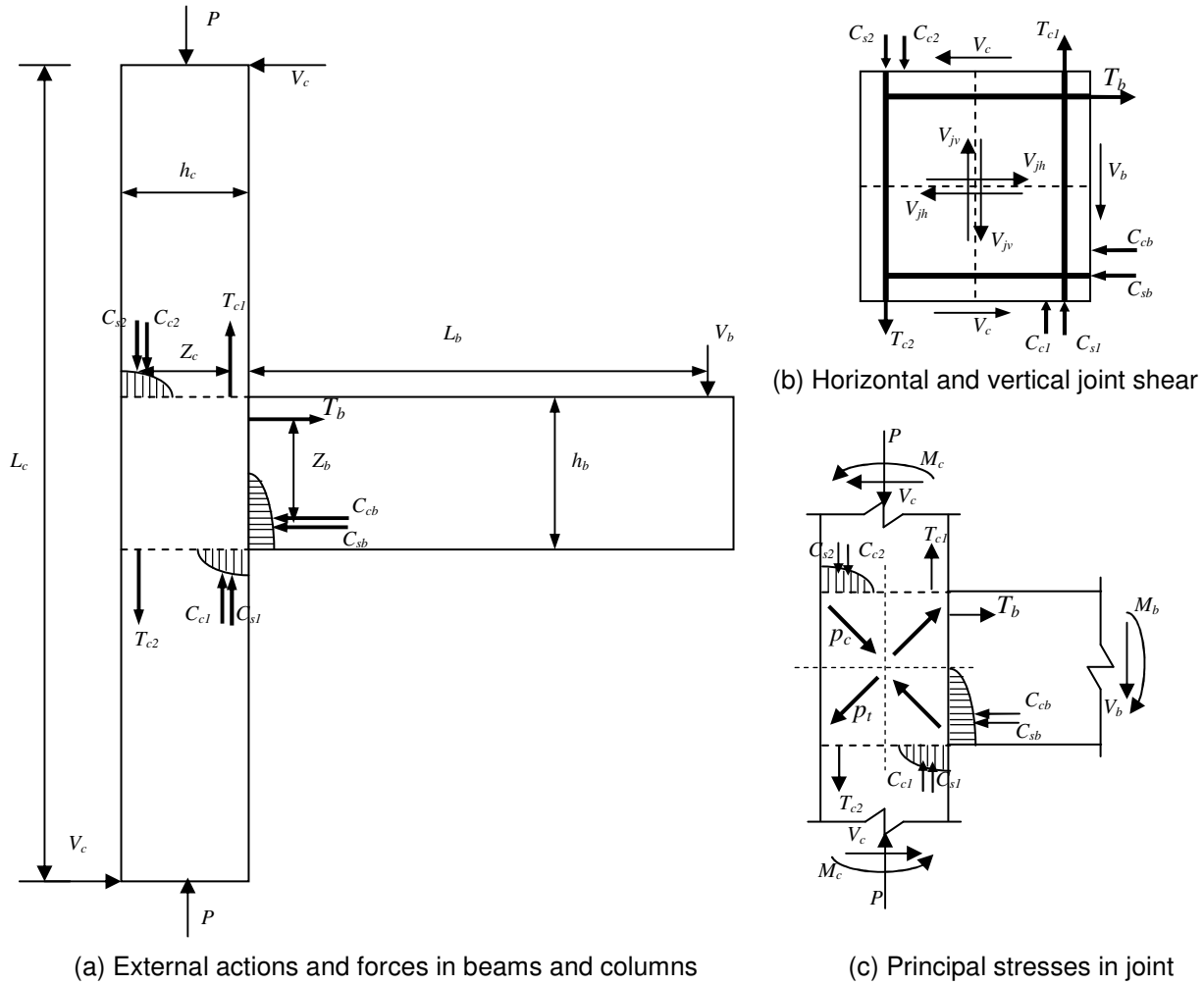


Figure 2.4 Actions and Forces on an Exterior Joint

Also, from the equilibrium of external actions, we have,

$$V_c = V_b(L_b + 0.5h_c)/L_c \quad (2.3)$$

Substituting (2) and (3) in (1), we get,

$$V_{jh} = V_b \left(\frac{L_b}{Z_b} - \frac{L_b + 0.5h_c}{L_c} \right) \quad (2.4)$$

The horizontal joint shear stress can be obtained as

$$\tau = \frac{V_{jh}}{h'_c b'_c} \quad (2.5)$$

where, h'_c and b'_c are the length and width of joint core respectively.

In general, for sufficient accuracy, we can consider,

$$Z_b = d_b - d'_b \quad (2.6)$$

Where,

d_b = Effective depth of the beam

d'_b = Effective cover to compression reinforcement

Similarly, from equilibrium in vertical direction, we can get vertical joint shear. However, it has been shown that (Park and Paulay, 1975; CEN 250; Paulay and Park, 1984; Tsonos, 2007)

$$\frac{V_{jv}}{V_{jh}} = \frac{h_b}{h_c} = \alpha \quad (2.7)$$

where, α is the joint aspect ratio.

Now, vertical joint shear stress is given by,

$$\sigma = \frac{V_{jv}}{h'_c b'_c} \quad (2.8)$$

Thus, (5), (7) and (8), we have,

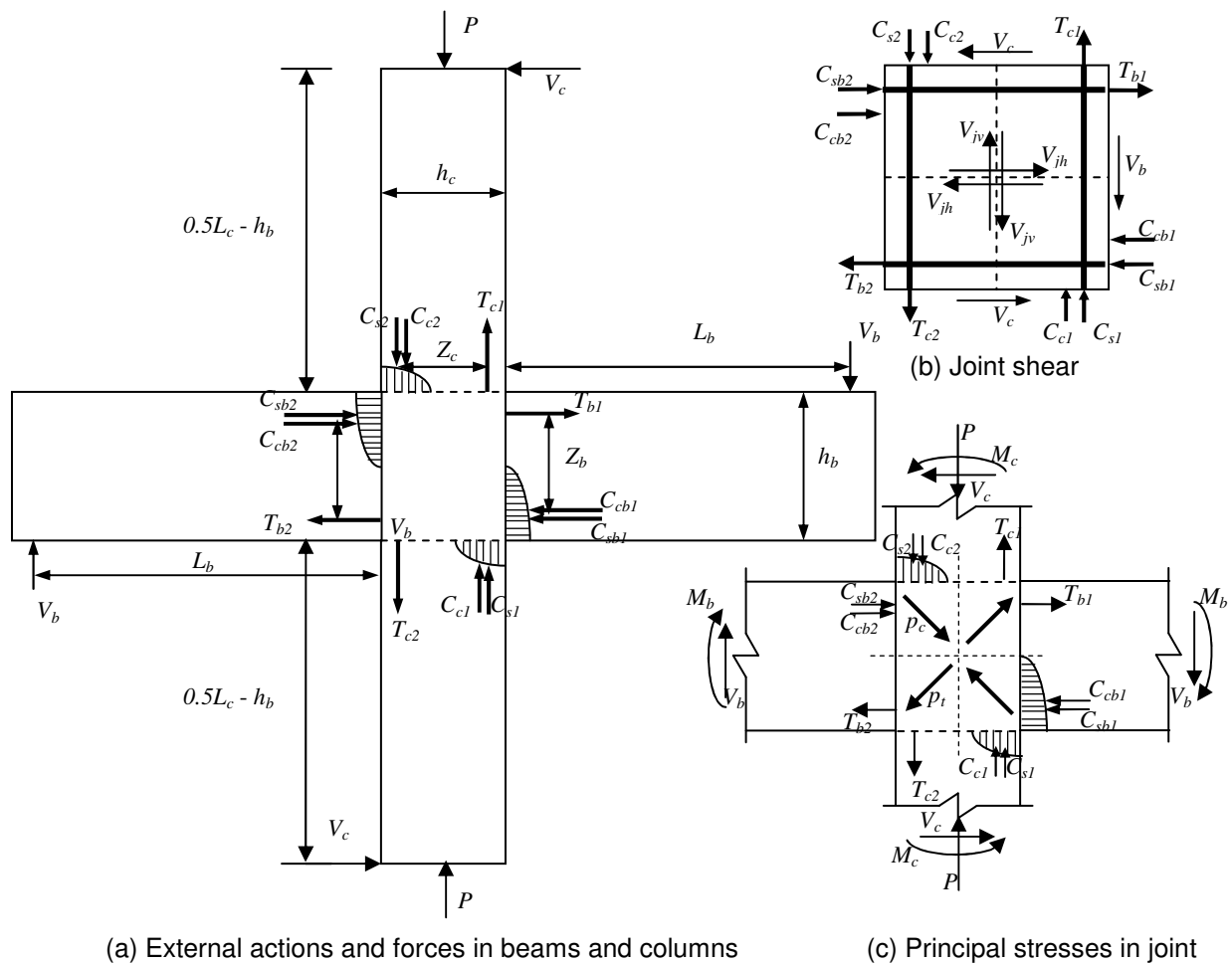
$$\sigma = \alpha \tau \quad (2.9)$$

The principal compressive stress, p_c and tensile stress p_t can be calculated as

$$p_{c,t} = \frac{\sigma}{2} \pm \frac{\sigma}{2} \sqrt{1 + \frac{4\tau^2}{\sigma^2}} \quad (2.10)$$

2.3.2 Interior Joints

In case of interior joints, the beam runs through the column. In order to calculate the horizontal shear force in the joint core, let us consider the equilibrium of the joint. Let M_h and M_s be the hogging and sagging moments respectively acting on either side of the joint core as shown in Figure 2.5 (a).



(a) External actions and forces in beams and columns (c) Principal stresses in joint
Figure 2.5 Mechanics of interior joint under seismic actions

T_b and C_b are the tensile and compressive forces in the beam reinforcements. V_b is vertical beam shear and V_{col} is horizontal column shear. Similar to the expressions for exterior joints, we can obtain relations for joint shear and principal stresses for interior joint as shown in Figure 2.5. The horizontal joint shear force can be obtained as

$$V_{jh} = 2V_b \left(\frac{L_b}{Z_b} - \frac{L_b + 0.5h_c}{L_c} \right) \quad (2.11)$$

In a similar way, the vertical joint shear force can be obtained. In the above expressions, L_b is always the distance from the face of the column to the point of contra-flexure of the beam.

2.3.3 Mechanism of resistance

The most acceptable mechanism for shear forces resistance in a joint is by a system of diagonal compression strut and tension tie. Various models on the basis of such strut-and-tie model have been proposed by literature which will be discussed in chapter 3. The basic philosophy behind this approach is that the internal forces generated in the concrete combine

to develop a diagonal strut (Paulay and Priestley, 1992; Paulay et al, 1978; Hakuto et al, 2000), while other forces transmitted to the joint core from beam and column bars by means of bond necessitate a truss mechanism. The strength of the diagonal strut controls the joint strength before cracking. The transverse reinforcement in the joint helps confine the concrete diagonal strut in the joint core thereby contributing to increased joint strength. If the joint shear forces are large, diagonal cracking in the joint core occurs followed by the crushing of concrete in joint core. The joint reinforcement alone is not sufficient to avoid undesirable pinching in hysteretic loops at this stage (Murty et al, 2003; ACI 352, 2002; Stevens et al, 1991).

2.4 Problem of bond in beam-column joints

The joint resistance mechanism depends on bond forces along its perimeter so that a truss mechanism can be mobilized and on a compressed diagonal strut between corners. One of the most important reasons for stiffness degradation of beam-column joints under large cyclic excitations is the deterioration of bond between reinforcement and concrete (Fillipou et al, 1983). Tests by Soleimani et al (1979) showed that the fixed end rotations due to bond deterioration in the joint can contribute up to 50% of overall deflections of the sub-assembly.

The flexural forces from the beams and columns cause tension or compression forces in the longitudinal reinforcements passing through the joint (Figure 2.9). During plastic hinge formation, relatively large tensile forces are transferred through bond. After the first cycle in the inelastic range, the contribution of the diagonal strut reduces significantly necessitating the truss mechanism to come into action. This may be explained as follows. High inelastic deformation causes permanent elongation of the beam bars, which leads to full depth open cracks at the beam-joint interface (Costa, 2003). This essentially means that the flexural compression due to concrete in beams becomes negligible and the compressive forces are transmitted through the longitudinal reinforcement. This significantly increase the bond stresses in the reinforcing bars passing through the joint. This leads to a drastic reduction in the contribution of the concrete strut to the transfer of horizontal joint shear and a consequent increase in the contribution of the truss mechanism. The efficiency of the truss mechanism depends on the effectiveness of bond between the steel bars and the surrounding concrete.

The bond has a very poor response in terms of energy dissipation, stiffness and strength degradation under inelastic cycling. As per Rehm and Eligehausen (1977), the bond strength decreases with increasing number of cycles between constant bond stresses (fatigue strength of bond). The slip under peak load and the residual slip increase considerably as the number of cycles increases. Although many factors related to early concrete damage (micro-cracking and micro-crushing due to high local stresses at the lugs) may be involved in this bond behaviour during repeated loads, the main cause of the slip increase under constant peak bond stress is creep of concrete between lugs (Rehm and Eligehausen 1977).

Joints whose columns are low axially loaded are the most sensitive to bond deterioration since compression helps to maintain the bond mechanism (Costa, 2003). Joint horizontal shear reinforcement improves anchorage of beam bars (Ichinose, 1991), but there is an upper bound to the beneficial effects of confinement. At this limit, maximum bond strength is attained beyond which the crushing of concrete in front of the rib portion of the deformed bar occurs. Research indicates better bond performance when the clear distance between the longitudinal bars is less than 5 times the diameter of the bar (Eligehausen et al, 1983). As expected, the deformed bars give better performance in bond. The behaviour of the reinforcing bar in bond also depends on the quality of concrete around the bar.

In exterior joints, the beam longitudinal reinforcement that frames into the column terminates within the joint core. After a few cycles of inelastic loading, the bond deterioration initiated at the column face due to yield penetration and splitting cracks, progresses towards the joint core. Repeated loading aggravates the situation and a complete loss of bond up to the beginning of the bent portion of the bar may take place. The longitudinal reinforcement bar, if terminating straight, will get pulled out due to progressive loss of bond. The pull out failure of the longitudinal bars of the beam results in complete loss of flexural strength. This kind of failure is unacceptable at any stage. Hence, proper anchorage of the beam longitudinal reinforcement bars in the joint core is of utmost importance.

In an interior joint, the force in a bar passing continuously through the joint changes from compression to tension. This causes a push-pull effect which imposes severe demand on bond strength and necessitates adequate development length within the joint. The development length has to satisfy the requirements for compression and for tension forces in the same bar. As per Filippou et al (1983), the most unfavourable bond conditions exist in the interior beam-column joints.

Insufficient development length and the spread of splitting cracks into the joint core may result in slippage of bars in the joint. Slippage of bar occurs when the limiting bond stress is exceeded within the available development length. In the case of interior joints, the column depth is the available development length for the straight longitudinal bars passing through the joint. Hence, for a given limiting bond stress, the ratio of development length to the bar diameter becomes a constant value. Research has shown that when the development length is greater than 28 bar diameters little or no bond degradation was observed with respect to various shear stress levels in the joint (Leon 1990).

3. LITERATURE REVIEW

This thesis is primarily focussed on developing practical models to simulate the inelastic seismic behaviour of beam-column joints in non-seismically deigned RC frame structures. For predicting joint shear strength, empirical models, models based on single strut mechanism, strut and tie mechanism and average plane stress approach are reported in literature. The joint element models following various approaches include, lumped plasticity models, multi-spring models, finite element simulations and fracture mechanics based approaches. Before presenting the models developed in this work, it is essential to critically review the models presented earlier by various researchers along with the strength and limitations of the same. This chapter gives a brief overview of the models available in literature to predict the joint shear strengths and to simulate the behaviour of RC beam-column joints.

3.1 Review of Existing Shear Strength Models

Currently there are several empirical and analytical models available in literature, to predict the shear strength of the joints, that have been developed based on experimental database and/or mechanistic concepts. These models can be classified on the basis of approach followed or the failure mechanism assumed to derive the models.

3.1.1 Empirical models

The approach followed to derive empirical model consists of mainly in extracting certain parameters affecting the joint shear strength from the tests and performing statistical regression analysis under the assumption that each parameter is uncorrelated to other parameters.

Probably, the first empirical model to predict the shear strength of beam-column joints was presented by Taylor (1974). An analogy between the effective depth ratio of beam to column framing into the joint and the ratio of shear span to effective depth in a deep beam was assumed as basis for the model. The ultimate joint shear strength was compared with the nominal shear strength of a column without stirrups and it was also assumed that the column shear is negligible because it is very small compared to the joint shear force provided by the beam reinforcement. The ultimate joint strength, τ_u was given by

$$\tau_u = \left(3 + 2 \frac{d_c}{z_b} \right) \tau_c \quad (3.1)$$

Where,

d_c = effective depth of column

z_b = lever arm of internal forces in beam at column face

τ_c = nominal shear strength of a column without stirrups

The ratio d_c/z_b is analogous to the shear span to effective depth ratio of a deep beam. To predict the first cracking of the joint, Taylor (1974) used an approximate principle stress analysis approach and the shear stress within the joint corresponding to initial diagonal cracking was proposed to be

$$\tau_{c,cr} = 0.67\sqrt{f_t^2 + f_c f_t} \quad (3.2)$$

Where, f_t is the tensile strength of concrete and f_c is the axial stress on the column obtained by dividing the axial load on column by gross area of the column.

On the basis of fourteen full scale tests on interior beam-column joints, investigated the influence of column load, concrete strength and amount of reinforcement in joint and column. The following equation was proposed on the basis of regression analysis to predict the stress corresponding to joint cracking, τ_{cr} :

$$\tau_{cr} = 0.0124(f_c')^{0.85} \left(\frac{P}{A_g} \right)^{0.485} \quad (3.3)$$

Where,

f_c' = Cylinder compressive strength of concrete, in psi

P = Axial load on column, in kips

A_g = Gross area of column, in in^2

For prediction of ultimate strength of the joint, the following equation was proposed, again on the basis of regression analysis

$$\tau_u = 5.492(f_c')^{0.660} (1 + \rho_s)^{0.5371} \quad (3.4)$$

Where, ρ_s is the ratio of joint reinforcement to joint area.

It is interesting to notice that in predicting the joint cracking, no credit is given to the joint reinforcement, while in predicting the ultimate strength, axial load on column is ignored.

Sarsam and Phipps (1985) proposed an equation for the design of exterior beam-column joints under monotonic loading while considering the concrete strength, the column longitudinal reinforcement ratio and axial load.

$$\tau_c = 5.08(f_{cu}\rho_c)^{0.33} \left(\frac{h_c}{h_b}\right)^{1.33} b_c h_c \sqrt{1 + 0.29 \frac{P}{A_g}} \quad (3.5)$$

Where,

f_{cu} = cubic compressive strength of concrete, MPa

ρ_c = ratio of the area of the layer of longitudinal steel in column farthest from maximum compression face of column to the gross column area

h_b = beam depth, mm

h_c = column depth, mm

b_c = column width, mm

The effect of axial stress on column was considered to increase the joint cracking strength as seen in equation (3.5), but the same was not considered to increase the ultimate strength capacity of the joint.

Scott et al. (1994) tested fifteen exterior beam column joints and proposed equations to predict the cracking and ultimate strength of the joint. The equation to predict the cracking strength, τ_{cr} was proposed as

$$\tau_{cr} = \tau_c \sqrt{1 + \frac{P}{A_g \tau_c}} \quad (3.6)$$

Where, τ_c = design concrete shear strength for a reinforced concrete section.

To predict the ultimate shear strength of exterior beam-column joints, the following equation was proposed assuming a transfer of shear force through the joint by a single diagonal strut:

$$\tau_u = \frac{2\sqrt{f_{cu}}}{\begin{pmatrix} z_c & z_b \\ z_b & z_c \end{pmatrix}} \quad (3.7)$$

Where,

f_{cu} = cubic compressive strength of concrete

z_b = lever arm of internal forces in beam at column face

z_c = lever arm of internal forces in column at joint face

Vollum (1998) proposed the following equation to obtain a lower bound estimate of the shear strength of concrete for the joints with aspect ratio (ratio of beam to column depth) between 1.33 and 2.0:

$$\tau_u = 0.642\beta \left(1 + 0.555 \left(2 - \frac{h_b}{h_c} \right) \right) f'_c \quad (3.8)$$

Where, β is a reduction factor, not less than 0.8.

An empirical model based on SI units was developed Bakir and Boduroğlu (2002). Beam reinforcement ratio, and the joint aspect ratio were included as parameters in the proposed equation for evaluating contribution of concrete to joint shear strength.

$$\tau_u = \frac{0.71\beta\gamma \left(\frac{100A_{sb}}{b_b d_b} \right)^{0.4289} \left(\frac{b_b + b_c}{2} \right) h_c \sqrt{f'_c}}{\left(\frac{h_b}{h_c} \right)^{0.61}} \quad (3.9)$$

Where,

β and γ depend on reinforcement detailing

A_{sb} = total area of beam reinforcement in tension

d_b = effective depth of beam

h_b = total depth of beam

h_c = total depth of column

b_b = width of beam

b_c = width of column

Hegger et al. (2003) developed the following empirical model including the parameters of column reinforcement ratio and joint aspect ratio:

$$\tau_u = 2\alpha_1 \sqrt[3]{f'_c} \left(1.2 - 0.3 \frac{h_b}{h_c} \right) \left(1 + \frac{\rho_{col} - 0.5}{7.5} \right) \quad (3.10)$$

Where,

α_1 represents anchorage detail

ρ_{col} = ratio of longitudinal column reinforcement in tension

The evaluation of results shows consistent overestimation of the joint shear strength (Park and Mosalam, 2009).

Russo and Somma (2004) examined the behavior at failure of 50 exterior beam-column joints tested by various researchers and proposed a model for computing the shear strength of exterior beam-column joints. The equation giving concrete shear strength contribution was proposed as:

$$\tau_u = f_{ct} \sqrt{1 + \frac{\sigma_a + f_v}{f_{ct}}} \quad (3.11)$$

Where,

$$f_v = k_v \frac{A_v f_{yv}}{A_g} \quad (3.12)$$

σ_a = Mean axial compressive stress on column
 f_{yv} = yield strength of longitudinal column reinforcement
 A_v = cross-section of longitudinal column reinforcement
 A_g = gross area of joint cross section
 f_{ct} = tensile strength of concrete
 k_v = numerical coefficient

Mainly on the basis of 3D FE modelling of RC beam-column joints, Mahajan (2009) proposed an equation to predict the joint shear strength.

$$V_{ch} = b_j h_c \cos \theta \left(1.4 \sqrt{f'_c} - 2.2 \right) \left(0.24 \sqrt{\frac{\rho_s f_{sh}}{f'_c}} + 1.68 \right) \quad (3.13)$$

Where,

f_{sh} = stress in joint transverse reinforcement at failure in MPa
 ρ_s = volumetric ratio of ties in %

$$\theta = \tan^{-1} \left(\frac{h_b}{h_c} \right)$$

3.1.2 Strut and Tie Models

Strut and tie models are popular among researchers to predict the behaviour of beam-column joints. The basic idea of the strut and tie mechanism is explained by Paulay and Priestley (1992), When the joint is subjected to external forces, the internal forces generated in the concrete combine to form a diagonal strut, while the other forces transmitted through reinforcing bars by means of bond, necessitate a truss mechanism. Consequently, in a strut and tie model, the struts represent the compressive stress fields, while the ties account for the tensile reinforcement. Thus, the strut and tie model is an idealization of the stress state in the structure at the limit state under consideration (Vollum, 1998). However, the model is limited in its applicability due to inherent complexities associated with the same such as pre-judgement of the stress field (Genesio, 2012).

Strut-and-tie concept was used by Ortiz (1993) to predict the shear strength of exterior beam-column joints with and without transverse reinforcement. Figure 3.1 shows the free body diagram of the joint as proposed by Ortiz (1993).

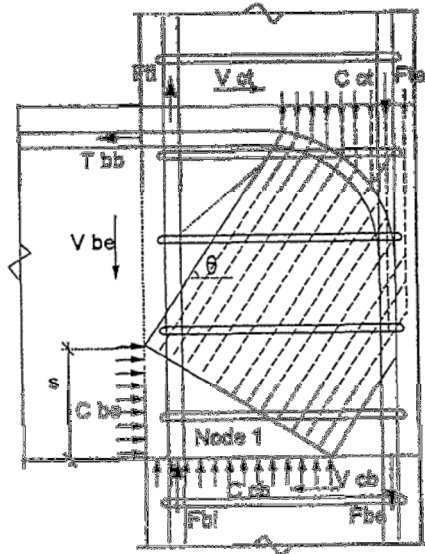


Figure 3.1 Equilibrium of the beam-column joint as considered by Ortiz (1993)

The boundary forces were calculated on the basis that plane sections remain plane adjacent to the joint block. The rectangular-parabolic stress block of the CEB Model Code (1990) was adopted for the concrete in compression and a bilinear stress-strain diagram, with no strain hardening, for the reinforcement. A semi-empirical approach was adopted by Ortiz to evaluate the strength of the diagonal strut. The concrete strength was considered as the design strength for cracked concrete proposed by the CEB Model Code (1990) and the width of the inclined strut was chosen to give a good fit to her experimental results for specimens without joint stirrups.

Parker and Bullman (1997) developed a model to predict the shear strength of the joint. The equilibrium of the joint as proposed by Parker and Bullman (1997) is shown in Figure 3.2. It was assumed that the shear force is resisted by an inclined compression field or strut in the concrete. The inclination of the struts and its dimensions were determined on the basis of the minimum potential energy principle.

A strut and tie model was developed by Vollum (1998) for exterior beam-column joints with and without transverse reinforcement. The model defines the joint shear failure when the maximum diagonal stress at the top node reaches the cracked concrete strength. The model includes the detrimental effect of the joint aspect ratio but it does not consider the change of the joint shear strength with the variation of beam reinforcement (Park and Mosalam, 2009). Figure 3.3 displays the model proposed by Vollum (1998) as adapted from Bakir and

Bodurođlu (2001). The direct strut was divided into ten trapezoidal elements and the strain was calculated at the centre of each and then added up to find the axial extension of the direct strut. A similar approach was carried out for indirect struts. A stiffness approach was embedded in a virtual work approach for the whole procedure. The model becomes overly complex for practical design usage.

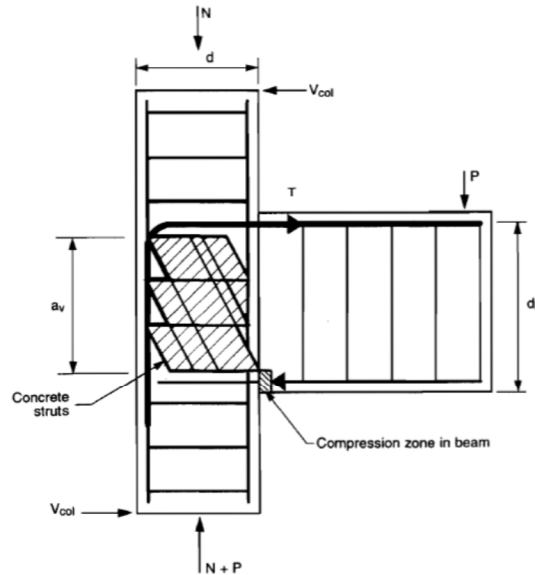


Figure 3.2 Parker and Bullman (1997) model for beam-column joints strength prediction

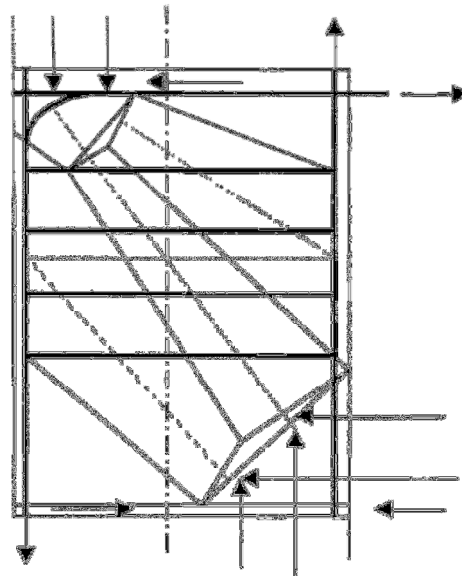


Figure 3.3 Model by Vollum (1998)

Another joint shear strength model known as “softened strut and tie model” was developed by Hwang and Lee (1999) considering the equilibrium, compatibility, and constitutive laws for cracked reinforced concrete. The model assumes that the joint shear resisting mechanism

(Figure 3.4) is composed of: (1) the diagonal strut mechanism, (2) the horizontal mechanism, and (3) the vertical mechanism. The equilibrium requirement is satisfied by equating the sum of horizontal components of compression force in diagonal strut, tension force in horizontal ties and the horizontal component of tension force in vertical tie to the horizontal joint shear force. The concrete strength in the diagonal strut was assumed to follow the softening concrete model by Belarbi and Hsu (1995), and the two-dimensional compatibility condition is constructed by considering the average strains in the joint panel. Due to the assumptions of horizontal and vertical strain in unreinforced joints, this model is not able to predict the joint shear failure without beam reinforcement yielding. Moreover, only beneficial effects of column axial load on joint shear strength are included in the model.

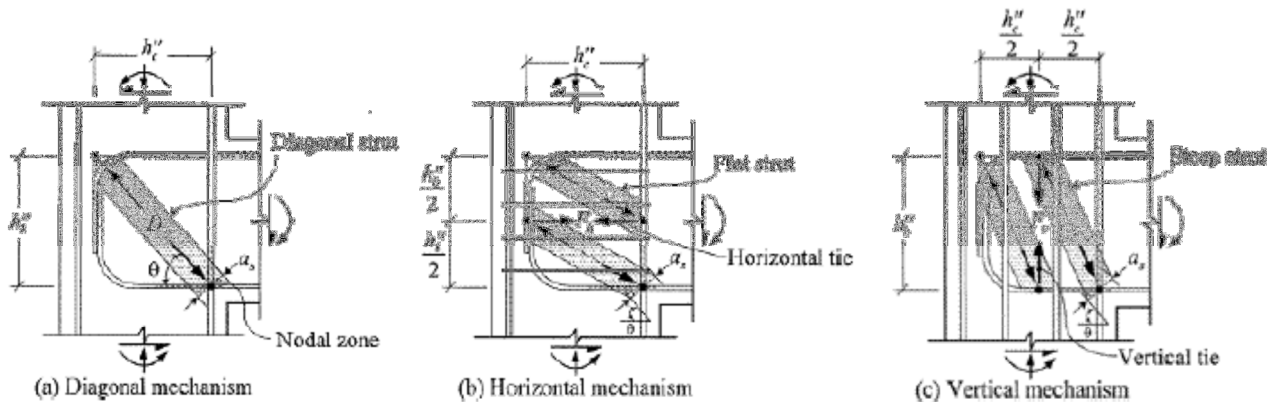


Figure 3.4 Mechanism for joint shear resistance (Hwang and Lee, 1999)

3.1.3 Models based on average plane stress plane strain approach

The average plane stress plane strain approach consists of evaluating the average stress generated in the joint panel due to external loads and comparing them with certain critical values. The critical values of allowable stress are suggested for different limit states such as joint cracking and ultimate strength. The approach, owing to its simplicity in application, has found its place in various design codes such as ACI 352 (2002), NZS 3101 (1995) etc, where the average horizontal joint shear stress is compared with the allowable stresses.

Pantazopoulou and Bonacci (1992) developed a shear strength model for interior beam-column joints, under the assumption that the joint is well confined such that average stress and strain values can be used. A relationship between average joint shear stress and strain before joint reinforcement yielding was formulated and it was concluded that the principal tensile strain increases with increasing column axial load as well as shear stress, which leads to decrease in the compressive strength of the diagonal strut. Based on this conclusion, the detrimental effect of column axial load on the joint shear strength was supported. However, this conclusion is drawn by the unrealistic assumption that the principal direction is not changed regardless of column axial load (Park and Mosalam, 2009). They defined two types

of failure without yielding of joint reinforcement: (a) column reinforcement yielding and (b) concrete crushing in the principal compressive stress direction.

A so-called Modified Rotating-Angle Softened-Truss Model was proposed by Wong (2005) to predict the shear strength of exterior joints. The model was based on the compatibility equation proposed by modifying (i) modified compression field theory, (ii) rotating-angle softened truss-model, and (iii) fixed-angle softened truss model. The aspect ratio is considered by accounting for the effect of the shear span to depth ratio as in deep beams. However, as pointed out by Park and Mosalam (2009), the boundary condition of the exterior joints is completely different from that of a deep beam. The model calls for an extensive numerical iteration to obtain joint shear strength values.

A relatively new formulation to predict the ultimate shear strength for the beam-column joints of modern structures was proposed by Tsonos (2007), based on the strut-and-tie mechanism. The basic assumption in the model is that the summation of vertical and horizontal forces acting on the joint is equal respectively to the vertical and horizontal joint shear forces. The normal compressive stress was given by equation (2.8) and the horizontal joint shear stress by eq (2.5). Eq (2.7) has been considered valid and the maximum and minimum principal stresses are calculated using eq (2.10). A fifth-order polynomial equation was assumed to represent the biaxial concrete strength curve and the confined concrete strength was considered based on the model by Scott et al (1982). The fifth order polynomial equation is solved to obtain the values of ultimate joint shear strength. The model led to, in general, very good comparison with the experiments performed by various researchers on joints having shear reinforcement. However, a comparison only for three unreinforced joints was given in the paper which showed that the model generally over-predicts the shear strength of such joints by around 15-17%, but the same was not further discussed. This overestimation might have resulted due to the use of over-simplified average stress equilibrium equation (Park and Mosalam, 2009).

Priestley (1997) suggested a principal tensile stress model to assess the shear strength of beam-column joints without joint reinforcement which needs to compare the average principal tensile stress of the joint panel with some critical values representing diagonal cracking and shear failure. Priestley suggested the critical values of principal tensile stresses as $p_t = 0.29(f_c')^{0.5}$ for first shear crack and $p_t = 0.42(f_c')^{0.5}$ for maximum shear strength for the case of exterior joints having beam reinforcement bent into the joint (Figure 3.5). The model has the advantage of being very simple and the joint shear strength degradation is also considered in terms of joint rotation. Moreover the effect of axial force is also considered. However, it is sometimes argued that the principal tensile stress approach may be conservative because more joint shear can be carried by the diagonal compression strut mechanism (Hakuto et al, 2000). However, the author is of the opinion that for the normally found ranges of axial loads on columns in structures (less than 30% of column capacity), it seems that the principal tensile stress approach may be appropriate.

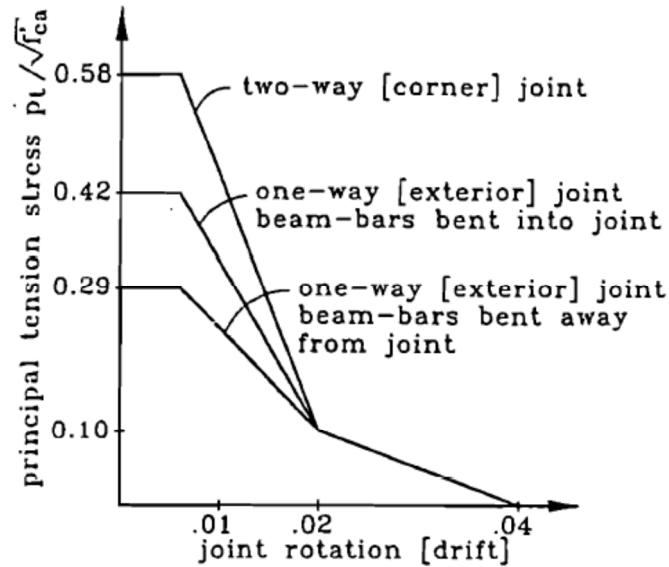


Figure 3.5 Critical principal tensile stress values suggested by Priestley (1997)

Based on same principle, Pampanin et al (2002) suggested the plots of principal tensile stress v/s joint shear deformation for exterior joints with smooth bars having end hooks (Figure 3.6).

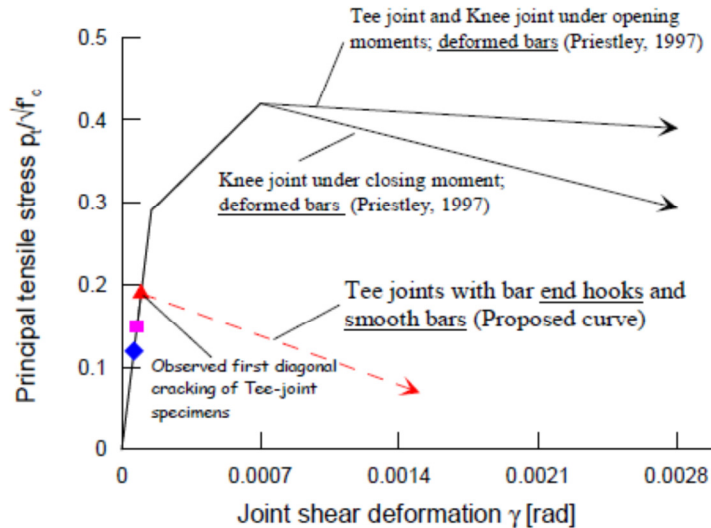


Figure 3.6 Suggested principal tensile stress v/s joint shear deformation relationship (Pampanin et al, 2002)

Based on experiments, and a vast numerical parametric study, Genesio (2012) extended the recommendations for the critical values of principal tensile stress and corresponding joint shear deformations. He suggested formulations giving due consideration to the joint aspect ratio, beam longitudinal reinforcement ratio and the axial load on the column. Genesio (2012) followed a detailed 3D Finite element analysis approach using microplane model with relaxed

kinematic constraint (Ožbolt et al, 2001) as constitutive law for concrete and using discrete springs to model bond between solid concrete elements and bar elements modelling steel reinforcement (Figure 3.7). The basic modelling philosophy for the joints was the same as explained in Appendix C.

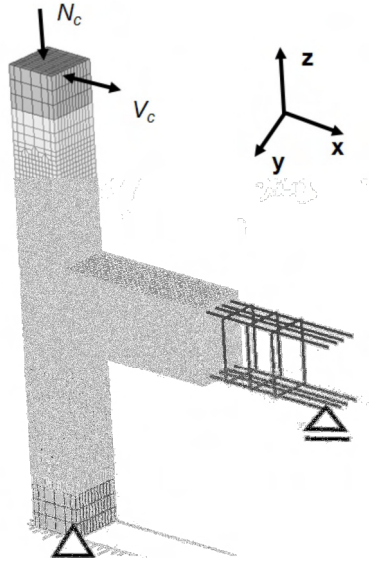


Figure 3.7 Typical 3D FE model for the beam-column joint modelled by Genesis (2012)

Genesis (2012) suggested that the strength corresponding to first diagonal cracking and ultimate joint strength can be considered as given by eq. (3.14) and (3.15a, b) respectively:

$$\text{First diagonal cracking: } \frac{P_t}{\sqrt{f'_c}} = k_0 + k_1 \left(2 - \frac{h_b}{h_c} \right) \quad (3.14)$$

Ultimate strength:

$$\frac{P_t}{\sqrt{f'_c}} = k_0 + k_1 \left(2 - \frac{h_b}{h_c} \right) + k_2 \frac{(n_{c,0} - n_c)}{100} \rho_b, \text{ for } n_c \leq n_{c,0} \quad (3.15a)$$

$$\frac{P_t}{\sqrt{f'_c}} = k_0 + k_1 \left(2 - \frac{h_b}{h_c} \right), \text{ for } n_c > n_{c,0} \quad (3.15b)$$

where k_0 and k_1 are non-dimensional empirical coefficients depending from the joint detailing; h_b/h_c is the joint aspect ratio; n_c is the axial load on the column; $n_{c,0}$ is the upper limit value of axial load after which the peak load is coincident with the first joint cracking; and ρ_b is the beam longitudinal reinforcement ratio.

3.2 Review of Joint Element Models

Joint shear strength is an important criterion to design the beam-column joints. However, in order to assess the complete seismic performance of a joint, it is essential to determine its load-deformation response, preferably with hysteretic behaviour. Therefore, joint element

models are required that can be used in predicting the seismic response of the joints. In general, the models proposed for RC beam-column joints can be classified as

1. Models based on experiments
2. Models based on analytical or numerical studies

These are discussed in details as under.

3.2.1 Models based on experiments

Some of the earliest work to simulate the inelastic response of reinforced concrete frames relied on the calibration of the “plastic-hinges” within beam-column line elements to introduce the inelastic action of the beam-column joint. These models are essentially based on experiments conducted on full or reduced scale beam-column joints under cyclic excitations. Several geometric curves and rules defining the hysteretic behaviour of the connections are proposed.

Townsend and Hanson (1973) introduced a set of polynomial expressions which represent the hysteretic behaviour of beam-column connections and account for the observed stiffness degradation. Anderson and Townsend (1977) proposed a degrading trilinear joint model whose parameters are determined to match a series of experimental results from exterior beam-column joint tests. Soleimani et al (1979) introduced the concept of effective length by which the curvature at the beam-column interface if multiplied to yield the fixed end rotation.

The parameters defining the hysteretic behaviour of the connection were selected to best fit the observed behaviour and were not derived from physical interpretation of the mechanisms contributing to such behaviour. Therefore, the generalization and objectivity of such models so as to make them applicable for different configurations and loading conditions is doubtful. Such models therefore remained rather unpopular and will not be discussed further here.

3.2.2 Models based on analytical or numerical studies

Several models have been proposed in the past based on analytical or numerical studies by various researchers. These models can be further subdivided as

1. Rotational hinge models
2. Multiple spring models

3.2.2.1 Rotational Hinge Models

These models are typically composed of a bilinear or trilinear monotonic envelope curve and an associated set of hysteretic rules defining behaviour under cyclic load reversals. Several researchers proposed such models.

Otani (1974) used a bilinear idealization of the envelope curve and computed the characteristic points of this bilinear envelope curve with an assumption that bond stresses are constant along the development length of the reinforcing bars and that the reinforcing embedment length is long enough to develop steel forces of required magnitude. The fixed end rotation was found to be proportional to the square of the moment acting at the beam-column interface. Takeda (1970) rule was used as the associated hysteretic rule.

Banon et al (1981) also followed basically the same assumptions as Otani and employed a bilinear envelope curve in connection with Takeda's hysteretic rule. However, they included the observed pinching effect due to bond slip and shear sliding. The model was used to represent the inelastic deformations due to slippage of the reinforcement.

The assumptions followed in the above two models do not agree with the experimental evidences and they appear to be on unsafe side with respect to the strength and stiffness of the joint. Moreover they have one shortcoming in common that the experimentally observed slip-through of reinforcing bars in interior joints of commonly used dimensions is not taken into account. This leads to an interaction between the two column ends so that no unique moment-rotation relationship can be derived for one end, unless the actions at the other end are accounted for. Also, they fail to provide an understanding and analytical description of mechanisms leading to the observed significant stiffness degradation in RC joints.

Filippou et al (1983, 1988) proposed model that can give due consideration to the effect of bond deterioration on hysteretic behaviour of the joints. Figure 3.7 shows the analytical model of the joint sub-element that accounts for the fixed-end rotations which arise at the beam-column interface of RC members due to bond deterioration and slippage of reinforcement in the joint and in the girder region adjacent to the joint. The proposed model consists of a concentrated rotational spring located at each girder end. The two springs are connected by an infinitely rigid bar to form the joint sub-element. The moment-rotation relation of the rotational springs is derived using the detailed model by Filippou et al. (1983) which accounts for the geometry, material properties and reinforcement layout of the connection. A different moment-rotation relation can be prescribed at each connection. The moment-rotation relation of the rotational springs of the joint sub-element is based on a bilinear elastic-strain hardening envelope curve.

The envelope curves are established with the aid of the joint model in Filippou et al. (1983) once the dimensions of a particular joint and the arrangement of the reinforcement are known. This process takes place as follows: the beam-column joint model which represents a particular connection of the frame under investigation is subjected to monotonically increasing girder end moments. These give rise to concentrated rotations due to reinforcing bar pull-out at the beam-column interface. Thus, the model presented by Filippou et al (1983, 1988) was detailed and was based on pure mechanics of the joints. The model was easier to

implement and also, the results matched reasonably well with the experiments. However, the biggest limitation was that the model did not give due consideration to the joint shear and diagonal cracking in the hysteretic behaviour of beam-column joints.

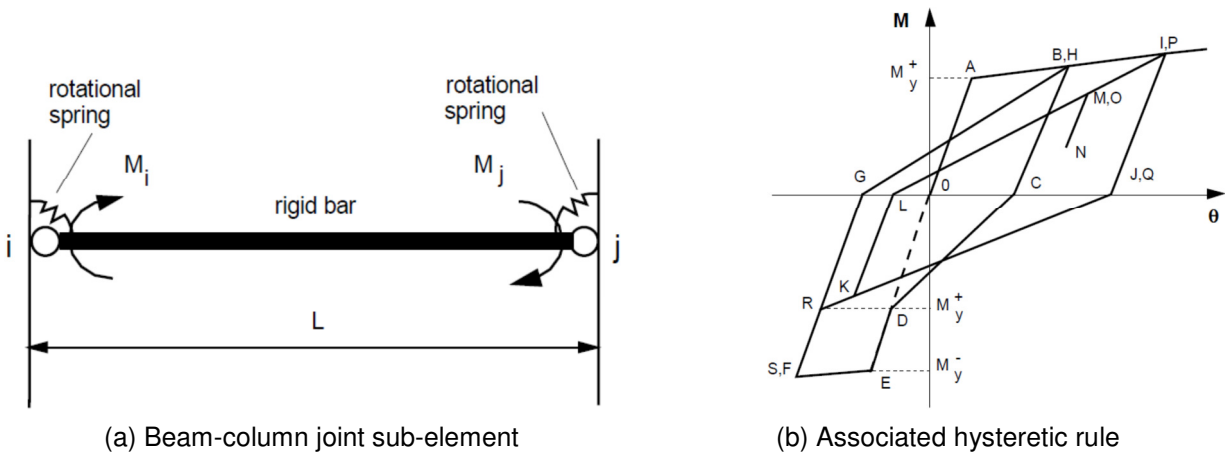


Figure 3.7 Beam-column joint sub-element by Fillipou et al (1983, 1988)

El-Metwally and Chen (1988) modelled the joint mechanically as a concentrated rotational spring and utilized the thermodynamics of irreversible processes to obtain spring stiffness. In the proposed model, the connection is assumed to be properly designed and have adequate shear strength. Thus, the joint is modelled mechanically as a concentrated rotational spring using the assumptions that (1) anchorage failure for longitudinal reinforcement embedded in the joint controls inelastic joint action under earthquake loading and (2) total energy dissipation due to anchorage failure is approximately constant for all beam-column joints. The biggest disadvantage of the model is that it requires the moment rotation data from beam-column joint experiments to calculate the required parameters.

Kunnath et al. (1995) modified the flexural capacities of the beams and columns of gravity load designed RC frames to model insufficient positive beam bar anchorage and inadequate joint shear capacity implicitly (Celik and Ellingwood, 2008). To account for insufficient positive beam bar anchorage, the pullout moment capacity of the beam was approximated as the ratio of the embedment length to the required development length per ACI 318–89 multiplied by the yield moment of the section. This approximation required that the yield strength of the discontinuous steel be reduced by the ratio of the actual to the required anchorage length. To model inadequate joint shear capacity, the flexural capacities of the beams and columns framing into the joint were reduced to a level that would induce shear failure of the joint. The proposed procedure was utilized in inelastic dynamic time history analyses of typical three-, six-, and nine-story gravity designed RC frames, which revealed that they are susceptible to damage from joint shear failures and weak column-strong beam effects leading to soft-story collapses (Celik and Ellingwood, 2008).

Alath and Kunnath (1995) modeled the joint shear deformation with a rotational spring model with degrading hysteresis. The finite size of the joint panel was taken into account by introducing rigid links (Figure 3.8). The envelope to the shear stress-strain relationship was determined empirically, whereas the cyclic response was captured with a hysteretic model that was calibrated to experimental cyclic response (Celik and Ellingwood, 2008). The model was validated through a comparison of simulated and experimental response of a typical GLD RC frame interior beam-column joint subassembly.

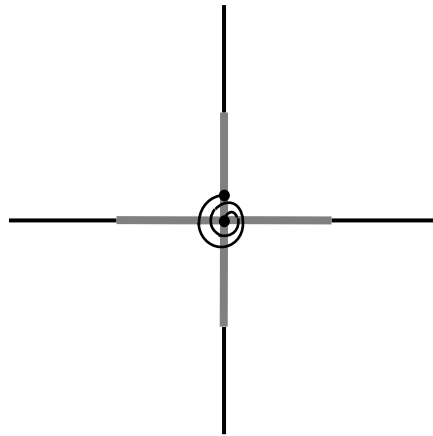


Figure 3.8 Beam-Column Joint model by Alath and Kunnath (1995)

Again, the biggest disadvantage of the above mentioned models is that they require the moment rotation data from beam-column joint experiments to calculate the required parameters.

A simple model has been more recently proposed by Pampanin et al. (2002) that consists of a non-linear rotational spring that permits to model the relative rotation between beams and columns converging into the node and to describe the post-cracking shear deformation of the joint panel (Figure 3.9). Beam and column elements are modelled as one dimensional element with lumped plasticity in the end sections with an associated moment-curvature relationships defined by a section analysis. The effect of moment-axial load interaction is taken into account for columns. To represent the real geometric dimensions of the joint panel region, rigid elements are used to connect the beam and column members to the rotational spring.

The definition of the moment-rotation relationship of the rotational spring is based on the results of experimental tests performed at the Department of Structural Mechanics of the University of Pavia (Pampanin et al., 2002). A relation between the shear deformation and the principal tensile stress in the panel region was found and transformed into a moment-rotation relation to be assigned to the rotational spring. The shear deformation is assumed to be equal to the rotation of the spring and the moment is deduced as corresponding to the principal tensile stress evaluated on the basis of Mohr's theory.

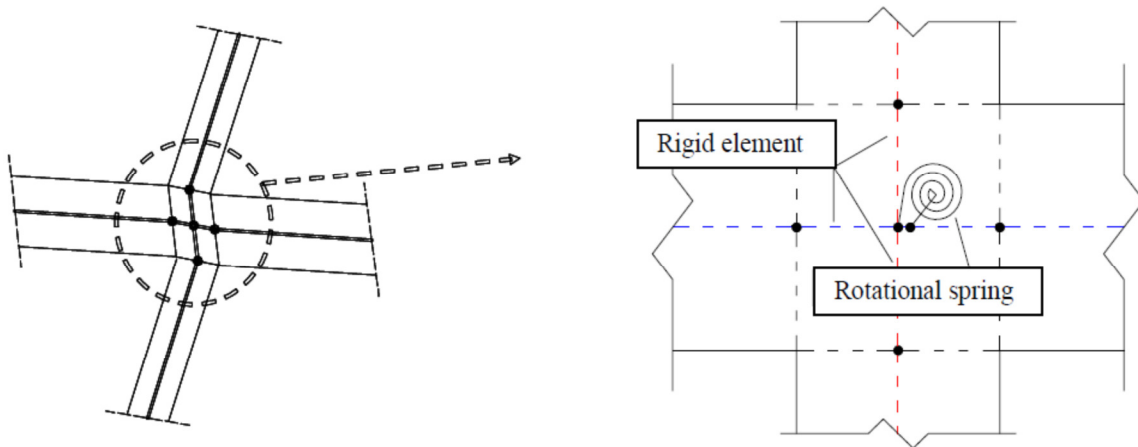


Figure 3.9 Model for RC beam-column joints by Pampanin et al (2002)

The rotational-hinge joint model provides a means of independently characterizing inelastic joint action with only a moderate increase in computational effort. But, this approach does not facilitate the development of objective and accurate calibration procedures. It requires that data from experimental testing of beam-column joint sub-assemblages be used to develop a one-dimensional joint moment-rotation relationship.

Developing such a model that can be used to predict the response of joints with different design details requires either a large number of data sets and a sophisticated calibration procedure or multiple models for joints with different design details. Currently, there are not sufficient data in the literature to support the development of models that are appropriate for a broad range of joint designs.

3.2.2.2 Multiple Spring Models

Multiple spring models is a more realistic and objective extension of the rotational spring models. Instead of using a single rotational spring, this approach recommends to use various springs to model different mechanisms of the joints. A nice review of multiple spring models is given by Celik and Elingwood (2008).

Biddah and Ghobarah (1999) modeled the joint with separate rotational springs that modelled the joint shear and bond-slip deformations (Figure 3.10). The shear stress-strain relationship of the joint was simulated using a tri-linear idealization based on a softening truss model (Hsu, 1988), while the cyclic response of the joint was captured with a hysteretic relationship with no pinching effect (Celik and Elingwood, 2008). The bond-slip deformation was simulated with a bilinear model based on previous analytical and experimental data. The cyclic response of the bond-slip spring was captured with a hysteretic relationship that accounts for pinching effects. They utilized this joint element in performing dynamic analyses of three- and nine-story gravity load designed RC buildings. They compared the dynamic response of three and nine-story frames modelled with joint elements to the response of

similar frames with rigid joints when subjected to strong motion records. The comparisons revealed that accounting for joint shear and bond-slip deformations in modelling results in significantly larger drifts, particularly for the nine-story frame.

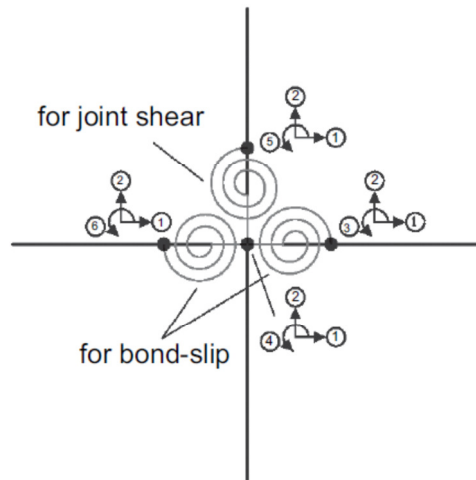


Figure 3.10 Beam-Column Joint model by Biddah and Ghobarah (1999)
Source: Celik and Elingwood (2008)

Elmorsi et al (2000) proposed an approach where beams and columns are described by elastic elements and are connected to the joint through the interposition of non-linear transitional elements. The effective node panel region is modelled with another element constituted by 10 joints (Figure 3.11). This model allows describing the material behaviours with the introduction of the stress-strain relationships of steel and concrete. Concrete is defined by two different relationships defining the pre and post cracking behaviour. Longitudinal reinforcing steel bars are modeled with non-linear elements placed along the upper and lower sides of the joint panel. Furthermore this model allows the introduction of a "bond-slip element" to represent the slipping of steel bars.

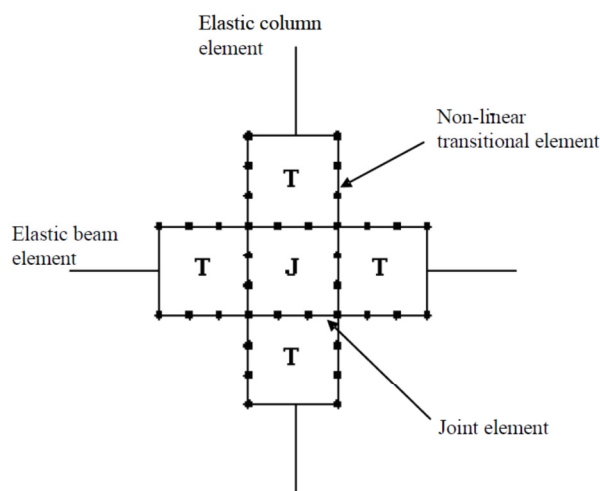


Figure 3.11 Beam column joint model by Elmorsi et al (2000)

Youssef and Ghobarah (2001) proposed a joint element (Figure 3.12) in which two diagonal translational springs connecting the opposite corners of the panel zone simulate the joint shear deformation; 12 translational springs located at the panel zone interface simulate all other modes of inelastic behaviour (e.g., bond-slip, concrete crushing)—elastic elements were used for the joining elements. The model was validated using experimental test results of ductile and non-ductile exterior beam-column joints. This model requires a large number of translational springs and a separate constitutive model for each spring, which may not be available and restricts its applicability (Celik and Ellingwood, 2008).

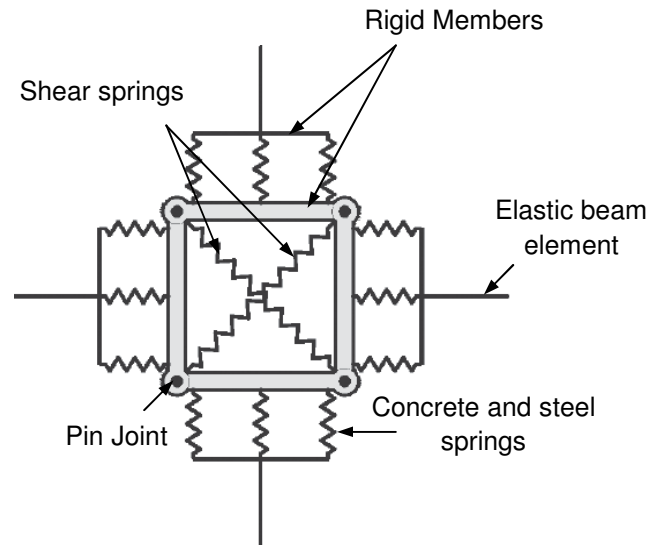


Figure 3.12 Beam-column joint model by Youssef and Ghobarah (2001)
Source: Celik and Ellingwood (2008)

Lowes and Altoontash (2003) proposed a 4-node 12-degree-of-freedom (DOF) joint element (Figure 3.13) that explicitly represents three types of inelastic mechanisms of beam-column joints under reversed cyclic loading. Eight zero-length translational springs simulate the bond-slip response of beam and column longitudinal reinforcement; a panel zone component with a zero-length rotational spring simulates the shear deformation of the joint; and four zero-length shear springs simulate the interface-shear deformations (Celik and Ellingwood, 2008).

The envelope and cyclic response of the bar stress versus slip deformation relationship were developed from tests of anchorage-zone specimens and assumptions about the bond stress distribution within the joint. To define the envelope to the shear stress-strain relationship of the panel zone, the modified-compression field theory (MCFT) (Vecchio and Collins, 1986) was utilized. The cyclic response of the panel zone was modelled by a highly pinched hysteresis relationship, deduced from experimental data provided by Stevens *et al.* (1991). A relatively stiff elastic load-deformation response was assumed for the interface-shear components.

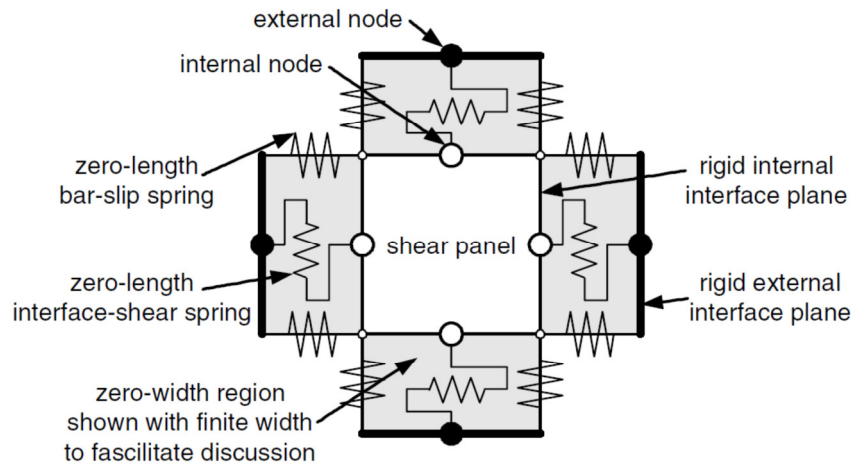


Figure 3.13 Beam-column joint model by Lowes and Altoontash (2003)

Lowes et al. (2004) later attempted to model the interface-shear based on experimental data; this effort also predicted a stiff elastic response for the interface-shear. Mitra and Lowes (2007) subsequently evaluated the model by comparing the simulated response with the experimental response of beam-column joint subassemblies. The experimental data included specimens with at least a minimal amount of transverse reinforcement in the panel zone, which is consistent with the intended use of the model. Joints with no transverse reinforcement, a reinforcing detail typical in GLD RC frames, were excluded from this study. It was noted that in joints with low amounts of transverse reinforcement, shear is transferred primarily through a compression strut, a mechanism, which is stronger and stiffer than predicted by the MCFT. The model is therefore not suitable for the analysis of the joints of gravity load designed frames with no transverse reinforcement (Celik and Ellingwood, 2008).

Altoontash (2004) simplified the model proposed by Lowes and Altoontash (2003) by introducing a model consisting of four zero-length rotational springs located at beam- and column-joint interfaces, which simulate the member-end rotations due to bond-slip behaviour, while the panel zone component with a rotational spring remains to simulate the shear deformation of the joint as shown in Figure 3.14 (Celik and Ellingwood, 2008).

The constitutive relationship (i.e., the envelope and the cyclic response) for the panel zone from Lowes and Altoontash (2003) was retained, enabling the calculation of constitutive parameters based on material properties, joint geometry, joint reinforcing steel ratio, and axial load. However, calibration of constitutive parameters was still required for joints with no transverse reinforcement to overcome the limitation of the MCFT for such joints. He adapted the constitutive model developed for the translational bond-slip springs in Lowes and Altoontash (2003) in a fiber section analysis to derive the constitutive model for the member-end rotational springs, but noted that detailed information on bond-slip response is needed. Furthermore, the development length was assumed to be adequate to prevent complete pullout. The model is still not suitable for the analysis of the joints of gravity load designed frames with no transverse reinforcement (Celik and Ellingwood, 2008).

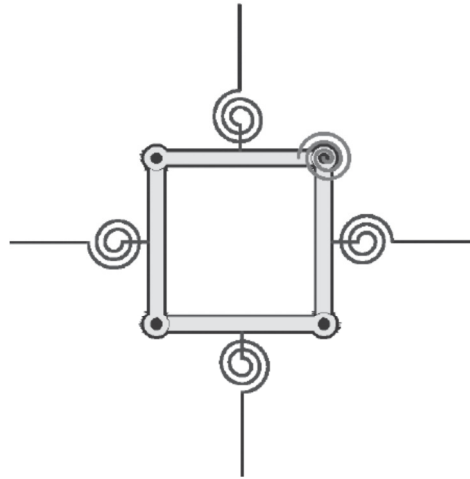


Figure 3.14 Beam-column joint model by Altoontash (2004)
Source: Celik and Elingwood (2008)

Shin and LaFave (2004) represented the joint by rigid elements located along the edges of the panel zone and rotational springs embedded in one of the four hinges linking adjacent rigid elements as displayed in Figure 3.15 (Celik and Ellingwood, 2008).

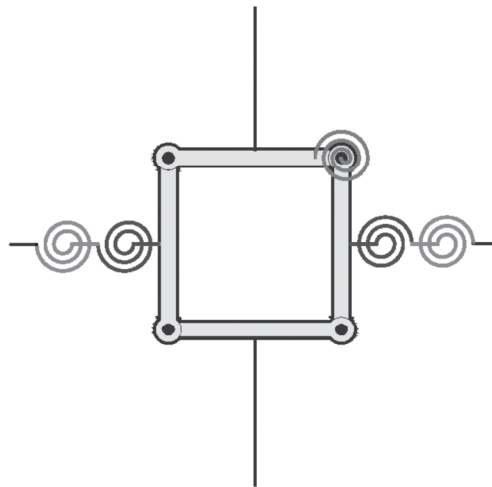


Figure 3.15 Beam-column joint model by Shin and LaFave (2004)
Source: Celik and Elingwood (2008)

The envelope to the joint shear stress-strain response was approximated by the MCFT, whereas experimental data were used to calibrate the cyclic response. Two rotational springs (in series) located at beam-joint interfaces simulate the member-end rotations due to bond-slip behaviour of the beam longitudinal reinforcement and plastic hinge rotations due to inelastic behaviour of the beam separately. The proposed joint model is intended for RC beam-column joints of ductile moment frames designed and detailed following modern seismic code requirements.

LaFave and Shin (2005) discussed the use of the MCFT in defining the envelope to the shear stress-strain relationship of the panel zone. The authors collected from the literature experimental joint shear stress and strain data of 50 RC interior joint subassemblies that failed in joint shear. The envelope responses to the experimental data typically follow a quad-linear curve that connects three key points (corresponding to joint shear cracking, reinforcement yielding, and joint shear strength) starting from the origin and has a degrading slope once past the joint shear strength. For each of the experimental subassemblies, the authors applied the MCFT as described by Lowes and Altoontash (2003) to determine the ordinates of the envelope points, particularly the maximum joint shear stress (i.e., joint shear strength). Comparison of the ratio of analytical (MCFT) to experimental maximum joint shear stress versus the ratio of transverse joint shear reinforcement provided to that required by ACI 318–02 (2002) revealed that the MCFT approach consistently underestimates the joint shear strength for joints that do not satisfy the joint reinforcement requirement per ACI 318–02. Hence, the MCFT may be inappropriate for modeling GLD RC frames, which have little or no joint transverse shear reinforcement (Celik and Ellingwood, 2008).

The multiple spring models are in general more accurate and are based on mechanics of joints. However, in certain cases, they also need large experimental data for calibration. The limitations of such models are:

1. They need larger computational effort as compared to rotational hinge models.
2. Often need a special element incorporated in software.
3. Most of the available models are not suitable for joints of gravity designed frames.

3.2.3 Summary of Existing Models

Many researchers have proposed various models to capture the inelastic behaviour of reinforced concrete beam-column connections under seismic excitations. Various theories towards the prediction of the shear strength of the beam-column joints exist, which include the empirical equations, strut and tie models, 3D FE simulation based approach, average plane stress-plane strain approach etc. The strut and tie models and 3D FE simulation based approach is good for research purpose, but the application of the same on practical problems is complicated and time consuming. The empirical equations are simple to use but different researchers have proposed various equations, which give the shear strength predictions as a function of different parameters. The suitability of the equation is dependent on the number and type of parameters considered. It is sometimes found that the equations are suitable only for a limited range of parameters. Average plane stress plane strain approach is by far the simplest approach and therefore, it has found place in most of the design codes (ACI 318, NZS 3101). However, the plane stress approach based only on horizontal joint shear stress cannot consider the influence of axial load on the column or the anchorage of reinforcement bars into the joint. The approach suggested by Priestley (1997), which is based on the critical values of principal tensile stresses and joint distortion for different limit states and considers

the degradation of joint strength seems simple enough to be used in practice as well as reasonably accurate. The same is followed in this work to estimate the strength of the beam column joint.

The first joint element models begin with the experimental studies based models but they were found to be un-objective. As the understanding of the behaviour of beam-column connections grew, more detailed and accurate models could be proposed. Rotational spring models recommend modelling the joint as a rotational spring connecting beam and column elements, even though it is not so straightforward in reality. The moment-rotation characteristics determination in such a case needs large and careful calibration. The multiple spring models definitely recommend models that are much closer to reality by modelling shear behaviour and slip behaviour by different springs but they need special purpose programs or elements for implementation. Moreover, many of such models are not suitable for the joints of gravity designed RC frames without any transverse reinforcement, the case that is most critical and needs maximum consideration. Therefore, there is still a large scope to develop realistic models that can not only predict the behaviour of even poor detailed beam-column connections well but are also implementable in general purpose nonlinear analysis programs e.g. SAP2000, STAADPro, Sofistik to name a few. At the same time, it is also needed that the model is closer to reality from the consideration of deformation behaviour and load resisting mechanism. An attempt is made in this work to propose such a model, which is explained in next chapter.

4. THE PROPOSED JOINT MODEL

4.1 Need for the joint model

In chapters 1 and 2, it has been emphasized that under seismic loading, beam-column joints are subjected to very high shear forces that lead to their failure. While designing a structure, conventionally, the joint core is considered as rigid and the frame members are assumed to be connected forming a single node that symbolizes the joint. New codes (ACI 318, NZS, EC8) suggest an indirect approach to design the joint by limiting the joint shear stresses. However, in older codes, no such provisions existed.

For seismic assessment of RC frame structures, performance based approach using inelastic displacement based analysis has been in forefront. Inelastic dynamic analysis is recognized as the most accurate form of seismic analysis for RC structures. However, it is found to be computationally too expensive for practical problems today. Due to prohibitive computational time and efforts required to perform a complete nonlinear dynamic analysis, researchers and designers all over the world are showing keen interest in nonlinear static pushover analysis. Nonlinear static pushover analysis requires determination of nonlinear force-deformation curve called 'pushover curve' or 'capacity curve' that signifies the load as well as deformational capacity of the structure. This simplifies the structural model while providing insight information about the likely nonlinear behaviour of the structure. Therefore, it can be said that a vital step towards good seismic performance estimation of the structure is reliable and accurate determination of force-deformation curve popularly known as "pushover curve" or "capacity curve".

In order to capture the complete picture of the nonlinear behaviour of the frame structure, it is required to model various nonlinearities such as flexural, shear, axial and torsional behaviour (with interactions) for beams and columns as well as to predict more complex behaviour at the connections e.g. joint shear failure, bond failure etc. Especially, for the structures designed and detailed as per the non-seismic detailing practice, the nonlinear behaviour of the beam-column joints plays a dominant role in determining the seismic response of the structure. The modelling of inelastic behaviour of the members under flexure, shear, torsion and axial forces are well documented and the same have been described in Annexure-I.

Even though today it is well-known that the beam-column joints, especially the poorly designed ones, behave highly nonlinearly during the earthquakes, still the analysis approach mainly revolves around considering concentrated plasticity at the member ends and assuming the joint core as rigid. This is not due to negligence of the designers or analysts but is attributed to the fact that the models available in literature generally are not simple enough to be used in commercial programs being at the same time able to predict the shear behaviour of the joints nicely.

Moreover, the models either require large computational efforts so that they are not practically useful for analyzing the global structural behaviour or they need a special element with various nodes and springs or a special purpose program to implement the joint nonlinearity. This makes it difficult for the designers and analysts to follow the recommended approaches using the commercial programs. Based on the above discussion, it can be said that there is a need to develop, realistic, objective and easily implementable model that can enable not only researchers but also the designers using general purpose programs to give due consideration to the inelastic behaviour of RC beam-column connections.

In this work, a new model for predicting the nonlinear shear behaviour of beam-column joints is suggested that can reasonably accurately capture the shear behaviour of the joints and also is practical enough to be used with existing commercial software programs available. The model is based on practical deformational behaviour of the joint sub-assembly in a structure and follows the principal stress failure criteria so that due consideration may be given to the axial load acting on the column. The formulations needed to generate the joint characteristics are given in this chapter. The model has also been described in Sharma et al (2011).

4.2 Basis for the model

4.2.1 Contribution of Joint Shear Deformation to Storey Drift

The typical deformed shape of a reinforced concrete frame structure under an earthquake is shown in Figure 4.1 below. The inter-storey drift is given as the difference in the deformation of two successive stories.

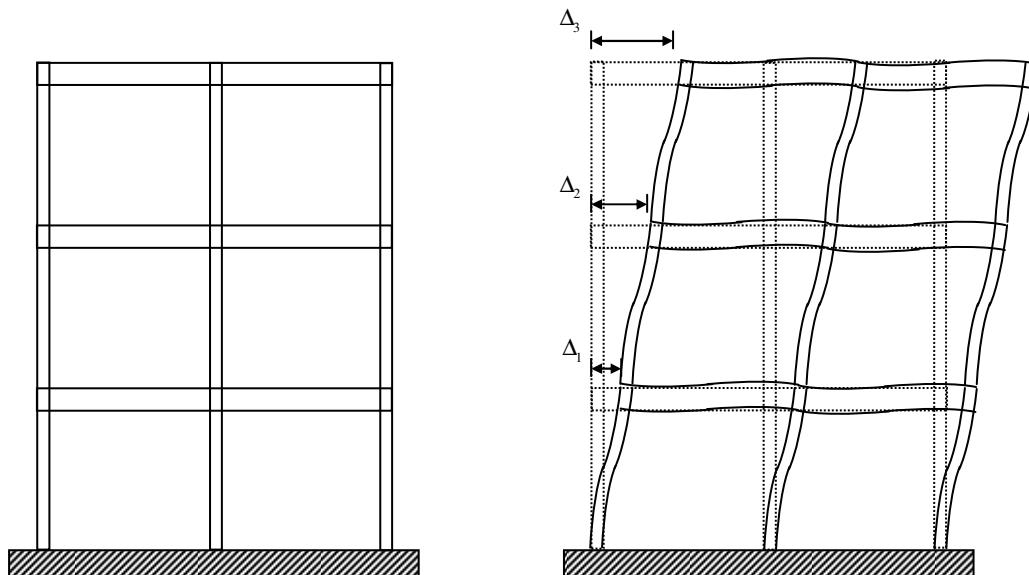


Figure 4.1 Typical deformed shape of framed structures under earthquakes

For a beam-column joint sub-assembly formed between the mid-span of beams and mid-height of columns (assumed points of contraflexure), the contribution of joint shear deformation to storey drift is shown in Figure 4.2 for exterior joints and in Figure 4.3 for interior joints.

Now, due to the joint shear deformation, γ_j , the column experiences a relative shear displacement of $\gamma_j h_b$, where h_b is the total depth of the beam. This deformation can be divided into two as $\Delta_c = \gamma_j h_b / 2$ for the column half above the beam centre line and $\Delta_c = \gamma_j h_b / 2$ for the column half below the beam centre line (Figures 4.2 and 4.3). This deformation is in addition to any shear deformations in the column due to external shear forces. Further, due to joint shear deformation, the beam experiences a rotation of γ_j due to which the beam tip displacement is equal to $\Delta_c = \gamma_j L_b$, where L_b is the length of the mid span of beam from the face of the column. Again, this rotation is due only to the shear deformation of the joint and is in addition to any rotation in the beam that occurs due to external bending moment.

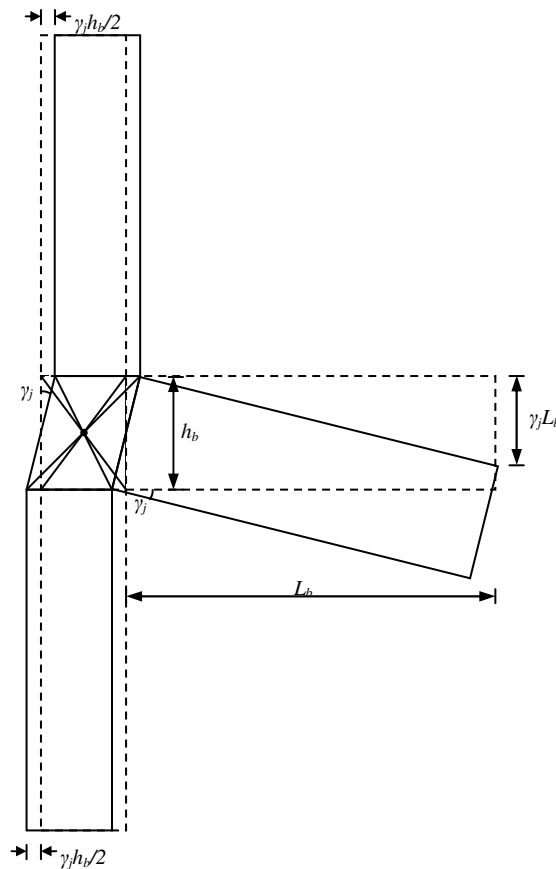


Figure 4.2 Contribution of joint deformation to storey drift for exterior joints

4.2.2 Modelling the Contribution of Joint Shear Deformation to Storey Drift

Based on the above discussed deformational behaviour of joint, it seems most reasonable to model the contribution of joint shear deformation to overall storey drift in a way that can

consider the shear deformations in column and rotation in beam due to joint shear deformation.

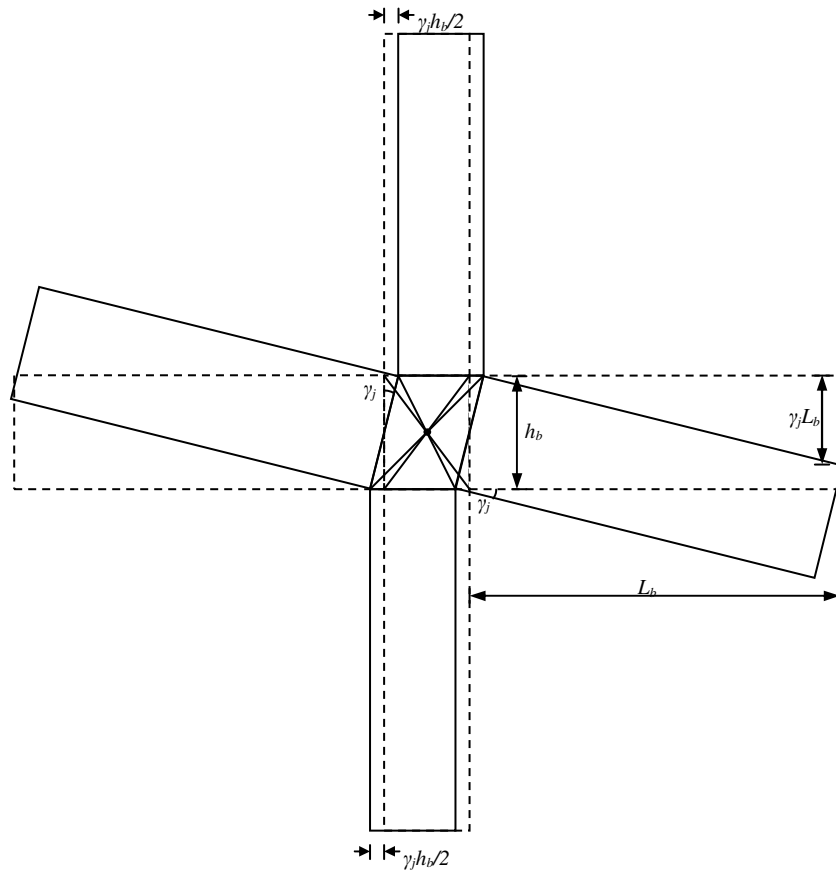


Figure 4.3 Contribution of joint deformation to storey drift for interior joints

One way to model this behaviour is as shown in Figure 4.4 where shear springs in the column portion and a rotational spring in the beam region are assigned to take into account the joint deformational behaviour. Thus, in a frame analysis by software packages, in addition to hinges assigned at the ends of the members (beams and columns), a joint core may be modelled by dividing the frames and hinges are provided in the core region to consider the shear deformations of the joint as shown in Figure 4.5. For interior joints, a rotational spring on the other side of beam needs to be included. This kind of model can be, in a very straightforward manner, applied to general purpose programs where the beam and column members are modelled as frame elements with 6 degrees of freedom at both ends and the springs are the regions of concentrated plasticity with user defined characteristics.

4.3 Characterization of springs for joint model

Physically, the springs should have characteristics as moment in beam, M_b v/s shear deformation of joint, γ_j for the rotational spring and joint horizontal shear force, V_{jh} v/s shear deformation in column portion of joint, $\Delta_c = \gamma_j h_c / 2$. However, in most commercial programs that

are based on matrix analysis using frame elements, it is not possible to model the reinforcement details explicitly and therefore it is not possible to calculate horizontal joint shear force directly. Therefore, in order to make this model suitable for implementation in such programs, we need to provide the characteristics for shear springs as shear force in column, V_c v/s shear deformation in column portion of joint, $\Delta_c = \gamma_j h_b/2$.

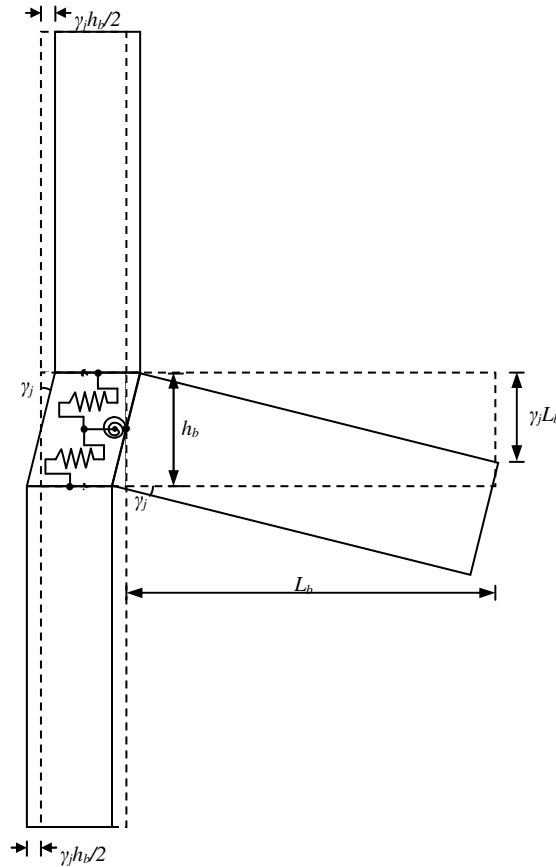


Figure 4.4 Modelling of joint deformational behaviour

Once these characteristics are generated for the joints, the model can be implemented in the computer model of the structure so that the joint behaviour can be taken into account. There are different ways to generate these characteristics as described under:

1. Using results of experiments on beam-column joints tests.
2. Using results of detailed finite element analysis of joints.
3. Analytical computation of characteristics from mechanics of the joints.

4.3.1 Obtaining spring characteristics using experimental results

While performing the experiments on beam-column joints, the column shear force can be directly measured using load cell. Also corresponding joint shear deformations can be measured.

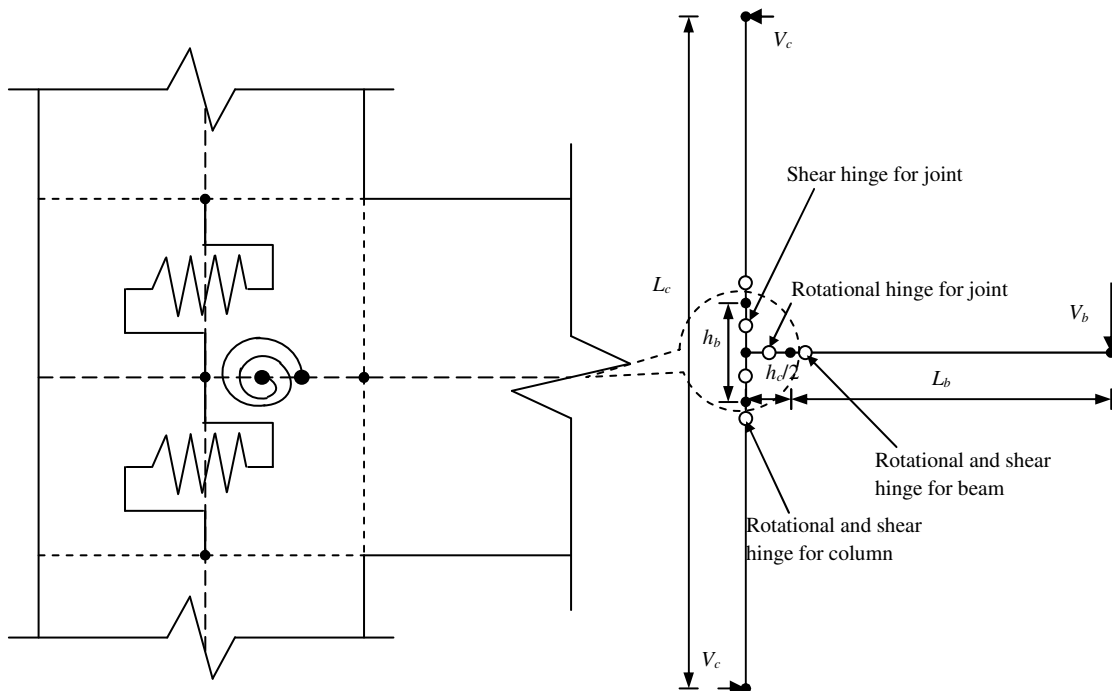


Figure 4.5 Implementation of model in frame elements approach

The most popular method to measure the joint shear deformations is to use cross configuration of linear variable differential transformers (LVDTs) as shown in Figure 4.6 (Genesio and Sharma, 2010).

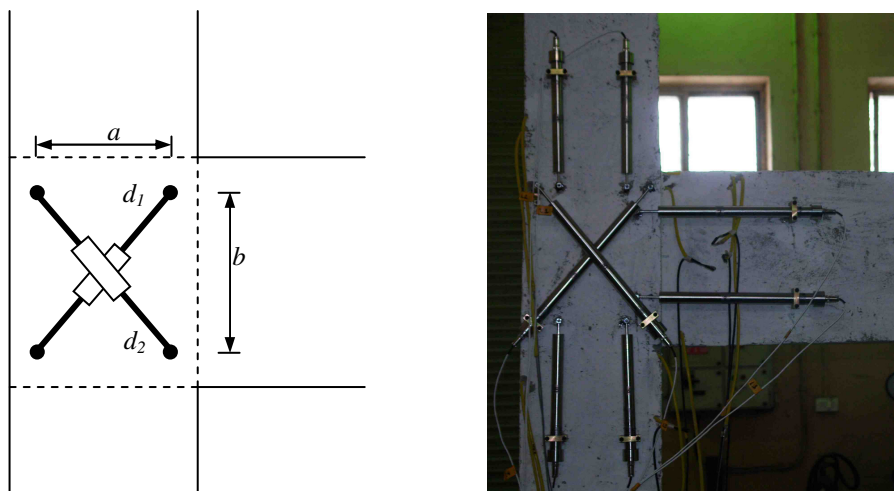


Figure 4.6 Measuring joint shear deformations in tests

The joint shear deformation can be then calculated using the measured values of the LVDT as

$$\gamma_j = \frac{\sqrt{a^2 + b^2}}{2ab} (\delta d_2 - \delta d_1) \quad (4.1)$$

where,

δd_2 is the change in length measured by LVDT, d_2

δd_1 is the change in length measured by LVDT, d_1

a is the horizontal distance between the end points of the LVDTs

b is the vertical distance between the end points of the LVDTs

Figure 4.7 shows a typical beam-end load v/s joint shear distortion plot obtained from the test on an exterior joint with gravity load design detailing (Genesio and Sharma, 2010). Using such plots from experiments, the required characteristics of shear force in column, V_c v/s shear deformation in column portion of joint, $\Delta_c = \gamma_j h_j / 2$ can be generated. Although, this method may be the most accurate and reliable one, it is highly prohibitive from the point of view of cost, time and resources required. Moreover, considering the different types of joints that may be present in a structure, this method is highly impractical too. However, this method can be used for calibration and validation of results.

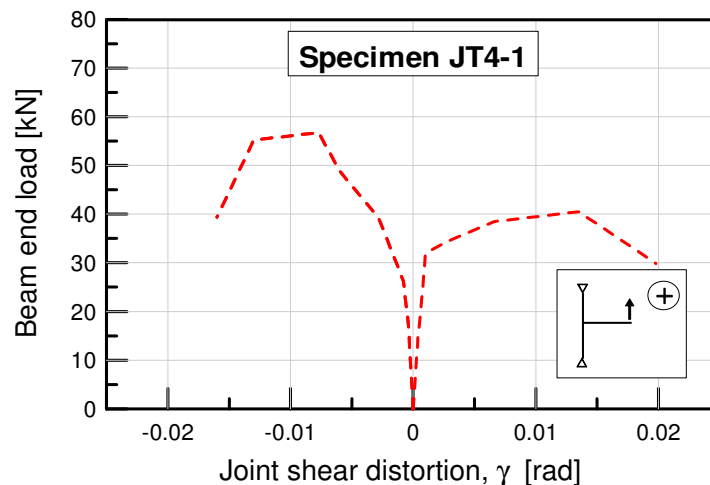


Figure 4.7 Typical measured beam load v/s joint shear distortion in tests (Genesio and Sharma, 2010)

4.3.2 Obtaining spring characteristics using results of detailed FE analysis

Another method to obtain the characteristics is to perform detailed finite element analysis of the joints. The accuracy and reliability of this method relies on the accuracy and reliability of the modelling techniques. One such method is explored and reported by Eligehausen et al (2006) and Sharma et al (2008) where a finite element approach specially developed for detailed modelling of fracture in quasi brittle materials has been proposed (Figures 4.8, 4.9).

MASA, a finite element program for 3D nonlinear analysis of concrete and reinforced concrete structures, developed at the Institut für Werkstoffe im Bauwesen, Universität Stuttgart (IWB and Ožbolt, 2005, 2008) was used in these works. The microplane material model with relaxed kinematic constraint is used for modelling the concrete and a discrete one

dimensional bond element model is used for modelling the bond behaviour of the reinforcement bars. Mahajan (2009) and Genesio (2012) used this approach for analysis of the joints for validation and parametric study to propose assessment models for joints. It is shown in all these studies that the model can predict the behaviour of the joints with high accuracy and can capture various failure modes. Further details can be obtained from the reference (Sharma et al, 2008; Genesio, 2012).

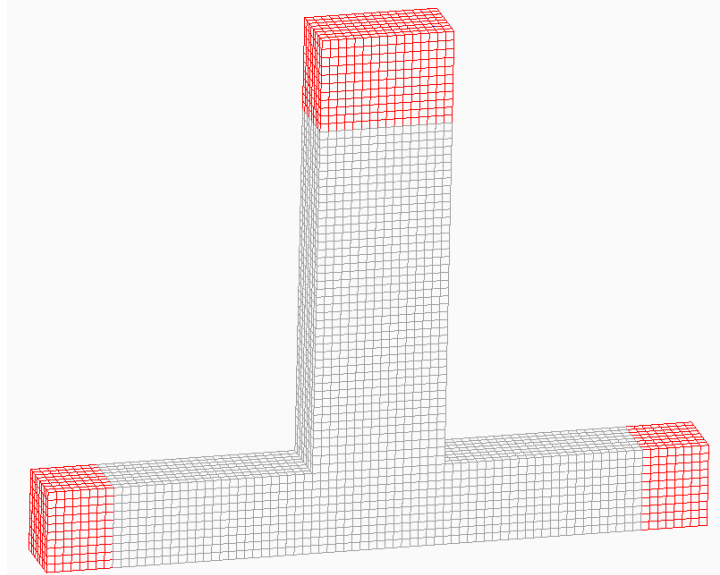


Figure 4.8 FE Model of the joint (Sharma et al 2008)

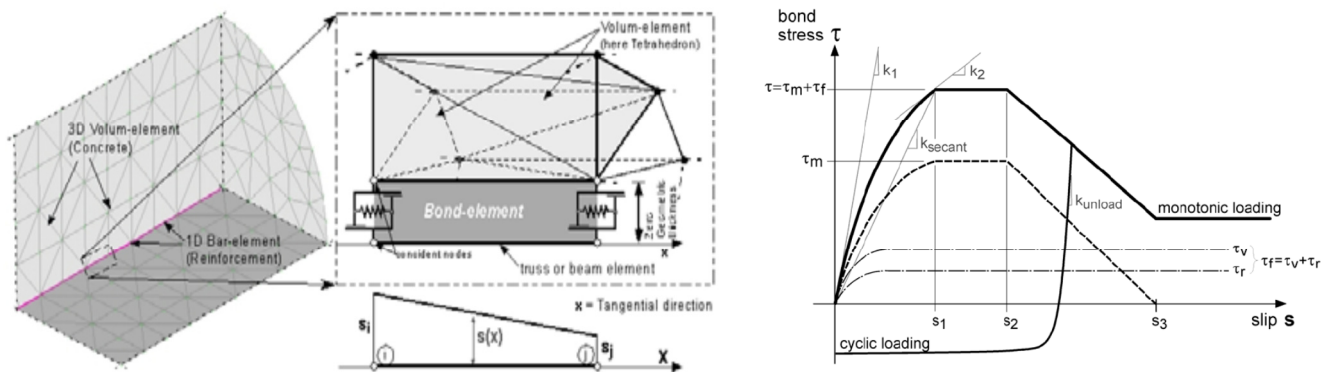


Figure 4.9 Discrete bond element and characteristics for bond element

This method has lesser cost implications but needs lot of modelling and computational time and effort. Again, considering the fact that there may be several different kinds of joints existing in a structure, the computational time and effort in this method becomes prohibitive. However, once the model is validated against experiments, the method can be useful in characterizing different types of joints by performing parametric study as shown by Genesio (2012). Thus, the method can principally work as replacement of experiments. However, it must be kept in mind that this procedure is useful to study sub-assemblies in details but a detailed FE analysis of the whole structure using this method is impractical.

4.3.3 Analytical computation of characteristics from mechanics of the joints

The most practical and computationally competitive method for obtaining spring characteristics for joint model is the analytical method. Once, a failure criterion for the joints is selected, the spring characteristics can be computed following the mechanics of the joint. Various failure criteria for the joints have been discussed in chapter 3. However, the objective of this work is to develop a model that is practical, computationally non-prohibitive, accurate and applicable to different structures. The shear strength models based on strut and tie approach are considered accurate but are known to be computationally expensive and too complicated for practical implementation. On the other hand, horizontal shear stress criterion is simple but is not accurate enough since it cannot differentiate between joints with different axial loads on columns.

Reviewing the various models discussed in chapter 3, the principal stress criterion seems to be most appropriate since it is simple and practical and at the same time provides a rational basis of predicting joint failure giving due consideration to the axial stresses in the column. Based on these arguments, in this work, the principal stress v/s joint distortion curve is considered to serve as the failure envelope for the beam-column joint core. Once this curve is obtained for any given joint, it can be utilized to develop the spring characteristics to model the joint behaviour.

For joints with deformed bars as reinforcement, Priestley (1997) suggested plots of principal tensile stress v/s inter-storey drift for interior and exterior joints with different reinforcement anchorage types (Figure 4.10). Pampanin (2002) suggested the plots of principal tensile stress v/s joint shear deformation for exterior joints with smooth bars having end hooks (Figure 4.11).

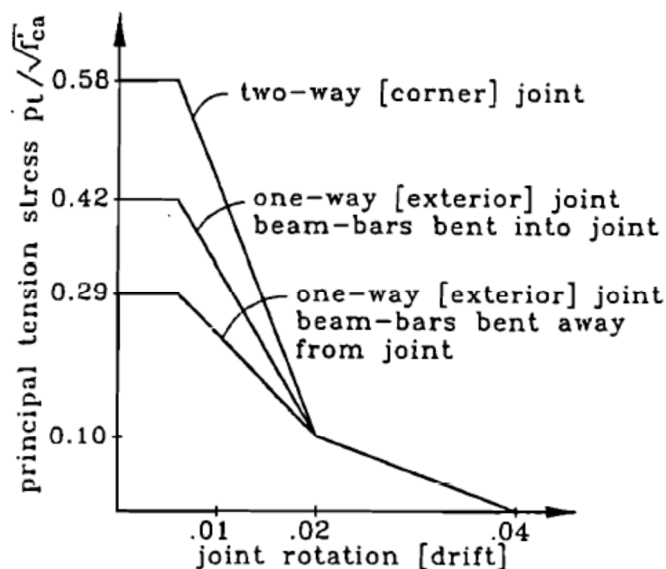


Figure 4.10 Principal tensile stress v/s inter-storey drift (Priestley, 1997)

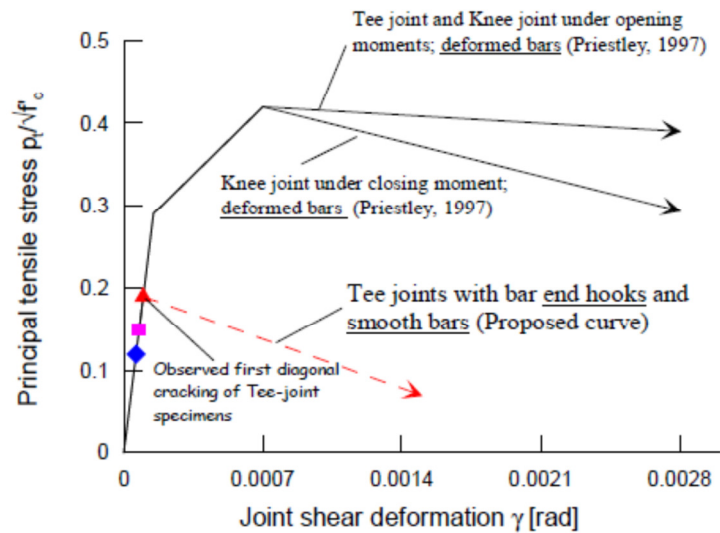


Figure 4.11 Suggested principal tensile stress v/s joint shear deformation relationship (Pampanin et al, 2002)

Priestley (1997) proposed the values for the limit states of first cracking and ultimate failure of joints with beam bars bent out (Figure 4.12 a) and with beam bars bent in (Figure 4.12 b). As per Priestley (1997), for exterior joints with deformed bars, a lower limit of critical principal tensile stress, p_t of $0.29\sqrt{f_c'}$ seems appropriate for first diagonal cracking, where f_c' is the cylindrical compressive strength of the concrete. He explained that for exterior joints, when the beam reinforcement is anchored by bending away from the joint (Figure 4.12 a), the diagonal struts in the joint cannot be stabilized and the joint failure occurs at an early stage. Thus, no further hardening after the cracking is considered for such joints. On the other hand, for exterior joints with beam bars bent in a hardening behaviour with increase of principal stress levels, up to $0.42\sqrt{f_c'}$ is suggested that corresponds to more severe diagonal cracking and damage in the joint panel zone (ultimate shear failure).

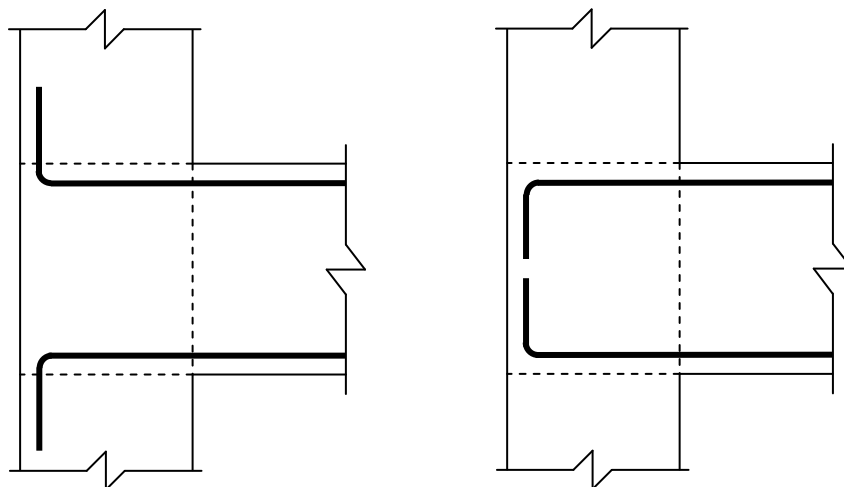


Figure 4.12 Exterior joints with (a) beam bars bent out (b) beam bars bent in

The principal tensile stress v/s joint shear deformation relation essentially serves as a failure envelope for the beam-column joints, using which the spring characteristics for the proposed joint model can be evaluated. As mentioned earlier, to model the springs in the joint model, we need to convert the principal tensile stress v/s shear deformation relation into (i) beam moment v/s joint rotation (same as joint shear deformation) for rotational hinge and, (ii) column shear v/s shear deformation of column element.

The formulations to generate these spring characteristics from the known principal tensile stress v/s joint deformation plots are given below for two cases:

1. Joints without axial load on column
2. Joints with axial load on column

4.3.3.1 Joints without axial load on column

The principal tensile stress is given by (Tsonos 2007),

$$p_t = \frac{\sigma}{2} - \frac{\sigma}{2} \sqrt{1 + \frac{4\tau^2}{\sigma^2}} \quad (4.2)$$

where, σ is the vertical joint shear stress given by,

$$\sigma = \frac{V_{jv}}{b_c h_c} \quad (4.3)$$

and τ is the horizontal joint shear stress given by,

$$\tau = \frac{V_{jh}}{b_c h_c} \quad (4.4)$$

Here,

b_c = breadth of the joint core

h_c = depth of the joint core

V_{jh} = Horizontal joint shear force

V_{jv} = Vertical joint shear force

Using equations (4.3) and (4.4), we get,

$$\sigma = \frac{V_{jv}}{V_{jh}} \times \tau \quad (4.5)$$

Also, it is shown (Park and Paulay, 1975; CEN 250; Paulay and Park, 1984; Tsonos, 2007) that:

$$\frac{V_{jv}}{V_{jh}} = \frac{h_b}{h_c} = \alpha \quad (4.6)$$

where,

h_b is the depth of the beam

α is known as the aspect ratio of the joint

Putting (4.6) in (4.5), we get,

$$\sigma = \alpha\tau \quad (4.7)$$

Replacing σ from equation (4.7) in (4.2), we get,

$$p_t = \frac{\alpha\tau}{2} - \frac{\alpha\tau}{2} \sqrt{1 + \frac{4\tau^2}{\alpha^2\tau^2}}$$

or,

$$p_t = \frac{\alpha\tau}{2} \left(1 - \sqrt{1 + \frac{4}{\alpha^2}} \right) \quad (4.8)$$

Rearranging equation (4.8), we get,

$$\tau = \frac{2p_t}{\alpha \left(1 - \sqrt{1 + \frac{4}{\alpha^2}} \right)} \quad (4.9)$$

Thus, from equation (4.4), we get,

$$V_{jh} = \frac{2p_t b_c h_c}{\alpha \left(1 - \sqrt{1 + \frac{4}{\alpha^2}} \right)} \quad (4.10)$$

Therefore, for a given value of critical principal tensile stress, p_t , we can calculate corresponding horizontal joint shear, V_{jh} by using (4.10).

Now, shear force in the column is given by,

$$V_c = T_b - V_{jh} \quad ; \text{ for exterior joints (Figure 2.4), and} \quad (4.11 a)$$

$$V_c = C_{sb2} + C_{cb2} + T_{b1} - V_{jh} \quad ; \text{ for interior joints (Figure 2.5)} \quad (4.11 b)$$

To calculate, V_c corresponding to V_{jh} , we need to follow an iterative procedure as given below:

1. Calculate moment in beam, M_b v/s tensile force in the beam bar, T_b curve for beam section in case of exterior joints and M_b v/s $(C_{cb} + C_{sb} + T_b)$, for interior joints (Same procedure as followed for obtaining Moment v/s curvature diagram). Detailed procedure to obtain moment v/s curvature curve is given in Appendix A.
2. Assume a value of T_b or $(C_{cb} + C_{sb} + T_b)$, as appropriate.
3. Calculate column shear using equation 4.11 (a or b), as appropriate.
4. Calculate beam shear from global equilibrium of the joint
e.g., $V_b = \frac{V_c L_c}{L_b + h_c / 2}$ (for exterior joints without gravity load) (4.12)
5. Calculate moment in the beam,
 $M_b = V_b \times l_b$ (4.13)
6. From M_b v/s T_b diagram or M_b v/s $(C_{cb} + C_{sb} + T_b)$ find the value of T_b or $(C_{cb} + C_{sb} + T_b)$.
7. If the value obtained in step 6 is close to the corresponding assumed value in step 2, then the obtained value of M_b corresponding to V_{jh} is correct. Else, go to step 2 and iterate.

By this iterative procedure, we can obtain the values of V_c and M_b corresponding to V_{jh} (and in turn corresponding to p_t). Corresponding to a given value of γ_j , we can calculate $\Delta_c = \gamma_j h_b / 2$. Thus, we can have a V_c v/s Δ_c relationship for shear hinge in column region of the joint and M_b v/s γ_j relationship for rotational hinge in beam region of the joint. A flowchart to derive V_c v/s Δ_c and M_b v/s γ_j relationships from given p_t v/s γ_j for no axial load case and exterior joints is given in Figure 4.13. The same is applicable for interior joints with T_b replaced by $C_{cb} + C_{sb} + T_b$.

4.3.3.2 Joints with axial load on column

Let the axial load on the column be 'P'. In this case, σ is the vertical joint shear stress given by,

$$\sigma = \frac{V_{jv} + P}{b_c h_c} \quad (4.14)$$

while, the horizontal joint shear stress, τ is given by equation (4.4).

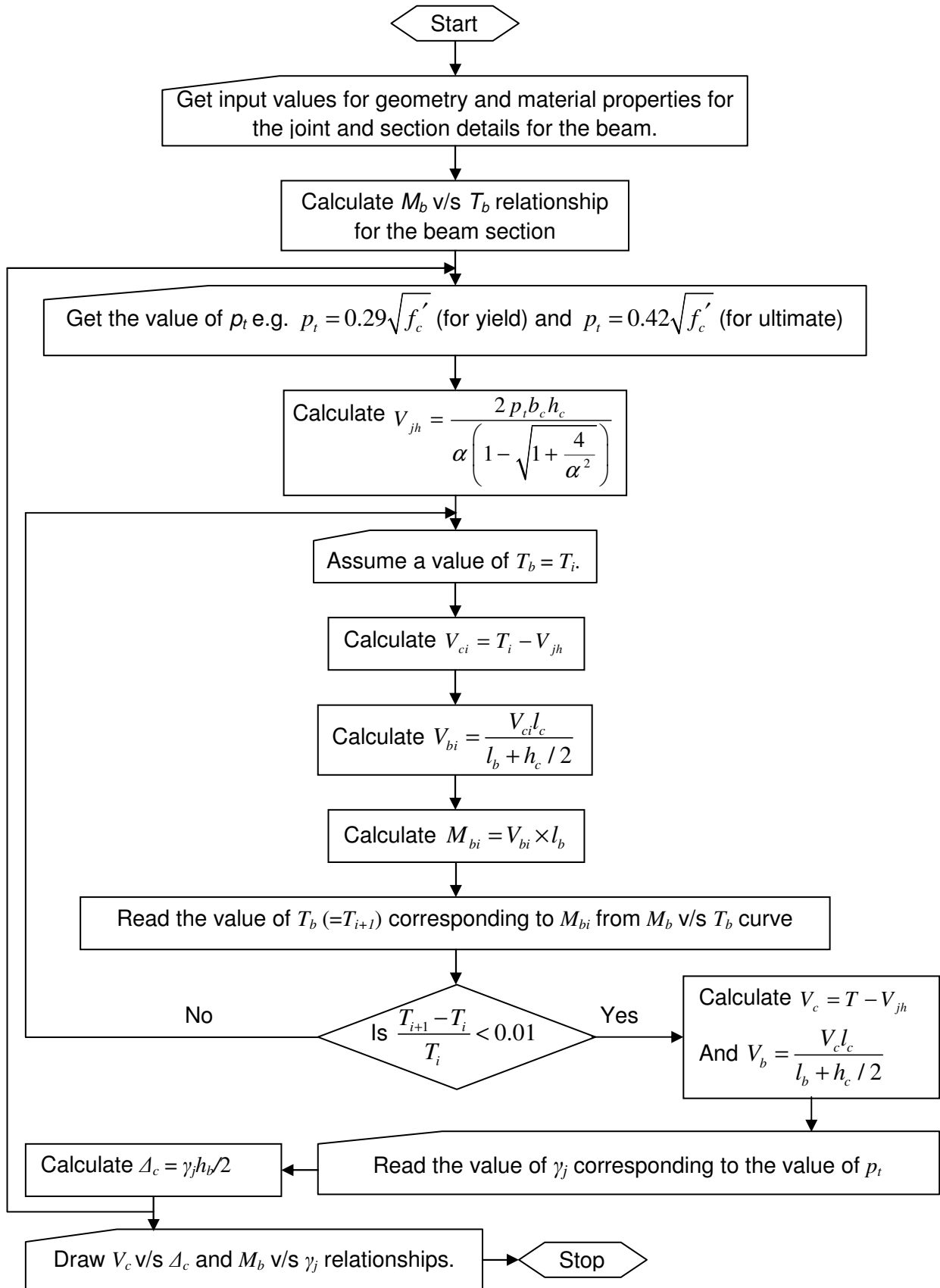


Figure 4.13 Flowchart for obtaining spring characteristics for no axial load case

Using equation (4.6) in (4.14), we get,

$$\sigma = \frac{V_{jv}}{b_c h_c} + \frac{P}{b_c h_c}$$

$$\Rightarrow \sigma = \frac{\alpha V_{jh}}{b_c h_c} + \frac{P}{b_c h_c} \quad (4.15)$$

Thus,

$$\sigma = \alpha \tau + \sigma_a \quad (4.16)$$

or,

$$\tau = \frac{\sigma - \sigma_a}{\alpha} \quad (4.17)$$

Putting (4.17) in (4.2), we get,

$$p_t = \frac{\sigma}{2} - \frac{\sigma}{2} \sqrt{1 + \frac{4(\sigma - \sigma_a)^2}{\alpha^2 \sigma^2}} \quad (4.18)$$

Rearranging equation (4.18), we get,

$$1 - \frac{2p_t}{\sigma} = \sqrt{1 + \frac{4(\sigma - \sigma_a)^2}{\alpha^2 \sigma^2}} \quad (4.19)$$

Squaring both the sides and simplifying, we get,

$$\sigma^2 - (2\sigma_a + \alpha^2 p_t)\sigma + (\sigma_a^2 - \alpha^2 p_t^2) = 0 \quad (4.20)$$

Solving (4.20), we get,

$$\sigma = \frac{2\sigma_a + \alpha^2 p_t + \alpha \sqrt{\alpha^2 p_t^2 + 4p_t(\sigma_a + p_t)}}{2} \quad (4.21)$$

Thus, for a given value of p_t , σ_a and α , we can obtain the corresponding value of σ . Now, from eq (4.14), we can get,

$$V_{jv} = \sigma b_c h_c - P \quad (4.22)$$

By equation (4.6), we have,

$$V_{jh} = \frac{V_{jv}}{\alpha} \quad (4.23)$$

Thus, for a given value of p_t , we can calculate corresponding horizontal joint shear, V_{jh} by using equations (4.22) and (4.23).

Now, we have, shear force in column,

$$V_c = T_b - V_{jh} \quad (\text{for exterior joints, Figure 2.}), \text{ and} \quad (4.24 \text{ a})$$

$$V_c = C_{sb2} + C_{cb2} + T_{b1} - V_{jh} \quad (\text{for interior joints, Figure 2.}) \quad (4.24 \text{ b})$$

To calculate, V_c corresponding to V_{jh} , we need to follow an iterative procedure as given below,

1. Calculate moment in beam, M_b v/s tensile force in the beam bar, T_b curve for beam section in case of exterior joints and M_b v/s $C_{cb} + C_{sb} + T_b$, for interior joints.
2. Assume a Value of T_b or $C_{cb} + C_{sb} + T_b$, as appropriate.
3. Calculate column shear using equation 4.24 (a or b) as appropriate.
4. Calculate beam shear from statics of the joint

$$\text{e.g., } V_b = \frac{V_c L_c}{L_b + h_c / 2} \quad (\text{for exterior joints}) \quad (4.25)$$

5. Calculate moment in the beam,

$$M_b = V_b \times L_b \quad (4.26)$$

6. From M_b v/s T_b diagram or M_b v/s $C_{cb} + C_{sb} + T_b$, find the value of T_b or $C_{cb} + C_{sb} + T_b$.
7. If the value obtained in step 6 is close to the corresponding assumed value in step 2, then the obtained value of M_b corresponding to V_{jh} is correct. Else, go to step 2.

By this iterative procedure, we can obtain the values of V_c and M_b corresponding to V_{jh} (and in turn corresponding to p_t). Corresponding to a given value of γ_j , we can calculate $\Delta_c = \gamma_j h_b / 2$. Thus, we can have a V_c v/s Δ_c relationship for shear hinge in column region of the joint and M_b v/s γ_j relationship for rotational hinge in beam region of the joint. A flowchart to derive V_c v/s Δ_c and M_b v/s γ_j relationships from given p_t v/s γ_j for with axial load case and exterior joints is

given in Figure 4.14. The same is applicable for interior joints with T_b replaced by $C_{cb} + C_{sb} + T_b$. Once the V_c v/s Δ_c and M_b v/s γ_j relationships are derived from given p_t v/s γ_j and details of the joint, the characteristics can be used as spring characteristics to model the joint shear.

4.4 Recommended principal tensile stress v/s shear deformation relations

Following the formulations given in previous section, the characteristics for the springs representing joint behaviour can be derived, provided the principal tensile stress v/s shear deformation relations are known. In this section, the recommended principal tensile stress v/s shear deformation relations for different types of joints are given. The relations are provided on the basis of the experimental data of tests where joint deformations were measured (e.g. Clyde et al, 2000; Pantelides et al, 2002; Pampanin et al, 2002; Anderson et al, 2008; Genesio and Sharma, 2010). Based on the data obtained on shear deformations in these tests and utilizing the recommendations made by Priestley (1997), the following plots of principal tensile stress v/s shear deformations are recommended to derive the spring characteristics. The characteristics are recommended for joints with deformed bars as reinforcement in beams and columns. For joints with plain round reinforcing bars, the relationships recommended by Pampanin et al (2002) can be utilized. It shall be noted that the formulations for the principal tensile stress v/s shear deformations recommended by Genesio (2012) as given in eqs. (3.14) and (3.15) can also be used to derive joint spring characteristics. A comparison of formulations used in this work and those proposed by Genesio (2012) is given at the end of this chapter.

4.4.1 Exterior Joints

4.4.1.1 Exterior Joints with beam bars bent in

As per Priestley (1997), the lower limit of principal tensile stress for the first shear cracking in the joint panel can be considered as $p_t = 0.29(f'_c)^{0.5}$. When the beam bars are bent into the joint (Figure 4.15), the diagonal struts in the joint are nicely stabilized and therefore, after the first cracking, the joint can offer further resistance and therefore a hardening behaviour till the principal tensile stress reach a value of $p_t = 0.42(f'_c)^{0.5}$ can be assumed (Priestley 1997). Based on these recommendations and using the experimental plots of shear deformations obtained by Clyde et al (2000), Pantelides et al (2002) and Anderson et al (2008) on similar joints, the plot of principal tensile stress v/s joint shear deformation, as shown in Figure 4.15 is recommended for calculating the spring characteristics.

4.4.1.2 Exterior Joints with beam bars bent out

When the beam bars are bent out of the joint (Figure 4.16), again the first cracking can be assumed to occur at $p_t = 0.29(f'_c)^{0.5}$ since the stress at first cracking will not be affected by bond requirements.

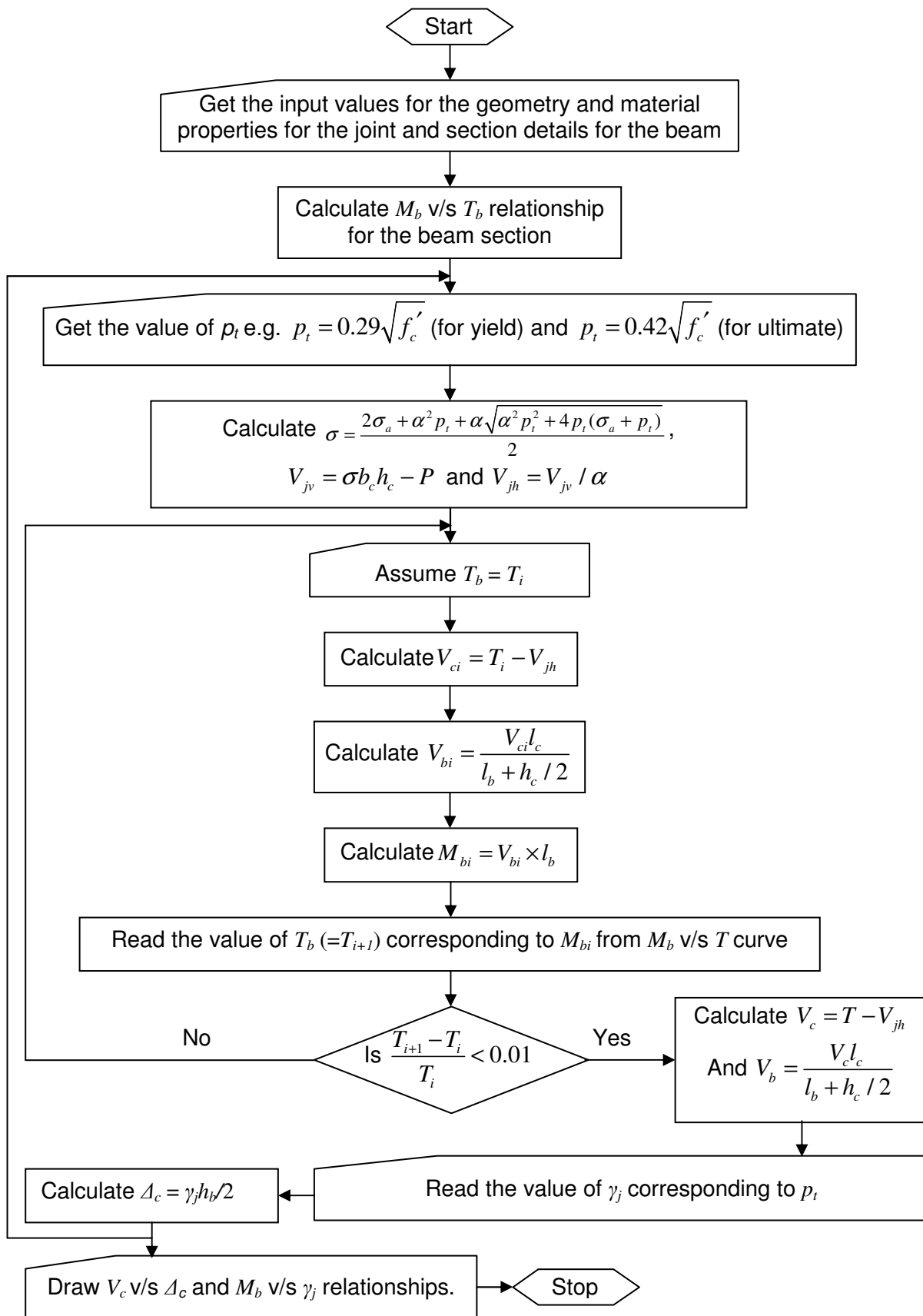


Figure 4.14 Flowchart to evaluate spring characteristics for joints with axial load

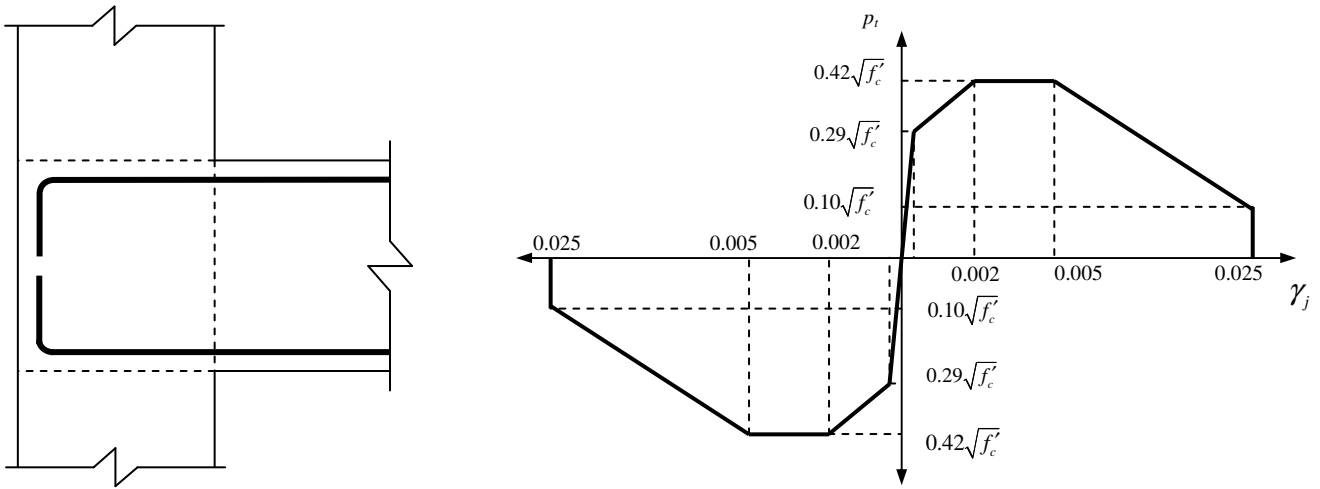


Figure 4.15 Recommended principal tensile stress-shear deformation relation for exterior joints with bars bent in

However, after the first cracking, the diagonal struts in the joint cannot be stabilized and therefore, the joint failure occurs at early stage and thus, no hardening can be assumed in such cases after the first cracking. Further joint resistance cannot be relied upon in such cases and therefore the principal tensile stress value of $p_t = 0.29(f'_c)^{0.5}$, is assumed as the limiting value (Priestley, 1997). Based on these recommendations and using the experimental plots of shear deformations obtained for similar joints (Genesio and Sharma, 2010), the plot of principal tensile stress v/s joint shear deformation, as shown in Figure 4.16 seems appropriate for calculating the spring characteristics.

In certain cases (e.g. Kurose, 1987), the top beam bars are bent into the joint and the bottom beam bars are bent out of the joint. For such cases, the plot of principal stress v/s shear deformation may be obtained by the superposition of Figure 4.15 and 4.16 as shown in Figure 4.17.

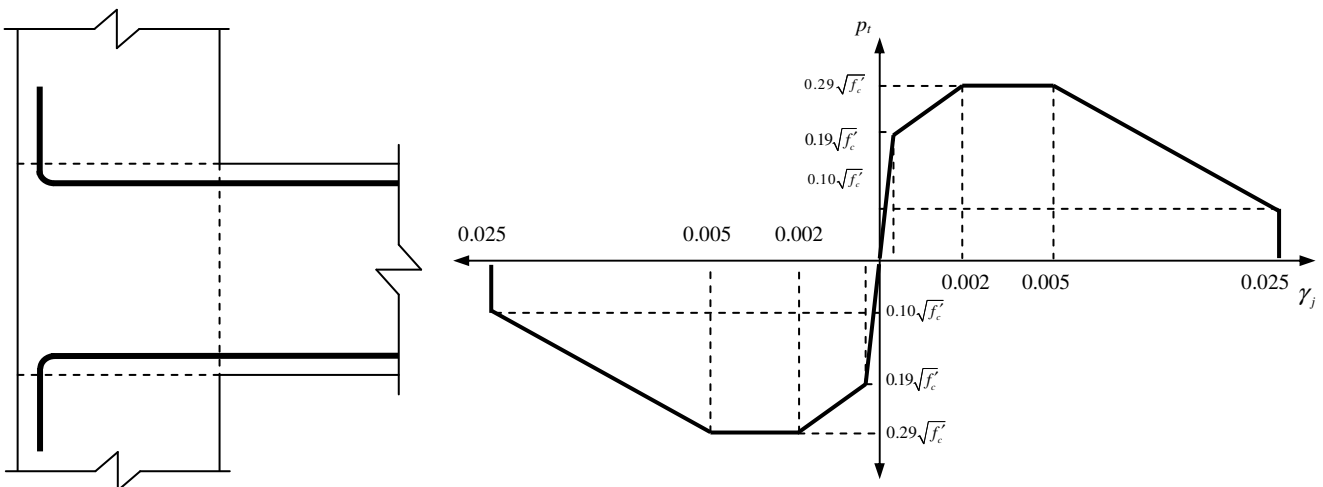


Figure 4.16 Recommended principal tensile stress-shear deformation relation for exterior joints with bars bent out

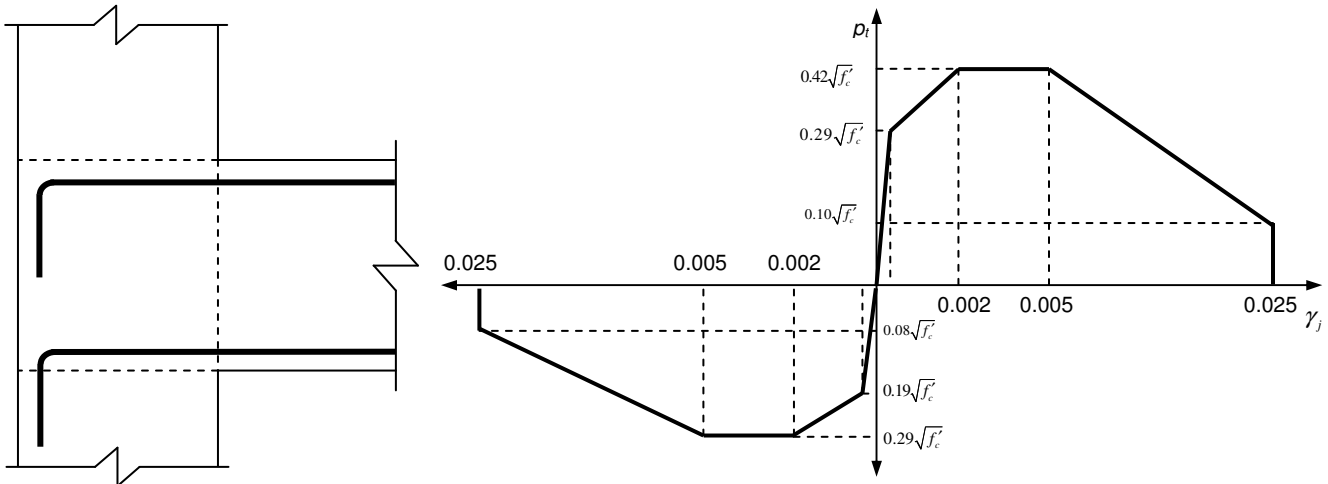


Figure 4.17 Recommended principal tensile stress-shear deformation relation for exterior joints with top bars bent in and bottom bars bent out

4.4.1.3 Exterior joints with straight bottom beam bars with full development length embedment

When the beam bars are not bent into the joint but kept straight, again the diagonal struts in the joint cannot be stabilized and therefore, the joint failure occurs at early stage $p_t = 0.29(f'_c)^{0.5}$. No hardening can be assumed in such cases after the first cracking. In cases where the beam bars are embedded into the joint for full development length, bond failure is unlikely and therefore, the same plot as shown in Figure 4.17 shall apply.

4.4.1.4 Exterior joints with bottom beam bars straight with 150mm embedment

In case of joints of gravity load designed (GLD) frames, where the bottom beam bars are embedded only up to 150mm (6 inches) inside the joint, the bond between concrete and rebars becomes the critical parameter. In such cases, the bond failure occurs much before the diagonal compressive strut could be fully activated and therefore the critical tensile stress at first cracking and ultimate state are significantly affected. To decide on the critical values for such joints, data of the tests performed by Pantelides et al (2002), Murty et al (2003), El-Amoury and Ghobarah (2002) and Genesio and Sharma (2010) was considered. The principal tensile stresses were calculated corresponding to the peak load in the direction that induces tension in the straight anchored bars. The values obtained for the peak principal tensile stresses are given in Table 4.1.

Although the database is not very large, but due to a small scatter, the critical values for principal tensile stress corresponding to 1st shear crack and the peak load as $p_t = 0.13(f'_c)^{0.5}$ and $p_t = 0.19(f'_c)^{0.5}$ respectively were considered appropriate for the joints having deformed bars with straight anchorage upto 150 mm embedment.

Table 4.1 Calculated principal tensile stresses corresponding to peak load for joints with bottom beam bars having 150mm embedment

Joint Name	Pantelides et al 1	Pantelides et al 2	Murty et al S1	El-Amoury & Ghobarah T0	Genesio & Sharma JT31
$p_t / \sqrt{f'_c}$ corresponding to 1 st shear crack	0.1545	0.1498	0.1348	0.1404	0.1413
$p_t / \sqrt{f'_c}$ corresponding to peak load	0.2164	0.2054	0.1919	0.2127	0.2033

Incidentally, Pampanin et al (2002) have proposed the same value, corresponding to peak load, as the critical principal tensile stress for smooth bars with end hooks. Moreover, it can be seen that the ratio of critical principal tensile stress corresponding to 1st shear crack to that corresponding to peak load is around 0.68 which is very close to the corresponding ratio for the joints with beam bars bent in. Though, the joint rotation values till the peak were considered same as for the joints with beam bars bent in, the ultimate rotation value was significantly reduced on the basis that the bar slip would not allow too much shear deformation of the joint. This is supported by the results of measured shear deformations during the tests on beam-column joints provided in the literature (Pantelides et al, 2002). The plot proposed for such joints is shown in Figure 4.18.

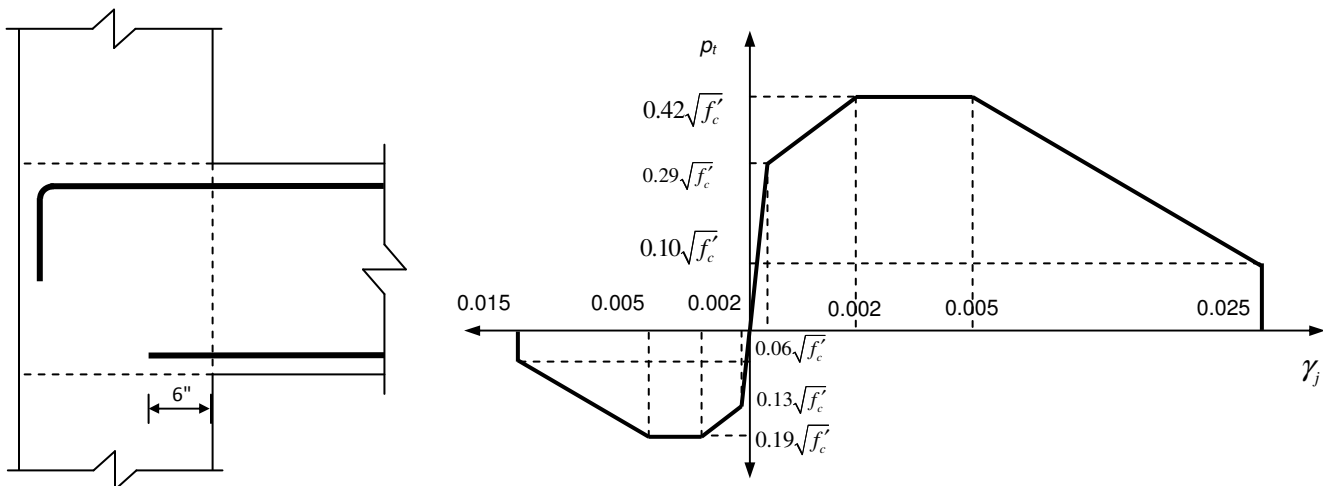


Figure 4.18 Recommended principal tensile stress-shear deformation relation for exterior joints with top bars bent in and bottom bars straight with 150mm embedment

4.4.2 Interior Joints

The principal tensile stress values that could be resisted by an interior joint are generally much higher than the exterior joints. Based on the test result data by Dhakal et al (2005) and Hakuto et al (2000), the relationship between principal stress v/s shear deformation as shown in Figure 4.19 is recommended for the interior joints with deformed bars.

4.4.3 Considerations of joint aspect ratio

Research, experimental (Wong and Kuang, 2008) and numerical (Shiohara, 2004; Mahajan, 2010; Genesis, 2012) has shown that the strength of a joint decreases with increase in the aspect ratio of joint, i.e., ratio of total depth of beam to total depth of column. Based on the experimental investigations, Wong and Kuang observed the reduction in joint shear strength with increase in aspect ratio as shown in Figure 4.20. The column depth for all the cases was 300mm and beam depth was varied as 300mm, 450mm and 600mm leading to the joint aspect ratios of 1.0, 1.5 and 2.0 respectively.

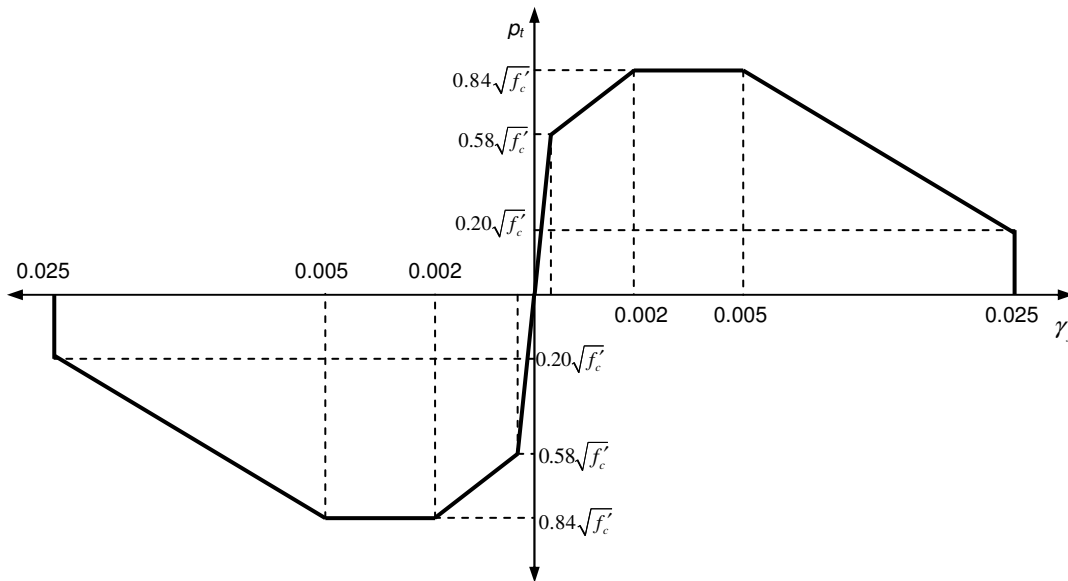


Figure 4.19 Recommended principal tensile stress-shear deformation relation for interior joints

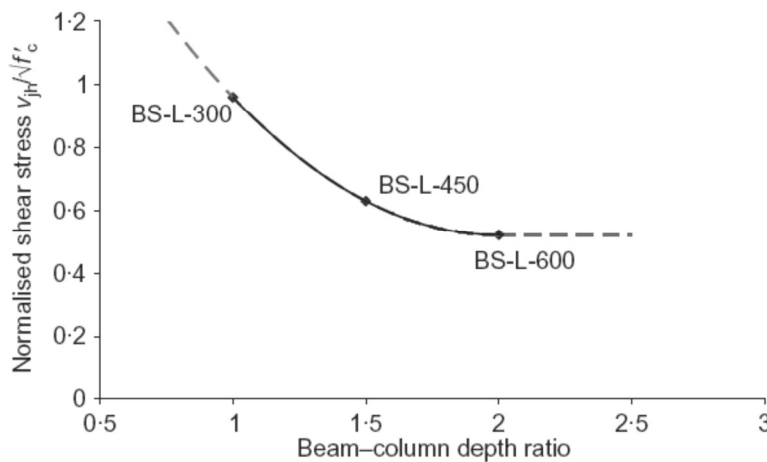


Figure 4.20 Variation of joint shear strength with increasing aspect ratio (Wong and Kuang, 2008)

This can be explained with the argument that with larger aspect ratios, the angle of the concrete strut with horizontal is larger and hence the horizontal component of the diagonal strut that resists the tensile force from beam reinforcing bars is less. Therefore to maintain equilibrium, for same tensile force in the beam bars, higher compression force in the concrete strut is required. Due to this increased demand in the concrete strut, the joint shear strength reduces due to increase in aspect ratio.

In this work, based on the curve recommended by Wong and Kuang (2008) as shown in Figure 4.20, it is recommended to consider the effect of aspect ratio by multiplying the critical principal tensile stress values for cracking and/or failure by the factor k_α , given as:

$$k_\alpha = \frac{1}{\alpha} \quad (4.27)$$

Where, $\alpha = \frac{h_b}{h_c}$ is the aspect ratio.

Hence, for a joint having aspect ratio α , the critical principal tensile stress corresponding to a particular limit state (e.g. 1st cracking) can be obtained as:

$$p_{t,\alpha} = k_\alpha p_{t(\alpha=1)} \quad (4.28)$$

The critical principal tensile stress values for different limit states for various types of joints with aspect ratio = 1.0 are given in Figures 4.15 through 4.19.

However, it may be noted that another way of considering the joint aspect ratio as recommended by Genesio (2012) may be utilized to obtain spring characteristics for joints with aspect ratios different than unity. A comparison of the criteria recommended by Genesio (2012) and that used in this work is given at the end of this chapter.

4.4.4 Considerations of eccentricity in joints

Often, the breadth of the beam is smaller than that of the column, it is framing into. For architectural purposes, the centre line of the beams and those of columns may not be coincident in such cases leading to eccentric joints. The eccentricity between beam and column centerlines induces torsional moment in the joint region, in addition to the horizontal joint shear in their concentric counterpart, when the joint is subjected to seismic loading (Li et al, 2009). This torsion produces additional joint shear stresses and thereby reduces the joint shear strength.

The most popular and acceptable way to account for the eccentricity in joints is to consider the effective joint width (instead of whole column width as joint width) while evaluating the failure load for the joint. Various equations are available for considering the effective width of the joint. Considering the good predictions obtained by Mahajan (2010), the following formulation is recommended to evaluate the equivalent joint width, $b_{j,eq}$ in this work (Mahajan, 2010).

$$b_{j,eq} = \beta b_b \quad (4.29)$$

$$\beta = 1 + \left\{ 1.10 \left(1 - \frac{b_b}{b_c} \right) \right\} - \left\{ 0.75 \frac{e / b_b}{h_b / h_c} \right\} \quad (4.30)$$

Where,

b_b = Width of the beam

b_c = Width of the column

e = Eccentricity = Distance between centre line of beam and centre line of column

h_b = Depth of the beam

h_c = Depth of the column

4.5 Summary

In this chapter, a new joint model has been proposed to simulate the inelastic seismic behavior of poorly detailed joints. The model is based on practical deformational behaviour of the joint sub-assembly in a structure and follows the principal stress failure criteria so that due consideration may be given to the axial load acting on the column. The formulations as given in this chapter were used to derive the monotonic envelopes for the joint springs and they were used along with the characteristics derived for structural members i.e. beams and columns (Appendix-A) to carry out the monotonic pushover analysis for joint sub-assemblies and structures following the procedure explained in Appendix-B. These properties were associated with appropriate hysteretic laws to perform cyclic and dynamic analysis of sub-assemblies and structures as will be shown in later chapters. The numerical analysis was performed using commercial software SAP2000.

The relationships used for critical principal tensile stress v/s joint shear deformation in this work are primarily based on the recommendations of Priestley (1997) with extended values proposed by Pampanin (2002) and Sharma (2011) to cover different types of joints. The influence of aspect ratio is considered based on equation (4.27), which is deduced from the work of Wong and Kuang (2008). Influence of eccentricity on joint strength is considered by equivalent joint width concept and the equivalent joint width is considered as per recommendations of Mahajan (2009). As mentioned earlier, the formulations for the principal tensile stress v/s shear deformations recommended by Genesio (2012) as given in eqs. (3.14) and (3.15) can also be used to derive joint spring characteristics, though influence of

eccentricity is not included in the recommendations of Genesio (2012). Here the formulations used in this work are briefly compared with those suggested by Genesio (2012).

Based on a numerical parametric study, Genesio (2012) proposed the formulations for critical principal tensile stresses as a function of joint aspect ratio for both first cracking and ultimate strength of the joint. For ultimate strength, he further included axial load ratio and beam reinforcement ratio as variables (eqs. 3.14 and 3.15). The first cracking of the joint was considered to be independent of both axial load and beam reinforcement ratio.

According to Genesio (2012), with increasing axial load on the column, the difference between critical principal tensile stress corresponding to 1st cracking and ultimate strength reduces. He suggested values for a critical axial load beyond which the critical principal tensile stress value for the 1st cracking as well as ultimate strength are essentially equal. In other words, after a certain critical axial load level, the cracking of the joint corresponds to its ultimate strength also. This essentially meant (also see eq. 3.15) that the joint has highest strength at no axial load and the joint strength gradually reduces with increasing axial load. For joints with beam bars bent in, Genesio (2012) suggested the critical axial load beyond which the ultimate strength and first cracking of the joint coincide as 20% of axial load carrying capacity. However, this is in contrast to commonly accepted statement that testing of joint sub-assemblies without axial load on the column is on conservative side.

Though, there is no clear consensus on the influence of column axial load on joint strength (Park and Mosalam, 2009), it is generally agreed that low levels of axial loads lead to increased joint shear strength. Furthermore, the rise in shear strength of concrete under compression is vastly studied and is also incorporated in almost every recognized design standard. However, in the opinion of the author of this thesis, this increase in shear strength applies only to the horizontal joint shear strength. The axial load need not be considered separately by increasing critical principal tensile stress value, since the influence of axial load on joint strength is implicitly considered through equation (4.21). This is the major advantage of following the limiting principal tensile stress criterion instead of limiting horizontal joint shear stress (Priestley, 1997).

Further, Genesio (2012) suggested that with increasing beam bar reinforcement ratio, the ultimate principal tensile strength increases. However, this increase is also valid only upto the critical axial load. The argument given for consideration of beam reinforcement ratio was that the lateral area of the reinforcement is directly proportional to the force transmitted via the bond of the reinforcement with the concrete (Genesio, 2012). This effect is not considered in the formulations used in this work. It is true that a better bond performance of beam reinforcement can lead to a better performance by the joint panel itself (Park and Paulay, 1975). However, author of this thesis opines that to consider this effect, total surface area instead of cross-sectional area of beam reinforcement, which is directly related to bond performance, should serve as a better parameter to consider beam reinforcement while

evaluating joint strength. However, author believes that the best way to consider this aspect should be by explicitly modelling the bond characteristics, instead of altering the joint strength itself. This aspect is currently not considered in this thesis.

A comparison of joint strength values for joints with beam bars bent in used in this work and those proposed by Genesio (2012), as a function of joint aspect ratio, is given in Figure 4.21. Aspect ratio range is considered from 0.75 to 2.50. As the expressions by Genesio (2012) also depend on the beam longitudinal reinforcement ratio, for comparison, 1% beam longitudinal reinforcement ratio is considered. Further, two values of axial loads are considered. For joints with beam bars bent in, Genesio (2012) suggested the critical axial load ratio as 20%. For comparison, in Figure 4.21, axial loads equal to 0% and 20% are considered, which form the extremities of formulations by Genesio (2012).

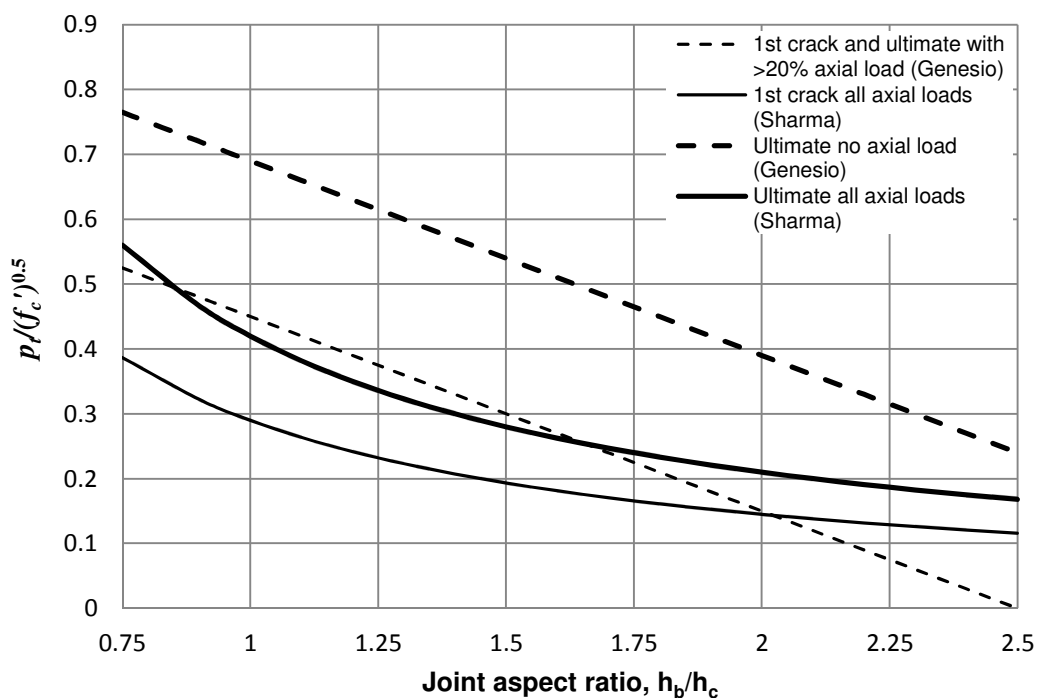


Figure 4.21 Comparison of critical principal tensile stress values recommended in this work with those by Genesio (2012) for joints with beam bars bent in

Based on equations (3.14) and (3.15), a linear variation with aspect ratio of the joints is suggested by Genesio (2012). As discussed earlier, the highest strength for the joint is given for the case of no axial load on the column, while for axial load of more than or equal to 20% of the load carrying capacity of the column, the first cracking and ultimate strength of the joints are given as equal. It is very interesting to note that in the formulation by Genesio (2012), for the case of a joint having aspect ratio equal to 2.50 (in case of beam bars bent in), the joint strength becomes zero, which means that a joint with aspect ratio of 2.50 or more is not feasible, which is not realistic. In the formulations used in this study, an asymptotically reducing strength of the joint is considered, which seems more realistic and it matches well

with experimentally reported values (Wong and Kuang, 2008; Park and Mosalam, 2009). This essentially means that the formulations recommended by Genesio (2012) are applicable only for the range of aspect ratios considered in his work, i.e. between 1.0 and 2.0. It can be observed that within this range of joint aspect ratio, the values of ultimate strength used in this work match closely with the values suggested by Genesio (2012) for joints with more than the critical axial load.

As discussed above, the author believes that the influence of axial load is automatically considered by using principal tensile stress criteria following the formulations given in section 4.3.3.2. Therefore reducing/increasing the critical principal tensile stress values as a function of axial load is not required. As will be shown in chapter 12, the values used in this work are able to nicely simulate the experimentally obtained behaviour of joints with various aspect ratios, various axial loads as well as a large range of beam reinforcement. Moreover, the formulations used in this work are able to capture the behaviour of eccentric joints as well, which is shown by means of simulation of a structural level experiment.

5. PIVOT HYSTERESIS MODEL PARAMETERS FOR MEMBERS AND JOINTS

Seismic loads are inherently dynamic and reversing (cyclic) in nature. Due to the dynamic nature, the inertia and damping of the system plays a very important role, while due to cyclic nature, hysteresis of the system comes into play. To simplify the problem, both at experimental and analytical front, monotonic tests/analysis as well as cyclic tests/analysis are performed. The influence of dynamic loads is then indirectly considered. Cyclic tests/analyses are more acceptable as they give information on the load and deformation capacity as well as the hysteretic response of the structures. However, dynamic tests (such as shake table tests) as well as dynamic analysis (nonlinear time history analysis) are known to provide the most accurate representation of seismic response of structures.

Today the performance based analysis of RC structures revolves mainly around the nonlinear static procedures (such as pushover). This is due to the fact that the nonlinear dynamic analysis is considered to be complex and time consuming for real life problems. Nevertheless, the importance of performing complete nonlinear dynamic analysis to have a realistic prediction of seismic response of structures cannot be denied. Especially, given the fact that current nonlinear static procedures still have certain deficiencies, it is essential to have models to perform realistic nonlinear dynamic analysis. The information thus obtained is complete and can be used to improve the performance analysis procedures.

The most popular form of dynamic analysis is the direct-integration time history analysis, which involves in numerically solving the equation of motion for the structure

$$[M]\{\ddot{x}(t)\}+[C]\{\dot{x}(t)\}+[K]\{x(t)\}=\{F(t)\} \quad (5.1)$$

Where,

$[M]$ is the mass matrix of the structure

$[C]$ is the damping matrix of the structure

$[K]$ is the stiffness matrix of the structure

$\{\ddot{x}(t)\}$ is the acceleration vector as a function of time, t

$\{\dot{x}(t)\}$ is the velocity vector as a function of time, t

$\{x(t)\}$ is the displacement vector as a function of time, t

$\{F(t)\}$ is the force vector as a function of time, t

The mass matrix and the elastic damping as well as elastic stiffness matrix can be evaluated from the structural dimensions and material properties. To consider the inelastic response of the structures in such an analysis, it is essential to define the stiffness variation as and when

the structure goes in the inelastic range. Due to cyclic nature of the problem, this must also be dependent on the history of the loading. To define the inelastic response of RC structural members under reversing loading, hysteretic rules are defined.

Over the years, various researchers have proposed various models to predict the hysteretic behavior of concrete and reinforced concrete structural elements. In the past, elasto-plastic hysteretic rules that idealize the hysteretic loops in bilinear format were frequently used. Such an idealization, though reasonable for steel members, were found to be more often than not, an over-simplification for reinforced concrete structures. Some other models give more consideration to effects like stiffness degradation, pinching due to opening and closing of cracks, bond slip etc. but they become computationally more demanding.

5.1 Pivot Hysteresis Model by Dowell et al (1998)

In 1998, Dowell et al (1998) proposed a so-called Pivot Hysteresis model for nonlinear dynamic analysis of reinforced concrete circular bridge columns. The model was shown to accurately capture the hysteretic behavior of reinforced concrete circular columns following a simple set of hysteretic rules. The model is based on the observations made on several experimental data on reinforced concrete circular columns. These observations show (Figure 5.1) that the unloading, back to zero force from any displacement level is generally guided towards a single point in the force-displacement plane, on the idealized stiffness line (Dowell et al, 1998).

Further, it was observed that all force-displacement paths tend to cross the elastic loading line at approximately the same point. The first point was named as “primary pivot point” and the second point was named as “pinching pivot point” (Figure 5.1). Thus, the model basically needs to define only two parameters, namely, α parameter that defines the so-called primary pivot point and controls the unloading stiffness of the member and β parameter that defines the pinching pivot point and controls the pinching behavior of the member.

5.1.1 Assumptions of pivot hysteresis model (Dowell et al, 1998)

The pivot hysteresis model utilizes the following two observations made from experimental hysteretic results of reinforced concrete members (Dowell et al, 1998):

- (1) Unloading stiffness decreases as displacement ductility increases, and
- (2) Following an inelastic excursion in one direction, upon load reversal, the force-displacement path crosses the idealized initial stiffness line prior to reaching the idealized yield force (unlike elasto-plastic response).

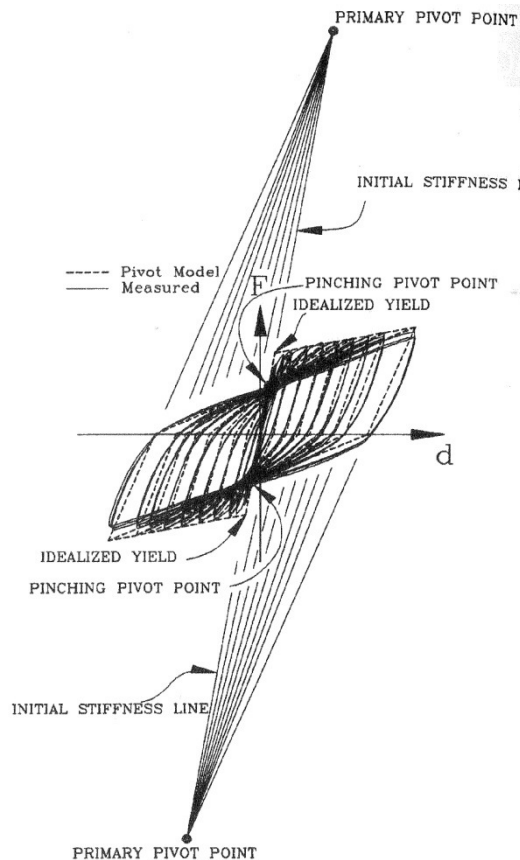


Figure 5.1 Hysteretic characteristics of a typical RC circular column and the idealisation (Dowell et al, 1998)

Further closer look in the experimental hysteretic results suggest the following two basic assumptions on which the pivot hysteretic model is based (Dowell et al, 1998):

- (1) Unloading, back to zero force from any displacement level, is generally guided toward a single point called primary pivot point (Figure 5.1). Similar approach was used by Kunnath et al (1990).
- (2) Force-displacement paths tend to cross the elastic loading line at approximately the same point, called as pinching pivot point (Figure 5.1).

5.1.2 Hysteretic Rules

The pivot model is governed by a set of rules that depend on the properties of the member and loading history. The two basic parameters that define the pivot hysteretic model are ' α ' parameter and ' β ' parameter (Figure 5.2) to control unloading and pinching respectively. Once, the monotonic envelopes of the load-displacement curves are obtained, the hysteretic rules can be assigned if these parameters, ' α ' and ' β ' are assigned. To account for unsymmetry in the section, the monotonic envelopes as well as ' α ' and ' β ' parameters need to

be assigned for the two loading directions. Figure 5.3 (Dowell et al, 1998) explains this concept.

Parameters, ' α_1 ' and ' β_1 ' control the response in one loading direction and the parameters ' α_2 ' and ' β_2 ' control the response in the other loading direction. The primary pivot points P_1 through P_4 in Figure 5.3, control the amount of softening expected with increasing displacement, and the pinching pivot points PP_2 and PP_4 fix the degree of pinching following a load reversal. Once, the yield deformation is exceeded in either direction, a subsequent strength envelope is developed. The modified strength envelope, acting as upper bound for future cyclic loading, is defined by lines joining point PP_4 to s_1 and point PP_2 to s_2 (Figure 5.3). The points s_1 and s_2 move along the strength envelope and are defined by the previous maximum displacements.

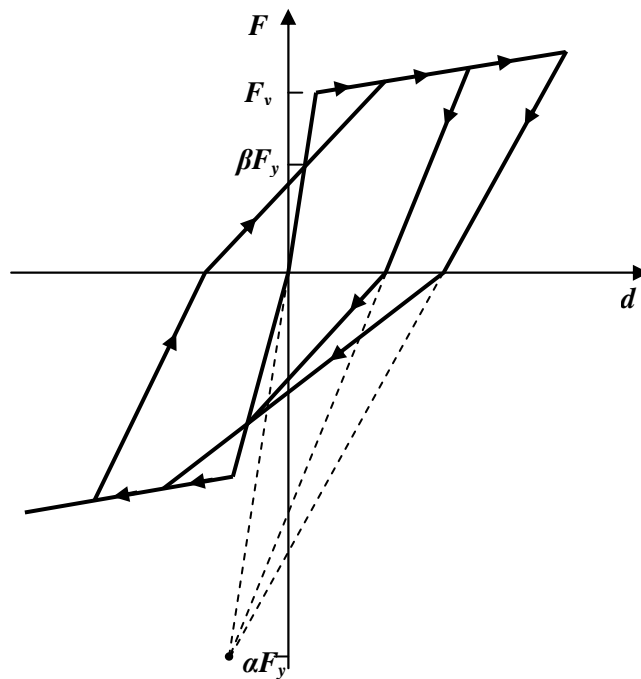


Figure 5.2 Basic parameters for pivot hysteretic model

5.1.3 Parameters controlling hysteretic response

Dowell et al (1998) provided the contours for ' α ' and ' β ' as a function of axial load ratio and longitudinal reinforcement ratio. Figure 5.4 shows the contours as reproduced from the reference (Dowell et al 1998). The contours were developed using the fibre element analysis of various circular RC columns and were validated with the experimental results. Since, the model was originally developed for circular bridge columns, the axial load ratio was considered only up to 20% of the axial load capacity of the column (Figure 5.4), appropriate for bridge columns. Both ' α ' and ' β ' were considered to be varying only with respect to longitudinal reinforcement and axial load ratio, neglecting the transverse reinforcement ratio.

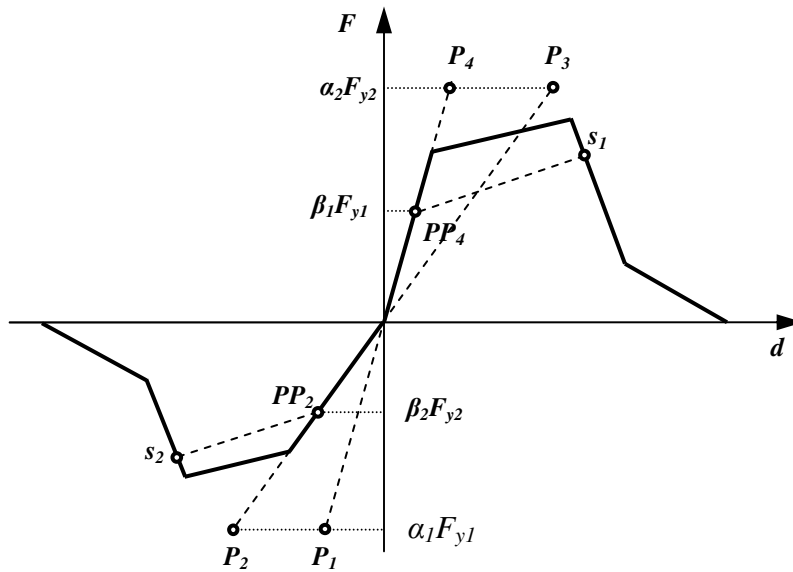


Figure 5.3 Pivot point designations (Dowell et al, 1998)

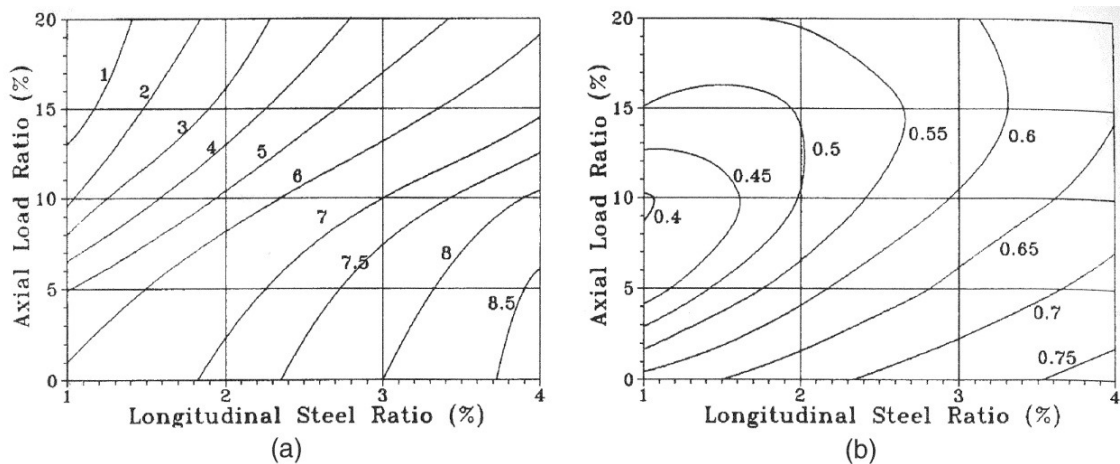


Figure 5.4 Contours for (a) α parameter and (b) β parameter for circular RC columns as suggested by Dowell et al (1998)

5.1.4 Need for new parameters to control hysteretic response of non-seismically detailed frame structures

In contrast to the bridge columns, the beams and columns of RC frame structures are generally rectangular in shape. Also, in case of frame structures, the axial load level on columns can be much higher than 20% of the axial capacity. Due to these two major differences, the parameters proposed by Dowell et al (1998) for circular columns of bridges cannot be applied for beams and columns of the frame structures. Also, in order to realistically capture the nonlinear cyclic/dynamic behaviour of non-seismically designed structures, the parameters are required to capture the hysteretic behaviour of beam-column joints. Furthermore, in case of non-seismically detailed RC structures, the transverse

reinforcement in the columns may be quite sparse while the same in the beams may be dense. It is known (Park and Paulay, 1975) that the pinching behaviour of the members is significantly influenced by the transverse reinforcement. In the parameters suggested by Dowell et al (1998) as seen in Figure 5.4 above, both primary as well as pinching pivot points were governed by the axial load ratio and longitudinal reinforcement only, giving no credit to the transverse reinforcement.

Due to the above reasons, it was required to develop and propose the parameters that can extend the applicability of the pivot model to capture the hysteretic response of:

- (a) RC members with rectangular sections subjected to a whole range of axial loads and giving due credit to transverse reinforcement ratio; and
- (b) Beam-column joints of non-seismically designed structures.

5.1.5 Methodology to develop parameters for frame structures

To capture the hysteretic response of non-seismically detailed frame structures, it is required to develop the parameters that control the response of the members (beams and columns) as well as of the beam-column joints. In this work, the parameters for rectangular RC beams, columns and non-seismically detailed beam-column joints are suggested that can be used with the original pivot hysteresis model, which was proposed for circular columns (Dowell et al, 1998). To derive the parameters that control the hysteretic response, the following approach was followed.

1. First, the database of results of experiments on columns and beam-column joints subjected to cyclic loads was collected. The database was made with tests on columns of varying cross-sections, longitudinal reinforcement ratio, transverse reinforcement ratio, axial load ratio and loading history.
2. The experimentally reported cyclic hysteretic loops were idealized as shown in Figure 5.5 and from these results, the parameters, α and β were evaluated.
3. The parameters thus obtained were plotted against the factors considered responsible for the change in these parameters e.g. axial load ratio (ALR), longitudinal reinforcement %, volumetric shear reinforcement % etc.
4. A regression analysis using least sum of the square of residues was performed for curve fitting and equations for α and β were obtained as a function of these factors. For columns, ALR from 0 to 100% of column capacity was considered and the effect of transverse reinforcement on pinching behaviour was taken into consideration.
5. Validation of the parameters calculated by the proposed equations was performed against the experimental results.

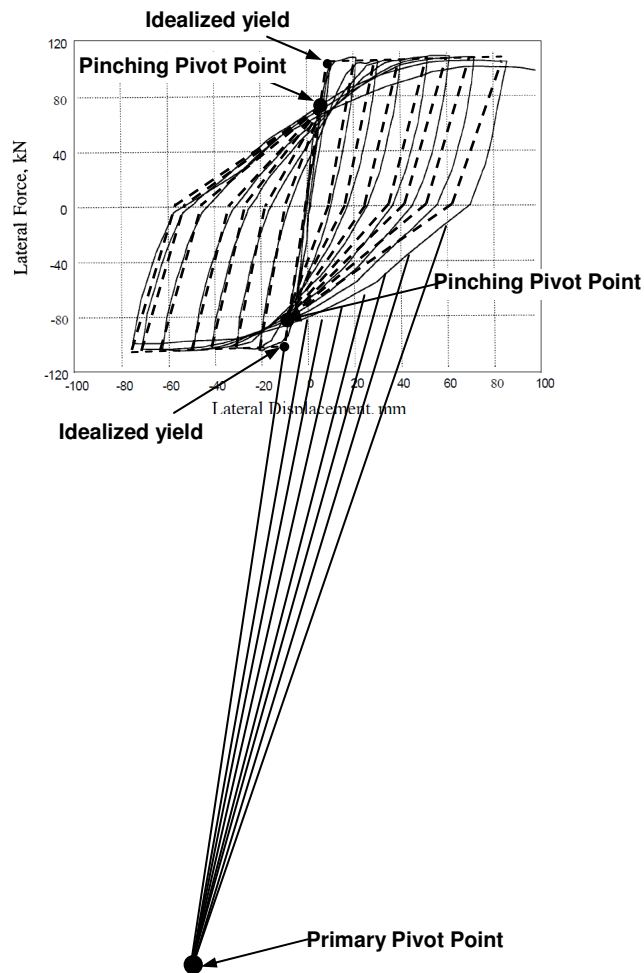


Figure 5.5 Typical experimental and idealized hysteretic behavior of a rectangular RC column tested by Ohno and Nishioka (1984)

5.2 Determination of parameters for rectangular sections beams/columns

Considering the simplicity and capabilities of the pivot hysteretic model to predict the hysteretic response of RC circular columns, an attempt is made in this work to suggest the parameters based on experimental evidence for members with rectangular cross-sections. The basic assumptions and rules of the original model were retained. However, the ' α ' and ' β ' parameters were defined in somewhat different way. The first step towards the definition of the ' α ' and ' β ' is to determine the key factors influencing these parameters. Dowell et al (1998) considered these factors as longitudinal reinforcement ratio and axial load ratio for both ' α ' and ' β '. These two factors take into account the strength of concrete, dimensions of the section, amount of longitudinal reinforcement and amount of axial load applied on the member.

In addition to the above-mentioned factors, in this work, amount of transverse reinforcement in the form of volumetric shear reinforcement was also considered. This accounts for the size

and spacing of the transverse reinforcement. This was done due to the fact that transverse reinforcement is known to significantly influence the pinching behaviour of the RC members.

A database of around 100 simulated seismic tests on rectangular RC columns was collected. The hysteretic loops were idealized as shown in Figure 5.5 and data of α and β parameters was plotted individually against axial load ratio, longitudinal reinforcement ratio and volumetric reinforcement ratio. It was found that since the database consisted of various tests performed by different researchers, in each test series all three parameters were significantly varied. Therefore, a clear pattern of variation of α or β parameter was not obtained.

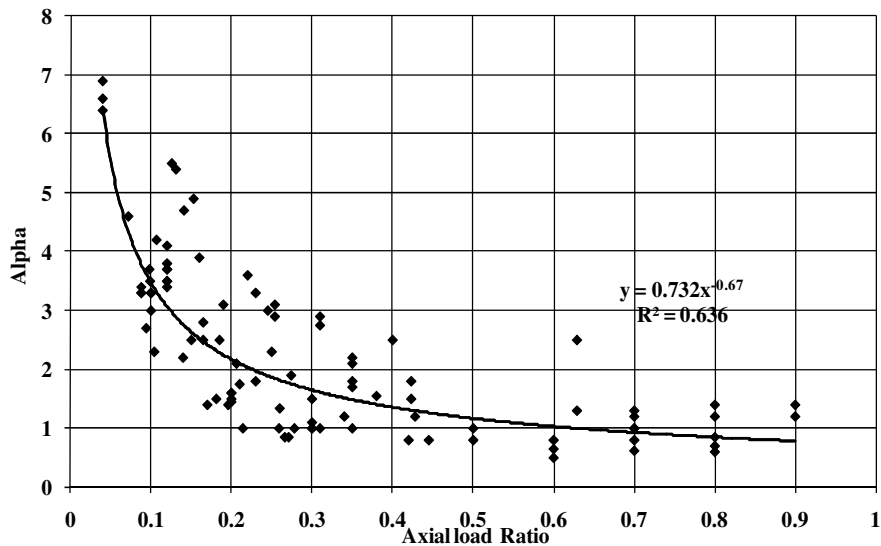


Figure 5.6 Variation of ‘ α ’ parameter with axial load ratio for rectangular columns

Figure 5.6 shows the variation of ‘ α ’ parameter with the axial load ratio. It should be noted that in the tests, in addition to axial load ratio, longitudinal reinforcement ratio and volumetric shear reinforcement ratio were also varied, but here the variation is shown only with respect to axial load ratio neglecting the other factors. A trend line is also fitted to the database. It can be seen that as the axial load ratio increases, the value of ‘ α ’ parameter seems to decrease. However, the regression coefficient is not very good.

Similarly, variation of ‘ α ’ parameter with the % longitudinal reinforcement is plotted in Figure 5.7 and a trend line is fitted to the data points. Although the trend line shows a rising trend for ‘ α ’ with respect to the % longitudinal reinforcement, the scatter is quite large and the regression coefficient is too small. Also shown in Figure 5.8 is the variation of ‘ α ’ parameter with the % volumetric shear reinforcement. The scatter is found to be too high to reach any conclusion.

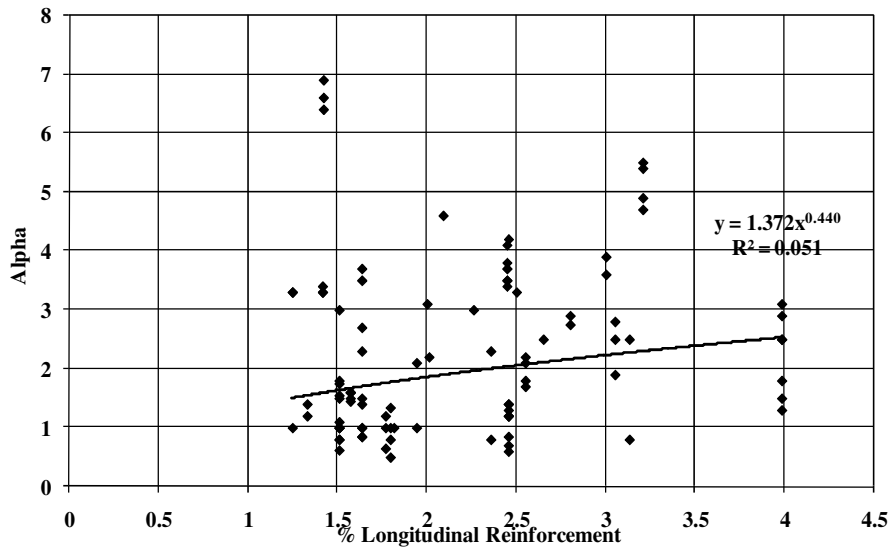


Figure 5.7 Variation of ‘ α ’ parameter with % longitudinal reinforcement for rectangular columns

As seen from Figures 5.6, 5.7 and 5.8, a clear variation of ‘ α ’ is observed only with the axial load ratio and a conclusion cannot be reached on variation of ‘ α ’ with respect to % longitudinal and shear reinforcement as the scatter is very high and the coefficient of regression is very poor. This is due to the fact that in the tests both the axial load ratio and % longitudinal reinforcement were varied.

Similar exercise was performed for ‘ β ’ parameter also. Figures 5.9, 5.10 and 5.11 show the variation of ‘ β ’ parameter with respect to axial load ratio, % longitudinal reinforcement and % volumetric shear reinforcement respectively. As can be seen, again no clear trend can be observed from these figures to define the ‘ β ’ parameter.

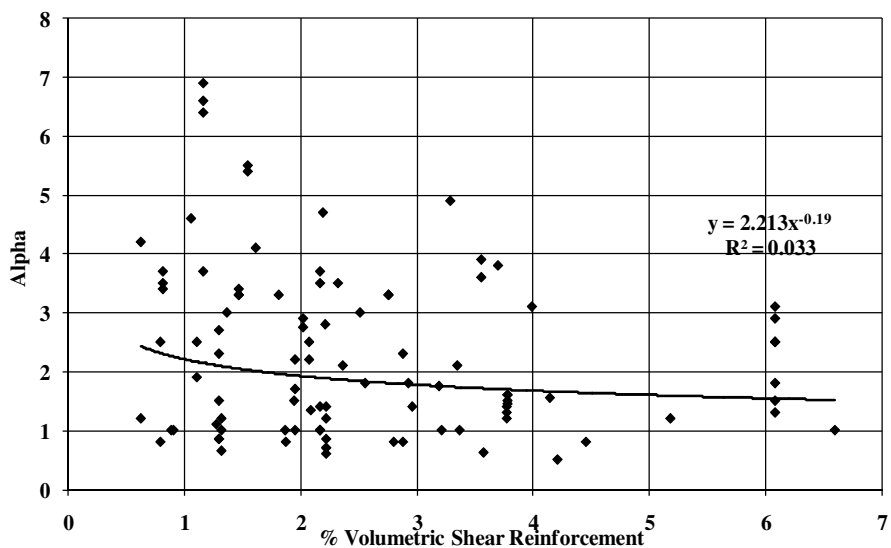


Figure 5.8 Variation of ‘ α ’ parameter with % volumetric shear reinforcement for rectangular columns

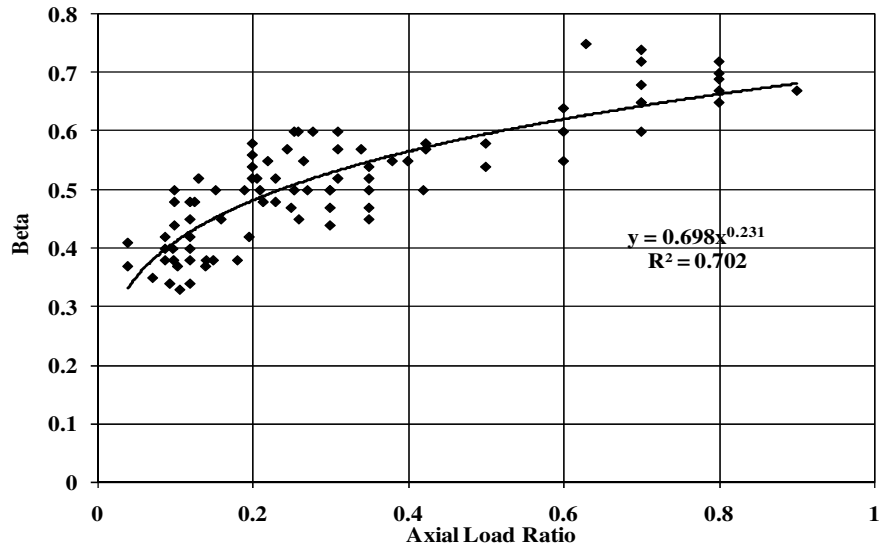


Figure 5.9 Variation of ‘ β ’ parameter with axial load ratio for rectangular columns

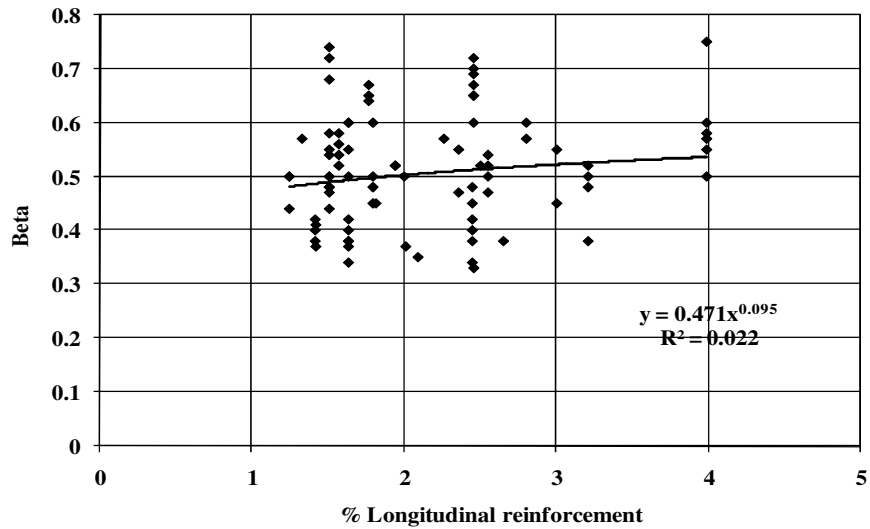


Figure 5.10 Variation of ‘ β ’ parameter with % longitudinal reinforcement for rectangular columns

As seen above, a clear pattern of variation of α or β parameter was not obtained. To solve this problem, the following postulates were made:

1. Higher value of α , signifies more energy dissipation. Therefore, as longitudinal steel ratio increases, α should increase. This is also observed in the contours for α suggested by Dowell et al (1998) as shown in Figure 5.4.
2. Axial load increases the brittleness of a member; therefore, as axial load ratio increases the value of ‘ α ’ should decrease. This also is observed in the contours for α suggested by Dowell et al (1998) as shown in Figure 5.4.

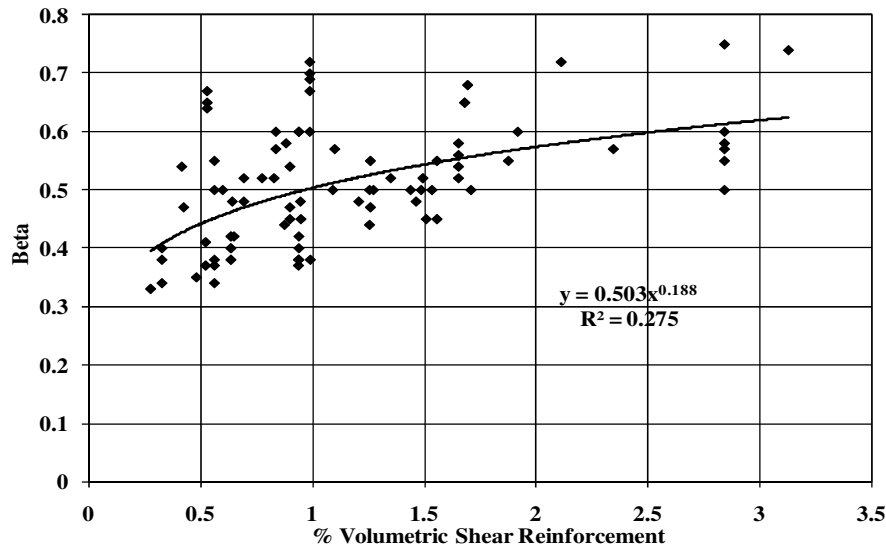


Figure 5.11 Variation of ‘ β ’ parameter with % volumetric shear reinforcement for rectangular columns

3. In general, as volumetric shear reinforcement ratio increases the value of ‘ β ’ should increase due to better confinement (Gill et al, 1979; Paulay and Priestley, 1992). This cannot be verified with the charts given in Figure 5.4 by Dowell et al (1998), since the volumetric shear reinforcement ratio is neglected in the same. However, tests on columns by Kishimoto et al (2004) confirm this postulate.
4. Since higher axial load also means better confinement and therefore less pinching, in general as the axial load ratio increases, the value of ‘ β ’ should also increase, since the confinement by stirrups is essentially passive (Park and Paulay, 1975; Paulay and Priestley, 1992).

Based on above postulates and curve fitting of the data, using regression analysis and the method of minimum sum of the square of residues, two new parameters namely k_α and k_β , which could consider the effect of longitudinal and transverse reinforcement as well as the axial load on the columns, were proposed. The parameters are defined as

$$k_\alpha = p_t / ALR \quad (5.2)$$

$$k_\beta = (ALR)^{0.25} \times (p_{sh})^{0.2} \quad (5.3)$$

where,

p_t = percentage longitudinal reinforcement,

p_{sh} = percentage volumetric shear reinforcement

ALR = Axial load ratio = applied axial load on the column / ultimate axial load capacity of the column

Since ' α ' is expected to increase with % longitudinal reinforcement and decrease with axial load ratio, now, it can be expected that ' α ' should increase monotonically with the factor ' k_α '. Figure 5.12 shows a plot of ' α ' v/s the factor ' k_α ' for the tests and the plot clearly display the expected trend. It can be seen that the parameter ' α ' almost linearly increase with the factor ' k_α ' and a linear trend line can be fitted to the data points. The equation relating ' α ' and ' k_α ' is given as

$$\alpha = 0.170 k_\alpha + 0.415 \quad (5.4)$$

Similarly, linear trend line was fitted to the data points of ' β ' v/s the factor ' k_β '. The equation relating β and k_β is given as

$$\beta = 0.485 k_\beta + 0.115 \quad (5.5)$$

Based on expressions given by equations (5.2) through (5.5), ' α ' and ' β ' parameters can be evaluated. The expressions cover the whole range of axial load ratios and also give due consideration to transverse reinforcement. The validation of these expressions against experimental results will be addressed in chapter 13.

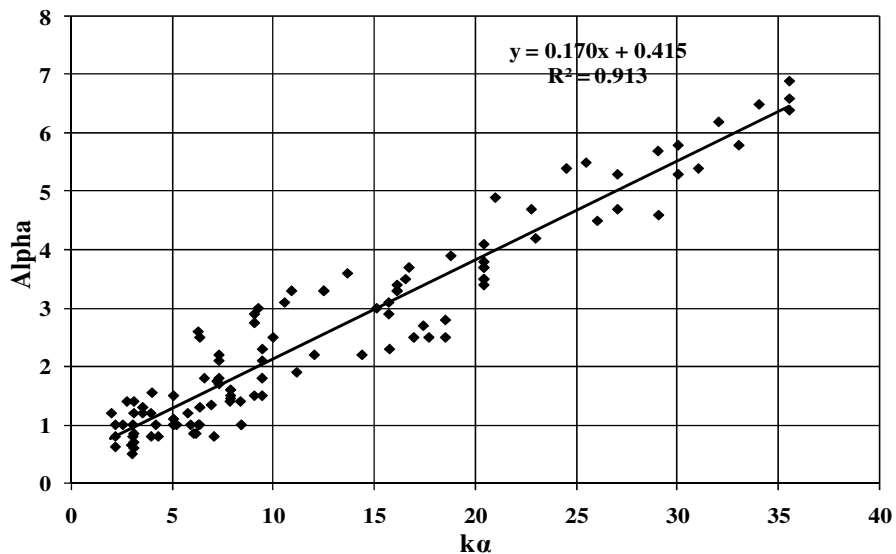


Figure 5.12 Variation of ' α ' parameter with factor ' k_α ' for rectangular columns

5.3 Determination of parameters for non-seismically detailed beam-column joints

In order to make this model suitable for the nonlinear cyclic/dynamic analysis of RC beam-column joints, it is required to define ' α ' and ' β ' parameters for the joint springs. The monotonic envelopes for the joint springs (one rotational and two shear) as described in chapter 4, are first generated following the principal tensile stress criteria. Once the spring

properties are generated, the ' α ' and ' β ' parameters assigned to the springs should control the hysteretic response of the joints.

In literature, many results are available from the tests conducted on the beam-column joint sub-assemblages. However, a joint sub-assemblage response is governed by the behaviour of beam, column and the joint core forming the sub-assembly. Therefore, the overall load-deformation curves for the joint sub-assembly cannot be used for the development of ' α ' and ' β ' parameters. In order to do so, test data on joint stress v/s shear deformation is essentially required. Unfortunately, earlier, due to unavailability of good instrumentation such data were not collected and till now only limited test data is available in literature (Clyde et al, 2000; Pantelides et al, 2002; Hwang et al, 2005; Hertanto, 2005; Genesio and Sharma, 2010) though the data base is increasing.

It has been shown that 3D Finite element modelling of beam-column joints using Microplane model for concrete and giving due consideration to re-bar slip provide good results for poorly detailed joints (Sharma et al, 2009). In order to make up for the unavailable test data, such analyses were performed using 3D FE program MASA developed at University of Stuttgart (IWB and Ožbolt, 2008). Microplane model for concrete with relaxed kinematic constraint (Ožbolt et al, 2001) was used as constitutive law for concrete and bond between rebar and concrete was modelled using the inbuilt 1D elements based on Eligehausen et al (1983) and Lettow (2006). The overview of the same is given in Appendix-C.

From the analysis, principal tensile stress v/s joint shear deformation data were obtained and the same was used to obtain the ' α ' and ' β ' parameters for joint hysteresis. It may be noted that the software MASA was utilized only to make up for gaps in test data, but the actual analysis to verify the parameters was performed with SAP2000 with the lumped plasticity approach. The analysis results for the joints performed with MASA can be obtained from Sharma et al (2008) and Genesio (2012). Since in this work, only poorly detailed joints are considered, joint core reinforcement is not a criterion for deciding on ' α ' and ' β ' parameters. However, the type of beam anchorage significantly affects the pinching behaviour of the joint and thus ' β ' parameter should depend on the beam bar anchorage. Otherwise, for joints with no joint reinforcement, axial load ratio is the only critical parameter that affects the values of ' α ' and ' β ' parameters. Based on available test and 3D FE analysis data collected and generated for poorly detailed joints, the relation between ' α ' parameter with the axial load ratio (ALR) for poorly detailed joints with beam bars bent in was obtained as

$$\alpha = 4.4 - 25.38*(ALR); \quad \text{for } 0 \leq ALR \leq 0.13, \text{ and} \quad (5.6)$$

$$\alpha = 1.0; \quad \text{for } ALR > 0.13 \quad (5.7)$$

Similarly, the relation between ' β ' parameter with the ALR was obtained as

$$\beta = 0.125 + 0.44*(ALR) \quad (5.8)$$

For joints with deformed bars terminating straight into the joint with 150mm embedment and for joints with plain reinforcing bars with end hooks, the alpha and beta parameters were considered as $2/3^{\text{rd}}$ of the values obtained for deformed bars. This was postulated based on the knowledge that straight terminating bars and plain round bars have a poorer bond behaviour compared to deformed bars bent in and therefore they result in more severe pinching and poorer hysteretic loops. This is consistent with the original pivot model (Dowell et al, 1998) and was also confirmed by the results of a few tests conducted on the exterior joints with plain round bars (Liu, 2006; Genesio and Sharma, 2010).

Using equations (5.6) through (5.8), the parameters controlling the hysteretic response of non-seismically detailed beam-column joints can be evaluated. The validation of these expressions against experimental results will be addressed in chapter 13.

6. ASSESSMENT MODEL FOR FULLY FASTENED HAUNCH RETROFIT SOLUTION

6.1 Background and motivation

Haunch retrofit solution (HRS) has been relatively recently investigated as a viable alternative for retrofitting of beam-column joints of reinforced concrete (RC) frame structures (Pampanin et al, 2006). The retrofit solution was proposed as an extension of the haunch retrofit solution developed for steel moment resisting frames. The solution consists of a haunch element, which primarily consists of a diagonal axial element in the form of a machined bar/plate connected to plates at both ends, connected to beam and column. The underlying principle of the HRS is to relocate the plastic hinge away from the vulnerable joint panel/core while enhancing the global response of non-seismically designed RC joint sub-assembly by altering the hierarchy of strength suitably.

In order to connect the haunch element, Pampanin et al. (2006) studied two types of connections between diagonal axial element and plates namely, hinged and welded. In one specimen, a yielding type fuse element was used as axial element. In order to connect the haunch element with beams and columns, two partially prestressed external rods along with two anchors directly fastened to both beam and column were used. Figure 6.1 shows the schematic of the HRS used by Pampanin *et al.* (2006).

It was reported (Pampanin *et al.*, 2006) that the retrofitted specimens displayed a substantially enhanced response when compared to the non-retrofitted specimens: damage to the joint was eliminated and a flexural plastic hinge was formed in the beam at the location of the beam–haunch connection. This resulted in an increase in the system lateral strength, a stable hysteretic behavior and enhanced energy dissipation capacity. Further, it was reported that the stiffness of the haunch element measured in the case of welded connection was very close to the expected value. Certain guidelines to design the retrofit solution, using external rods, for a beam-column joint sub-assembly were provided by Pampanin et al (2006).

The tests conducted by Pampanin et al. (2006) clearly displayed that the HRS can be very effective in improving the behavior of beam-column joints of non-conforming RC structures. However, one prohibitive requirement of the connection proposed by them was to use external partially prestressed rods to connect the haunch to the frame. Though, in laboratory tests, it could be easily achieved, to do the same in real structures would require drilling through holes in the slabs of the structure, which renders the solution prohibitive.

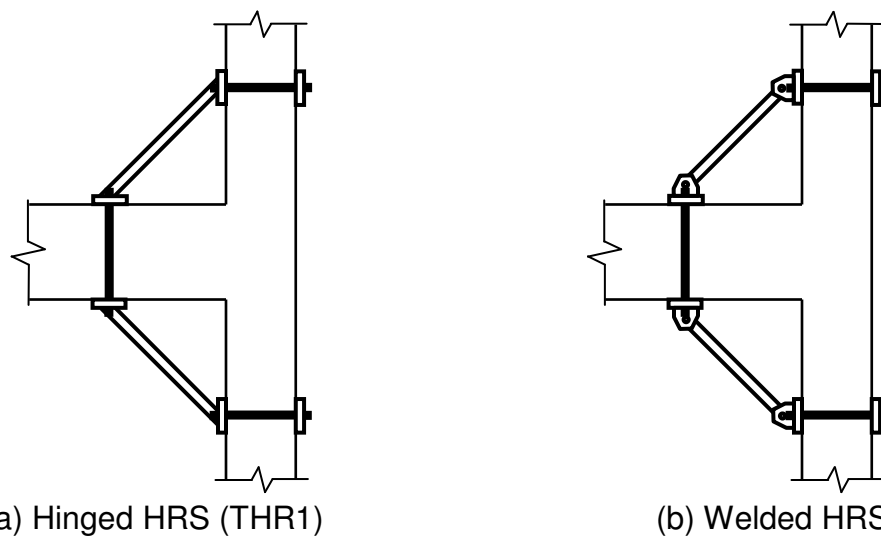


Figure 6.1 Schematic of haunch retrofit solutions tested and validated by Pampanin et al (2006)

To eliminate this limitation, Genesio (2012) investigated the performance of haunch elements connected to the frame members by using post-installed mechanical anchors. In order to investigate the feasibility of this “fully fastened HRS (FFHRS)”, experiments were first carried out in University of Canterbury (Genesio and Akgüzel, 2009) and later at BARC, Mumbai (Genesio and Sharma, 2010; Genesio et al, 2010; Sharma et al 2010). The major aims of these tests, which will be discussed in more detail in chapter 10, were to fully understand the behaviour of the FFHRS along with its strengths and limitations and to adapt it to the implementation of post-installed anchors. Genesio (2012) extended the design guidelines suggested by Pampanin et al (2006) for the fully fastened HRS using post-installed anchors.

However, in order to verify the performance of FFHRS, it is required to have an assessment model that, in addition to member, joint and haunch stiffness and deformability, can also give due consideration to non-linear anchor group behaviour. In the tests by Genesio and Sharma (2010b), it was found that the efficiency of the retrofit solution depends highly on the performance of the anchorage system. It was clearly shown that if the anchorage system performs well, then a high efficiency of the haunch retrofit solution can be expected. Therefore, considering perfect connection of haunch element with frame members, ignoring nonlinear anchor behaviour can be quite unconservative.

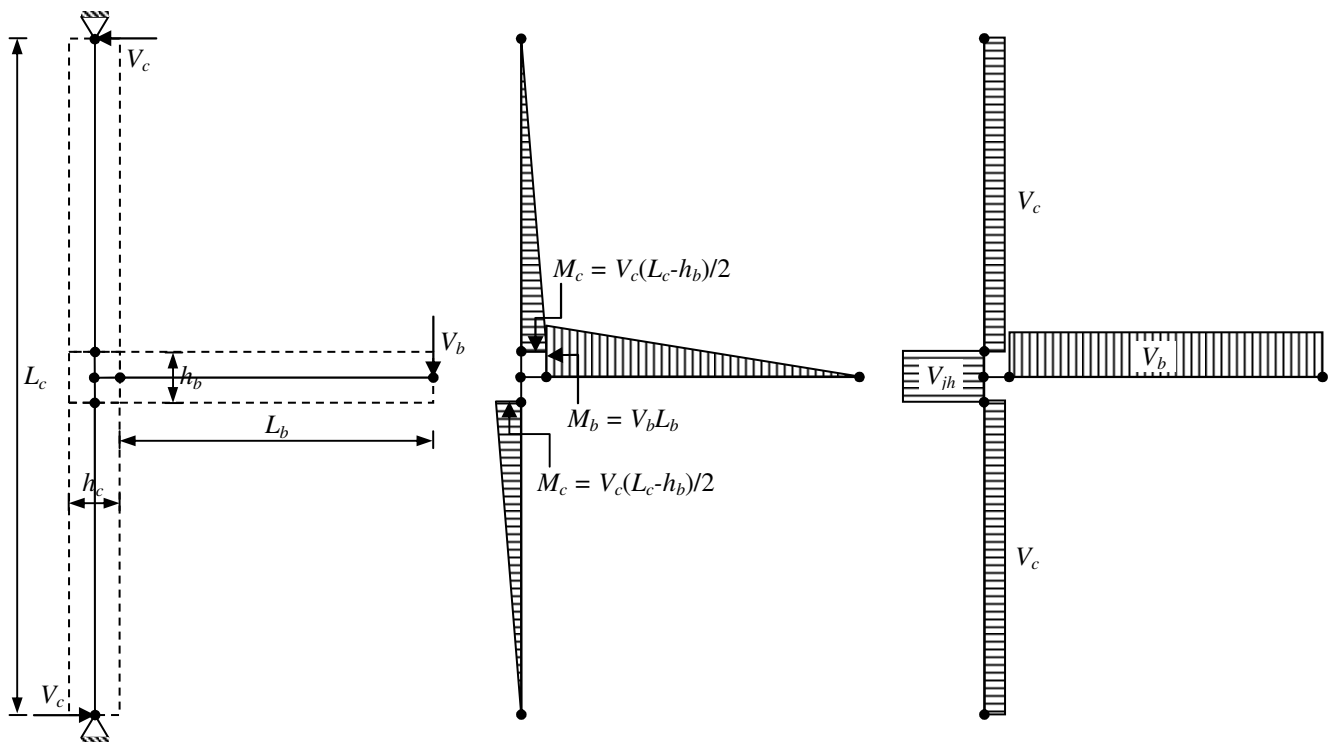
This work is aimed at developing an assessment model to evaluate the seismic performance of joints retrofitted with fully fastened haunch retrofit solution. This chapter presents the theoretical background and model to assess the seismic performance of the joints retrofitted with HRS connected using anchor fasteners.

6.2 Mechanics of joints retrofitted with HRS

To understand the behaviour of beam-column joints retrofitted with HRS, it is important to understand the effect of the same in redistributing the forces and moments in a joint. Let us consider an exterior beam-column joint subassembly formed by the assumed points of inflexion at mid height of columns and mid span of beams, as shown in Figure 6.2 (a). The dashed lines depict the physical dimensions of the members while the solid lines with rounded ends depict the frame element to model the members and their end nodes respectively. Let the joint be applied by a beam end load, V_b . The bending moment and shear force diagrams for the joint sub-assembly are as depicted in Figure 6.2 (b) and (c) respectively. As derived in chapter 2, due to the applied load, V_b , joint panel is subjected to a horizontal joint shear force given by

$$V_{jh} = \frac{M_b}{Z_b} - V_c = V_b \left(\frac{L_b}{Z_b} - \frac{L_b + 0.5h_c}{L_c} \right) \quad (6.1)$$

Where, Z_b is the lever arm of internal forces in the beam at column face. Other symbols are explained in Figure 6.2. This shear force is the major cause of failure of the joint panel.



(a) Joint sub-assembly (b) Bending Moment Diagram (c) Shear Force Diagram

Figure 6.2 Mechanics of conventional exterior joint

Now, let us consider the same joint sub-assembly, retrofitted with two diagonal haunch elements as shown in Figure 6.3 (a). The physical dimension of the joint is shown by dotted

line and the central solid line depicts the frame element to model the same. To take into account for the physical dimensions of beam and column, rigid link is used to connect the end nodes of haunch element to the beam and column. The bending moment and shear force diagrams for the joint sub-assembly are as depicted in Figure 6.3 (b) and (c) respectively. As seen in Figure 6.3 (b), under the applied beam end load, V_b , the maximum bending moment in beam occurs at the point of connectivity of haunch, M_{bh} , given by

$$M_{bh} = V_b (L_b - L_h) \tag{6.2}$$

Where, L_h is the horizontal projected length of the haunch element.

Beyond the point of connectivity of the haunch element, the bending moment in the beam gradually reduces. The rate of reduction on bending moment depends on the relative stiffness of the beam and the haunch element.

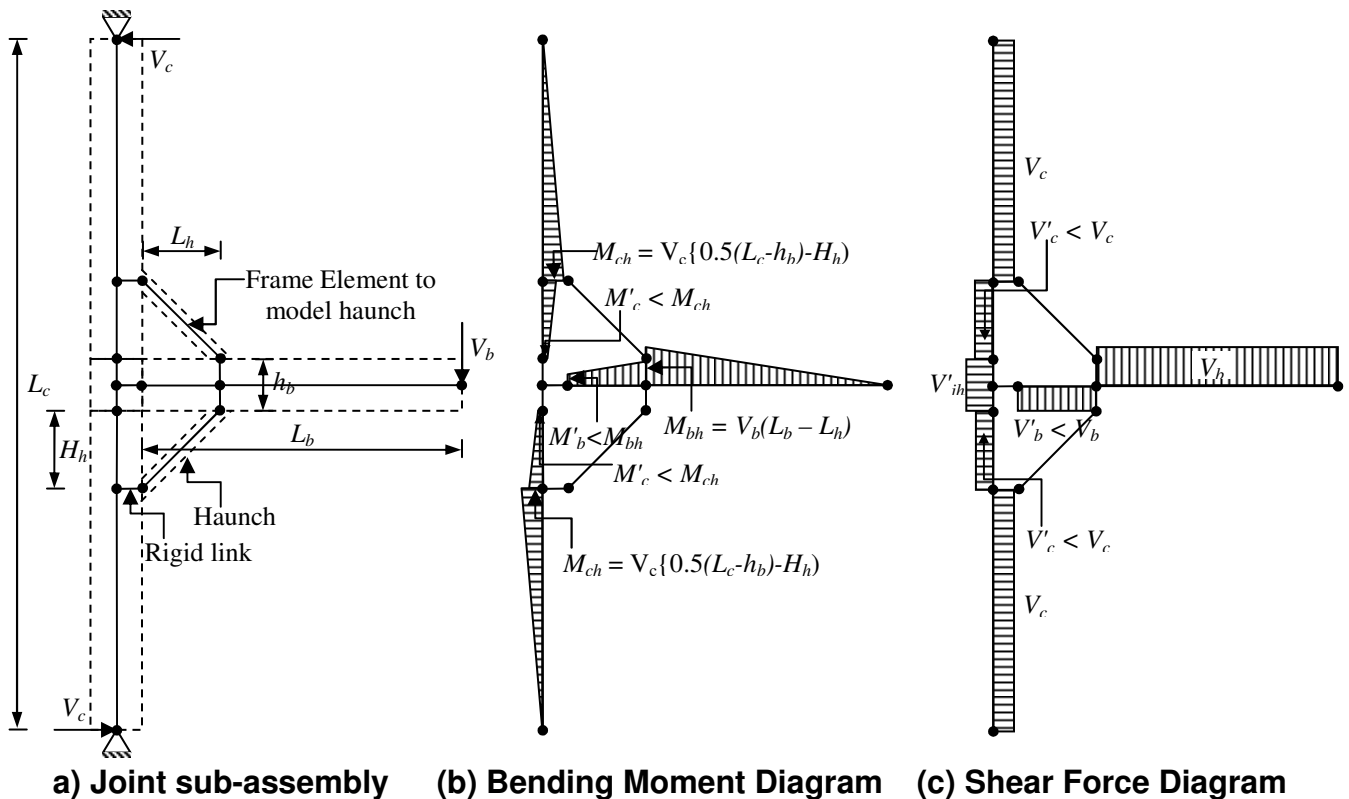


Figure 6.3 Mechanics of joint retrofitted with diagonal haunch elements

Thus, at the face of the column, the moment in the beam, M'_b is less than the moment, M_{bh} . Similarly, we have reduced bending moment in the column at the face of the beam, M'_c and the reduced shear forces in beam, V'_b and column, V'_c , beyond the haunch element. The reduced joint horizontal shear force for the haunch retrofitted joint, V'_{jh} , can now be obtained as

$$V_{jh} = \frac{M'_b}{Z'_b} - V'_c \quad (6.3)$$

Where, Z'_b is the lever arm of the internal forces in the beam at the face of the column.

Based on above discussed mechanics, it can be observed that the effect of haunch in reducing the joint horizontal shear force is essentially two-fold:

- (i) Modifying the critical section for flexure and thereby reducing the maximum bending moment in the beam for a given applied load (Effect of geometry).
- (ii) Further reducing the bending moment at the face of the column, due to redistribution of forces (Effect of stiffness).

Therefore, by designing the haunch element suitably, the horizontal joint shear stress can be significantly reduced compared to the as-built joint. However, it must be considered that at the point of connectivity of haunch with beam/column, the shear force suddenly rises. Therefore, this system must not be used for the case where the members are or may become shear critical due to the haunch element.

6.3 Assessment model for fully fastened haunch retrofit solution

6.3.1 Basic modelling philosophy

In order to evaluate the seismic performance of a joint retrofitted with FFHRS, an assessment model is required. The stiffness and deformability of the members (beam and column) and the joint panel can be duly accounted for by following the procedure explained in Appendix-A and chapter 4. To include the behaviour of the FFHRS in the joint model, the modelling of stiffness and deformations in the anchor group need to be incorporated over the complete linear-nonlinear range. As a good design approach, the haunch element itself shall be designed in such a way that it remains in the elastic range throughout loading history.

Figure 6.4 shows the proposed model for the seismic assessment of joints retrofitted with FFHRS. In Figure 6.4, for clarity, only flexural springs are shown in the members but the shear springs for the same can also be included if required. For beams and columns, we need to provide springs at all the critical locations as shown in Figure 6.4 (b). Additionally, springs are required to model the anchor group behaviour. To model that one possible way is to provide one spring to model each anchor behaviour individually, e.g. if the haunch element is connected to the frame member using six anchors as shown in Figure 6.4 (a), six springs can be used to model their individual behaviour. This way of modelling can better simulate the anchor slip behaviour. However, there are two problems in doing so: (i) the model becomes complicated, and (ii) in case of concrete cone failure, the contribution of individual capacity of the anchor becomes difficult to ascertain.

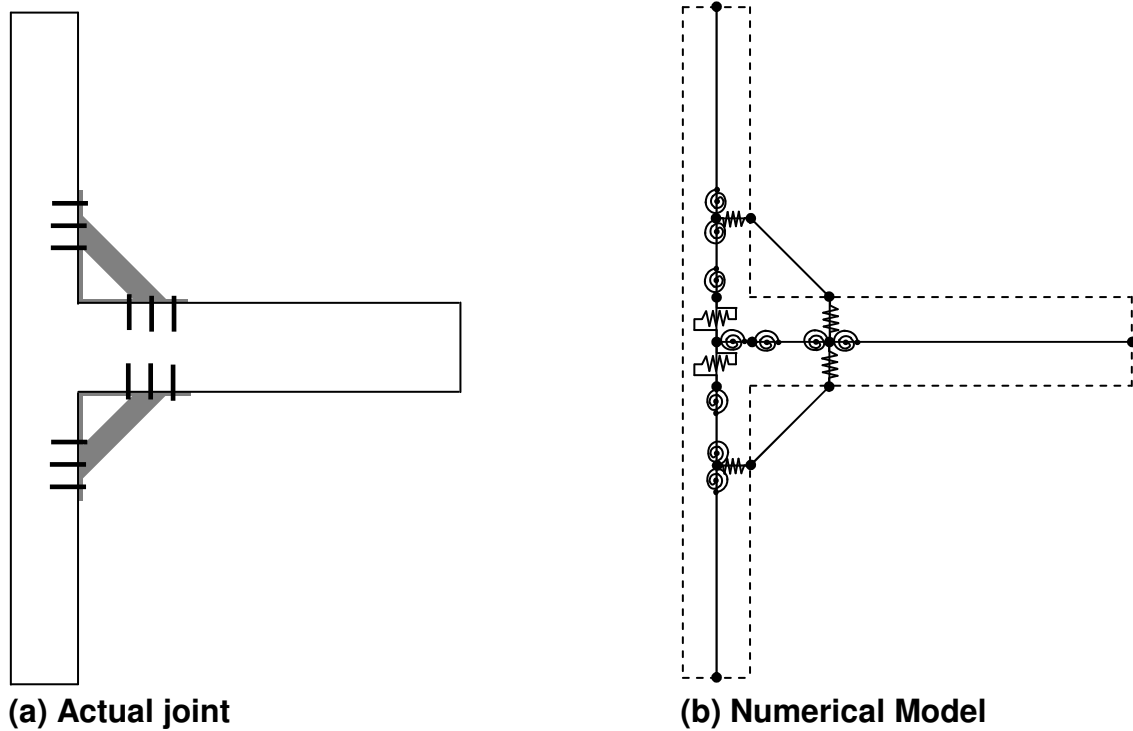


Figure 6.4 Joint details and idealized analytical model

Another possibility is to model the anchor group behaviour by a single spring as shown in Figure 6.4 (b). This simplifies the model and can also predict the concrete cone/bond slip behaviour of the group with sufficient accuracy.

6.3.2 Assumptions behind the model

During cyclic loads such as in case of earthquakes, an anchorage system is subjected to cyclic tension and cyclic shear loads. Additionally, if the anchor is intercepted by a crack, it may also be subjected to crack cycling (opening and closing of cracks). The assumptions made in development of the model for FFHRS along with their basis are given below:

Assumption 1: Only tension loads are critical for the anchorage system and the same can therefore be modelled using axial spring (Figure 6.4 (b)).

Basis for assumption: In case of a planar beam-column joint loaded in its own plane, the shear loads will not be critical unless the steel strength of anchor is insufficient. Also, in case of structures, due to the slab, shear capacity of the anchorage system would be high enough and the system will not be shear critical.

Assumption 2: The axial spring used to model the anchorage system is considered as stiff and linear elastic when loaded in compression.

Basis for assumption: The haunch element consists of steel plates welded together and the plate is connected using the anchors. In case of tension, only the anchors resist the load, but under compression, almost all of compression is transferred through bearing of base plate on

the member. Therefore, the spring modelling the anchorage system can be considered as stiff and in linear elastic range.

Assumption 3: The concrete breakout strength for anchor group can be calculated using Concrete Capacity (CC) Method (Fuchs et al, 1995).

Basis for assumption: The major possible failure modes for an anchor in tension are steel failure, concrete cone failure, pull-out failure and side face blow-out failure (Eligehausen et al, 2006; ACI 318, 2011). The steel failure can be evaluated by multiplying the effective steel area with the strength of anchor steel. For pullout failure, experimental results are required to estimate the strength. Concrete cone failure is generally considered as most critical failure mode for the anchors (Eligehausen and Sharma, 2011) and is also the most studied failure mode. It has been shown by Fuchs et al (1995) that the CC method can predict the failure load in case of concrete cone failure quite realistically taking into account the size effect (embedment depth) as presented in Figure 6.5 (Eligehausen et al, 2006).

Assumption 4: Unless special provisions are made to prevent cracks in the anchorage zone, cracked concrete shall be assumed.

Basis for assumption: Due to the low tensile strength, concrete members will invariably experience cracking either due to external loading or due to thermal constraints. There is a high probability that fasteners installed in non-cracked concrete will be intercepted by a crack when cracks form (Eligehausen et al, 2006) as depicted in Figure 6.6.

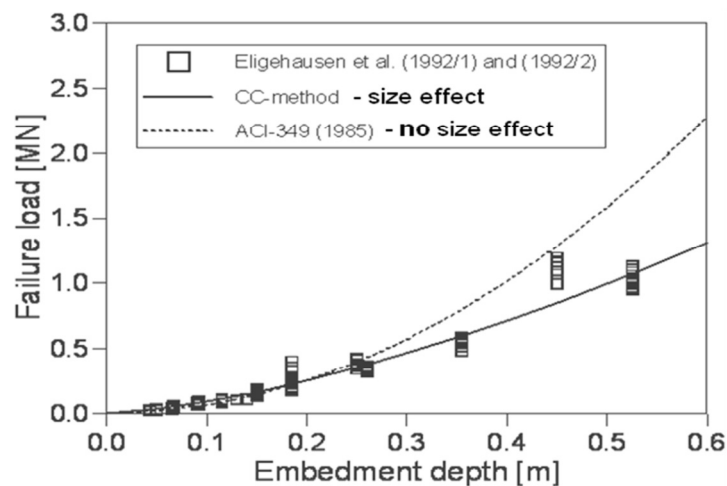


Figure 6.5 Effectiveness of CC method in predicting the breakout strength of concrete

This is mainly due to the fact that high tensile stresses are caused due to prestressing and loading of the anchor and the drill holes act as notches leading to stress concentration (Eligehausen et al, 2006). The effect of cracking on anchor concrete breakout capacity is two-fold. First, due to the presence of crack, for equilibrium, the distribution of hoop stresses change as shown in Figure 6.7. This affects all types of anchors. Second, there is a degradation of force-transfer mechanism due to opening of hole that affects especially bonded anchors and expansion anchors (Eligehausen et al, 2006).

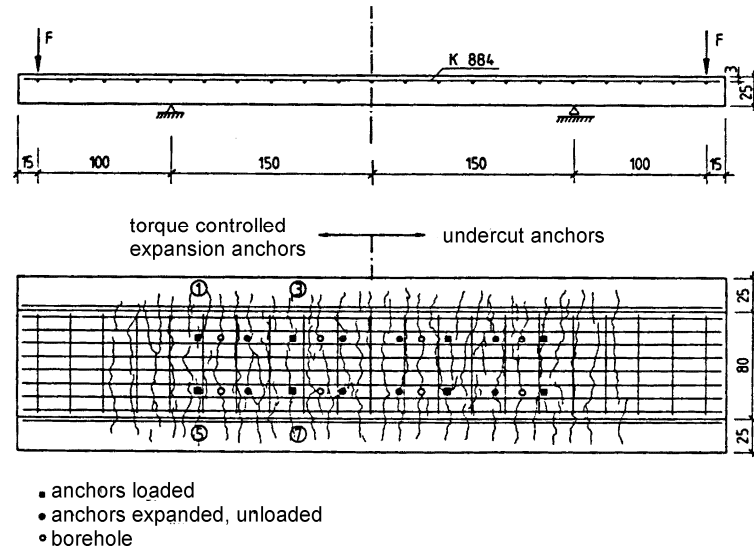


Figure 6.6 Crack patterns in flexurally loaded slab at service load and position of anchors (Eligehausen et al, 2006)

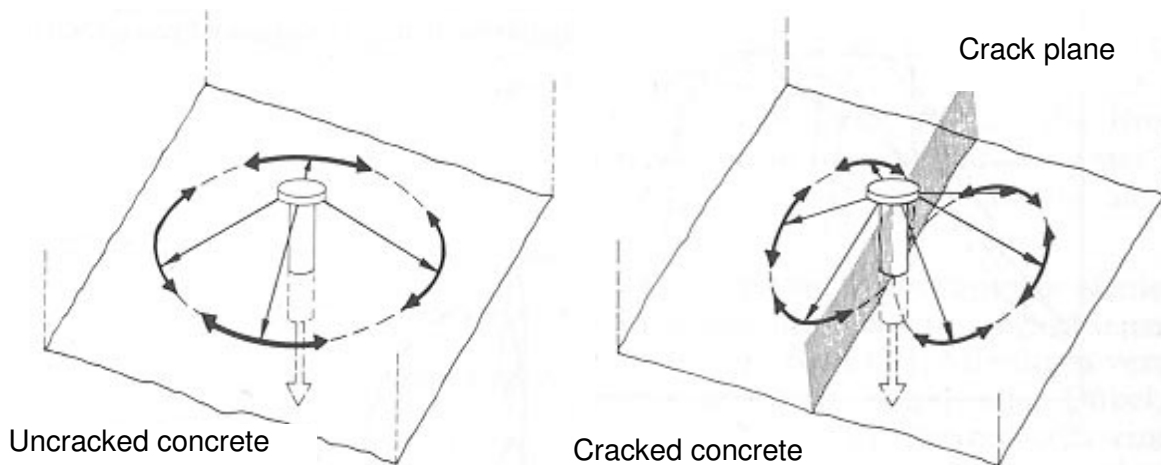


Figure 6.7 Hoop stresses around anchor in uncracked and cracked concrete (Eligehausen et al, 2006)

It has been shown by various tests (Eligehausen et al, 2006) that the anchor load-displacement behaviour is adversely affected by the crack and its width in which the anchor may be located. Figure 6.8 shows the influence of cracking on (a) Load-displacement behaviour and (b) peak load of sleeve type torque-controlled expansion anchors (Eligehausen et al, 2006). Since cracks have a significant negative influence on the anchor performance, the assumption that the anchor is situated in a crack is conservative.

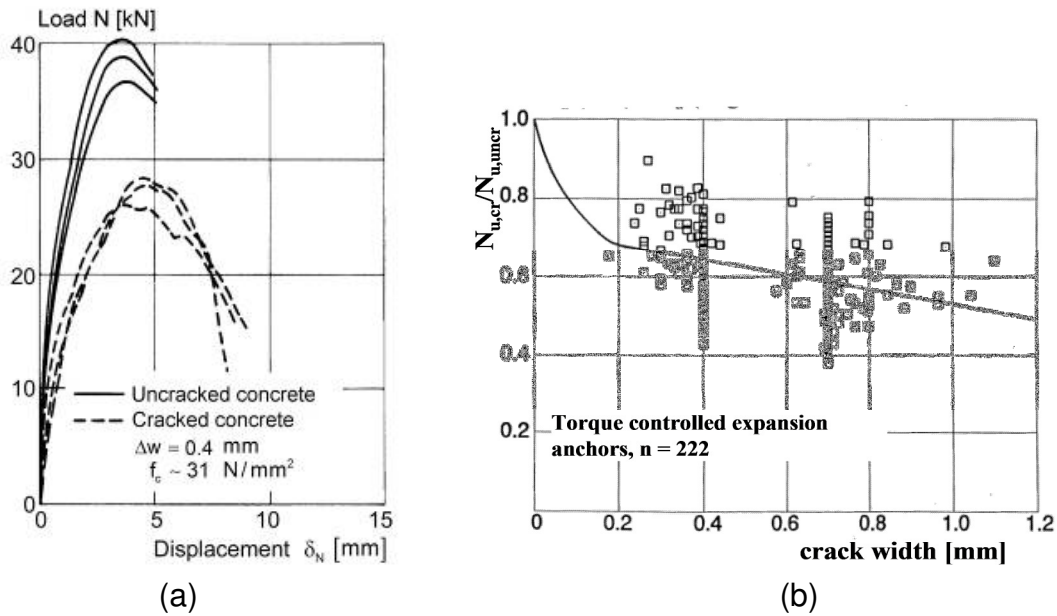


Figure 6.8 Effect of cracking on behaviour of torque-controlled expansion anchors (sleeve type) suitable for cracked concrete (Eligehausen et al, 2006)

Assumption 5: The model is applicable only for anchors suitable for cracked concrete

Basis for assumption: Anchors, not suitable for cracked concrete, may experience large deterioration in the load carrying capacity as well as displacement behaviour, when tested in cracked concrete (Eligehausen and Sharma, 2011). The load-displacement curves in Figure 6.9 depict the behaviour of torque-controlled expansion anchors (bolt type) which were developed for applications in un-cracked concrete, but tested in un-cracked and cracked concrete. It can clearly be seen that in cracked concrete the anchors do not function properly, resulting in very large displacements and unpredictable low ultimate capacities. Due to the unreliable behaviour of such anchors in cracked concrete, they shall not be used to connect haunch elements and therefore the model proposed is not considered valid for the same.

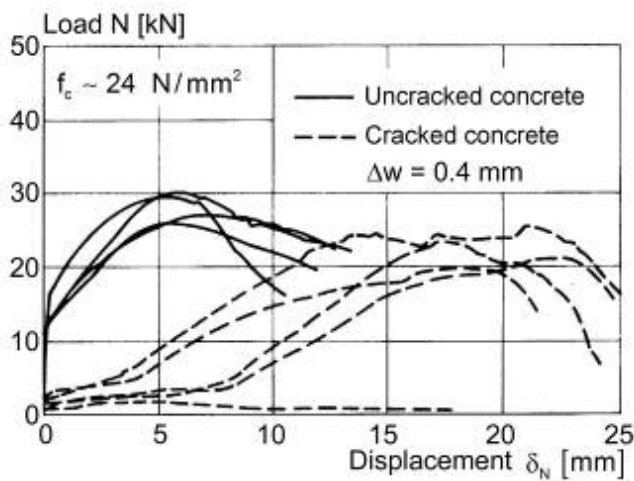


Figure 6.9 Load-displacement curves of torque-controlled expansion anchors not suitable for cracked concrete (Eligehausen et al, 2006)

6.3.3 Characteristics for spring to model anchorage system behaviour

In this work, the load-displacement behaviour of the anchorage system is idealized in a penta-linear format as shown in Figure 6.10. The penta-linear format shown in Figure 6.10 is selected since it can reasonably well represent the typical load-displacement behaviour of the anchors as depicted in Figure 6.8 (a). The coordinates of points A, B, C and D as shown in Figure 6.10 depend of the estimated failure mode for the anchor group. In case of anchors subjected to tension loads, the concrete cone failure is known to be most brittle while the steel failure is known to be most ductile. The pull out or pull through or bond failure fall in between concrete and steel failure in terms of ductility. This phenomenon can be accounted for in the model by varying the distance between points B and C as well as between points C and D in Figure 6.10. Let the failure load calculated for the anchor group following the CC method (Eligehausen et al, 2006) is N_u . The tension load corresponding to points B and C is considered as N_u , that for Point A is considered as 80% of N_u and point D corresponds to 20% of N_u .

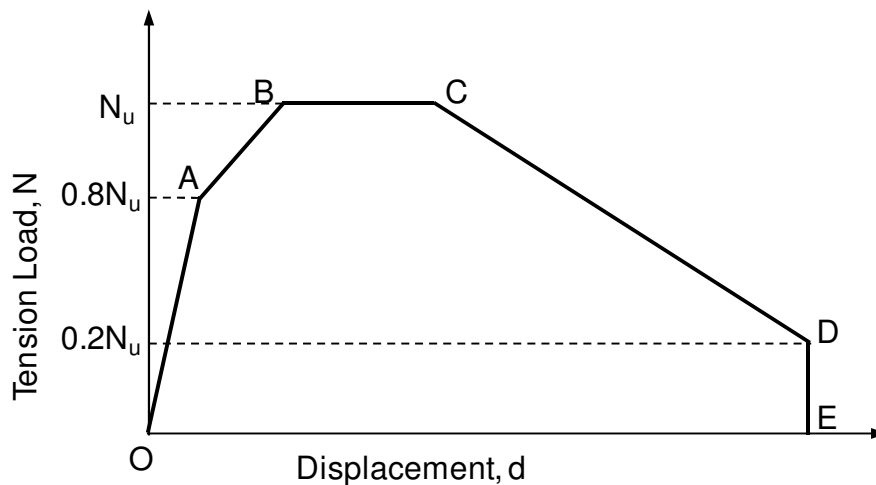


Figure 6.10 General Idealized Load-Displacement Behaviour for the anchorage system

Table 6.1 gives the values of load and corresponding displacement of points A, B, C and D to be used in the model for anchor spring.

In table 6.1, the following terminology is followed:

N = tension load on anchor group

d = displacement of the spring modelling anchor group corresponding to load, N

N_u = Ultimate load for the group calculated using CC method

$K_{0.5N_u}$ = Secant stiffness of the anchor group corresponding to 50% of N_u

k_{N_u} = Secant stiffness of the anchor group corresponding to N_u

$k_{N_u,cr}$ = Secant stiffness of the anchor group corresponding to N_u considering cracked concrete

$k_{N_u,uncr}$ = Secant stiffness of the anchor group corresponding to N_u considering uncracked concrete

Table 6.1 Salient points for the spring characteristics for anchorage system

Failure Mode	Point	N	d	$k_{N_u,cr} / k_{N_u,uncr}$
Concrete Cone	A	$0.8N_u$	$0.8N_u/k_{0.5N_u}$	0.45
	B	N_u	N_u/k_{N_u}	
	C	N_u	$1.25N_u/k_{N_u}$	
	D	$0.2N_u$	$2N_u/k_{N_u}$	
Pull out / Pull Through / Bond Failure	A	$0.8N_u$	$0.8N_u/k_{0.5N_u}$	0.30
	B	N_u	N_u/k_{N_u}	
	C	N_u	$2N_u/k_{N_u}$	
	D	$0.2N_u$	$4N_u/k_{N_u}$	
Steel Failure	A	$0.8N_u$	$0.8N_u/k_{0.5N_u}$	1
	B	N_u	N_u/k_{N_u}	
	C	N_u	$3N_u/k_{N_u}$	
	D	$0.2N_u$	$5N_u/k_{N_u}$	

The stiffness of the anchors loaded in tension/shear is generally evaluated corresponding to the load equal to 50% of the peak load. This is due to the fact that the scatter in the displacement at 50% of the mean residual capacity is somewhat limited, since it is in the beginning of load displacement curve (Mahrenholtz et al, 2009). Moreover, this parameter is recognized by many technical approvals (ETAG 001) for the initial stiffness of the anchors. Based on the large number of tests on anchors under monotonic tension loads (Eligehausen et al (2006), Mahrenholtz, 2011) in this model, it is assumed that this stiffness, $k_{0.5N_u}$, is valid up to point A i.e. till $0.8N_u$. This simplifies the model while still being able to capture the anchor behaviour reasonably accurately. This stiffness value can be obtained either by technical approval or from the tension tests performed on anchors.

For point B, the corresponding displacement can be obtained by dividing the peak load by k_{N_u} . Again, k_{N_u} can be obtained from technical approval for the anchors or from experimental results of monotonic tension tests. However, it has been found from various test data that $k_{0.5N_u} = 2k_{N_u}$ can be used as a reasonable estimate for k_{N_u} , if $k_{0.5N_u}$ is known or vice-versa (Mahrenholtz, 2011).

As mentioned above (assumption 4), while evaluating the load carrying capacity of the anchor group, cracked concrete shall be assumed. From tests it has been shown that the load carrying capacity of the anchors reduces with increasing crack width (Figure 6.8 (b)). However, it is considered reasonable to consider the load carrying capacity of the anchorage system in cracked concrete as 70% of the peak load carrying capacity of the anchorage system in uncracked concrete, i.e., $N_{u,cracked} = 0.7 * N_{u,uncracked}$ (Eligehausen et al, 2006).

As seen from Figure 6.8 (a), due to the presence of the crack, not only the load carrying capacity but also the stiffness of the anchors is significantly affected. If not obtained by tests

or from technical approval, the ratio of stiffness of the anchor group in cracked concrete, $k_{Nu,cr}$ to the stiffness in uncracked concrete, $k_{Nu,uncr}$ can be considered as given in last column of Table 6.1, which is based on values obtained from a number of tests by Mahrenholtz (2011).

The stiffness values are generally obtained for single anchors. The stiffness values for the group of anchors may be estimated from the individual stiffness of the anchor by using the geometrical arrangement of anchors in the group and the estimated failure mode. For concrete cone failure, the load carrying capacity of the anchor group is estimated by comparing the projected area of the group with the projected area for one anchor with fully developed concrete cone. Similar philosophy is proposed in this work to estimate the stiffness ($k_{0.5Nu}$ or k_{Nu}) for the group with the estimated failure mode as concrete cone failure. Thus, for concrete cone failure:

$$k_{group} = \frac{A_{c,N}}{A_{c,N}^0} k_{individual} \quad (6.4)$$

Where, $A_{c,N}$ = Projected area of the group, and $A_{c,N}^0 = 9h_{ef}^2$

In case of pull out failure, pull through failure, bond failure or steel failure, the stiffness of the group can be obtained as:

$$k_{group} = n \cdot k_{individual} \quad (6.5)$$

Where, n = number of anchors in the group

Based on the above discussion and Table 6.1, Figure 6.11 shows the normalized load-displacement curves for the anchorage system.

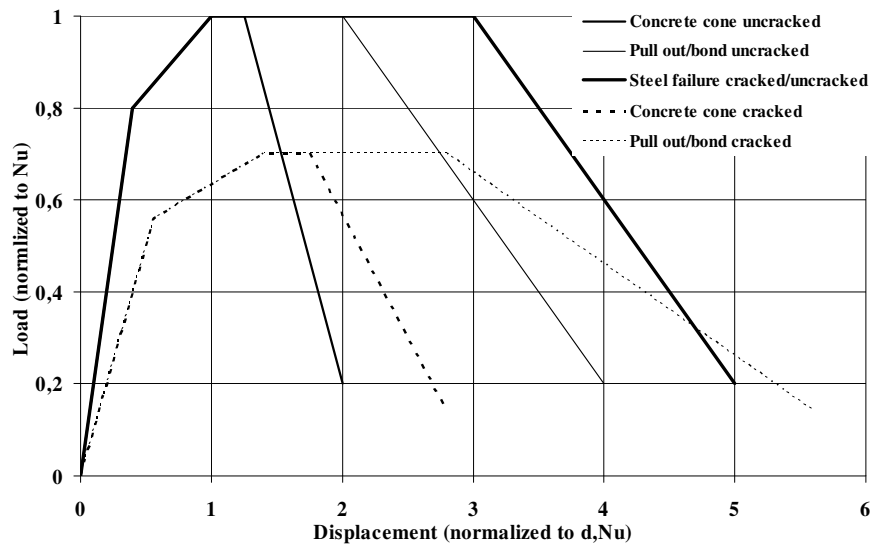


Figure 6.11 Normalized load-displacement curves for anchorage system

The steps to be followed to evaluate tension spring characteristics for anchorage system in haunch retrofit solution can be summarized as:

1. Evaluate the ultimate load capacity of the anchorage system and estimate the most probable failure mode using CC Method.
2. Corresponding to the failure mode, read the values of relevant points on the load-displacement curve for the anchor system (Table 1)
3. For cracked concrete, consider $N_{u,cracked} = 0.7 * N_{u,uncracked}$
4. Read the stiffness of individual anchors from technical approvals/test results and evaluate the group stiffness. If unavailable otherwise, take $k_{0.5N_u} = 2k_{N_u}$
5. Consider compression side anchor as stiff and linear elastic
6. Perform the analysis by modelling anchor group by a tension spring

The validation of the proposed model is presented in chapter 14. The numerical analysis was performed using commercial software SAP2000.

7. EXPERIMENTAL PROGRAM ON AS BUILT BEAM-COLUMN JOINTS

To understand the seismic behaviour of non-seismically designed and detailed RC beam-column joints, an experimental program was carried out. Five beam-column joints were tested under the program. The tests were carried out within the framework of the thesis of Genesio (2012) and the complete details of the experimental work are available in Genesio and Sharma (2010a) and Genesio (2012). However, these tests also serve as the basic tests within the framework of this thesis to study the behaviour of as-built joints and also for validation of the models proposed earlier. Therefore, a brief discussion of the experiments is provided in this chapter. The objectives of these tests were

- (i) to understand the seismic behaviour of non-seismically designed beam-column joints;
- (ii) to investigate the influence of beam bar anchorage on joint behaviour;
- (iii) to serve as control specimen for verification of haunch retrofit solution at sub-assembly level; and
- (iv) to provide database for validation of the numerical models described earlier.

7.1 Experimental Program

The experimental program on as-built beam-column joints consisted of performing static-cyclic tests on non-seismically designed full-scale RC exterior joints. Five joints were tested under the program. The test matrix is shown in Table 7.1.

Table 7.1 Test matrix for experimental program on as-built joints

Joint Name	Type of Rebar	Anchorage of beam top bars	Anchorage of beam bottom bars	Expected failure mode
JT1-1	Deformed	Bent in	Bent in	Joint shear
JT2-1	Plain	180° hook	180° hook	Joint shear
JT3-1	Deformed	Bent in	150 mm straight embedment	Joint shear / Pullout of bottom beam bars
JT4-1	Deformed	Bent in	Bent out	Joint shear
JT5-1	Deformed	Bent in	Bent in	Joint shear/ beam yielding

7.2 Description of Joints

7.2.1 Geometry

Figure 7.1 shows the typical details of the joints tested under the program. Five different joints were tested under the program, with different beam bar anchorage in the joint panel as

shown in Figure 7.1. The joints were named as JT1-1 through JT5-1. The cross-section details for the columns for all the joints were same, while the cross-section of beam was different for joint JT5-1 compared to other specimens (Figure 7.1). By design, for JT1-1 through JT4-1, joint shear failure prior to beam/column failure is imminent. However, for joint JT5-1, the yielding of beam longitudinal reinforcement follows the joint shear cracking but happens before ultimate joint shear failure.

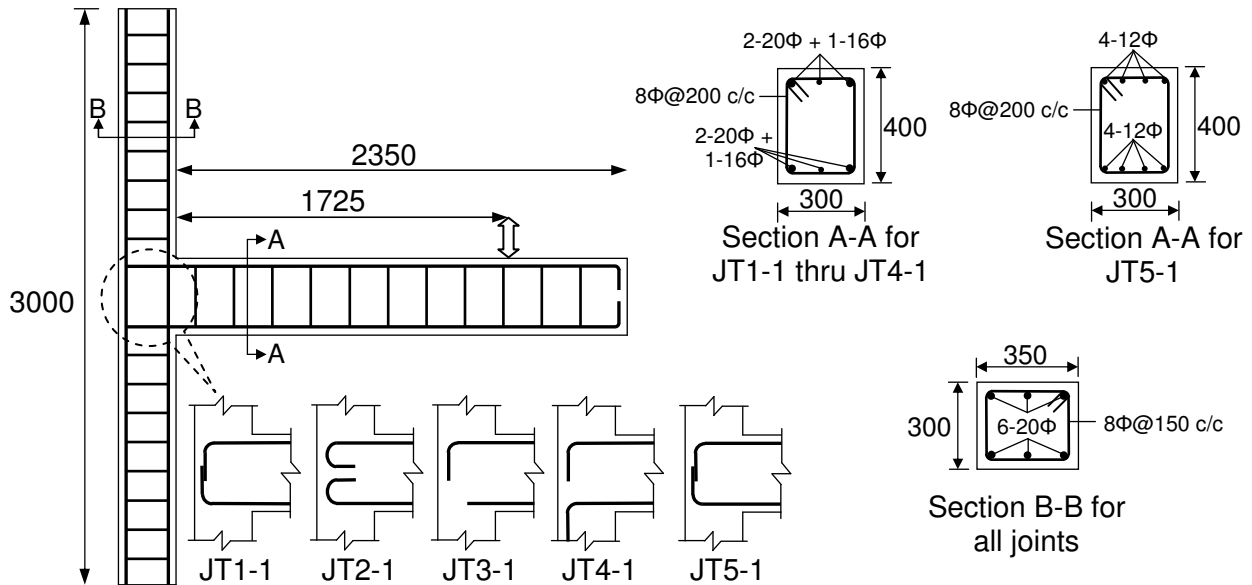


Figure 7.1 Dimensions and reinforcement details of the specimens

7.2.2 Material Properties

The average compressive strength of concrete on testing day, obtained by performing tests on 150mm size cubes are reported in Table 7.2 for each joint. Fe500 (IS 1786:2008) grade reinforcing bars were used in the specimens JT1-1 through JT4-1, while Fe250 grade plain round bars (Mild steel) were used for JT2-1. The actual properties of reinforcing bars used in the joints are tabulated in Table 7.3.

Table 7.2 Average compressive strength for concrete

Joint	Average Compressive Cube Strength (MPa)
JT1-1	31.75
JT2-1	30.44
JT3-1	34.32
JT4-1	35.29
JT5-1	30.79

Table 7.3 Properties of Reinforcing Bars used for as-built joints

Diameter of bar (mm)	Deformed bars				Plain round bars			
	Yield (MPa)	Strength	Ult. (MPa)	Strength	Yield (MPa)	Strength	Ult. (MPa)	Strength
8	548		652		301		485	
12	543		640		--		--	
16	558		688		312		478	
20	552		672		308		482	

7.3 Test Setup

7.3.1 Loading and Reaction Frame

The beam-column joints were tested in erect position, with column vertical. Both ends of the columns were held by elastic hinge sub-assembly. The top hinge was connected rigidly to a steel portal frame, while the test setup was connected to the strong floor. The beam was connected to a servo-hydraulic actuator at the loading point. Figure 7.2 shows the schematic of the test setup, while Figure 7.3 shows the test setup as assembled.

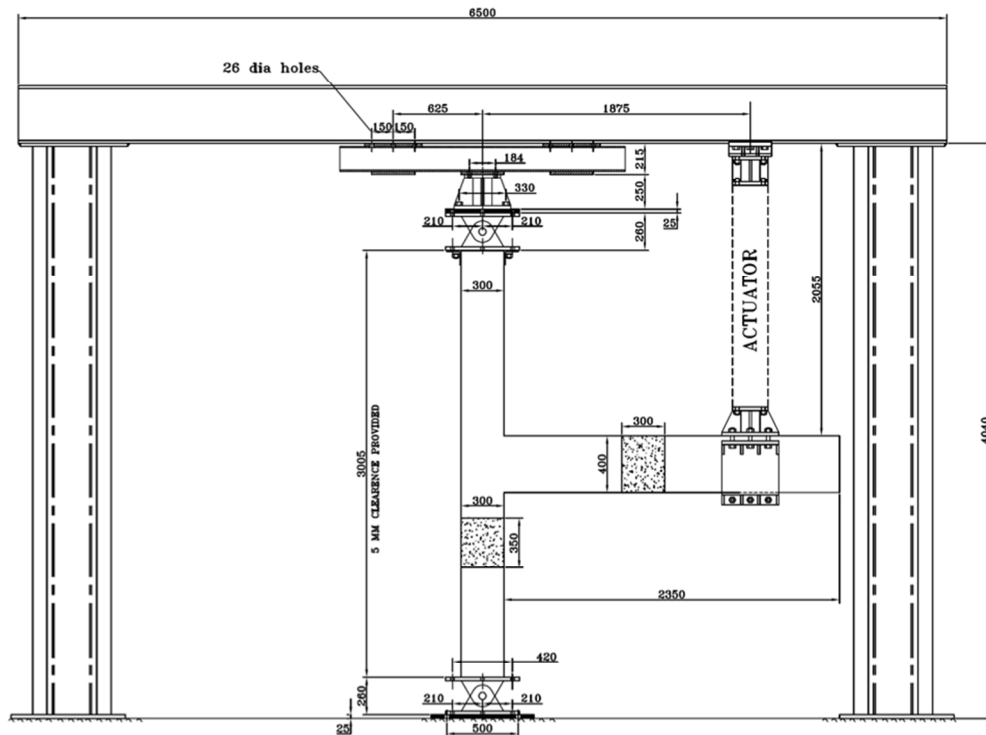


Figure 7.2 Schematic of Test Setup



Figure 7.3 Test Setup as built

Axial load was not applied on the column in any of the cases. This may be considered to be on conservative side since the moderate level of axial load is expected to increase the joint shear strength (Paulay and Priestley, 1992).

7.3.2 Test Facility

The experiments were carried out in the component testing facility (CTF) of BARC, Mumbai. The facility consists of servo-hydraulic actuators of 250 kN capacity along with a strong cast iron machine floor and a portal frame for fixing actuators and other accessories for the tests. The high performance actuators are integrated with displacement transducer, load cell, high capacity 2 stage servo valve attached to a pre-loaded swivel base and swivel rod end for both static and dynamic test applications. The actuators are operated by control system software with programming facilities to impart both pre-programmed and custom profiles for facilitating static and dynamic tests on components under load, displacement or strain control modes.

7.3.3 Instrumentation

The instrumentation for a typical as-built joint included the following:

- Load cell (inbuilt in actuator) to measure beam end load
- Displacement Transducer (inbuilt in actuator) to measure beam end displacement
- Strain gauge on reinforcing bars to measure strains at critical locations
- Potentiometers to measure beam, column and joint deformations

The strain gauges were provided on the reinforcing bars at the three faces of the joint, where bending moments, and hence strains, shall be maximum. Figure 7.4 shows the locations for strain gauges on reinforcing bars in an as-built joint.

To evaluate the element deformations, linear potentiometers were used. Total eight potentiometers were used, two for beam, four for column and two for joint as shown in Figure 7.5. The pair of potentiometers 1-2 and 5-6 were used to evaluate the rotation of column members, potentiometer pair 7-8 was used to evaluate the rotation of the beam and the pair 3-4 was used to evaluate the joint shear distortion.

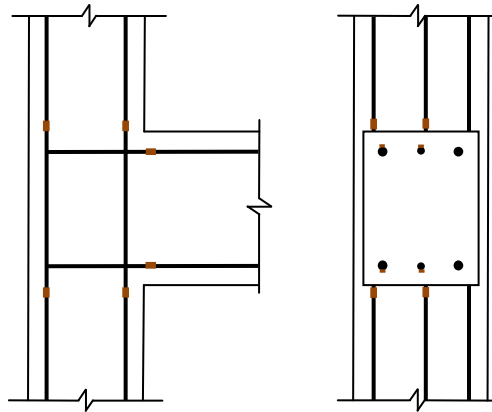


Figure 7.4 Location of strain gauges on as-built joint

The member fixed end rotation can be obtained by dividing the difference of the readings of potentiometer by the distance between the potentiometers. The joint shear deformation can be obtained from geometry as explained below.

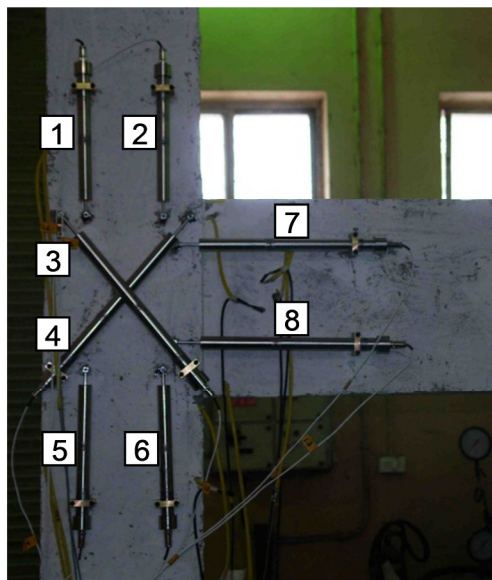


Figure 7.5 Potentiometers to measure element deformations

Let the undeformed length of potentiometer 4 be l_j and it makes an angle α_j with horizontal. Now let us suppose that the joint deforms in such a way that potentiometer 4 is elongated by an amount δ_j and corresponding compression in potentiometer 3 is δ_j' . The joint deformation can then be obtained as

$$\gamma_j = \gamma_1 + \gamma_2 = \frac{\delta_j - \delta_j'}{2l_j} \cdot \left(\tan \alpha_j + \frac{1}{\tan \alpha_j} \right) \quad (7.1)$$

7.3.4 Loading Pattern

The experiment was carried out by applying cyclic load at the beam end in displacement control. The beam end displacement cycles as per the loading protocol used in the tests are shown in Figure 7.6. Since the actuator stroke was limited to 150mm (total), the maximum beam end displacement was restricted to +/-70mm. Two cycles were provided for each level of beam end displacements.

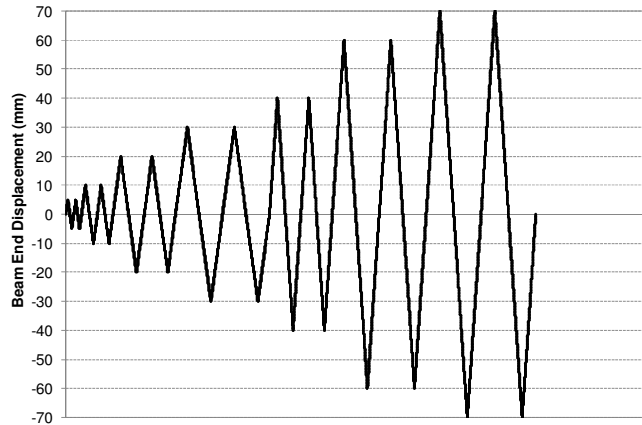


Figure 7.6 Loading pattern used for the tests

7.4 Experimental Results

7.4.1 JT1-1

Joint JT1-1 was constructed using deformed bars and had both top and bottom beam reinforcing bars bent into the joint (Figure 7.1). Figure 7.7 shows the hysteretic load-displacement curves obtained for the joint. In the plots, the load is considered as positive when the beam is pulled up and negative when pushed down. The peak load in the positive direction was obtained as 79.9 kN and that in the negative direction was 61.5 kN. In both sides, the peak load was obtained during 60mm cycle. The difference in positive and negative peak loads is rather unusual for a joint having symmetric reinforcement detailing and

no axial load. This is also replicated in the crack patterns as shown in Figure 7.8 corresponding to various displacement levels.

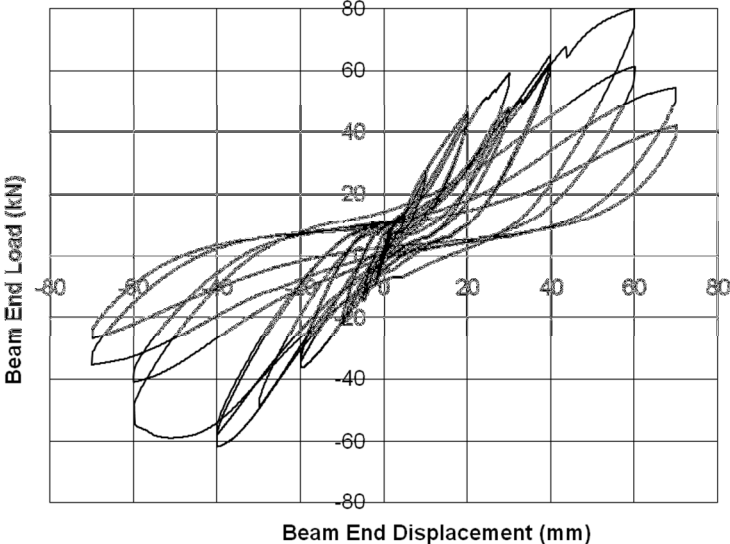


Figure 7.7 Hysteretic loops obtained from test on JT1-1

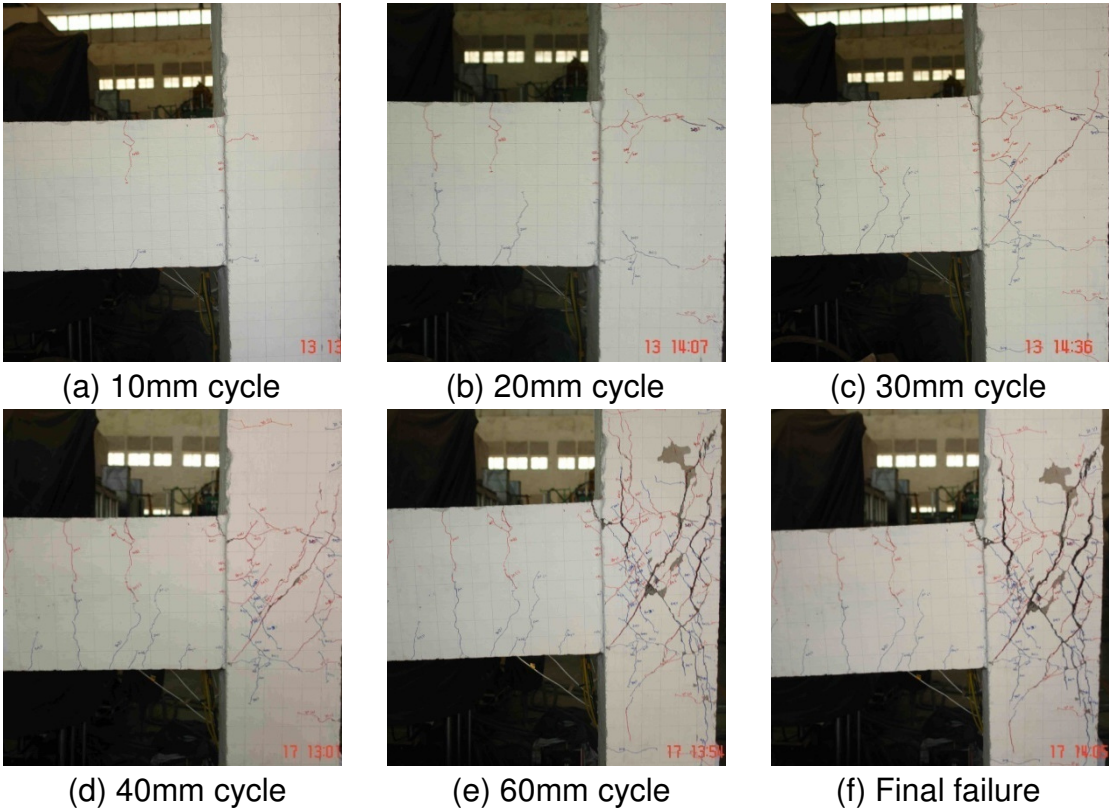


Figure 7.8 Crack patterns observed for joint JT1-1

The first cracks were observed in the beam at column face (Figure 7.8a) due to flexure corresponding to 10mm cycle. When the beam end displacement was increased to 20mm,

the beam bars experienced large bond stresses which led to splitting bond cracks in the joint (Figure 7.8b). When the beam end displacement was further increased, the first joint shear crack occurred for negative loading direction (beam being pulled up) as seen in Figure 7.8c. Although, in absence of axial load on column, it is expected to observe symmetric diagonal cracking in both loading directions, the same was not observed in the test. Even at 40mm cycle, the clear diagonal cracking of the joint did not occur for the positive cycle but several smaller cracks did appear in the joint region (Figure 7.8d). This corresponds to higher load obtained for the positive cycle in this test and may be attributed to certain local phenomenon.

On further increasing the beam end displacement, the diagonal crack appeared in the joint while loading in positive direction too (Figure 7.8e). The final failure clearly was due to joint shear failure, which was marked by severe diagonal cracking as well as vertical cracks along column longitudinal reinforcement (Figure 7.8f). The vertical cracks are attributed to the fact that when joint cracks, it tends to dilate horizontally placing the cover concrete at the back of the joint in curvature which leads to vertical cracking on the weak plane at the line of column reinforcement (Priestley, 1997).

7.4.2 JT2-1

Joint JT2-1 had essentially the same configuration as JT1-1 except that plain round bars were used as reinforcement and the beam bars had hooks instead of bends (Figure 7.1). Figure 7.9 shows the hysteretic load-displacement curves obtained for the joint. The peak load for the positive loading cycle was obtained as 41.5 kN and that for negative loading cycle as 39.1 kN. This shows a practically symmetric behavior of the joint as is expected for a joint with symmetric reinforcement detailing and no axial load on column. The same corresponds with the crack patterns as well. Figure 7.10 shows the crack patterns observed in the test at various displacement levels.

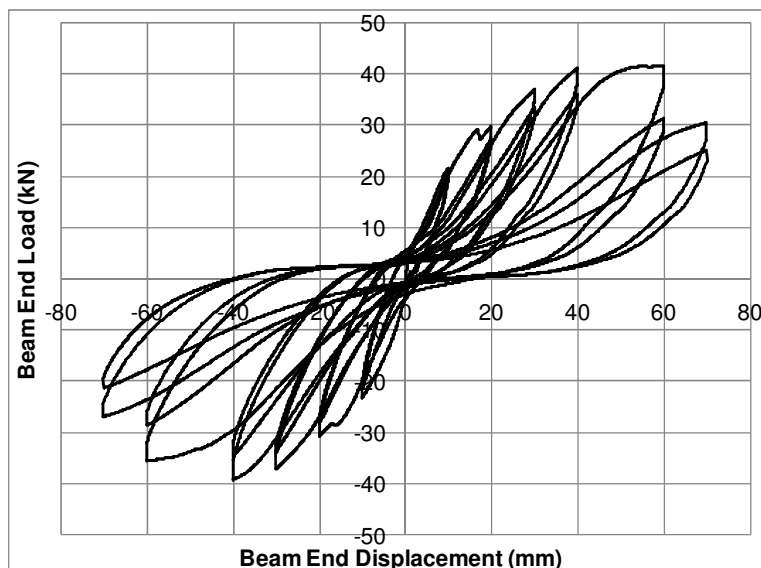


Figure 7.9 Hysteretic loops obtained from test on JT2-1

At the beam end displacement cycle of +/- 10mm, flexural cracks appeared on the beam (Figure 7.10a). On increasing the displacement level to 20mm, diagonal shear cracks appeared in the joint in a practically symmetric fashion (Figure 7.10b). No bond cracks appeared in this case. This was in contrast to joint JT1-1 where the bond cracks appeared at the same displacement cycle. This is attributed to the type of reinforcing bars used in the two joints. In case of JT1-1 deformed bars were used which are capable of developing high bond stresses, whereas the plain round bars used in case of JT2-1 are not capable of the same.

Further increase in beam end displacement resulted in the extension of the existing cracks and opening of the diagonal cracks in the joint (Figure 7.10 c, d, e). The diagonal cracks of the joint further propagated along the column longitudinal reinforcement. The final failure is attributed to the shear failure of the joint along with certain cracks in beam and column (Figure 7.10f).

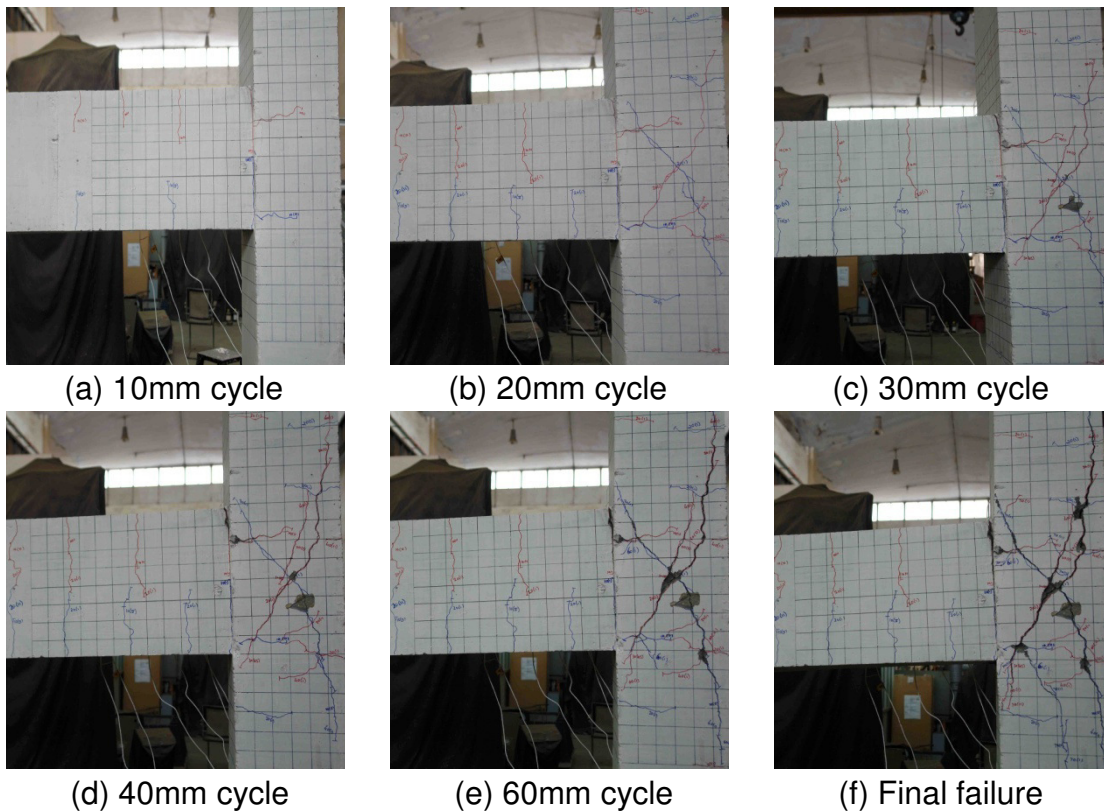


Figure 7.10 Crack patterns observed for joint JT2-1

7.4.3 JT3-1

Joint JT3-1 was constructed using deformed bars with a typical gravity load designed detailing with top beam bars bent in and bottom beam bars embedded 150mm from the face of the column inside the joint core. Thus, for this joint it is expected that during the positive loading (beam being pulled up), the bond slip of the beam bars may occur. Therefore the full

strength development of the joint in the positive direction is not expected. This is replicated in the hysteretic loops obtained for the joint as shown in Figure 7.11. The peak loads for positive and negative loading directions were obtained as 38.0 kN and 53.5 kN respectively.

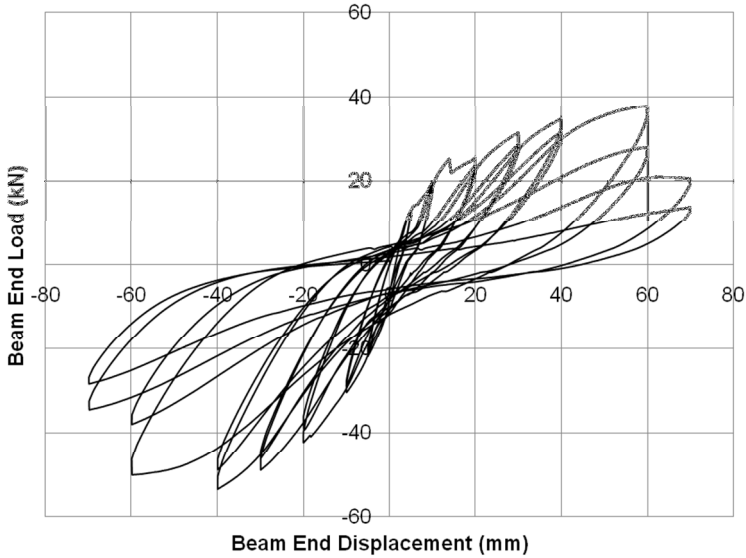


Figure 7.11 Hysteretic loops obtained from test on JT3-1

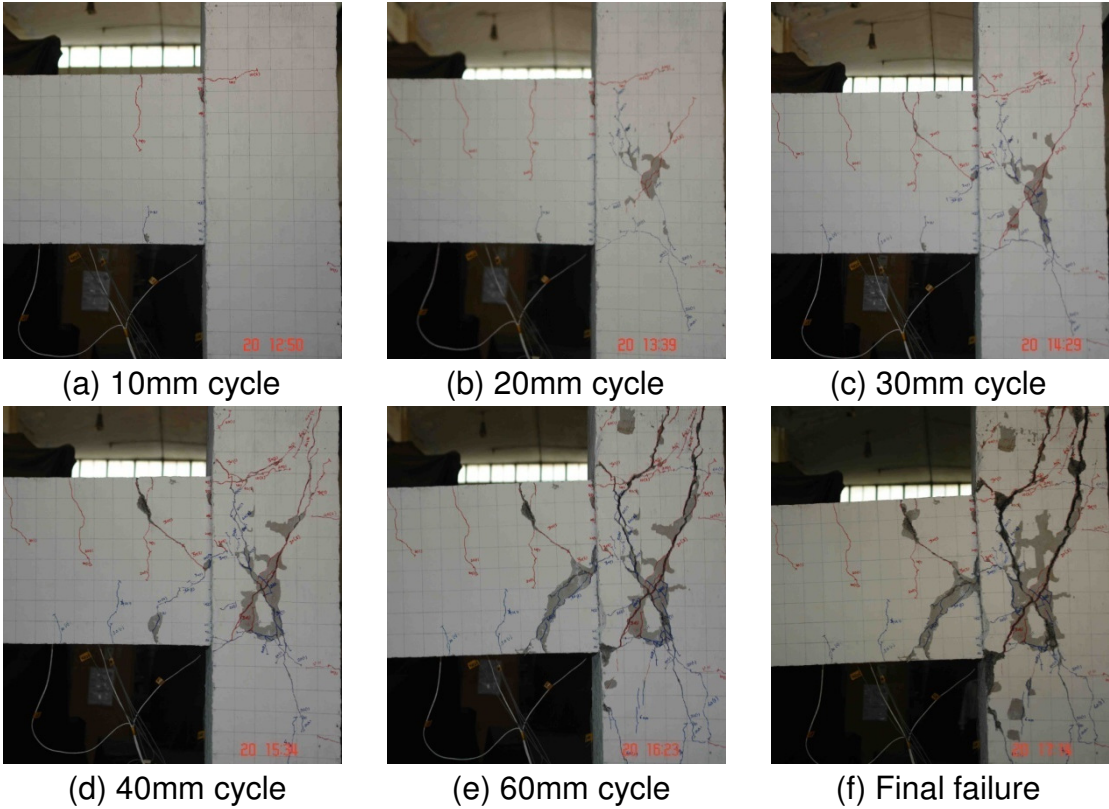


Figure 7.12 Crack patterns observed for joint JT3-1

The crack patterns observed in the test for joint JT3-1 are presented in Figure 7.12 for various displacement levels. In the first displacement cycle of +/-10mm, the first crack appeared at the beam-joint interface and the second flexural crack appeared in the beam (Figure 7.12a). When the beam was pulled up for the first 20mm cycle, the first diagonal crack appeared in the joint starting from the end of the anchorage of straight beam bars almost at mid depth of column (Figure 7.12b).

While loading in the negative direction, another diagonal crack appeared in the joint (Figure 7.12b), which extended similar to the crack in case of JT1-1 on further loading (Figure 7.12c). At 30mm cycle (Figure 7.12c), pullout of the bottom beam bars initiated, which is characterized by the crack (marked in red) propagating from mid height of beam to the top of beam. On further loading, the concrete spalling occurred at this pullout crack (Figure 7.12d). On further loading, the existing cracks propagated, opened up and significant spalling was observed (Figure 7.12e). Again the diagonal cracks propagated along the column longitudinal reinforcement. The final failure is attributed to joint shear combined with pullout failure of bottom beam bars (Figure 7.12f).

7.4.4 JT4-1

Joint JT4-1 was constructed using deformed bars and was detailed with beam top bars bent into and beam bottom bars bent out of the joint. As discussed in chapter 4, when the beam bars are bent out, after the first cracking, the diagonal struts in the joint cannot be stabilized and therefore, the joint failure occurs at early stage compared to when beam bars are bent in. The same can be observed in Figure 7.13 where the peak load in positive loading direction is obtained as 40.5 kN while in the negative direction, the same is obtained as 57.8 kN.

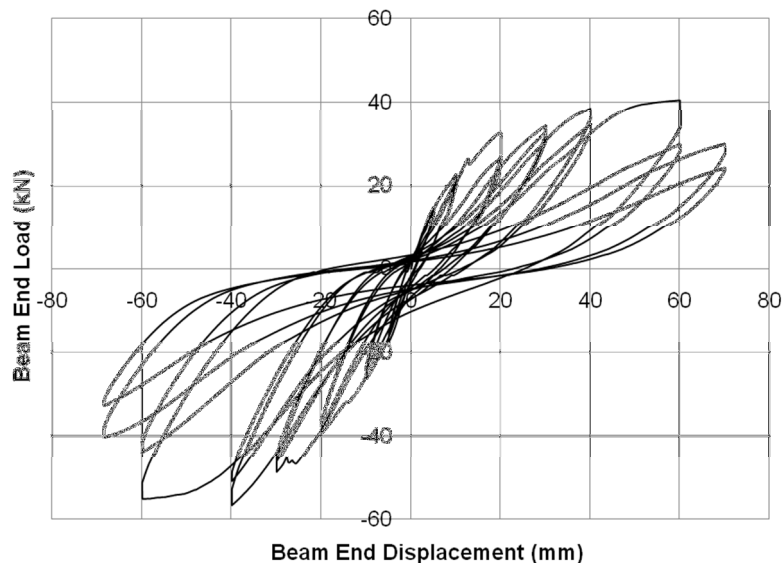


Figure 7.13 Hysteretic loops obtained from test on JT4-1

The failure patterns as observed in the test for various beam end displacement levels are depicted in Figure 7.14. During the first cycle of $\pm 10\text{mm}$, the flexural cracks in the beam as well as the bond cracks in the joint appeared (Figure 7.14a). Till this point, the crack pattern was practically symmetric. When the beam end displacement was increased to 20mm , the first diagonal shear crack appeared in the positive loading side (Figure 7.14b). The diagonal crack in the negative loading direction appeared in the next cycle when the beam end displacement was increased to 30mm (Figure 7.14c). During the 40mm cycle, new shear cracks appeared in the joint panel (Figure 7.14d) in the negative loading direction, however in the positive loading direction, there was essentially a single diagonal crack.

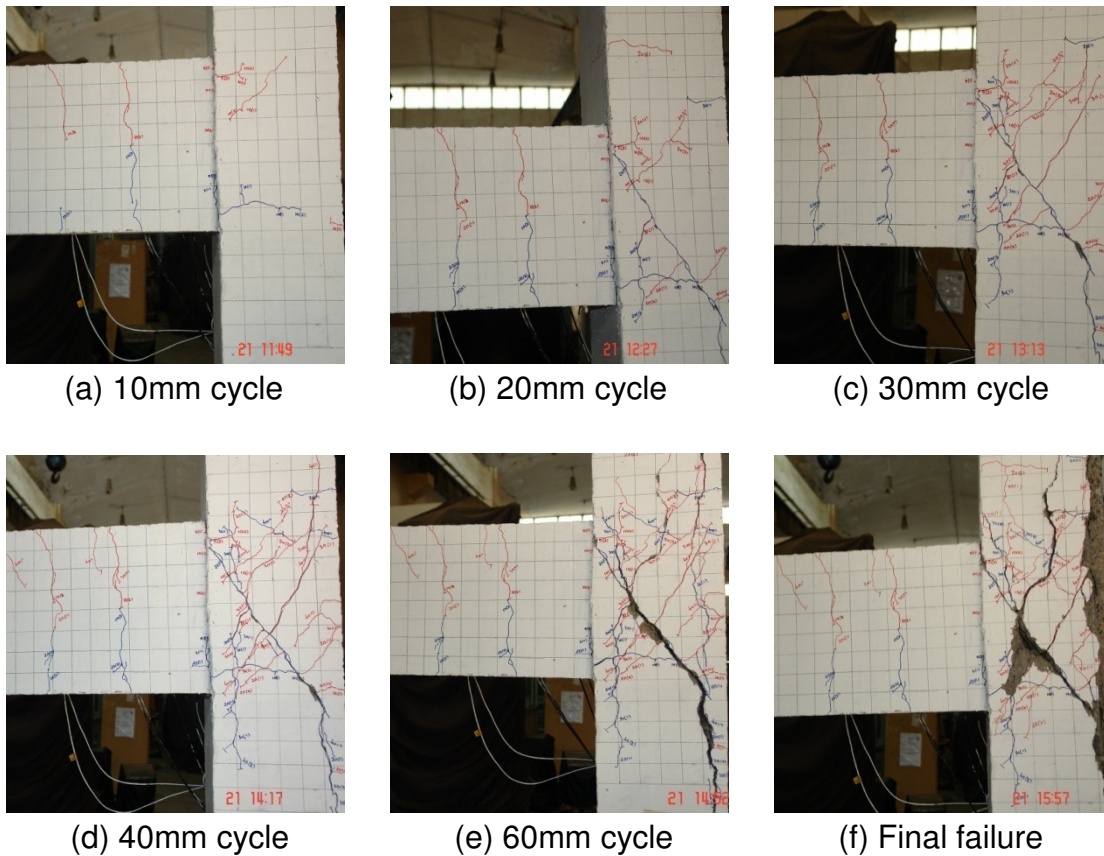


Figure 7.14 Crack patterns observed for joint JT4-1

During the cycle with beam end displacement of $\pm 60\text{mm}$, the crack in the positive direction opened up largely and significant amount of spalling was observed (Figure 7.14e). This was not the case in the negative loading direction, justifying the theory of Priestley (1997) stating the stabilization of diagonal strut and therefore hardening behaviour is not possible when the beam bars are bent out. It was also observed that the diagonal crack propagated along the beam bars bent out of the joint and due to the lateral thrust, the cover to column longitudinal bars was fractured. During the last cycle, large amount of spalling in the joint as well in the column was observed (Figure 7.14f). Again the failure is characterized as joint shear failure.

7.4.5 JT5-1

Joint JT5-1 was constructed using deformed bars as reinforcement and both beam top and bottom bars bent into the joint, but it had a major difference from all other joints tested. The beam reinforcement for joint JT5-1 consisted of 4-12mm diameter bars (Figure 7.1). This modification in the design was done in order to induce the yielding of beam reinforcement after the first shear cracking of the joint but before its ultimate failure due to joint shear. Figure 7.15 presents the hysteretic loops obtained for joint JT5-1. The peak load in the positive displacement cycle was obtained as 51.0 kN and that in negative direction as 39.50 kN, though the detailing was essentially symmetric. The theoretical load corresponding to yielding of beam reinforcement was approximately 50 kN. In neither of the loading direction was hardening observed after joint shear cracking suggesting that the strength of the sub-assembly is limited by beam yielding. It is interesting to observe that there is no increase in ductility (compared to earlier tests), even though the beam yields. This clearly suggests that beam yielding after the joint cracking does not form any desirable failure mode.

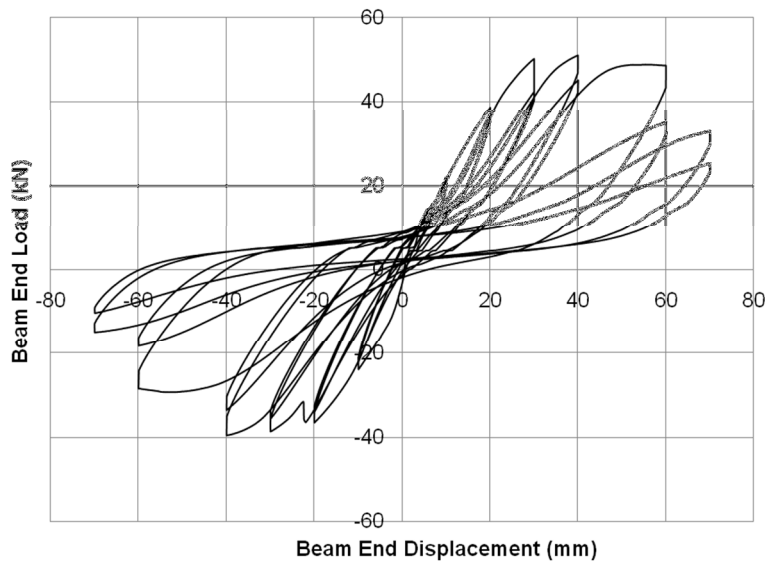


Figure 7.15 Hysteretic loops obtained from test on JT5-1

Figure 7.16 presents the crack patterns during progressive increasing beam end displacement cycles. During the first cycles of ± 10 mm (Figure 7.16a) and ± 20 mm (Figure 7.16b), flexural cracks in beam and bond cracks in the joint were observed. The first diagonal cracks appeared on the joint in both the directions while loading the beam to the end displacement of ± 30 mm (Figure 7.16c). On further increasing the beam end displacement to 40mm (Figure 7.16d), more flexural cracks in the beam as well as diagonal cracks in the joint appeared. Also, little spalling from the joint panel was observed.

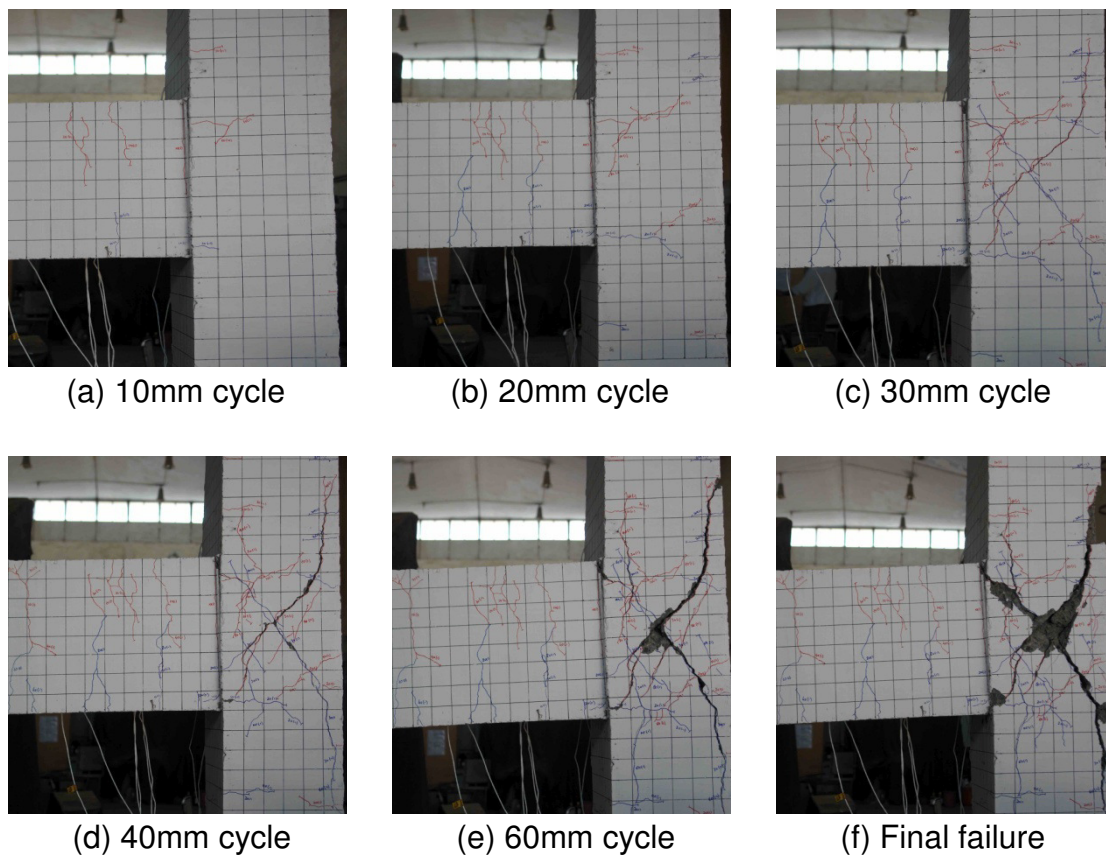


Figure 7.16 Crack patterns observed for joint JT5-1

On increasing the beam end displacements to 60 mm (Figure 7.16e), further cracking and spalling in the joint panel was observed. Also, it was interesting to note that the crack width of the flexural cracks in beam and column reduced during this cycle. This suggests that the deformation of the joint is mainly (almost fully) contributed by joint shear cracks. The final failure is characterized by two major diagonal shear cracks along with dilation of the joint leading to vertical cracks (Figure 7.16f).

7.5 Summary

Five tests were performed on poorly detailed full-scale RC beam column joints. The tests clearly confirmed the vulnerability of non-seismically designed joints subjected to seismic loads. The test program provided a great insight into the shear behaviour of poorly detailed beam column joints. In all the tests, joint shear failure was the major failure mode. The influence of type of anchorage of beam reinforcing bars in the joint panel on seismic behaviour of the joints was clearly displayed. The experiments served their purpose well as the control specimens for assessing the performance of haunch retrofit solution and also provided data that could be used for validation of the joint model.

8. EXPERIMENTAL INVESTIGATION ON INELASTIC SEISMIC BEHAVIOR OF RC FRAME STRUCTURES

Experiments at joint sub-assembly level, as discussed in chapter 7 clearly demonstrated the vulnerability of the joints of non-seismically designed frame structures against seismic forces. However, it is important to understand the behavior of joints when they are an integral part of a whole structure where the joint failure modes also interact with other possible failure modes in the structure. This requires performing experiments at structural level against simulated seismic loads till failure of the structure. It is true that a shake table test provides the best representation of the seismic behavior of structures; such a test is almost always limited by the limitations of the shake table such as pay load capacity, maximum acceleration, velocity and displacement capacity etc. On the other hand, pushover type static tests can be performed at bigger scale. In this work, both types of tests have been performed on the structures. The details of shake table tests on scaled down structures will be discussed in next chapter. This chapter describes a pushover test performed under the framework of the thesis on a full-scale RC structure. The experimental work has also been described in Sharma et al (2012).

The objectives of this test were:

- (i) to understand the behavior of beam-column joints when they are an integral part of structure
- (ii) to investigate the interactions between various failure modes in a structure
- (iii) to provide database for validation of numerical models described earlier at structural level

8.1 Description of the structure

A full-scale four storey reinforced concrete structure was tested under monotonically increasing lateral pushover loads with an inverse triangular loading pattern. In order to keep the structure as close to reality as possible, no special design for the structure as such was performed and instead a portion of a real life existing office building was selected. The structure tested was the replica of a part of the existing office building in Mumbai and was deliberately selected in such a way that it shall exhibit all major failure mode types for a typical RC frame structure. The various failure modes exhibited by the structure included failure due to flexure along with interactions with axial force (both tension and compression) as well as shear, failure due to torsion, shear failure of joints and bond failure.

8.1.1 Geometry

Figure 8.1 shows the general geometric arrangement of the structure.

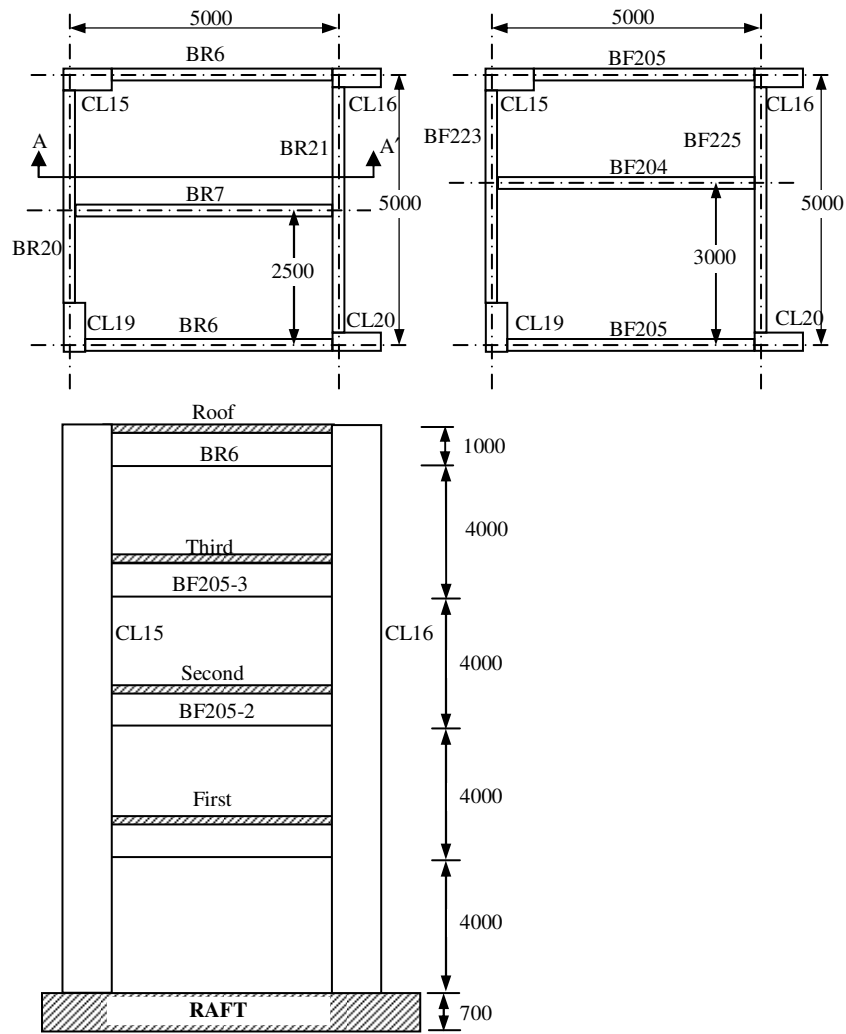


Figure 8.1 Geometry of the Structure

As seen in Figure 8.1, the secondary beam (BF204) in all floors was eccentric, whereas the same for fourth floor (BR7) was in the centre of the slab. This was as provided in original structure to support the load from partition wall on 1st, 2nd and 3rd floor slabs, whereas there was no such wall on the roof.

Figure 8.2 gives the details of floor beams and Figure 8.3 that of roof beams. The sections are uniform throughout the length of the member. Under the cross beams, additional reinforcements were provided as given in Figure 8.4.

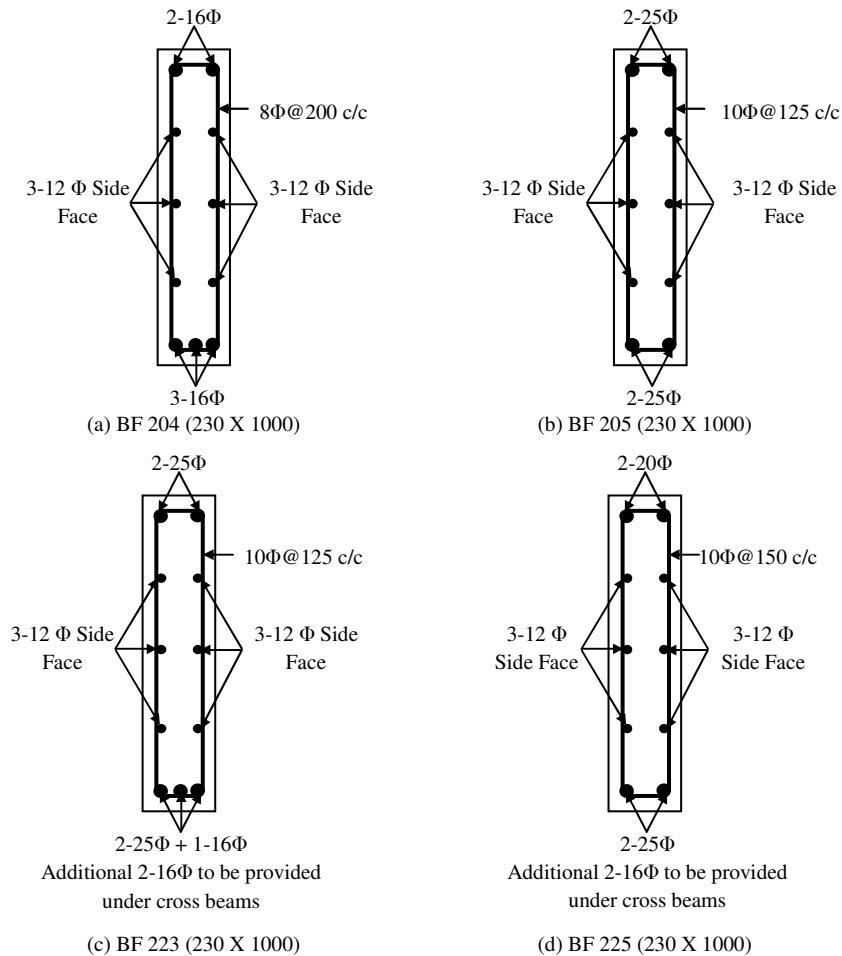
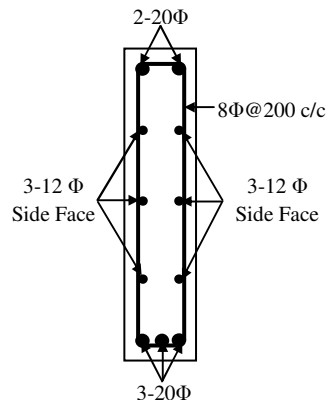


Figure 8.2 Details of Floor Beams

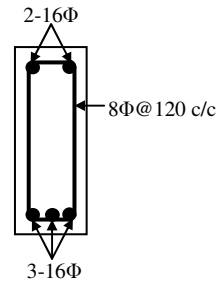
Figure 8.5 gives the sectional details of columns at different levels. The figures in brackets beside the name of the section indicate the size of the section as (Breadth x Depth). All dimensions are given in millimeters (mm).

Although the overall geometry of the structure tested in this work was kept same as the portion of the original structure, there were few major differences in the reinforcement detailing as mentioned below.

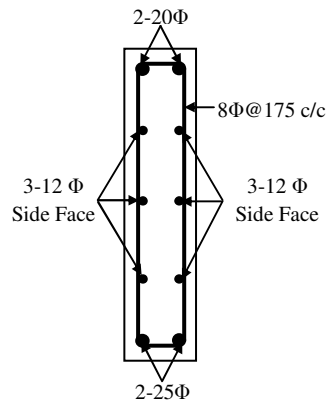
1. Although the original structure was detailed according to new conforming seismic detailing practice, the structure for the experiment followed the non-seismic detailing practice. The reason for this is the fact that pushover analysis is mostly used for retrofit of old structures, which have not followed the seismic detailing practice. Therefore, no shear reinforcement in the beam-column joints was provided. Figure 8.6 shows a typical non-conforming joint detail as was provided in the structure. The beam longitudinal reinforcement bars were extended beyond the face of the column into the joint up to a length equal to the development length for the bar as calculated by Indian standard code of practice, (IS 456:2000).



(a) BR 6 (230 X 1000)

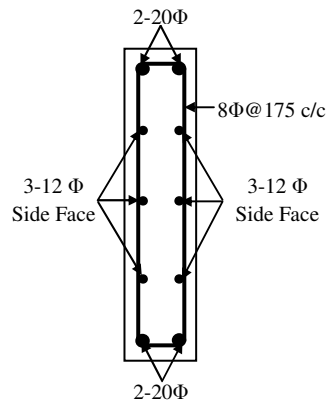


(b) BR 7 (230 X 600)



Additional 2-16Φ to be provided under cross beams

(c) BR 20 (230 X 1000)



Additional 2-16Φ to be provided under cross beams

(d) BR 21 (230 X 1000)

Figure 8.3 Details of Roof Beams

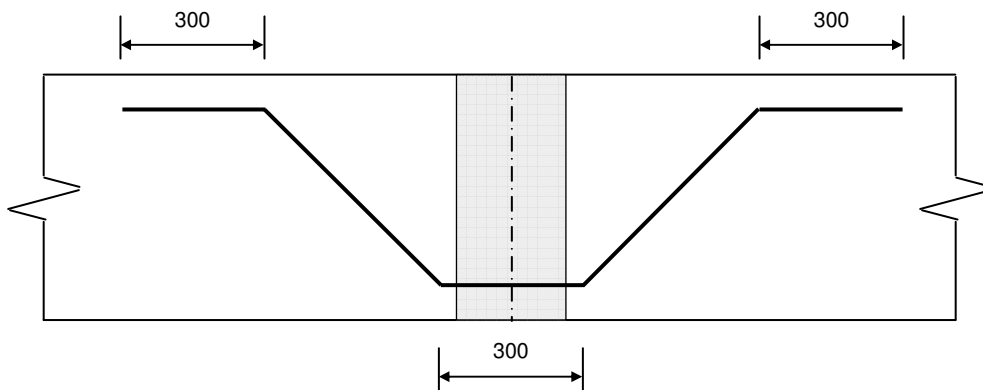


Figure 8.4 Additional Reinforcement under cross beams

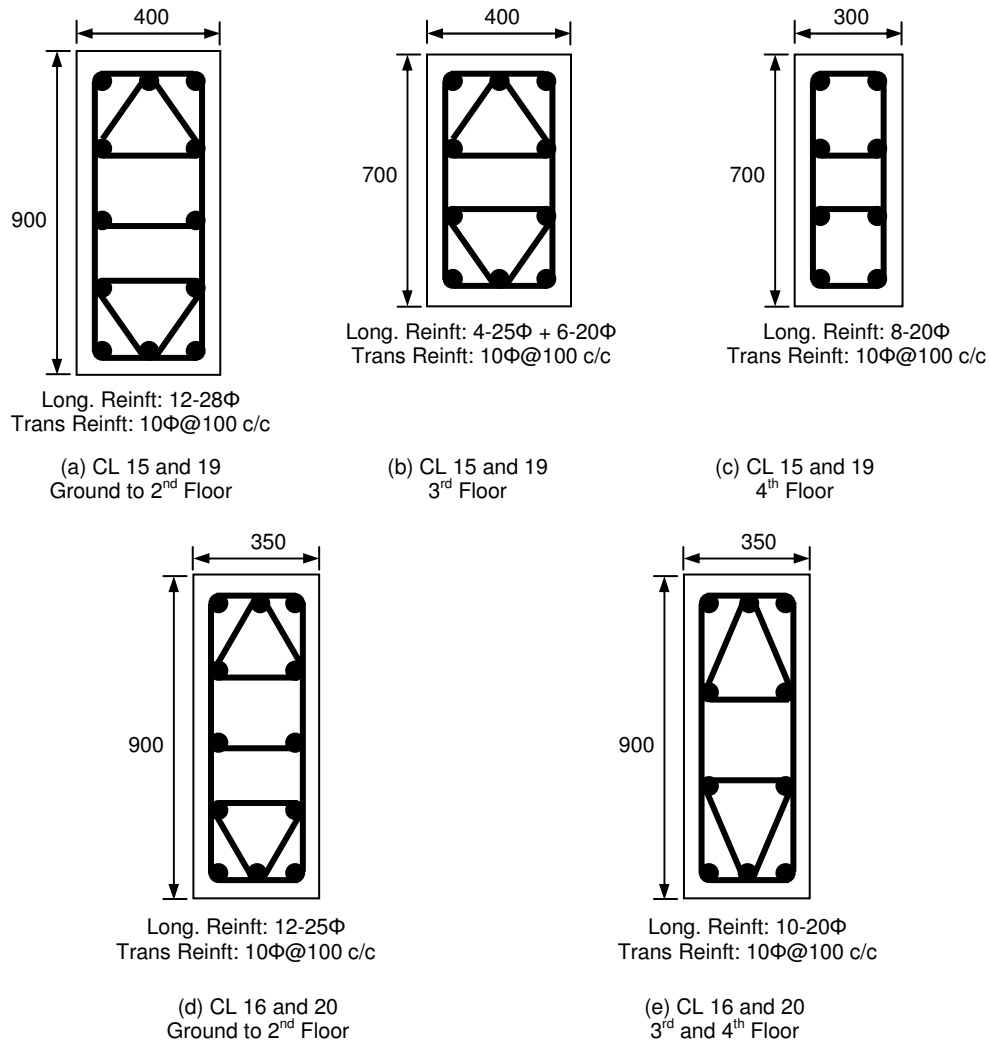


Figure 8.5 Details of Columns at various levels

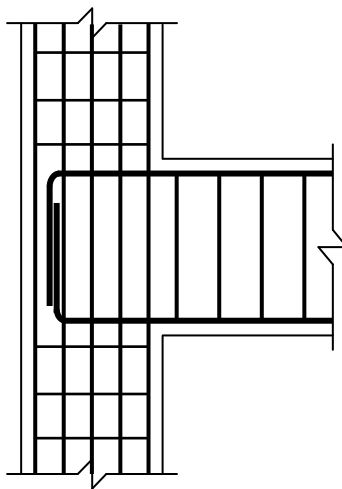


Figure 8.6 Typical non-conforming joint details as provided in the structure

2. Since the structure tested is replica of a small portion of the large original structure, the continuous reinforcements in the slab and beams were suitably modified to fit as per the requirement. The reinforcement details for floor/roof slab are shown in Figure 8.7 and Table 8.1. The thickness of the slab is 130 mm.

3. Another major difference is in the foundation system. In order to avoid any nonlinear behaviour of the foundation, a raft foundation with a number of rock anchors were provided. The details of the same are given later in the section on construction of frame.

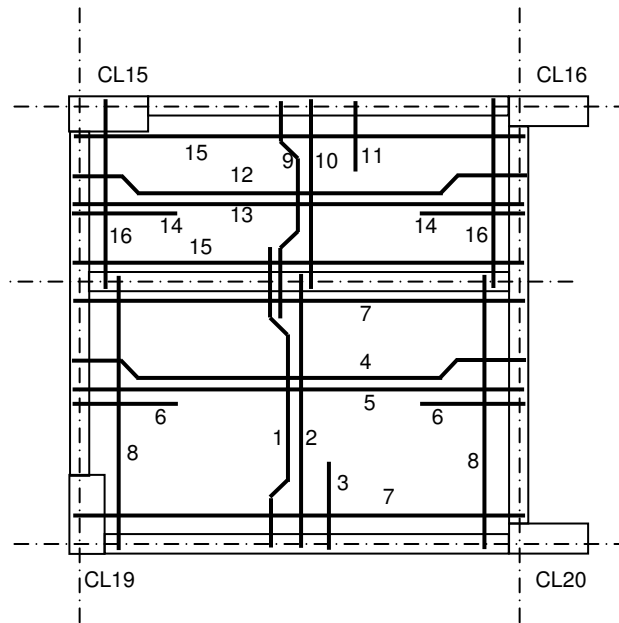


Figure 8.7 Reinforcement Details for Floor/Roof Slab

Table 8.1 Reinforcement Details for Floor/Roof Slab

Detail No.	Diameter of bar (mm)	C/C Spacing (mm)	Type/ Location
1	10 Φ	450	Alternately bent up
2	10 Φ	450	Bottom
3	10 Φ	450	Top
4	10 Φ	500	Alternately bent up
5	10 Φ	500	Bottom
6	10 Φ	500	Top
7	8 Φ	250	Top (Distribution)
8	8 Φ	250	Top (Distribution)
9	10 Φ	450	Alternately bent up
10	10 Φ	450	Bottom

11	10 Φ	450	Top
12	10 Φ	500	Alternately bent up
13	10 Φ	500	Bottom
14	10 Φ	500	Top
15	8 Φ	250	Top (Distribution)
16	8 Φ	250	Top (Distribution)

8.1.2 Material Properties

For each floor level and for columns extending from one floor to another, six standard 150mm cubes were tested under compressive loads and the average 28 day strength was obtained. Table 8.2 depicts the values of compressive strength obtained for different levels.

Table 8.2 Average compressive strength for concrete

Location	Average Compressive Cube Strength (MPa)
Raft	32.88
Columns 1 st Floor	28.86
Beams and Slab 1 st Floor	27.73
Columns 2 nd Floor	33.30
Beams and Slab 2 nd Floor	31.09
Columns 3 rd Floor	32.24
Beams and Slab 3 rd Floor	29.86
Columns 4 th Floor	31.24
Beams and Slab 4 th Floor	30.56

Cold worked deformed bars with a nominal strength of 415 MPa (IS456:2000) were used in construction. The actual properties for bars of different diameters as obtained from tests are given in Table 8.3.

Table 8.3 Properties of Reinforcing Bars

Diameter of reinforcing bar (mm)	Yield Strength (MPa)	Ult. Strength (MPa)
8	456.06	604.91
10	517.81	599.94
12	539.88	620.78

16	490.96	615.02
20	488.93	614.60
25	523.37	629.49
28	498.42	622.33

8.2 Construction of the frame

8.2.1 Construction of Raft foundation

One of the major challenges during the construction of the frame was to restrict the very likely rotation of the foundation of the structure. This was practically not possible if simple footings were made. Therefore, foundation for the structure was formed as a uniform raft for all columns. The substratum was found to be hard rock and therefore, in order to avoid any possible rotation of the foundation, rock anchors were provided. In total, 144 numbers of 1500 mm long rock anchors were used with 700mm embedment in concrete and 800 mm in rock. The rock anchors were basically high strength bolts that were inserted in pre-drilled holes in the rock and the holes are then grouted with non-shrinkable epoxy mortar grout.

It is important to note that this man-made fixity has an effect on the contribution of structural modes of vibration, since in a flexibly supported system the modal mass activated by the first mode is lower than that of a corresponding fixed based system. However, since the objective of this work was to study and model the inelastic behaviour of the structure, such a simplification was deemed necessary to avoid any soil-structure interaction effects, which is a separate research topic of its own.

The raft was constructed in such a way that the clear overhang of the raft is equal to 750mm from the face of each column on both sides. Thus, the raft dimensions were 7.40 m x 6.73 m. The design details of the foundation along with the rock anchor details are shown in Figure 8.8 and Figure 8.9 respectively. Figure 8.10 depicts the construction of raft foundation for the structure with rock anchors.

8.2.2 Construction of super-structure

Once the foundation was set, the superstructure was cast in stages as any other normal building construction with a quality control similar to the general quality control followed during the construction of normal residential buildings in India. Once, the reinforcement cage was ready, strain gauges were mounted on the reinforcement bars of beams and columns. Figure 8.11 shows the location of strain gauges on each floor, where T and B in braces indicate the strain gauge number for top and bottom beam reinforcement, respectively. The strain gauges were provided with suitable protective coating to protect the same from getting damaged during concreting.

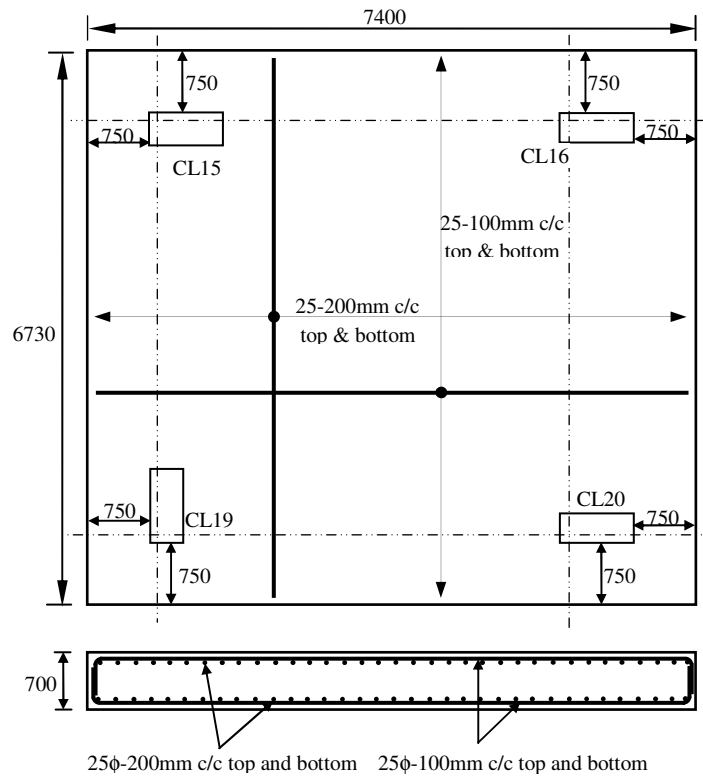


Figure 8.8 Design details of the raft foundation for the structure

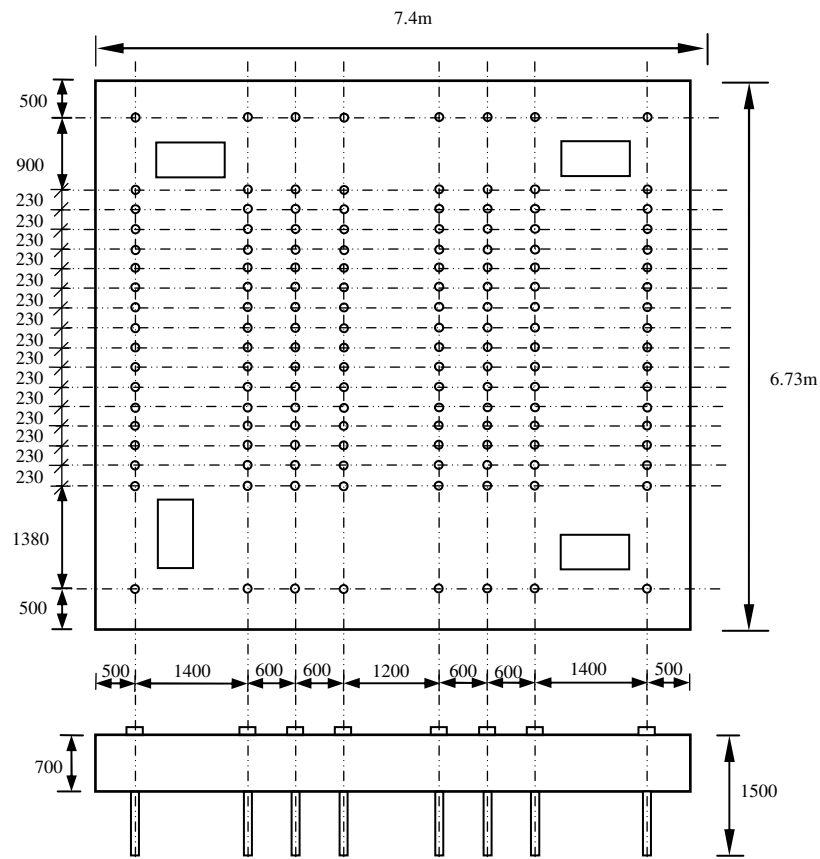


Figure 8.9 Rock anchor details for the raft foundation



Figure 8.10 Construction of Raft Foundation with Rock Anchors

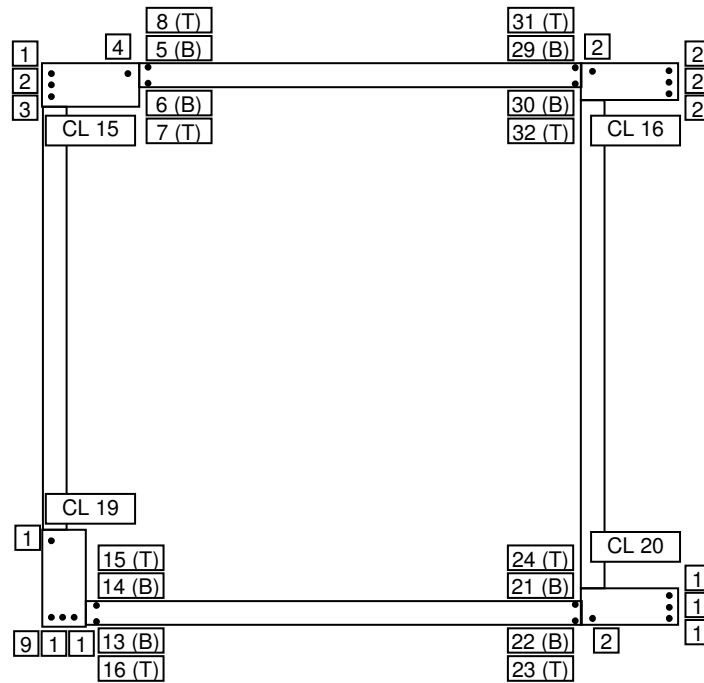


Figure 8.11 Locations of strain gauges on reinforcement bars

8.2.3 Loading arrangement

Pushover loads can acceptably be applied in inverse triangular fashion, parabolic fashion or in the ratio of the first mode shape etc (ATC40, 1996). In view of the existing tower test facility, it was found that the best possible control of loading would be through the inverse triangular loading. Therefore, the load on the structure was applied in an inverted triangular fashion and the load ratio was maintained at P: 2P: 3P: 4P corresponding to 1st floor: 2nd floor: 3rd floor: 4th floor, respectively. In order to distribute loads in a better way, loading

arrangement using steel plates and bolts were provided in the slabs. Figure 8.12 shows the design details of the loading arrangement.

In order to maintain the required applied load ratio at different floors, one such loading assembly was provided at 1st floor slab, two at 2nd floor slab, three at 3rd floor slab and four at 4th floor slab. Figure 8.13 shows the construction of the same in the slab of 3rd floor.

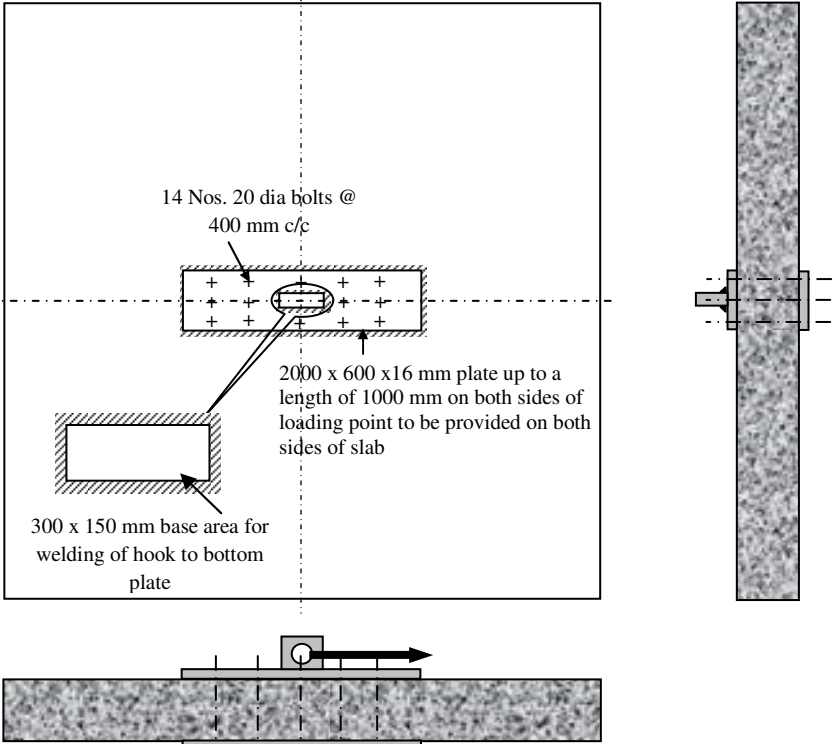


Figure 8.12 Details of Loading Arrangement



Figure 8.13 Loading arrangement at 3rd floor slab

8.3 Experimental Setup

8.3.1 Test facility

The test was conducted at tower testing facility of Central Power Research Institute, Bangalore, India. The facility is generally and regularly used to perform monotonic load tests on full-scale transmission line towers. The test facility is well equipped with high strength cables, pulleys, calibrated load cells, electro mechanical winches with Programmable Logic Control (PLC) for accurate and simultaneous load application in a predefined pattern. It has to be noted that the facility could perform the test only in load-controlled mode. This may not truly be a limitation since the pre-peak curve is generally accepted to be more accurate in the case of load-control, though a displacement control is required to capture post-peak degradation. Therefore, it would be best to perform the test under load-control in pre-peak region and under displacement control in post-peak region. However, keeping in mind the technical capabilities of the facility and also financial and time considerations, the whole experiment was conducted in load-control mode.

The load was applied remotely by means of high strength cables passing through pulleys using electro-mechanical winches controlled through a programmable logic control PLC (SCADA) system. The applied loads were continuously monitored using tension-type load cells. Figure 8.14 depicts the structure being tested at the tower test facility.



Figure 8.14 Structure being tested at tower testing facility

8.3.2 Instrumentation

The instrumentation used in the experiment included:

- (i) Load cells to monitor and apply the load on the structure in controlled manner.
- (ii) Digital theodolites on either side of the structure (one towards CL 16 and one towards CL 20 side), to measure displacements and laser based displacement measuring devices to verify the recorded displacements.
- (iii) Strain gauges on reinforcement bars to obtain strain data (as mentioned above)
- (iv) Tilt meters for measuring member and joint rotations, which were mounted directly on the structure at the beam and column intersecting at the joint.
- (v) Digital dial gauges to provide information on surface strains at the base of the columns at raft level. It was anticipated that the strains will be maximum at the base of the columns and therefore, the survival of reinforcement strain gauges or concrete surface strain gauges was doubtful. Therefore, in order to obtain average surface strains over a gauge length, at the base of the columns, dial gauge potentiometers were installed on the tension side of all the four columns.

8.3.3 Loading sequence

The loading sequence during the test was kept such that the load in the first floor was increased in the steps of 1tn (9.81 kN). Thus, the load in the second floor was incremented with the steps of 2tn (19.62 kN), that in 3rd floor in steps of 3tn (29.43 kN) and in 4th floor in steps of 4tn (39.24 kN). Thus the ratio of 1:2:3:4 is always maintained.

8.4 Experimental results

The pushover curves as obtained for CL16 and CL20 are shown in Figure 8.15. Since the experiment was conducted under load control, the dropping part of the curves could not be obtained. Though the flat portion of Figure 8.15 cannot be used for evaluation of ductility or post-yield behavior, it is still provided in order to illustrate the effect of eccentricity of the columns on the global behavior of the structure. As it can be seen in Figure 8.15, the maximum displacement for CL16 side was equal to 537mm and that on CL20 was equal to 765mm. The considered structure is non-symmetrical in plan with one column (CL 19) section having its major axis perpendicular to the major axis of the other three columns (Figure 8.1).

This eccentricity and the loading arrangement design leads to a situation where the point of application of the resultant force at a particular floor does not coincide with the centre of rigidity of structure in plan. Therefore, as the lateral load is applied on the structure, the eccentricity between the point of application of resultant force and the centre of rigidity leads to storey twist in the structure (Paulay and Priestley, 1992). Since the stiffness of the frame formed by CL 19 and CL 20 is less than that of the frame formed by CL16 and CL20 side, the

storey twist results in larger displacements of the CL20 side than CL 16 side. The average top drift is equal to approximately 4% of the total height of the building.

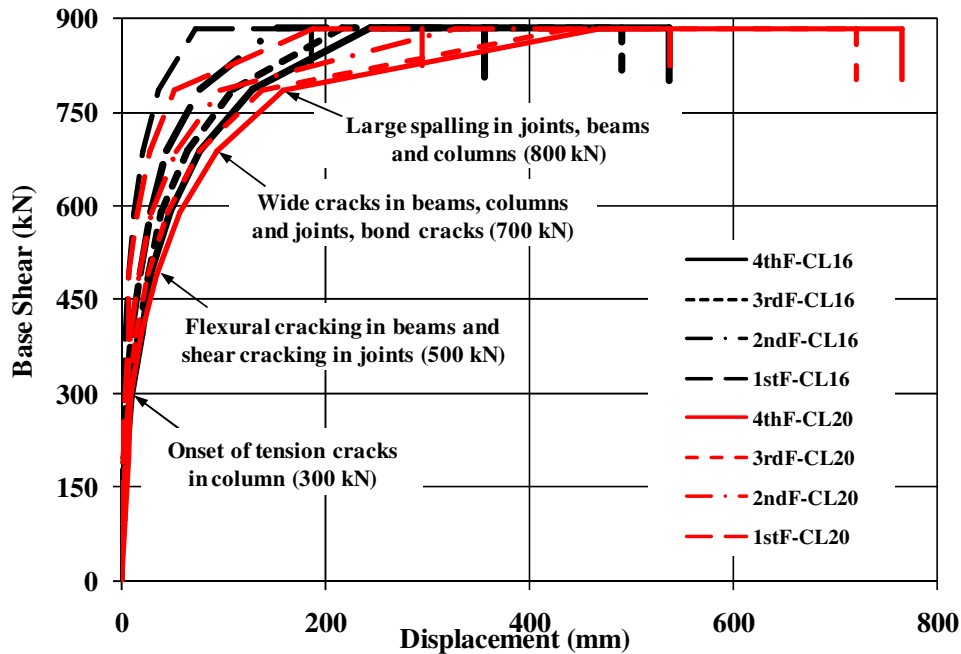


Figure 8.15 Experimental pushover curves obtained for the structure

When subjected to lateral forces, the structure acts as a vertical cantilever. The resulting total horizontal force and overturning moment is transmitted at the foundation level (Paulay and Priestley, 1992). It is evident that the structure behaved linearly up to a base shear value of approximately 300 kN. At this point the bending moments at the base of the columns caused the flexural tension cracks to appear and the structure displayed a reduced stiffness thereon (Figure 8.15). The structure possesses a strong column-weak beam configuration. On further increasing the load, at a base shear value of approximately 500 kN, the cracks at the base of the columns became wider and failures at other locations, namely beams and beam-column joints began to appear. As a result the stiffness of the structure further decreased, as it can be observed in the pushover curves. Though, the formation of hinges in beams after the hinge formation of the base of the columns results in a kinematically admissible mechanism (Paulay and Priestley, 1992), the failure of beam-column joints is undesirable. This is one of the prime weaknesses of non-seismically detailed structures. The joint failures are observed due to inadequate shear resistance of the core and/or poor bond behavior of bars extending into the joint, both brittle and undesirable failure modes for a structure. When the structure is subjected to cyclic loads, such failures lead to ill-formed hysteretic loops with significant pinching behavior, mainly due to slippage of reinforcing bars. Therefore, the energy absorbed by the structure due to hysteresis becomes significantly lower than that would be expected in a structure displaying only desirable beam flexural failure modes.

The failure of beam-column joints is inherently brittle and results in limited ductility, thus, degrading the seismic behavior of the overall structure as well. After reaching the base shear value of 700 kN, the joints of the structure displayed rapid degradation and the inter-storey drift increased progressively. On further increase of the lateral load, the structure displayed a very soft behavior with large displacement increase for the same increase in the base shear. For a base shear of 90tn (882.90 kN), i.e., 9tn load at first floor, 18tn at second floor, 27tn at third floor and 36tn at fourth floor, the structure started undergoing increasing displacement and its resistance reduced. However, due to load control, the load decrease could not be recorded. Hence, since the load could not be increased any further, the test was stopped and the load was removed.

Though, it is rather intuitive to deduce information on the seismic capacity of non-seismically detailed structures based on the results of the experiment, it must be noted that in this experimental setup no superimposed dead loads (e.g., floor finish), no live loads, no masonry walls, etc were included. Furthermore, the foundation of the structure was artificially fixed. These aspects prohibit a direct deduction on the seismic capacity, in terms of load or ductility, from this experiment. The objective of this experiment is to highlight the failure modes and the corresponding important aspects that must be considered while modeling the structure to obtain realistic predictions. Once an accurate and reliable simulation technique and numerical analysis procedure is established, it can be utilized to assess the seismic capacity of any real-life structure. Therefore, the above-discussed results were not used to draw any conclusions on the seismic capacity of structures with non-conforming detailing.

Figure 8.16 shows the displacement profiles of the structure due to the applied load. Each curve corresponds to the displacement profile of a particular load step. Initially, when the structure was loaded, it behaved fairly linearly till the third load step corresponding to a base shear of 300 kN. As the lateral load on the structure was increased, the inter-storey drift increased and the structure entered the inelastic (nonlinear) range. It was observed that as the displacement increases, the contribution of relative displacement between third and fourth floor is smaller which is attributed to the joint failure at the third floor level.

8.4.1 Failure patterns

Figures 8.17 to 8.19 show various failure modes and patterns observed during the experiment. As the test started, the initial cracks were observed on the tension face at the base of the columns and at the tension face on beam ends for the beam BF 205-1 at first floor level. The corresponding base shear at this step was approximately 300 kN. In the next step, the beam BF205-2, i.e., at 2nd floor level started to display cracks and also the already formed cracks at the column bases and beams became wider. However, up to this point the beam-column joints had no signs of distress. At a base shear equal to 500 kN, the first shear cracks started to appear at the beam-column joints at 1st floor level. These cracks opened with the further increase in the load and more cracks at higher elevation (2nd and 3rd level)

were also observed in the beams and beam-column joints. Additionally, at a base shear of approximately 500 kN, first cracks in the beam BF225-1 appeared at the ends of the beam near CL16 and CL20. Further increase in load led to significant widening of the existing cracks, spalling of concrete and formation of new cracks at upper floor levels. The failures at various locations in the structure at the peak load are described below.

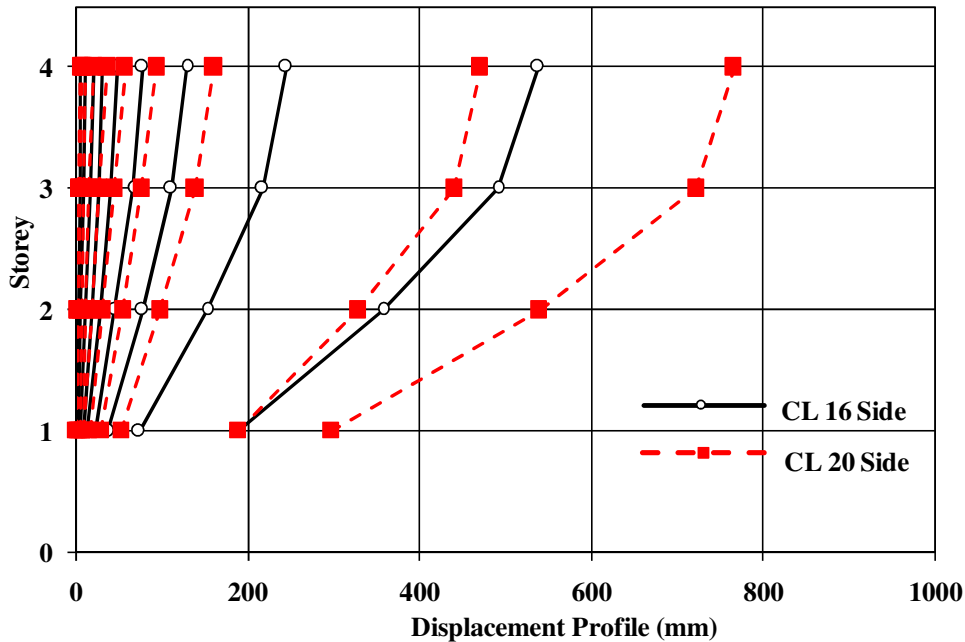


Figure 8.16 Displacement pattern for increasing top drift

Figure 8.17 (a and b) presents the failure of bottom storey columns on compression side, namely columns CL16 and CL20. The columns exhibited well-known failure modes of combined axial compression and bending. As the lateral load was applied and gradually increased on the structure, columns CL 16 and CL20 were exposed to increasing compressive forces combined with bending moment. Thus, due to this combined axial compression and bending, the column section started having tension cracks on the rear face. Further increase of the loads resulted in higher bending moments as well as axial forces on the column, and these tension cracks became bigger along the depth of the section due to the shifting of neutral axis towards the front face of the columns. Moreover, due to the shift of neutral axis, less area was available to resist higher compressive forces. Consequently, crushing of concrete on front face of the column occurred. The state of the columns at peak load is depicted in Figure 8.17 (a and b).

Figure 8.17 (c and d) illustrates the failure pattern of columns on tension side of CL15 and CL19, which were subjected to combined axial tension and bending moments. The columns were initially under compression due to self load of the building, but as the lateral load on the structure increased, the tensile forces on the two columns started to develop, along with bending moments. Under the action of the combined axial tension and bending moments, the

columns started developing cracks from the rear face of the columns that propagated as the load increased, towards the front face of the columns. The spalling on the front face was nominal compared to that of CL16 and CL20 and major tension cracks were observed.



(a) CL 16 (Flexure-Compression)



(b) CL 20 (Flexure-Compression)



(c) CL 15 (Flexure-Tension)



(d) CL 19 (Flexure-Tension)

Figure 8.17 Failure of columns at base under combined axial load and bending

Figure 8.18 (a) depicts the failure mode of the beam BF 205, which is connected to CL15 at 1st floor, in flexural mode combined with bond slippage of the beam tension reinforcing bars. Due to lateral loading, bending moments were generated in the beam with hogging moments towards the end fixed with column CL16 and sagging moments towards the end fixed with column CL15. As a result, flexural tension cracks were observed initiating from the soffit of the beam and propagating towards the slab as shown in Figure 8.18 (a). Due to high tensile stresses generated in the beam bottom bars, a slippage of the bars seems to have occurred. Spalling of concrete was observed on both the tension and compression faces of the beam due to extensive cracking and crushing, respectively.

Figure 8.18 (b) shows the failure of the beam BF 225, which is transverse to the direction of loading. As shown in Figure 8.12, the load was applied on the structure through the slabs of each floor. As the lateral load increased, the beams transverse to the direction of loading in the front, namely BR21 and BF225, were pushed by the slab. This push was resisted by the stiffness provided at the ends due to restraining action of columns CL16 and CL20. Due to the end restraints, the beams suffered high compatibility torsion moments at the fixed ends. Nevertheless, this is not a typical seismic failure mode, since it can be attributed to the design of loading arrangement.



(a) Flexural failure of beam BF 205-1



(b) Torsional failure of beam BF223-1

Figure 8.18 Failure modes observed in beams of the structure

Figure 8.19 presents different types of joint failures observed in the structure. Under the action of lateral forces, beam-column joints are subjected to large shear stresses in their core. Typically, high bond stress requirements are also imposed on reinforcement bars passing through the joint. The axial and joint shear stresses result in principal tension and compression that leads to diagonal cracking and/or crushing of concrete in the joint core. The flexural forces from the beams and columns cause tension or compression forces in the longitudinal reinforcements passing through the joint. During plastic hinge formation, relatively large tensile forces are transferred through bond. When the longitudinal bars at the joint face are stressed beyond yield, splitting cracks are initiated along the bar at the joint face. If the concrete cover of the reinforcement bars is inadequate and if the joint core is not confined by confining reinforcement in the form of stirrups, the cover concrete is spalled off due to the pressure exerted by the beam reinforcement bars. Most severe joint failures were found in the case of column CL 19. This might be attributed to the relatively low column depth (400mm) compared to beam depth (1000mm). In such cases, plasticization of columns can occur, which may also lead to damage ingress in the joint core. Moreover, there was high eccentricity between the beam and the column, since the beam of width 230mm was joined at the face of the column having width of 900 mm.

Figure 8.19 (a) illustrates the failure of joint of CL 19 at first floor. High stresses in the joint resulted in diagonal cracks in the core, followed by cover spalling due to the pressure exerted by the beam longitudinal reinforcement. Figure 8.19 (b) shows the failure of joint of CL 19 at 2nd floor level, which shows the beam bar bursting out of the joint. This is a typical failure mode for joints with unrestrained bars. This occurred since in order to provide the development length of the beam main reinforcement, the bent bars had a long free length beyond the bending length and there were no transverse reinforcement to provide any restraint at this region. Such a failure can, in general, be prevented if proper confining reinforcement is provided in the joint core. Figure 8.19 (c) depicts the failure of the joint of CL16 at first floor level that exhibited bond failure along with beam flexural failure and spalling of side cover due to pressure exerted by the reinforcement. High tension force in the beam reinforcement resulted in bond deterioration and ultimately failure with splitting of concrete. Furthermore, large cracks along with spalling of concrete can be observed at the beam-column interface. Figure 8.19 (d) shows a typical diagonal (shear) crack in the joint of CL16, 2nd floor with flexural cracks in the beam. The diagonal cracks in the joints are formed due to principal tensile stresses generated as a result of axial and joint shear stresses. As the lateral forces were increased on the structure, the joint shear stress increased and in combination with the axial stresses, resulted in diagonal tension that was responsible for the development of diagonal tension cracks. Figure 8.19 (e) presents diagonal shear crack in the joint of CL20, 2nd floor during the test with flexural cracks in the beam and bond failure of the tension reinforcement. It can be observed that a clear diagonal shear crack appeared in the joint during the test, but it was not further opened and essentially the failure was transferred through bond mechanism. Although the beam longitudinal reinforcement was bent up to the required development length inside the column, it appears that such bending may not be adequate to prevent bond failure.

8.4.2 Inter-storey drifts

Figure 8.20 illustrates the inter-storey drifts between ground to 1st floor, 1st to 2nd floor and so on, as a function of base shear on CL 16 side. Furthermore, in the same plot, the roof drift obtained as the lateral roof deflection divided by the total height of the structure is given. Maximum inter-storey drifts were obtained between the ground to first floor and first to second floor and were of the order of 4.5%. Drifts between second to third floor was equal to 3.5%, which was also the order of global drift. The inter-storey drifts between the third and roof level were in the range of 1-1.5%, which explains why greater damage levels were concentrated within lower floors.



(a) Joint shear failure of CL 19 (1st floor)



(b) Beam bars bursting out of cover for the joint of CL 19 (2nd floor)



(c) Flexural and bond failure of beam at joint CL16 (1st Floor)



(d) Joint shear cracking and flexural cracking of beam at CL16 (2nd floor)



(e) Joint shear, beam-flexure and bond failure of beam bars at CL20 (2nd floor)

Figure 8.19 Failure modes observed in beam-column joints of the structure

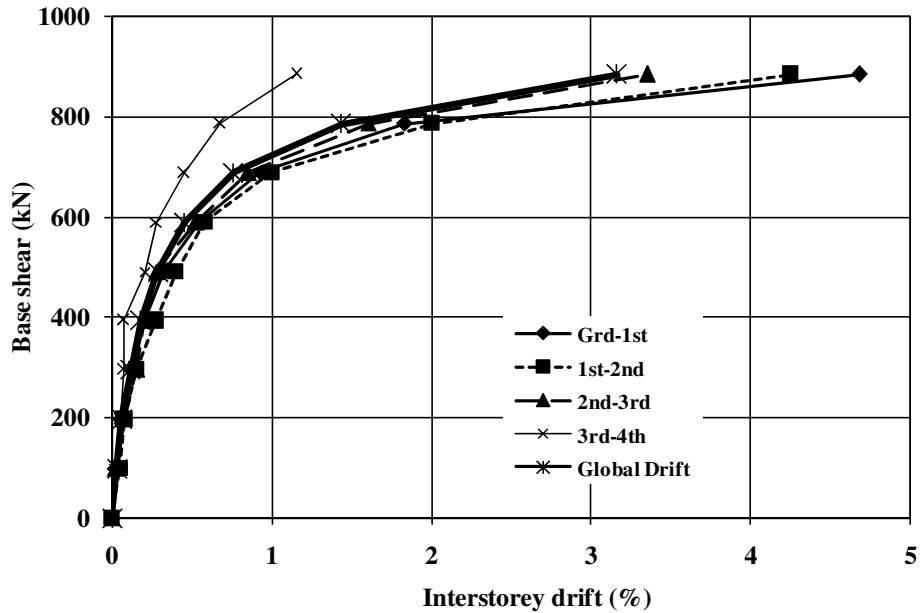


Figure 8.20 Inter-storey drift as a function of base shear

8.4.3 Strain data

The average beam bar strains of beams BF 205 are plotted in Figure 8.21 for 1st, 2nd, 3rd and 4th floor levels of the structure. The plot clearly shows that as the base shear increased, the average beam bar strain increased almost linearly up to a base shear value of 500 kN and thereafter going in the non-linear range.

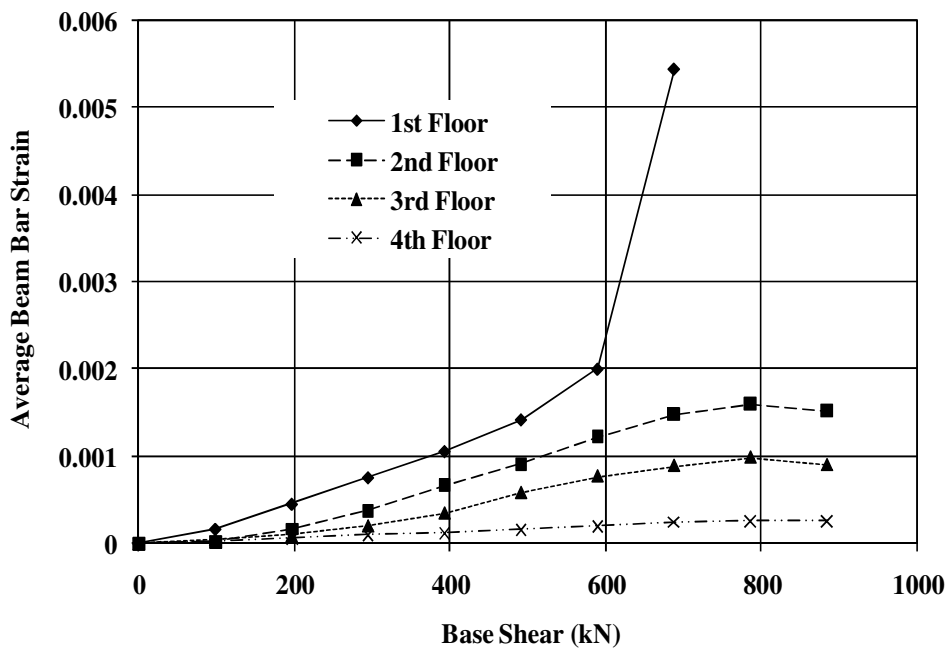


Figure 8.21 Average beam re-bar strains for BF 205 at different floor levels

As expected, the maximum strains were obtained at 1st floor level and the strain gauges at that level broke after the yielding of the reinforcement bars. These strain gauges could read only up to a base shear of 700 kN. The strain gauges at other floors did not show very high values, which is mainly due to the fact that the failure modes at second and third floors were mainly governed by the bond failure of beam bars and the shear failure of the joint. The fourth floor beams were almost undamaged.

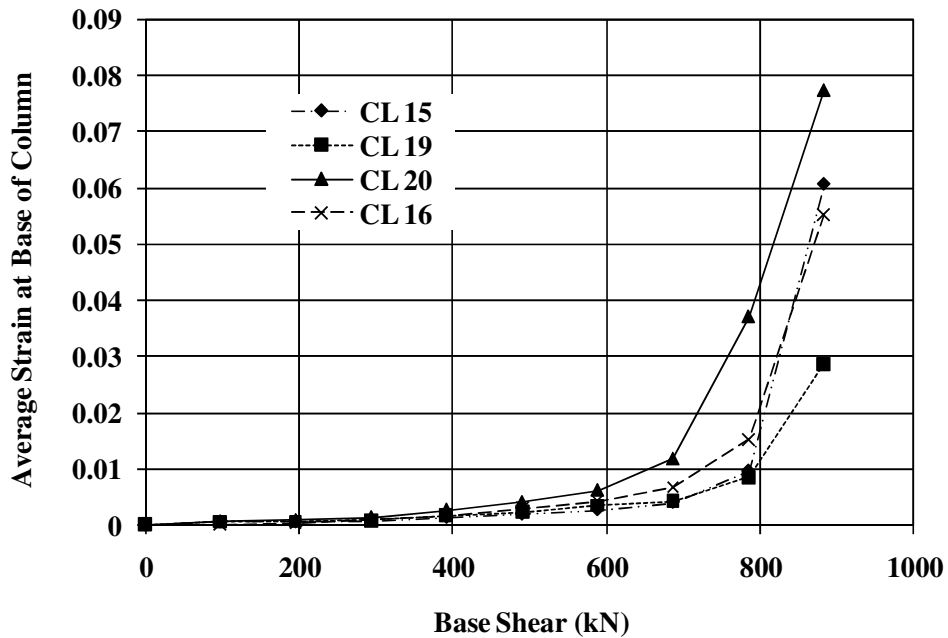


Figure 8.22 Average surface strains at the base of the columns

As discussed earlier, the dial gauges were installed on the tension face of the columns at the base. The dial gauges read the total extension over a gauge length, which was then converted to average surface strains at the base of the columns and plotted in Figure 8.22. It can be observed that the average strains grow linearly with base shear up to a base shear of approximately 400-500 kN, and thereafter start to increase at a higher rate. The rate of increase of strain becomes very high after a base shear of 700 kN. As expected and verified by failure modes, column CL 19 has minimum strains.

8.4.4 Rotations

The tilt meters were used in order to get the information on the rotation of members and joints. The relative rotation between beams and columns framing into the joints of CL15 and CL19 for different floors are given in Figure 8.23. Since the tilt meters were placed very close to the joint faces on beams and columns, this relative rotation is also a measure of rotation (shear distortion) of the joint. It is clear that the relative rotation is higher for the joints of CL19, which is attributed to the low column depth as compared to that for the joints of CL15.

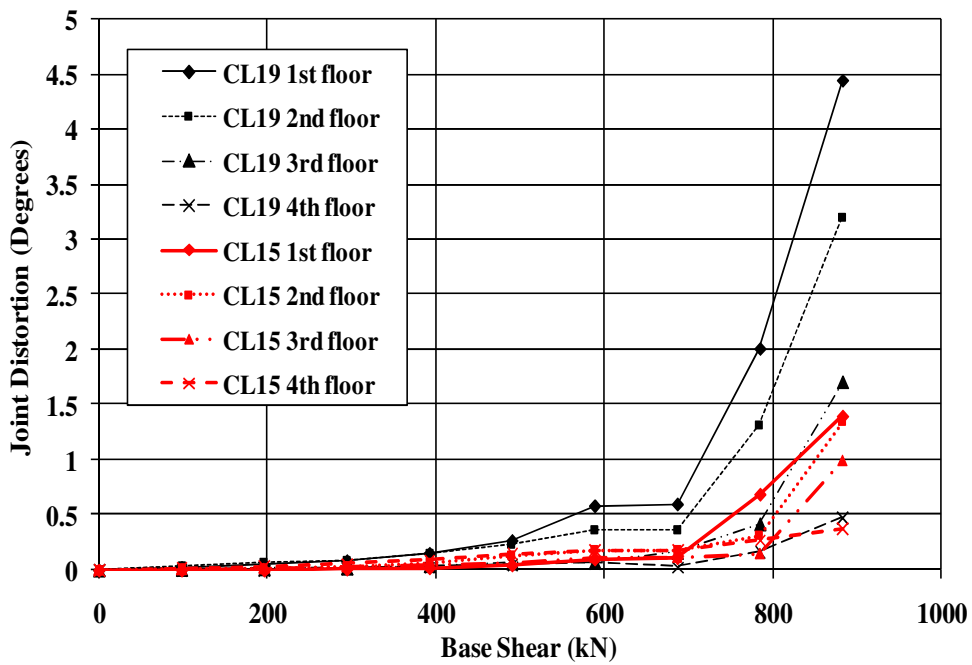


Figure 8.23 Relative rotations of beams and columns framing into joints of CL 15 and CL 19

Figure 8.24 shows the average tilt of the columns at various floors. In addition, the tilt increased till third floor and reduced in the case of fourth floor, which is also easily detected in the deflection profile of the structure.

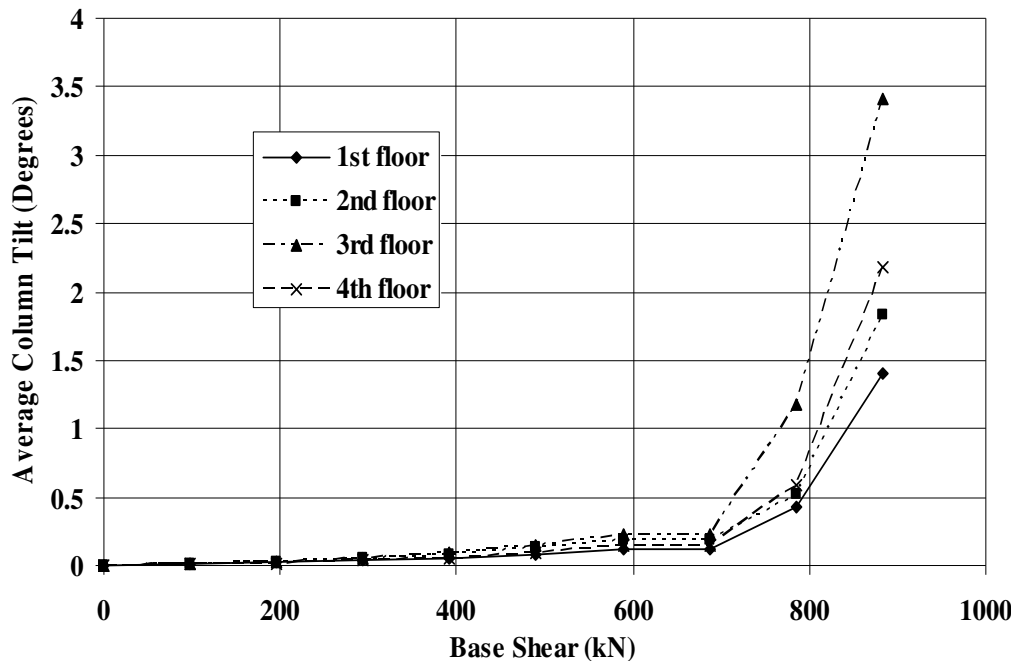


Figure 8.24 Average tilt of the column of the structure

8.5 Summary of the experiment

In this study, a full scale experiment was conducted on a RC frame which was a replicate of a substructure of an existing office building in India. The structure was constructed with non-seismic detailing and the foundation was constructed with rock anchors to avoid any possible rotation during the experiment. The failure patterns displayed the vulnerability of RC buildings with non-conforming detailing which tend to fail in undesirable failure mechanisms, such as joint shear failures, bond failures, etc.

The experiment was used as a benchmark problem to validate the modeling aspects for non-seismically detailed RC structures. The numerical modeling aspects of the same are discussed in chapter 12. It has been shown that in order to capture the overall behavior of RC structures, neglecting the inelasticity in the joints can lead to inaccurate results.

9. EXPERIMENTAL PROGRAM ON AS-BUILT RC FRAMES UNDER DYNAMIC LOADING (SHAKE TABLE TESTS)

In Chapter 7, an experimental program on RC exterior beam-column joints was discussed. The test program clearly displayed that non-seismically designed beam-column joints are highly vulnerable against seismic loads. Experiment at the full-scale RC frame structure as discussed in Chapter 8 further strengthened this opinion. The aim of the experiment at the full scale RC frame structure was to understand the various failure modes in the structure along with interactions and to provide database for validation of models explained earlier. However, the experiment was performed under pushover loads and also did not correspond directly to the tests on joints discussed in chapter 7.

To understand the real behaviour of beam-column joints in structures under seismic loads, shake table tests were performed on 2D RC frame structures. In order to have a direct comparison with the experiments at sub-assembly level discussed in chapter 7, the basic design of the frames was performed so that the exterior joints of the frames are 2/3rd scale replica of the joints tested earlier.

The objectives of this test were:

- (i) to understand the behaviour of RC structures (especially joints) under real seismic situation;
- (ii) to serve as the control specimen for the verification of haunch retrofit solution under seismic loads;
- (iii) to provide database for validation of models discussed earlier

9.1 Description of Test Structure

9.1.1 Geometry

The geometry of the structure considered for the experiments is shown in Figure 9.1. The structure is a plane frame RC structure with two storey and one bay configuration. The sizes and reinforcement details of the structural elements were decided so that a typical exterior joint of the structure corresponds to 2/3rd scale of the joint subassembly tested earlier (Chapter 7).

Typical non-seismic design philosophy was followed for the structure. The beam section was 200mm x 270mm while the column section was 230mm x 200mm. The details of the beam and column sections for the structure are given in Figure 9.2. The clear cover to reinforcing bars of beam was kept as 20mm while that for column was kept as 25mm. The beam reinforcement bars were bent in to the joint core for all the joints. The details of the corner and exterior beam-column joints of the frame are shown in Figure 9.3.

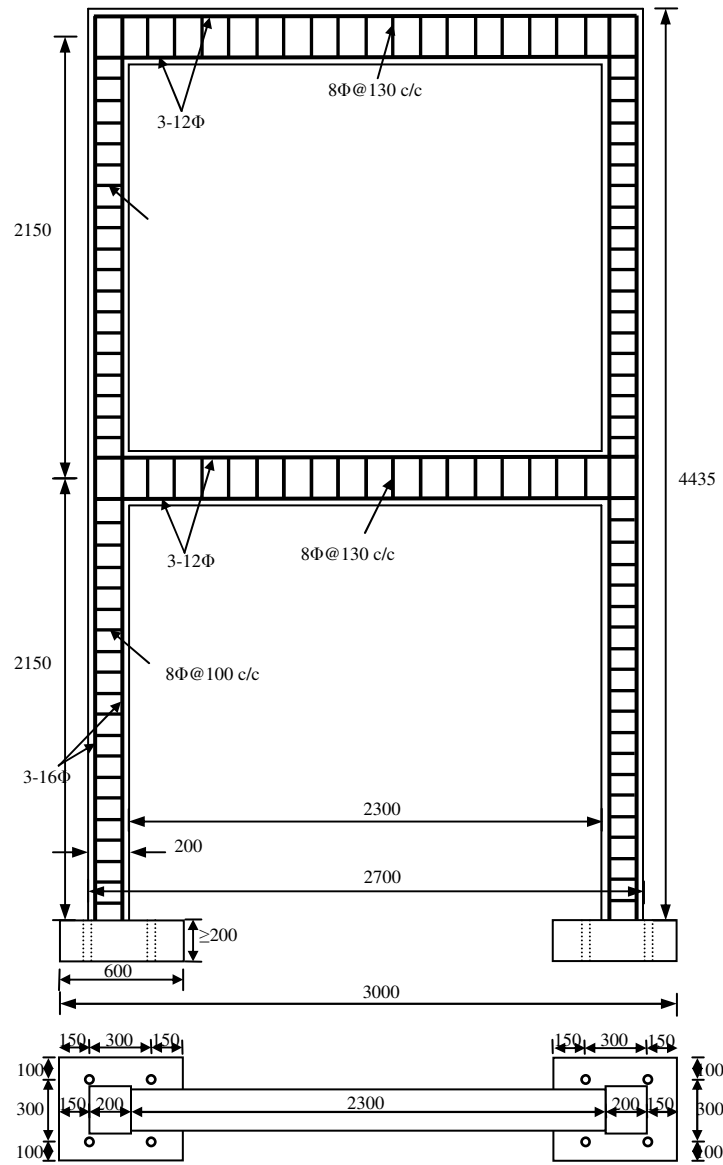


Figure 9.1 Geometry of the frame structure

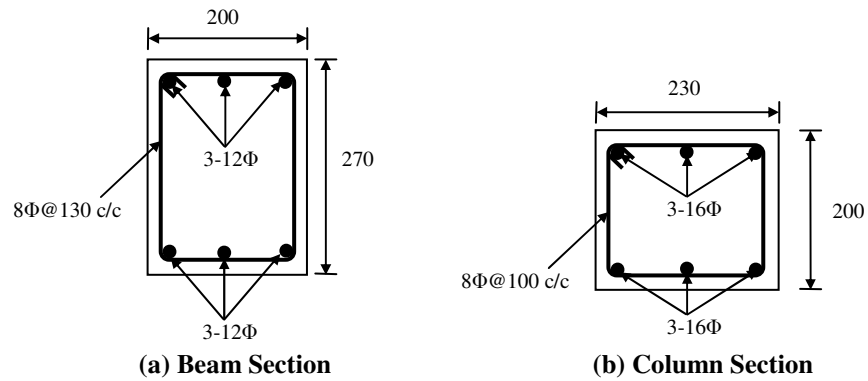


Figure 9.2 Section Details for the structure

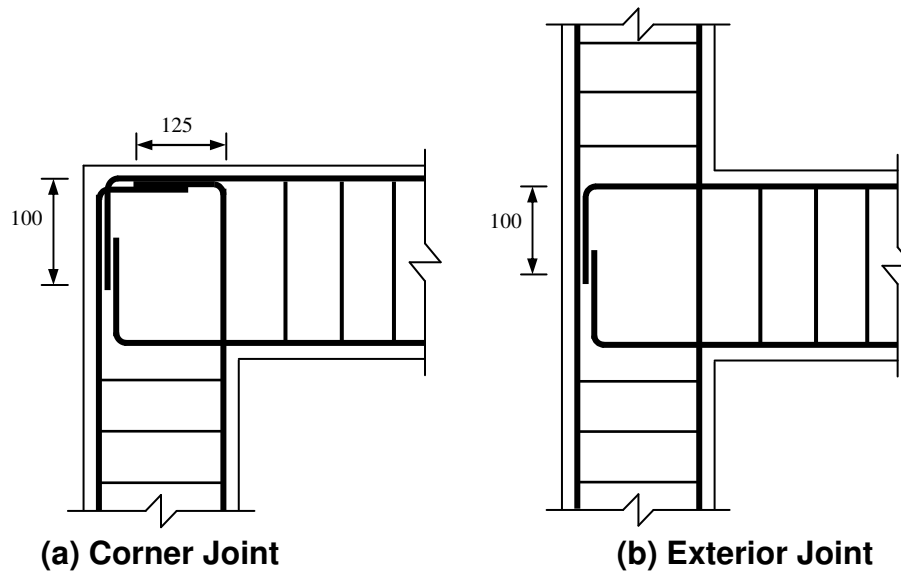


Figure 9.3 Joint Details

9.1.2 Material Properties

The average cubic concrete compressive strength at the day of testing was obtained as 28.29 MPa for as built specimen. The properties of the reinforcing bars are tabulated in Table 9.1.

Table 9.1 Properties of reinforcing bars used for construction of frames

Bar Diameter (mm)	Yield Strength, f_y (MPa)	Ultimate Strength, f_u (MPa)	Elongation (%)
8	526	608	24
12	541	619	21
16	507	614	22

9.2 Scaling Philosophy

As mentioned earlier, the test structure under this program was designed in such a way that an exterior joint of the same corresponds to $2/3^{\text{rd}}$ scale model of the beam-column joints tested earlier as described in chapter 7. One of the biggest technical limitations of the shake table tests is to design the structure suitable enough to represent the real life structures without much distortion. Mostly this limitation comes due to the size and weight capacity of the shake table. Though, theoretically it would be possible to design a specimen that can almost accurately simulate the real life structure at a smaller scale by following dimensional analysis (Buckingham, 1914), the construction of a ‘true replica’ model that satisfies all the similitude requirements needed by dimensional analysis is almost an impossible task due to material limitations (Morcarz et al, 1981; Quintana-Gallo et al 2010). Therefore, the challenge is to design a least distorted model within the constraints of shake table capacity and material availability. The scaling was performed using the following principles.

9.2.1 Linear Dimension Scaling

As mentioned earlier, due to the shake table size limitation, a linear scale factor of $S_L = 1/(2/3) = 1.50$ was enforced. While scaling, the point of contraflexure was assumed at mid column height and mid beam length. Thus, the centre-to-centre beam length for the structure was obtained as (refer Figure 7.2) $1875 \times 2/S_L = 2500\text{mm}$. Similarly the centre to centre column height was obtained as $3260/S_L \approx 2150\text{mm}$. The beam width was obtained as $300/S_L = 200\text{mm}$ and depth as $400/S_L \approx 270\text{mm}$. Column width was calculated to be $350/S_L \approx 230\text{mm}$ and column width as $300/S_L = 200\text{mm}$.

9.2.2 Material Scaling

The materials for construction of the frame were kept similar to the materials used for construction of beam-column joints and no scaling was done. However, certain variation in the material properties was inevitable. The actual material properties of both concrete and reinforcing steel for beam-column joints and frame structure were reported in the respective sections. However, to maintain similitude, the maximum size of aggregate (msa) of around 14mm was used in concrete for construction of frame structure (corresponding to msa of 20mm in case of beam column joints).

9.2.3 Reinforcement Area Scaling

According to similitude requirements (Sabnis et al, 1983), the required model reinforcement area, A_m to provide the scaled bar yielding force is calculated as

$$A_m = \frac{A_p}{S_{FS} \times S_L^2} \quad (9.1)$$

Where,

A_p = Area of reinforcement in prototype (in this case joint)

A_m = Area of reinforcement in model (frame structure)

S_L = Linear scaling factor = 1.5

S_{FS} = Strength scaling factor for steel (= 1.0 in this case)

The number of bars in beams and columns of the frame structure were kept same as the number of bars in beams and columns of the joints. The model reinforcement area were scaled according to the law given by eq (9.1), though, a perfect scaling could not be done due to size and type of reinforcements available.

9.2.4 Mass Scaling

Since the density and modulus of elasticity of the concrete in prototype and model were essentially equal (at least theoretically), a mass simulation approach suggested by Quintana-Gallo et al (2010) that corresponds to an extension of what is suggested by Morcarz et al. (1981) was followed. The additional inertial mass on the i^{th} floor level in the model structure, ΔM_i corresponding to a unit mass in prototype is given by eq (9.2).

$$\Delta M_i = \frac{1}{S_L^2} \left(1 - \frac{1}{S_L} \right) \quad (9.2)$$

Therefore for every ton of mass located at a storey level of the prototype structure, 0.148 tons of mass was to be applied at the corresponding storey level for model structure. The total mass placed at each storey was 1.0 tonnes.

9.3 Test Setup

The experiment was performed under real dynamic loads using the shake table. Shake table tests provide the base acceleration which generates the inertial forces due to the mass in the structure, as in the case of real earthquakes.

9.3.1 Test Facility

The experiment was carried out at the tri-axial shake table system at the Earthquake Engineering and Vibration Research Centre (EVRC) of Central Power Research Institute (CPRI), Bangalore, India. The system features a 100kN payload capacity shake table of all-welded steel construction with an advanced control system which allows the reproduction of earthquake ground motions with high precision on specimen of maximum size 3m x 3m and height up to 10m. Figure 9.4 shows the shake table system at CPRI. Though, the table is capable of reproducing three dimensional earthquake excitation, in this work only unidirectional tests were performed due to the 2D geometry of specimen and to have a direct comparison with the beam-column test results.

9.3.2 Support Structure

Although the shake table is capable of accurately producing unidirectional excitation, certain out of plane small vibrations are inevitable. Since the test structures were two dimensional, there was a possibility to experience the out of plane movement under dynamic loads. In order to prevent any accidental out of plane movement of the 2D frame structures, two steel frames were fabricated and the same were placed on either side of the frame on shake table.

Figure 9.5 shows the steel frames used as support structure. The frames were provided with rollers, capable of rolling about vertical axis, at the first and top storey level.



Figure 9.4 3D Shake Table at CPRI Bangalore

9.3.3 Added Mass on the structure

In order to simulate the floor mass, 1.0 tonnes of mass was added at each floor level. The mass was fabricated using various steel sections welded together. The fabricated mass was placed on the structure using overhead crane and fork lift (Figure 9.6). The centre of the mass was around 200 mm from the top of the beam. The flanges of the mass were tightly bolted so that the mass has a tight grip on the beam and slipping is prevented.



Figure 9.5 Support structures to prevent out of plane movement



Figure 9.6 Added mass being placed on the structure

9.3.4 Layout on shake table

Figure 9.7 shows the layout of the test structure and supporting structure on the shaking table. The shaking table has a grid of holes at 300mm c/c spacing to which the foundation of the test structure was bolted. The supporting structures were placed on either side of the frame in such a way that the rollers at each floor level just barely touched the flange of the mass to prevent out of plane motion. Figure 9.8 shows the close up view of the rollers on supporting structures touching the flange of the mass.



Figure 9.7 Layout on Shake Table

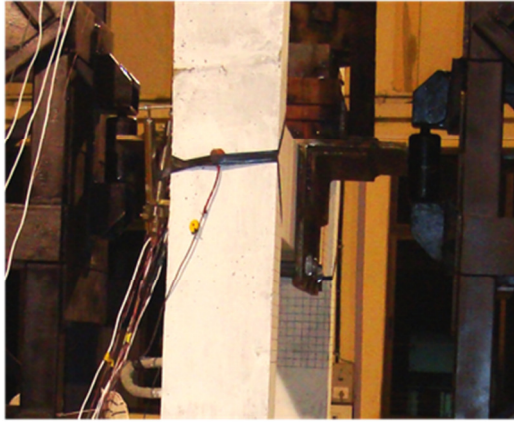


Figure 9.8 Close up view of rollers to prevent out of plane movement

9.4 Instrumentation

The instrumentation for the 2D frame consisted of the following:

- Accelerometers at each floor to measure the response acceleration history
- Accelerometers at the shake table to record the input time history
- Strain gauge on reinforcing bars to measure strains at critical locations
- Potentiometers to measure beam, column and joint deformations

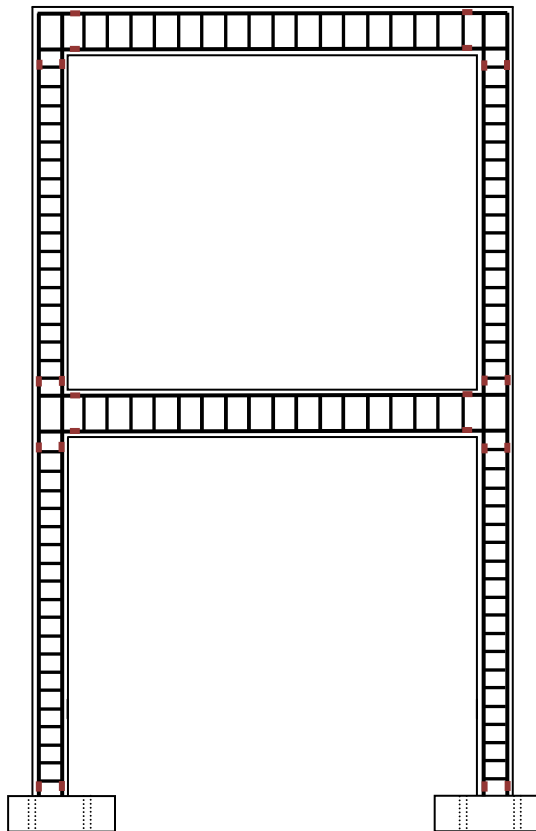


Figure 9.9 Location of strain gauges in as-built frame

The strain gauges were provided on the reinforcing bars of beams and columns at all critical locations, where bending moments and hence strains, shall be maximum. Figure 9.9 shows the locations for strain gauges on reinforcing bars for the structure.

To evaluate the element deformations, linear potentiometers were used. In a typical exterior joint, total eight potentiometers were used, two for beam, four for column and two for joint. For corner joints, six potentiometers were used, two for beam, two for column and two for joint. Two potentiometers were used at the column base to measure the elemental column deformations at the fixed base. Figure 9.10 shows the schematic arrangement of potentiometers used in the experiment. The elemental deformations were evaluated using the readings of potentiometers as explained in chapter 8.

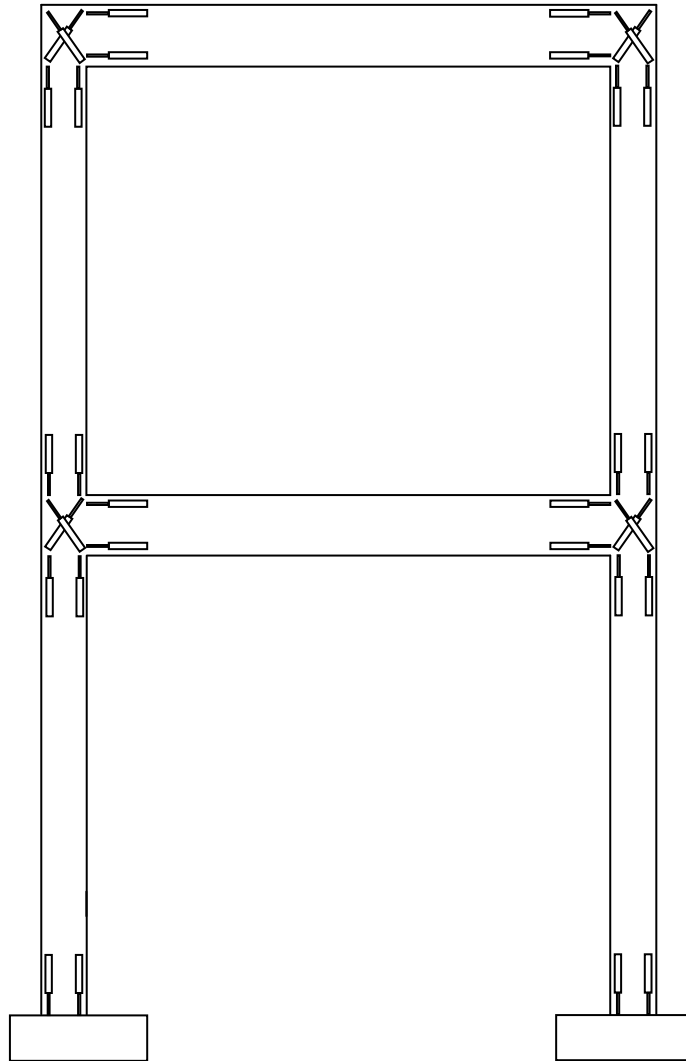


Figure 9.10 Arrangement of potentiometers used in the test

9.5 Loading Pattern and test matrix

The experiments were performed under uni-directional earthquake excitation. The acceleration time history was provided to the shake table. The time history compatible to the shape of the site specific response spectrum used for seismic design of safety related structures in Mumbai was used in the tests. Figure 9.11 shows the 5% damped target response spectrum for a peak ground acceleration (PGA) of 0.2g and the achieved response spectrum as obtained by the compatible acceleration time history, which was used in the experiment (Figure 9.12).

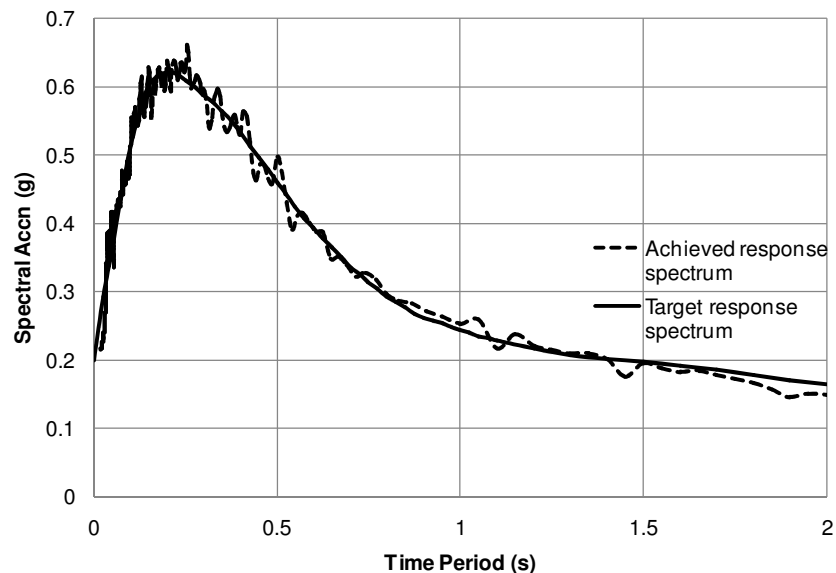


Figure 9.11 Response spectrum corresponding to 0.2g PGA and 5% damping used as target response spectrum for the experiment

After completing the test setup, initially a sine sweep loading was provided to the structure. The maximum acceleration of the sine sweep loading was kept as 0.1g and the frequency of sinusoidal loading wave was swept from 0.1Hz to 50 Hz at the rate of one octave per minute, i.e. the frequency of loading wave got doubled in one minute. The natural time periods were obtained by the half power bandwidth method (Chopra, 1995).

Once the sine sweep test was over, the structure was then subjected to simulated seismic loading by providing the acceleration time history corresponding to the spectral shape as shown in Figure 9.11. The tests started with the time histories corresponding to the PGA of 0.1g and gradually it was increased in steps of 0.1g till 1.0g, which was the limit of the shake table facility. After each loading wave, the test was paused to mark the crack patterns on the structure. Table 9.2 shows the test matrix of the experimental program.

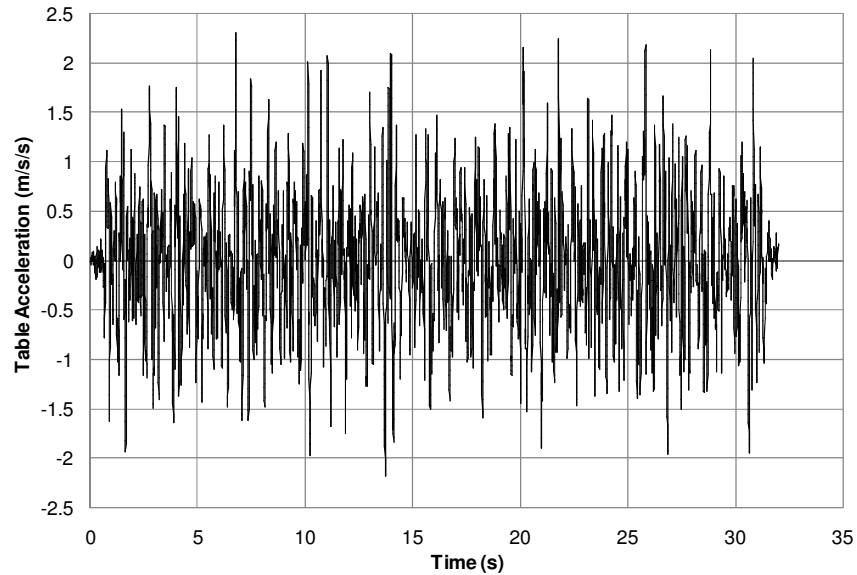


Figure 9.12 Input Time history corresponding to 0.2g PGA used for the experiment

Table 9.2 Test Matrix of experimental program

S. No.	Ground Motion	PGA (g)
1	Sine sweep 0.1Hz to 50 Hz @1 octave /min	0.1
2	Simulated Seismic	0.1
3	Simulated Seismic	0.2
4	Simulated Seismic	0.3
5	Simulated Seismic	0.4
6	Simulated Seismic	0.5
7	Simulated Seismic	0.6
8	Simulated Seismic	0.7
9	Simulated Seismic	0.8
10	Simulated Seismic	0.9
11	Simulated Seismic	1.0

9.6 Experimental Results

9.6.1 Natural time periods of the structure

As mentioned above, the structure was first subjected to a sine sweep test to evaluate the natural time periods/frequencies of the structure. The time period corresponding to the first mode was obtained as 0.31 seconds (3.22 Hz), while the same for second mode was obtained as 0.076 seconds (13.13 Hz).

9.6.2 Simulated seismic test with PGA = 0.1g

The structure was subjected to a base excitation corresponding to a PGA of 0.1g. The responses in the form of acceleration time history at both the floors were recorded using accelerometers. Figure 9.13 represents the acceleration time history recorded at first floor and Figure 9.14 depicts the same recorded at the roof.

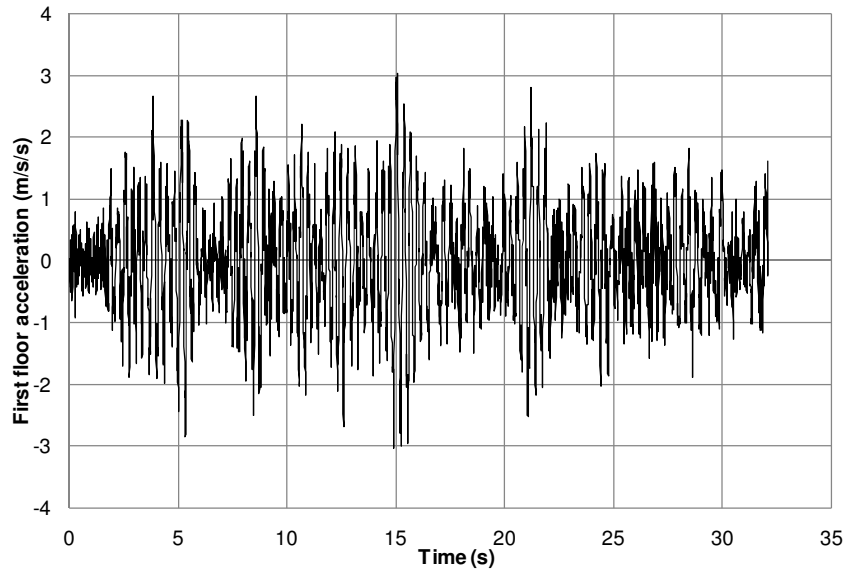


Figure 9.13 Recorded acceleration-time history at the first floor level for input ground motion corresponding to PGA = 0.1g

The peak floor acceleration was obtained as 3.03 m/s^2 for first floor and 4.82 m/s^2 for roof level. During the ground motion of 0.1g, no cracks were observed in the structure suggesting that the structure behaved essentially in linear elastic fashion.

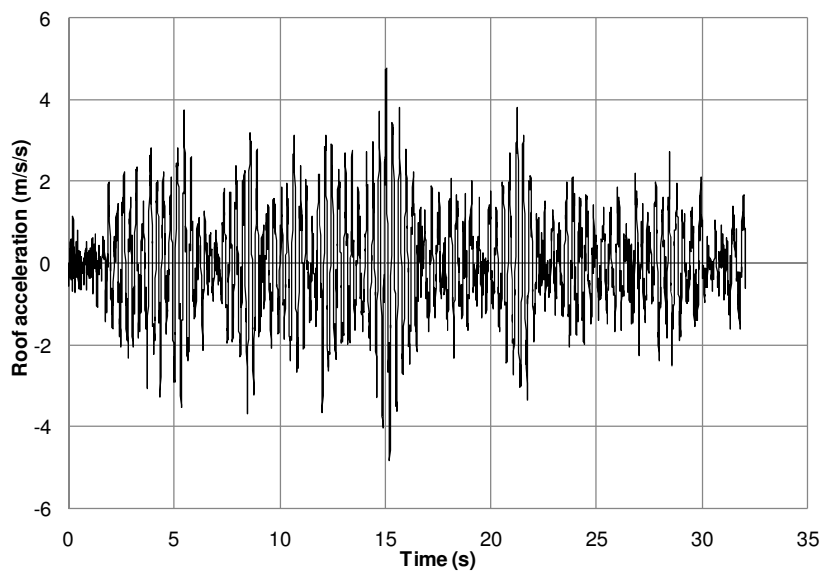


Figure 9.14 Recorded acceleration-time history at the roof level for input ground motion corresponding to PGA = 0.1g

9.6.3 Simulated seismic test with PGA = 0.2g

The structure was next subjected to a base excitation corresponding to a PGA of 0.2g (Figure 9.11). Figure 9.15 represents the acceleration time history recorded at first floor and Figure 9.16 depicts the same recorded at the roof.

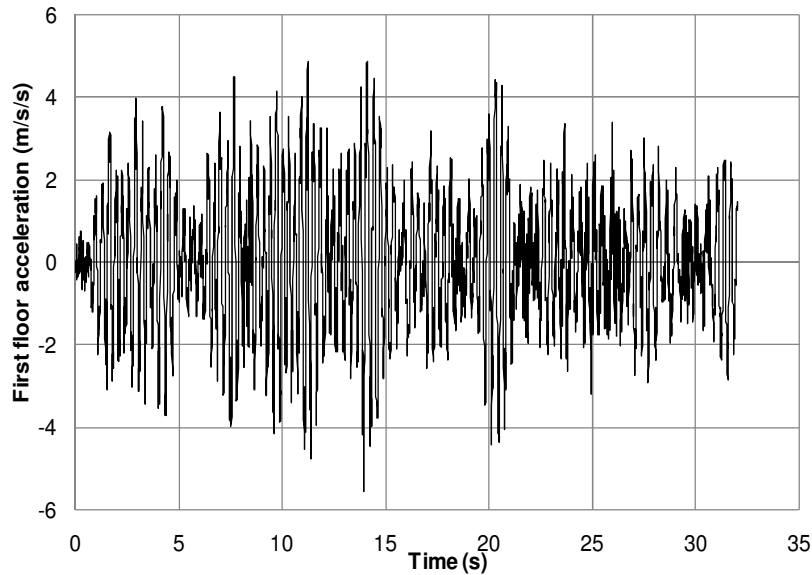


Figure 9.15 Recorded acceleration-time history at the first floor level for input ground motion corresponding to PGA = 0.2g

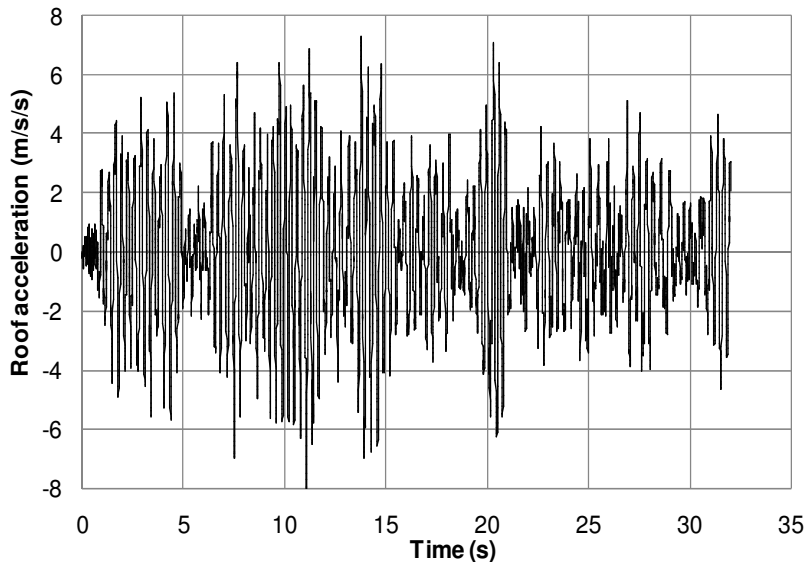


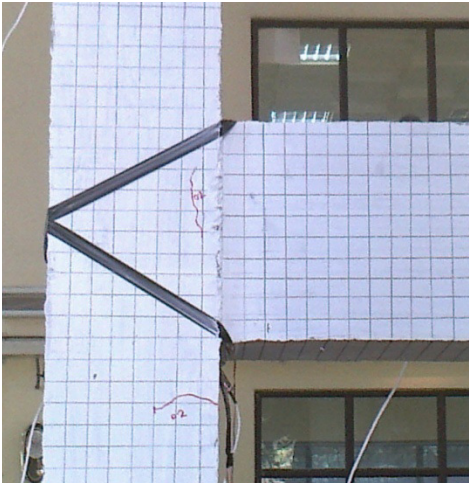
Figure 9.16 Recorded acceleration-time history at the roof level for input ground motion corresponding to PGA = 0.2g

The peak floor acceleration was obtained as 5.58 m/s^2 for first floor and 8.14 m/s^2 for roof level. Since on doubling the input acceleration, the peak floor acceleration is not doubled, it suggests cracking of concrete in the structure. This is confirmed by the crack initiation in the

structure as shown in Figure 9.17. The very first cracks, as expected, appeared at the base of the column (Figure 9.17a) and on the column just below the first floor beam (Figure 9.17b).



(a) At the base of the column



(b) At column and beam ends of 1st floor

Figure 9.17 Crack patterns observed after the base excitation of 0.2g

9.6.4 Simulated seismic test with PGA = 0.3g

Figure 9.18 represents the acceleration time history recorded at first floor and Figure 9.19 depicts the same recorded at the roof corresponding to the input ground motion with a PGA of 0.3g. The peak floor acceleration was obtained as 8.27 m/s² for first floor and 11.98 m/s² for roof level.

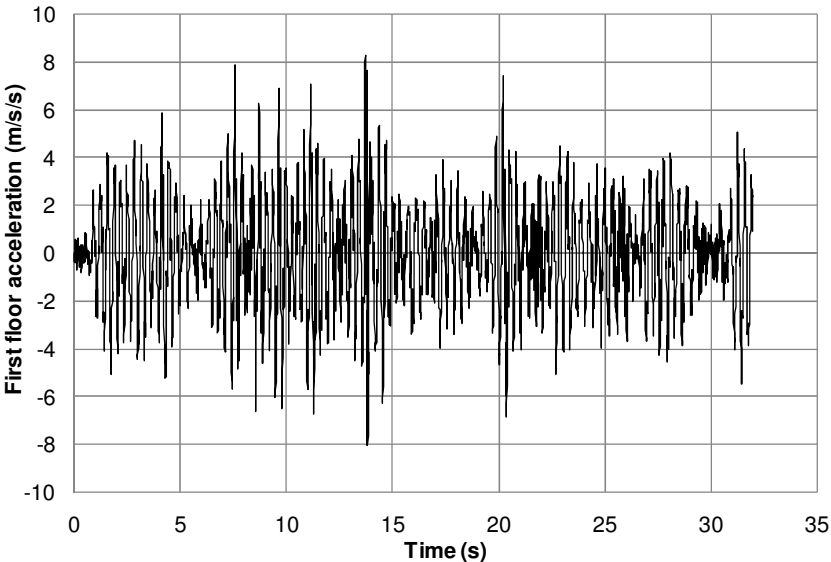


Figure 9.18 Recorded acceleration-time history at the first floor level for input ground motion corresponding to PGA = 0.3g

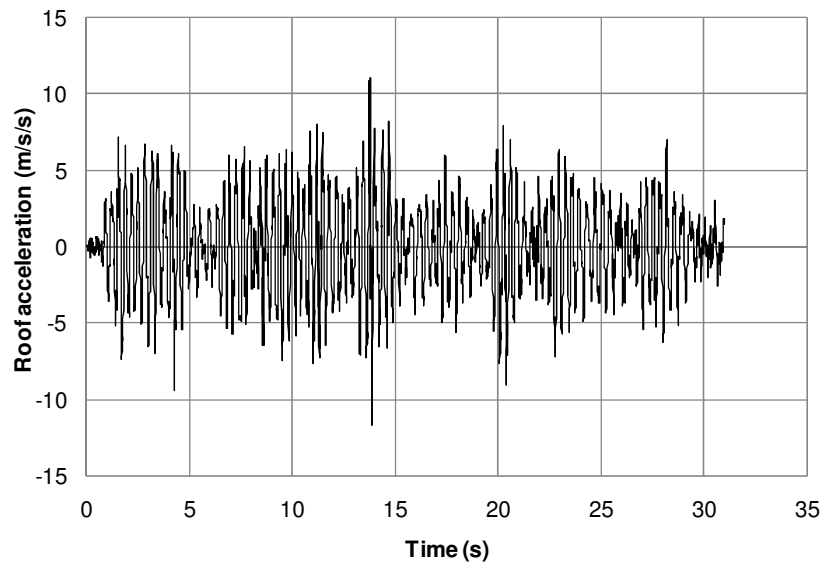
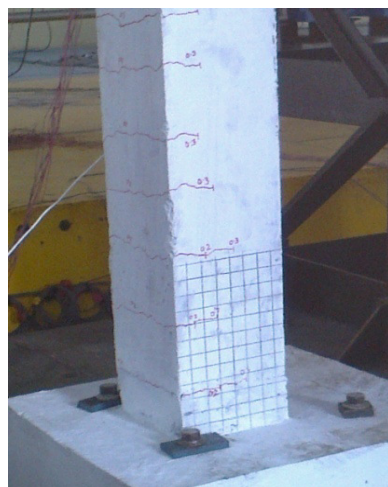


Figure 9.19 Recorded acceleration-time history at the roof level for input ground motion corresponding to PGA = 0.3g

The crack patterns observed after the loading wave corresponding to a PGA of 0.3g are presented in Figure 9.20. Several new cracks at the base of the column on tension face were observed (Figure 9.20a). At the beam of first floor level, the earlier formed cracks were extended (Figure 9.20b), and minor cracks extending into the joint core on right side beam were observed. It is well known from the fundamental structural mechanics that for such frame structures subjected to lateral loads as in case of earthquakes, the maximum bending moments occur at the base of the structure which is the reason for typical flexural cracking at the base of the columns.



Left Side Column



Right Side Column

a) At the base of left column



Left Side



Right Side

(b) At column and beam ends of 1st floor

Figure 9.20 Crack patterns observed after the base excitation of 0.3g

9.6.5 Simulated seismic test with PGA = 0.4g

Figure 9.21 shows the acceleration time history recorded at first floor and Figure 9.22 depicts the same for the roof corresponding to the input ground motion with a PGA of 0.4g. The peak floor acceleration was obtained as 11.21 m/s^2 for first floor and 15.34 m/s^2 for roof level.

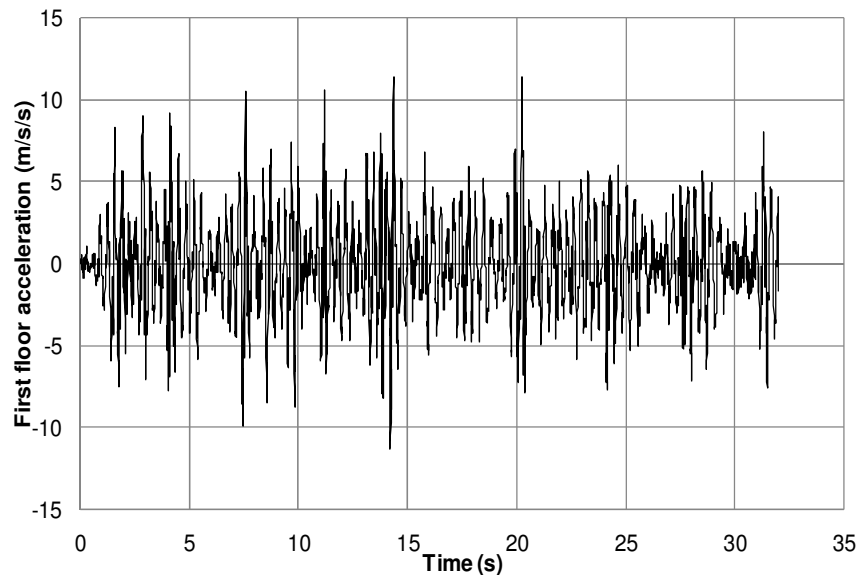


Figure 9.21 Recorded acceleration-time history at the first floor level for input ground motion corresponding to PGA = 0.4g

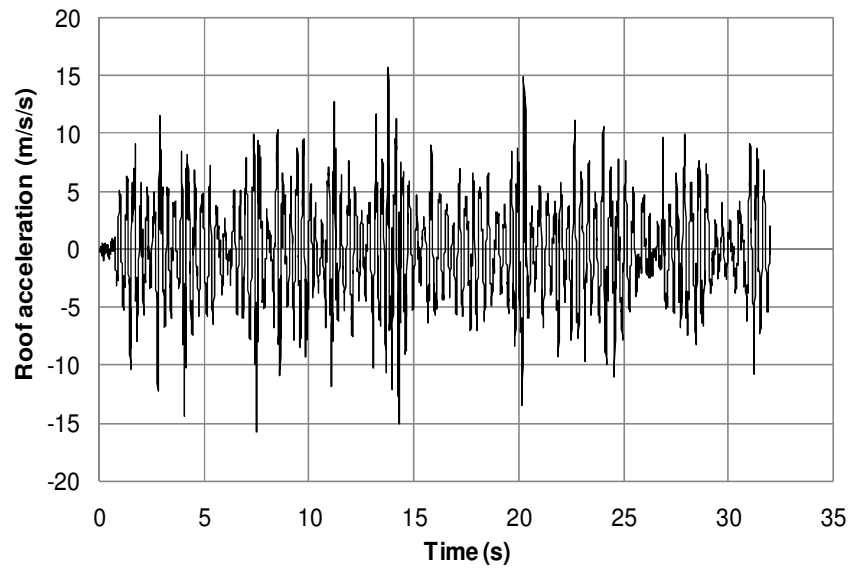
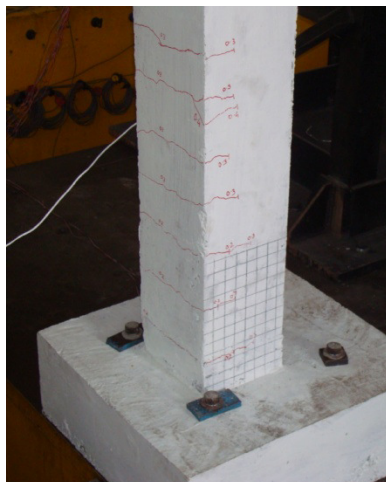
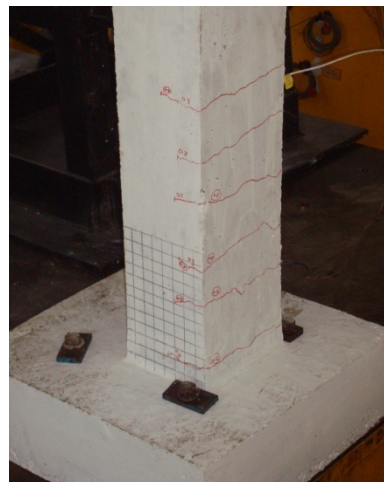


Figure 9.22 Recorded acceleration-time history at the roof level for input ground motion corresponding to PGA = 0.4g

The crack patterns observed in this case (Figure 9.23) displayed different behaviour compared to previous cases. The cracks at the base of the column were almost not altered compared to 0.3g case (Figure 9.23a), however, several new cracks were observed at the first floor beam level on both sides (Figure 9.23b). This is attributed to the fact that once the cracks form at the base of the column, the local stiffness reduces and the rise in moment there is not observed. Consequently, beam is subjected to higher bending moments resulting in significant cracking.

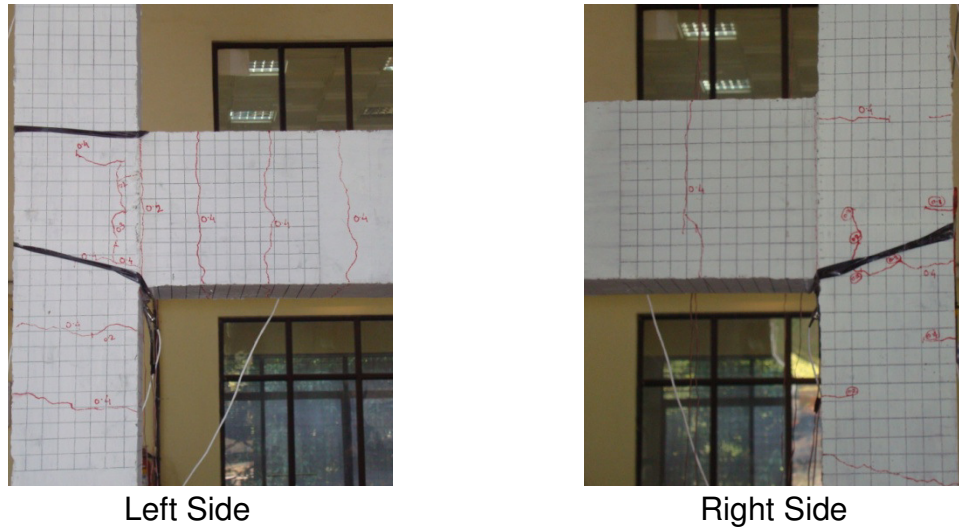


Left Side Column



Right Side Column

a) At the base of left column



(b) At column and beam ends of 1st floor
Figure 9.23 Crack patterns observed after the base excitation of 0.4g

9.6.6 Simulated seismic test with PGA = 0.5g

Figure 9.24 and 9.25 show the acceleration time history recorded at first floor and roof, respectively, corresponding to the input ground motion with a PGA of 0.5g. The peak floor acceleration was obtained as 13.23 m/s² for first floor and 16.78 m/s² for roof level.

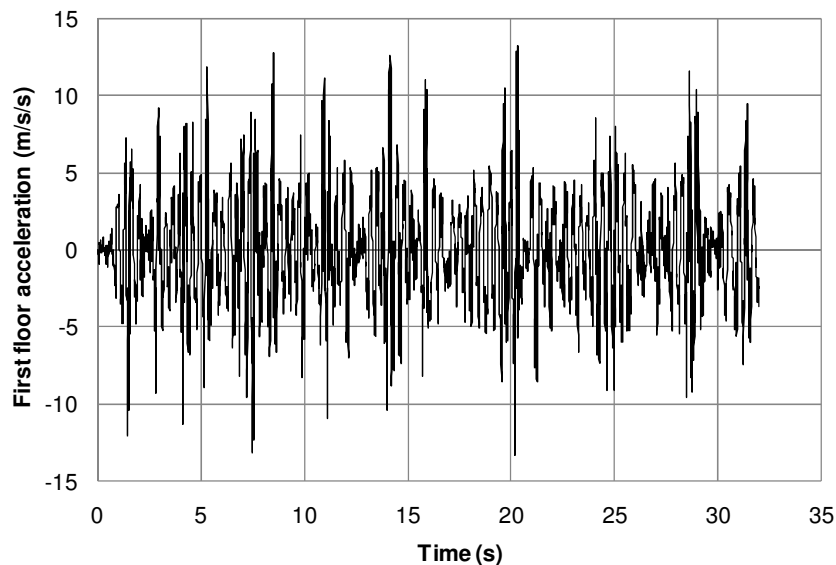


Figure 9.24 Recorded acceleration-time history at the first floor level for input ground motion corresponding to PGA = 0.5g

During the loading wave of 0.5g PGA, the first diagonal shear cracks appeared at the joint. Figure 9.26 shows the cracking at the first floor joint for (a) left side joint, and (b) right side joint. At the base of the columns, two more flexural tensile cracks appeared (Figure 9.26c).

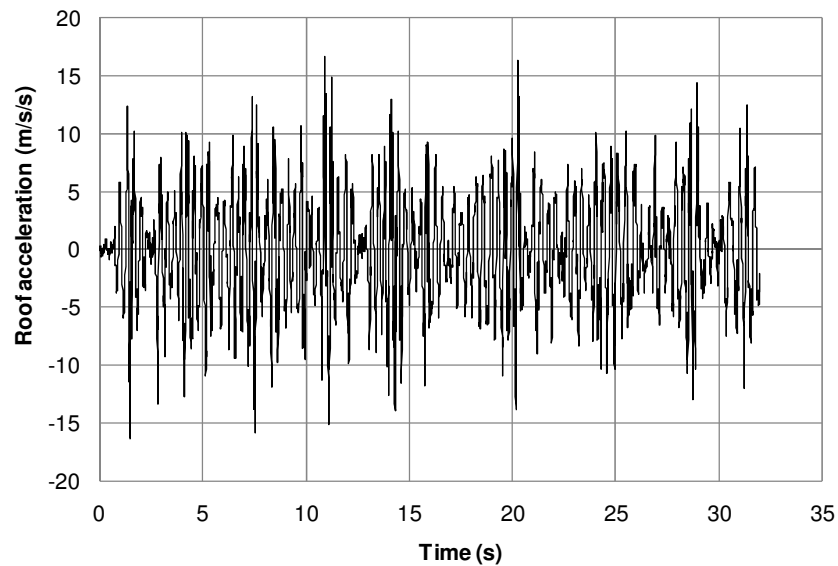


Figure 9.25 Recorded acceleration-time history at the roof level for input ground motion corresponding to PGA = 0.5g

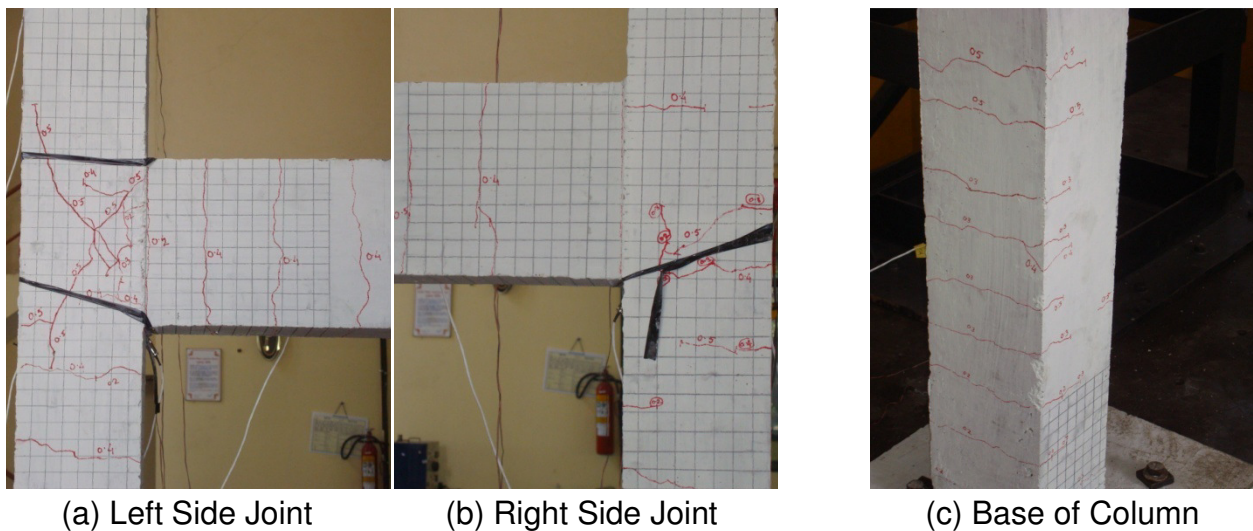


Figure 9.26 Crack patterns observed after the base excitation of 0.5g

As mentioned earlier, the exterior joint of the structure was the 2/3rd replica of the joints tested earlier, specifically joint JT1-1 (Chapter 7). It can be observed that the crack patterns obtained in the shake table test of the frame structure resemble the crack patterns observed for the joint JT1-1 (Figure 7.8) quite closely. Similar to the sub-assembly level tests, after a few cracks in the beam (but before yielding of reinforcement bars), joint shear cracking occurs. This highlights the vulnerability of the beam-column joints of non-seismically designed structures subjected to earthquakes. Further, this confirms that in order to develop a suitable retrofit for this structure, the joints are required to be strengthened or safeguarded, which is essentially one of the major focuses of this thesis.

Although the structure is symmetric in geometry, the crack patterns on both left and right side are not identical (Figure 9.26 a and b). This may be attributed to the inevitable scatter and uncertainties in the RC structures. However, given the design and detailing of the joint, the shear cracking of the right side joint is also expected in next loading waves. Also, it is expected that, similar to the tests at sub-assembly level, beyond this loading wave, most of the damage may be concentrated in the joint region.

9.6.7 Simulated seismic test with PGA = 0.6g

Figure 9.27 and 9.28 show the acceleration time history recorded at first floor and roof, respectively, corresponding to the input ground motion with a PGA of 0.6g. The peak floor acceleration was obtained as 13.80 m/s^2 for first floor and 17.87 m/s^2 for roof level.

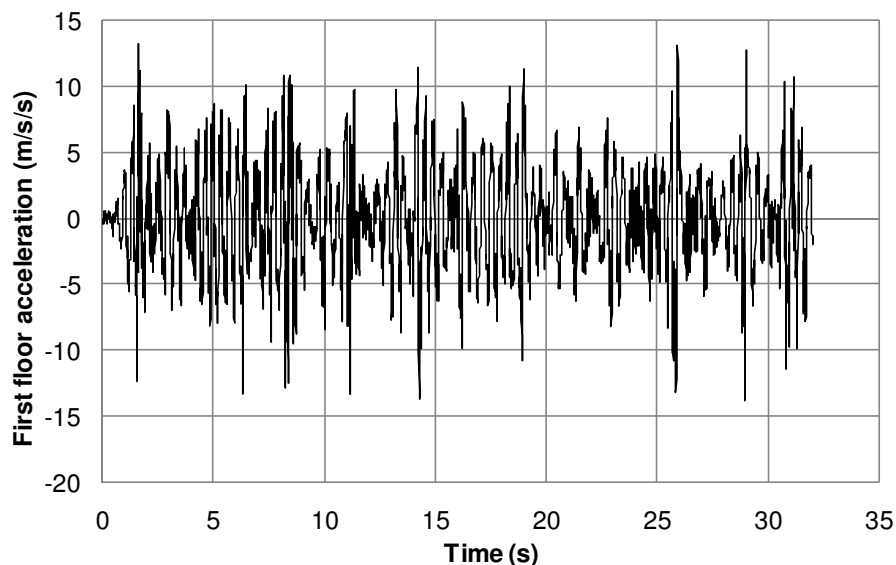


Figure 9.27 Recorded acceleration-time history at the first floor level for input ground motion corresponding to PGA = 0.6g

The crack patterns observed in the experiment are presented in Figure 9.29. As expected, during the loading wave of 0.6g PGA, the diagonal shear cracks appeared on the right side joint as well. A few small cracks also appeared on the joint. On left side joint the existing diagonal cracks propagated further and the existing cracks opened up. At the base of column, few more flexural tensile cracks appeared.

9.6.8 Simulated seismic test with PGA = 0.7g

The acceleration response histories obtained from the experiment corresponding to the input ground motion with a PGA of 0.7g are presented in Figures 9.30 and 9.31 respectively. The peak floor acceleration was obtained as 16.57 m/s^2 for first floor and 20.21 m/s^2 for roof level.

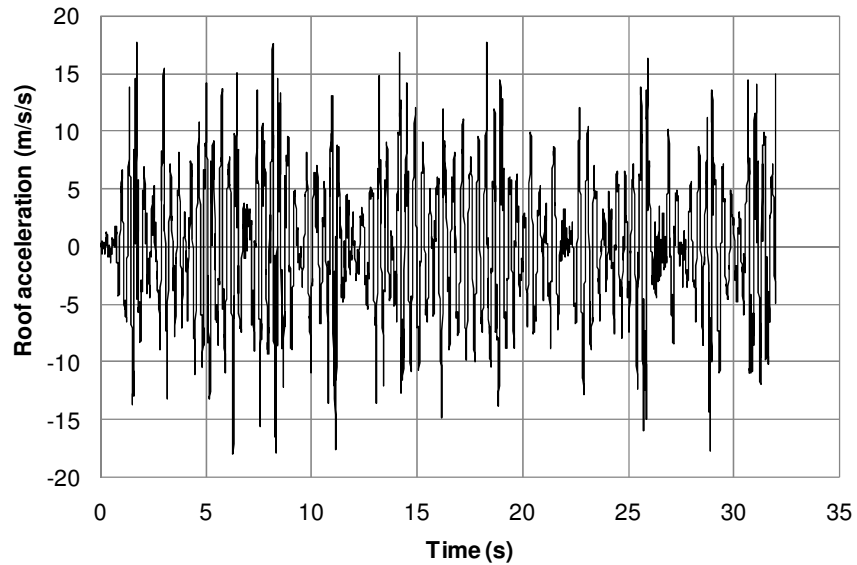
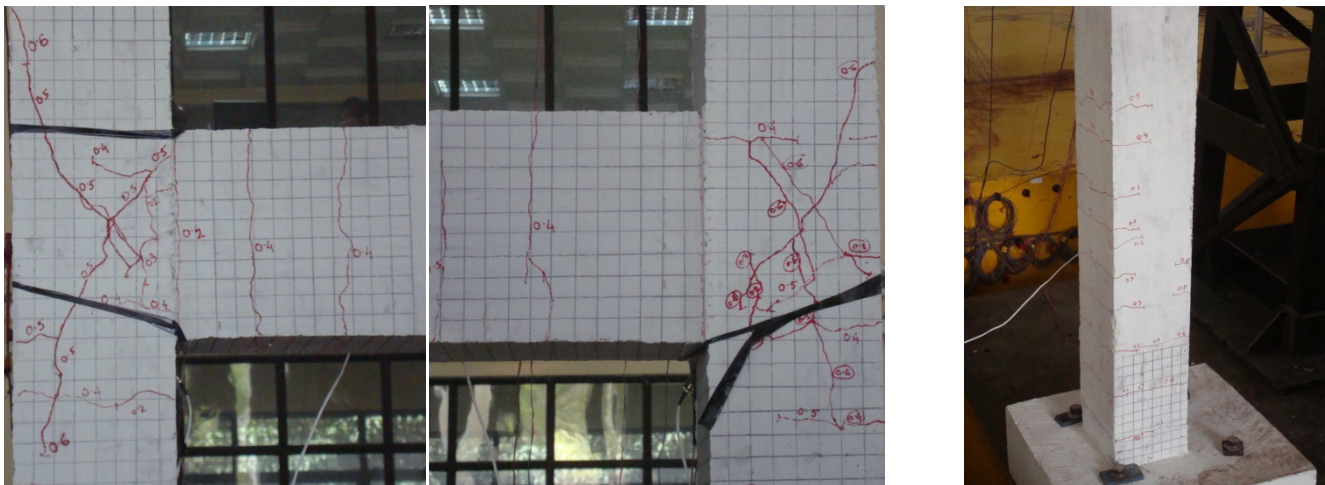


Figure 9.28 Recorded acceleration-time history at the roof level for input ground motion corresponding to PGA = 0.6g



(a) Left Side Joint

(b) Right Side Joint

(c) Base of Column

Figure 9.29 Crack patterns observed after the base excitation of 0.6g

The crack patterns observed in the experiment are shown in Figure 9.32. On the left side joint (Figure 9.32a), the existing cracks opened and a little amount of spalling was observed from the point of intersection of diagonal cracks. On the right side joint, the earlier formed diagonal shear cracks extended and a few more cracks appeared (Figure 9.32b). The base of the column showed no new cracks (Figure 9.32c). This again is in tune with the experimental results on the beam-column joints, where the damage was limited to the extension and opening of existing cracks.

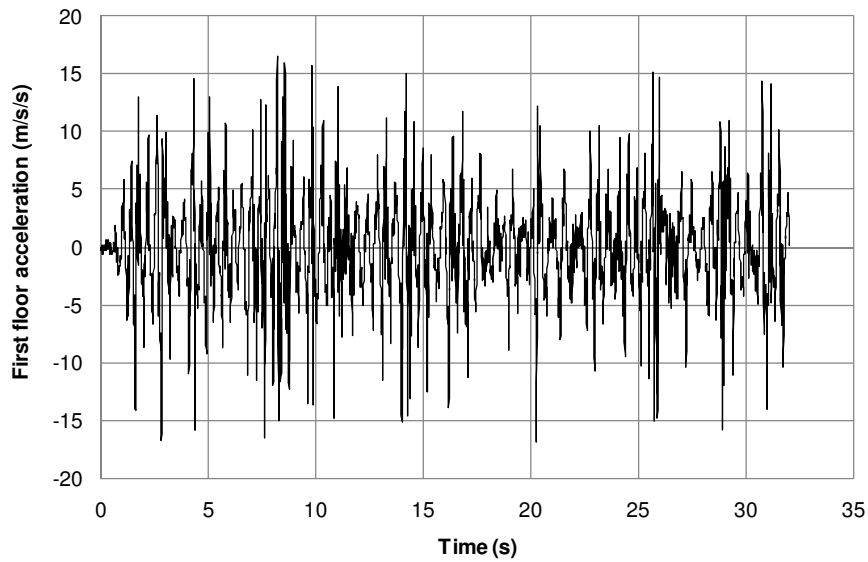


Figure 9.30 Recorded acceleration-time history at the first floor level for input ground motion corresponding to PGA = 0.7g

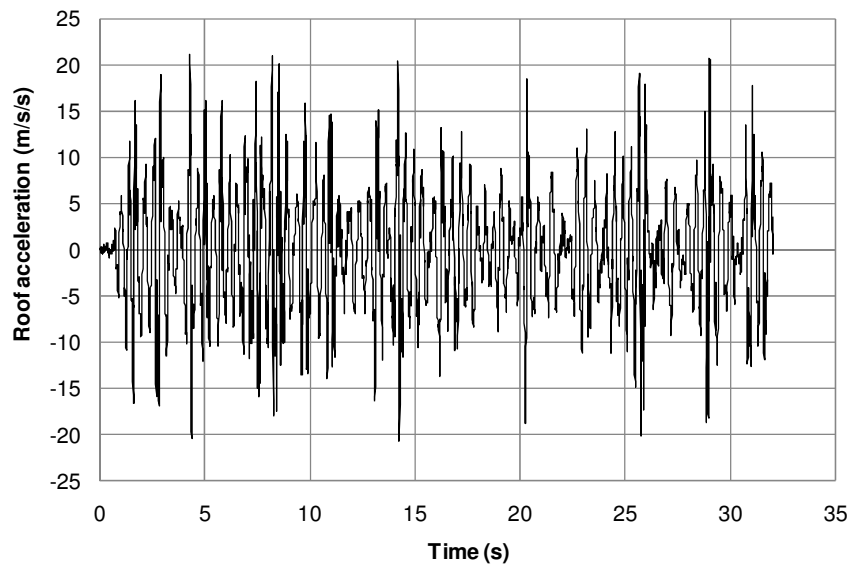
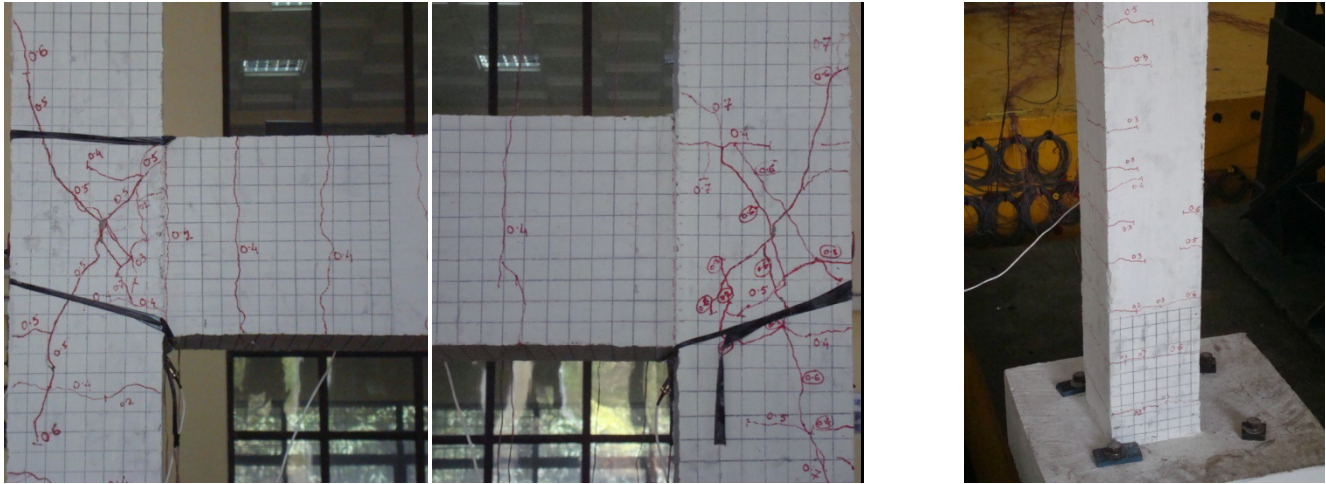


Figure 9.31 Recorded acceleration-time history at the roof level for input ground motion corresponding to PGA = 0.7g

9.6.9 Simulated seismic test with PGA = 0.8g

Figures 9.33 and 9.34 show the acceleration response histories recorded at the first floor and roof level respectively for the structure when subjected to a loading wave of 0.8g PGA. The peak floor acceleration was obtained as 18.88 m/s^2 for first floor and 22.34 m/s^2 for roof level.



(a) Left Side Joint (b) Right Side Joint (c) Base of Column

Figure 9.32 Crack patterns observed after the base excitation of 0.7g

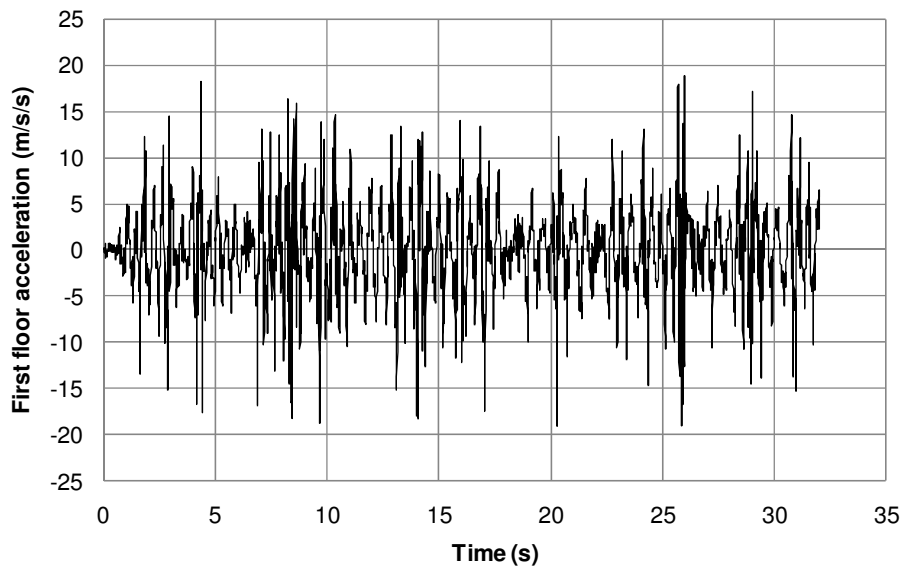


Figure 9.33 Recorded acceleration-time history at the first floor level for input ground motion corresponding to PGA = 0.8g

Figure 9.35 presents the crack patterns observed on the joints of left side and right side columns of the structure. The column base did not show any more new cracks and therefore is not shown here. From this point onwards the existing cracks opened and more spalling was observed from the joints.

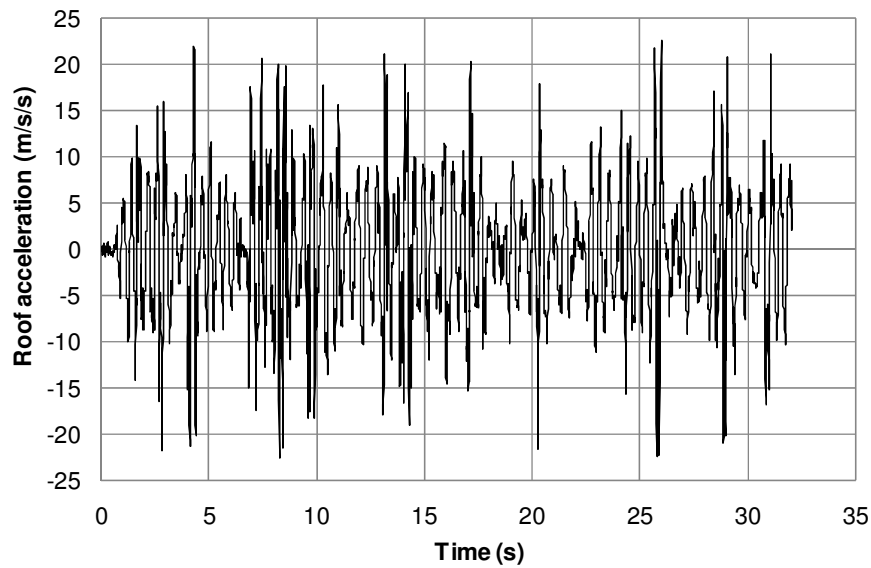
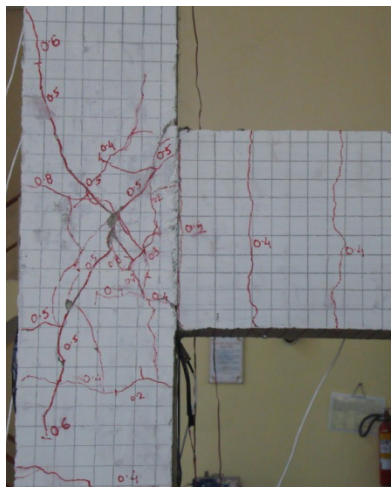
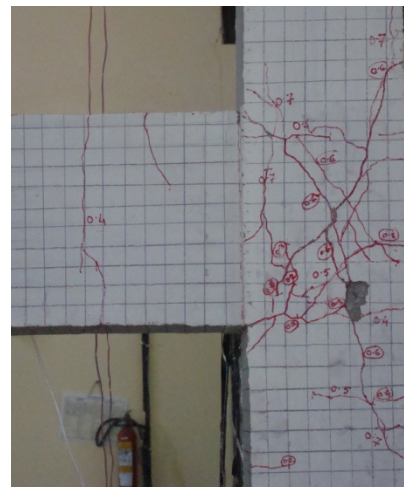


Figure 9.34 Recorded acceleration-time history at the roof level for input ground motion corresponding to PGA = 0.8g



(a) Left Side Joint



(b) Right Side Joint

Figure 9.35 Crack patterns observed after the base excitation of 0.8g

9.6.10 Simulated seismic test with PGA = 0.9g

Figures 9.36 and 9.37 show the acceleration response histories recorded at the first floor and roof level respectively for the structure when subjected to a loading wave of 0.9g PGA. The peak floor acceleration was obtained as 18.92 m/s^2 for first floor and 23.44 m/s^2 for roof level. Since no significant new cracks were observed, the crack pattern is not shown for this case.

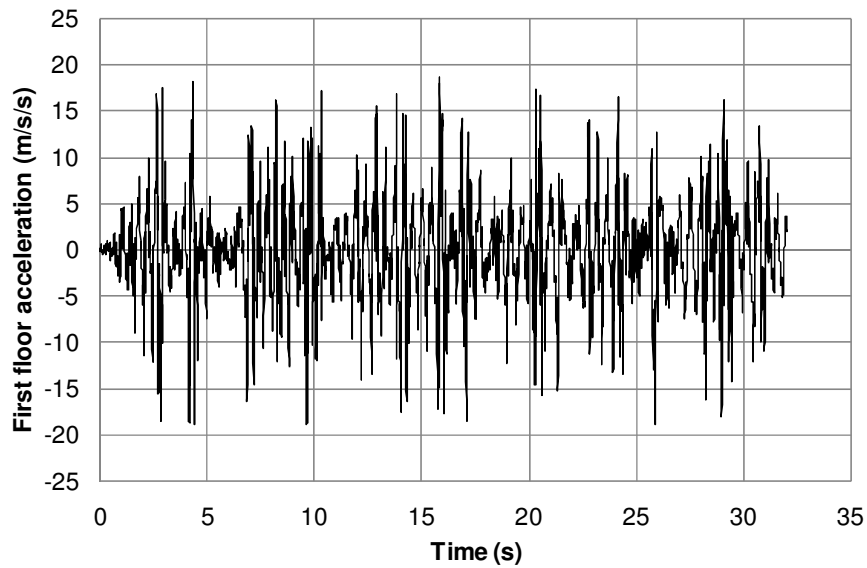


Figure 9.36 Recorded acceleration-time history at the first floor level for input ground motion corresponding to PGA = 0.9g

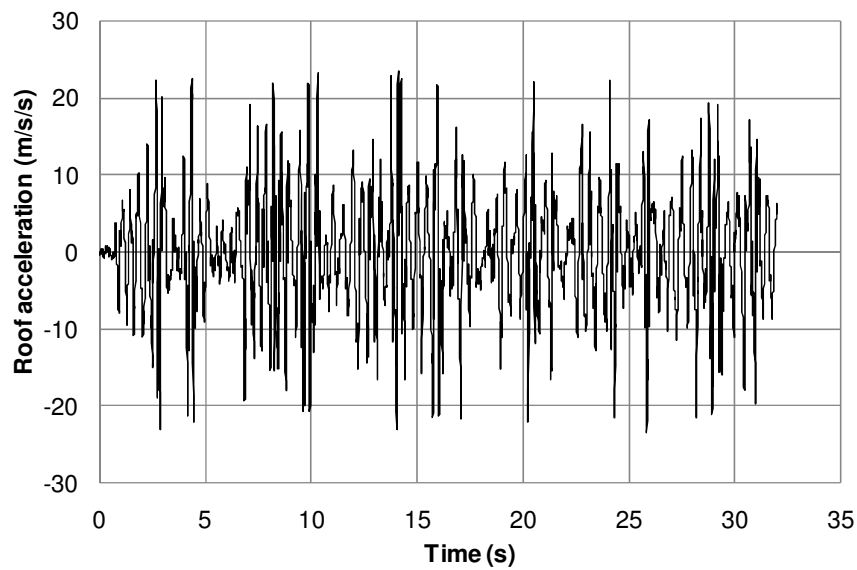


Figure 9.37 Recorded acceleration-time history at the roof level for input ground motion corresponding to PGA = 0.9g

9.6.11 Simulated seismic test with PGA = 1.0g

Figures 9.38 and 9.39 show the acceleration response histories recorded at the first floor and roof level respectively for the structure when subjected to a loading wave of 1.0g PGA. The peak floor acceleration was obtained as 18.82 m/s^2 for first floor and 24.14 m/s^2 for roof level.

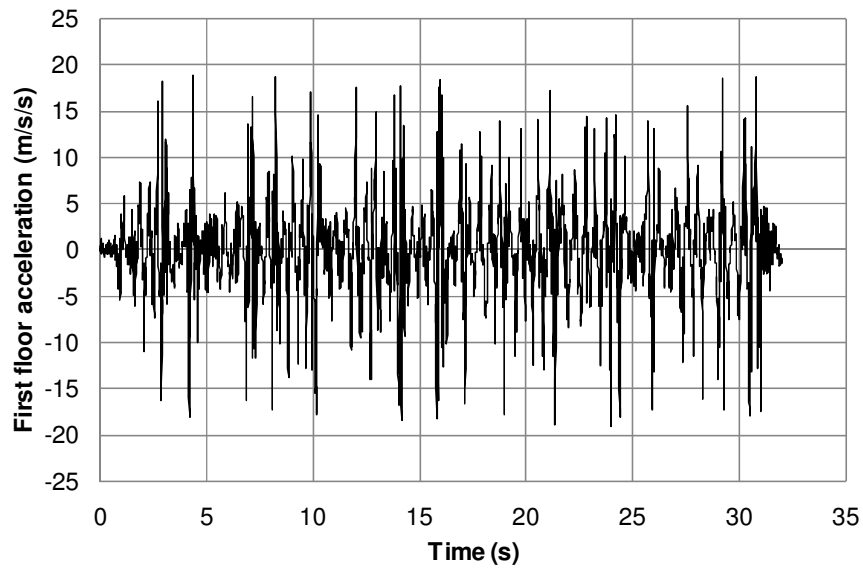


Figure 9.38 Recorded acceleration-time history at the first floor level for input ground motion corresponding to PGA = 1.0g

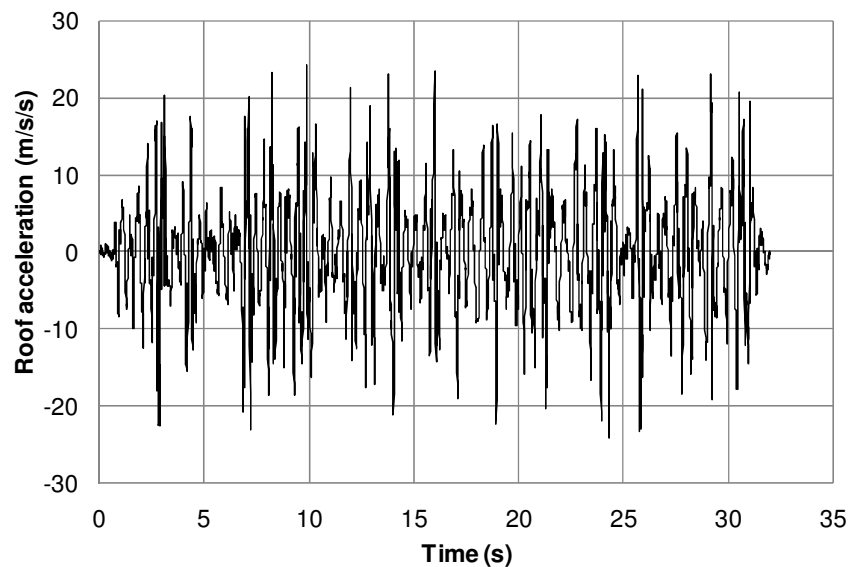
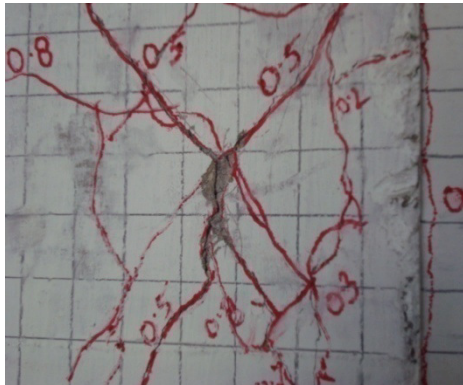


Figure 9.39 Recorded acceleration-time history at the roof level for input ground motion corresponding to PGA = 1.0g

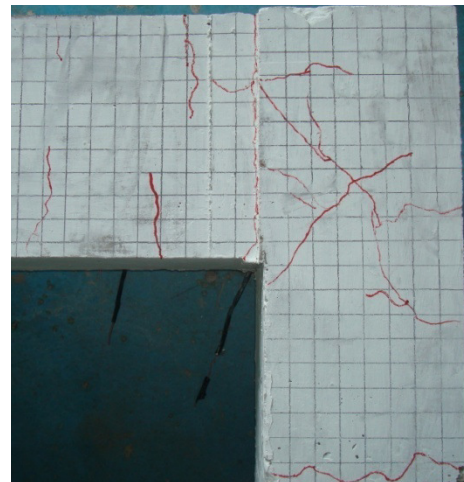
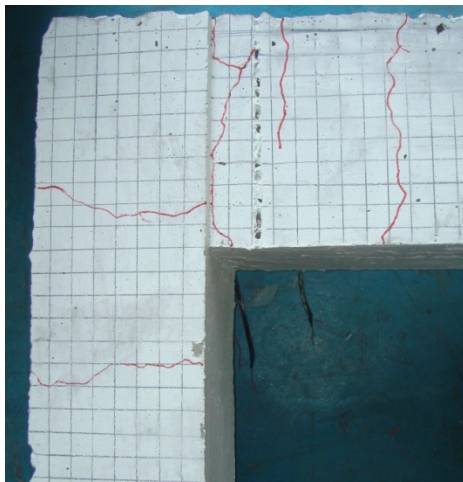
9.7 Summary of Experimental Results

A 2D RC frame structure was tested on shake table and was subjected to gradually increasing levels of excitation. The crack patterns were marked at the end of each loading wave and it was concluded that joint shear failure was the fundamental mode of failure for the structure. At the end of the test series, opened diagonal cracks were observed in the joint (Figure 9.40a). Further, certain spalling was observed from the column just adjacent to the top face of the beam (Figure 9.40b). After the test series was over, the structure was took off the table and laid on the floor to facilitate the marking of cracks on the 2nd floor level (roof).

Figure 9.40c and 9.40d represents the crack patterns observed at the roof on left and right side corner joints, respectively. Diagonal cracks could be observed on right side corner joint but not on the left one. Nevertheless, as expected, the damage suffered by the roof corner joints was much less in comparison to the exterior joints of first floor.



(a) Opened diagonal shear cracks in the joint panel (b) Spalling at top face of beam



(c) Crack pattern for the left corner joint (d) Crack pattern for the right corner joint

Figure 9.40 Crack patterns observed after the completion of test series

In figure 9.41, the peak floor acceleration (PFA) recorded in the experiment for 1st floor level and roof level are plotted as a function of the peak ground acceleration (PGA). It can be observed that during the initial loading waves, the PFA rises linearly (though not proportionally) with the increasing PGA. When the PGA reaches a value of 0.5g (4.9 m/s²), the rise in PFA is blocked which is attributed to the joint cracking at this stage. The PFA again rises in with increasing PGA before it gets saturated for PGA values of 0.8g, 0.9g and 1.0g. This is attributed to the corresponding increase in hysteretic damping of the system due to induced damage. This also explains why no further damage was observed in the tests during last three few loading waves. A summary of experimental results on as built structure are given in Table 9.3.

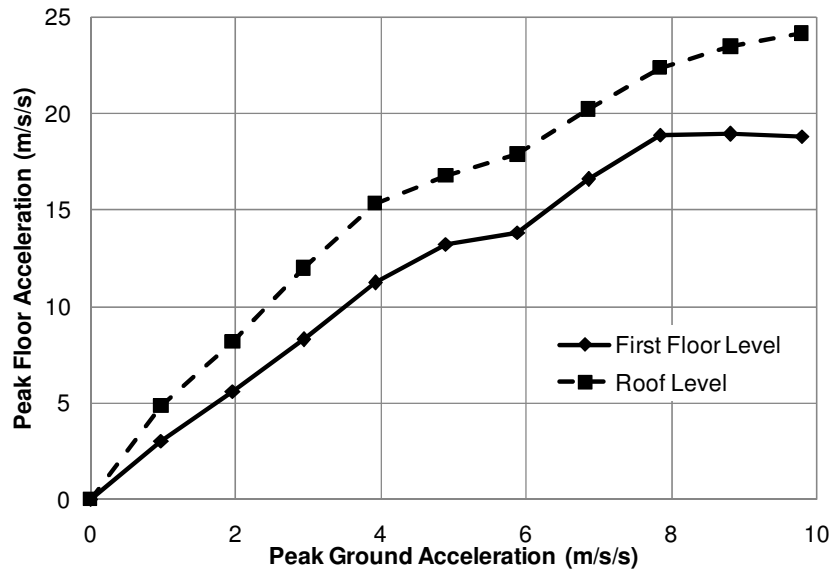


Figure 9.41 Peak floor acceleration as a function of peak ground acceleration as recorded during tests

Table 9.3 Summary of experimental results on as built structure

PGA (g)	Peak Response Accel. (g)		Observations
	Roof	1 st floor	
0.1	0.48	0.30	No cracks
0.2	0.81	0.56	Flexure cracks at the base and top of bottom column
0.3	1.20	0.83	New flexural cracks at the base of bottom column and at the ends of 1 st floor beam
0.4	1.53	1.12	New cracks at the ends of 1 st floor beam
0.5	1.68	1.32	Diagonal shear cracks on left side exterior joint (1 st floor level)
0.6	1.79	1.38	Diagonal shear cracks on right side exterior joint. New cracks in column
0.7	2.02	1.66	Diagonal shear cracks opened and propagated. Little spalling observed
0.8	2.23	1.89	Existing cracks opened and propagated
0.9	2.34	1.89	Existing cracks opened and propagated
1.0	2.41	1.88	Existing cracks opened and propagated

Joint deformation was measured in the test using diagonal LVDTs. The plot of the exterior joint deformation with increasing PGA for the as built structure is displayed in Figure 9.42. It can be seen that at the PGA of 0.5g, the joint deformation suddenly rises, which is attributed to the joint cracking occurring at this point in the experiment. A significant amount of joint distortion clearly displays the poor performance of the exterior joints in the test. To further investigate the system characteristics, the time history obtained from the experiment corresponding to each PGA level was used to generate Fourier spectrum from which the

natural frequency of the structure corresponding to fundamental mode was obtained. Figure 9.43 shows the plot of the variation of frequency corresponding to first mode as a function of the PGA.

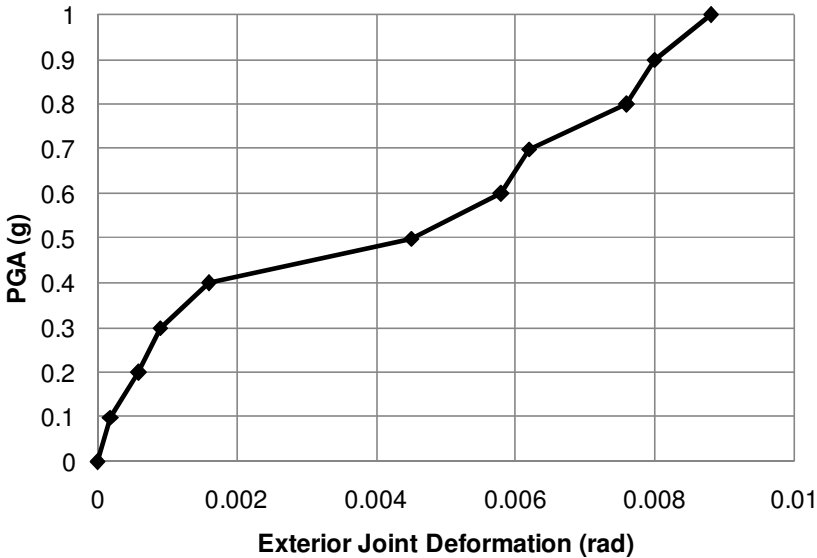


Figure 9.42 Joint shear deformation for exterior joint as a function of PGA

The plot in Figure 9.43 clearly shows that the time period elongates with increasing PGA due to the damage inflicted in the structure. The fundamental time period was increased from 0.31s (for undamaged structure) to 0.45s after completion of whole test series. This implies that the structural stiffness for damaged structure is approximately 50% of the structural stiffness of undamaged structure. This elongation in fundamental time period is a direct consequence of the damage inflicted in the structure.

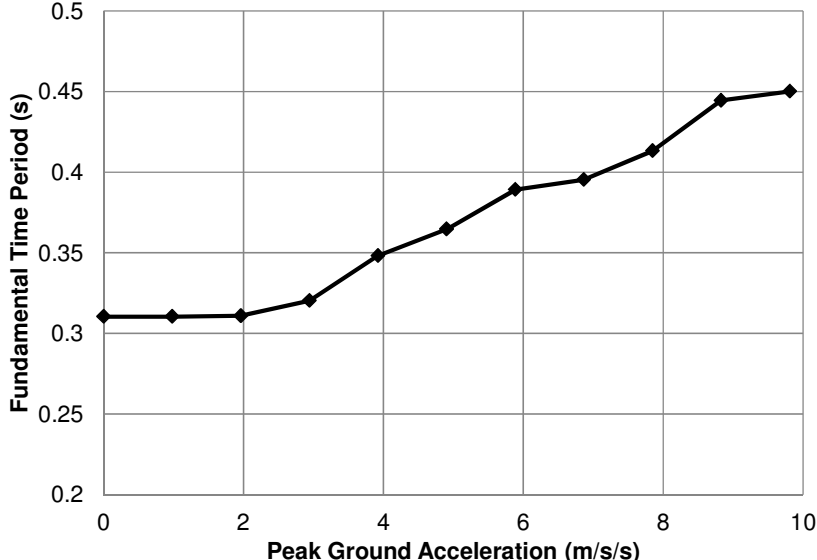


Figure 9.43 Variation of fundamental time period of first mode with PGA

As can be seen from Figure 9.11, the spectral acceleration reduces with increasing time period beyond approximately 0.23 s. This implies that with elongated time period, the structure would attract less seismic forces compared to undamaged structure. Further, more damage implies more energy dissipation and hence higher damping. These two reasons are responsible for the saturation of peak floor accelerations and damage in the structure. Though, with further increase in PGA, or with higher duration of loading, more damage could possibly be inflicted, the same was not the objective of the test. The experiment clearly displayed the vulnerability of the non-seismically designed frames subjected to earthquake loading and successfully served its purpose as benchmark specimen. However, to obtain further information on the behaviour of the specimen, numerical analysis for the structure was performed till higher PGA as will be discussed in chapter 13.

Exact replica of the same specimen was retrofitted using fully fastened haunch retrofit solution and the details of the same are given in chapter 11.

10. EXPERIMENTAL PROGRAM ON BEAM-COLUMN JOINTS RETROFITTED WITH FULLY FASTENED HAUNCH RETROFIT SOLUTION

In chapter 7, the details of the experimental program on as built exterior beam-column joints were provided. The experiments clearly displayed the vulnerability of the non-seismically designed joints under seismic loads. As a retrofit solution to upgrade such joints and improve their seismic behaviour, fully fastened haunch retrofit solution (FFHRS) was evaluated in this work. The basic concept and fundamental mechanics of the joints retrofitted with FFHRS was discussed in chapter 6.

In this chapter, the details of the experimental program carried out on beam-column joints to study the behaviour of joints retrofitted with FFHRS are presented. The tests were carried out within the framework of the thesis of Genesio (2012) and the complete details of the experimental work are available in Genesio and Sharma (2010a) and Genesio (2012). However, these tests also serve as the basic tests within the framework of this thesis to study the behaviour of joints retrofitted with FFHRS and also for validation of the models proposed earlier. Therefore, a brief discussion of the experiments is provided in this chapter.

The objectives of these tests were

- (i) to understand the seismic behaviour of non-seismically designed beam-column joints retrofitted with FFHRS;
- (ii) to investigate the influence of anchorage type on the behaviour of retrofit solution;
- (iii) to evaluate the strengths and limitations of the retrofit solution and to determine the best suited retrofit philosophy; and
- (iv) to provide database for validation of the numerical models described earlier.

10.1 Experimental Program

The experimental program on retrofitted beam-column joints consisted of performing static-cyclic tests on non-seismically designed full-scale RC exterior joints. Total five joints were tested under the program namely JT1-2 through JT1-6. However, in the first test (JT1-2), the support sliding took place and hence the same was repeated as JT1-3. In other four tests (JT1-3 through JT1-6), there was no problem in the setup and hence those four tests are reported here. In all the cases, deformed bars were used with both top and bottom beam bars bent into the joint core. For joints JT1-3, JT1-5 and JT1-6, retrofitting involved only installation of FFHRS while the same for JT1-4 involved installation of FFHRS as well as selective weakening of beam. The test matrix is shown in Table 10.1.

Table 10.1 Test matrix for experimental program on joints retrofitted with FFHRS

Joint Name	Type of Anchors	Retrofit type	Remarks
JT1-2	Bonded Anchors	FFHRS	Discarded
JT1-3	Bonded Anchors	FFHRS	Repeat of JT1-2
JT1-4	Bonded Anchors	FFHRS + Selective weakening	--
JT1-5	Concrete Screws	FFHRS	--
JT1-6	Expansion Anchors	FFHRS	--

10.2 Description of Joints

10.2.1 Geometry

The geometry and reinforcement details of all the joints were same as that of joint JT1-1 tested earlier (Figure 7.1) that served as the benchmark for all the tests.

10.2.2 Material Properties

The average compressive strength of concrete on testing day, obtained by performing tests on 150mm size cubes are reported in Table 10.2 for each joint.

Table 10.2 Average compressive strength for concrete for retrofitted joints

Joint	Average Compressive Cube Strength (MPa)
JT1-3	37.74
JT1-4	42.03
JT1-5	34.63
JT1-6	29.07

The actual properties of reinforcing bars used in the joints are tabulated in Table 10.3.

Table 10.3 Properties of Reinforcing Bars (All Deformed Bars)

Diameter of bar (mm)	Yield Strength (MPa)	Ult. Strength (MPa)
8	548	652
16	478	590
20	501	575

10.3 Description of Fully Fastened Haunch Retrofit Solution (FFHRS)

10.3.1 Haunch Elements

The haunch elements used in the retrofitting of beam-column joints essentially consisted of three machined steel plates welded together. Figure 10.1 shows the schematic drawing of the haunch elements used in this work and Figure 10.2 shows the photographic view of the fabricated haunch element. All plates used were 16 mm thick.

The two plates were placed orthogonally and welded so that they act as the base plates to facilitate the connection of haunch elements with the beam and column. The third plate was placed diagonally inside the orthogonal plates and welded. This diagonal plate acts as the main haunch. On the base plates, six holes three on either side of central diagonal plate were drilled as shown in Figure 10.1. The slots were made in the base plates to bring out the wires of strain gauges to be applied on anchors safely.

10.3.2 Anchorage System

Three different types of anchors were used to fasten the haunch elements with the beam and column of the sub-assembly, namely bonded anchors, expansion anchors and concrete screws (refer Table 10.1). Bonded anchors were used in case of JT1-3 and JT1-4. In JT1-4, selective weakening of beam was also employed as retrofit strategy. JT1-5 employed concrete screws and JT1-6 used expansion anchors for fastening the haunch elements.

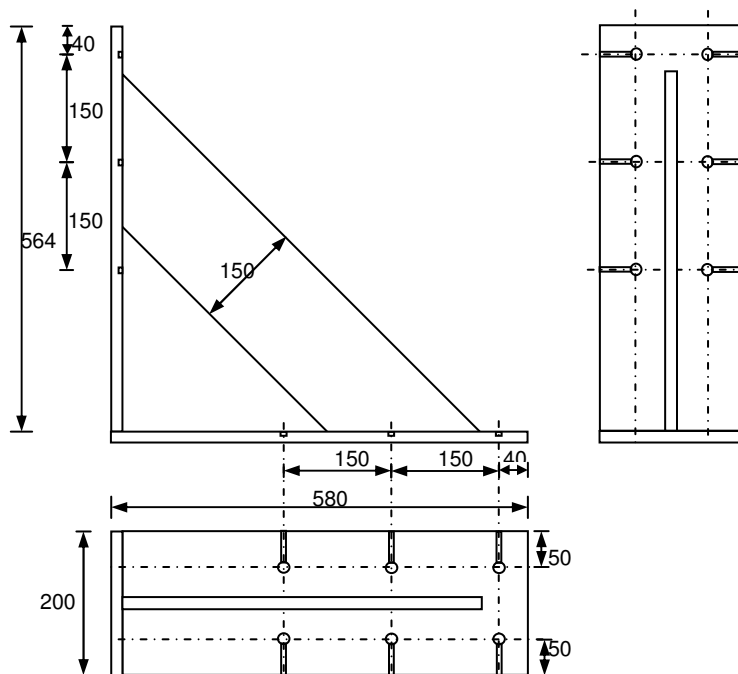


Figure 10.1 Schematic of the haunch elements



Figure 10.2 Fabricated haunch elements

10.3.2.1 Bonded Anchors

The bonded anchors comprised of high strength threaded rods (Figure 10.3a), which was glued using two component epoxy based mortar WIT-PE 500 from manufacturer Würth (Figure 10.3b). On the threaded rods, strain gauges were applied to measure the forces attracted by individual anchors (Figure 10.3a). The installation involves (in chronological order): drilling the hole to desired depth; cleaning of hole as per specifications given in anchor approval; filling the drilled hole with epoxy mortar; inserting the threaded rod; curing of mortar; tightening of nut (with washer) to specified torque. Bonded anchors are known to be quite susceptible to hole cleaning and therefore special cleaning procedure using steel brush and air blower is needed. The complete installation procedure is given in Genesio and Sharma (2010) and Genesio (2012).



(a) Threaded rods with applied strain gauge



(b) Epoxy based Mortar

Figure 10.3 Bonded anchors used to connect haunch elements for JT1-3 and JT1-4

10.3.2.2 Concrete Screws

Würth make concrete screws (W-SA) were used to connect the haunch elements in case of JT1-5. These types of anchors are known to have relatively easy installation procedure. The installation involves in drilling and cleaning holes and then setting the anchors using torque wrench till the specified torque (Figure 10.4). The cleaning of hole in this case basically require only air blowing. The complete installation procedure is given in Genesio and Sharma (2010) and Genesio (2012).



Figure 10.4 Concrete screws used for retrofitting of JT1-5

10.3.2.3 Expansion Anchors

Bolt type expansion anchors (W-FAZ) from manufacturer Würth, were used to connect haunch elements for joint JT1-6. The installation involves: drilling and cleaning of hole; light hammering on the anchor to insert it till desired depth; tightening of nut (with washer) till desired torque. The complete installation procedure is given in Genesio and Sharma (2010) and Genesio (2012). Figure 10.5 shows expansion anchor being installed for JT1-6.



Figure 10.5 Expansion anchors used for retrofitting of JT1-6

10.3.2.4 Anchor Installation Parameters

The installation parameters for different anchors used for retrofitting are given in Table 10.4. It must be noted that in order to simulate the relaxation of preload during the service life of anchor, the anchors were first tightened with full specified torque, loosened after ten minutes and then re-tightened to 50% of the specified torque.

Table 10.4 Installation parameters for anchors used for retrofitting

Parameter	Units	Bonded anchor M 12	Concrete Screw d 14	Expansion anchor M 16
Effective embedment depth, h_{ef}	mm	150	71.5	115
Drill diameter, d_0	mm	14	12	16
Drill bit diameter, d_{cut}	mm	14.50	12.50	16.50
Drill hole depth, h_0	mm	150	105	140
Installation moment, T_{inst}	Nm	20*	Contact of anchor head with base plate	90*
Fixture thickness, t_{fix}	mm	16	16 ~ 20	16 ~ 20
Fixture hole diameter	mm	14	15	17

10.4 Test Setup

The basic test setup for testing of retrofitted joints was exactly same as the joints tested in as-built condition and reported in section 7.3. Again no axial load was applied on the column in any of the cases. However, additional instrumentation was provided for the retrofitted joints.

The instrumentation for a typical retrofitted joint included the following:

- Load cell (inbuilt in actuator) to measure beam end load
- Displacement Transducer (inbuilt in actuator) to measure beam end displacement
- Strain gauge on reinforcing bars to measure strains at critical locations
- Strain gauge on diagonal haunch elements to measure strains in haunch element
- Strain gauge on bonded anchors to measure strains in anchors
- Potentiometers to measure beam, column and joint deformations

In addition to the strain gauges on the reinforcing bars in case of as-built joint, twelve more strain gauges were applied on the beam reinforcing bars to obtain the strain profile that helps in understanding the efficiency of the haunch element. Figure 10.6 shows the locations for strain gauges on reinforcing bars in a retrofitted joint. To evaluate the element deformations, linear potentiometers were used. Again, in addition to the eight potentiometers used, in case

of as built joints, four more potentiometers were used to measure beam deformations as shown in Figure 10.7.

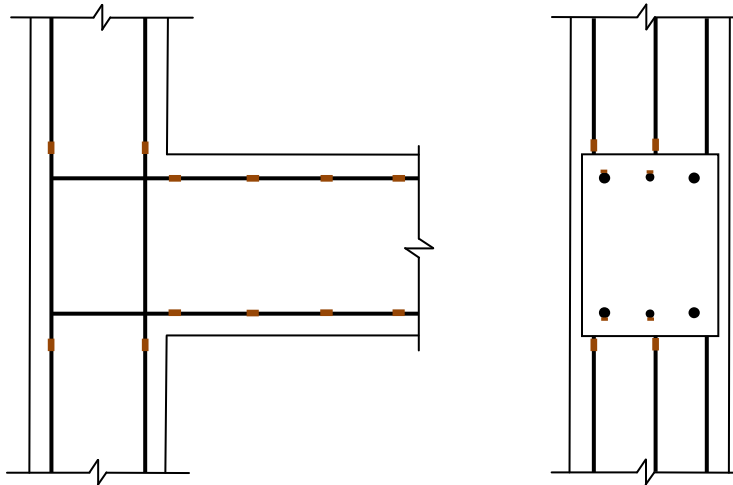


Figure 10.6 Location of strain gauges on retrofitted joint



Figure 10.7 Potentiometer arrangement for retrofitted joint

The experiment was carried out by applying cyclic load at the beam end in displacement control as per the loading protocol shown in Figure 7.6.

10.5 Experimental Results

10.5.1 JT1-3

Joint JT1-3 was retrofitted using the bonded anchors with the parameters listed in table 10.4. Figure 10.8 shows the hysteretic load-displacement curves obtained for the joint. In the plots, the load is considered as positive when the beam is pulled up and negative when pushed down. The peak load in the positive direction was obtained as 111.9 kN and that in the negative direction was 120.9 kN, which was much higher than the peak loads obtained during

the test on as-built joint JT1-1. In both sides, the peak load was obtained during 60mm cycle. However, as can be seen, during the positive cycles for 40mm beam end displacement, the load was close to the peak load, which was not the case for the negative cycles. However, for either side, no softening was observed in the load-deflection curves till the capacity of the actuator (for +/- 70mm) was exhausted. Thus, the test suggested a significant increase in the capacity of the retrofitted joint.

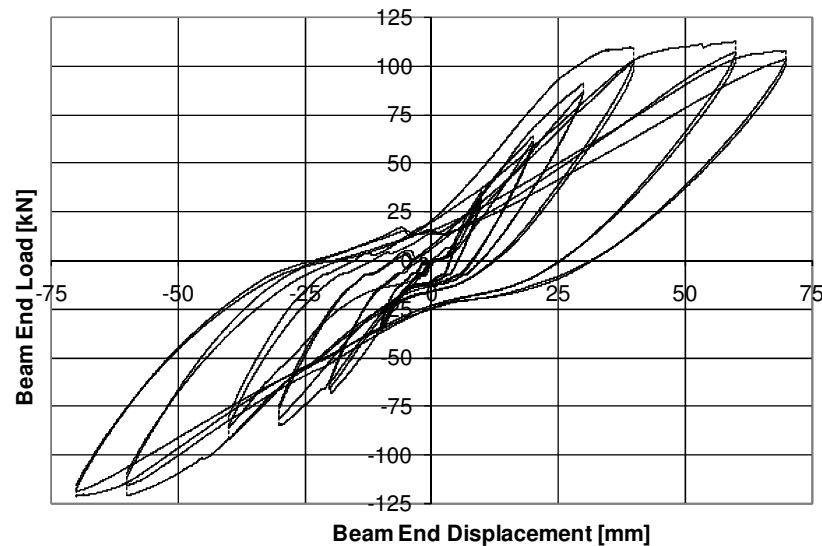


Figure 10.8 Hysteretic loops obtained from test on JT1-3

Figure 10.9 presents the crack patterns as observed in the experiment. The first cracks were observed in the beam, corresponding to 10mm cycle, at the shifted critical section at the location of the farthest anchors in the haunch element (Figure 10.9a). When the beam end displacement was increased to 20mm, many more cracks were formed in the beam. The cracks appeared at all three anchor lines in the beam as well as at certain distance away from the haunch towards the loading point (Figure 10.9b). This is, to some extent, expected since the anchor holes act as notch and it results in stress concentration, which results in crack formation (Eligehausen et al, 2006). When the beam end displacement was further increased, further flexural cracks were formed in the beam as well as column at the anchor locations as seen in Figure 10.9c.

However, during this loading cycle, the crack in the beam appeared also in the region between the face of the column and the anchors connecting haunch element. This essentially suggests that due to cracking, the anchors and hence the FFHRS loses the stiffness and therefore the efficiency of the same to redistribute the forces reduces. During the 40mm cycle, further cracks appear in beam and column and the anchor group starts to undergo concrete cone failure (Figure 10.9d). On further increasing the beam end displacement, the anchor group at the top face of the beam undergoes concrete cone failure, which results in higher shear forces in the joint leading to diagonal cracking (Figure 10.9e). During the final loading cycles, diagonal cracks appeared during positive cycles as well. The concrete cone

failure clearly occurred and the chunk of concrete was removed from the top face of the beam at the anchor group (Figure 10.9f).

The test showed that so far the anchor group serves its purpose well, the FFHRS is very effective in safeguarding the joint core. However, once the anchor group fails, the joint shear rises and the joint failure can occur. This test definitely proved the efficacy of the FFHRS in safeguarding the joint and significantly increased the load carrying capacity of the joint, but due to the concrete cone failure occurring prior to the beam flexure failure, the failure mechanism of the joint (concrete cone + joint shear) is brittle and undesirable.

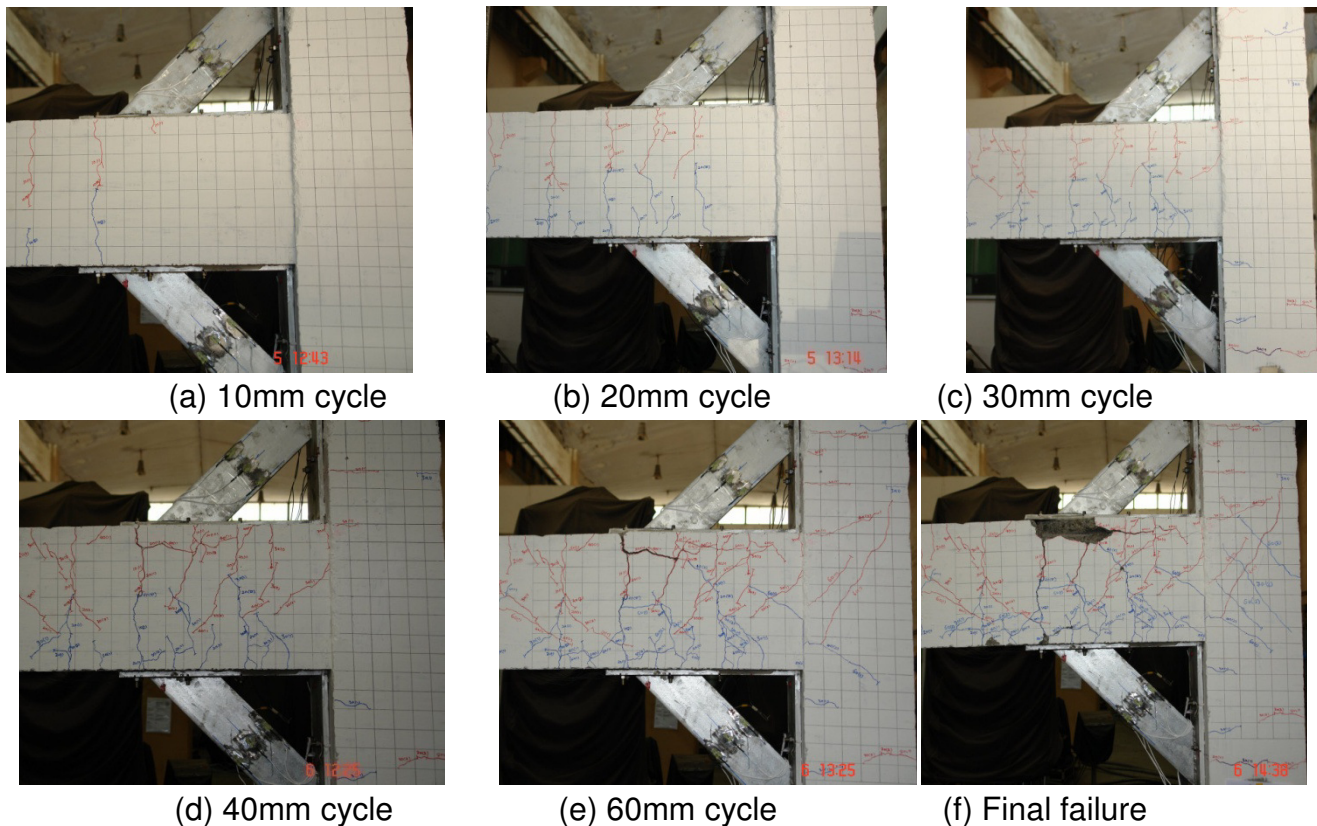


Figure 10.9 Crack patterns observed for joint JT1-3

10.5.2 JT1-4

Joint JT1-4 was also retrofitted using bonded anchors as was JT1-3. However, since JT1-3, underwent undesirable concrete cone and joint shear failure mode, slight modification was made in JT1-4 to prevent the same. As seen in Figure 7.1, the beam was reinforced with 2-20 mm dia bars and 1-16 mm dia bar. It was observed in case of JT1-3 that this reinforcement in beam makes it too strong and therefore, a ductile beam flexural failure could not be induced. In case of JT1-4, the central 16mm dia bar in the beam was cut, to make it selectively weak, very close to the end of base plate of haunch element connected to the beam.

Figure 10.10 shows the hysteretic load-displacement curves obtained for the joint. Since the maximum actuator stroke was 150mm in one direction, after the completion of 70mm cycles, one monotonic push till 150mm downward displacement was provided. The peak load for the positive loading cycle was obtained as 102.37 kN and that for negative loading cycle as 96.56 kN. The peak loads are less than those obtained in case of JT1-3, which is expected due to reduced beam strength, but a very high increase in the ductility was obtained in this case. The load displacement was obtained till a displacement of 150mm in negative direction (beam pushed down), though the cyclic behavior could be obtained only up to ± 70 mm due to actuator stroke limitation. The curve displays a very ductile behavior till the beam end displacement of 150mm which suggests a ductile beam flexure as the governing failure mode. This is confirmed by the crack patterns observed in the test as shown in Figure 10.11.

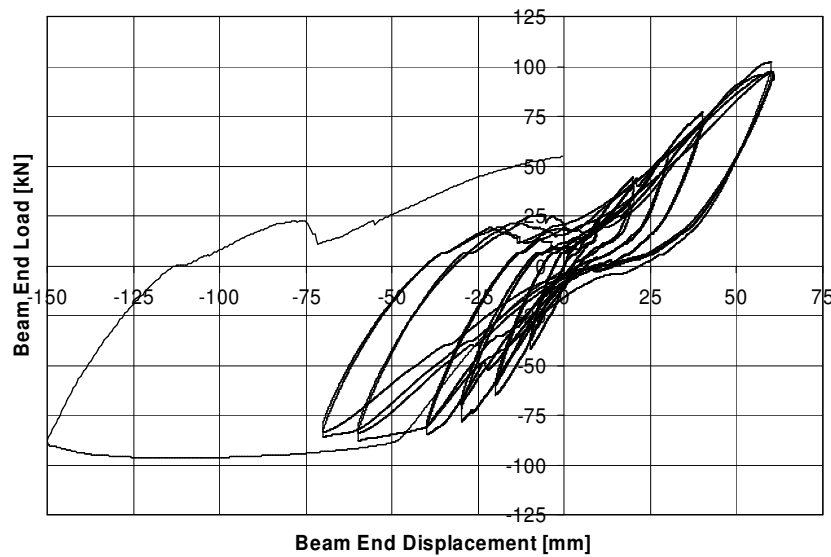


Figure 10.10 Hysteretic loops obtained from test on JT1-4

At the beam end displacement cycle of ± 10 mm, first flexural cracks appeared on the beam at the critical section (Figure 10.11a), though only while being pushed down (negative load cycle). On increasing the displacement level to 20mm, further flexural cracks appeared on the beam in a practically symmetric fashion (Figure 10.11b). Also during this displacement cycle, cracks appeared at the anchor location on the beam.

On further increase in beam end displacement, many new cracks were formed in the beam (Figure 10.11c). The crack in the beam appeared also in the region between the face of the column and the anchors connecting haunch element, which suggests loss of stiffness of FFHRS due to crack formation. However, no diagonal cracks were formed in the joint region. As the beam end displacements were increased, more and more flexural cracks were formed in the beam, while no shear cracks appeared in the joint (Figure 10.11d, e). After the completion of 70mm cycle, one monotonic push was given till -150mm displacement level.

During this push, very large and wide cracks formed at the critical section (end of the base plate of haunch element) as shown in Figure 10.11f.

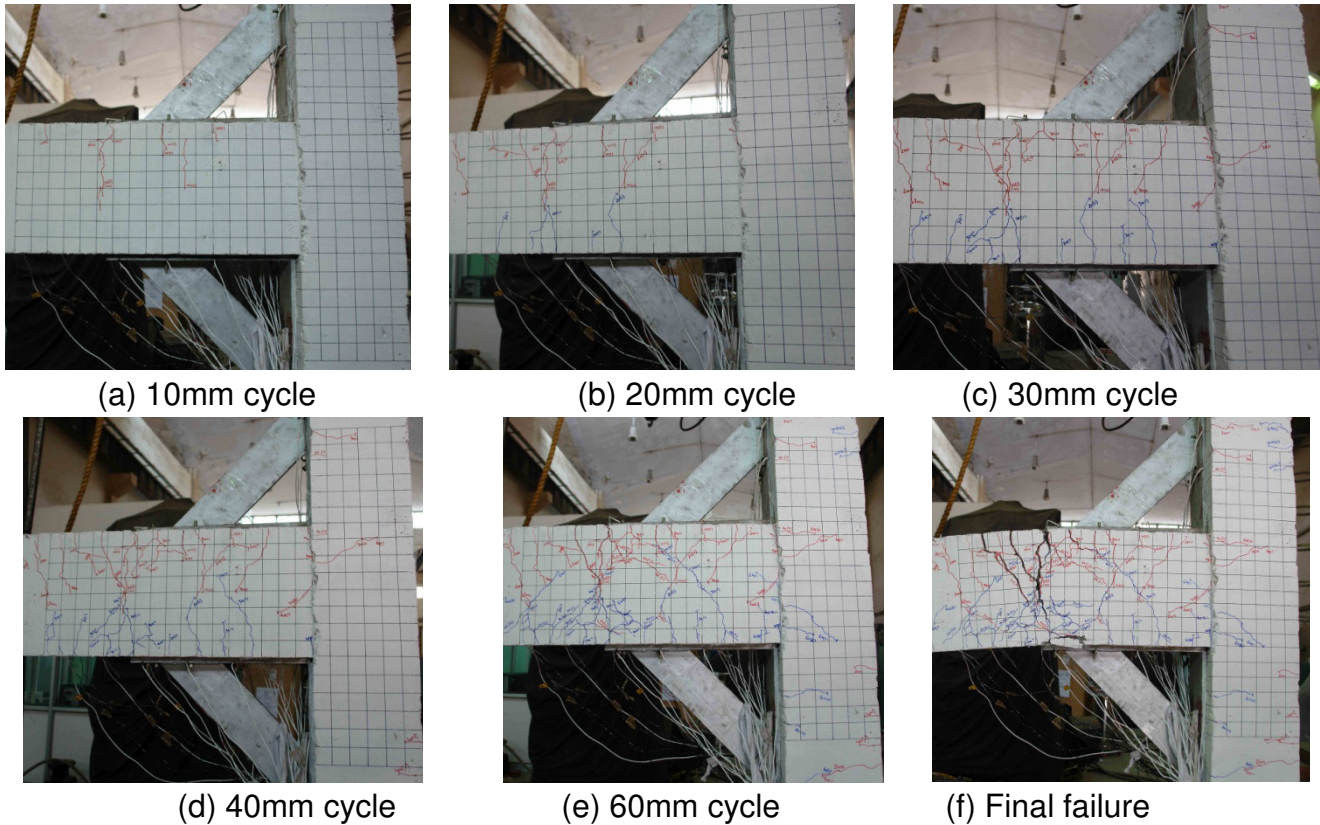


Figure 10.11 Crack patterns observed for joint JT1-4

The cracking pattern observed for joint JT1-4 is typical for the flexural failure mode with reinforcing bars yielding prior to compression failure of concrete (under reinforced section). A clear flexural hinge was developed at the critical section (end of haunch element). Thus, the final failure mode in case of joint JT1-4 was essentially beam flexure failure, which is a desirable mode of failure since it is inherently ductile. Thus, selective weakening of the beam combined with the FFHRS proved to be a highly effective and efficient solution to modify the failure mode from brittle shear to ductile flexure.

10.5.3 JT1-5

Joint JT1-5 was retrofitted using concrete screws with parameters as listed in table 10.4. Selective weakening was employed in this case, since its efficiency was already proved by test on JT1-4. The test was essentially the same as JT1-3 with concrete screws in place of bonded anchors. The hysteretic loops obtained for JT1-5 are shown in Figure 10.12. The peak loads for positive and negative loading directions were obtained as 81.91 kN and 67.97 kN respectively. The peak loads are significantly lower than those obtained in case of joint JT1-3 or JT1-4. Given the fact that no selective weakening was employed in this case, it

suggests a sub-optimal retrofit. In this case also, after completion of +/-70mm cycle, the beam was pushed monotonically till 150mm beam end displacement in negative (downward) direction. The hysteretic loops shown in Figure 10.12 signify significant bond slip.

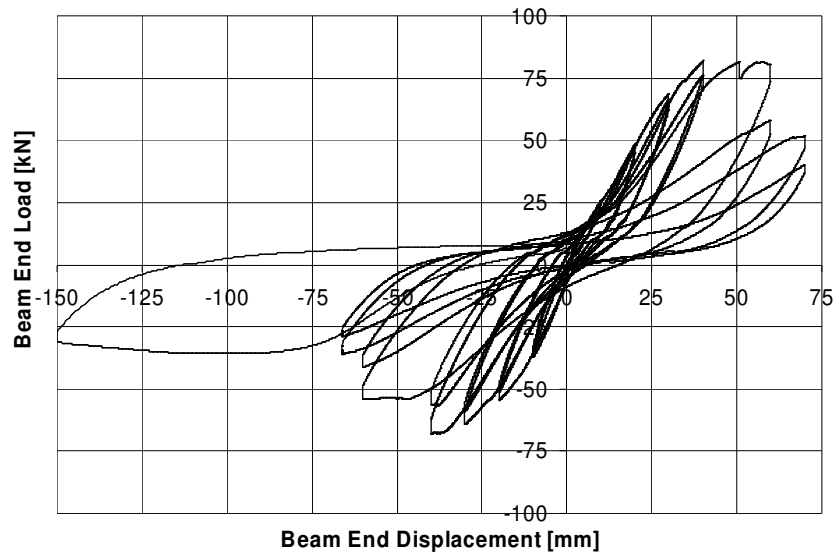


Figure 10.12 Hysteretic loops obtained from test on JT1-5

The crack patterns observed in the test for joint JT1-5 are presented in Figure 10.13 for various displacement levels. In this case, during the first displacement cycle of +/-10mm, several cracks appeared in the beam at regular intervals (Figure 10.12a). Cracks appeared at the anchor locations, at and beyond critical section as well as between haunch and column face. The number of cracks during this cycle for JT1-5 was much higher than JT1-3 or JT1-4.

During the +/-20mm displacement cycle (Figure 10.13b), several new flexural cracks appeared in the beam, few cracks appeared in the column and bond cracks were visible in the joint region, suggesting a sub-optimal function of the anchors and hence the FFHRS. On further loading, during 30mm cycle (Figure 10.13c), shear crack appeared in the joint while loading in negative direction, and the crack appeared on the top column haunch at the anchor location suggesting premature failure of the anchor group.

The shear crack also appeared in the joint while loading in positive direction during 40mm cycle (Figure 10.13d). The bottom column haunch anchor group also started cracking at this loading cycle, while the crack at the anchor group location for top column haunch opened significantly. Further loading aggravated the problem of concrete cone failure at the top and bottom column haunch elements and at both locations the anchor group failed (Figure 10.13e). This premature failure of the anchors resulted in high shear forces transmitted to the joint core and ultimately the joint failed under joint shear (Figure 10.13f).

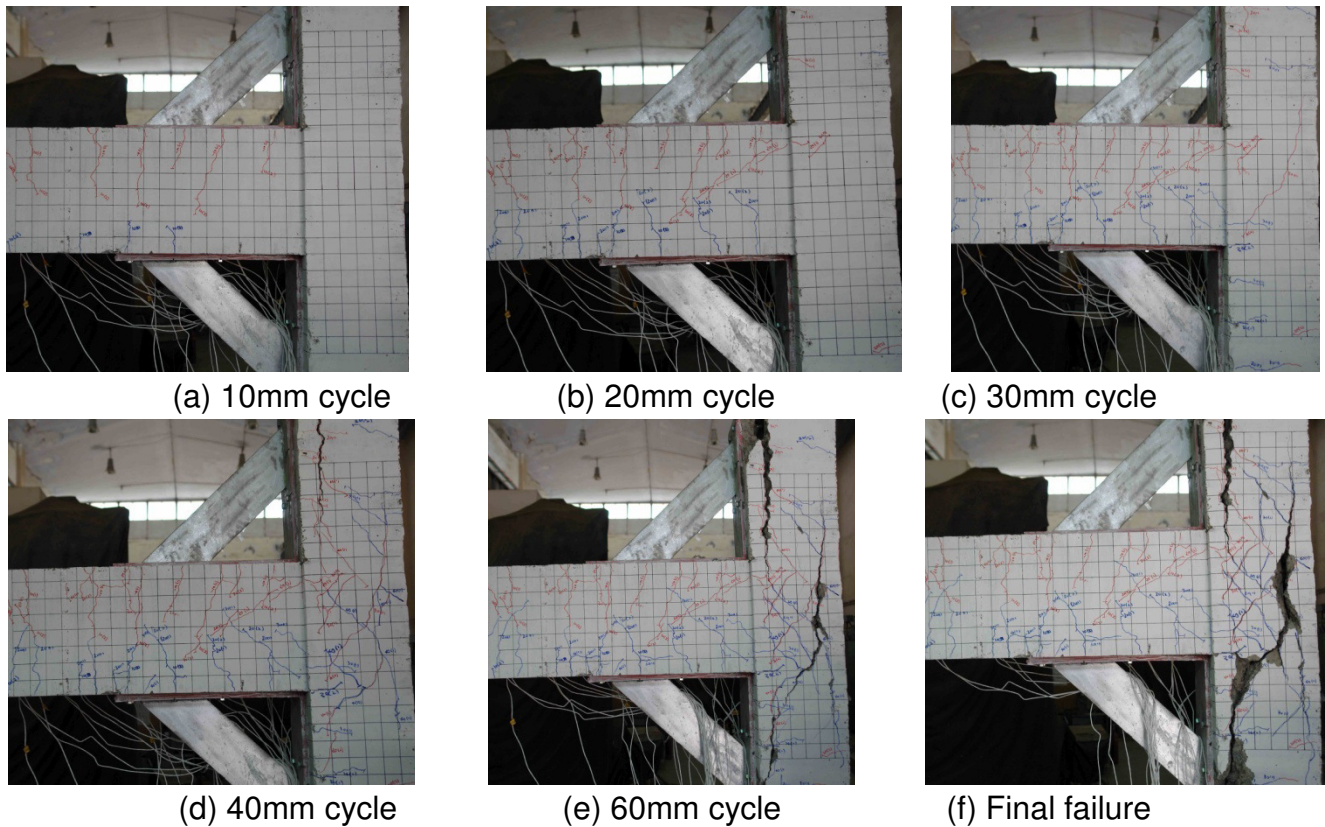


Figure 10.13 Crack patterns observed for joint JT1-5

This test highlighted the importance of anchor behaviour in effectiveness of the FFHRS. The test displayed that in case of the premature anchorage failure, the FFHRS loses its effectiveness in redistributing the forces around joint core, leading to undesirable and brittle failure modes. Thus, correct assessment of the anchorage behaviour is the most essential part of designing the FFHRS.

10.5.4 JT1-6

Joint JT1-6 was retrofitted using the bolt type expansion anchors as per the parameters listed in table 10.4. The hysteretic loops obtained for the joint are depicted in Figure 10.14. The peak load in positive loading direction is obtained as 116.40 kN while in the negative direction, the same is obtained as 85.41 kN.

The load in positive loading direction (beam pulled up) is close to the one obtained for JT1-3, however the load in negative direction is significantly less. Again, since no selective weakening was employed, it suggests sub-optimal retrofit behaviour. The failure patterns as observed in the test for various beam end displacement levels are depicted in Figure 10.15. During the first cycle of +/-10mm, the flexural cracks appeared in the beam at the critical section, similar to joint JT1-3 (Figure 10.15a). New flexure cracks were observed in the beam and column when the beam end displacement was increased to 20mm (Figure 10.15b).

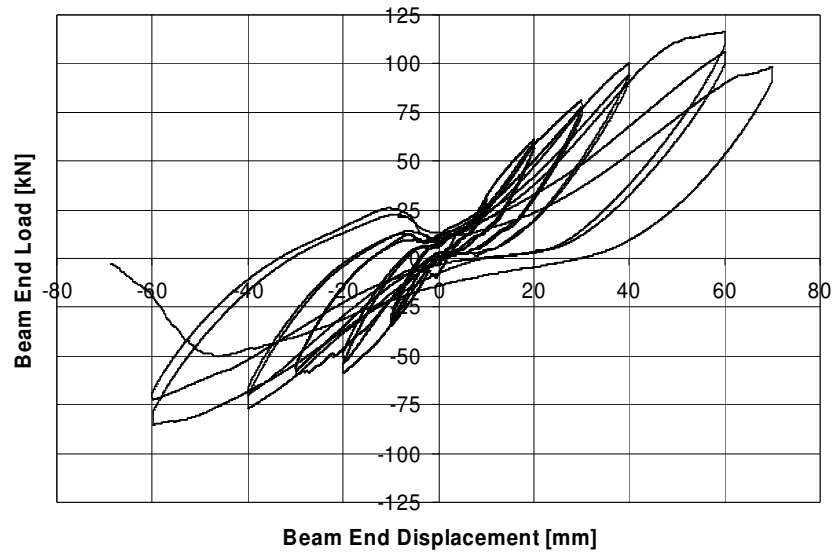


Figure 10.14 Hysteretic loops obtained from test on JT1-6

Additionally, a bond crack appeared in the joint region. On further increasing the beam end displacement to 30mm, flexural cracks appeared in the beam near the face of the column (Figure 10.15c). The existing cracks propagated and new flexural and bond cracks formed during 40mm loading cycle (Figure 10.15d). Also, during this loading cycle, the anchor slippage started to occur.

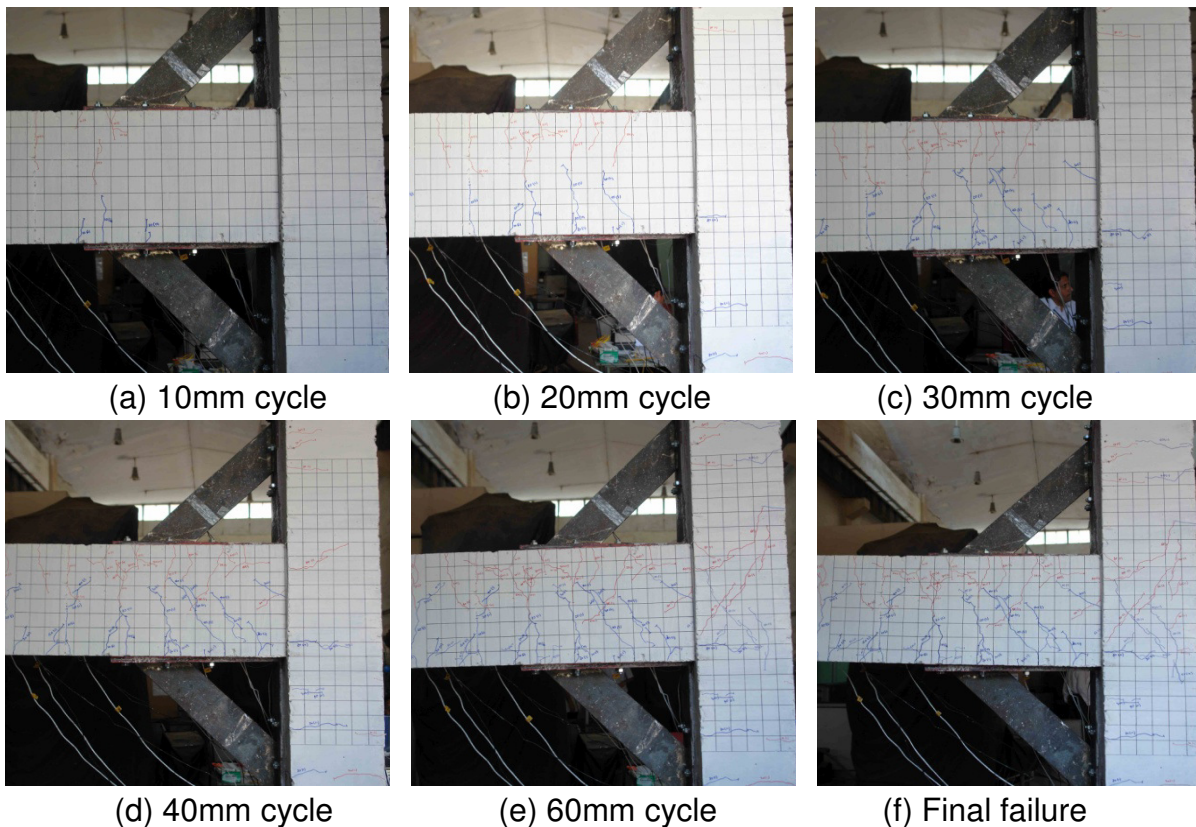


Figure 10.15 Crack patterns observed for joint JT1-6

During the cycle with beam end displacement of +/- 60mm, the diagonal shear crack appeared (Figure 10.15e), which is attributable to the significant slippage of anchors (up to 5mm). The test setup displayed some problem during this stage and 70mm cycle could not be completed. The final crack pattern (Figure 7.14f) showed several cracks in the joint depicting sub-optimal retrofit.

10.6 Summary

The experimental program on retrofitted beam-column joints was carried out which consisted of performing static-cyclic tests on non-seismically designed full-scale RC exterior joints. Total five joints were tested under the program namely JT1-2 through JT1-6. However, in the first test (JT1-2), the support sliding took place and hence the same was repeated as JT1-3. In other four tests (JT1-3 through JT1-6), there was no problem in the setup and hence those four tests are reported here. In all the cases, deformed bars were used with both top and bottom beam bars bent into the joint core. For joints JT1-3, JT1-5 and JT1-6, retrofitting involved only installation of FFHRS while the same for JT1-4 involved installation of FFHRS as well as selective weakening of beam.

It was concluded that the effectiveness of the FFHRS is directly related to the efficiency of the anchor group used to fasten the haunch elements. In case where the anchor group performed very well (JT1-4), a ductile flexural failure in the beam could be induced, while in case where the anchor group suffered concrete cone failure (JT1-5), joint shear failure occurred. Also, it was observed that the most efficient retrofit solution is achieved when the anchor behaves almost in linear range. As the anchors lose stiffness (e.g. in case of JT1-6), the efficacy of the FFHRS to redistribute the forces reduces.

11. EXPERIMENTS ON RC FRAMES RETROFITTED WITH FULLY FASTENED HAUNCH RETROFIT SOLUTION UNDER DYNAMIC LOADING

In Chapter 9, details of the experimental program on a 2D as built RC frame structure tested under dynamic loads on shake table were presented. The basic design of the frame was such that the exterior joints of the frame are $2/3^{\text{rd}}$ scale replica of the exterior joints tested earlier (see chapter 7). The test clearly displayed the vulnerability of the beam-column joints of non-seismically designed RC frame structures under dynamic earthquake excitation.

The experimental program on beam-column joints retrofitted with fully fastened haunch retrofit solution (FFHRS) as detailed in chapter 10 produced encouraging results proving the efficacy of the FFHRS to prevent the joint failure. The tests clearly displayed that provided the anchor group serves its purpose well, FFHRS can be very effective in modifying the hierarchy of the joint sub-assembly, thus leading to desirable failure modes such as beam flexure.

For any structure the type of test closest to reality is the shake table test. In order to verify the suitability of the FFHRS for retrofitting of the joints of structures when subjected to dynamic earthquake loading, an exact replica of the frame tested earlier (chapter 9) was retrofitted with FFHRS and tested under dynamic loads. This chapter provides the details of the test on 2D frame structure retrofitted with FFHRS using bonded anchors. The objectives of this test were:

- (i) to understand the seismic behaviour of RC structures with joints retrofitted with FFHRS under real seismic situation;
- (ii) to evaluate the efficacy of the FFHRS when subjected to dynamic seismic loads;
- (iii) to provide database for validation of models discussed earlier

11.1 Description of Test Structure

11.1.1 Geometry

The geometry of the structure considered for the experiments was exactly same as that of the benchmark specimen as discussed in section 9.1.1 and shown in Figure 9.1.

11.1.2 Material Properties

The average cubic concrete compressive strength at the day of testing was obtained as 28.86 MPa for the retrofitted specimen. The properties of the reinforcing bars are same as those tabulated in Table 9.1.

11.1.3 Fully Fastened Haunch Retrofit Solution (FFHRS)

The haunch elements used in the retrofitting of the frame structure consisted of three machined steel plates welded together. Figure 11.1 shows the schematic drawing of the haunch elements used in this work. All plates used were 10 mm thick.

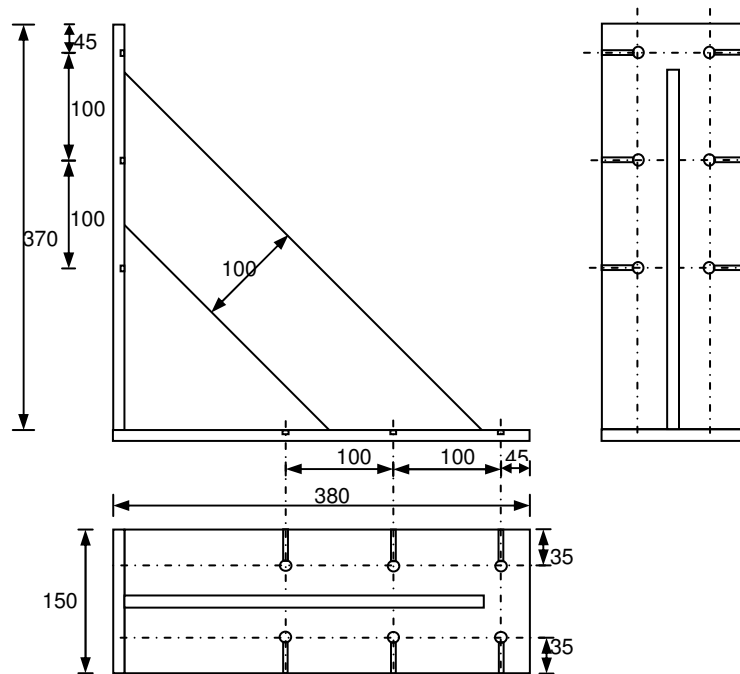


Figure 11.1 Schematic of the haunch elements used for retrofitting of frame

The haunch elements were connected to the frame using bonded anchors which comprised of 10mm diameter high strength threaded rods glued using two component epoxy based mortar. Figure 11.2 represents an installed haunch element using bonded anchors.



Figure 11.2 Haunch element installed using bonded anchors

11.2 Test Setup

The experiment was carried out at the tri-axial shake table system at the Earthquake Engineering and Vibration Research Centre (EVRC) of Central Power Research Institute (CPRI), Bangalore, India. In order to prevent any accidental out of plane movement of the 2D frame structures, steel frames same as in case of test on as-built structure were placed on either side of the frame on shake table. Again, 1.0 tonnes of mass was added at each floor level. Figure 11.3 shows the layout of the test structure and supporting structure on the shaking table. The instrumentation for the 2D frame consisted of the following:

- Accelerometers at each floor to measure the response acceleration history
- Accelerometers at the shake table to record the input time history
- Strain gauge on reinforcing bars to measure strains at critical locations
- Potentiometers to measure beam, column and joint deformations

In addition to strain gauges provided on the reinforcing bars of beams and columns for as built structure, eight more strain gauges were provided on either end of both beams to capture the strain profile due to haunch. Figure 11.4 shows the locations for strain gauges on reinforcing bars for the retrofitted structure. To evaluate the element deformations, linear potentiometers were used.



Figure 11.3 Layout of retrofitted structure on Shake Table

The experiments were performed under uni-directional earthquake excitation with the test protocol as discussed in chapter 9 for as built specimen.

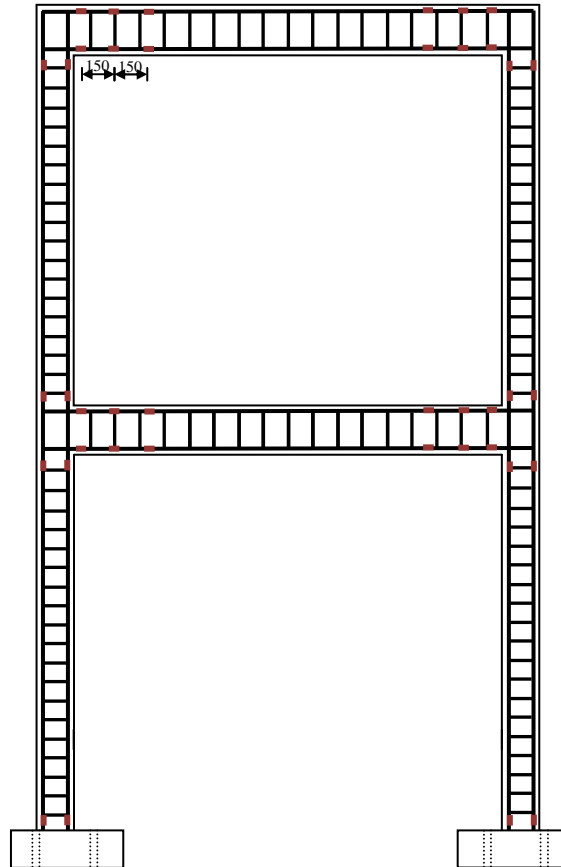


Figure 11.4 Location of strain gauges in as-built frame

11.3 Experimental Results

11.3.1 Natural time periods of the structure

As mentioned above, the structure was first subjected to a sine sweep test to evaluate the natural time periods/frequencies of the structure. The time period corresponding to the first mode was obtained as 0.234 seconds (4.27 Hz), while the same for second mode was obtained as 0.062 seconds (16.26 Hz).

11.3.2 Simulated seismic test on retrofitted structure with PGA = 0.1g

The retrofitted structure was subjected to a base excitation corresponding to a PGA of 0.1g. Figure 11.5 represents the acceleration time history recorded at first floor and Figure 11.6 depicts the same recorded at the roof.

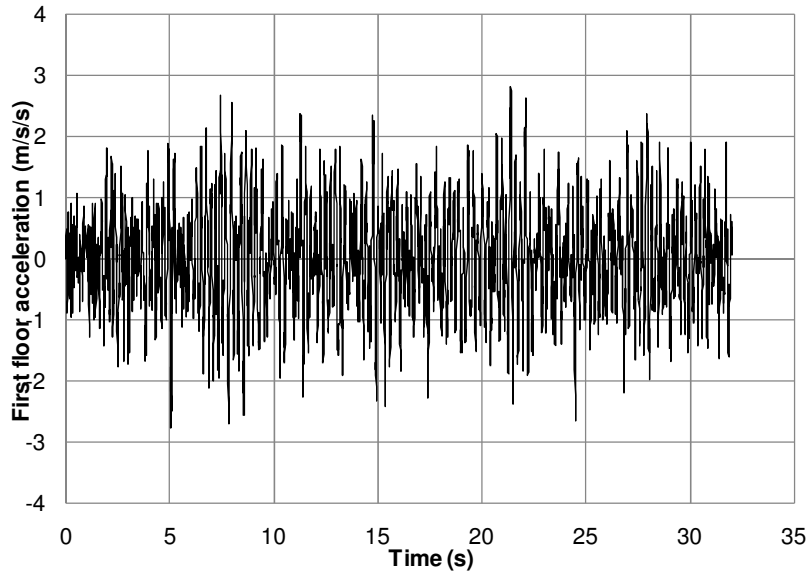


Figure 11.5 Recorded acceleration-time history at the first floor level for input ground motion corresponding to PGA = 0.1g for retrofitted structure

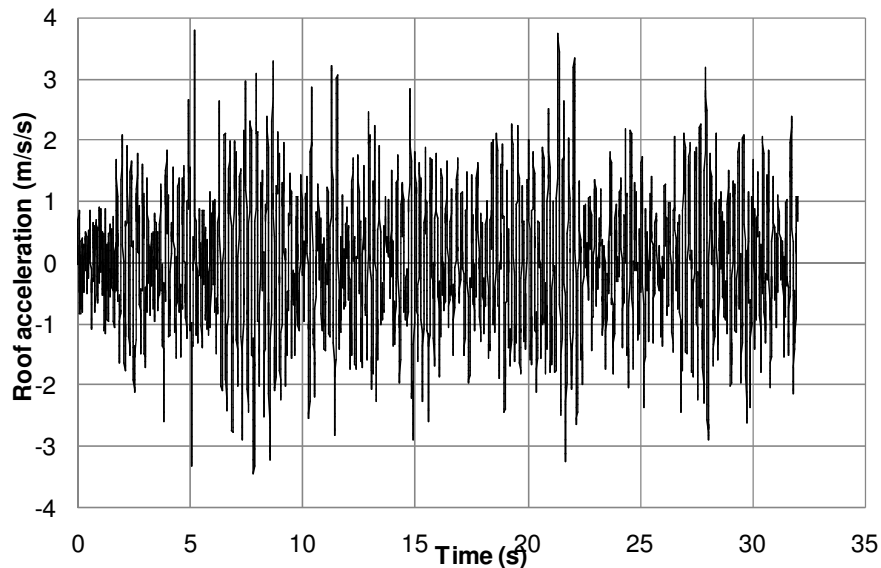


Figure 11.6 Recorded acceleration-time history at the roof level for input ground motion corresponding to PGA = 0.1g for retrofitted structure

The peak floor acceleration was obtained as 2.80 m/s^2 for first floor and 3.84 m/s^2 for roof level. During the ground motion of $0.1g$, no cracks were observed in the structure.

11.3.3 Simulated seismic test on retrofitted structure with PGA = 0.2g

Figure 11.7 represents the acceleration time history recorded at first floor and Figure 11.8 depicts the same recorded at the roof. The peak floor acceleration was obtained as 5.09 m/s^2

for first floor and 6.74 m/s^2 for roof level. At this acceleration level, a single crack at the column-foundation interface was observed (Figure 11.9).

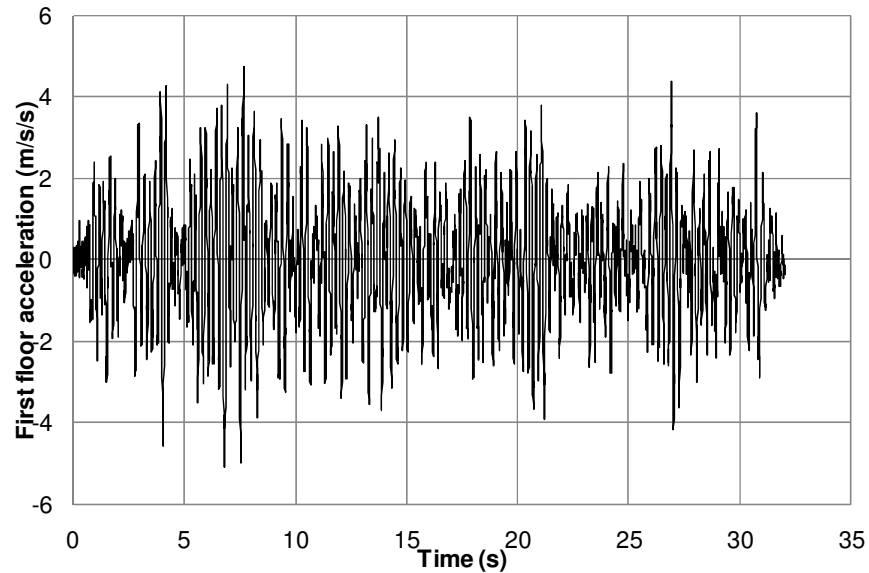


Figure 11.7 Recorded acceleration-time history at the first floor level for input ground motion corresponding to PGA = 0.2g for retrofitted structure

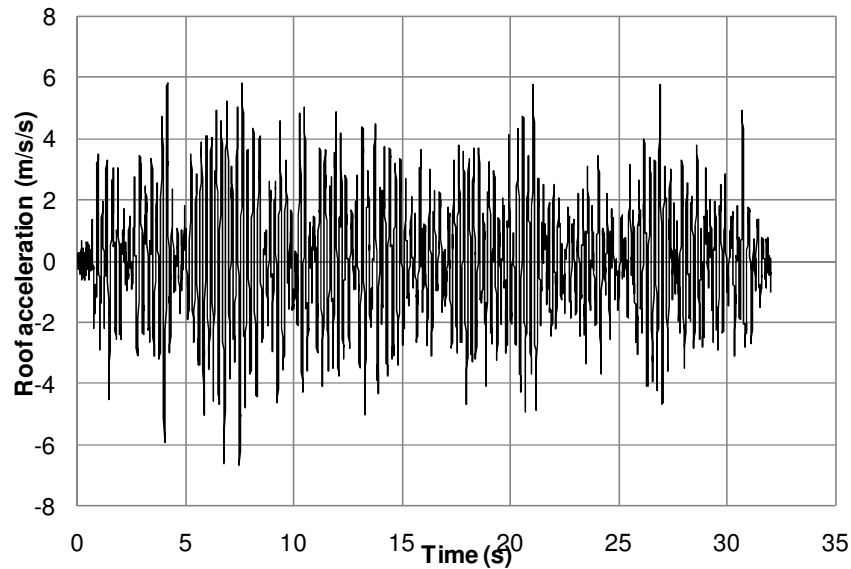
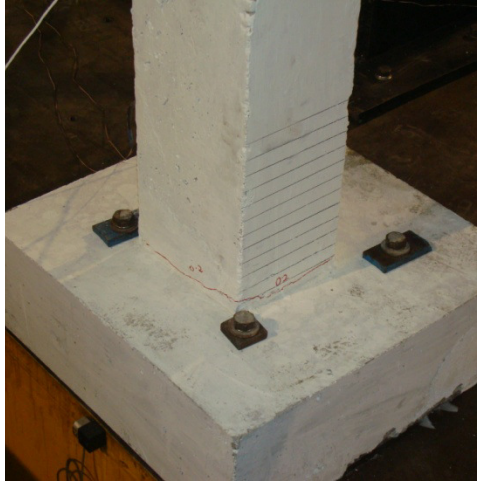


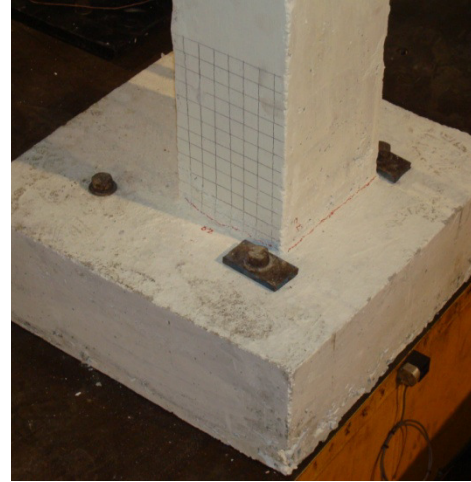
Figure 11.8 Recorded acceleration-time history at the roof level for input ground motion corresponding to PGA = 0.2g

11.3.4 Simulated seismic test on retrofitted structure with PGA = 0.3g

Figure 11.10 represents the acceleration time history recorded at first floor and Figure 11.11 depicts the same recorded at the roof corresponding to the input ground motion with a PGA of 0.3g. The peak floor acceleration was obtained as 7.47 m/s^2 for first floor and 9.68 m/s^2 for roof level.



(a) Left side column



(b) Right side column

Figure 11.9 Crack patterns observed at the base of column for base excitation of 0.2g

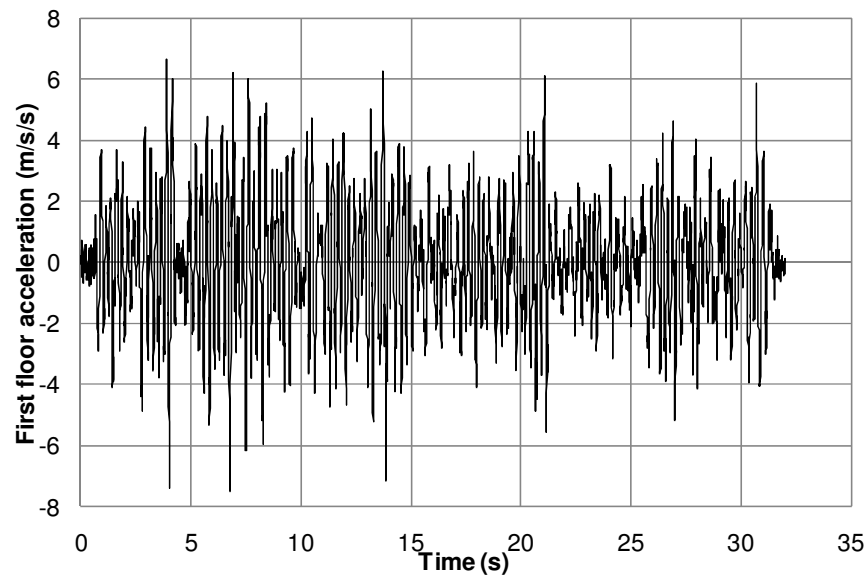


Figure 11.10 Recorded acceleration-time history at the first floor level for input ground motion corresponding to PGA = 0.3g for retrofitted structure

The crack patterns observed after the loading wave corresponding to a PGA of 0.3g are presented in Figure 11.12.

Several new cracks at the base of the column were observed (Figure 11.12a). However, no cracks were observed at the beam of first floor level, which was in contrast to the test on as-built structure where the cracks appeared at the beam of first floor level also.

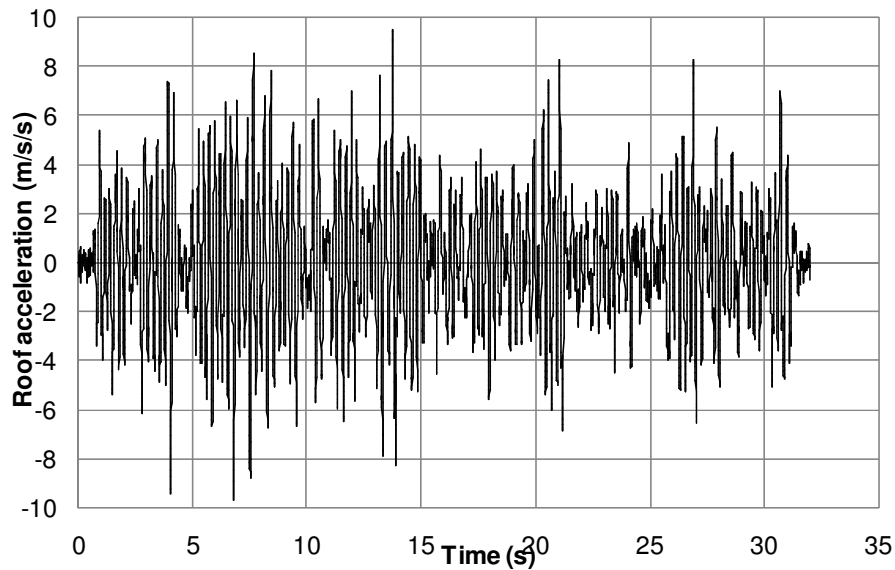
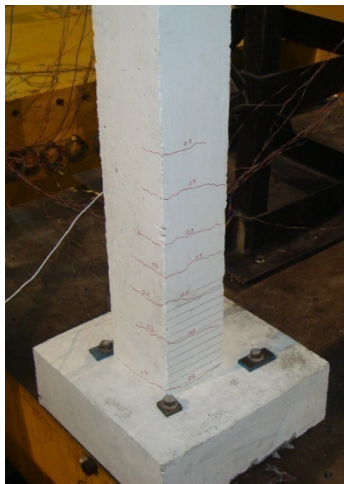


Figure 11.11 Recorded acceleration-time history at the roof level for input ground motion corresponding to PGA = 0.3g for retrofitted structure



(a) Left side column



(b) Right side column

Figure 11.12 Crack patterns observed after the base excitation of 0.3g

11.3.5 Simulated seismic test on retrofitted structure with PGA = 0.4g

Figure 11.13 shows the acceleration time history recorded at first floor and Figure 11.14 depicts the same for the roof corresponding to the input ground motion with a PGA of 0.4g. The peak floor acceleration was obtained as 9.57 m/s^2 for first floor and 12.66 m/s^2 for roof level. At this acceleration level, two more cracks appeared on the left side column (Figure 11.15a), however, on the right side column no new cracks appeared.

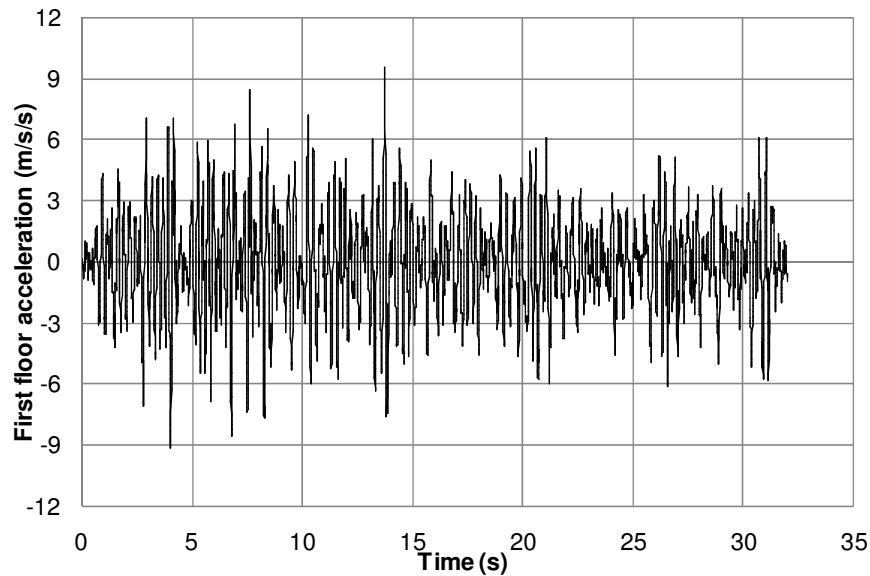


Figure 11.13 Recorded acceleration-time history at the first floor level for input ground motion corresponding to PGA = 0.4g for retrofitted structure

A single crack appeared also on the beam (Figure 11.15b) at the farthest anchor of the haunch. The anchor farthest from the face of the column serves as the critical section for flexure in the beam for the retrofitted structure, and therefore, the first flexural crack appears there. However, no flexural cracks appeared on the column in vicinity of the first floor level. This shows that the desirable hierarchy of strength is maintained in the joint region with beam cracking before joint or column.

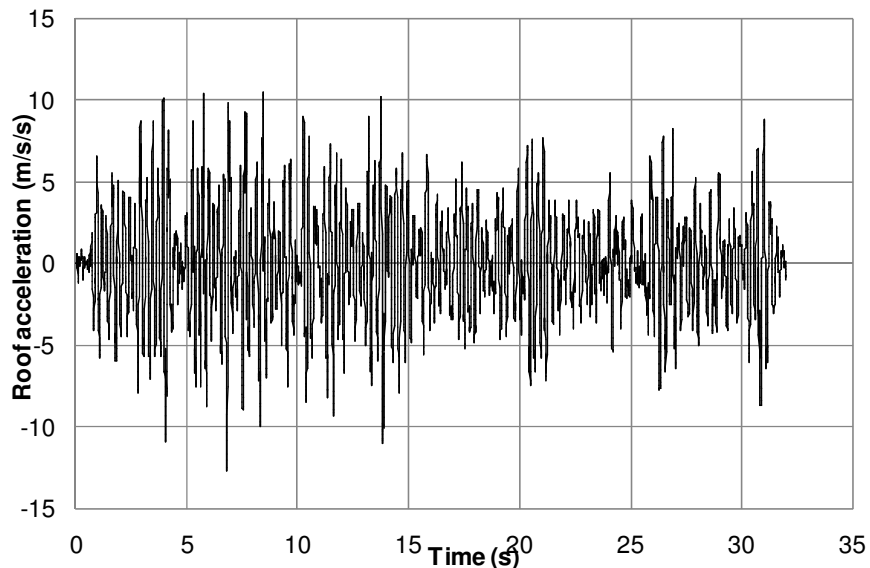
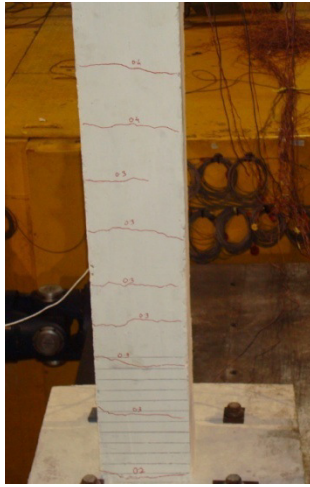


Figure 11.14 Recorded acceleration-time history at the roof level for input ground motion corresponding to PGA = 0.4g for retrofitted structure



(a) At the base of left Side Column (b) On the beam of first floor (left side joint)
Figure 11.15 Crack patterns observed after the base excitation of 0.4g

11.3.6 Simulated seismic test on retrofitted structure with PGA = 0.5g

Figure 11.16 and 11.17 show the acceleration time history recorded at first floor and roof, respectively, corresponding to the input ground motion with a PGA of 0.5g for retrofitted structure. The peak floor acceleration was obtained as 11.43 m/s^2 for first floor and 15.57 m/s^2 for roof level.

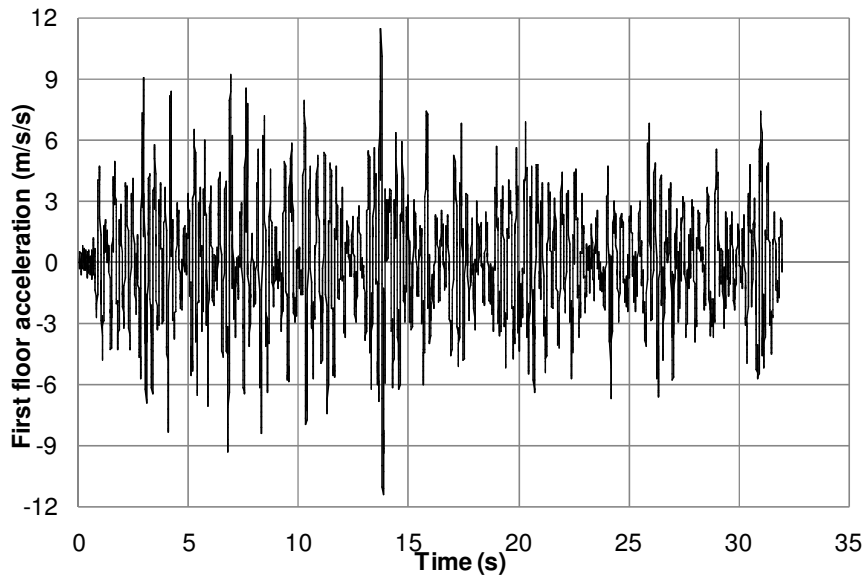


Figure 11.16 Recorded acceleration-time history at the first floor level for input ground motion corresponding to PGA = 0.5g for retrofitted structure

During the loading wave of 0.5g PGA, on the left side column, the cracks appeared on the column just below the first floor beam at the farthest anchor location of the haunch and nearby (Figure 11.18a). Also, the crack initiated in the beam during 0.4g level excitation got extended. On the right side joint, two cracks appeared on the beam from the top and also

cracks appeared on the outer face of the column just below the first floor beam (Figure 11.18b). This essentially shows that on the left side column, the moments due to seismic loads are such that the tension is coming on the inside face of column and lower face of beam while on the right hand side column it is on the outer face of column and top face of beam.

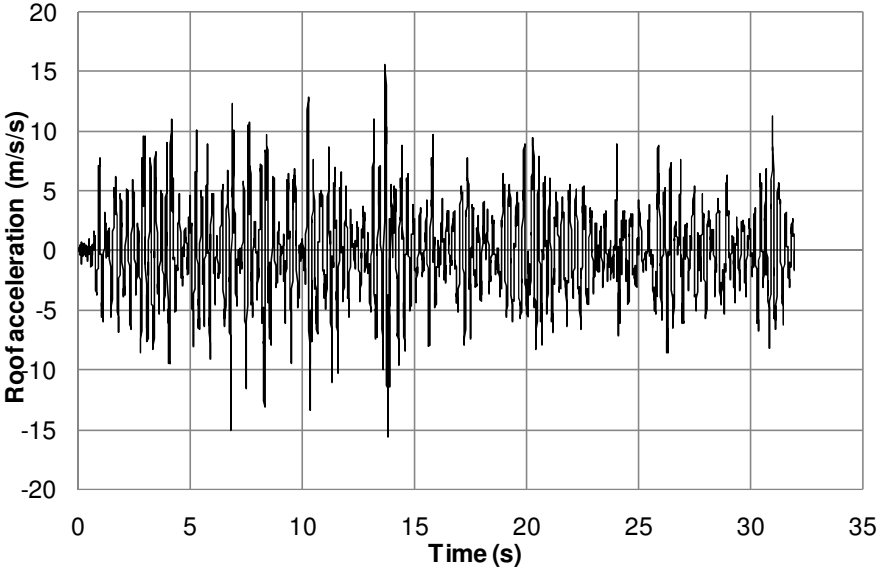


Figure 11.17 Recorded acceleration-time history at the roof level for input ground motion corresponding to PGA = 0.5g for retrofitted structure

Though, in the shake table test, the forces are dynamic and reversing in nature and it is expected to generate symmetric cracks, the same is not happening and the crack pattern is similar to what is expected when the forces applied were monotonic and non-reversing.



(a) Left Side Joint



(b) Right Side Joint

Figure 11.18 Crack patterns observed after the base excitation of 0.5g

During the tests on as built structure, at the base excitation level of 0.5g, clear shear cracks appeared in the joint (Figure 9.26). However, the same is not the case for retrofitted structure, proving the efficacy of the haunch retrofit solution.

11.3.7 Simulated seismic test on retrofitted structure with PGA = 0.6g

Figures 11.19 and 11.20 show the acceleration time history recorded at first floor and roof, respectively, for retrofitted structure, corresponding to the input ground motion with a PGA of 0.6g. The PFA was obtained as 13.04 m/s² for first floor and 17.48 m/s² for roof level.

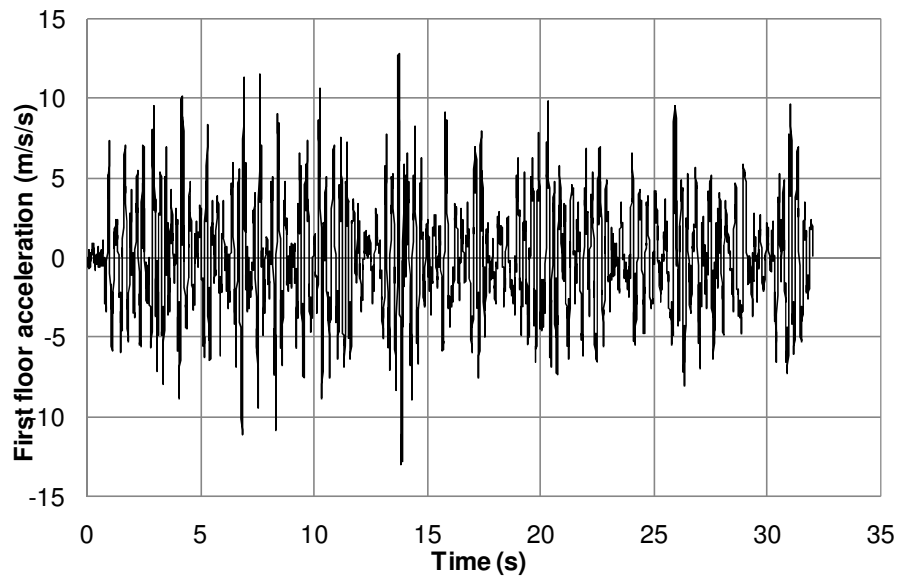


Figure 11.19 Recorded acceleration-time history at the first floor level for input ground motion corresponding to PGA = 0.6g for retrofitted structure

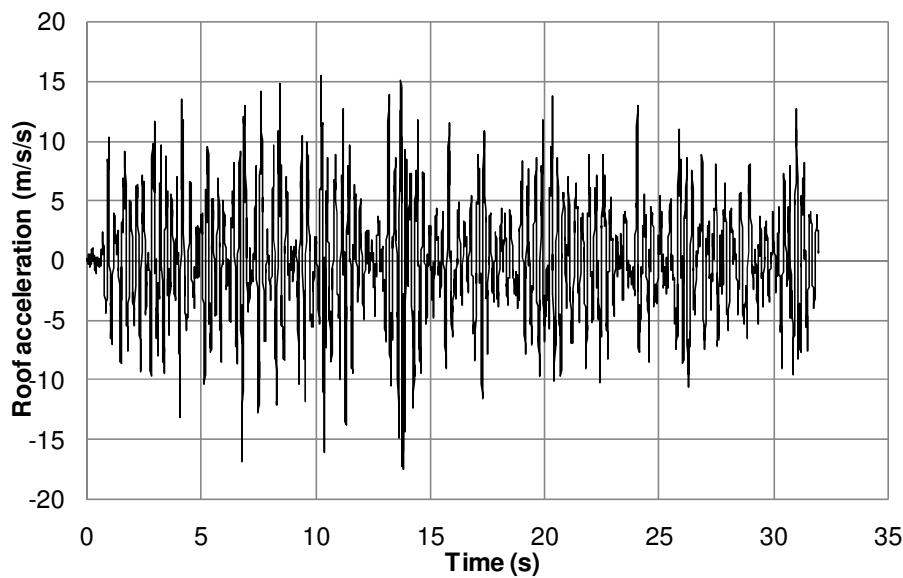


Figure 11.20 Recorded acceleration-time history at the roof level for input ground motion corresponding to PGA = 0.6g for retrofitted structure

The crack patterns observed in the experiment corresponding to the base excitation with 0.6g PGA are presented in Figure 11.21. The crack patterns were essentially the extension of the previously formed cracks on the beams (Figure 11.21a and b). No new cracks were formed at the base of the columns (Figure 11.21c).

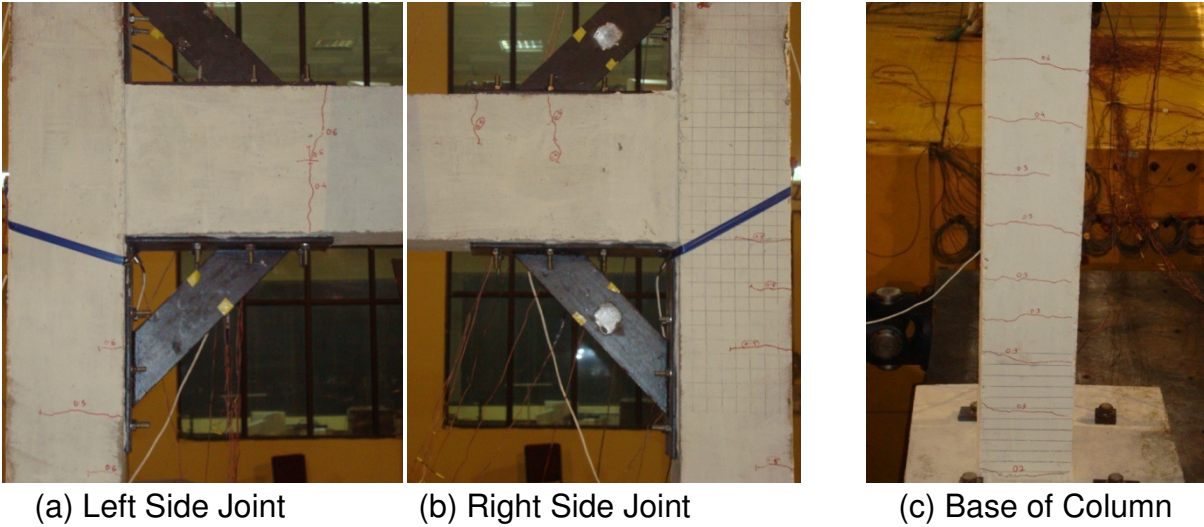


Figure 11.21 Crack patterns observed after the base excitation of 0.6g

11.3.8 Simulated seismic test on retrofitted structure with PGA = 0.7g

The acceleration response histories obtained from the experiment on retrofitted structure corresponding to the input ground motion with a PGA of 0.7g are presented in Figures 11.22 and 11.23 respectively. The peak floor acceleration was obtained as 15.07 m/s² for first floor and 20.44 m/s² for roof level.

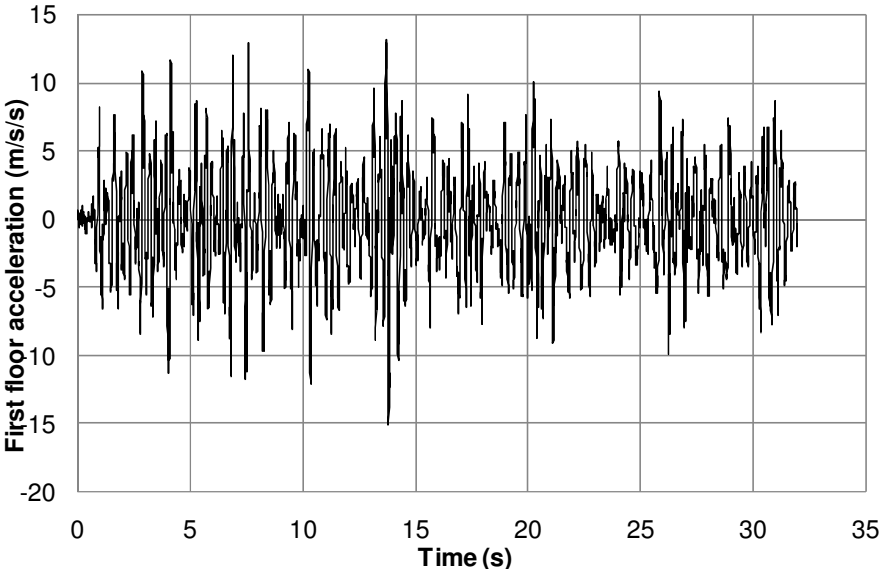


Figure 11.22 Recorded acceleration-time history at the first floor level for input ground motion corresponding to PGA = 0.7g for retrofitted structure

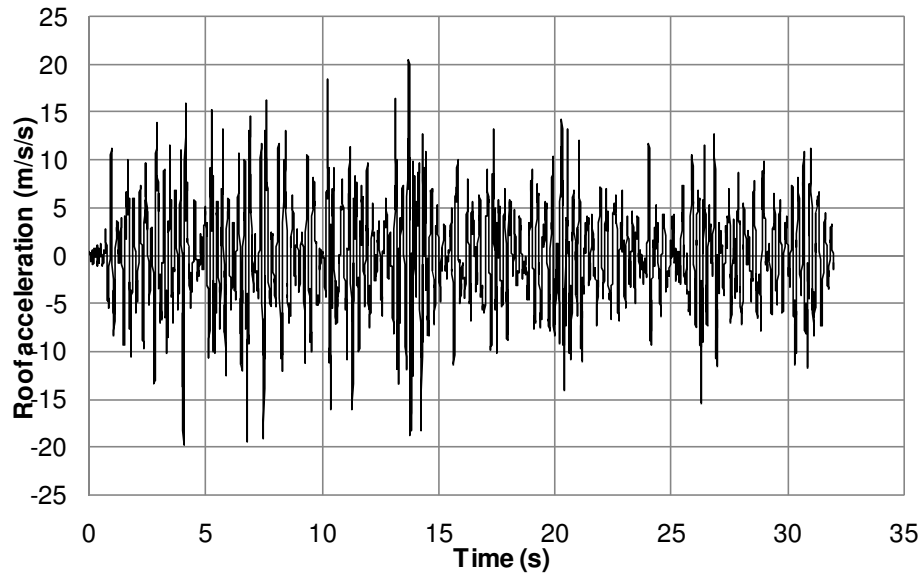
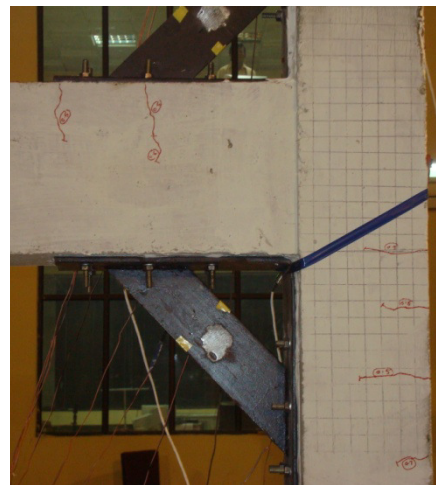


Figure 11.23 Recorded acceleration-time history at the roof level for input ground motion corresponding to PGA = 0.7g for retrofitted structure

The crack pattern obtained for the test performed for a PGA of 0.7g is depicted in Figure 11.24. One crack appeared on the bottom face of the beam close to left side joint (Figure 11.24 a) and another cracks appeared on the outer face of the right side column (Figure 11.24 b). No new cracks appeared at the column base.



(a) Left Side Joint



(b) Right Side Joint

Figure 11.24 Crack patterns observed after the base excitation of 0.7g

11.3.9 Simulated seismic test on retrofitted structure with PGA = 0.8g

Figures 11.25 and 11.26 show the acceleration response histories recorded at the first floor and roof level respectively for the structure subjected to a loading wave of 0.8g PGA. The peak floor acceleration was obtained as 15.70 m/s^2 for first floor and 23.82 m/s^2 for roof level.

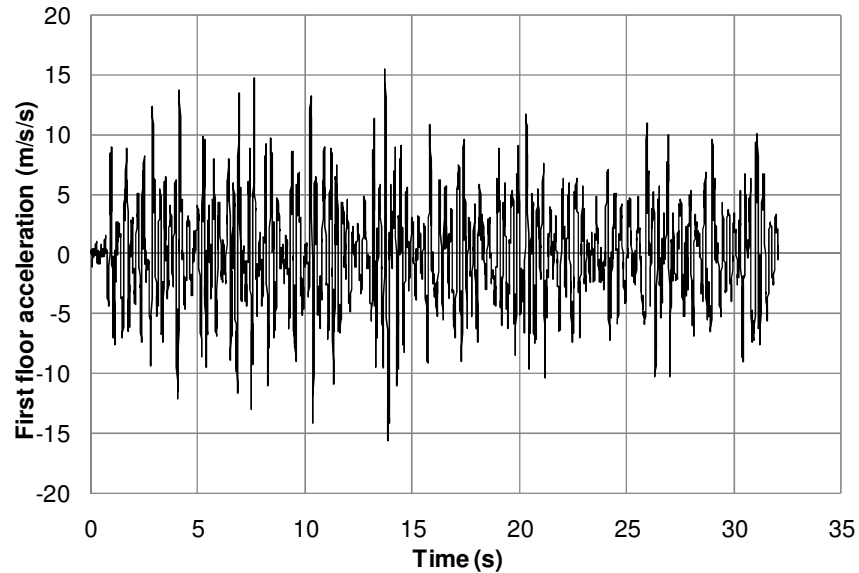


Figure 11.25 Recorded acceleration-time history at the first floor level for input ground motion corresponding to PGA = 0.8g for retrofitted structure

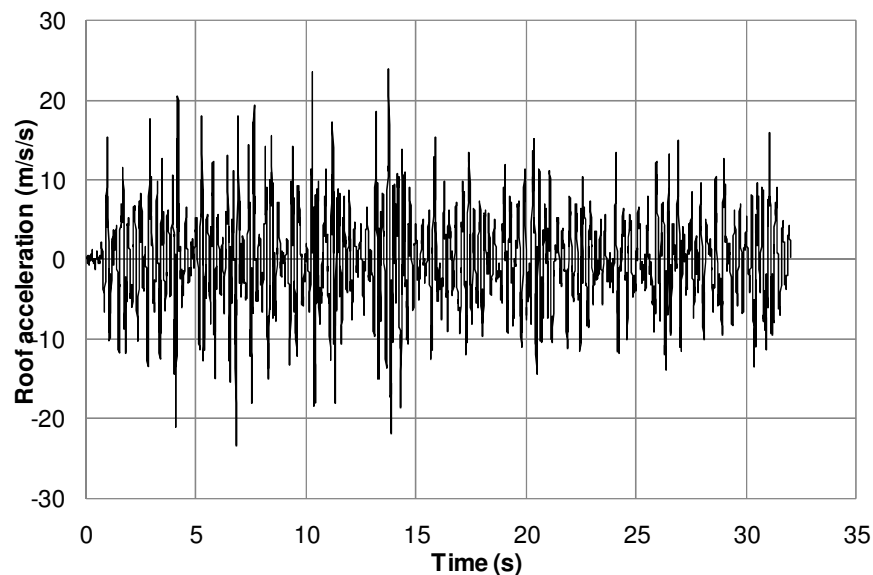


Figure 11.26 Recorded acceleration-time history at the roof level for input ground motion corresponding to PGA = 0.8g for retrofitted structure

Figure 11.27 presents the crack patterns observed on the joints of left side of the structure. On the left side joint, the existing cracks on beam and column got extended and a new crack was observed on the beam close to the position of the mass. No new cracks were observed on the right side joint or on the column base and the same are therefore not shown here.



Figure 11.27 Crack patterns observed after the base excitation of 0.8g

11.3.10 Simulated seismic test on retrofitted structure with PGA = 0.9g

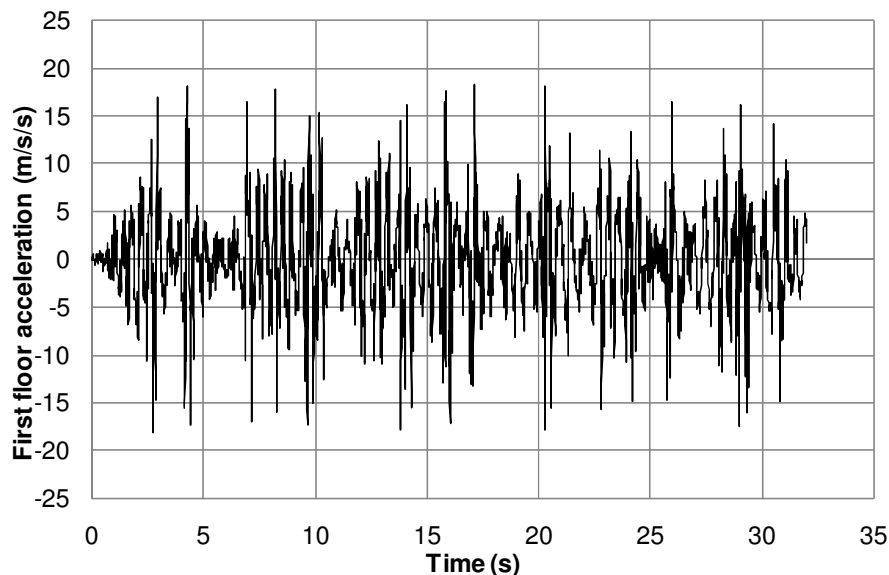


Figure 11.28 Recorded acceleration-time history at the first floor level for input ground motion corresponding to PGA = 0.9g for retrofitted structure

Figures 11.28 and 11.29 show the acceleration response histories recorded at the first floor and roof level respectively for the retrofitted structure subjected to 0.9g PGA loading wave. The peak floor acceleration was obtained as 18.24 m/s^2 for first floor and 27.12 m/s^2 for roof level.

The crack pattern observed for this loading case is depicted in Figure 11.30. On the left side joint, only the earlier formed crack extended by a small amount (Figure 11.30 a). On the right side joint, a new crack from the bottom of the beam just at the end of the haunch element appeared, which propagated and joined the earlier formed crack above it (Figure 11.30 b). No new cracks were formed on the column base.

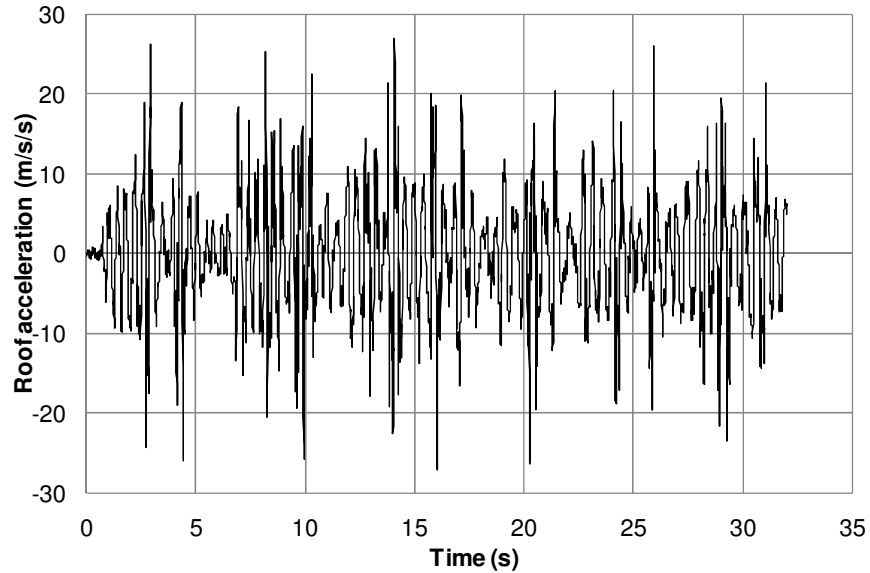
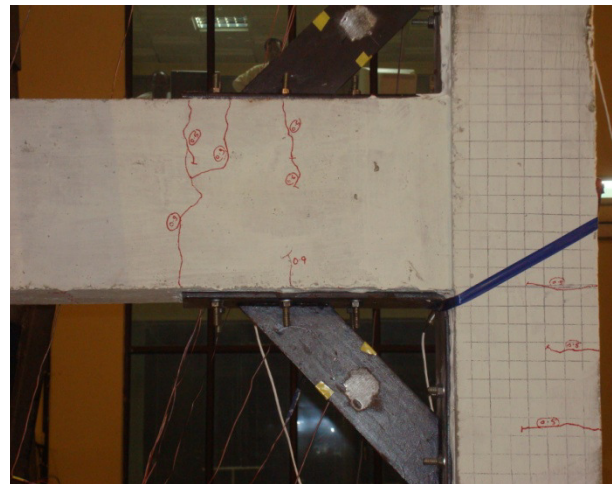


Figure 11.29 Recorded acceleration-time history at the roof level for input ground motion corresponding to PGA = 0.9g for retrofitted structure



(a) Left Side Joint



(b) Right Side Joint

Figure 11.30 Crack patterns observed after the base excitation of 0.9g

11.3.11 Simulated seismic test on retrofitted structure with PGA = 1.0g

Figures 11.31 and 11.32 show the acceleration response histories recorded at the first floor and roof level respectively for the retrofitted structure when subjected to a loading wave of 1.0g PGA. The peak floor acceleration was obtained as 19.75 m/s^2 for first floor and 28.48 m/s^2 for roof level.

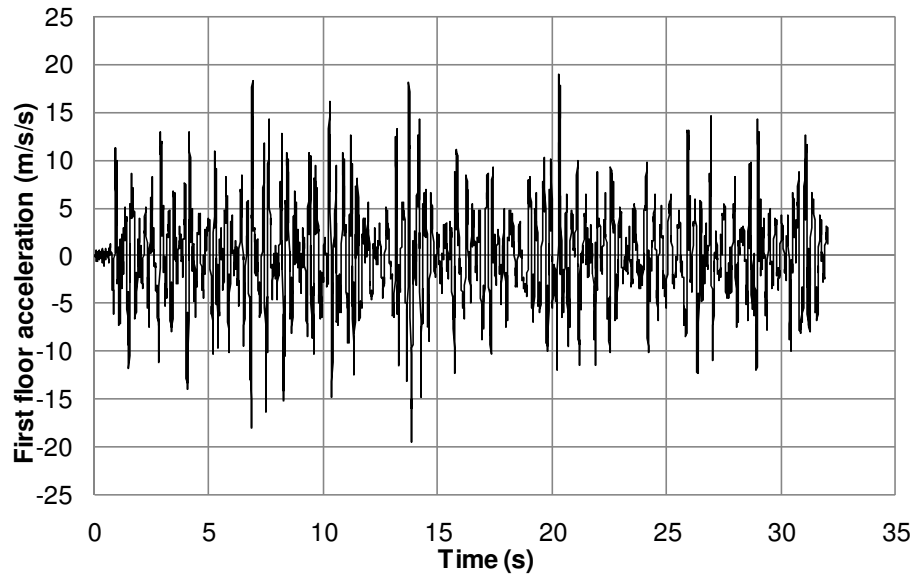


Figure 11.31 Recorded acceleration-time history at the first floor level for input ground motion corresponding to PGA = 1.0g for retrofitted structure

The crack pattern observed for the structure corresponding to a loading wave with PGA = 1.0g is presented in Figure 11.33. The earlier formed cracks propagated further in the beams on left as well as right side. However, no new cracks were observed at the column base or in the joint panel, which clearly proves the efficacy of the haunch retrofit solution in safeguarding the beam-column joints.

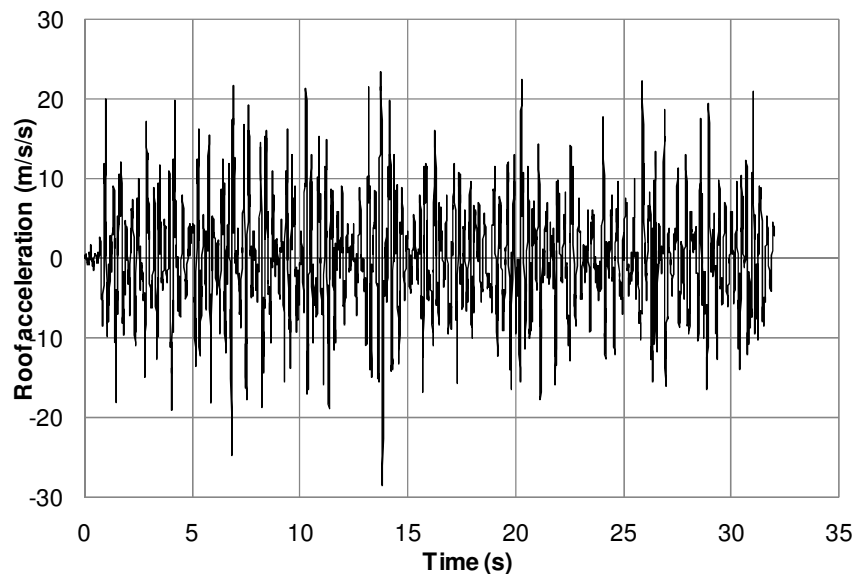
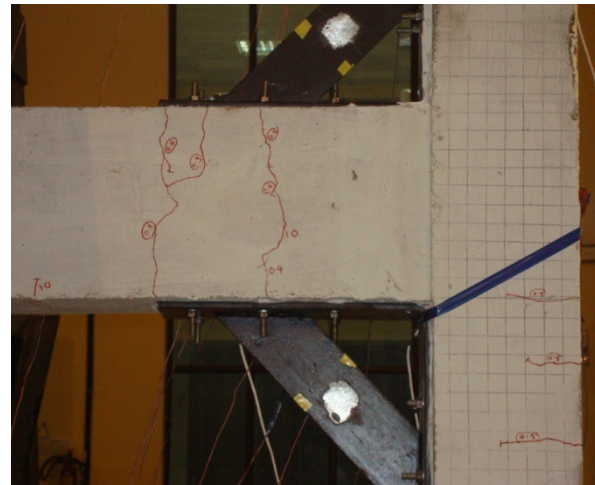


Figure 11.32 Recorded acceleration-time history at the roof level for input ground motion corresponding to PGA = 1.0g for retrofitted structure



(a) Left Side Joint



(b) Right Side Joint

Figure 11.33 Crack patterns observed after the base excitation of 1.0g

11.4 Summary of Experimental Results

The replica of the 2D RC frame structure tested earlier was retrofitted using the fully fastened haunch retrofit solution and tested on shake table with the same loading protocol as the as built structure by subjecting the structure to gradually increasing levels of excitation. The crack patterns were marked at the end of each loading wave. Unlike the test on as built structure, no diagonal shear cracks were observed in the joint panels for the retrofitted structure clearly showing the efficacy of the FFHRS in safeguarding the beam-column joints. The crack patterns were limited to the crack formation in beams and columns, while the joint region was essentially crack free. Also, the cracks formed in beams and columns were only hair line cracks. No spalling was observed in the test. Again, after the test series was over, the structure was taken off the table and laid on the floor to facilitate the marking of cracks on the 2nd floor level (roof).

Figures 11.34a and 11.34b represent the crack patterns observed at the roof on left and right side corner joints, respectively. No diagonal cracks were observed in the corner joints and only a few minor cracks were observed at the bottom of the beam. As expected, the damage at the roof members was much less in comparison to that at first floor.

In figure 11.35, the peak floor acceleration (PFA) recorded in the experiment on retrofitted structure for 1st floor level and roof level are plotted as a function of the peak ground acceleration (PGA). In case of retrofitted structure, this plot is practically linear till the end of the test series unlike as built structure. This is expected since the damage in the structure is minimal and therefore large hysteretic damping is not expected in the system. A summary of the results obtained for the retrofitted structure is given in Table 11.1.



(a) Crack pattern for the left corner joint (b) Crack pattern for the right corner joint
Figure 11.34 Crack patterns observed at the roof level for the retrofitted after the completion of test series

Table 11.1 Summary of experimental results on retrofitted structure

PGA (g)	Peak Response Accel. (g)		Observations
	Roof	1 st floor	
0.1	0.39	0.29	No cracks
0.2	0.69	0.52	Single flexural crack at the base of the bottom column
0.3	0.96	0.76	New cracks at the base of bottom column
0.4	1.29	0.98	Single crack on 1 st floor beam at the farthest anchor of haunch
0.5	1.59	1.17	Cracks on top of bottom column at the farthest anchor
0.6	1.78	1.33	Extension of earlier cracks in the beam
0.7	2.08	1.54	Extension of earlier cracks
0.8	2.43	1.60	Extension of earlier cracks
0.9	2.76	1.86	Extension of earlier cracks
1.0	2.90	2.01	Extension of earlier cracks

Figure 11.36 shows the plot of the variation of fundamental time period corresponding to first mode as a function of the PGA as obtained from the Fourier spectrum of the response corresponding to each PGA level. In this case, the change in fundamental frequency of the structure is nominal with increasing PGA. The fundamental time period increased from 0.23s (for undamaged structure) to 0.26s after completion of whole test series. The only significant variation in the frequency occurs for a PGA of 0.3g, which corresponds to various cracks formed at the column base (Figure 11.12). For better comparison, the variation of time period v/s PGA is also plotted for as built structure in the same graph.

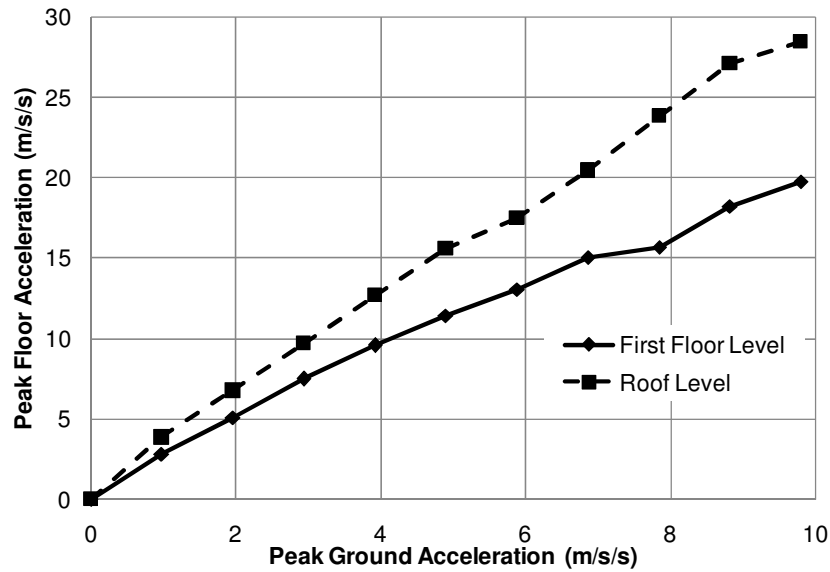


Figure 11.35 Peak floor acceleration as a function of peak ground acceleration as recorded during tests on retrofitted structure

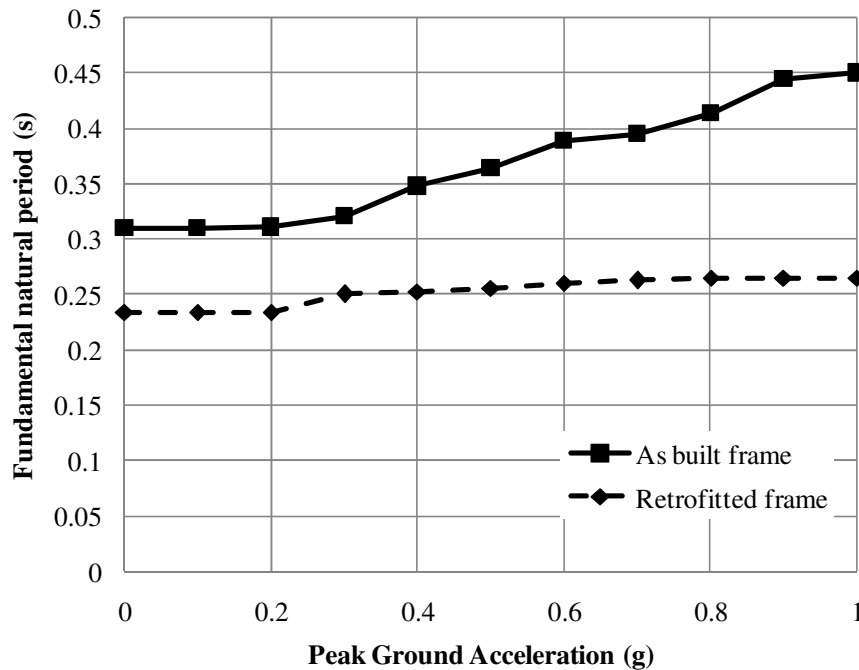


Figure 11.36 Variation of fundamental time period with PGA

Figure 11.37 presents the comparison of maximum joint deformation for exterior joints of the frame as a function of increasing PGA for the as built and retrofitted structure. It can be observed that the joint shear deformation in this case (0.0032 radians) is much less compared to that obtained in case of as built structure (0.0088 radians). The measured shear deformation suggests no significant distortion of the joint as seen from the crack patterns too.

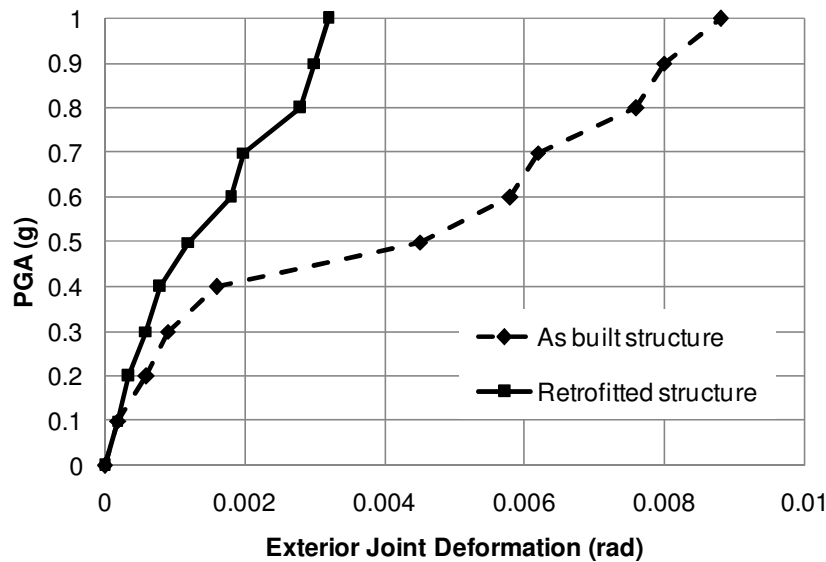


Figure 11.37 Comparison of exterior joint distortion as a function of increasing PGA for as built and retrofitted structure

It was very interesting to note that in case of beam-column joints retrofitted with FFHRS, once a crack appears at the anchor location, it propagates and grows wider with each loading cycle, finally resulting in anchorage failure. Whereas, in case of the structure tested on shake table, even though the crack appeared at the anchor location during the PGA of 0.4g, the crack did not grow wider and the anchor group performed its function very well. It can be attributed to two reasons: (i) under dynamic loads, due to fast loading, the crack does not get enough time to propagate; and (ii) the probability of the anchor loaded to its maximum at the same time when the crack width is maximum, is rather low (Sharma et al, 2010). Therefore, the performance of the anchors under dynamic loads is much better than that under cyclic loads.

Figure 11.38 displays the plot of the peak displacement for first floor and roof as a function of PGA for as built and retrofitted structure. For the as built structure, it can be seen that with the increasing PGA, the storey displacements keep rising, which is attributed to increasing PFA as well as elongated time period. From the theory of structural dynamics, it is known that the flexible structure (elongated time period) has higher displacement response for the same acceleration. Thus, in case of as built structure, the displacement demand is as high as 121mm (4.76in) at the roof (approx. 2.8% global drift). Whereas, in case of retrofitted structure, the maximum displacement demand is around 50.54mm (1.99in) at the roof (approx. 1.18% global drift). Thus, due to lower time period of the retrofitted structure till the end of the test, the displacement demands are rather limited compared to that of as built structure. The results of the tests on retrofitted structure and their comparison with the results on as built structure clearly displayed that the structure retrofitted with the haunch retrofit solution behaved almost in linear fashion till the end of the test and successfully proved the efficacy of retrofit solution.

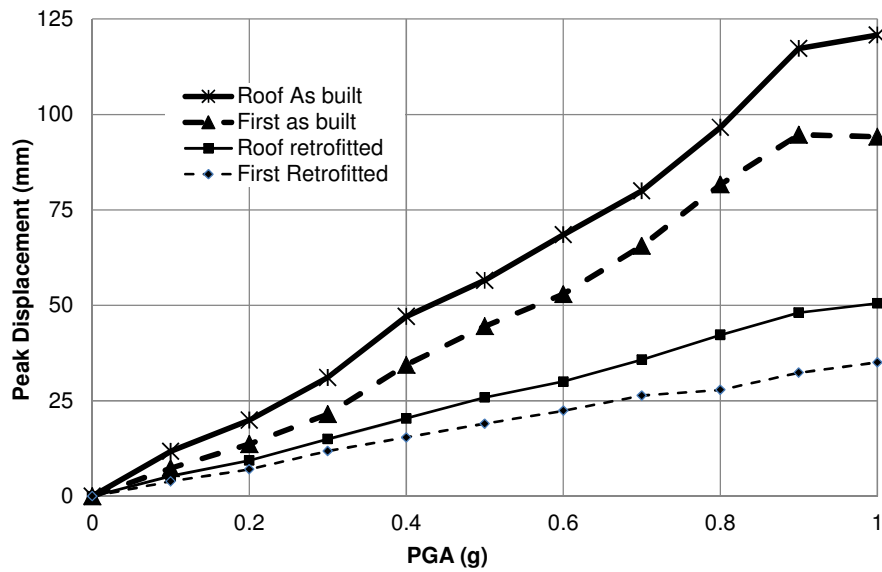


Figure 11.38 Peak floor displacements as a function of PGA for as built and retrofitted structure

Though, due to the limitation of the test setup, the experiment could not be continued further, the behaviour of the two structures under further higher seismic excitations has been numerically assessed. The results are discussed in chapter 14.

12. VALIDATION OF PROPOSED JOINT MODEL AGAINST EXPERIMENTS

This chapter provides the validation of the proposed joint model at sub-assembly as well as structural level. The analysis was performed using the proposed joint model following the formulations and assumptions given in chapter 4. The results of analysis are validated by and comparing them with their experimental counterparts. In this chapter, only the results of monotonic analysis are provided. The load-displacement curve obtained from the analysis is compared with the envelope of the cyclic hysteretic loops obtained from experiments. The comparison of full hysteretic loops for certain cases is provided in next chapter.

The procedure to obtain the nonlinear characteristics required to perform monotonic analysis of RC members (beams and columns) using the constitutive laws, equilibrium equations and strain compatibility conditions are well documented in literature. Since, in this work no new formulations were suggested for the monotonic analysis of the members, and only already proven techniques were used to model the inelastic monotonic behaviour of the members, such an analysis was not repeated in this work. However, the laws, assumptions and procedure followed to obtain the same are detailed in Appendix-A. The procedure to perform inelastic static analysis is explained in Appendix-B. Further validation of the model and complete analysis procedure is performed at structural level against the experiment reported in chapter 8 as well as experiments reported in literature. The details of the same are provided in this chapter. The numerical analysis was performed using commercial software SAP2000.

12.1 Validation of model against experiments at sub-assembly level

To verify the applicability of the joint model, and to validate the same, various joints of different configurations tested by different researchers were analyzed. To understand the concepts and applicability, the model was first used to analyze the exterior joints. Various exterior joints were analyzed in this work to include joints having different type of beam reinforcement embedment, different levels of axial loads, aspect ratios far from unity, different failure modes etc. Once the model was thoroughly validated against exterior joints, the same was validated against interior joints as well.

12.1.1 Exterior Joints

The exterior joints analyzed under this work include joints with beam bars bent in, joints with beam bars bent out, joints with top beam bar bent in and bottom beam bar straight with 150 mm embedment as well as joints with plain round bars and end hooks. The analyses of the same are presented here.

12.1.1.1 Tests by Clyde et al (2000)

Clyde et al (2000) performed cyclic tests on exterior beam-column joints with varying axial loads. The beam bars were bent into the joint in all the cases. The joints were designed in a way to have joint shear failure before the yielding of the beam bars. A typical exterior beam-column joint in a reinforced concrete frame building built in 1964 was chosen as a model for the project. The overall dimensions of the original joint were reduced by half, and reinforcing details were reduced based on shear stress calculations. The longitudinal reinforcement in the beam was increased to prevent early degradation of the beam, forcing a shear mode of failure in the joint. There is no transverse reinforcement within the joint core, and the beam longitudinal bars are not adequately anchored in the connection. Four joints were tested under the program with an axial stress on the column as $0.1 f_c'$ in two cases and $0.25 f_c'$ in other two cases. The reinforcement yield and ultimate strength values are given in Table 12.1 below.

Table 12.1 Properties of reinforcement bars used by Clyde et al (2000)

Reinforcement Type	Bar Size No. (dia in mm)	Yield strength, f_y (MPa)	Ultimate strength, f_u (MPa)
Beam longitudinal	#9 (28.58)	454.4	746.0
Column longitudinal	#7 (22.23)	469.5	741.9
Stirrups/ties	#3 (9.53)	427.5	654.3

Typical reinforcement details and dimensions of the joints tested are given in Figure 12.1 and the test setup is shown in Figure 12.2.

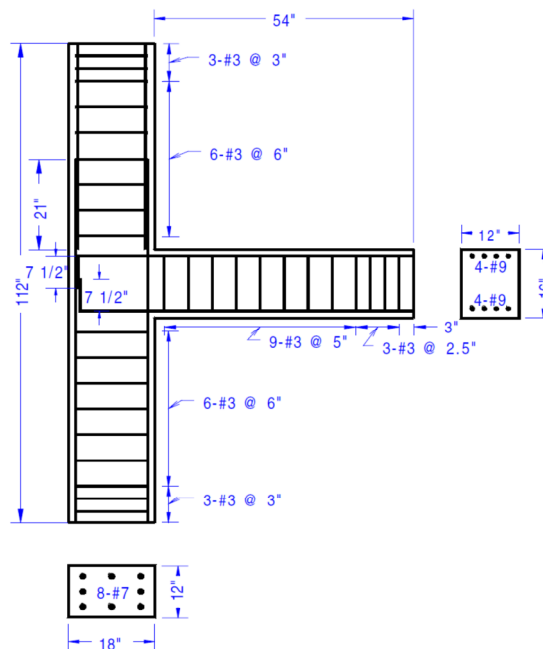


Figure 12.1 Details of joints tested by Clyde et al (2000)

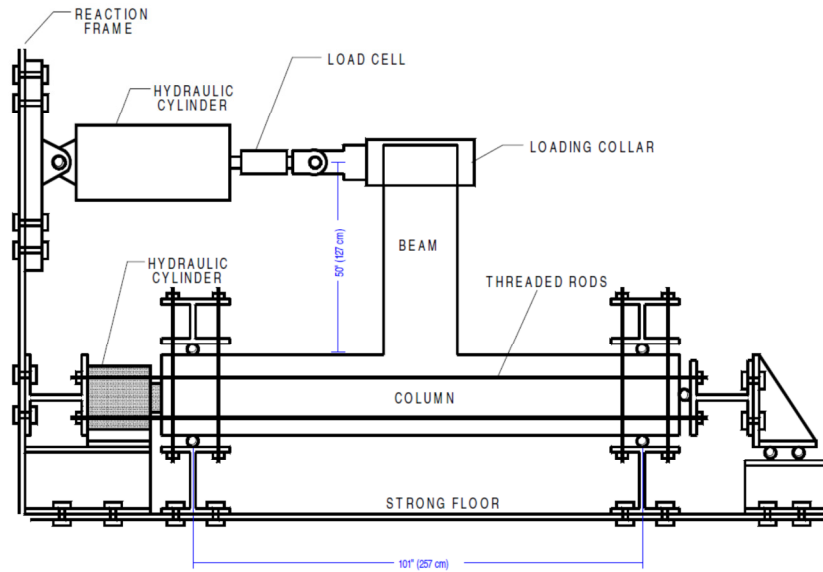


Figure 12.2 Test setup of joints tested by Clyde et al (2000)

12.1.1.1.1 Test #2 (10% axial load)

Test #2 was performed with an axial load corresponding to an axial stress on the column as $0.1 f_c'$. The cylindrical concrete compressive strength f_c' was 46.2 MPa (Clyde et al, 2000).

For the given geometry, reinforcement details and material properties, the beam and column flexural and shear characteristics were generated following the procedure given in Appendix. The joint spring characteristics were evaluated following the procedure explained in chapter 4. A sample calculation is given below.

Let us consider the point,

$$p_t = 0.29\sqrt{f_c'}$$

$$p_t = 0.29\sqrt{f_c'} = 0.29\sqrt{46.2} = 1.97\text{MPa}$$

and the axial stress is given as

$$\sigma_a = 0.1f_c' = 0.1 \times 46.2 = 4.62 \text{ MPa}$$

The aspect ratio,

$$\alpha = h_b/h_c = 16/18 = 0.89$$

Substituting the values in eq (4.21), we get,

$$\sigma = \frac{2 \times 4.62 + 0.89^2 \times 1.97 + 0.89 \sqrt{0.89^2 \times 1.97^2 + 4 \times 1.97 \times (4.62 + 1.97)}}{2} = 8.70 \text{ MPa}$$

Thus,

$$V_{jv} = (\sigma - \sigma_a) b_c h_c = (8.70 - 4.62) \times 304.8 \times 457.2 \text{ N}$$

Or, $V_{jv} = 568.6 \text{ kN}$

From (4.23), we get,

$$V_{jh} = \frac{V_{jv}}{\alpha} = \frac{568.6}{0.89} = 638.84 \text{ kN}$$

Let us assume, $T = 750 \text{ kN}$

Thus, $V_c = T - V_{jh} = 750 - 638.84 = 111.16 \text{ kN}$

Thus, we have,

$$V_b = \frac{V_c l_c}{l_b + h_c / 2} = \frac{111.16 \times 2.57}{1.27 + 0.457 / 2} = 190.64 \text{ kN}$$

Moment in beam at the face of the column,

$$M_b = V_b l_b = 190.64 \times 1.27 = 242.11 \text{ kNm}$$

The corresponding tensile force in the reinforcement can be obtained as 780 kN. Since this is more than the assumed value of 750 kN, another trial is required.

Performing the calculations for a few times, we can converge to a value of $T = 745 \text{ kN}$. The corresponding value of column shear is

$$V_c = T - V_{jh} = 745 - 638.84 = 106.16 \text{ kN}$$

and the bending moment in the beam is

$$M_b = V_b l_b = \frac{V_c l_c l_b}{l_b + h_c / 2} = \frac{106.16 \times 2.57 \times 1.27}{1.27 + 0.457 / 2} = 231.22 \text{ kNm}$$

Thus, corresponding to a principal tensile stress of $p_t = 0.29\sqrt{f'_c}$, the values of shear force in column and bending moment in the beam are $V_c = 106.16$ kN and $M_b = 231.22$ kNm respectively. Similarly, the values of shear force in column and bending moment in the beam corresponding to various levels of principal tensile stress can be calculated. In this case these values were calculated for principal stress values of $p_t = 0.29\sqrt{f'_c}$, $p_t = 0.42\sqrt{f'_c}$ and $p_t = 0.10\sqrt{f'_c}$. The values of M_b and V_c along with the corresponding rotation and deformation values were used as the characteristics for the rotational and shear springs used to model the joint behaviour as explained in chapter 4.

The comparison of experimentally and numerically obtained curves is shown in Figure 12.3 below. To better visualize and appreciate the significance of joint modelling, a comparison is given with the analysis results where the joint core was considered rigid i.e. when the numerical model did not have springs to model the joint shear behaviour. It should be noted that in this case also, the beam and column member had both flexural and shear spring characteristics assigned. The test was performed under quasi cyclic loading. Here, the envelope of the hysteretic loops is considered for comparison with numerical results. In chapter 13, the comparison of hysteretic loops will be given.

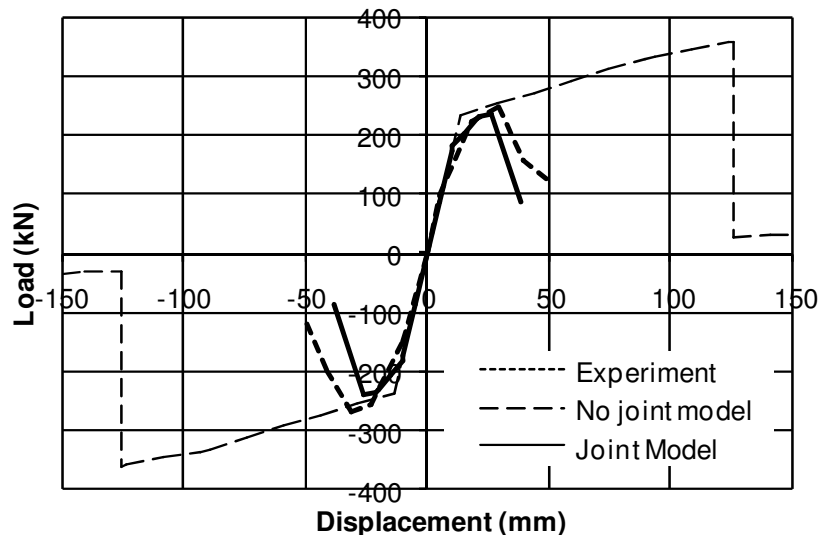


Figure 12.3 Validation of joint model with results for Test #2 by Clyde et al (2000)

From figure 12.3, it is very clear that the analysis considering the joint model is able to simulate the joint behaviour very well, whereas the model considering the joint as rigid provides very unsafe results. Thus, the significance of joint modelling is highlighted. As per the test report (Clyde et al, 2000), measurable flexural cracks in the beam and shear cracks in the joint appeared during the seventh load step corresponding to a lateral load of approximately 40 kips (178 kN). From the analysis, it can be seen that the load at the beam

end corresponding to a principal tensile stress of $p_t = 0.29\sqrt{f'_c}$ is 181.9 kN, which is quite close to the value of first significant cracking in the experiment.

In the experiment, the subsequent loading steps produced only slight increase in crack widths in the beam. Similar observations were made in the analysis. Figure 12.4 depicts the deformed state and hinge pattern of the joint as obtained in the analysis. Pink colour hinge in the beam represents a minor damage in the beam whereas red and yellow coloured hinges in the joint region depict extensive damage in the joint panel.

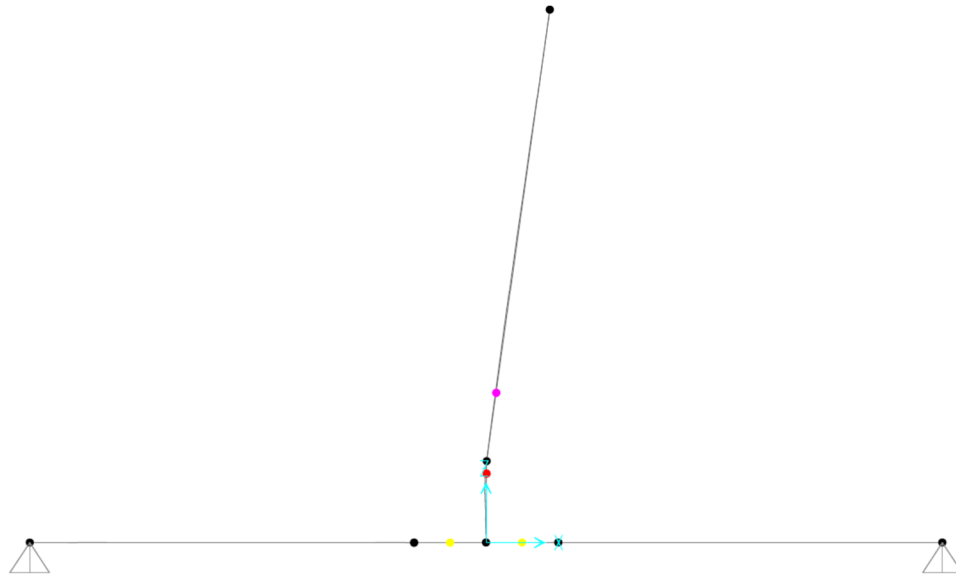


Figure 12.4 Hinge (Damage) pattern obtained from numerical analysis

The peak load was obtained as 267 kN in the experiment and 241 kN in the analysis, a value that corresponds to a principal tensile stress value of $p_t = 0.42\sqrt{f'_c}$. Thus, it can be concluded that not only the overall load deflection behaviour but also the failure modes were captured well in the analysis using joint model. In the case of model where the joint springs were not modelled, a large strain hardening behaviour after the first yield of beam bars was observed. The peak load in this case was obtained as 370 kN and the ultimate displacement as 135 mm which was found to be significantly on the unsafe side.

12.1.1.1.2 Test #6 (10% axial load)

Similar to test #2, test #6 was performed with an axial stress on the column as $0.1f'_c$. The cylindrical concrete compressive strength, f'_c was 40.1 MPa (Clyde et al, 2000). The characteristics for the members (beams and columns) were evaluated following the procedure described in Appendix, while the joint spring characteristics were derived following the procedure described in chapter 4. The yield and ultimate load from experiment was obtained as 156kN and 262kN, while the same were obtained as 166kN and 243kN

respectively in the analysis. The comparison of the envelope of experimental hysteretic loops and results of numerical analysis is given in Figure 12.5 below. Again, a good correspondence between experimental and numerical analysis results highlights the capability of the model to predict the joint behaviour well.

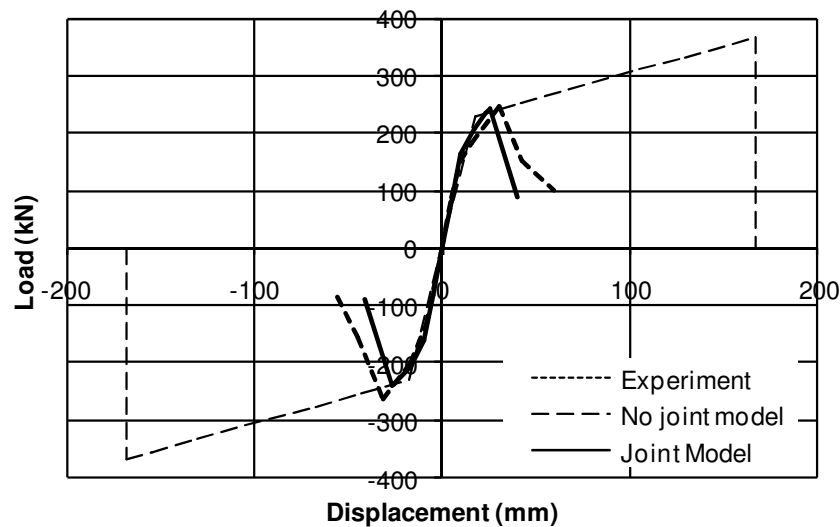


Figure 12.5 Validation of joint model with results for Test #6 by Clyde et al (2000)

12.1.1.1.3 Test #4 (25% axial load)

Test #4 was performed with axial stress on the column as $0.25 f_c'$. The cylindrical concrete compressive strength, f_c' was 41.0 MPa (Clyde et al, 2000). The comparison of envelope of experimental hysteretic loops and numerical results is given in Figure 12.6 below. As per the test report (Clyde et al 2000), yielding corresponded to a lateral load of 60 kips (267 kN), while the peak load was obtained as 276 kN in the experiment. . From the analysis, the load at the beam end corresponding to yield is 223 kN, while the peak load is 286 kN. Thus, it can be again concluded that even for a higher axial load, both the load deflection behaviour and the failure modes were captured nicely in the analysis using joint model. The model without joint springs again yielded results on unsafe side.

12.1.1.1.4 Test #5 (25% axial load)

Similar to test #4, test #5 also had an axial load on the joint corresponding to an axial stress on the column as $0.25 f_c'$. The cylindrical concrete compressive strength, f_c' was 37.0 MPa (Clyde et al, 2000). The yield and ultimate load were obtained as 231kN and 267kN in the experiment, while as 207kN and 268kN respectively, in analysis considering joint model.

The comparison of results of the experiment and numerical analysis curves is given in Figure 12.7. Same as in earlier cases, it can be observed that the numerical results using the

proposed joint model are very close to the experimental results, while the same considering joint as rigid (no joint model) leads to unsafe predictions.

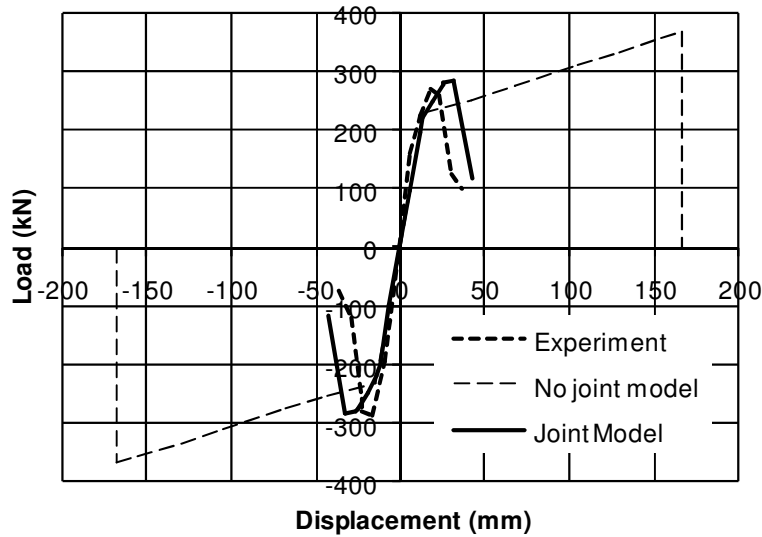


Figure 12.6 Validation of joint model with results for Test #4 by Clyde et al (2000)

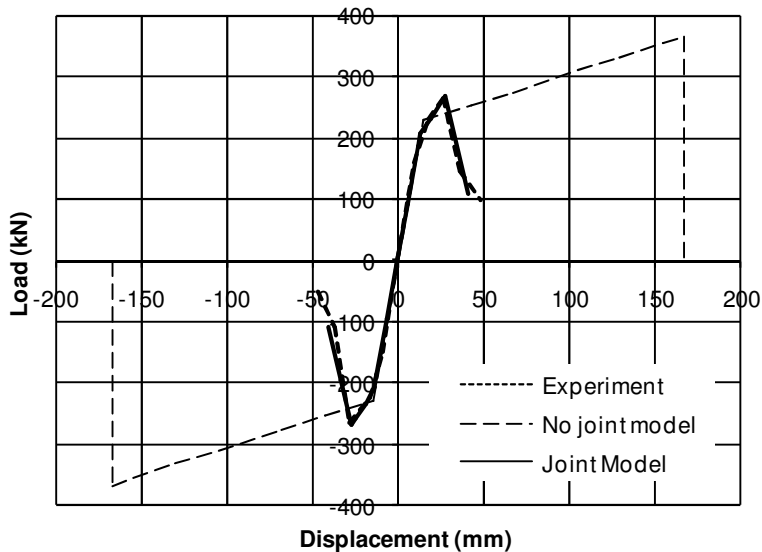


Figure 12.7 Validation of joint model with results for Test #5 by Clyde et al (2000)

12.1.1.2 Tests by Pantelides et al (2002)

Pantelides et al (2002) performed cyclic tests on exterior beam-column joints with varying axial loads. The six test units were full-scale models of typical exterior beam-column joints in RC buildings found in the United States before 1970. The longitudinal and transverse reinforcement in the beam and the column transverse steel was increased to prevent early degradation of the beam and column, forcing a shear mode of failure in the joint. There is no

transverse reinforcement within the joint core, and the beam longitudinal bottom bars did not have adequate embedment into the joint.

Analysis is performed for four units two of which were tested with an axial stress on the column as $0.1f_c'$ and other two were tested with an axial stress of $0.25f_c'$ on the column. The reinforcement details and dimensions of the joints tested are given in Figures 12.8 and 12.9. As seen in Figure 12.8, test units 1 and 2 had top beam bars bent into the joint in the form of a hook but covering full joint depth and the bottom bars were embedded only up to 6 inch (approx. 150mm) inside the joint.

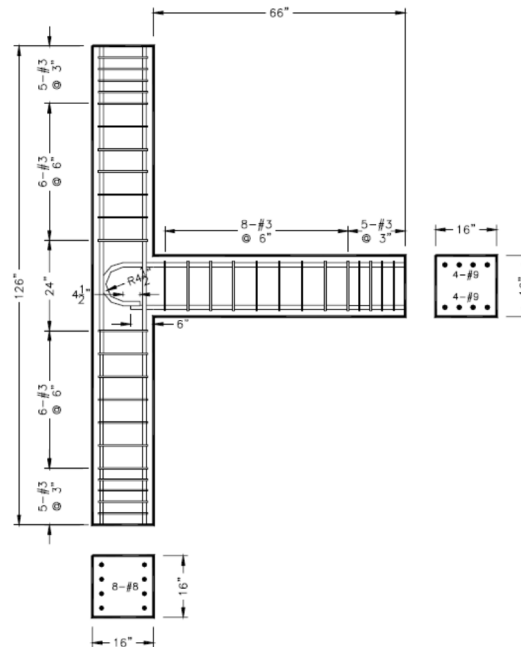


Figure 12.8 Details of test units 1 and 2 (Pantelides et al 2002)

The yield and ultimate strength values for reinforcement are given in Table 12.2 below.

Table 12.2 Properties of reinforcement bars used by Pantelides et al (2002)

Reinforcement Type	Bar Size No. (dia in mm)	Yield strength, f_y (MPa)	Ultimate strength, f_u (MPa)
Beam longitudinal	#9 (28.58)	458.5	761.2
Column longitudinal	#8 (25.4)	469.5	741.9
Stirrups/ties	#3 (9.53)	427.5	654.3

Test units 5 and 6 (Figure 12.9) had both top and bottom beam bars bent into the joint in the form of a hook covering full joint depth.

12.1.1.2.1 Test unit 1

Test unit 1 was tested with axial load on the column corresponding to an axial stress of $0.1f_c'$. The cylindrical concrete compressive strength, f_c' was 33.1MPa (Pantelides et al, 2002). The comparison of experimental and numerically obtained curves is given in Figure 12.10. To visualize the significance of joint modelling, a comparison is given with the analysis results when the model did not have springs to model the joint shear behaviour.

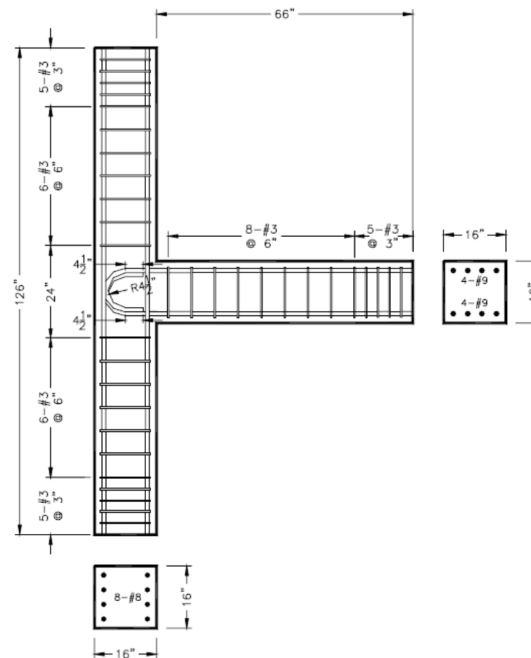


Figure 12.9 Details of test units 5 and 6 (Pantelides et al 2002)

The effect of unsymmetric detailing of the joint can be clearly seen in this case. Note that a positive load indicates that the load was applied in the upward direction. It is clear that the upward direction resistance is deficient because of the inadequate anchorage of the bottom beam bars into the joint. This effect can be considered in the joint model by using the critical principle tensile stress v/s joint deformation curve shown in Figure 4.18.

The peak load from the experiment was obtained as 93.8 kN for up direction and 198.6 kN for down direction. In the analysis, the corresponding values were obtained as 102.6 kN for up direction and 191.3 kN for down direction that matches closely the experimentally obtained values.

Obviously, the analysis considering joint as rigid cannot give any consideration to different embedment and hence predicts equal load-deflection behaviour for either side. It can be seen from Figure 12.10 that the model without joint springs yielded results on highly unsafe side for both the directions.

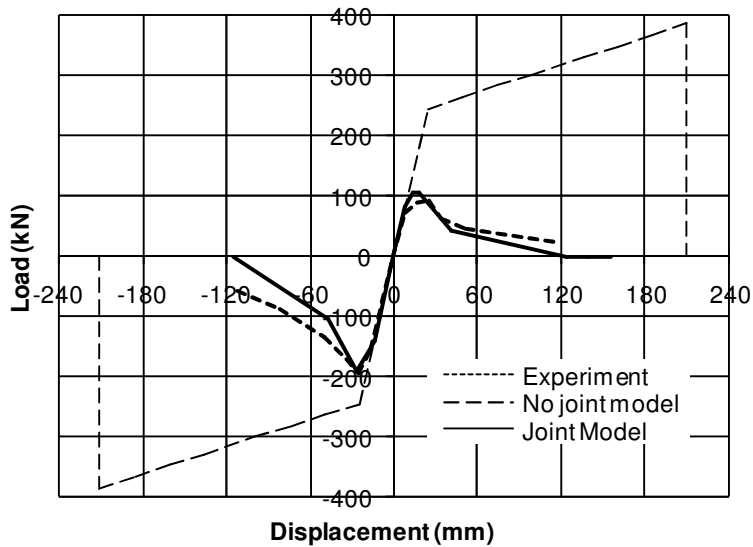


Figure 12.10 Validation of joint model with results for test unit 1 (Pantelides et al 2002)

These results show that the model works well not only for joints with bent in bars but also for joints with poorer end anchorages as in this case.

12.1.1.2.2 Test unit 2

Test unit 2 was tested with an axial load corresponding to an axial stress on the column as $0.25f'_c$. The cylindrical concrete compressive strength f'_c was 30.2MPa (Pantelides et al, 2002). The comparison of experimental and numerical results is given in Figure 12.11.

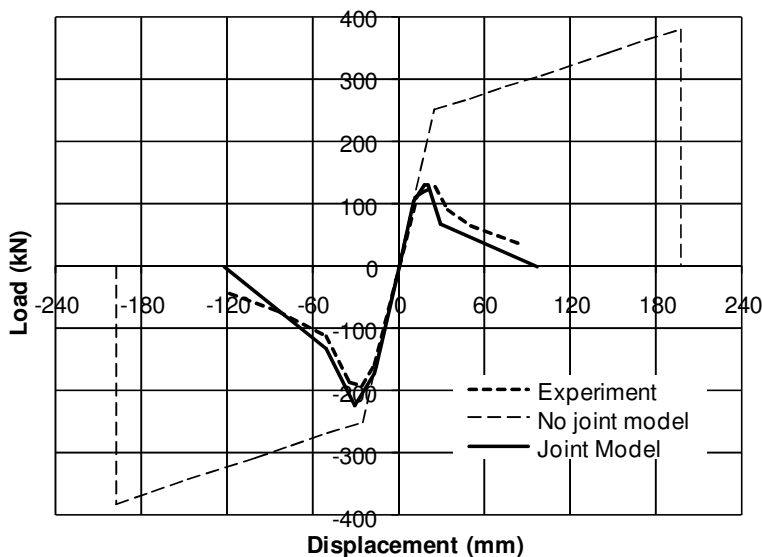


Figure 12.11 Validation of joint model with results for test unit 2 (Pantelides et al 2002)

The effect of unsymmetric detailing of the joint is somewhat attenuated due to the presence of higher axial load on the column which was beneficial in preventing early bond slip of the

bottom beam bars. The peak load from the experiment was obtained as 128.4 kN for up direction and 193.7 kN for down direction. In the analysis using joint model, the corresponding values were obtained as 131.6 kN for up direction and 221.4 kN for down direction that matches well with the experimentally obtained values. Nevertheless, considering joint as rigid is shown to be dangerous.

12.1.1.2.3 Test unit 5

Test unit 5 had an axial load on the joint corresponding to an axial stress on the column as $0.1f_c'$. The cylindrical concrete compressive strength f_c' was 31.7MPa (Pantelides et al, 2002). The comparison of experimental and numerical results is given in Figure 12.12 below.

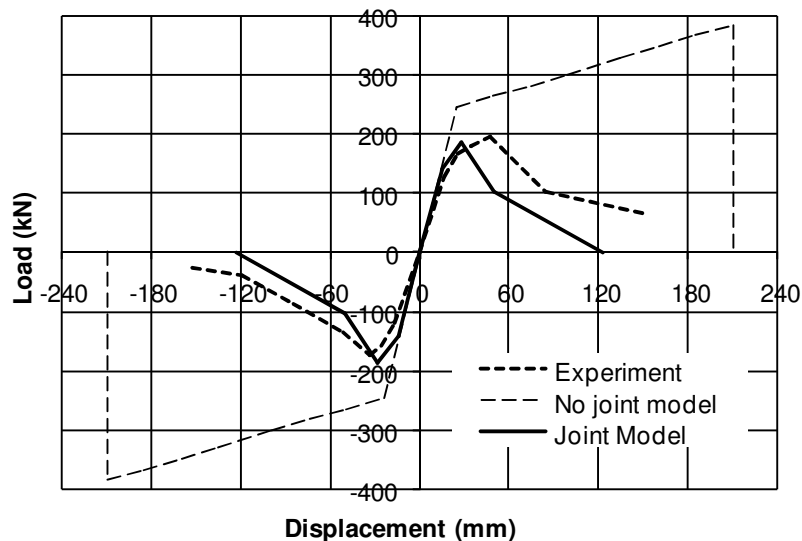


Figure 12.12 Validation of joint model with results for test unit 5 (Pantelides et al 2002)

The peak load from the experiment was obtained as 197.8 kN for up direction and 173.2 kN for down direction. Since in this case, the symmetric beam reinforcement embedment was provided, in the analysis, the peak load was obtained as 191.8 kN for both up and down directions, which agrees well with the experimental results. Same as in previous cases, the model considering joint as rigid is found as not applicable.

12.1.1.2.4 Test unit 6

Test unit 6 was tested with an axial load corresponding to an axial stress on the column as $0.25f_c'$. The cylindrical concrete compressive strength, f_c' was 31.0MPa (Pantelides et al, 2002). The comparison of experimental and numerical results is given in Figure 12.13.

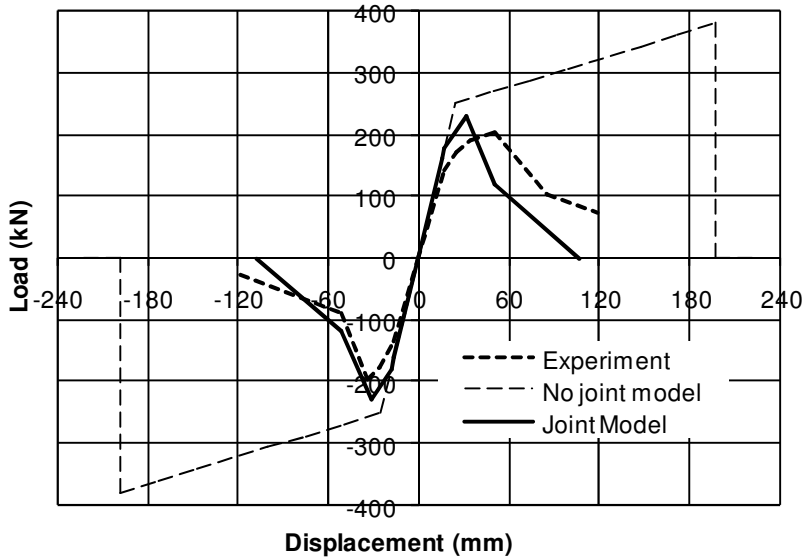


Figure 12.13 Validation of joint model with results for test unit 6 (Pantelides et al 2002)

The peak load from the experiment was obtained as 201.4 kN for up direction and 195.5 kN for down direction. In the analysis considering joint model, the peak load was obtained as 223.8 kN for both up and down directions. The overall behaviour predicted by the analysis is close to the experimental results.

12.1.1.3 Tests by El-Amoury and Ghobarah (2002)

El-Amoury and Ghobarah (2002) performed test on a gravity-designed exterior joint with details as shown in Figure 12.14.

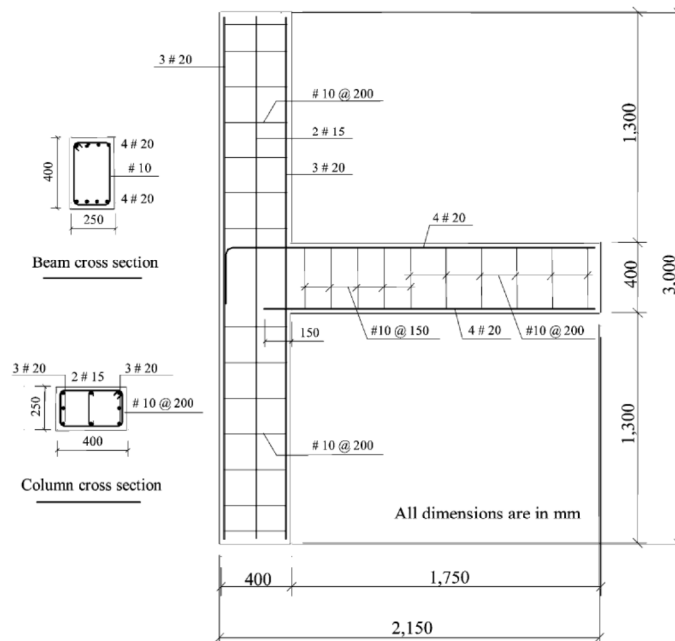


Figure 12.14 Details of the joint tested by El-Amoury and Ghobarah (2002)

The top longitudinal reinforcements in the beam are bent down into the column, whereas the bottom reinforcement was anchored 150 mm from the column face. No transverse reinforcement was installed in the joint region. The beam was reinforced using 4#20 as top and bottom longitudinal bars and #10 as transverse steel. The column was reinforced with 6#20 plus 2#15 as longitudinal bars and #10 ties spaced 200mm.

The concrete compressive strength on the test day was 30.6MPa and the yield strength of the steel bars #10, #15 and #20 was 450MPa, 408MPa and 425MPa, respectively. The specimen was tested in the column vertical position, hinged at the top and bottom column ends and subjected to a cyclic load applied at the beam tip. A constant axial load of 600kN was applied to the column.

The comparison of experimental and analytical curves is given in Figure 12.15. The peak load from the experiment was obtained as 60 kN for up direction and 86 kN for down direction. In the analysis, the peak load was obtained as 64 kN for up and 102 kN for down directions using joint model and 140 kN for both up and down directions without using joint model. The overall behaviour predicted by the analysis is close to the experimental results.

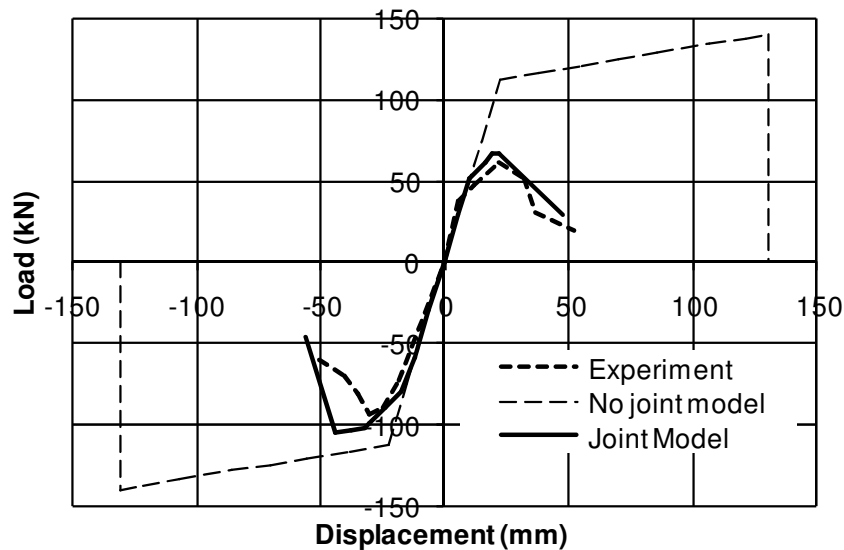


Figure 12.15 Validation of joint model with results for test by El-Amoury and Ghobarah (2002)

12.1.1.4 Test by Murty et al (2003)

Murty et al (2003) performed cyclic tests on exterior beam-column joints with various anchorages of beam bars and different types of joint reinforcement. Out of those, one joint, namely 'S1' had gravity design and no joint reinforcement and the same was considered suitable for further validation of the model. There was no axial load applied on the column. Figure 12.16 shows the details of the joint.

The top longitudinal reinforcements in the beam are bent down into the column, whereas the bottom reinforcement was anchored 150 mm from the column face. No transverse reinforcement was installed in the joint region. Complete information may be obtained from reference Murty et al (2003). The cylinder strength of the concrete used for the specimen was 27.8 MPa. The comparison of results for joint S1 tested by Murty et al (2003) is given in Figure 12.17.

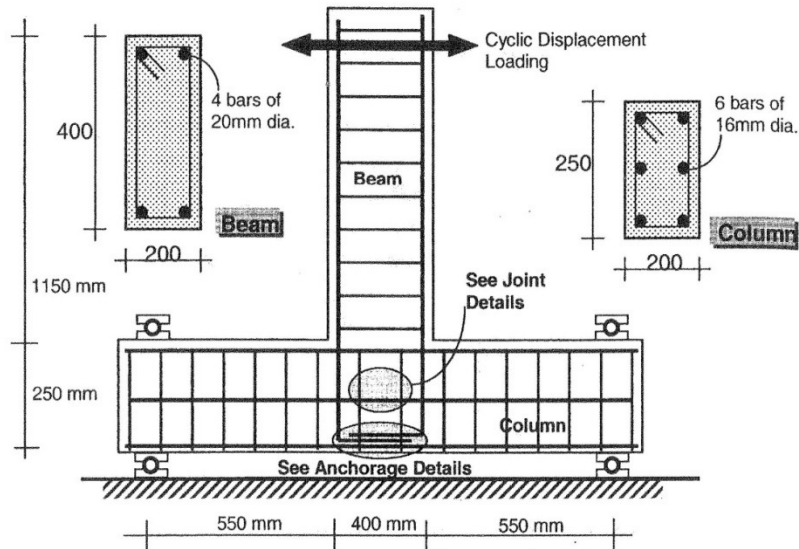


Figure 12.16 Details of joint tested by Murty et al (2003)

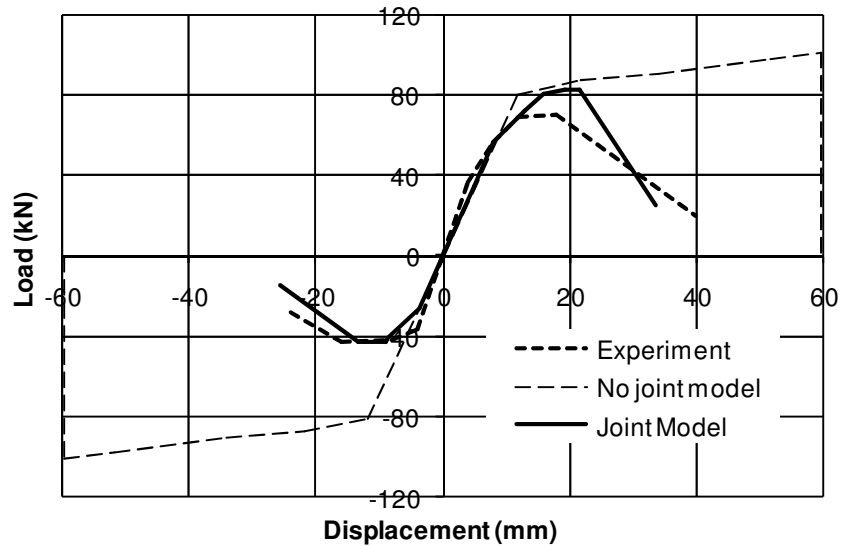


Figure 12.17 Validation of joint model with test S1 performed by Murty et al (2003)

The comparison shows that the analytical and experimental results are close when joint model is used and without using the same, the results can be misleading and unsafe.

12.1.1.5 Test by Hwang et al (2005)

Hwang et al (2005) performed tests on nine exterior joints having different joint reinforcement details. One test namely OT0 did not have any joint reinforcement and therefore was considered for validation. However, there was one major difference in this case compared to the earlier cases. Though, the joint did not have any ties, the specimen was designed to have sufficient shear strength according to strut and tie model (Hwang et al, 2005). It was written by the authors that Specimen OT0 was a lower bound limit that had just sufficient shear strength. Figure 12.18 shows the details of the joint. Complete information may be obtained from Hwang et al (2005). This test was selected to demonstrate that in case of joint sub-assemblies undergoing beam/column flexure instead of joint shear can also be analyzed using the same procedure.

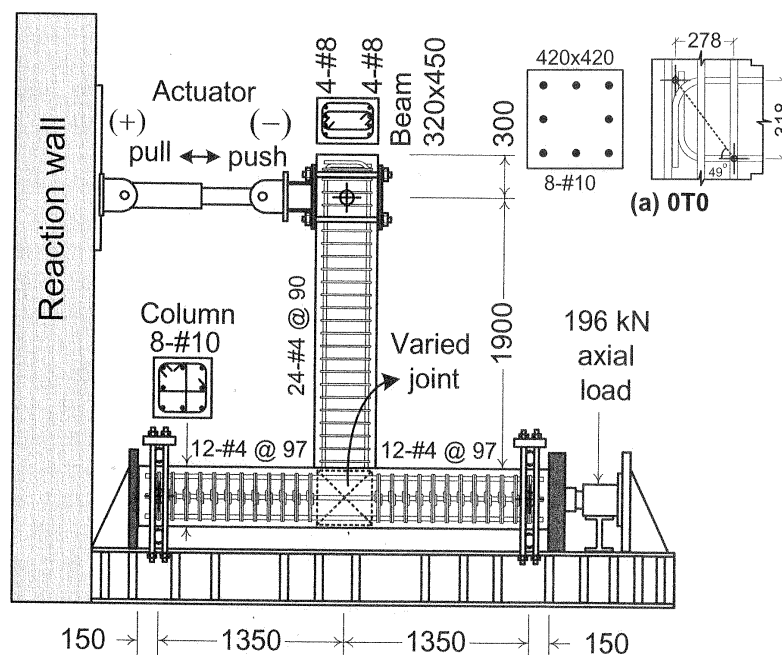


Figure 12.18 Details of joint tested by Hwang et al (2005)

A comparison of experimental and analytical results is shown in Figure 12.19. Interestingly, it can be seen that in this case the analysis with or without joint model leads to same result, which is attributed to the fact that the joint sub-assembly underwent a beam flexure failure before the joint shear failure. In contrast, in other joints, where we had a pure joint shear failure, the fact that we use joint model or not makes a big difference. However, this result shows that using joint model does not impose any failure mode deliberately and if joint failure does not occur, the joint springs simply don't get activated.

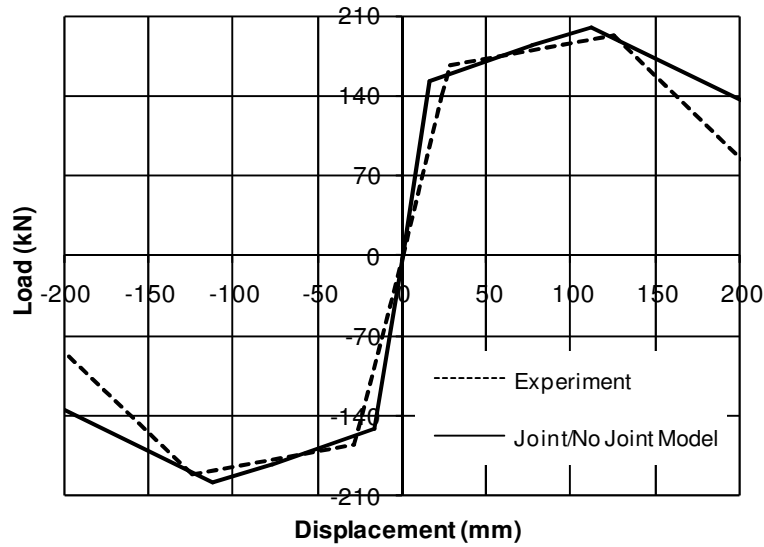


Figure 12.19 Validation of model with test OT0 performed by Hwang et al (2005)

12.1.1.6 Tests by Wong and Kuang (2008)

Wong and Kuang (2008) tested full scale exterior joints to investigate the influence of joint aspect ratio. One joint had the aspect ratio of unity that means that the depth of beam was same as the depth of the column. Two more joints had aspect ratios of 1.5 and 2.0 respectively. As suggested by Wong and Kuang (2008), the nominal joint shear strength reduces with increase in aspect ratio and therefore accordingly principal tensile stress v/s joint deformation envelope need to be adjusted. This was done by multiplying the relevant critical principal tensile stress values used to evaluate the spring characteristics (Figure 4.15) by the factors proposed by Wong and Kuang (2008) as shown in Figure 4.20.

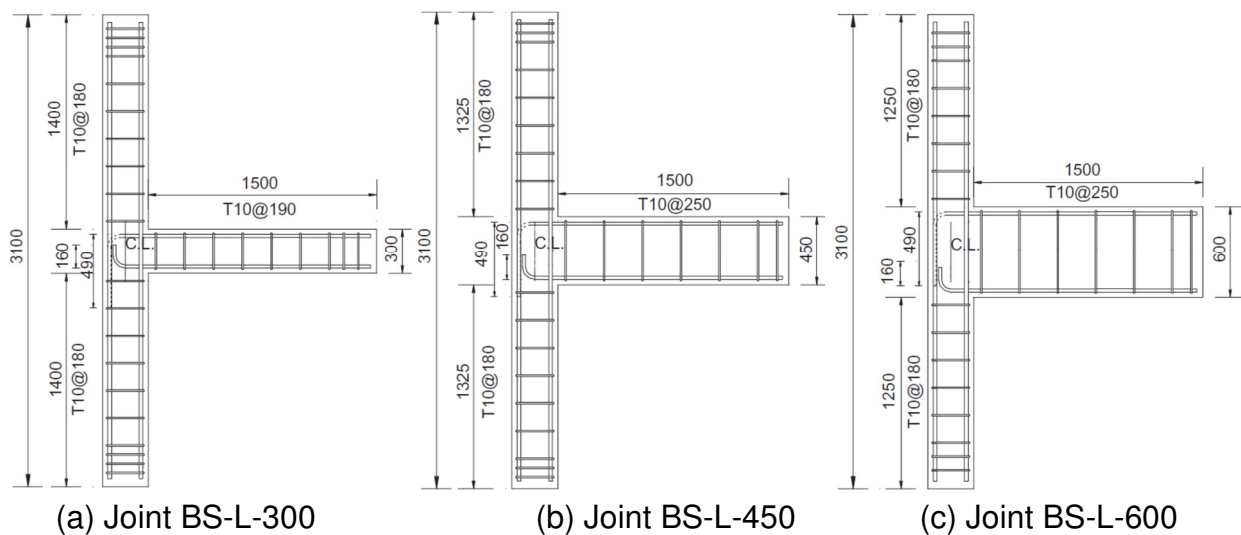


Figure 12.20 Details of joint tested by Wong and Kuang (2008)

Figure 12.20 shows the details of the joints tested by Wong and Kuang (2008). The concrete cube strength for joints BS-L-300, BS-L-450 and BS-L-600 were obtained as 42.6MPa, 38.6MPa and 45.5MPa respectively (Wong and Kuang, 2008). All columns were of size 300mm x 300mm reinforced with 4-25mm deformed bars having yield strength of 520MPa. The beam width was 260mm for all cases, while the depth was varied. Beam was reinforced with 3-20mm deformed bars on top and bottom face. 10mm bars were used as transverse reinforcement in beam and column as shown in Figure 12.20.

12.1.1.6.1 Test BS-L-300

Joint named BS-L-300 had beam depth equal to 300 mm, which is the same as its column depth (aspect ratio = 1.0). Figure 12.21 shows the comparison of experimental and numerical results. In this case, the beam capacity is quite close to the joint capacity, which can be verified from the experimental curves as well (Wong and Kuang, 2008). Therefore, even if joint springs are not considered, the failure load due to beam flexure failure is not significantly higher. As can be observed in Figure 12.21, the curve without considering joint model predicts almost the same failure load as was predicted by joint model. However, since the beam flexural failure is inherently ductile, a much higher ductility is predicted than in reality, which is dangerous.

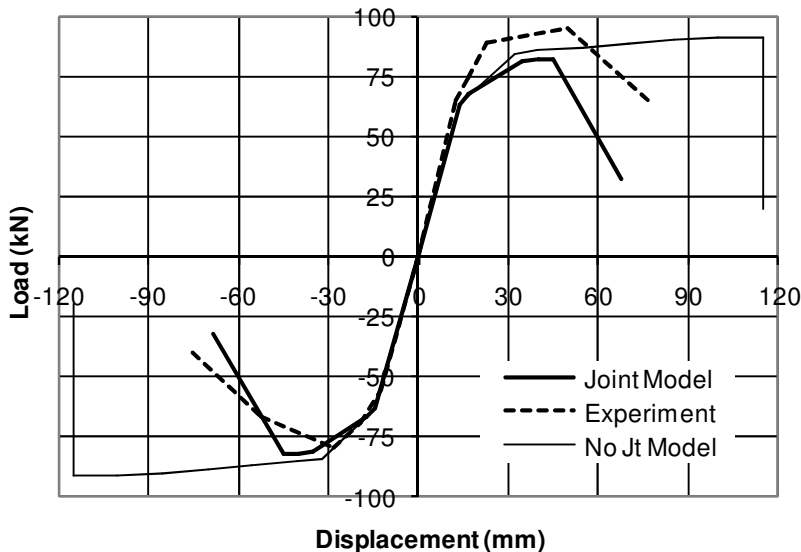


Figure 12.21 Validation of joint model with test BS-L-300 performed by Wong and Kuang (2008)

12.1.1.6.2 Test BS-L-450

Joint BS-L-450 had beam depth equal to 450 mm, resulting in the joint aspect ratio of 1.5. The critical principal tensile stresses were therefore modified by multiplying them with factors as per Figure 4.20. Figure 12.22 shows the comparison of results.

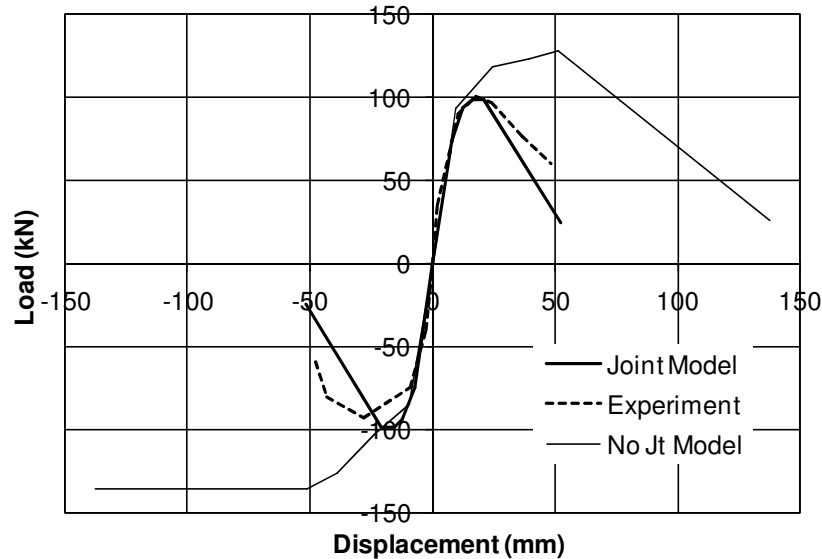


Figure 12.22 Validation of joint model with test BS-L-450 performed by Wong and Kuang (2008)

The peak load in the experiment was obtained as 101 kN on positive side and 93 kN on negative side, while the same was obtained as 99kN for either direction in the analysis. In this case, the beam strength was higher than the joint strength and therefore, the analysis considering joint as rigid lead to results on the unconservative side, while a good agreement is obtained in case of analysis with joint model. Thus, it can be said that the modification in the critical principle tensile stress values as per the recommendation of Wong and Kuang (2008), leads to consideration of the joint aspect ratio in the model, quite well.

12.1.1.6.3 Test BS-L-600

Joint BS-L-600 had beam depth equal to 600 mm, resulting in the joint aspect ratio of 2.0. The critical principal tensile stresses were therefore modified by multiplying them with factors proposed by Wong and Kuang (Figure 4.20). Figure 12.23 shows the comparison of experimental and analytical results.

The peak load in the experiment was obtained as 133 kN in positive direction, while 95 kN in negative direction. Though there is no discussion on the same in the reference (Wong and Kuang, 2008), this can be attributed to the fact that the bottom beam reinforcement was not embedded completely in the joint (see Figure 12.20c) and therefore the strut action is not totally mobilized after certain level. However, in the analysis with joint model, the peak load was obtained as 135kN in both directions. This is essentially due to the fact that the joint model does not explicitly model the bond behaviour and only indirectly considers the effects of detailing by modifying the critical principal tensile stress values. However, the kind of detailing used in BS-L-600 is not a popular detailing type and is rare in practice.

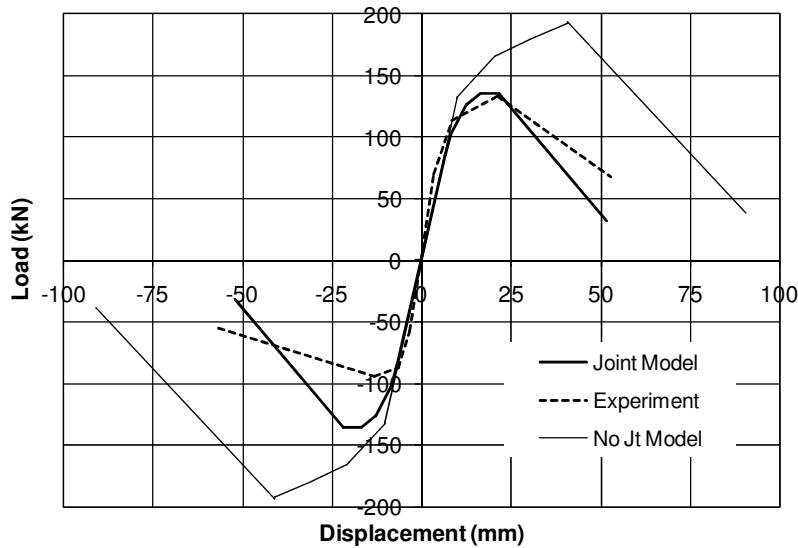


Figure 12.23 Validation of joint model with test BS-L-600 performed by Wong and Kuang (2008)

12.1.1.7 Tests by Genesio and Sharma (2010)

Genesio and Sharma (2010) performed experiments on exterior RC beam-column joints under cyclic loads. Five different joints were tested under the program, with different beam bar anchorage in the joint panel as shown in Figure 7.1, replicated as Figure 12.24 for ease of reference.

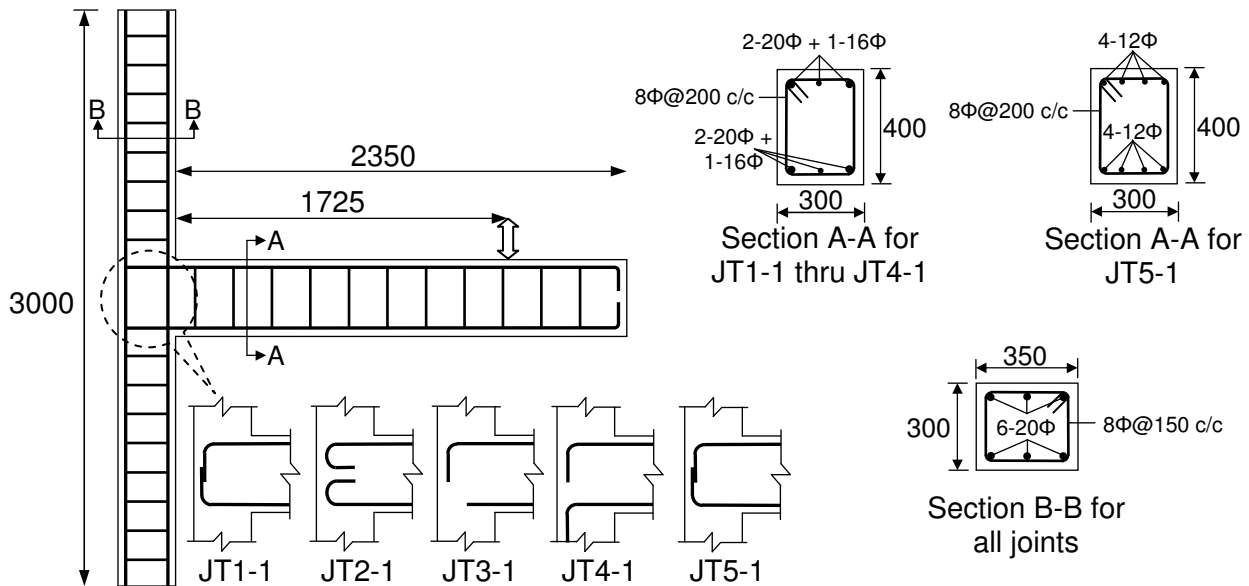


Figure 12.24 Details of joints tested by Genesio and Sharma (2010)

The cross-section details for the columns for all the joints were same, while the cross-section of beam was different for joint JT5-1 compared to other specimens (Figure 12.24). By design, for JT1-1 through JT4-1, joint shear failure prior to beam/column failure is imminent. However, for joint JT5-1, the yielding of beam longitudinal reinforcement follows the joint shear cracking but happens before ultimate joint shear failure.

The average compressive strength of concrete on testing day, obtained by performing tests on 150mm size cubes for JT1-1, JT2-1, JT3-1, JT4-1 and JT5-1 were obtained as 31.75MPa, 30.44MPa, 34.32MPa, 35.29MPa and 30.79MPa respectively. Fe500 (IS 1786:2008) grade reinforcing bars were used in the specimens JT1-1 through JT4-1, while Fe250 grade plain round bars (Mild steel) were used for JT2-1. The actual properties of reinforcing bars used in the joints are tabulated in Table 7.3. The beam-column joints were tested in erect position, with column vertical. Both ends of the columns were held by elastic hinge sub-assembly. No axial load was applied on the column in any case.

12.1.1.7.1 Joint JT1-1

Joint JT1-1 was constructed using deformed bars and had both top and bottom beam reinforcing bars bent into the joint (Figure 12.24). The comparison of experimental and numerical results for joint JT1-1 is given in Figure 12.25.

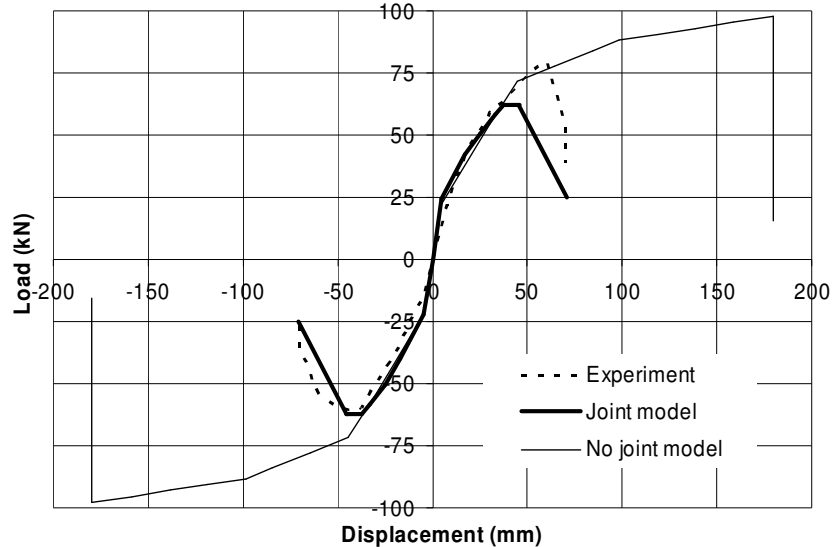


Figure 12.25 Validation of joint model against experiment on JT1-1

The analysis results follow the experimental results very closely, especially in the negative direction of loading. In the experiment, the peak load in the positive direction was obtained as 79.9 kN and that in the negative direction was 61.5 kN. Such significant difference in the experimental peak loads is quite rare for joints having symmetric beam reinforcement and no axial load and may be attributed to certain local in-homogeneity. However, the peak load was

obtained as 62.5kN for either side in the analysis. It can be observed, that the model considering joint as rigid leads to unsafe results, while the analysis considering joint model leads to good prediction of the response of the joint.

12.1.1.7.2 Joint JT2-1

Joint JT2-1 was constructed using plain round bars with end hooks for both top and bottom beam reinforcing bars (Figure 12.24). Therefore to generate joint spring characteristics, the failure criteria suggested by Pampanin et al (2002), which is essentially the same as the criteria shown in the third quadrant of Figure 4.18 was used.

The comparison of experimental and numerical results for joint JT2-1 is given in Figure 12.26. As seen from the results, the peak load attained in this case was much less compared to that in case of joint JT1-1, which is attributed to the use of plain round bars in this case. The peak load in the experiment was obtained as 41.5 kN for the positive loading cycle and as 39.1 kN for negative loading cycle. The peak load in the analysis using joint model was obtained as 39.2 kN for either side and that on the analysis considering joint as rigid (no joint model) was obtained as 68.3 kN for either side.

As can be seen from Figure 12.26, the analysis considering joint as rigid leads to very unsafe prediction of response, while the analysis using joint model leads to results in close agreement with their experimental counterparts.

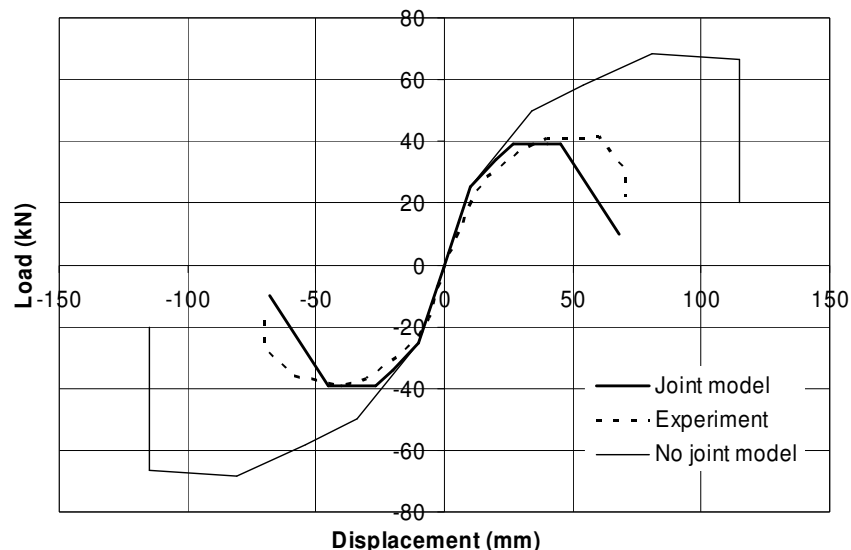


Figure 12.26 Validation of joint model against experiment on JT2-1

12.1.1.7.3 Joint JT3-1

Joint JT3-1 was constructed using deformed bars with top beam bar bent into the joint, while the bottom beam bar embedded straight up to 150mm into the joint (Figure 12.24). The comparison of experimental and numerical results for joint JT3-1 is given in Figure 12.27.

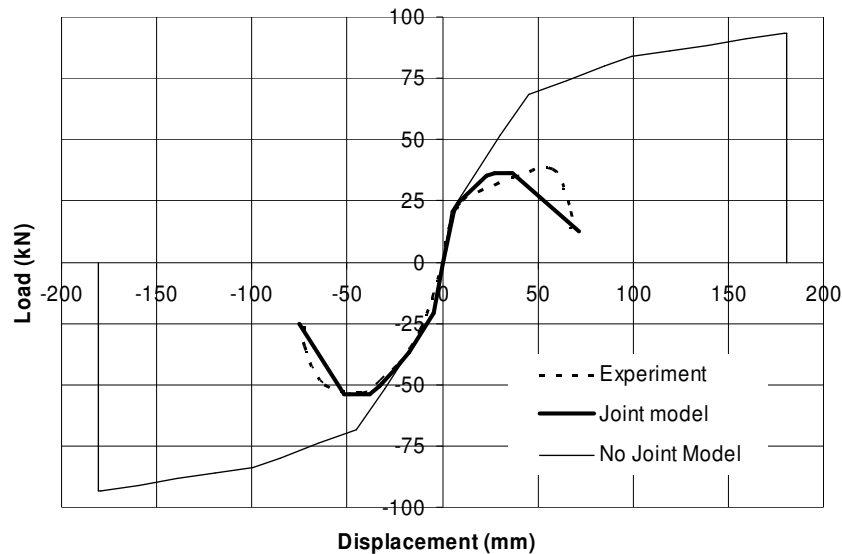


Figure 12.27 Validation of joint model against experiment on JT3-1

Due to un-symmetric embedment of beam reinforcing bars into the joint, the peak loads in the experiment for positive and negative loading directions were obtained as 38.0kN and 53.5kN respectively.

As discussed in chapter 4 earlier, this effect can be accounted for in the joint model and hence the results of the analysis with joint model are close to experimental ones. The peak load in the analysis with joint model was obtained as 36.4kN and 54.2kN for positive and negative loading direction respectively, which is very close to experimental results. However, the analysis performed considering the joint as rigid cannot consider the influence of unsymmetric embedment and hence the peak load in this case is obtained as 93.3kN for either side, which is very much on unsafe side.

12.1.1.7.4 Joint JT4-1

Joint JT4-1 was constructed using deformed bars with top beam bar bent into the joint, while the bottom beam bar bent out of the joint (Figure 12.24). The comparison of experimental and numerical results for joint JT4-1 is given in Figure 12.28.

In this case again due to unsymmetric embedment of beam reinforcing bars, the peak load in positive loading direction is obtained as 40.5kN while in the negative direction, the same is

obtained as 57.8kN. In the analysis with joint model, this effect can be considered and therefore the peak load was obtained as 41.5kN and 58.6kN for positive and negative directions, respectively. The analysis considering joint as rigid leads to a peak load of 96.8kN in either direction. Figure 12.28 again confirms the usefulness of the joint model to predict the load-displacement behaviour of the joints.

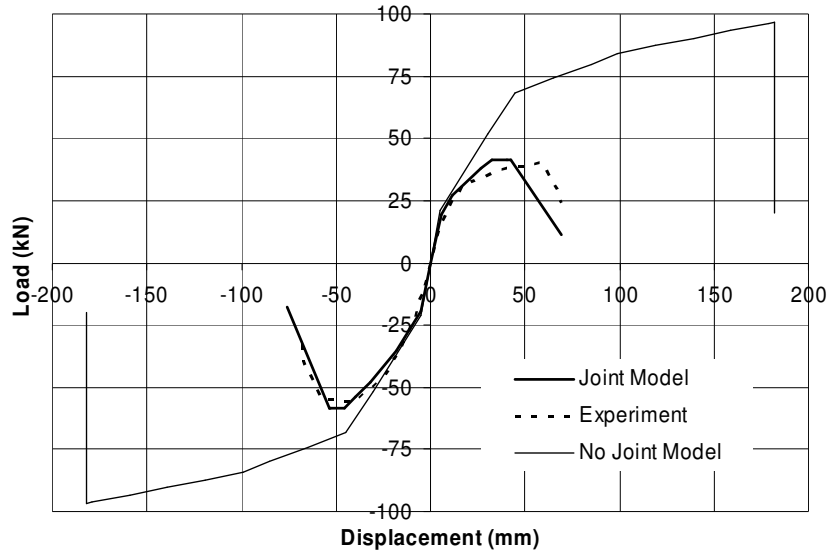


Figure 12.28 Validation of joint model against experiment on JT4-1

12.1.1.7.5 Joint JT5-1

Joint JT5-1 was constructed using deformed bars and had both top and bottom beam reinforcing bars bent into the joint, however it had different beam reinforcement (Figure 12.24). The comparison of experimental and numerical results for joint JT5-1 is given in Figure 12.29.

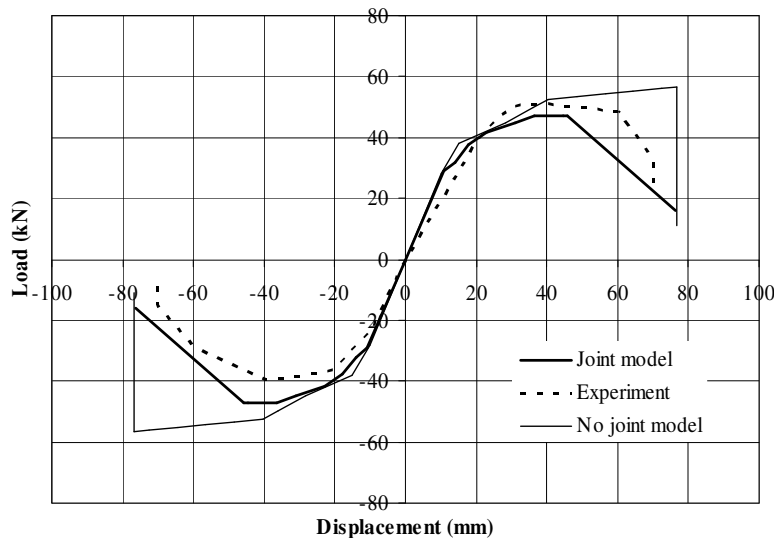


Figure 12.29 Validation of joint model against experiment on JT5-1

The experimental peak load in the positive displacement cycle was obtained as 51.0 kN and that in negative direction as 39.50 kN, though the detailing was essentially symmetric, which is unusual. From analysis with joint model, the peak load is obtained as 47.20kN for either direction and from analysis considering joint as rigid, the same was obtained as 56.70kN for both directions.

The difference in the analysis without and with joint model is not so severe in this case since the failure of joint was essentially a combination of beam flexure and joint shear (see chapter 7). Nevertheless, the analysis considering rigid joint predicts much higher ductility than in reality. The results considering joint model are again close to the experimental results.

12.1.2 Interior Joints

Once the joint model was extensively validated against the exterior joints and the various aspects of detailing, type of reinforcement, aspect ratio etc were considered, the model was validated against the experiments on interior joints.

12.1.2.1 Tests by Dhakal et al (2005)

Dhakal et al (2005) performed experiments on gravity designed interior beam-column joints as shown in Figure 12.30, that were part of frames designed according to the British standard BS8110.

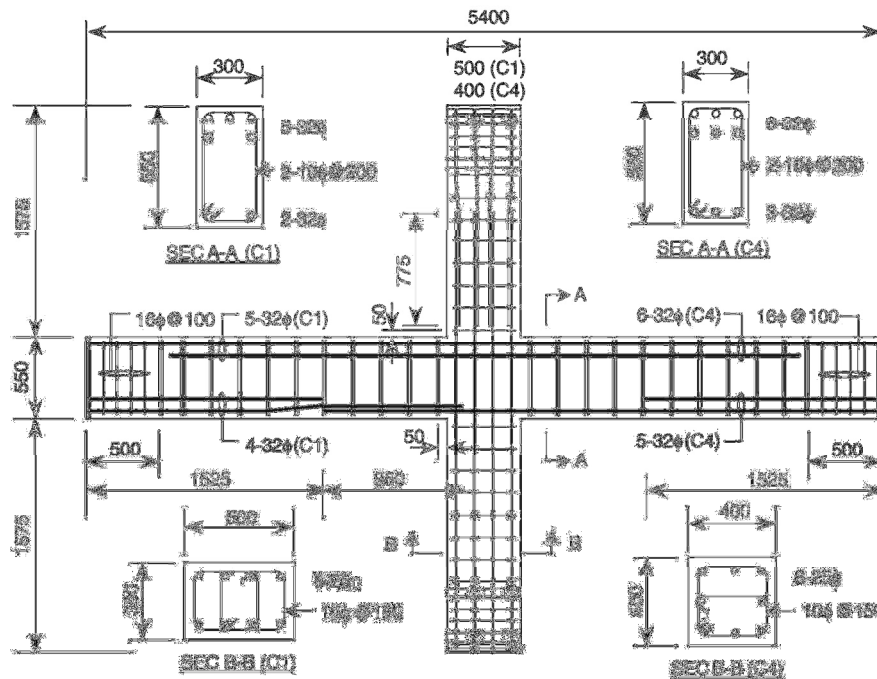


Figure 12.30 Details of specimens tested by Dhakal et al (2005)

The specimens were full-scale reproductions of a gravity designed frame between the points of contra-flexure, which are assumed to be the mid-heights of columns in two successive storeys and the centre-points of beams in two adjacent bays. The geometrical dimensions and reinforcement details of the C1 and C4 type specimens are illustrated in Figure 12.30. Specimens of both types had similar overall dimensions (3.7 m high column and 5.4 m long beam), and the cross-section of the beam (300 mm width × 550 mm depth) was the same in all specimens.

The beam in C1 type specimens had seven 32 mm diameter bars, five at the top (2.7% reinforcement ratio) and two at the bottom (1.1%), whereas C4 type specimens had six bars at the top (3.3%) and three bars at the bottom (1.6%) of the beam. C1 type specimens had columns with cross-section 350 × 500 mm, and two layers of four 25 mm diameter bars (2.4%) were laid parallel to the two longer sides. Similarly, in C4 type specimens, the 400 × 400 mm column included eight 25mm diameter bars (2.5%) arranged symmetrically along the perimeter. The stirrups in the beam comprised of four legs of 10 mm diameter bars spaced at 200 mm apart, and the ties in the column had three legs of 10 mm diameter bars with 150 mm spacing. Both the specimens were without any vertical or lateral hoops inside the joint core.

Standard compression test results on cylinders showed that the average compressive strength of concrete was 31.6MPa for the C1 type specimens and 32.7MPa for the C4 type specimens. Based on standard tension test results, the average yield strengths of the 32, 25 and 10 mm diameter bars were 538, 537.6 and 363.7 MPa respectively. Similarly, the average ultimate tensile strengths of these bars were 677.3, 675.3 and 571.5MPa respectively. All specimens were subjected to an axial compression of 10% axial capacity.

12.1.2.1.1 Joint C1

The comparison of experimental and analytical curves is given in Figure 12.31 below. To visualize the significance of joint modelling, a comparison is given with the analysis results when the model did not have springs to model the joint shear behaviour. The peak load from the experiment was obtained as 225 kN for both up and down directions. In the analysis, the peak load was obtained as 224 kN for both up and down directions using joint model, which is very close to the experiment, while the same was obtained as 332 kN for both up and down directions without using joint model. Thus, the model without joint springs again yielded results on highly unsafe side for both the directions.

12.1.2.1.2 Joint C4

Joint C4 had an aspect ratio of 1.375 (Figure 12.30). Therefore, the critical principle tensile stresses were multiplied by the factor to consider the reduction in critical joint stress due to aspect ratio.

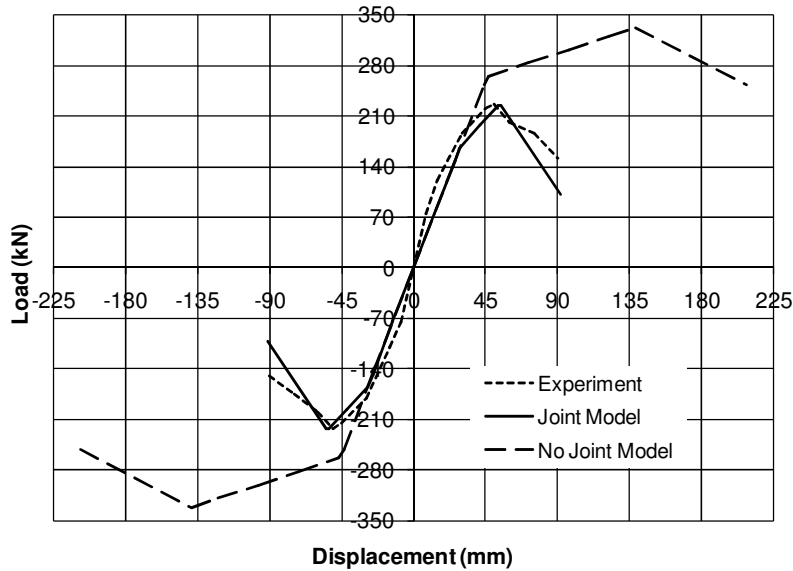


Figure 12.31 Experimental and analytical results for specimen C1 by Dhakal et al (2005)

The comparison of experimental and analytical curves is given in Figure 12.32 below. To visualize the significance of joint modelling, a comparison is given with the analysis results when the model did not have springs to model the joint shear behaviour.

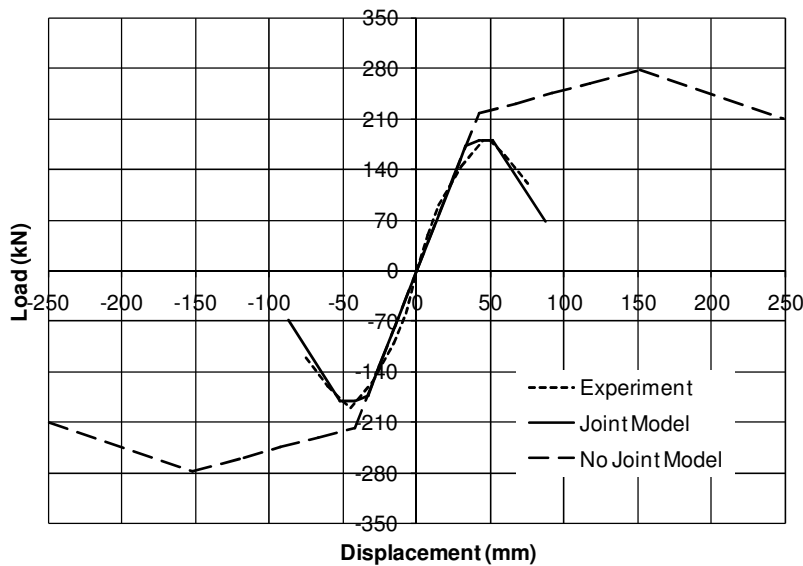


Figure 12.32 Experimental and analytical results for specimen C4 by Dhakal et al (2005)

The peak load from the experiment was obtained as 181 kN for both up and down directions. In the analysis, the peak load was obtained as 179 kN for both up and down directions using joint model, which is again very close to the experimental results. The peak load considering joint as rigid (no joint model) was obtained as 280 kN for both up and down directions. This further proves the validity and importance of modelling the joint using the proposed joint

model. Also, it is shown that the model without joint springs may yield results on highly unsafe side.

12.2 Validation of model against experiment at structural level

In chapter 8, details of a pushover test performed on a full scale RC frame structure were provided. The failure patterns displayed the vulnerability of RC buildings with non-conforming detailing which tend to fail in undesirable failure mechanisms, such as joint shear failures, bond failures, etc. In this section, the numerical modeling aspects of the same will be provided and the applicability of the joint model at structural level will be verified.

12.2.1 Modeling aspects

The beams and columns of the structure were modeled as 3D beam (frame) elements, with six degrees of freedom at both nodes. Frame members are modeled as line elements connected at points (joints). The slabs were modeled using four-noded quadrilateral shell elements. To capture the inelastic behavior of members, flexural springs (moment-rotation), shear springs (shear force-deformation) and torsional springs (torsional moment-rotation) were modeled following the formulations given in Appendix-I. The joint deformation characteristics were modeled using the joint model explained in chapter 4. The effect of aspect ratios was considered by modifying the principal tensile stress values as per Figure 4.20, while the influence of eccentricity between beam and column was accounted for using equations (4.27) and (4.28). The hinge characteristics, once obtained, were assigned to the frame members. The hinges assigned on a typical joint of the structure in the program and their physical significance is displayed in Figure 12.33. Since the loading was uni-directional, no joint hinges were provided for the transverse beams of the joints.

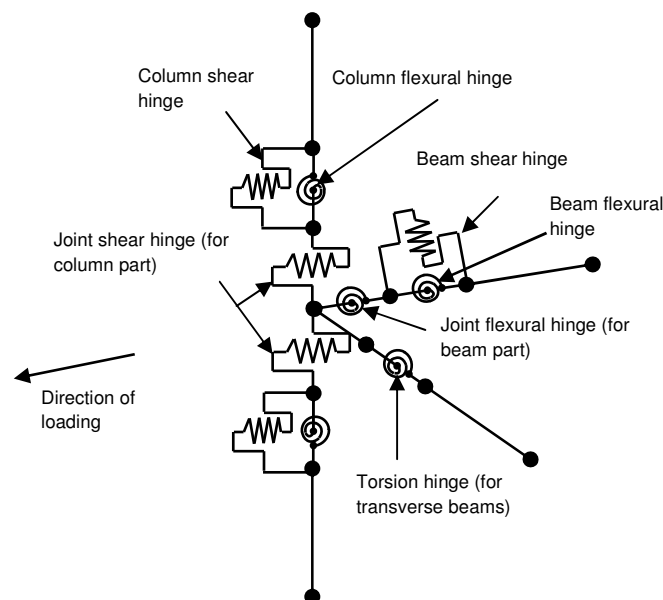


Figure 12.33 Hinges assigned to members and core of a typical joint of the structure

12.2.2 Numerical results

In order to have a comparison among modelling techniques, three cases were analyzed, with different types of nonlinear hinges models:

1. Model 1, with flexural and shear hinges only;
2. Model 2, with torsional hinges along with flexural and shear hinges;
3. Model 3, with joint characteristics along with torsional, flexural and shear hinges.

12.2.2.1 Pushover curves

Figure 12.34 shows the comparison of experimental and analytical results for the examined cases. It can be observed that the first model over-predicts the strength of the structure. However, the initial stiffness obtained from the analysis in this case is quite close to the experimentally obtained one. The over-prediction of strength was expected, since the analysis considered only moment and shear hinges, whereas in the experiment it was found that the torsional and joint failure were also dominant.

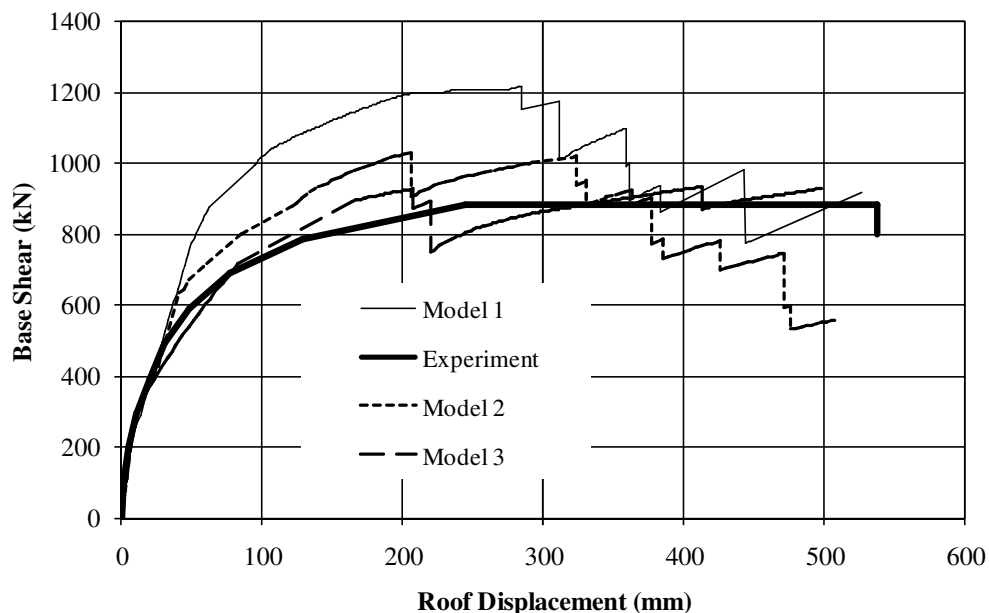


Figure 12.34 Comparison of results of various models against experiment

After considering the torsional effects, the predicted maximum base shear approximates better the experimentally obtained value. However, the predicted maximum base shear is still higher than the actual base shear. This is attributed to the fact that in this case the nonlinear characteristics of the joints were not modelled.

Finally, after considering the joint characteristics, torsional effects, moment and shear characteristics the analysis using third model predicted very well the load-deformation behaviour of the structure. The numerical results follow the experimental ones very closely. It has to be noted that the geometric nonlinearity in terms of P-delta effects was considered in all models and no calibration was performed to obtain the presented results.

12.2.2.2 Deflection profile

Figure 12.35 presents a comparison of the experimentally observed and numerically simulated deflected shape of the structure for each analysis case, with respect to the point when the structure reaches the first peak. Since the computational models and the experimental setup reach peak base shear at different displacement, for better comparison of the deflected shape, the actual values of the storey displacement were normalized with respect to roof displacement.

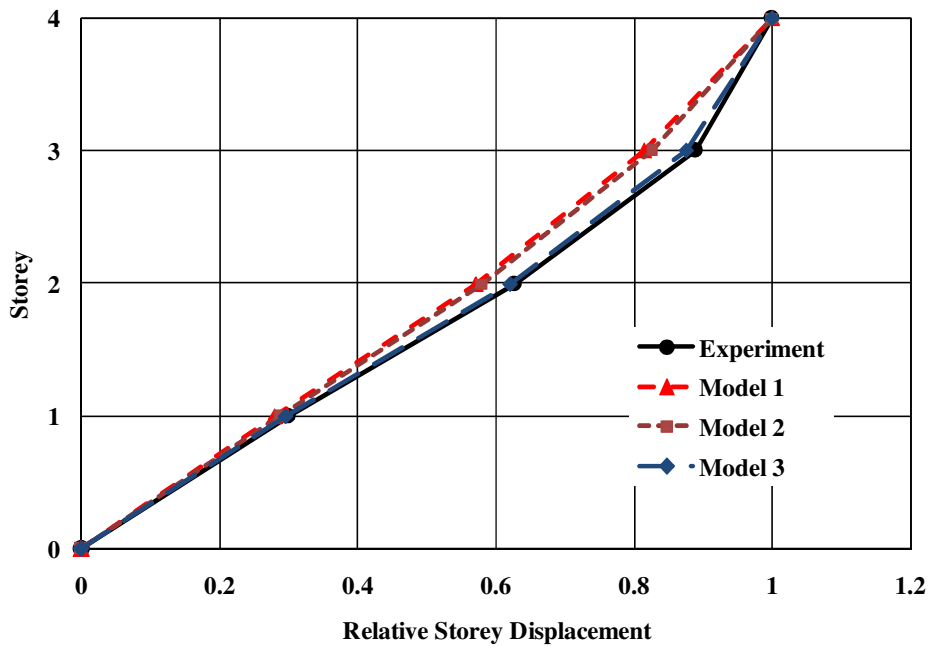


Figure 12.35 Comparison of deflected shape of the structure

It can be seen that the numerically obtained displacement shape for Models 1 and 2 display a parabolic shape for the structure and do not match the experimentally observed profile. This discrepancy is attributed to the rigid behavior of the joints. However, in the experiment, due to the failure at joint levels, the displacement of the roof level was much less than would be expected in the case of shear building behavior. In order to simulate this phenomenon, modeling of joint nonlinearities becomes extremely important and therefore explains why the deflected shape obtained from Model 3 matches closely the experimentally observed one.

Thus, it can be concluded that the third model could simulate almost all types of failure modes that were observed in the experiment, since not only the base shear, but also the deflected shape of the structure could be successfully captured.

12.2.2.3 Failure patterns

Figure 12.36 depicts the various hinges formed in the structure in the computational model with flexural, shear, torsional and joint hinges. A zoomed view of joint at 1st floor level for column CL19 is provided in Figure 12.36 to illustrate how the model is able to capture the real behavior of the joint. Similarly, an enlarged view of the first floor of the structural model is shown in Figure 12.38 where each hinge and its corresponding physical significance in real life case are shown. The consistency between the hinges obtained in the analysis and the failures in the experiment is remarkable.

Thus, it has been shown that in order to capture the overall behavior of RC structures, neglecting the inelasticity in the joints can lead to inaccurate results. The first two models over-predicted the base shear resistance of the structure and inaccurate deflected shapes were also derived. In contrast, it was found that via Model 3, not only the pushover curves, but also the deflected shape of the structure as well as the failure modes and locations could be satisfactorily simulated. Therefore, it can be concluded that the joint model works well at structural level and joint modeling is essential for correct prediction of the seismic behavior of RC structures detailed as per non-seismic guidelines.

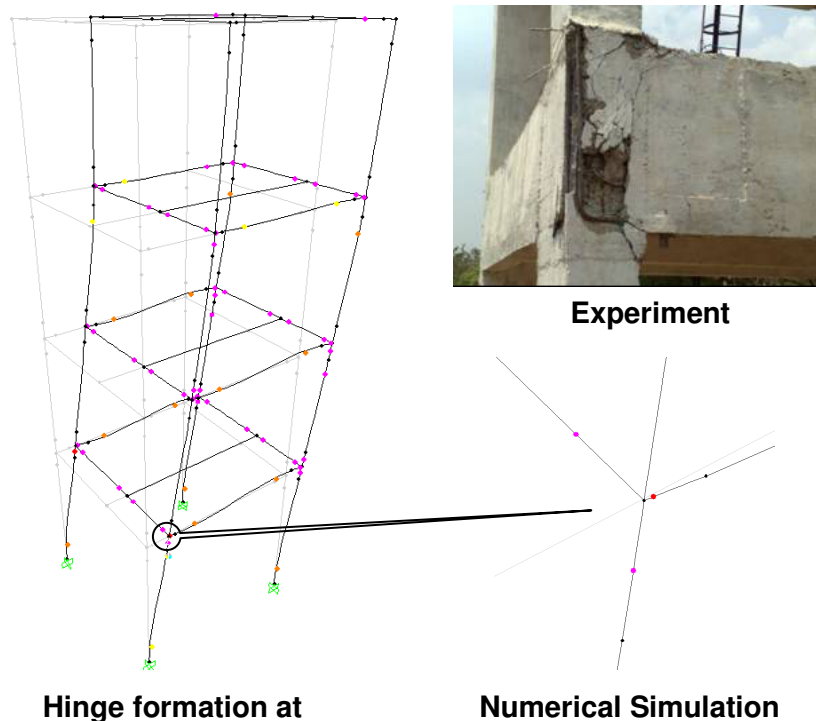


Figure 12.36 Failure mode of structure with emphasis on joint of CL 19 at 1st floor level

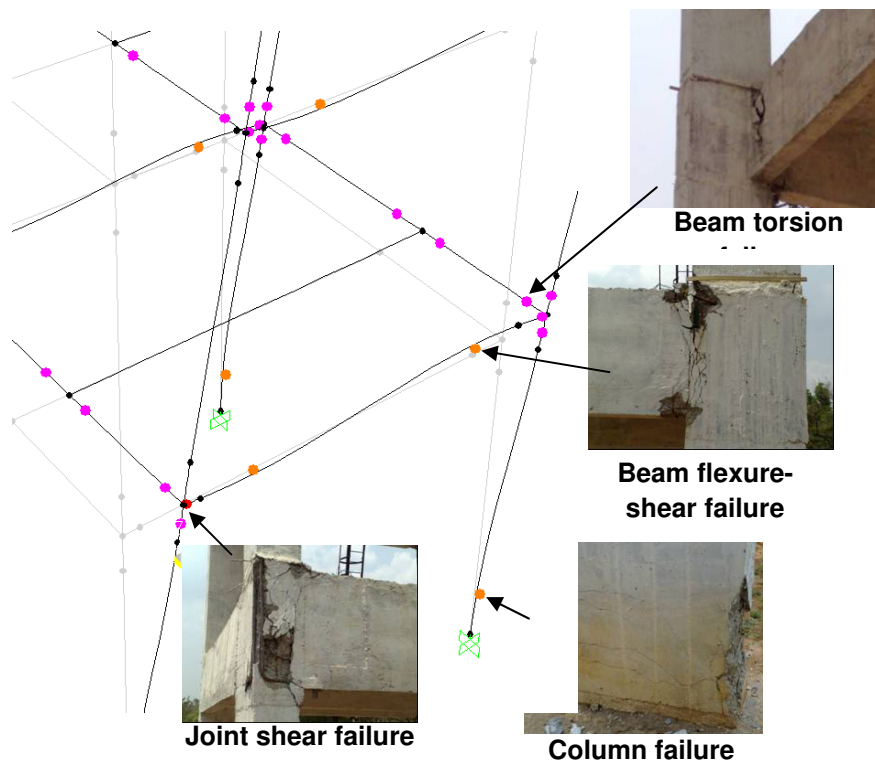


Figure 12.37 Comparison of failure modes as experimentally and numerically derived

13. VALIDATION OF PIVOT HYSTERETIC MODEL PARAMETERS FOR MEMBERS AND JOINTS AGAINST EXPERIMENTS

In chapter 5, the parameters were suggested to define hysteretic laws for rectangular sections having varying levels of axial load levels and reinforcement detailing as well as for poorly detailed beam-column joints with varying axial load levels. In this chapter, the verification of the applicability of the parameters to capture the hysteretic response of members, joints and structures is presented.

13.1 Validation of parameters for rectangular sections at member level

The parameters suggested in chapter 5 were validated against various experiments available in the literature. The numerical analysis was performed using commercial software SAP2000.

13.1.1 Tests by Gill et al (1979)

Gill et al (1979) tested full-size column sections loaded with different ranges of constant axial compressive loads and subjecting them to a static cyclic lateral load sequence. The well-known modified Kent and Park model (Park et al, 1982) was based on the results of this experimental program.

13.1.1.1 Specimen Details

Figure 13.1 explains the specimen details used by Gill et al (1979). The test configuration was a double ended simply supported column as shown in Figure 13.1 (a). Two different lateral tie arrangements were used as shown in Figure 13.1 (b) and (c). A self-reacting load frame with a hydraulic ram was used to apply cyclic lateral load, and a universal testing machine to apply constant axial load. The longitudinal reinforcement consisted of 12 numbers of 24mm diameter deformed bars at a 50 mm effective cover. The transverse reinforcement was made up of plain round bars and was varied for the specimens as shown in Table 13.1. The hoops within the plastic hinge region were closely spaced as compared to the hoops in outside plastic hinge region. The axial load, P was varied over a range of around 20% to 60% of the axial load capacity, P_{ult} of the columns.

Table 13.1 Transverse reinforcement arrangement for the specimens by Gill et al (1979)

Unit No.	In Plastic Hinge region			Outside Plastic Hinge region		
	No. of hoop sets	Bar Dia (mm)	Spacing (mm)	No. of hoop sets	Bar Dia (mm)	Spacing (mm)
2	8	12	75	3	12	210
3	8	10	75	6	10	105
4	10	12	72	3	12	200

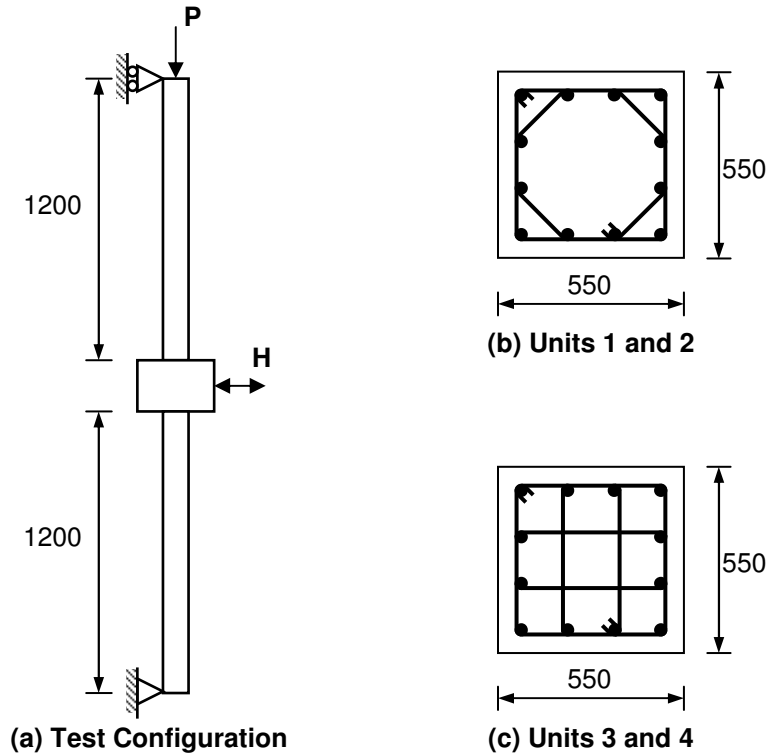


Figure 13.1 Specimen details for columns tested by Gill et al (1979)

Table 13.2 gives the details of the specimens tested by Gill et al (1979).

Table 13.2 Details of specimens tested by Gill et al (1979)

Unit No.	Concrete Strength (MPa)	Axial Load, P (kN)	P/P_{ult}	Longitudinal Reinforcement		Transverse Reinforcement	
				Ratio	f_y	Ratio	f_y
2	41.4	2680	0.214	0.0179	375	0.023	316
3	21.4	2719	0.420	0.0179	375	0.020	297
4	23.5	4265	0.600	0.0179	375	0.035	294

13.1.1.2 Experimental and numerical results

The experimental results were taken from the consolidated report on cyclic lateral load tests on rectangular reinforced concrete columns by Taylor et al (1997). Although, in experiment, two cycles were provided for each displacement level, in analysis only one cycle per each displacement level was provided. This is sufficient to verify the parameters suggested for the columns.

13.1.1.2.1 Unit 2

As given in Table 13.2, unit 2 was tested under an axial load of 2680 kN that accounted for around 21.4% of its axial load carrying capacity. This can be considered as moderate axial load on the column. For analysis, the complete nonlinear spring characteristics for the section were calculated using the formulations given in Appendix-I. For given values of axial load ratio, % longitudinal reinforcement and % transverse reinforcement, the values of α and β parameters were evaluated using equations (5.2) through (5.5).

Figure 13.2 shows the comparison of experimentally and numerically obtained results. Figure 13.2a shows the experimental hysteretic loops as reproduced from Taylor et al (1997), while figure 13.2b shows the numerically obtained hysteretic loops.

From figure 13.2, it can be clearly said that the analysis procedure as followed in this work can simulate the experimental behaviour of rectangular columns subjected to quasi-static-cyclic loads quite well. The yield loads, peak loads and corresponding displacements match very closely with the experimental values suggesting that the hinge characteristics as calculated offer good prediction capabilities. Similarly, observing that the hysteretic loops considering the unloading, reloading and pinching match quite closely with the experimentally observed values, signify that the associated hysteretic rule and the values of α and β parameters can predict the hysteretic behaviour of the column very nicely.

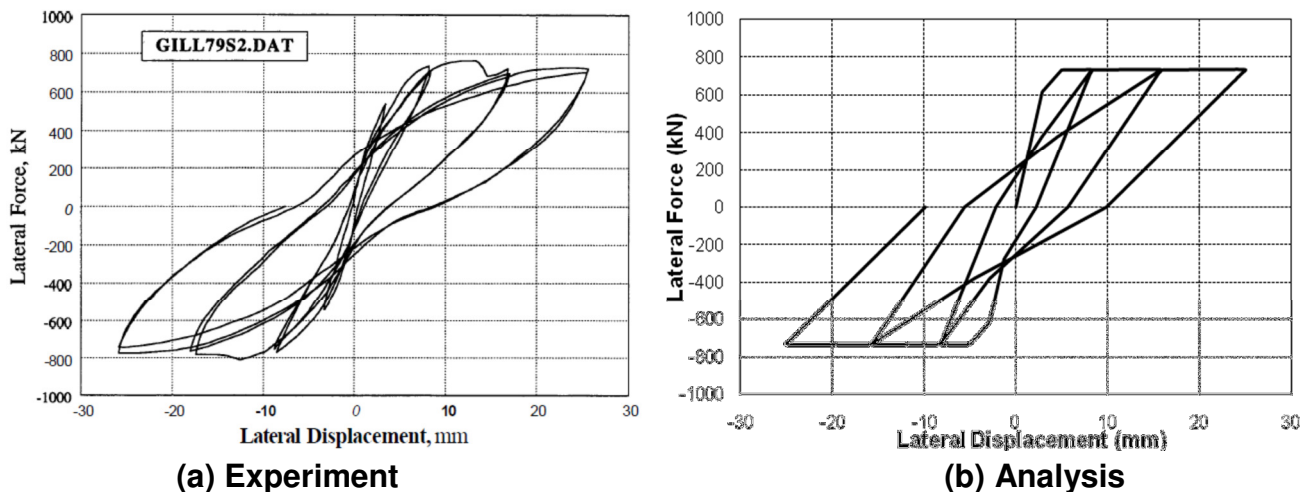


Figure 13.2 Validation of pivot hysteretic law parameters for rectangular sections against results of unit 2 tested by Gill et al (1979)

13.1.1.2.2 Unit 3

As given in Table 13.2, unit 3 was tested under an axial load of 2719 kN that accounted for around 42.0% of its axial load carrying capacity. This can be considered as moderate to high

axial load on the column. Figure 13.3 shows the comparison of experimentally and numerically obtained results.

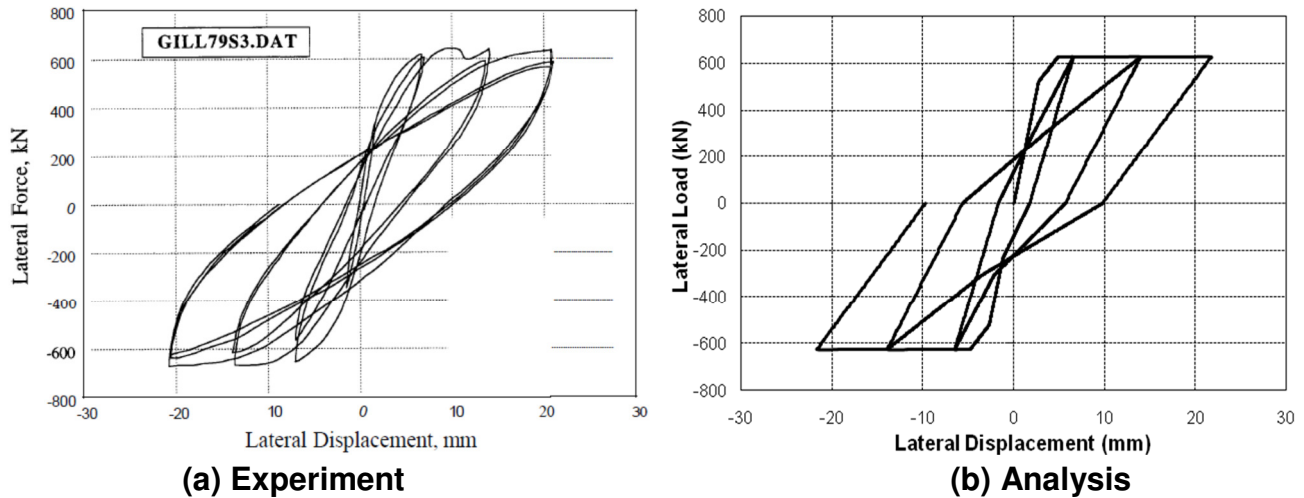


Figure 13.3 Validation of pivot hysteretic law parameters for rectangular sections against results of unit 3 tested by Gill et al (1979)

Figure 13.3a shows the experimental hysteretic loops as reproduced from Taylor et al (1997), while figure 13.3b shows the numerically obtained hysteretic loops. Comparing figure 13.3a and 13.3b, it can again be clearly said that the analysis procedure as followed in this work can simulate the experimental hysteretic behaviour of rectangular columns subjected to quasi-static-cyclic loads quite well.

13.1.1.2.3 Unit 4

As given in Table 13.2, unit 4 was tested under an axial load of 4265 kN that accounted for around 60.0% of its axial load carrying capacity. This can be considered as high axial load on the column. Figure 13.4a shows the experimental hysteretic loops as reproduced from Taylor et al (1997), while figure 13.4b shows the numerically obtained hysteretic loops. The validity of the parameters can be confirmed in this case also.

13.1.2 Tests by Ohno and Nishioka (1984)

Ohno and Nishioka (1984) tested cantilevered columns under constant axial load and cyclic lateral load. The variables studied were the lateral load pattern and the level of axial load. In this work, the analysis was performed for specimen L1 that was tested under a very severe lateral load pattern with only two high drift cycles applied and for specimen L2 that was tested under various cycles of slowly incrementing drift levels.

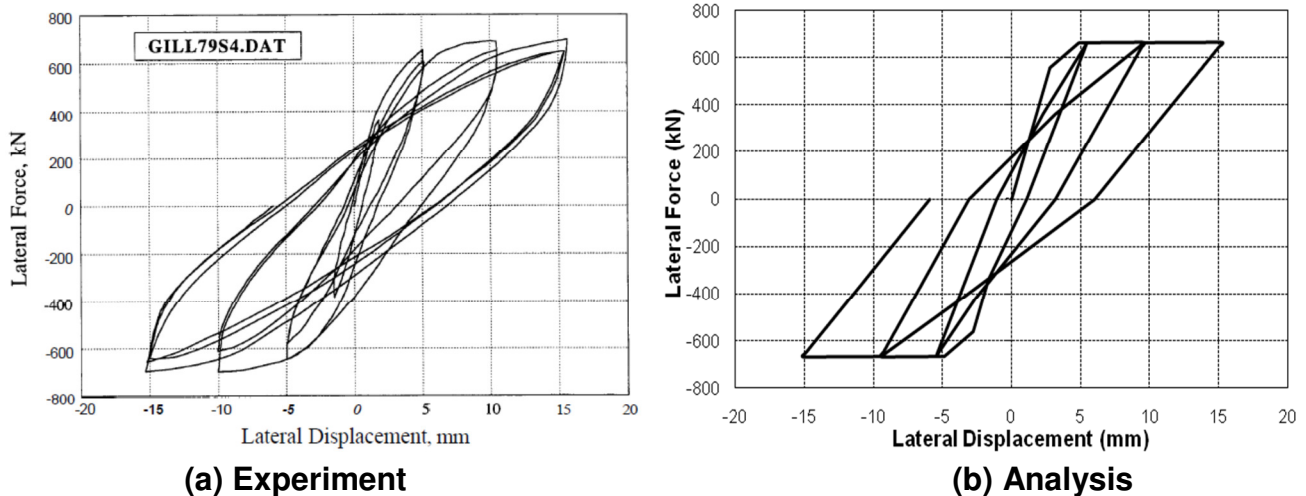


Figure 13.4 Validation of pivot hysteretic law parameters for rectangular sections against results of unit 4 tested by Gill et al (1979)

13.1.2.1 Specimen details

Figure 13.5 shows the details of the specimens tested by Ohno and Nishioka (1984). The concrete strength for both L1 and L2 specimens was reported as 24.8 MPa. The axial load was 157 kN corresponding to a ratio of axial load to the axial load capacity of 0.04 (or 4%), which can be considered as low axial load. The longitudinal steel ratio was 1.42% and the transverse reinforcement consisted of 9 mm diameter stirrups at a spacing of 100 mm.

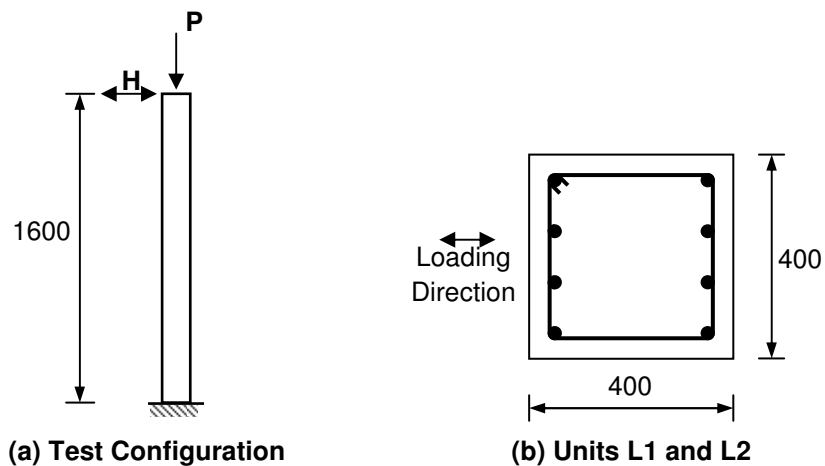


Figure 13.5 Specimen details of columns tested by Ohno and Nishioka (1984)

13.1.2.2 Experimental and numerical results

The experimental results were taken from the consolidated report on cyclic lateral load tests on rectangular reinforced concrete columns by Taylor et al (1997).

13.1.2.2.1 Unit L1

Unit L1 was tested under high drift levels. Only two cycles of high drifts were provided to the specimen. The experimentally obtained hysteretic loops as reproduced from Taylor et al (1997) are shown in Figure 13.6a and the corresponding numerical results are shown in Figure 13.6b.

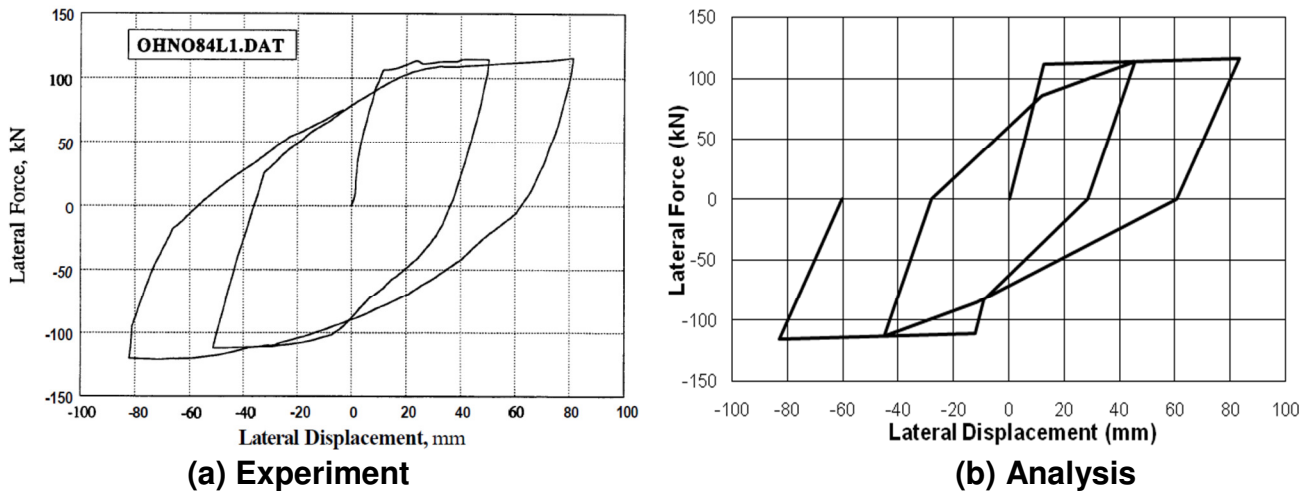


Figure 13.6 Validation of pivot hysteretic law parameters for rectangular sections against results of unit L1 tested by Ohno and Nishioka (1984)

Comparing Figure 13.6a and 13.6b, it can be clearly said that the analysis procedure and the parameters followed in this work can simulate the experimental behaviour of rectangular columns subjected to quasi-static-cyclic loads quite well, even for very high demand cycles.

13.1.2.2.2 Unit L2

Unit L2 was essentially the same as unit L1 except that it was tested under low drift levels. One cycle each for a drift of 10 mm, 20 mm, 30 mm and so on up to 80 mm was given to the specimen. The experimentally obtained hysteretic loops as reproduced from Taylor et al (1997) are shown in Figure 13.7a and the corresponding numerical results are shown in Figure 13.7b. Comparing the two figures, it can be clearly said that the parameters suggested in this work can simulate the experimental behaviour of rectangular columns subjected to quasi-static-cyclic loads quite well, for low demand cycles.

13.1.3 Tests by Atalay and Penzien (1975)

Atalay and Penzien (1975) tested columns with the main variables studied being the level of axial stress; the quantity of lateral reinforcement; and the displacement history applied to the specimen.

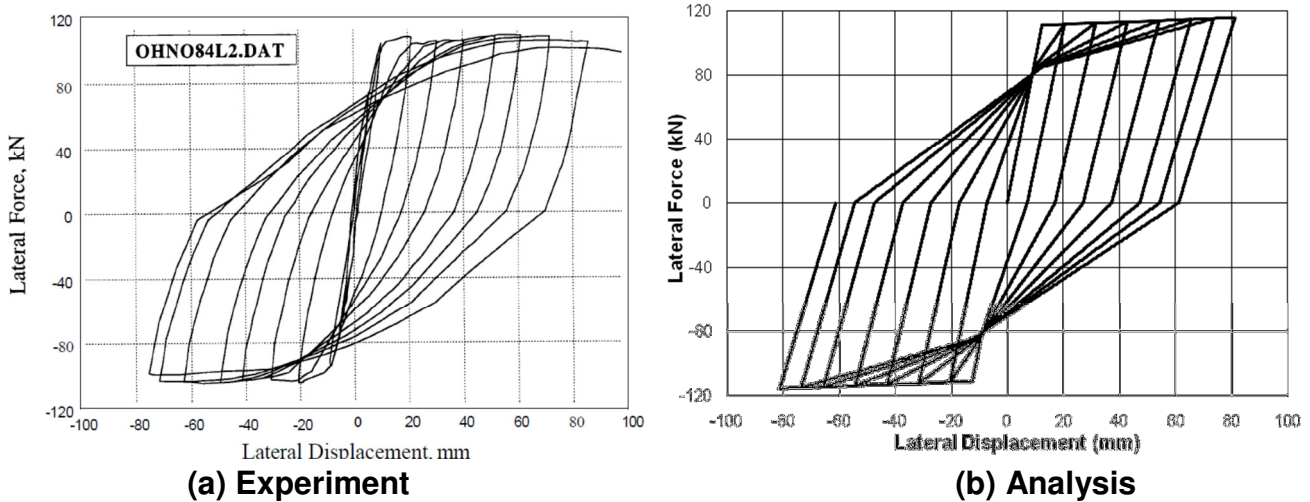


Figure 13.7 Validation of pivot hysteretic law parameters for rectangular sections against results of unit L2 tested by Ohno and Nishioka (1984)

13.1.3.1 Specimen Details

Figure 13.8 explains the specimen details used by Atalay and Penzien (1975). The test configuration was a double ended simply supported column. The two ends of each specimen had pinned boundary condition, and cyclic lateral displacements were applied to the central stub. Axial loads were applied by a hydraulic actuator reacting against a buttress.

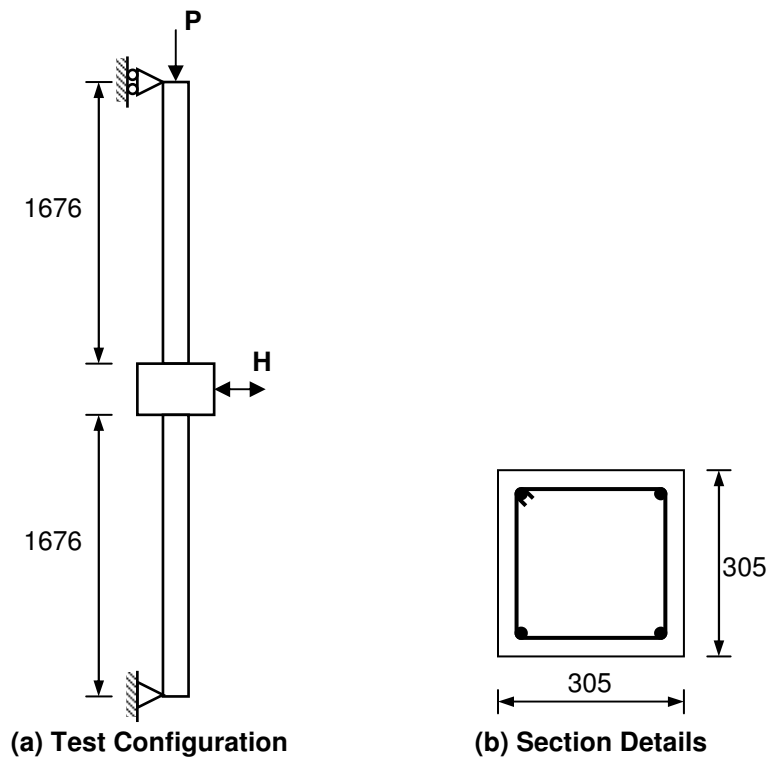


Figure 13.8 Specimen details for columns tested by Atalay and Penzien (1975)

The longitudinal reinforcement consisted of 4 numbers of 22mm diameter grade 40 bars at a 32 mm clear cover. The transverse reinforcement consisted of 9.5 mm diameter bars and two different spacing i.e. 76mm c/c and 127 mm c/c were studied. The axial load ratio was also varied. In order to validate the model parameters, four different columns, two having an axial load ratio of around 10% and two having an axial load ratio of around 20% were analyzed. Table 13.3 gives the information on the specimens tested by Atalay and Penzien (1975) and analyzed in this work.

Table 13.3 Details of specimens tested by Atalay and Penzien (1975)

Unit No.	Concrete Strength (MPa)	Axial Load, P (kN)	P/P_{ult}	Transverse reinforcement	
				Bar Dia (mm)	Spacing (mm)
1S1	29.1	267	0.099	9.5	76
2S1	30.7	267	0.094	9.5	127
5S1	29.4	534	0.196	9.5	76
6S1	31.8	534	0.181	9.5	127

13.1.3.2 Experimental and Numerical results

13.1.3.2.1 Unit 1S1

The test was carried out on the column having closely spaced ties and having an axial load of around 10% of its capacity. The specimen was loaded with cycles of +/- 10mm, 20mm, 30mm and 40mm. The experimentally obtained hysteretic loops as reproduced from Taylor et al (1997) are shown in Figure 13.9a, while the numerical results are reported in Figure 13.9b. A good correspondence between the experimental hysteretic loops and their numerical counterparts further prove the validity of parameters for rectangular sections.

13.1.3.2.2 Unit 2S1

The test was carried out on the column having closely spaced ties and having an axial load of around 10% of its capacity. The specimen was loaded with cycles of +/- 10mm, 20mm, 30mm, 40mm and 50 mm. The experimentally obtained hysteretic loops as reproduced from Taylor et al (1997) are shown in Figure 13.10a, while the numerical results are reported in Figure 13.10b. Again, a good correspondence between the experimental hysteretic loops and their numerical counterparts is obtained.

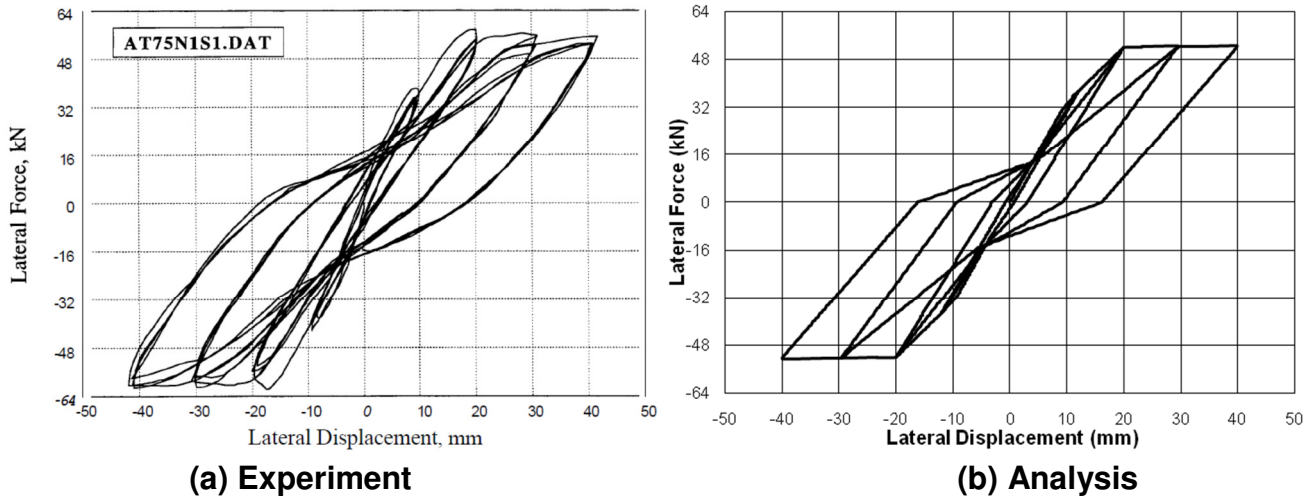


Figure 13.9 Validation of pivot hysteretic law parameters for rectangular sections against results of unit 1S1 tested by Atalay and Penzien (1975)

13.1.3.2.3 Unit 5S1

The test was carried out on the column having closely spaced ties and having an axial load of around 20% of its capacity. The specimen was loaded with cycles of +/- 10mm, 20mm, 30mm, 40mm and 50 mm. The experimentally obtained hysteretic loops as reproduced from Taylor et al (1997) are shown in Figure 13.11a. The main difference in this case from the earlier cases is that this column showed a post-peak softening in the load-deflection response.

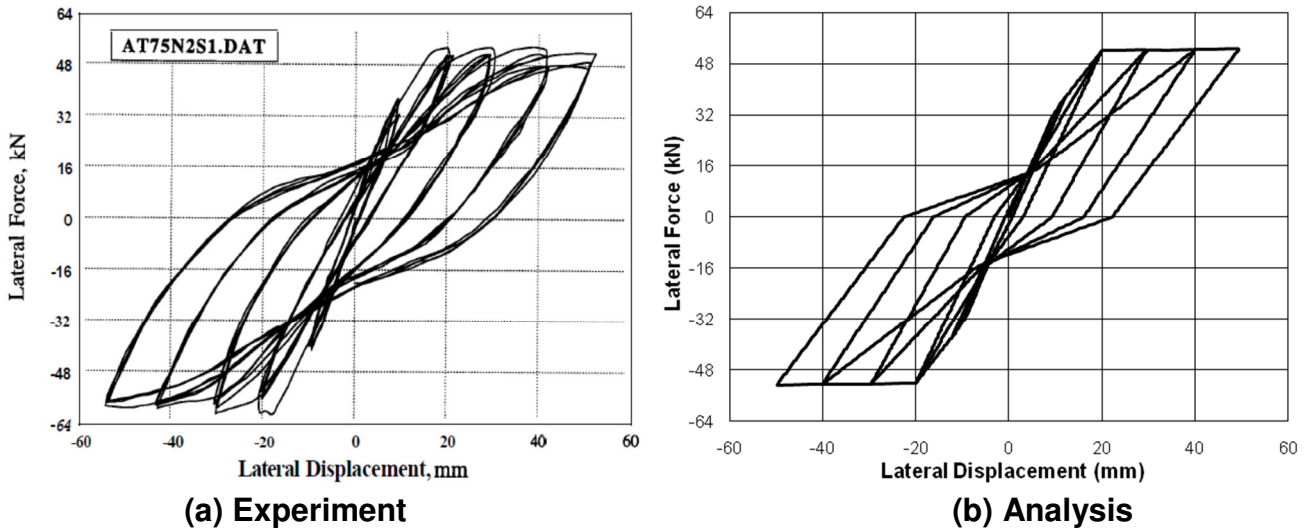


Figure 13.10 Validation of pivot hysteretic law parameters for rectangular sections against results of unit 2S1 tested by Atalay and Penzien (1975)

The numerical results are presented in Figure 13.11b. In this case, the post peak softening was obtained for the envelope as a result of moment-rotation analysis.

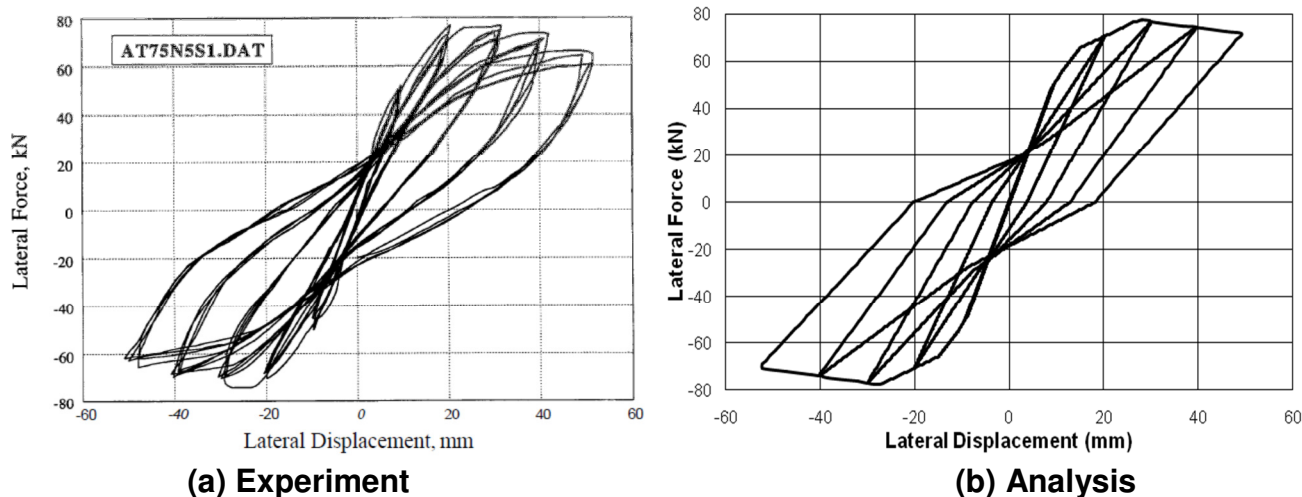


Figure 13.11 Validation of pivot hysteretic law parameters for rectangular sections against results of unit 5S1 tested by Atalay and Penzien (1975)

Comparison of experimental and numerical results proves that the analysis procedure followed in this work along with the suggested parameters for hysteretic behaviour can simulate the experimental behaviour of rectangular columns subjected to quasi-static-cyclic loads quite well. The effects such as post peak softening are automatically considered in the analysis.

13.1.3.2.4 Unit 6S1

The test was carried out on the column having closely spaced ties and having an axial load of around 20% of its capacity. The specimen was loaded with cycles of +/- 10mm, 20mm, 30mm, 40mm and 50 mm. The experimentally obtained hysteretic loops as reproduced from Taylor et al (1997) are shown in Figure 13.12a, while the numerical results are presented in Figure 13.12b. Again post-peak softening was observed in the load-deflection response. Comparison of experimental and numerical results proves the validity of the analysis procedure and suggested parameters for hysteretic behaviour.

13.1.4 Summary of analysis at member level

Based on the comparison of numerical analysis results with their experimental counterparts, it can be clearly said that the parameters suggested in this work can simulate the hysteretic behaviour of rectangular columns quite well. The hysteretic loops considering the unloading, reloading and pinching match quite closely with the experimentally observed values, signifying the applicability of the associated hysteretic rule and the values of α and β parameters. It is seen that different degrees of axial loads, transverse and longitudinal reinforcement ratios, different loading histories, post peak softening response etc, can be accounted for.

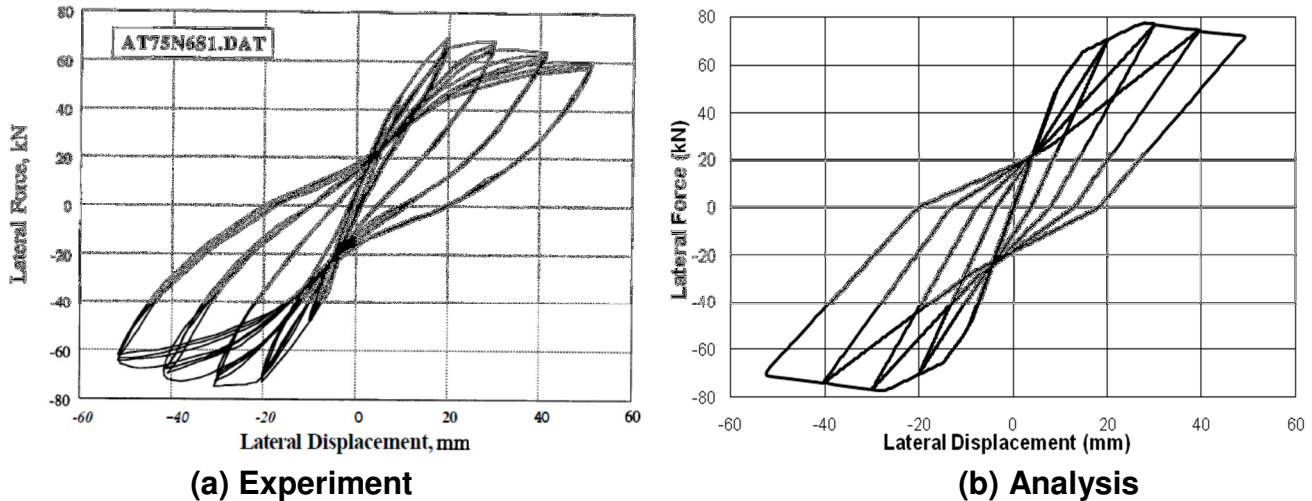


Figure 13.12 Validation of pivot hysteretic law parameters for rectangular sections against results of unit 6S1 tested by Atalay and Penzien (1975)

13.2 Cyclic Analysis of RC Beam-Column Joints

In the previous section, it was shown that the procedure followed to obtain the monotonic hinge characteristics for the members and the parameters used to associate the hysteretic rule with the same could very well predict the cyclic behaviour of the RC columns over a complete range of axial load ratio, with different details and under different levels of load cycles. In this section, the cyclic analysis of poorly detailed RC beam-column joints was performed with different types of detailing and having different axial load ratios.

13.2.1 Analysis of tests by Clyde et al (2000)

The tests performed by Clyde et al (2000) on poorly detailed joints, with beam bars bent in to the joint, were analyzed. The details of the specimens were given in chapter 12 and it was shown in that chapter that the joint model proposed can very well predict the monotonic load-deflection curve for such poorly detailed joints over a range of axial loads. The pivot hysteretic rule was associated with two shear and one rotational spring of the joint panel. The hysteretic parameters α and β were decided on the basis of equations (5.6) through (5.8). The results are reported as under.

13.2.1.1 Analysis of tests with 10% axial load

As mentioned in chapter 12, joint #2 and joint #6 were tested with the axial load on column equal to 10% of the axial load capacity of the column. In the experiment, three cycles per drift were given to the joint sub-assembly. However, in the analysis, only one cycle per drift

level was provided. This is sufficient to prove the validity of the parameters suggested for poorly detailed joints.

For the hinges in beam and column, monotonic curves were obtained using the procedure given in Appendix-I and for the springs of the joint panel, the characteristics were derived following the formulations given in chapter 4. The hysteretic parameters α and β for the member hinges were obtained from equations (5.2) through (5.5), whereas the same for the joint panel springs were obtained from equations (5.6) through (5.8).

The experimentally obtained result for joint #2 as reproduced from Clyde et al (2000) is shown in Figure 13.13a and the analytical result for the same is shown in Figure 13.13b.

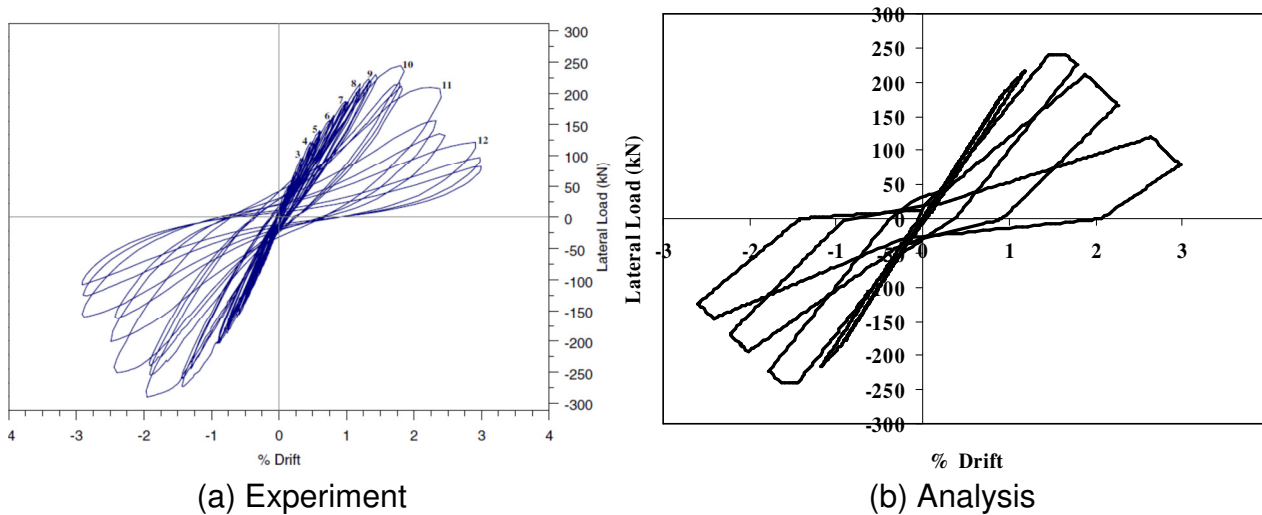
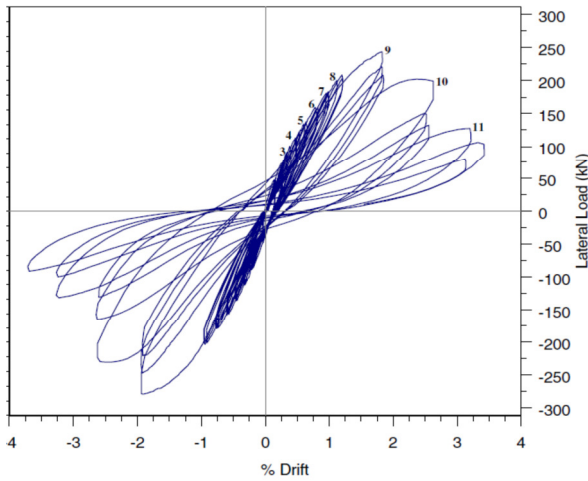


Figure 13.13 Hysteretic plots for joint #2 tested by Clyde et al (2000)

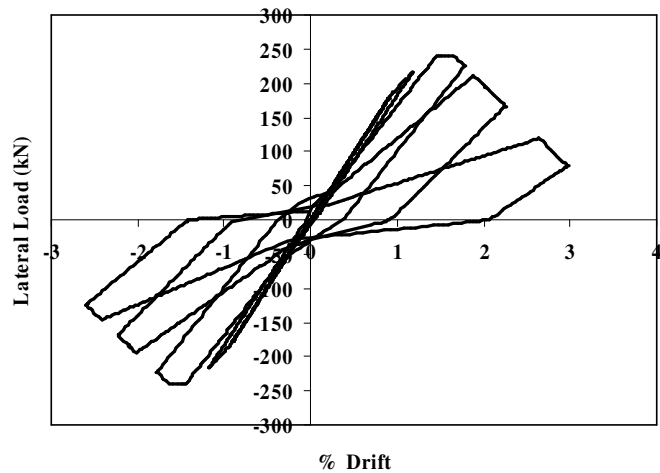
In the analysis for the joint using joint model (Figure 12.3), it was shown that the envelope of the experimental loops matches closely with the numerical results. The results shown in Figure 13.13 show that by associating the pivot hysteretic model to the springs for members and joint with the pivot point parameters as suggested in chapter 5, the hysteretic behaviour of the joint can be simulated nicely.

Similarly, the experimentally obtained result for joint #6 as reproduced from Clyde et al (2000) is shown in Figure 13.14a and the numerical result for the same is shown in Figure 13.14b.

Again it can be seen that the numerically obtained hysteretic loops for the joint are very similar to the experimentally obtained ones, thereby suggesting that the model for the joint along with the hysteretic parameters can be successfully employed to predict the hysteretic behaviour of poorly detailed RC beam-column joints.



(a) Experiment

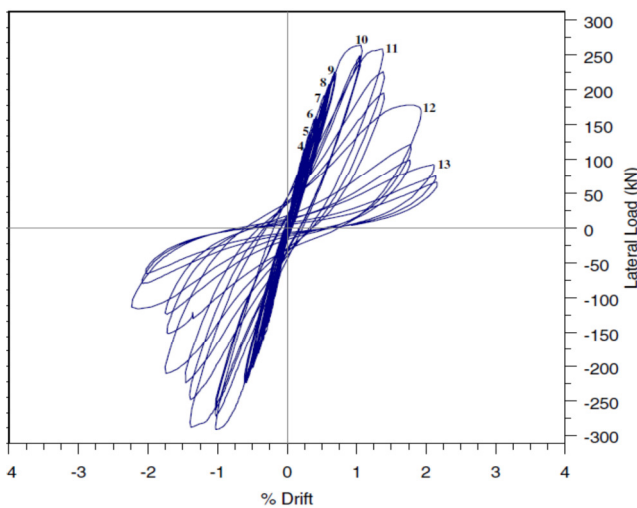


(b) Analysis

Figure 13.14 Hysteretic plots for joint #6 tested by Clyde et al (2000)

13.2.1.2 Analysis of tests with 25% axial load

As mentioned in chapter 12, joint #4 and joint #5 were tested with the axial load on column equal to 25% of the axial load capacity of the column. The experimentally obtained result for joint #4 as reproduced from Clyde et al (2000) is shown in Figure 13.15a, while the numerical result for the same is shown in Figure 13.15b. Similarly, the experimentally obtained result for joint #5 as reproduced from Clyde et al (2000) is shown in Figure 13.16a and the numerical result for the same is shown in Figure 13.16b.



(a) Experiment



(b) Analysis

Figure 13.15 Hysteretic plots for joint #4 tested by Clyde et al (2000)

Figures 13.15 and 13.16 show that the analytically obtained hysteretic loops for the joint are very similar to the experimentally obtained ones, thereby suggesting that the analytical model

for the joint along with the hysteretic parameters can be successfully employed to predict the hysteretic behaviour of poorly detailed RC beam-column joints for joints having different axial load ratios.

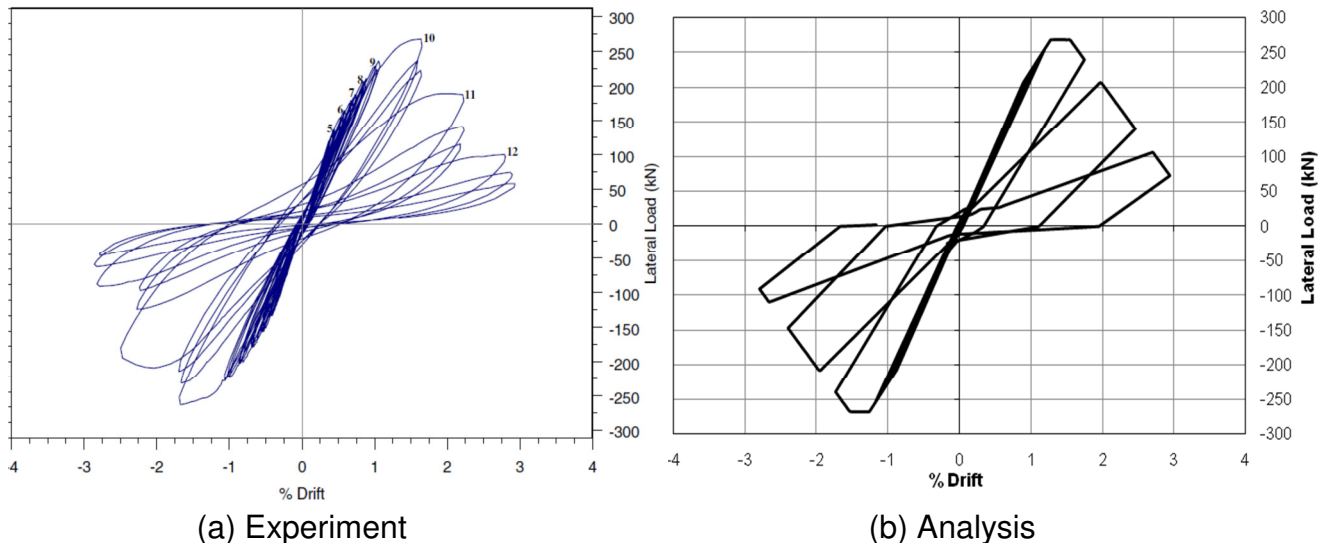


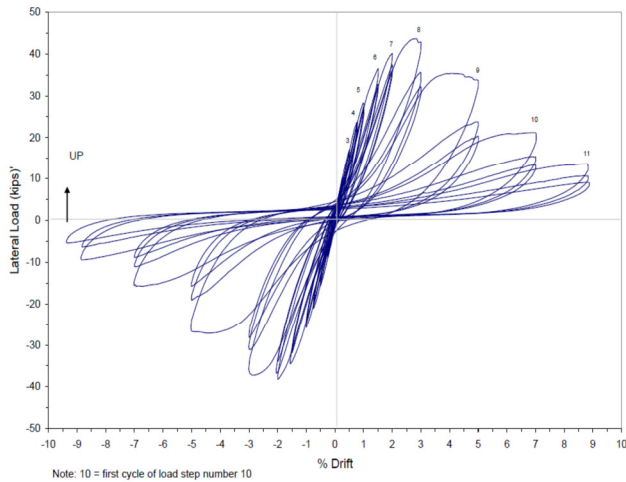
Figure 13.16 Hysteretic plots for joint #5 tested by Clyde et al (2000)

13.2.2 Analysis of tests by Pantelides et al (2002)

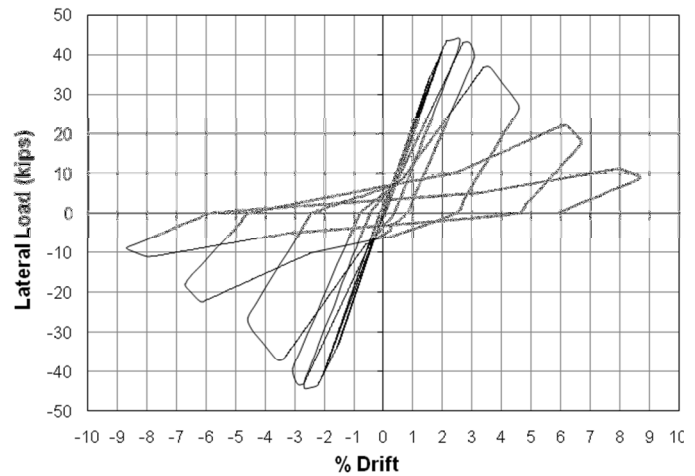
The tests performed by Pantelides et al (2002) on poorly detailed joints, only with beam bars bent in to the joint, were analyzed. The details of the specimens were given in chapter 12 and it was shown in that chapter that the joint model proposed can very well predict the monotonic load-deflection curve for such poorly detailed joints over a range of axial loads. The pivot hysteretic rule was associated with two shear and one rotational spring of the joint panel. The results are reported as under.

As mentioned in chapter 12, joint #5 was tested with the axial load on column equal to 10% of the axial load capacity of the column and joint #6 was tested with axial load on column equal to 25% of the axial load capacity of the column. Again, in the analysis, only one cycle per drift level was provided.

The experimentally obtained results for joint #5 as reproduced from Pantelides et al (2002) are shown in Figure 13.17a, while the numerical results for the same are shown in Figure 13.17b. Similarly, the experimentally obtained results for joint #6 as reproduced from Pantelides et al (2002) are shown in Figure 13.18a and their numerical counterparts are shown in Figure 13.18b. In this case, to have a direct visual comparison of experiment and analysis, lateral load is reported in kips, as was originally given in the reference (Pantelides et al, 2002).



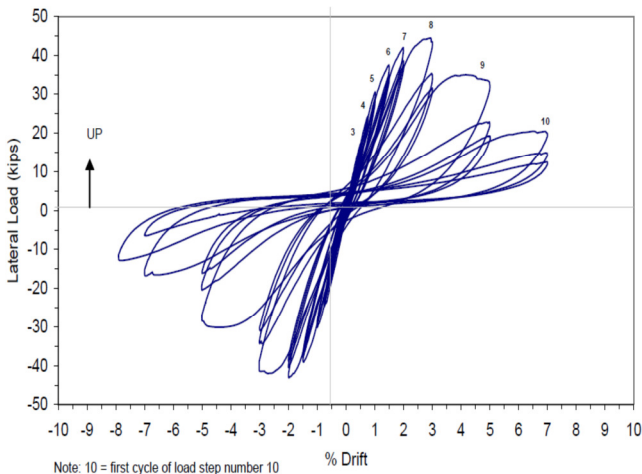
(a) Experiment



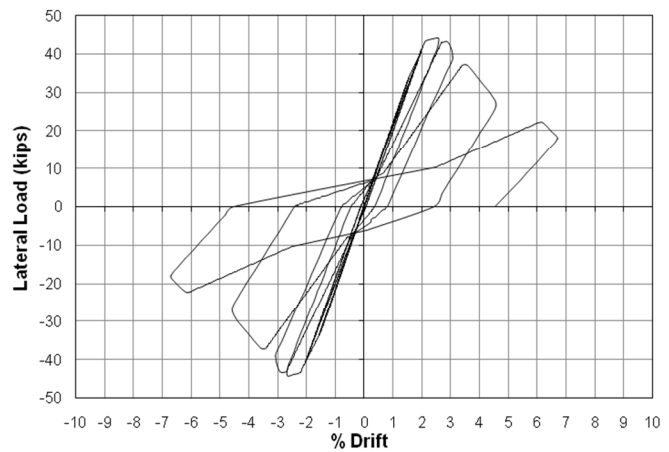
(b) Analysis

Figure 13.17 Hysteretic plots for joint #5 tested by Pantelides et al (2002)

Comparison of experimental and numerical results for both the joints shows that the hysteretic parameters within the framework of lumped plasticity approach can be successfully employed to predict the hysteretic behaviour of poorly detailed RC beam-column joints.



(a) Experiment



(b) Analysis

Figure 13.18 Hysteretic plots for joint #6 tested by Pantelides et al (2002)

13.3 Validation of parameters against quasi-static-cyclic analysis of RC structures

To demonstrate the efficacy of the model in predicting the cyclic hysteretic behaviour of non-seismically detailed RC structures, the results on a frame structure as tested by Calvi et al (2002) were used. The details of the structure as reproduced from original work (Calvi et al 2002) are given below.

13.3.1 Description of frame structure

The frame structure tested by Calvi et al (2002) was a 2/3rd scale replica of a three-storey structure. The geometrical and reinforcement characteristics of the test frame are given in Figure 13.19 as reproduced from Calvi et al (2002). To simulate a pre-1970's construction type, no transverse reinforcement was placed in the joint region and plain round bars were adopted for both longitudinal and transverse reinforcement. Beam bars in exterior joints were anchored with end-hooks.

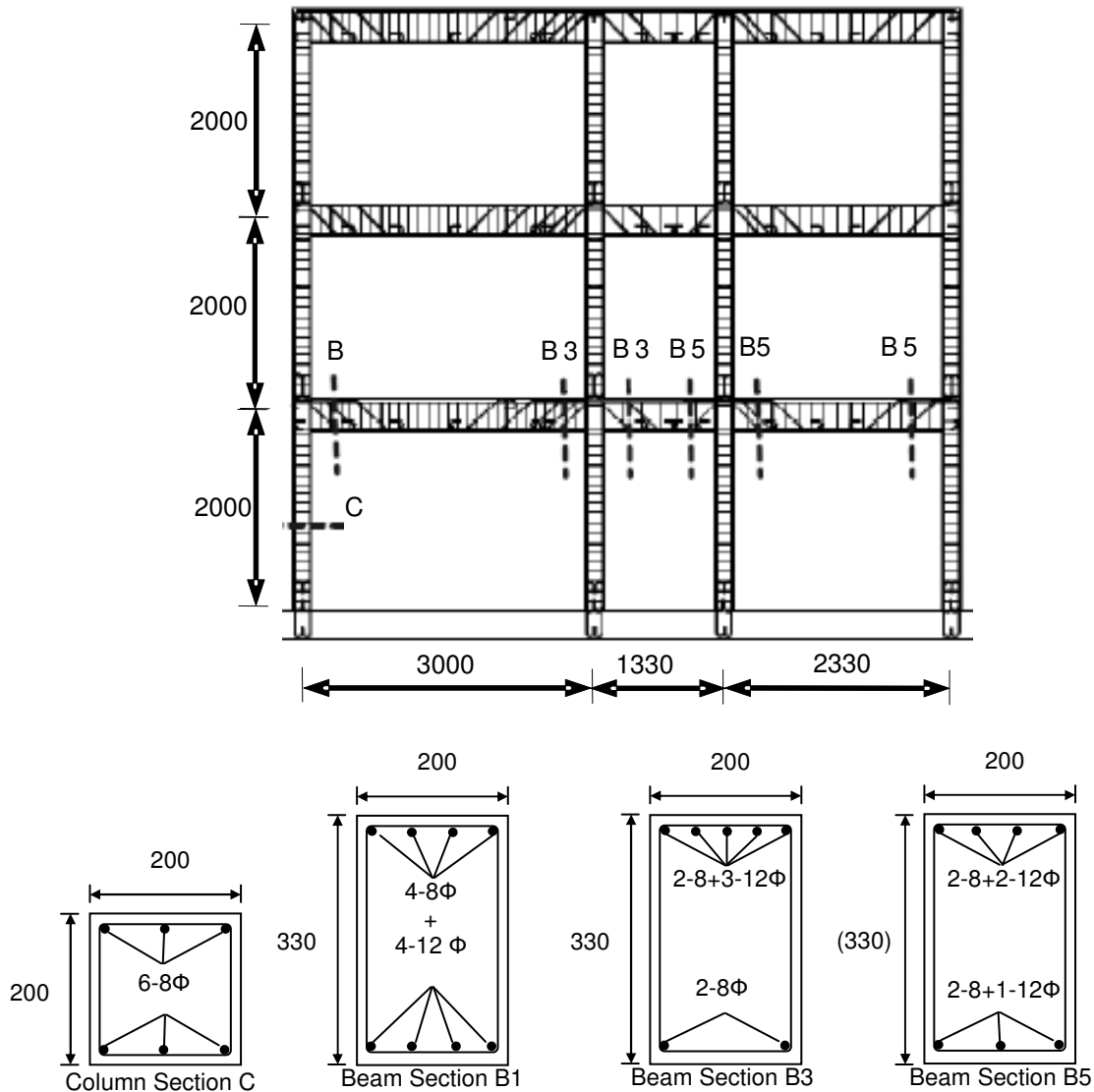


Figure 13.19 Geometry of the frame tested by Calvi et al (2002)

The average concrete cylinder strength on the test day was reported as 14.06MPa and the strength was found to be varying between 12.72MPa to 17.83MPa over different locations. The yield and ultimate strength of 8mm diameter bars was reported as 385.64MPa and

451.22MPa respectively, while the same for 12mm diameter bars was reported as 345.87MPa and 458.63MPa respectively.

The frame system was subjected to quasi-static cyclic loading at increasing levels of top displacement. The loading history consisted of a series of three cycles of top drift of $\pm 0.2\%$, $\pm 0.6\%$, $\pm 1.2\%$, and one conclusive cycle of $\pm 1.6\%$. At each loading step, the load at Roof level: second level: first level was kept fixed at 1:0.9:0.45 respectively. On 1st and 2nd floor, the weights in 1st, 2nd and 3rd bay were equal to 31.8kN, 14.1kN and 27.1kN respectively. Similarly on the roof level, the weights in 1st, 2nd and 3rd bay were equal to 22.4kN, 9.4kN and 22.4kN respectively.

13.3.2 Experimental and numerical results

Figure 13.20 shows (a) experimental hysteretic loops as obtained for the structure and (b) shows the analytical hysteretic loops. Again, although in the experiment, three cycles were given for each drift level, in the analysis only one cycle per drift level was provided.

For analysis, first the envelope of spring characteristics were evaluated and then pivot model parameters were assigned. However in this case, plain reinforcing bars were used instead of deformed bars. The procedure to obtain the member and joint hinge characteristics would not change due to the type of bars since the procedures as such are independent of the bar type. Only the appropriate bar strength has to be used. However, to obtain the joint hinge characteristics the principal tensile stress v/s shear deformation curve as recommended by Pampanin et al (2002) was followed which is essentially similar to the curve for the joint with beam bars anchored straight into the joint with 150 mm embedment as shown in the third quadrant of Figure 4.18.

For analysis, first the envelope of spring characteristics were evaluated and then pivot model parameters were assigned. Since in this case, plain reinforcing bars were used instead of deformed bars, the alpha and beta parameters were considered as $2/3^{\text{rd}}$ of the values obtained for deformed bars. This is consistent with the original pivot model (Dowell et al, 1998). This was postulated based on the knowledge that plain round bars have a poorer bond behaviour compared to deformed bars and therefore they result in more severe pinching and poorer hysteretic loops. This was also confirmed by the results of a few tests conducted on the exterior joints with plain round bars (Liu, 2006).

Comparing Figure 13.20 (a) with Figure 13.20 and (b), it is clearly observed that the numerical analysis procedure along with hysteretic parameters suggested can successfully capture the hysteretic response of gravity load designed frames.

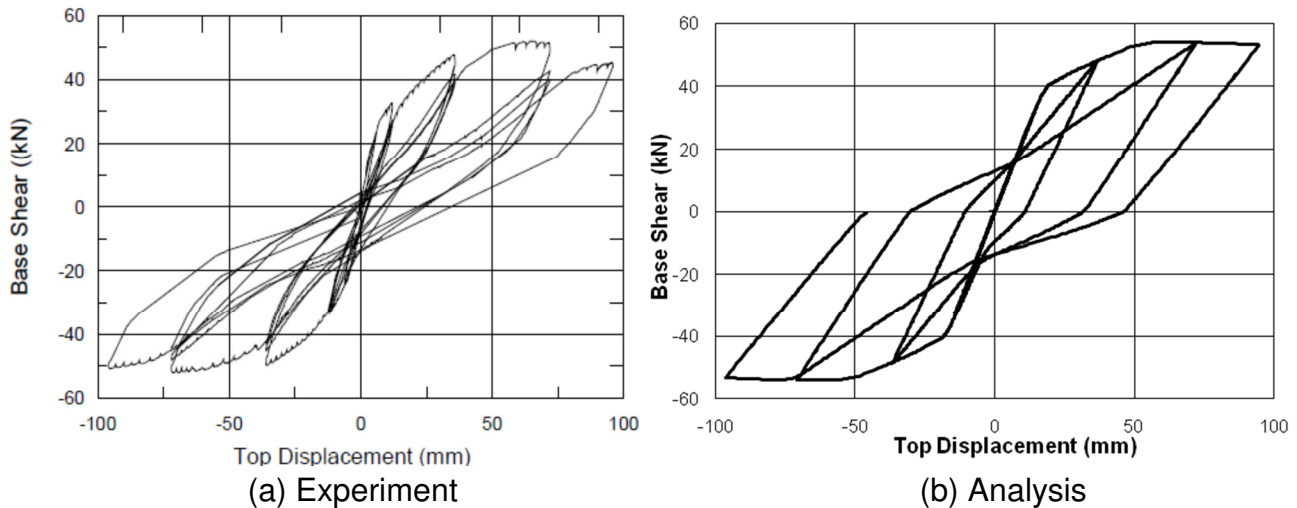
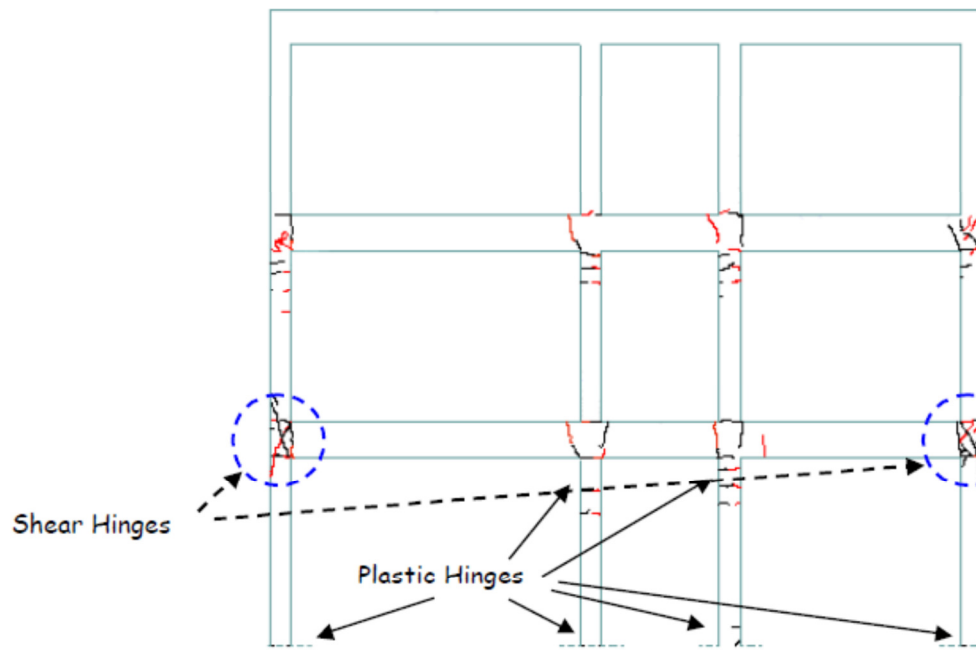


Figure 13.20 Hysteretic Base Shear v/s Top Displacement plots for the structure tested by Calvi et al (2002)

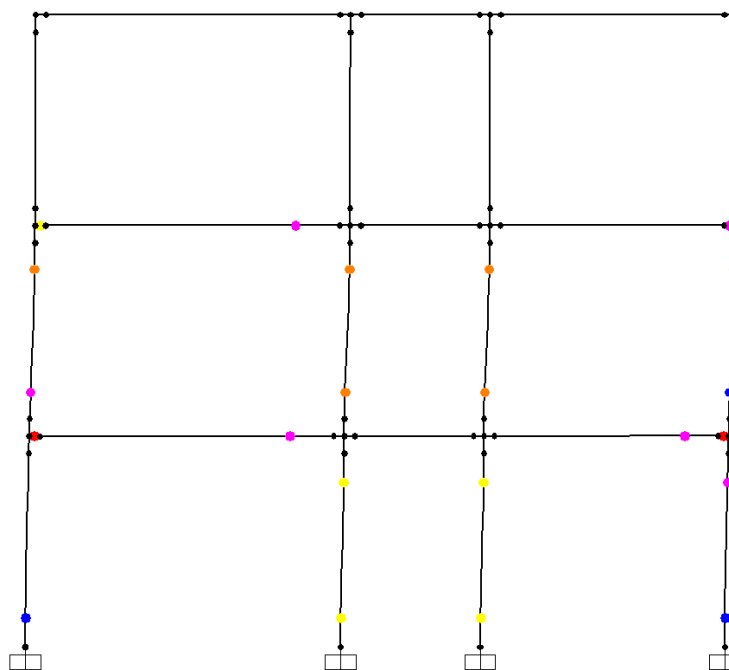
Figure 13.21 shows (a) failure patterns as observed during the test and (b) failure pattern as predicted by analysis. The typical failures observed in the test namely joint shear hinges for exterior joints as well as plastic hinges in beams and columns could be successfully replicated in the analysis. Thus, it can be said that the numerical modelling procedure followed in this work can correctly predict not only the hysteretic behaviour but also the expected failure patterns for the non-seismically detailed structures.

13.4 Validation of parameters and numerical modelling for dynamic analysis of non-seismically designed RC structures

In previous sections it was shown that the numerical modelling procedures as well the hysteretic parameters proposed in this work are capable of successfully simulation the inelastic seismic behaviour of members, joints and structures. The procedure has been extensively validated against the quasi-static-monotonic and quasi-static-cyclic analysis. However, it is well known that the earthquake induced forces are generated due to inertia of the structure and therefore a nonlinear dynamic analysis of the same can provide the best estimates for the seismic forces and displacements expected due to a particular ground motion. To validate the suitability of models and numerical analysis procedure, in this section, the results of a nonlinear dynamic analysis performed on a 1:3 scale three storey structure tested on shake table by Bracci et al (1992, 1995) are reported.



(a) Experiment



(b) Analysis

Figure 13.21 Failure patterns observed for the structure tested by Calvi et al (2002)

13.4.1 Description of Test Structure

Bracci et al (1992, 1995) tested a 1:3 scale model of a hypothetical but realistic prototype three storey gravity load designed structure. The geometry of the model structure tested, as reproduced from the reference (Bracci et al, 1992) is shown in Figure 13.22. The bay width

was 6 feet (1829mm) in both directions and the storey height was 4 feet (1219mm), which is suitable for 1/3rd model of a typical prototype structure.

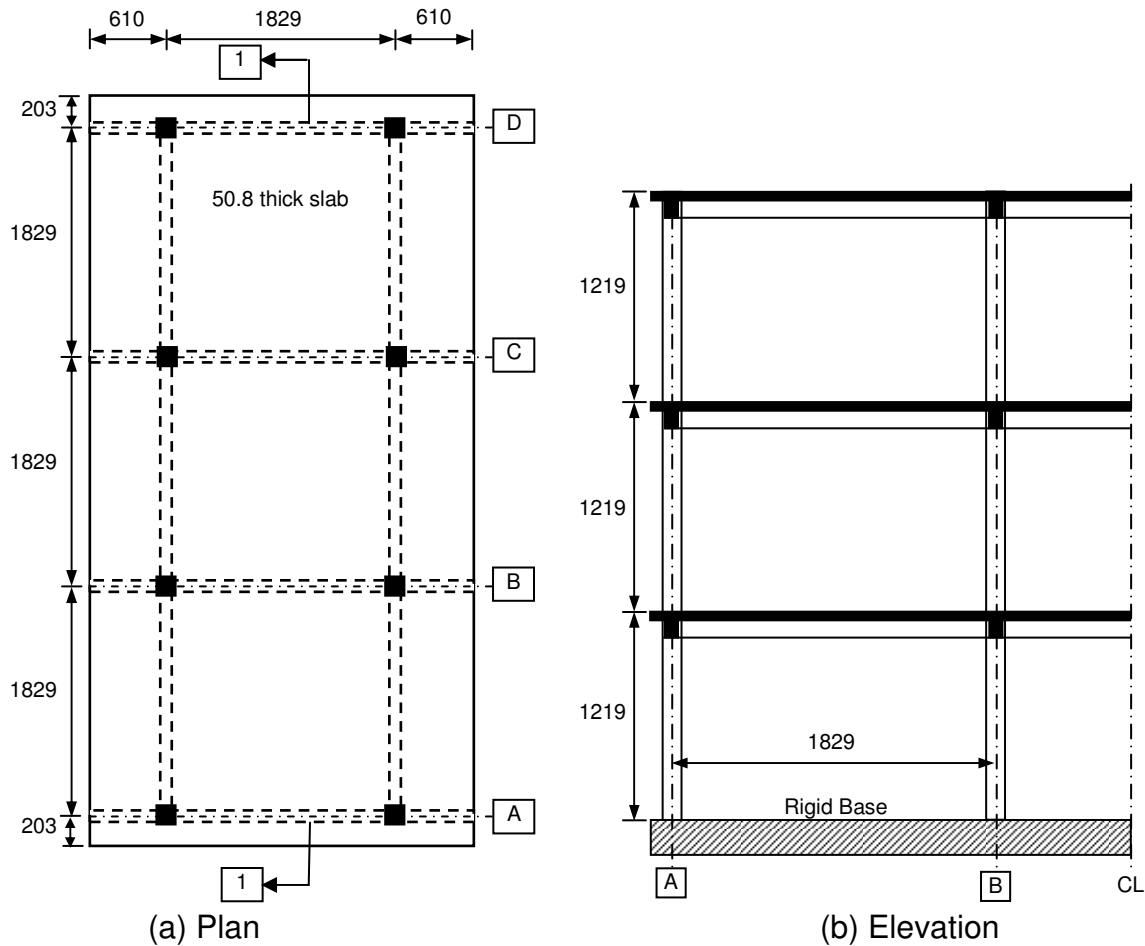


Figure 13.22 Geometry of the model structure tested by Bracci et al (1992)

To satisfy mass similitude requirements, additional weights were placed in the form of concrete blocks and lead bricks on the slab of different storey levels. The total weight provided at each floor level including the self weight of the model, the weight of concrete blocks and lead bricks was calculated to be 27.0 kips (120 kN).

The average concrete cylinder strength was reported as 3900 psi (26.90 MPa) and the range of concrete strength variation between different locations was reported from 2920 psi (20.13 MPa) to 4960 psi (34.20 MPa).

The reinforcement details for the beams of the structure are shown in Figure 13.23 (Bracci et al, 1992). The detailing conforms to the detailing of a typical gravity load designed structure with no negative reinforcement in mid span and only nominal positive reinforcement at the supports. The reinforcement details for the columns of the structure are shown in Figure 13.24 (Bracci et al, 1992). The lap splices were given at potential hinge locations similar to the old gravity load design detailing practice.

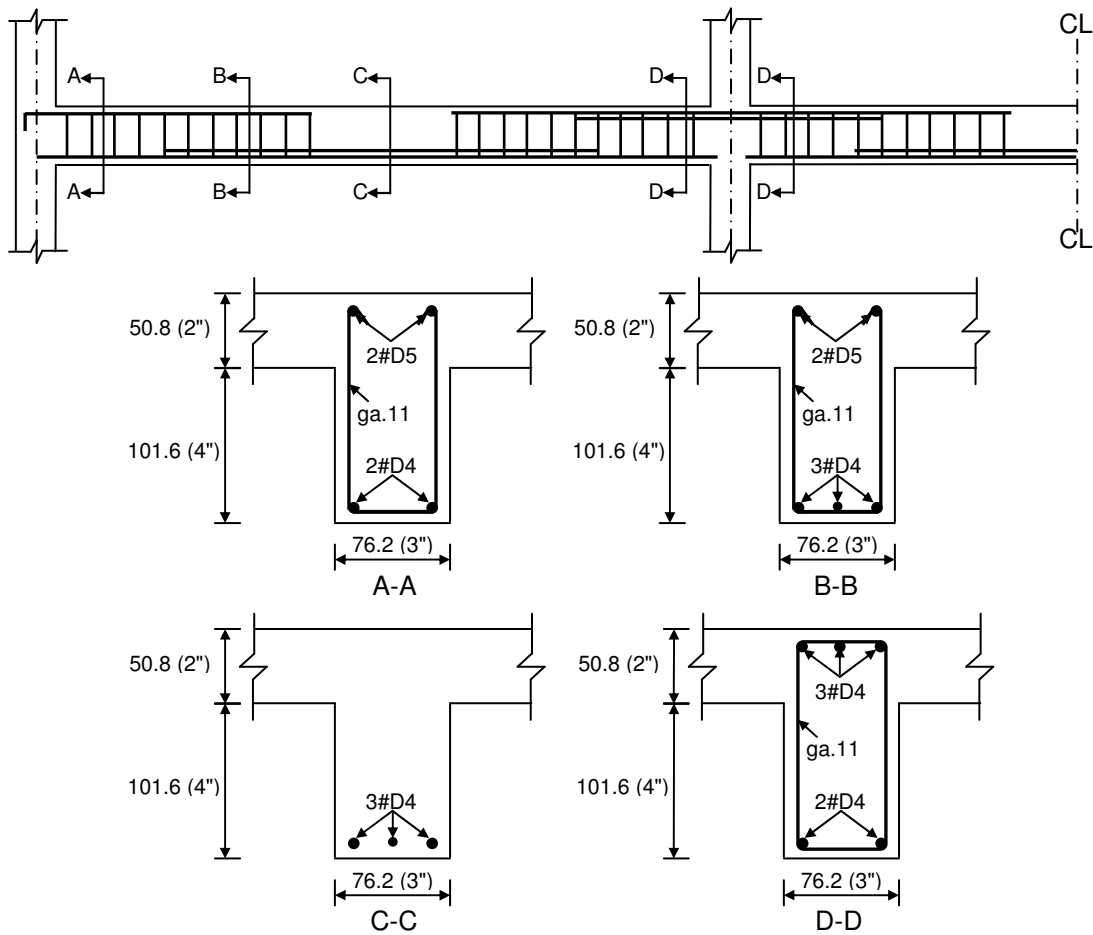


Figure 13.23 Typical beam reinforcement details for the model structure tested on shake table by Bracci et al (1992, 1995)

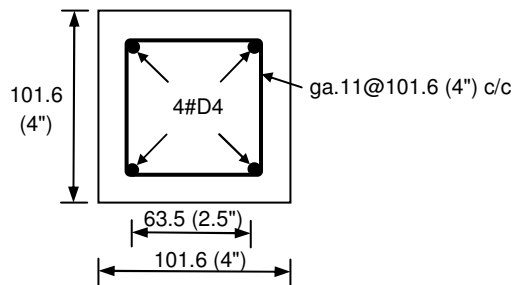


Figure 13.24 Typical column reinforcement details for the model structure tested on shake table by Bracci et al (1992, 1995)

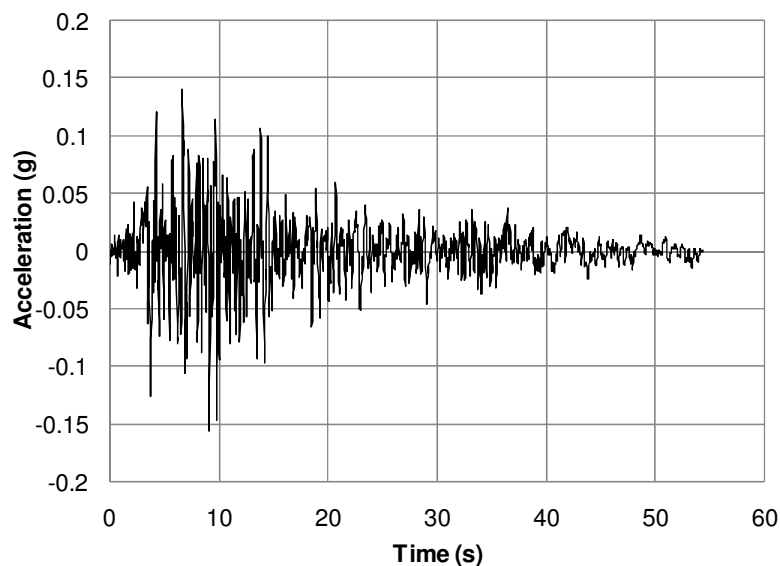
The reinforcing steel for the design of prototype structure was considered as #3, #5 and #6 deformed rebars with 40 ksi yield strength. Based on yield force similitude and tensile testing of selected reinforcement, annealed D4 and D5 rebars having diameters of 0.225 in (5.715 mm) and 0.252 in (6.40 mm) respectively were used as longitudinal reinforcement for beams and columns. The measured average yield and ultimate strength for the D4 rebars were 68 ksi (468.8 MPa) and 73 ksi (503.3 MPa) respectively and the corresponding values for D5 rebars were 38 ksi (262 MPa) and 54 ksi (372 MPa) respectively. The transverse

reinforcement was made of gauge 11 black wire with a diameter of 0.12 in (3.048 mm) and an average measured yield strength of 56 ksi (386 MPa) and ultimate strength of 70 ksi (441.3 MPa). The slab reinforcement was made of gauge 12 galvanized rebars with a diameter of 0.109 in (2.77 mm) having an average measured yield strength of 58 ksi (400 MPa) and ultimate strength of 64 ksi (482 MPa). All the rebars were confirmed to satisfy the similitude requirements.

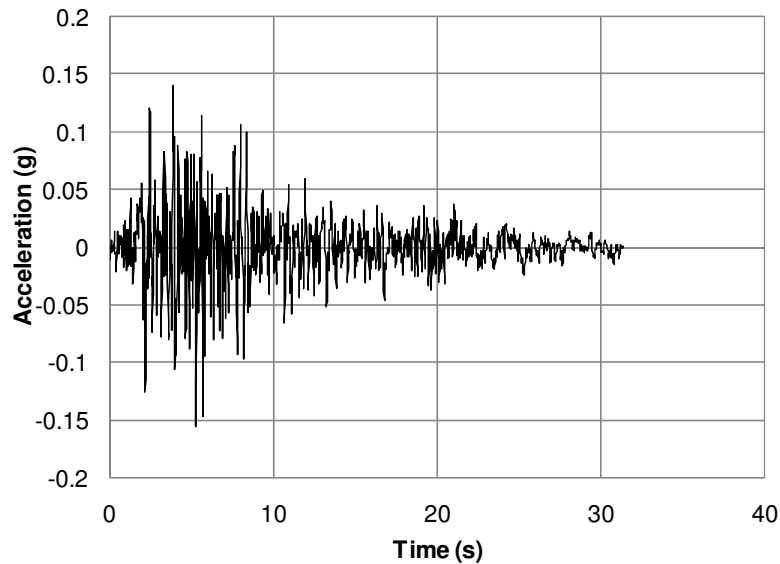
13.4.2 Experimental Program

The structure was tested on the shake table using the N21E ground acceleration component of the July 21, 1952 Taft earthquake at the Lincoln School Tunnel site in California. The original accelerogram has a total ground excitation time history of 54.4 seconds with peak ground acceleration (PGA) of 0.156 g. To satisfy the time similitude requirements of the actual earthquake for the one third scale model, a scale factor of $1/\sqrt{3}$ was used to compress the time history of the accelerogram (Bracci et al, 1992). The full scale Taft N21E component accelerogram and the scaled down accelerogram of the same as used by Bracci et al (1992) are shown in Figure 13.25a and 13.25b, respectively.

In the shake table tests to determine the seismic response of the structure, three levels of ground motions were used namely minor ground motion, by applying the time scaled accelerogram scaled down to a PGA of 0.05g; moderate ground motion with a scaled PGA of 0.2g; and severe ground motion with a scaled PGA of 0.3g. However, the complete test program comprised of the tests to determine the static and dynamic characteristics of the structure, in addition to the tests with the above-specified three ground motions.



(a) Full time history (original accelerogram)



(b) Scaled time history as used in the test

Figure 13.25 Ground motion records used for shake table tests on model structure by Bracci et al (1992, 1995)

13.4.3 Experimental and numerical results

In the numerical model, inelastic springs were used to model the characteristics of the members and joints following the concepts and modelling techniques discussed earlier. The structural model was subjected to ground acceleration time history and direct integration time history analysis was used to analyze the structure. However, before starting the nonlinear dynamic analysis, the suitability of the model to simulate the linear static and dynamic characteristics of the system were verified by simulating the pull back tests, snap back tests and frequency analysis for the structure.

13.4.3.1 Static characteristics of the structure

To obtain the static characteristics of the structure, the pull back tests were conducted on the structure. The flexibility matrix of the structure was experimentally obtained by statically loading the centre of the bay for each floor with horizontal loads (Bracci et al, 1992). The experimental flexibility matrix thus obtained is as shown below:

$$F_{ij, \text{experimental}} = \begin{bmatrix} 7.18 & 4.77 & 2.33 \\ 4.64 & 4.36 & 2.18 \\ 2.20 & 2.13 & 1.95 \end{bmatrix}$$

Where, the first element of the flexibility matrix is obtained by recording the displacement at roof level when the load is applied at the roof level.

Similarly, the pull back analysis was performed to obtain the linear flexibility matrix for the structural model with springs and to compare the same with the experimental flexibility matrix. The analysis was performed by statically loading the centre of the bay for each floor with horizontal loads and recording the various storey displacements. The analytical flexibility matrix thus obtained is as shown below:

$$F_{ij, \text{numerical}} = \begin{bmatrix} 7.12 & 4.68 & 2.05 \\ 4.87 & 4.44 & 2.03 \\ 2.27 & 2.25 & 1.85 \end{bmatrix}$$

Thus the static properties for the structure were very well be simulated in the numerical model with springs.

13.4.3.2 Dynamic characteristics of the structure

To obtain the dynamic characteristics for the structure, quick release snap back tests were performed on the model structure. Each floor of the model structure was statically loaded with a horizontal tensile force and quickly release so that the model could vibrate freely. Figure 13.26a shows the experimental displacement-time response for the third floor due to the snap load applied at third floor itself. The load applied was around 1.1 kips (4.89 kN) and the static displacement was obtained to be around 0.083 in (2.11 mm).

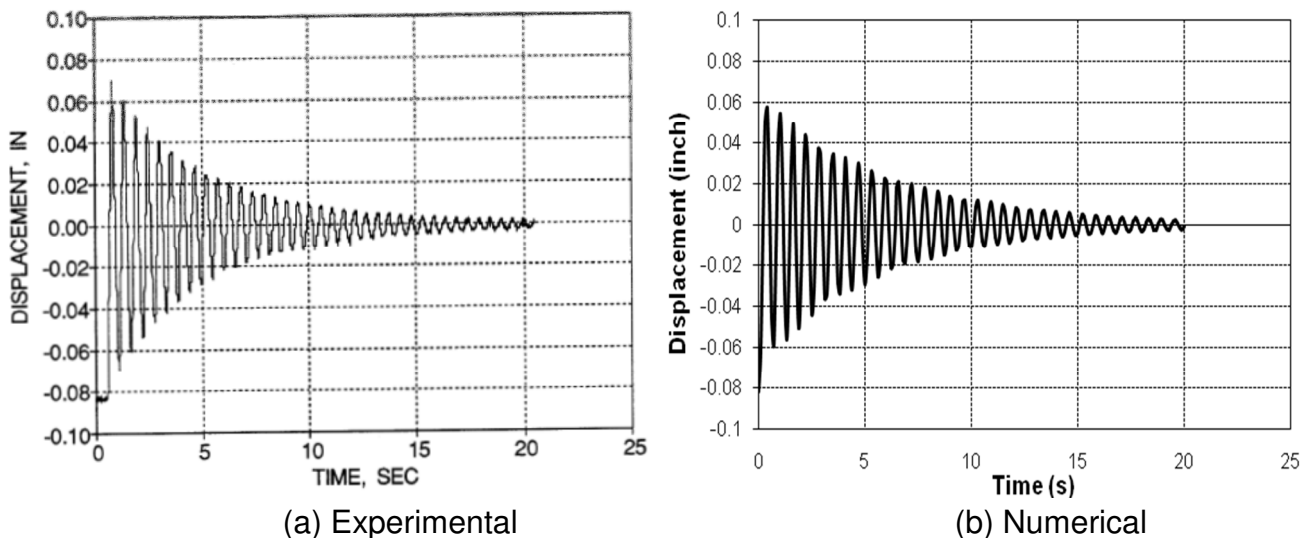


Figure 13.26 Third storey displacement response from third storey snap for the model structure tested by Bracci et al (1992)

Similar to the experiment, to obtain the dynamic characteristics for the structure, quick release snap back analysis was performed on the model of the structure. However, only

single analysis was performed where the load was applied at the roof level and then suddenly released leading to the free vibrations in the structure. Figure 13.26b shows the numerically obtained plot of the displacement-time response for this analysis. The results suggest that the linear dynamic characteristics of the structure could be nicely simulated in the numerical model with springs.

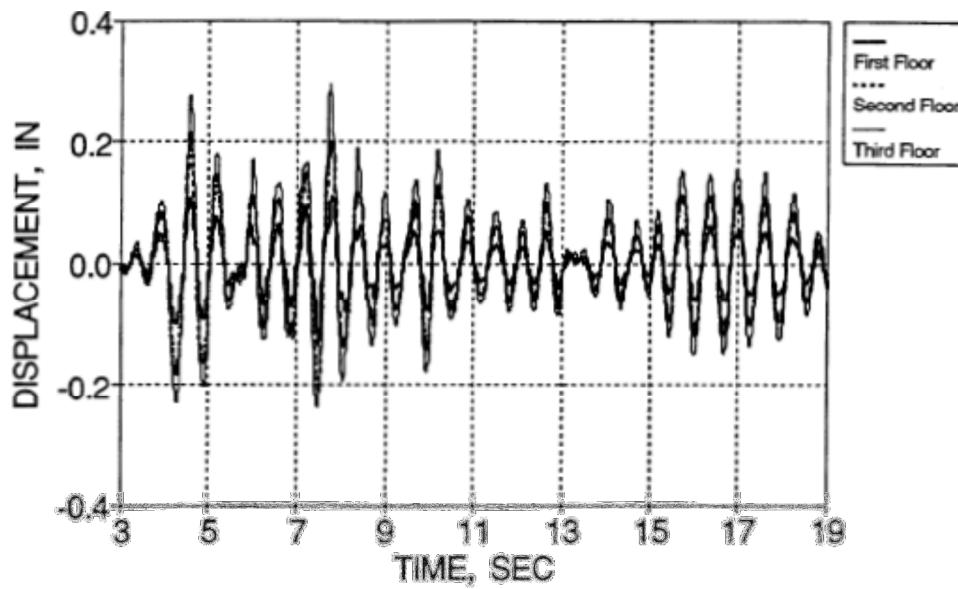
White noise tests were also performed to obtain the dynamic response of the model structure. From the white noise test (Bracci et al, 1992), it was found that the frequencies of the structure corresponding to the first three modes of vibration are 1.78 Hz, 5.32 Hz and 7.89 Hz respectively. In order to obtain the frequencies of vibration for the structure corresponding to various modes, an eigen vector based modal analysis was performed on the model of the structure with springs. The frequencies obtained numerically for the model were 1.77 Hz, 5.28 Hz and 8.26 Hz corresponding to 1st, 2nd and 3rd modes respectively.

Thus, based on the results of pull back analysis, snap back analysis and modal analysis, it was confirmed that the model with the inelastic springs was fully capable of reproducing the linear response of the structure in quite good agreement with the experimental results.

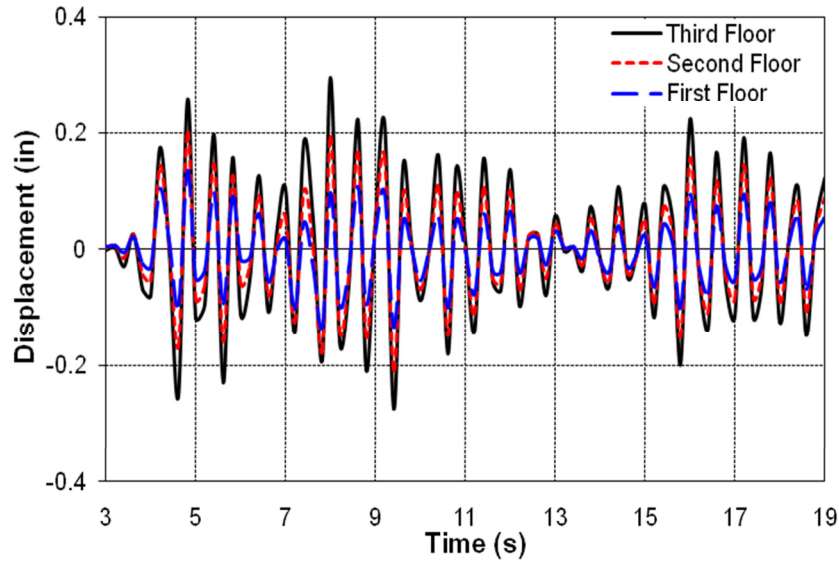
13.4.3.3 Simulated earthquake tests and analysis

The first simulated seismic test was performed on the structure with the ground motion corresponding to minor shaking (PGA = 0.05 g). This was followed by the tests with moderate shaking (PGA = 0.20g) and with severe shaking (PGA = 0.30g). Figure 13.27a shows the experimental displacement-time response of the various floors for the test with minor shaking (Bracci et al, 1992). As seen from the plot, for the minor shaking loading history, the maximum roof displacement was obtained as 0.3 in (7.6 mm), the maximum 2nd storey displacement was recorded as 0.22 in (5.6 mm) and the maximum 1st storey displacement was recorded as 0.14 in (3.6 mm).

The seismic analysis (nonlinear time history analysis) was performed on the computer model of the structure with the ground motion corresponding to minor shaking (PGA = 0.05 g). The initial conditions for the structure for this analysis were kept as unstressed. Figure 13.27b shows the numerical displacement-time response of the various floors for the analysis with minor shaking ground motion. As seen from the plot, for the minor shaking loading history, the maximum roof displacement was obtained as 0.29 in (7.37 mm), the maximum 2nd storey displacement was recorded as 0.208 in (5.28 mm) and the maximum 1st storey displacement was recorded as 0.134 in (3.4 mm).



(a) Experiment



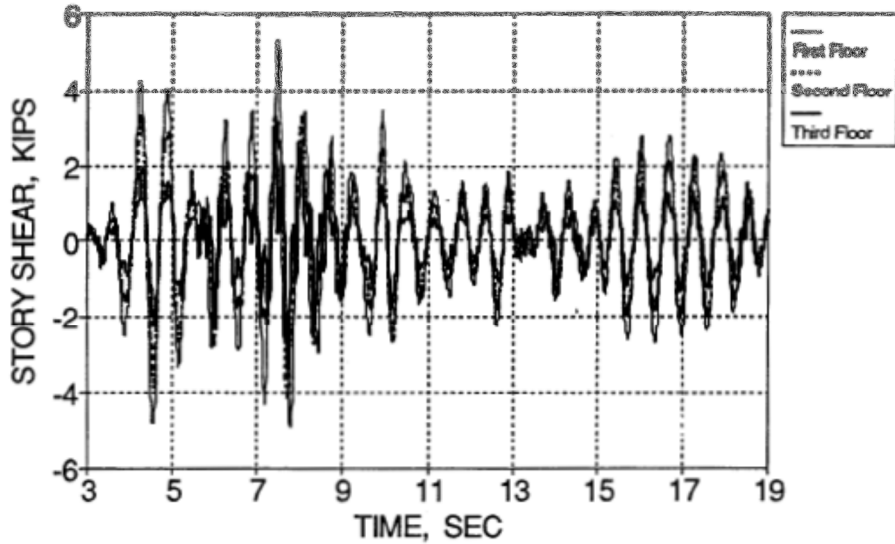
(b) Analysis

Figure 13.27 Displacement-time response obtained for the model structure tested by Bracci et al (1992) subjected to the ground motion with PGA = 0.05g

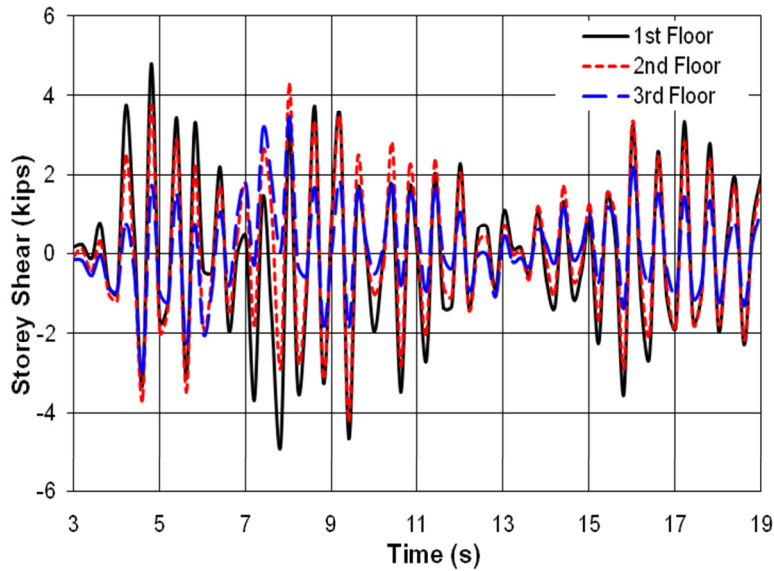
Comparing the plots shown in Figure 13.27 and the corresponding maximum displacement values, it is confirmed that the analysis can predict the response of the structure to this ground motion quite well.

Figure 13.28a shows the experimental storey shear-time response of the various floors for the test with minor shaking (Bracci et al, 1992). As seen from the plot, the maximum recorded base shear (storey shear for first floor) was recorded as 5.265 kips (23.42 kN) corresponding to 6.5% of the weight of the structure (81 kips = 360 kN). The maximum recorded storey shear for 2nd storey was 4.21 kips (18.72 kN) corresponding to 5.2% of the weight of the

structure and the maximum recorded storey shear for 3rd storey was 3.40 kips (15.12 kN) corresponding to 4.2% of the weight of the structure.



(a) Experiment



(b) Analysis

Figure 13.28 Storey shear-time response of various floor levels obtained for the model structure subjected to the ground motion with PGA = 0.05g

Figure 13.28b shows the numerically obtained storey shear-time response of the various floors for the test with minor shaking. The maximum recorded base shear (storey shear for first floor) was obtained as 4.80 kips (21.35 kN) corresponding to 5.9% of the weight of the structure (81 kips = 360 kN). The maximum recorded storey shear for 2nd storey was 4.28 kips (19.04 kN) corresponding to 5.29% of the weight of the structure and the maximum recorded storey shear for 3rd storey was 3.42 kips (15.21 kN) corresponding to 4.22% of the weight of the structure. Again, comparing these values with the corresponding experimental

values, it can be said that the analysis can predict the response of the structure to this ground motion quite well.

Similar records were obtained for the moderate and severe shaking time histories. The responses were also obtained for the moderate and severe shaking time histories from the numerical analysis. The nonlinear analysis for the minor ground motion was started from unstressed conditions; that for moderate ground motion was started from the stress state corresponding to the last point of the minor ground motion and that for severe ground motion was started from the stress state corresponding to last point of the moderate ground motion.

Table 13.4 gives the summarized results in the form of strength and deformation demand due to different ground motions on the structure along with the comparison with experimentally obtained values. The values given in Table 13.4 clearly suggest that the structure begins to go in the inelastic range from moderate shaking ground motion onwards since neither the storey shear nor the storey displacement rise in direct proportion to the PGA value. A one to one comparison of the values for the peak storey accelerations, maximum storey displacement as well as maximum storey shear clearly displays that the nonlinear dynamic analysis of the structure with the inelasticity and hysteretic behaviour at the hinge locations modelled using the formulations presented in this work can be quite effectively utilized to obtain a good idea of the inelastic dynamic behaviour of the RC structures due to earthquakes, while considering the joint distortion.

Table 13.4 Comparison of experimentally recorded and analytically obtained strength and deformation demand on the structure due to different ground motions for the model structure tested by Bracci et al (1995)

Ground Motion	Storey	Peak Storey acceleration (g)		Maximum storey displacement (mm)		Maximum storey shear (kN)	
		Experiment	Analysis	Experiment	Analysis	Experiment	Analysis
Minor shaking (0.05g)	Third	0.12	0.13	7.6	7.37	15.12	15.21
	Second	0.09	0.12	5.6	5.28	18.72	19.04
	First	0.09	0.10	3.6	3.40	23.42	21.35
Moderate shaking (0.20g)	Third	0.20	0.23	33.5	30.12	24.84	25.83
	Second	0.20	0.24	29.0	24.04	41.40	41.24
	First	0.25	0.21	16.3	14.13	54.72	49.22
Severe shaking (0.30g)	Third	0.25	0.29	59.7	50.10	31.68	25.71
	Second	0.22	0.32	52.1	44.21	51.48	44.38
	First	0.29	0.33	24.6	27.83	55.08	51.89

13.5 Nonlinear dynamic analysis of as built 2D RC frame structure

In chapter 9, the details of the shake table tests performed on a 2D RC frame structure were presented. The same structure was modelled, following the procedures and models explained in this work, and analyzed under dynamic loads. The results of the analysis are presented here. The numerical analysis was performed using commercial software SAP2000.

13.5.1 Modal analysis

Before starting the nonlinear dynamic analysis, modal analysis was performed for the structure to evaluate the natural time periods/frequencies of the structure. The time period corresponding to the first mode was obtained as 0.297 seconds numerically, while the same was obtained as 0.31 seconds experimentally. The same for second mode was obtained as 0.081 seconds numerically, while the same was obtained as 0.076 seconds experimentally. Thus, the model was able to simulate the linear dynamic characteristics of the system well.

13.5.2 Nonlinear dynamic analysis

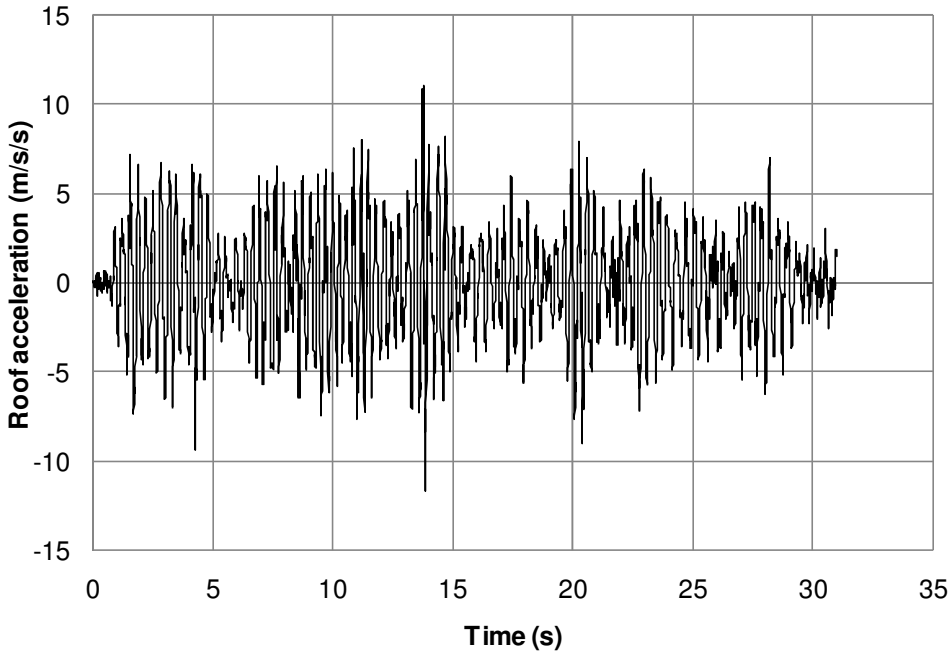
The numerical modelling of the structure to perform nonlinear dynamic analysis of the same was performed following the concepts and modelling techniques discussed earlier. The inelastic properties of the members (beams and columns) were derived on the basis of procedure described in Appendix-A, while the hysteretic characteristics for the same were simulated using pivot hysteretic model. The hysteretic parameters were evaluated on the basis of equations (5.2) through (5.5). The inelastic behaviour of the joints was modelled through the system of springs, with inelastic characteristics of the same derived on the basis of formulations explained in chapter 4, while the hysteretic characteristics for the same were simulated using pivot hysteretic model. The hysteretic parameters were evaluated on the basis of equations (5.6) through (5.8).

The structural model was subjected to ground acceleration time history and direct integration time history analysis was used to analyze the structure. The first input time history corresponded to the table time history for PGA of 0.1g. The analysis for the next higher loading wave (PGA = 0.2g) was started from the end conditions of the previous run. Similar to the experiment, the input ground motion was incremented with a PGA of 0.1g till the PGA of 1.0g was reached. Though, the analysis was run for all the loading cases, the comparison of experimental and numerical time histories is given for three critical loading waves, namely with PGA = 0.3g (cracking of columns), 0.5g (Joint cracking) and PGA = 1.0g (Final loading).

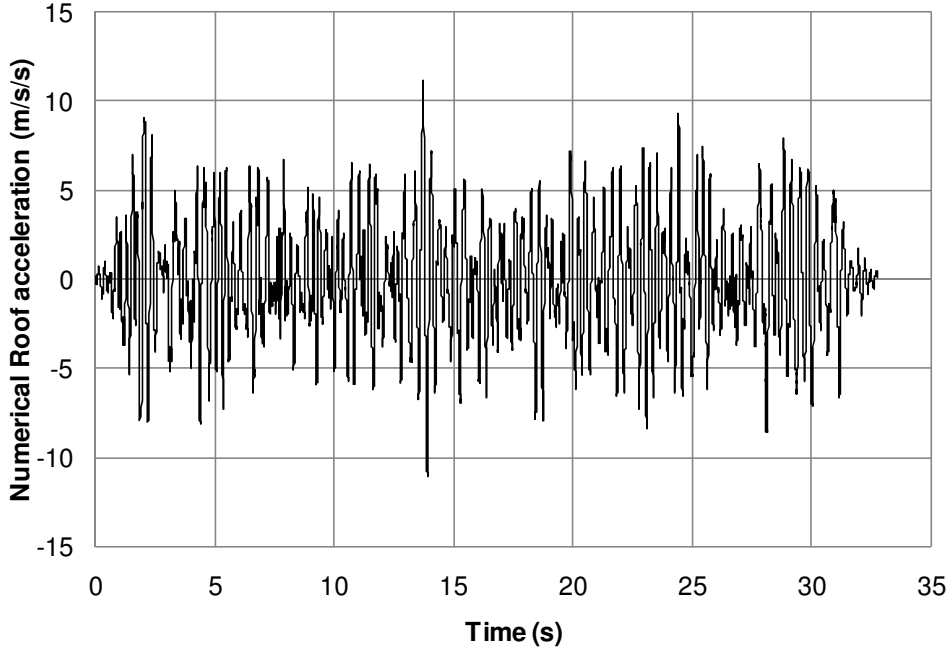
13.5.2.1 Analysis for the loading wave corresponding to PGA = 0.3g

Figure 13.29a and Figure 13.29b present the results of response in terms of roof acceleration time history, corresponding to PGA = 0.3g, as obtained in experiment and analysis

respectively. From figure 13.29, it can be observed that almost all the significant peaks along with their time of occurrence in the experiment could be well simulated in the numerical analysis. The peak acceleration for roof level was obtained as 11.98 m/s^2 in the experiment, while the same was obtained as 11.42 in the analysis. Thus, the numerical model could simulate the experimental behaviour of the structure with good accuracy.



(a) Experiment

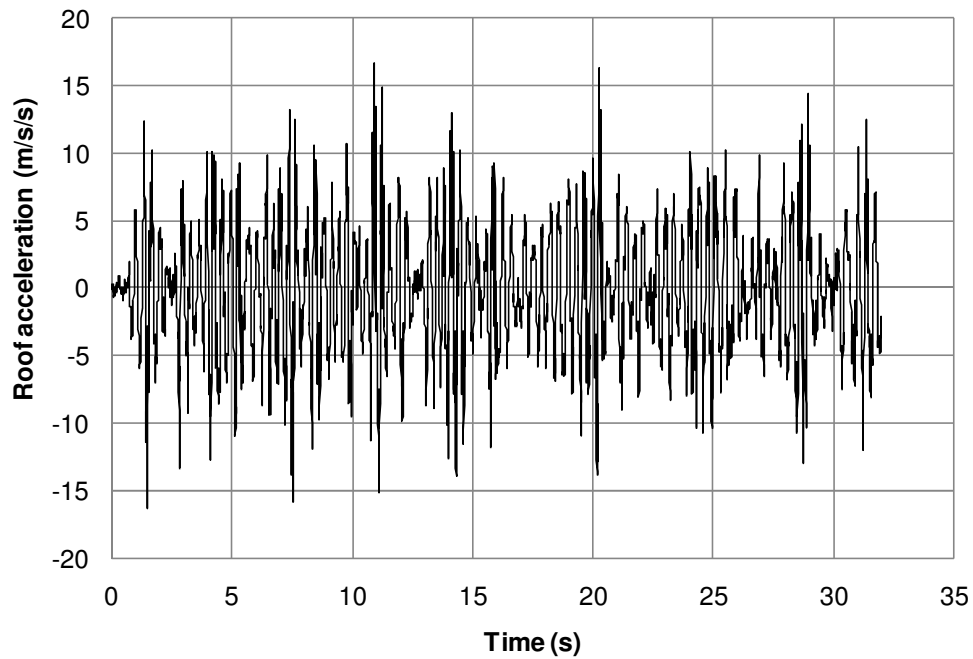


(b) Analysis

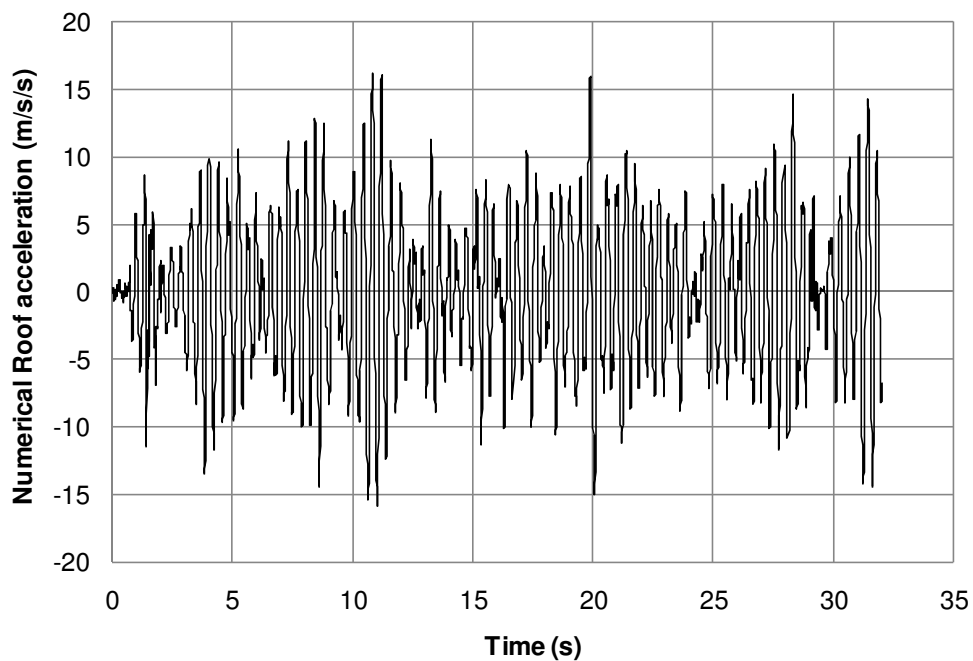
Figure 13.29 Response acceleration history obtained at roof of 2D structure corresponding to PGA = 0.3g

13.5.2.2 Analysis for the loading wave corresponding to $PGA = 0.5g$

Figure 13.30a and Figure 13.30b present the results of response in terms of roof acceleration time history, corresponding to $PGA = 0.5g$, as obtained in experiment and analysis respectively.



(a) Experiment



(b) Analysis

Figure 13.30 Response acceleration history obtained at roof of 2D structure corresponding to $PGA = 0.5g$

Again, from figure 13.30, it can be observed that almost all the significant peaks along with their time of occurrence in the experiment could be well simulated in the numerical analysis. The peak acceleration for roof level was obtained as 16.78 m/s^2 in the experiment, while the same was obtained as 16.20 in the analysis. Thus, the numerical model could simulate the experimental behaviour of the structure with good accuracy.

13.5.2.3 Analysis for the loading wave corresponding to $\text{PGA} = 1.0g$

Figure 13.31a and Figure 13.31b present the results of response in terms of roof acceleration time history, corresponding to $\text{PGA} = 1.0g$, as obtained in experiment and analysis respectively. The peak acceleration for roof level was obtained as 24.14 m/s^2 in the experiment, while the same was obtained as 23.65 in the analysis. Furthermore, from figure 13.31, it can be observed that almost all the significant peaks along with their time of occurrence in the experiment could be well simulated in the numerical analysis. Thus, it is again confirmed that the numerical model could simulate the experimental behaviour of the structure with good accuracy over the whole range of experiment.

13.5.2.4 Summary of nonlinear dynamic analysis

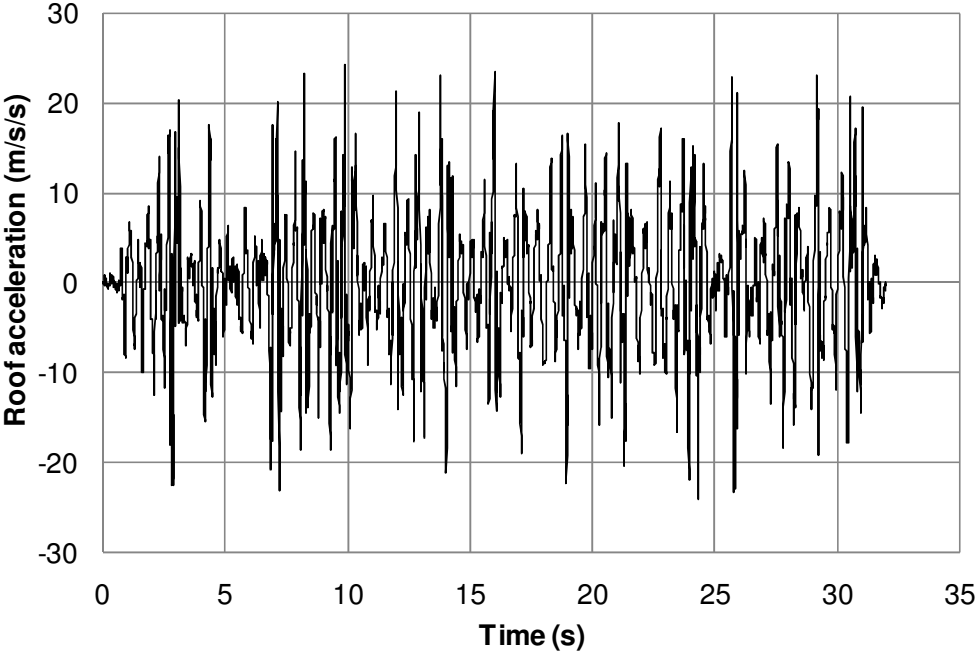
Figure 13.32 displays the comparison of experimentally and numerically obtained values of peak floor acceleration for the roof and first floor for as built structure. The accuracy of the nonlinear dynamic analysis in predicting the peak floor acceleration throughout the range of the experiment is remarkable.

13.5.2.5 Estimating damage in the structure from numerical analysis

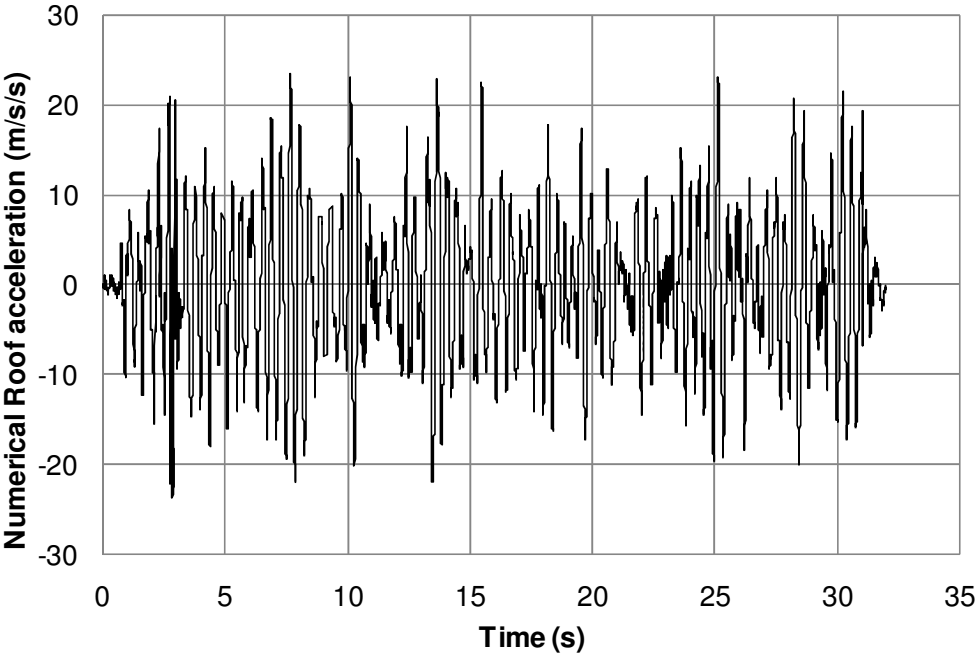
As described in chapter 9, the structure suffered severe damage in the exterior beam-column joints region. In order to estimate the damage suffered by the structure numerically, the hysteretic plots for the springs modelling various nonlinearities in the structure were evaluated. Figure 13.33 displays the complete hysteretic plot obtained for the base of the columns. The hysteretic plot shows that the spring used to model the base of the column just went into the inelastic range but the rotations were rather limited. This suggests limited amount of damage in the structure. This is in good agreement with the experimental results where certain cracking was observed at the column base but no spalling or wide cracks were observed. Thus, the numerical estimation of limited damage at the base of the columns holds good.

Similar hysteretic behaviour was obtained for the rotational springs at ends of beam on first floor as shown in Figure 13.34. The unsymmetry in the hysteretic behaviour is attributed to the moments existing due to gravity loads. The hysteretic plot shows that the spring used to model the rotational behaviour of the first floor beam also just went into the inelastic range

but the rotations were rather limited. This again suggests limited amount of damage in the structure. This is in good agreement with the experimental results where certain cracking was observed at the first floor beam ends but no spalling or wide cracks were observed. Thus, the numerical estimation of limited damage at the base of the columns holds good.



(a) Experiment



(b) Analysis

Figure 13.31 Response acceleration history obtained at roof of 2D structure corresponding to PGA = 1.0g

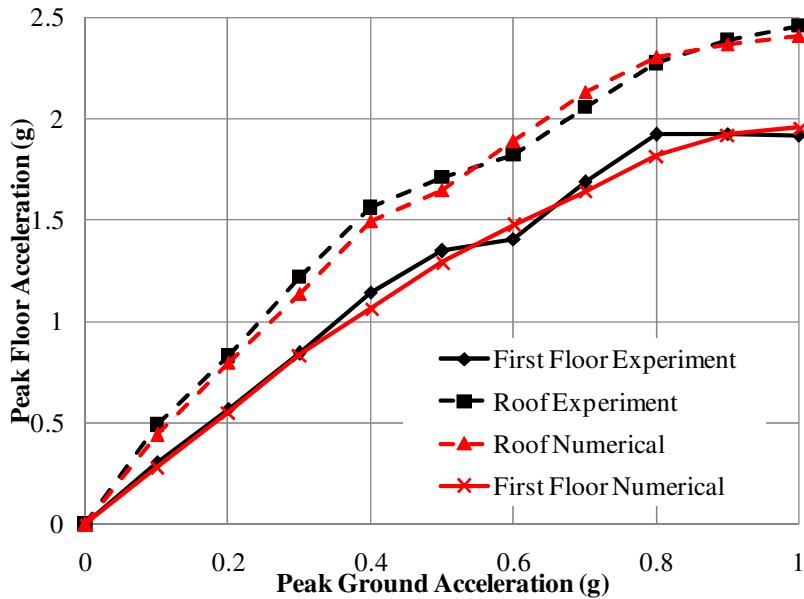


Figure 13.32 Comparison of peak floor acceleration obtained experimentally and numerically for as built structure

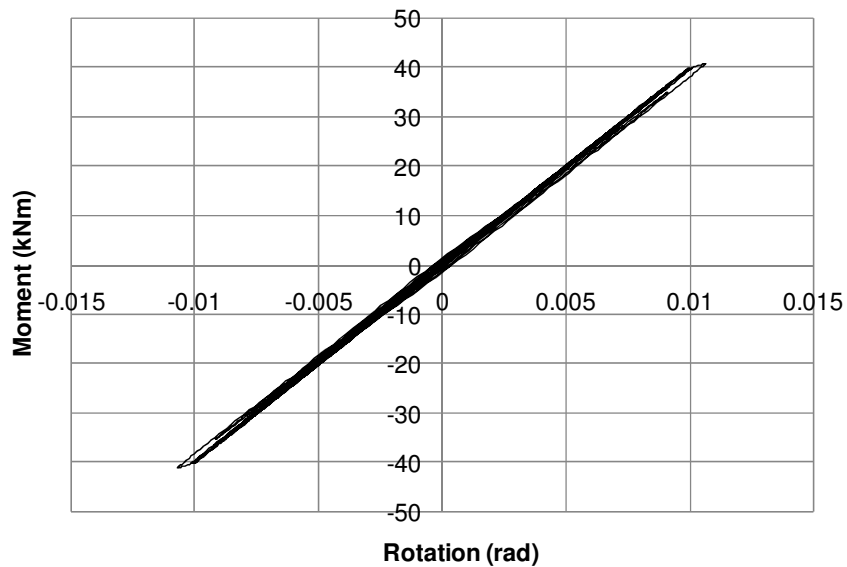


Figure 13.33 Hysteretic response obtained numerically for column base

Figure 13.35 displays the hysteretic behaviour obtained for the exterior joints. As can be seen, for exterior joints large hysteretic loops were obtained signifying significant damage in the exterior joints similar to that observed in the experiment. The maximum joint distortion was obtained as 0.008 radians, which was also close to the experimental value of 0.0087 radians as obtained in the experiment (Figure 9.42).

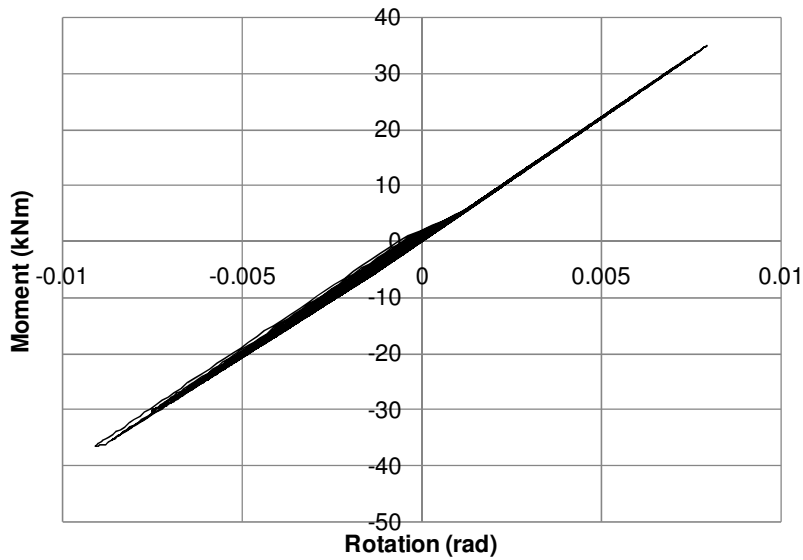


Figure 13.34 Hysteretic response obtained numerically for first floor beam end

The hysteretic loops of Figure 13.35 shows significant inelastic excursion in the joint, which signifies severe joint shear cracking. This behaviour is again in good agreement with the experimental findings where the joint shear cracking was concluded to be the major failure mode for the structure. Based on the comparison of experimentally and numerically obtained response time histories for various loading levels, as well as the failure modes of the structure, it is affirmed that the numerical modelling approach used in this work can be used to simulate the seismic response of non-seismically designed structures very well. The inelastic hysteretic behaviour of the members as well as joints can be successfully captured following the formulations given in chapter 4, chapter 5 and Appendix-A.

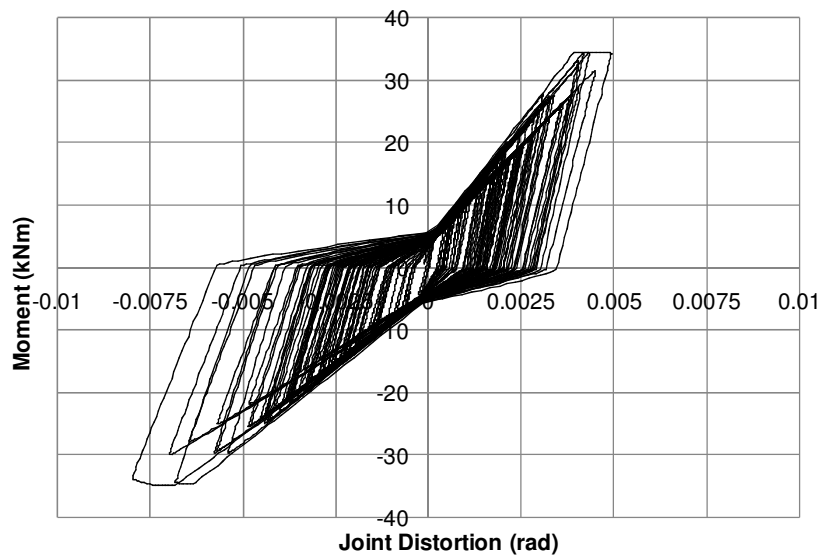


Figure 13.35 Hysteretic response obtained numerically for exterior joints

13.5.2.6 Numerical analysis results beyond experimental range

As was mentioned in chapter 9, the experiment could be performed only up to a PGA of 1.0g, due to the limitation of the test setup. Though, significant damage could be inflicted in the structure up to this level of PGA, the structure could not be termed as collapsed. In order to investigate the performance of the structure at further higher levels of PGA, after thorough validation of the model, the numerical analysis was continued on the same model under increasing levels of PGA. The results of the analysis are summarized in Figure 13.36. It can be seen that the peak floor acceleration after attaining the maximum values at PGA = 1.0g remain almost constant till a PGA of 1.2g. Thereafter a rapid degradation in the performance of the structure can be observed in both the roof response as well as response measured at the first floor. This kind of behaviour is typical of non-seismically designed structures and is attributable to the significant softening of the structure due to large damage.

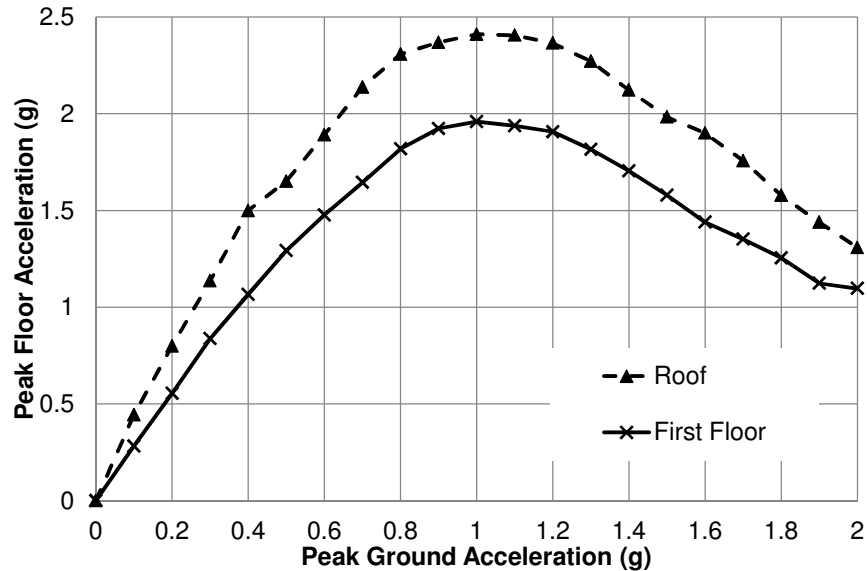


Figure 13.36 Summary of numerical results on as built structure including beyond experimental range

14. VALIDATION OF ASSESSMENT MODEL FOR FULLY FASTENED HAUNCH RETROFIT SOLUTION AGAINST EXPERIMENTS

In chapter 6, an assessment model was proposed to simulate the inelastic cyclic behaviour of beam-column joints and structures with joints retrofitted with fully fastened haunch retrofit solution (FFHRS). With the proposed model, inelastic behaviour of members, joint as well as anchorage could be simulated. In this chapter, the verification of the applicability of the model at joint and structural level is presented. Since such tests are not available in literature, the model is validated against the experiments performed by the author on beam-column joints as reported in chapter 10 and on 2D structure as reported in chapter 11. The numerical analysis was performed using commercial software SAP2000.

14.1 Validation of model against experiments at joint level

14.1.1 Validation against joint JT1-3

Joint geometry of joint JT1-3 was essentially the same as that of joint JT1-1, with both top and bottom beam bars bent into the joint. Bonded anchors with the parameters listed in table 10.4 were used to connect the haunch elements with beam and column. The characteristics to model the anchor group were obtained on the basis of procedure explained in chapter 6. A sample calculation for the same is shown below. Figure 14.1 shows the anchor group and its tributary area that is used to calculate the concrete cone capacity as per CC method (Eligehausen et al, 2006). Here,

$$f_{ck} = 37.74 \text{ MPa (150mm cube compressive strength)}$$

$$h_{ef} = 150 \text{ mm}$$

$$\text{Number of anchors} = 6$$

For bonded anchors, Eligehausen et al (2006) suggest the following equation to predict the failure load of a single anchor in tension, N_u^0 :

$$N_u^0 = 0.85 h_{ef}^2 \sqrt{f_{cc,200}} \quad (14.1)$$

Assuming $f_{cc,200} = 0.95 f_{ck}$, we get,

$$N_u^0 = 0.85 \times 150^2 \times \sqrt{0.95 \times 37.74} = 114515 \text{ N} = 114.52 \text{ kN}$$

For the anchor group, the failure load (N_u) can be obtained as:

$$N_u = \frac{A_{c,N}}{A_{c,N}^0} \psi_{s,N} \psi_{ec,N} N_u^0 \quad (14.2)$$

The calculation for $A_{c,N}$ is explained in Figure 14.1.

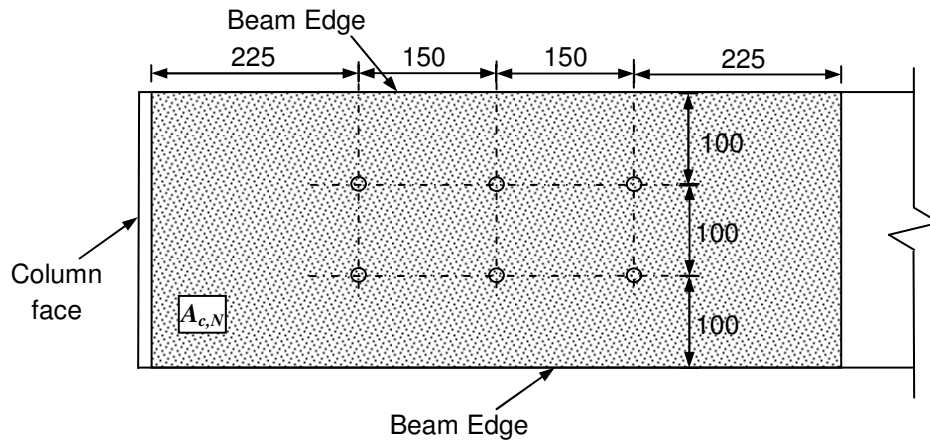


Figure 14.1 Calculation of anchor group tributary area as per CC method

As per Figure 14.1,

$$A_{c,N} = 300 \times 750 = 225000 \text{ mm}^2$$

$$A_{c,N}^0 = 9 \times n h_{ef}^2 = 9 \times 6 \times 150^2 = 1215000 \text{ mm}^2$$

$$\psi_{s,N} = 0.7 + 0.3 \frac{c}{c_{cr}}$$

Where,

c is the minimum edge distance (100 mm in this case)

c_{cr} is the critical edge distance = $1.5h_{ef}$ (Eligehausen et al, 2006)

Thus,

$$\psi_{s,N} = 0.7 + 0.3 \frac{100}{225} = 0.833$$

Considering the point of application of force transferred by the diagonal element at the center of the anchor group, $\psi_{ec,N}$ can be considered as unity in this case. Thus, the anchor group capacity is obtained as

$$N_u = \frac{225000}{1215000} \times 0.833 \times 1 \times 114.52 = 108.79 \text{ kN}$$

The stiffness values were obtained from the values recommended by Mahrenholtz (2011).

Figure 14.2 shows the comparison of the envelope of experimentally obtained hysteretic loops with the numerically obtained load-displacement plots for the joint. Two different cases were considered in the analysis, viz. (i) considering uncracked concrete to evaluate the anchor group behavior and (ii) considering cracked concrete to evaluate the same. As can be observed from Figure 14.2, the stiffness is better predicted by considering cracked concrete, while the load is closer in case of uncracked concrete assumption. This can be attributed to the scatter in the behavior of anchors (Eligehausen et al, 2006).

The experimentally obtained peak load in the positive direction (beam pulled up) was obtained as 111.9 kN and that in the negative direction (beam pushed down) was 120.9 kN. The same was obtained numerically as 111.67 kN assuming uncracked concrete, while 102.74 kN assuming cracked concrete. Nevertheless, it is important to note that the overall load-deflection behavior is predicted quite well with the model and the analysis using the cracked concrete assumption is reasonably conservative.

However, as a trial, the characteristics to model anchor behavior were developed in such a way that the stiffness was evaluated assuming cracked concrete, but the load was evaluated considering uncracked concrete. The model was analyzed under cyclic loads, similar to experiment. However, in contrast to experiment, only one cycle per displacement level was provided. Figure 14.3 displays the comparison of hysteretic loops obtained in the experiment and from numerical analysis.

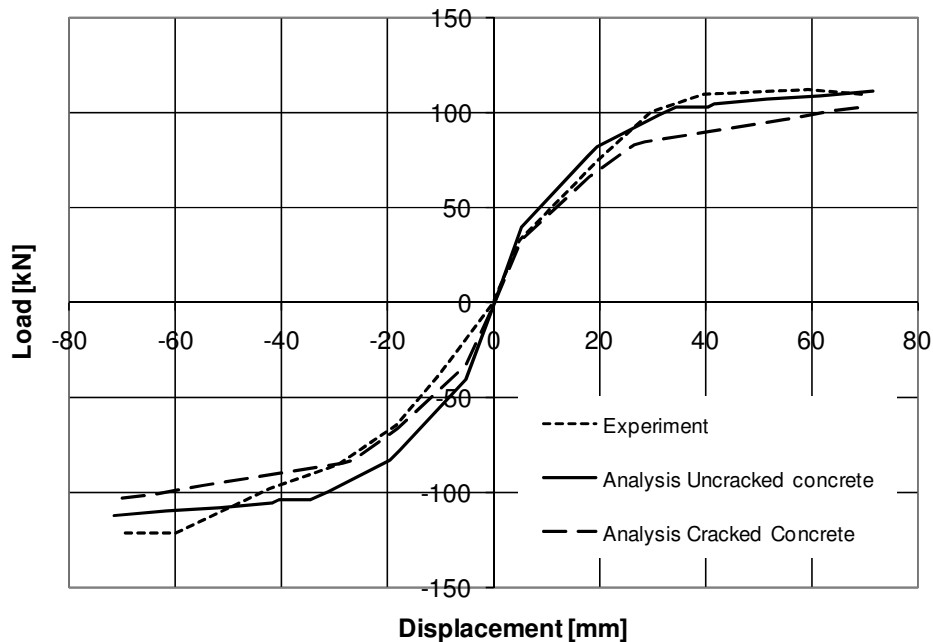


Figure 14.2 Validation of model for joints retrofitted with FFHRS against experiment on JT1-3 (Genesio and Sharma, 2010)

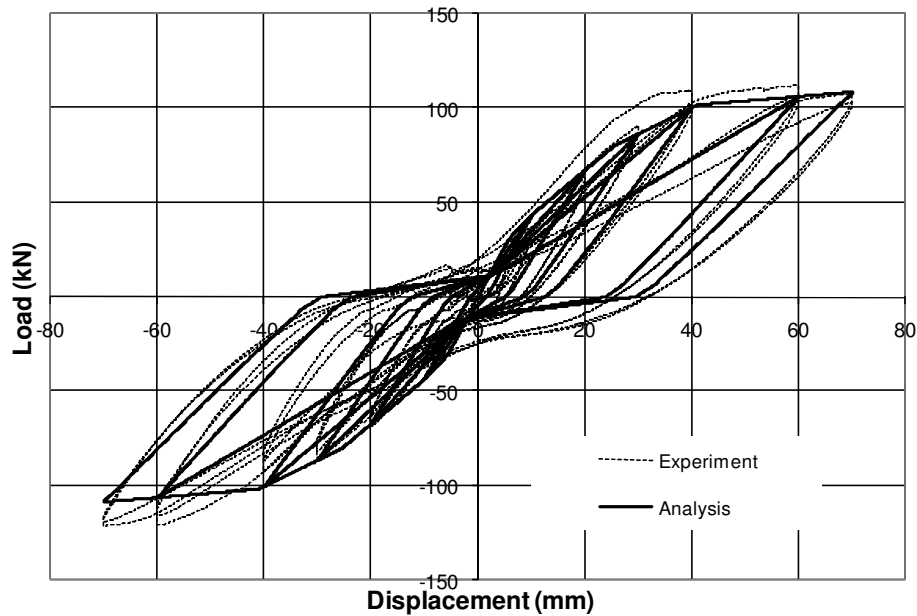


Figure 14.3 Validation of model for joints retrofitted with FFHRS against cyclic loads for joint JT1-3

From Figure 14.3, it can be inferred that the model can be successfully used to simulate the hysteretic behaviour of joints retrofitted with FFHRS.

14.1.2 Validation against joint JT1-4

Joint geometry as well as the retrofitting scheme used for joint JT1-4 was essentially the same as that of joint JT1-3. However, in this case, the beam was deliberately weakened in order to avoid anchorage failure. Also, in this case, after the completion of 70mm displacement cycle, one cycle till 150mm displacement in negative direction (beam pushed down) was provided. The numerical model was subjected to the same loading scenario with the exception that one cycle per displacement level was given in the analysis. Figure 14.4 displays the comparison of experimentally and numerically obtained hysteretic loops for the joint JT1-4.

It can be observed that the model is able to simulate the hysteretic behaviour of the retrofitted joint very well, especially in the negative (beam pushed down) direction. In the positive direction also, the load-displacement curve is having a good comparison with the experiment except for the initial stiffness, which may be attributed to certain non-homogeneity in the experiment.

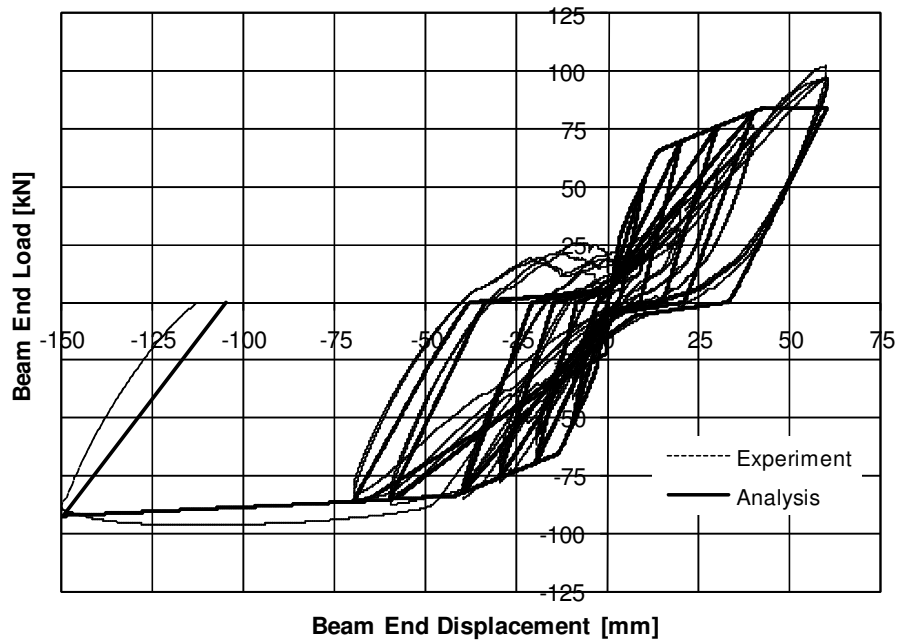


Figure 14.4 Validation of model for joints retrofitted with FFHRS against cyclic loads for joint JT1-4

14.1.3 Validation against joint JT1-5

Joint geometry for joint JT1-5 was essentially the same as that of joint JT1-3. However, in this case, the haunch retrofit was connected to beam and column using the concrete screws, with parameters as listed in Table 10.4. Same as in case of joint JT1-5, after the completion of 70mm displacement cycle, one cycle till 150mm displacement in negative direction (beam pushed down) was provided. The numerical model was subjected to the same loading scenario with the exception that one cycle per displacement level was given in the analysis. Figure 14.5 displays the comparison of experimentally and numerically obtained hysteretic loops for the joint JT1-5. Figure 14.5 again displays that the model can be successfully implemented to simulate the seismic behavior of beam-column joints retrofitted with FFHRS.

14.2 Nonlinear dynamic analysis of retrofitted 2D RC frame structure

In chapter 11, the details of the shake table tests performed on a 2D RC frame structure with its joints retrofitted with FFHRS were presented. The same structure was modelled, following the procedures and models explained in this work, and analyzed under dynamic loads. The results of the analysis are presented here. The numerical analysis was performed using commercial software SAP2000.

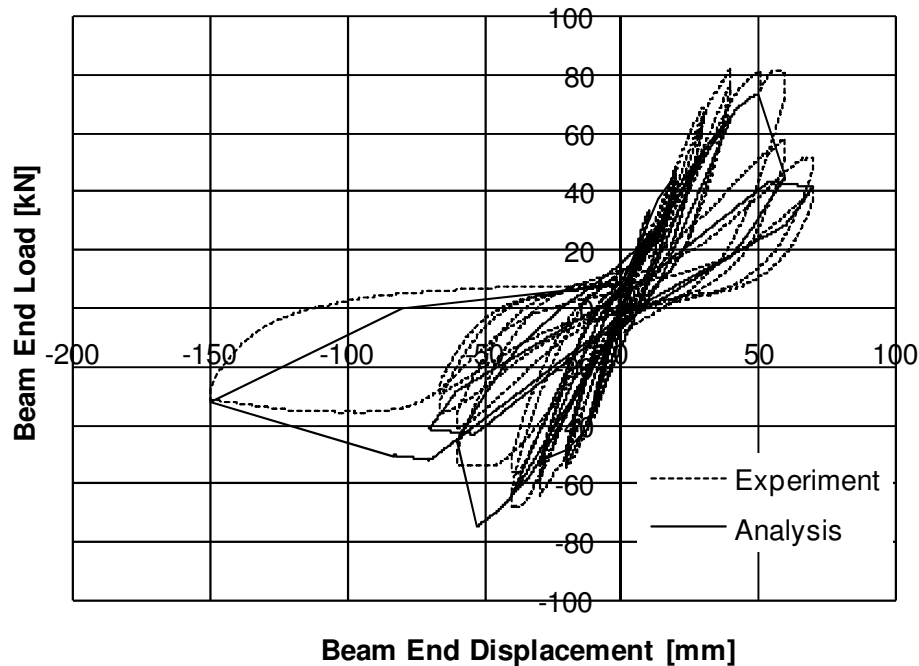


Figure 14.5 Validation of model for joints retrofitted with FFHRS against cyclic loads for joint JT1-5

14.2.1 Modal analysis

Before starting the nonlinear dynamic analysis, modal analysis was performed for the structure to evaluate the natural time periods/frequencies of the structure. The time period corresponding to the first mode was obtained as 0.229 seconds numerically, while the same was obtained as 0.234 seconds experimentally. The same for second mode was obtained as 0.067 seconds numerically, while the same was obtained as 0.062 seconds experimentally. Thus, the model was able to simulate the linear dynamic characteristics of the system well.

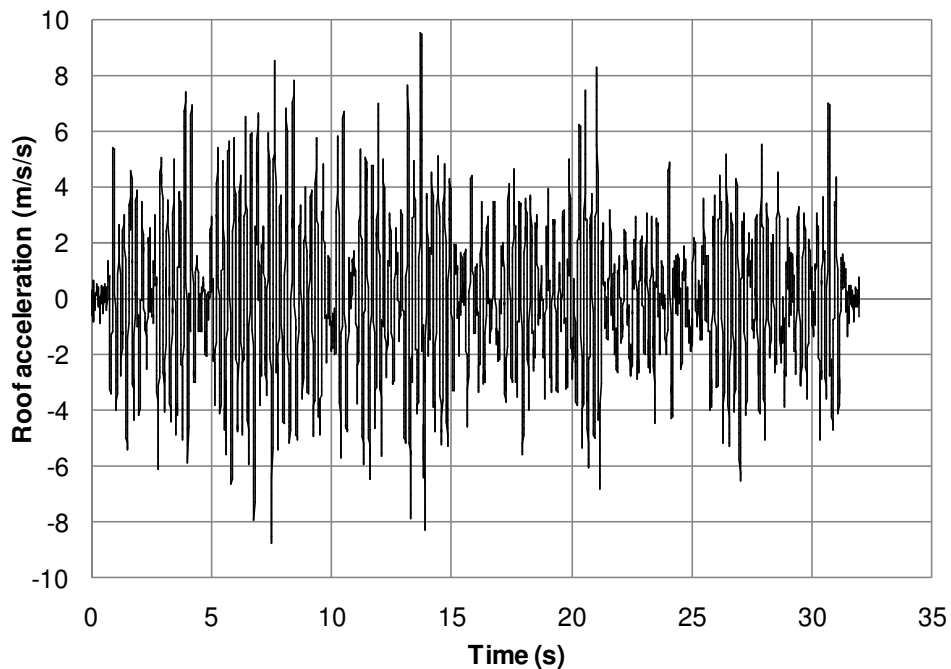
14.2.2 Nonlinear dynamic analysis

The numerical modelling of the structure to perform nonlinear dynamic analysis of the same was performed following the concepts and modelling techniques discussed earlier. The inelastic properties of the members (beams and columns) were derived on the basis of procedure described in Appendix-A, while the hysteretic characteristics for the same were simulated using pivot hysteretic model. The hysteretic parameters were evaluated on the basis of equations (5.2) through (5.5). The inelastic behaviour of the joints was modelled through the system of springs, with inelastic characteristics of the same derived on the basis of formulations explained in chapter 4, while the hysteretic characteristics for the same were simulated using pivot hysteretic model. The hysteretic parameters were evaluated on the basis of equations (5.6) through (5.8). The spring characteristics for the haunch retrofit solution were modelled following the procedure given in chapter 6.

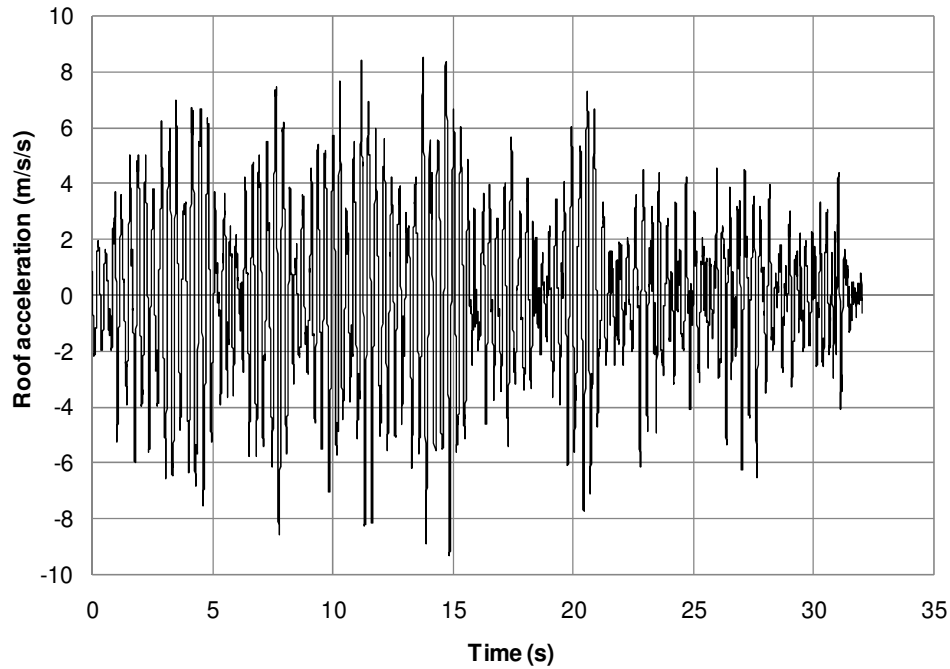
The structural model was subjected to ground acceleration time history and direct integration time history analysis was used to analyze the structure. The first input time history corresponded to the table time history for PGA of 0.1g. The analysis for the next higher loading wave (PGA = 0.2g) was started from the end conditions of the previous run. Similar to the experiment, the input ground motion was incremented with a PGA of 0.1g till the PGA of 1.0g was reached. Though, the analysis was run for all the loading cases, the comparison of experimental and numerical time histories is given for the same three loading waves as was done for the as built structure (chapter 13), namely with PGA = 0.3g (cracking of columns), 0.5g (Joint cracking) and PGA = 1.0g (Final loading).

14.2.2.1 Analysis for the loading wave corresponding to PGA = 0.3g

Figure 14.6a and Figure 14.6b present the results of response in terms of roof acceleration time history, corresponding to PGA = 0.3g, as obtained in experiment and analysis respectively for the retrofitted structure. It can be observed that almost all the significant peaks along with their time of occurrence in the experiment could be well simulated in the numerical analysis. The peak acceleration for roof level was obtained as 9.45 m/s² in the experiment, while the same was obtained as 9.53 in the analysis. Thus, the numerical model could simulate the experimental behaviour of the structure with good accuracy.



(a) Experiment



(b) Analysis

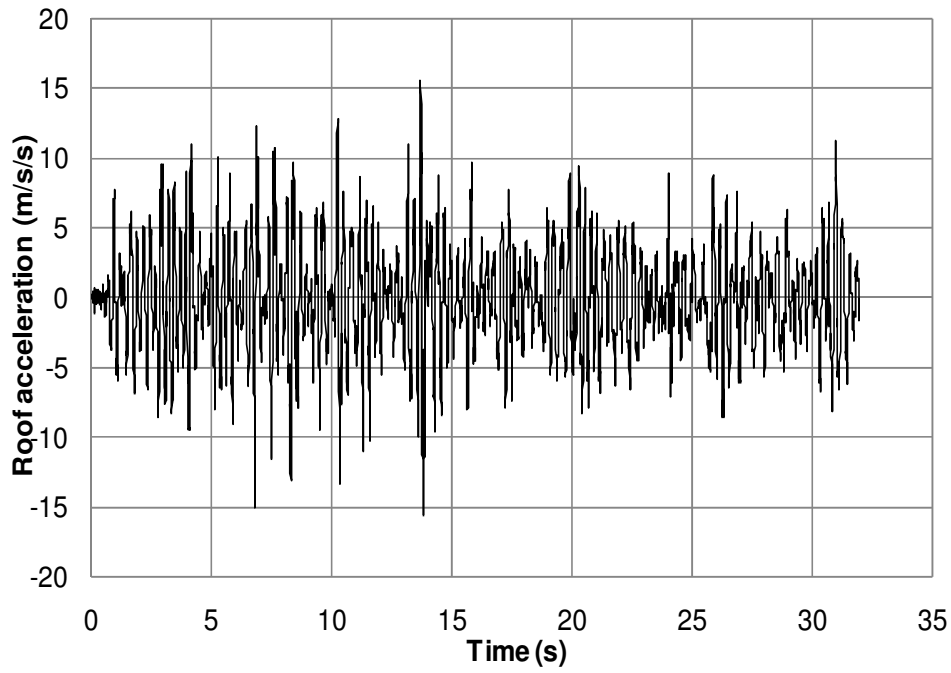
Figure 14.6 Response acceleration history obtained at roof of 2D retrofitted structure corresponding to PGA = 0.3g

14.2.2.2 Analysis for the loading wave corresponding to PGA = 0.5g

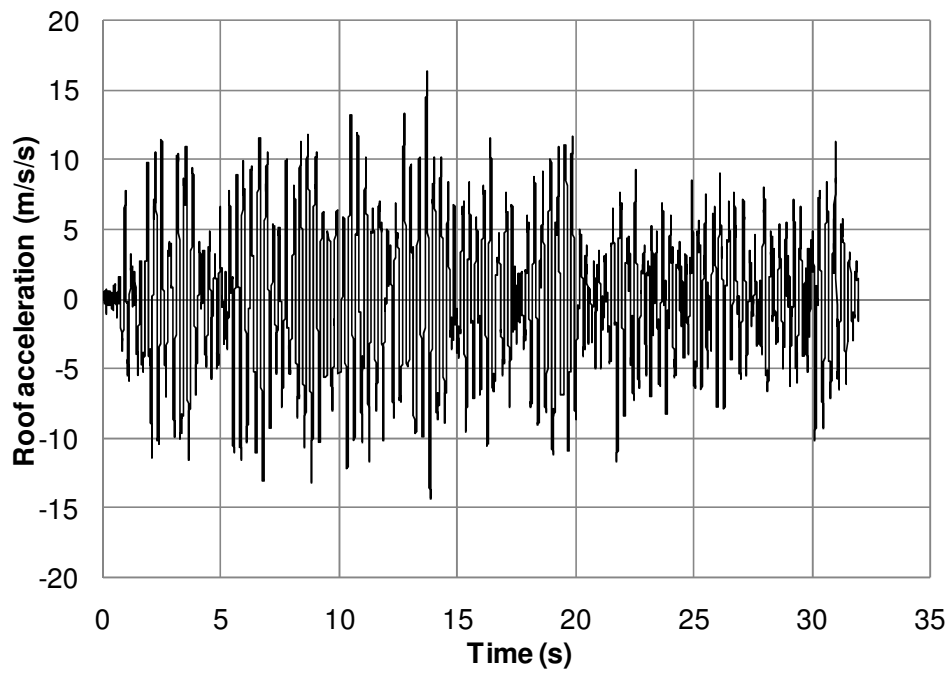
Figure 14.7a and Figure 14.7b present the results of response in terms of roof acceleration time history, corresponding to PGA = 0.5g, as obtained in experiment and analysis respectively for the retrofitted structure. Again, from figure 14.7, it can be observed that almost all the significant peaks along with their time of occurrence in the experiment could be well simulated in the numerical analysis. The peak acceleration for roof level was obtained as 15.57 m/s^2 in the experiment, while the same was obtained as 15.73 in the analysis. Thus, it can be said that the numerical model could simulate the experimental behaviour of the structure with good accuracy.

14.2.2.3 Analysis for the loading wave corresponding to PGA = 1.0g

Figure 14.8a and Figure 14.8b present the results of response in terms of roof acceleration time history, corresponding to PGA = 1.0g, as obtained in experiment and analysis respectively for retrofitted structure. The peak acceleration for roof level was obtained as 28.48 m/s^2 in the experiment, while the same was obtained as 28.65 in the analysis.

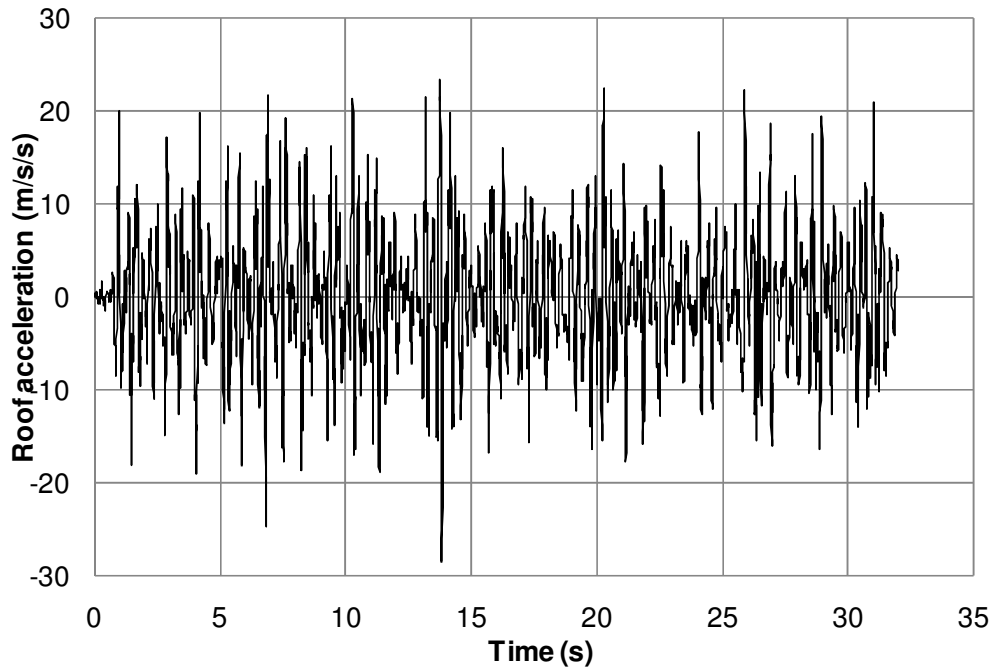


(a) Experiment

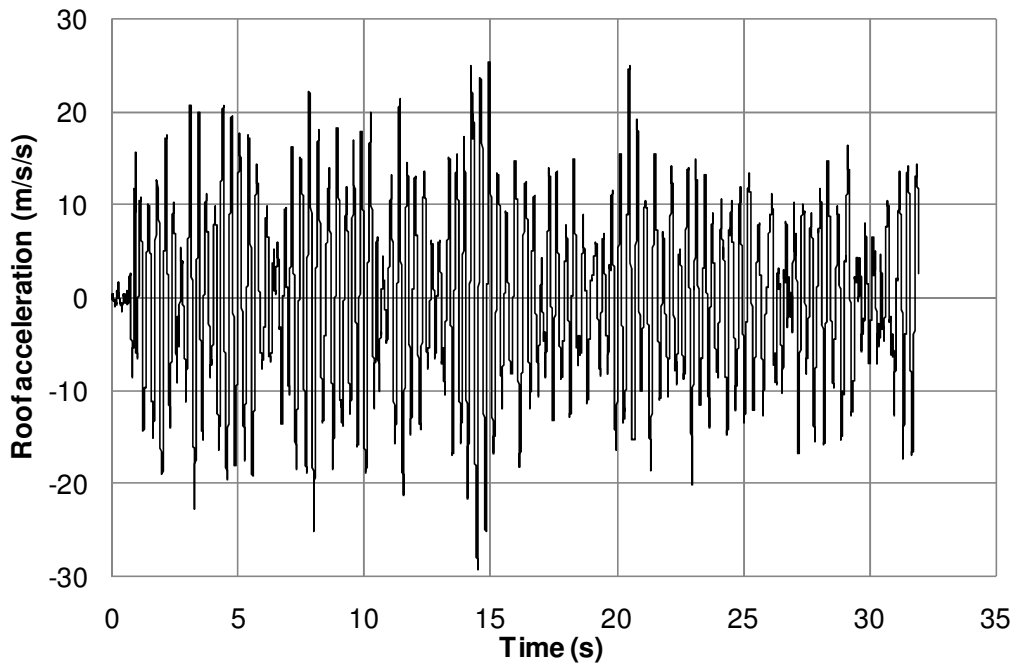


(b) Analysis

Figure 14.7 Response acceleration history obtained at roof of 2D retrofitted structure corresponding to $\text{PGA} = 0.5g$



(a) Experiment



(b) Analysis

Figure 14.8 Response acceleration history obtained at roof of 2D retrofitted structure corresponding to PGA = 1.0g

Furthermore, from figure 14.8, it can be observed that almost all the significant peaks along with their time of occurrence in the experiment could be well simulated in the numerical analysis. Thus, it is again confirmed that the numerical model could simulate the

experimental behaviour of the structure with good accuracy over the whole range of experiment.

14.2.2.4 Summary of Nonlinear Analysis

Figure 14.9 displays the comparison of experimentally and numerically obtained values of peak floor acceleration for the roof and first floor for the retrofitted structure. The accuracy of the nonlinear dynamic analysis in predicting the peak floor acceleration throughout the range of the experiment is remarkable.

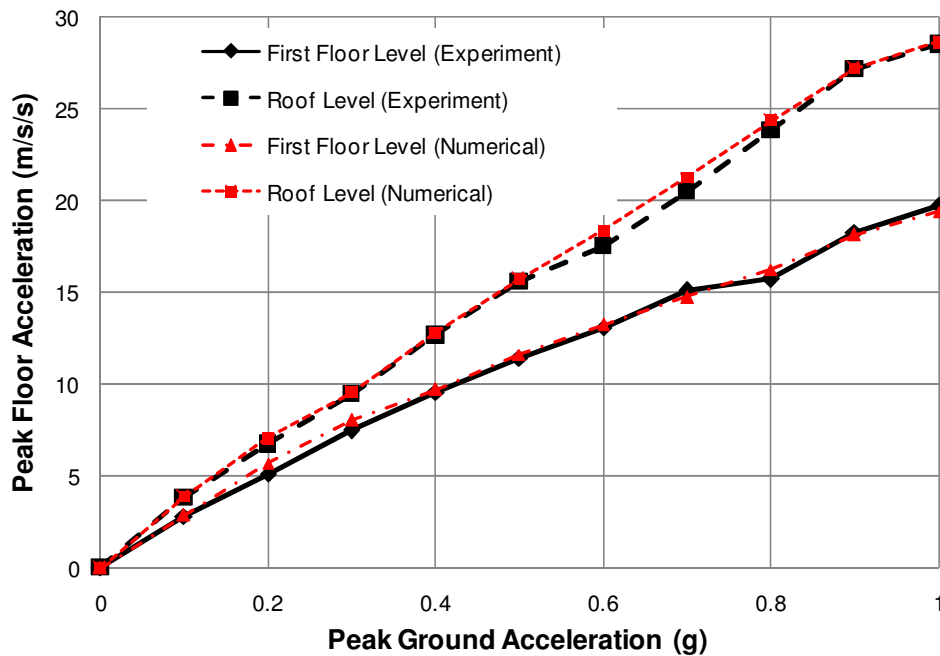


Figure 14.9 Comparison of peak floor acceleration obtained experimentally and numerically for the retrofitted structure

14.2.2.5 Estimating damage in the structure from numerical analysis

The retrofitted structure suffered no damage in the exterior beam-column joints region (chapter 11), while minor damage in the beams and certain cracking at the base columns was observed. In order to estimate the damage suffered by the structure numerically, the hysteretic plots for the springs modelling various nonlinearities in the structure were evaluated.

Figure 14.10 displays the complete hysteretic plot obtained for the base of the columns. The hysteretic plot shows that the spring used to model the base of the column just went into the inelastic range but the rotations were rather limited. There is a little bit increase in the moments compared to that for the as built structure. This suggests limited amount of damage

at the column base in the retrofitted structure. This is in good agreement with the experimental results where certain cracking was observed at the column base but no spalling or wide cracks were observed. Thus, the numerical estimation of limited damage at the base of the columns holds good.

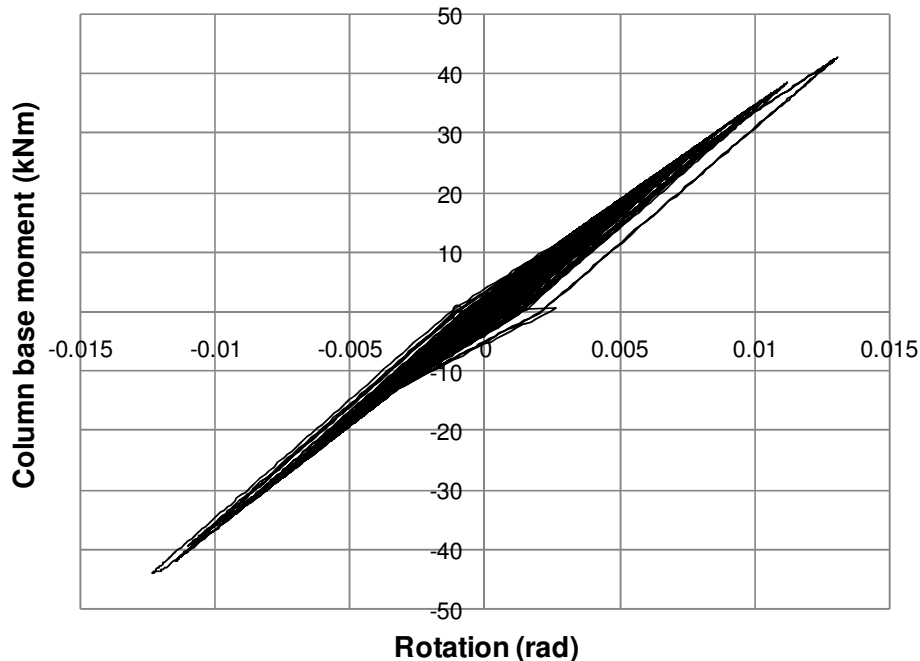


Figure 14.10 Hysteretic response obtained numerically for column base for the retrofitted 2D frame structure

Similarly, hysteretic behaviour was obtained for the rotational springs at ends of beam on first floor as shown in Figure 14.11. The hysteretic plot shows that the spring used to model the rotational behaviour of the first floor beam went into the inelastic range. The rotations were larger than that obtained in the as built structure, suggesting more cracking in the beam. This is in good agreement with the experimental results where more cracking was observed at the first floor beam ends in retrofitted structure compared to the as built structure. Thus, the numerical estimation of limited damage at the base of the columns holds good. This also shows that by the FFHRS, the hierarchy of strength was altered in such a way that beam failure occurs before the joint or column failure, which is a desirable failure mode for the moment resisting frame structures subjected to seismic loads.

Figure 14.12 displays the hysteretic behaviour obtained for the exterior joints. It can be seen that by the introduction of the FFHRS, for exterior joints, the bending moments and hence the corresponding joint shear reduces significantly. The joint remains essentially elastic, as observed in experiment also. Thus, the numerical prediction is again in good agreement with the experimental findings.

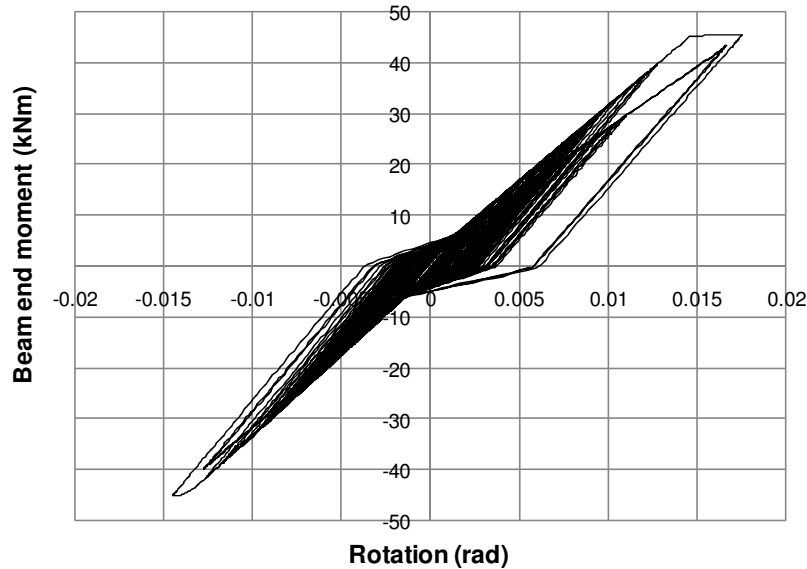


Figure 14.11 Hysteretic response obtained numerically for first floor beam end for the retrofitted 2D frame structure

Based on the comparison of experimentally and numerically obtained response time histories for various loading levels, as well as the failure modes of the structure, it is affirmed that the numerical modelling approach used in this work can be used to simulate the seismic response of non-seismically designed structures very well. The inelastic hysteretic behaviour of the members, joints and retrofitting can be successfully captured following the formulations given in chapter 4, chapter 5, chapter 6 and Appendix-A.

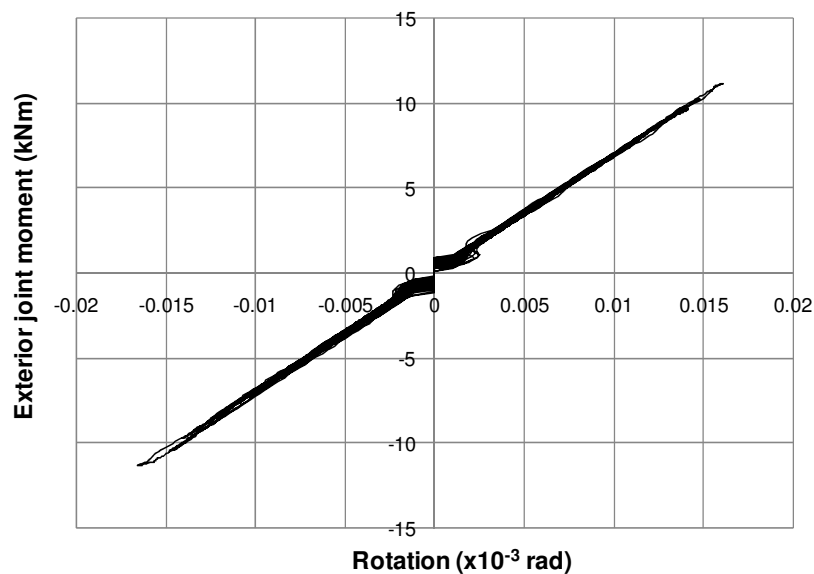


Figure 14.12 Hysteretic response obtained numerically for exterior joints for the retrofitted structure

14.2.2.6 Numerical analysis results beyond experimental range

As was mentioned in chapter 11, the experiment could be performed only up to a PGA of 1.0g, due to the limitation of the test setup. In order to investigate the performance of the structure at further higher levels of PGA, after thorough validation of the model, the numerical analysis was continued on the same model under increasing levels of PGA. The results of the analysis are summarized in Figure 14.13. It can be seen that in case of retrofitted structure, the peak floor acceleration keeps on increasing and attains a maximum value at PGA = 1.5g. However, beyond PGA = 1.6g, a degradation is observed in the performance of the structure, though the degradation is not as rapid as in case of as built structure.

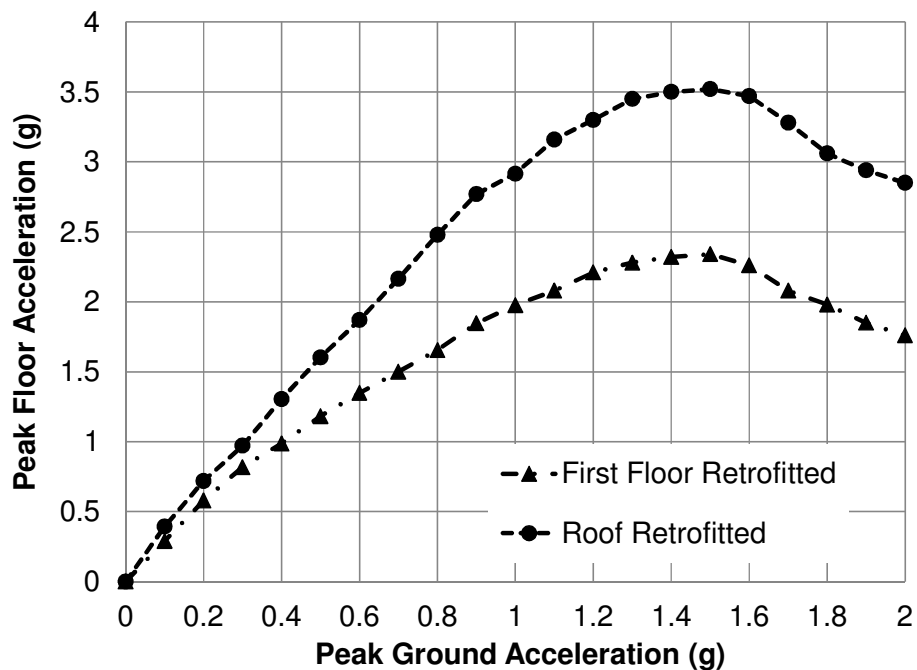


Figure 14.13 Summary of numerical results on retrofitted structure including beyond experimental range

Figure 14.14 shows a comparison of the performance of the as built and retrofitted structure, as obtained numerically. From Figure 14.14, it is clear that the structure with joints retrofitted using FFHRS could sustain much higher acceleration levels compared to the as built structure. These results prove the suitability of the FFHRS in improving the performance of non-seismically designed structures.

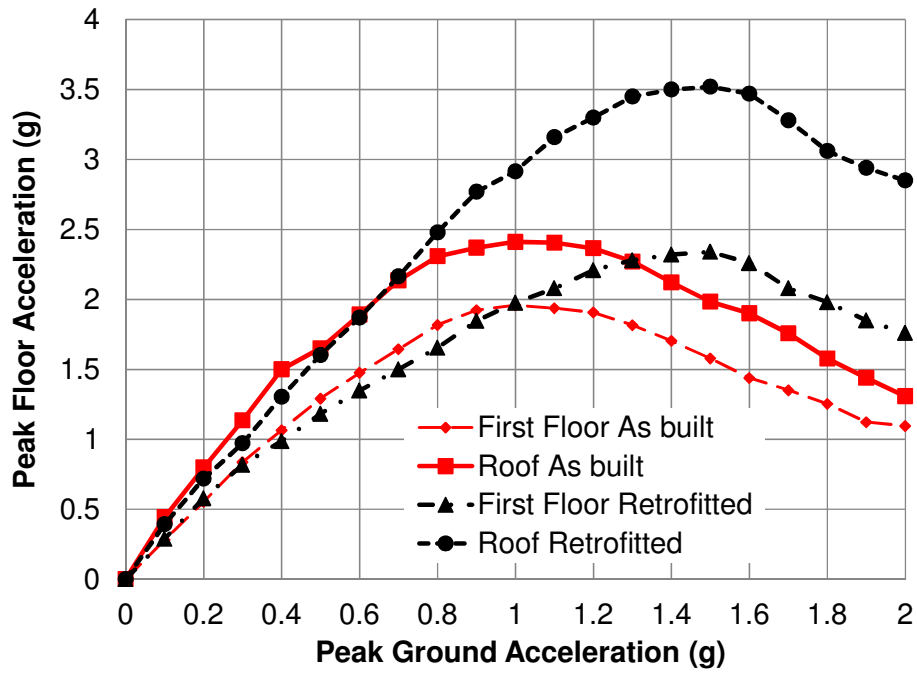


Figure 14.14 Comparison of numerical results obtained for as built and retrofitted structure including beyond experimental range

15. SEISMIC ASSESSMENT AND RETROFITTING OF A REAL LIFE RC FRAME STRUCTURE – A CASE STUDY

In this thesis, three different models have been presented viz. the joint model to simulate seismic behaviour of non-seismically designed beam-column joints, the extension to pivot hysteretic model and the model to simulate the behaviour of joints retrofitted with FFHRS. All the models have been widely validated against experimental results available in the literature as well as the experiments conducted by the author, which included tests on as built and retrofitted non-seismically designed beam-column joints; tests on a full scale RC frame structure under pushover loads; and tests on as built and retrofitted gravity load designed RC frame structure under seismic loads using shake table facility.

It is well known that the structures designed and constructed according to the non-seismic design philosophy are vulnerable to failure at the beam-column joints. Still, it is a common practice to consider the joints as rigid while assessing the structures under seismic loads. This is mainly due to the lack of practically implementable models to consider the inelastic behaviour of the joints. Such an analysis can consider only certain failure modes such as beam and column flexure failure, which are ductile in nature. Consequently, the analysis predicts much better seismic performance of the structure than is in reality. Such un-conservatism leads to either wrong qualification of the structure or to wrong retrofit design suggestions, e.g. strengthening of beam or column instead of the joint, which is the weakest link. The major objective of this work has been to develop practically implementable models and to demonstrate their suitability for application at structural level. In this chapter, the models developed and validated in this work will be used to assess the seismic performance of a real life existing RC frame structure under as built condition. Based on the results of seismic assessment, a suitable and economical retrofit design will be made and the structure will be again assessed in retrofitted condition.

The structure selected for this work is an existing residential building in New Delhi, India. The structure was designed in 1982 without giving due considerations to seismic design philosophy. The philosophy of seismic assessment and retrofit design, in practice, using the models presented in this work is presented herein.

15.1 Description of the structure

15.1.1 Geometry

The structure is a ground + 3 storey structure with the moment resisting beam-column framework as the load resisting system. The structure serves its purpose as a residential building in New Delhi, India, which is classified in seismic zone 4 (severe earthquake intensity) as per Indian Standard, IS 1893 (2002). Figure 15.1 shows the beam centre line

plan of the structure. The plan dimensions of the structure are 7.3m x 26.25m, with the bay dimensions as depicted in Figure 15.1. Figure 15.2 presents the line diagram showing the front elevation of the structure. The typical storey height is 2.9m while the foundation is 1.5m below plinth level (Figure 15.2). The beams and columns (frame members) for the structure were modelled in using the 3D beam elements, with 6 degrees of freedom (three translations and three rotations) at both nodes. The slabs were modelled using quadrilateral shell elements, which allow proper definition and distribution of loads and stiffness.

15.1.2 Section properties

The various section properties for the columns of the structure are summarized in Table 15.1, while the same for the beams are summarized in Table 15.2. In Tables 15.1 and 15.2, the longitudinal reinforcement is identified by number of bars and diameter of the same, e.g. 4-16+4-12 refer to 4 number of 16mm diameter + 4 number of 12mm diameter bars. The transverse reinforcement is identified by diameter of ties/stirrups and centre to centre spacing between ties/stirrups, e.g. 8-150 refer to 8mm diameter ties @ 150mm c/c. The assignment of sections to the members and the orientation of columns are identified in Figure 15.4.

Table 15.1 Column section details for the structure

Column	Location	B (mm)	D (mm)	Long. Reinf	Trans Reinf
C1	Foundation to Ground	300	500	4-16+4-12	8-200
	Ground to 1 st floor	300	450	4-16+4-12	8-200
	1 st floor to 2 nd floor	300	450	4-16+4-12	8-200
	2 nd floor to 3 rd floor	300	450	4-16+4-12	8-200
	3 rd floor to Roof	300	300	4-16	8-200
C2	Foundation to Ground	300	600	4-20+4-16	8-200
	Ground to 1 st floor	300	550	4-20+4-16	8-200
	1 st floor to 2 nd floor	300	500	4-20+4-16	8-200
	2 nd floor to 3 rd floor	300	450	4-16+4-12	8-200
	3 rd floor to Roof	300	450	4-16+4-12	8-200
C3	Foundation to Ground	300	700	10-20	8-150
	Ground to 1 st floor	300	600	10-20	8-150
	1 st floor to 2 nd floor	300	600	6-20+4-16	8-150
	2 nd floor to 3 rd floor	300	500	4-20+4-16	8-150
	3 rd floor to Roof	300	500	4-16+4-12	8-150
C4	Foundation to Ground	300	800	12-20	8-150
	Ground to 1 st floor	300	700	12-20	8-150
	1 st floor to 2 nd floor	300	600	6-20+6-16	8-150
	2 nd floor to 3 rd floor	300	500	4-20+4-16	8-150
	3 rd floor to Roof	300	500	4-16+4-12	8-150
C5	Foundation to Ground	300	800	4-25+6-20	8-150
	Ground to 1 st floor	300	700	4-25+4-20	8-150
	1 st floor to 2 nd floor	300	600	4-25+4-20	8-150
	2 nd floor to 3 rd floor	300	500	8-20	8-150
	3 rd floor to Roof	300	500	8-16	8-150

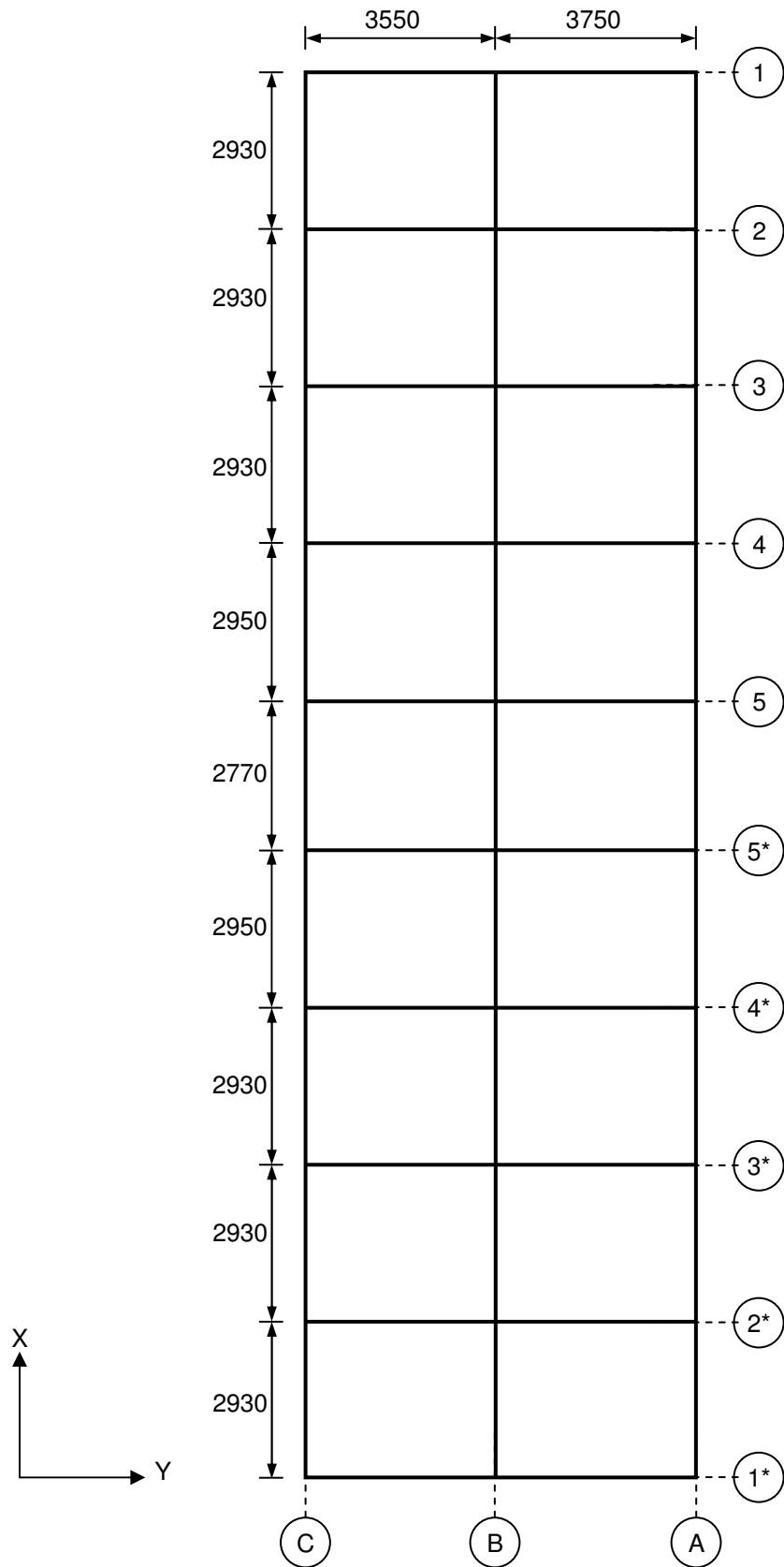


Figure 15.1 Typical floor beam plan of the building (line diagram)

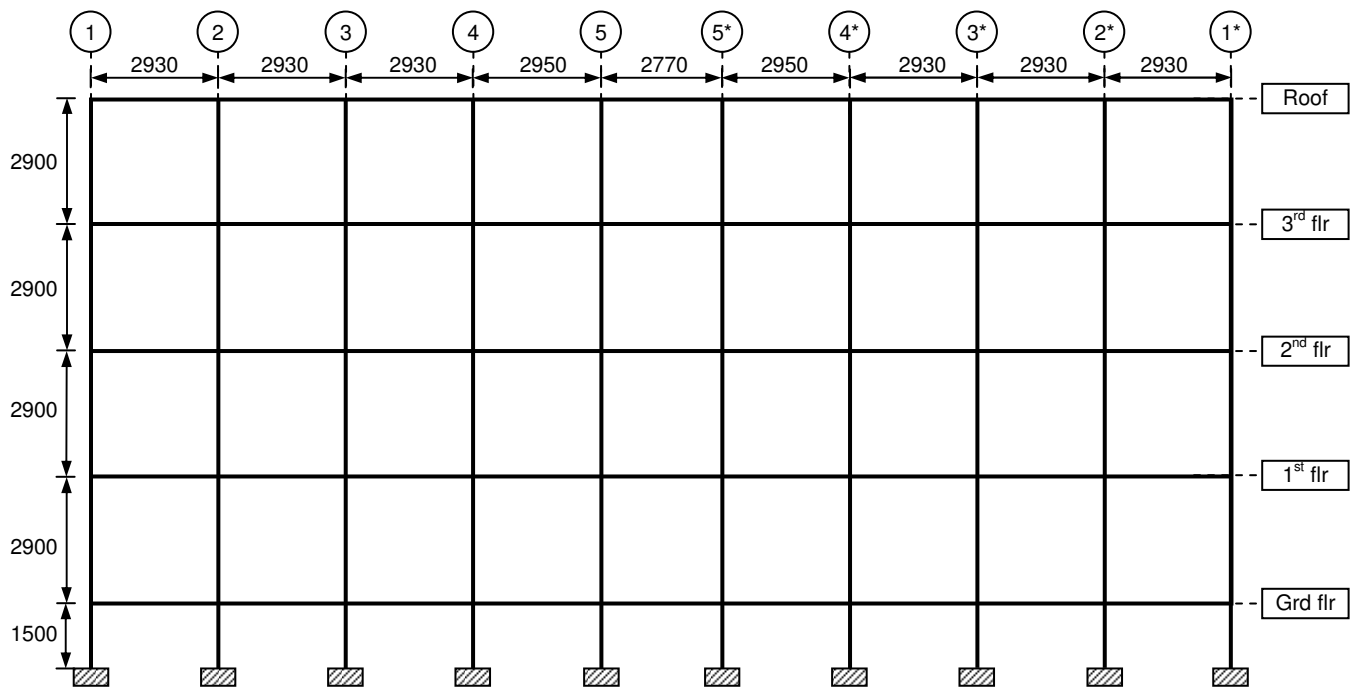


Figure 15.2 Front elevation of the building (line diagram)

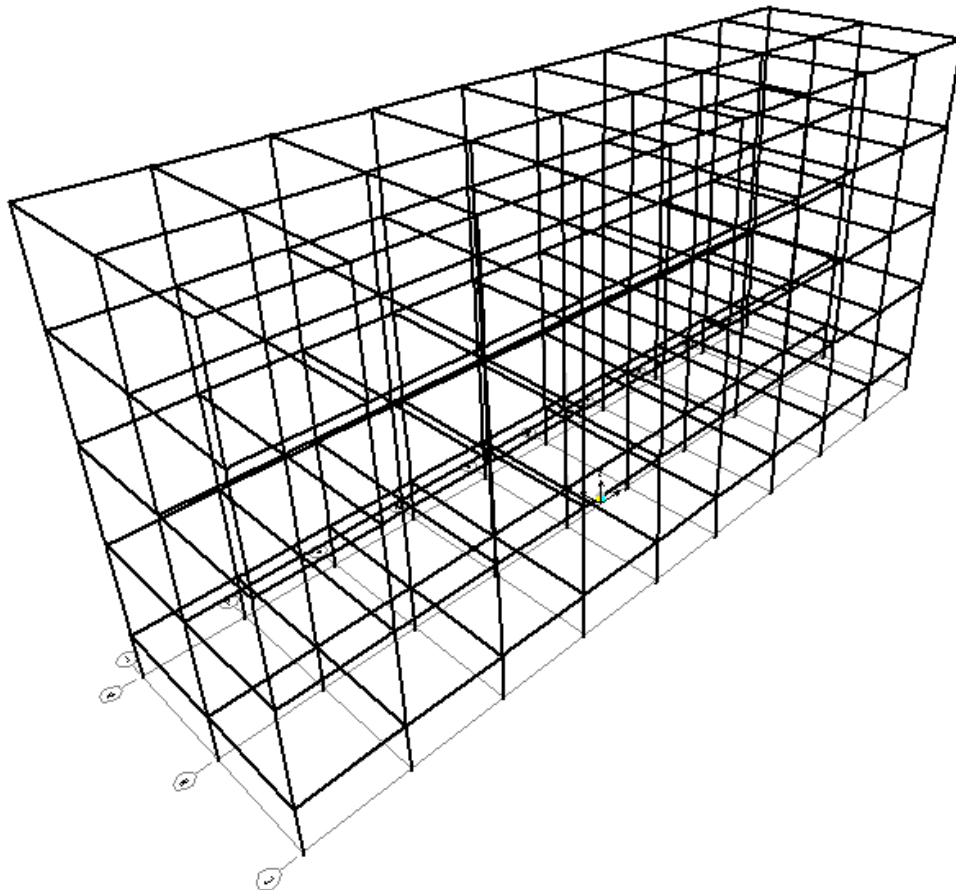


Figure 15.3 3D view of the computer model of the structure showing frame system

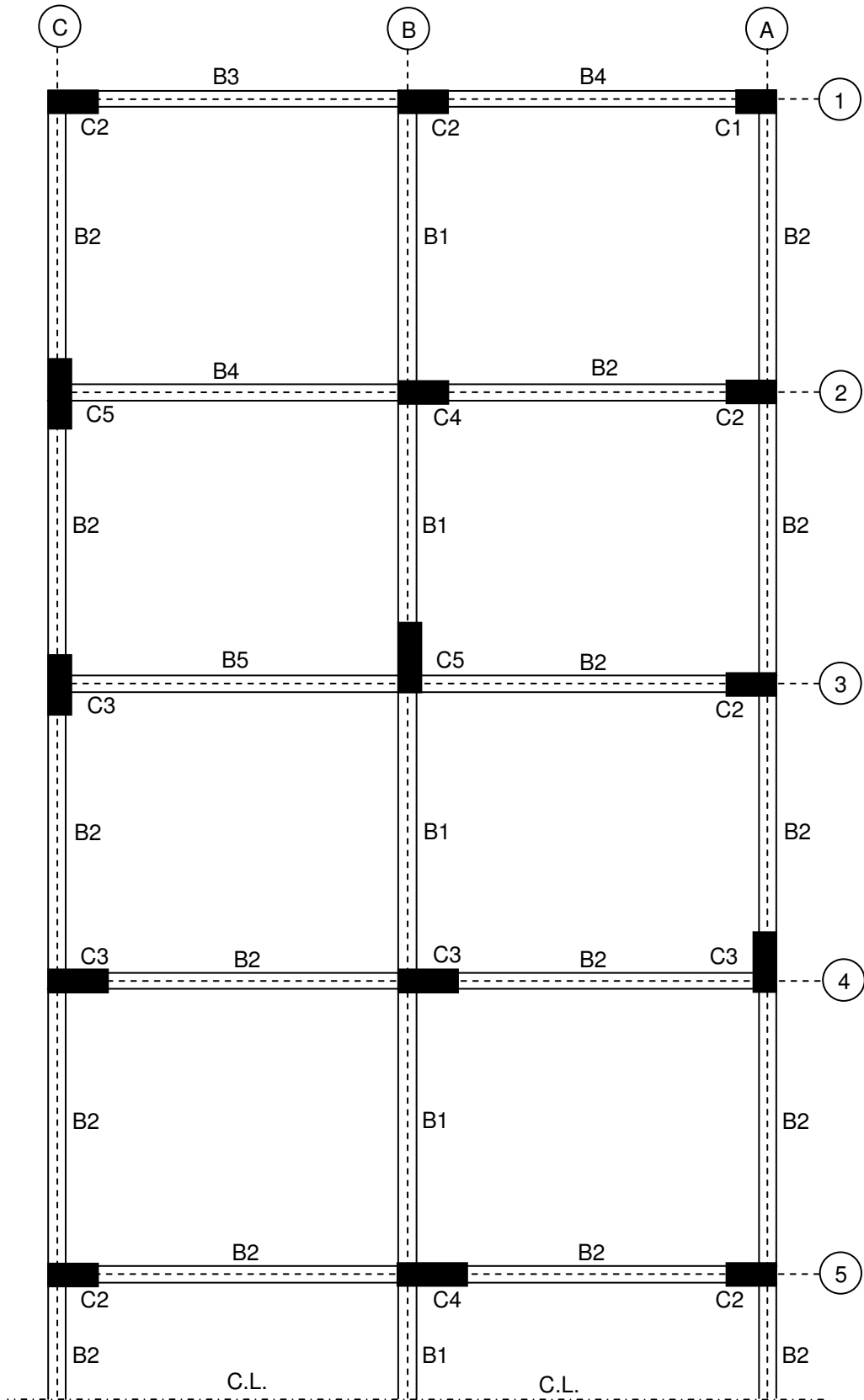


Figure 15.4 Identification of sections and orientation of columns

Table 15.2 Beam section details

Beam	B (mm)	D (mm)	End Support reinforcement		Mid Span reinforcement		Trans Reinf
			Top Reinf	Bottom Reinf	Top Reinf	Bottom Reinf	
B1	300	400	3-16	2-16	2-16	4-16	8-175
B2	300	500	4-16	2-16	2-16	4-16	8-175
B3	300	650	4-16	2-16	2-16	4-16	8-175
B4	300	750	4-16	2-16	2-16	4-16	8-150
B5	450	550	4-16	2-16	2-16	4-16	8-150

15.1.3 Material properties

The concrete of M20 (characteristic cubic compressive strength, f_{ck} of 20MPa) and reinforcement of grade Fe415 ($f_y = 415$ MPa) was used for the design and construction of the structure. The material properties considered for analysis and seismic assessment of the structure as recommended for Indian Standard (IS 456:2000) are tabulated in Table 15.3.

Table 15.3 Material properties used for analysis of the structure

Material	Grade	Elastic Modulus	Weight Density	Poisson's ratio
Concrete	M20	$5000 * (f_{ck})^{0.5} = 22360$ MPa	25 kN/m ³	0.2
Reinforcement	Fe 500	200000 MPa	78.5 kN/m ³	0.33

15.2 Loads on the structure

The following loads were considered for the assessment of the structure.

15.2.1 Dead Loads

The dead loads consist of two kinds of loads namely self loads and superimposed dead loads.

- (a) Self Loads: These loads are calculated and considered automatically by specifying unit weight of the material and dimensions of the members.
- (b) Superimposed dead loads: Permanently acting loads other than the self loads of the structure. In this case, the following loads are considered:
 - Floor finish: A floor finish of 75 mm thick is considered on all the floor slabs with a unit weight of 20 kN/m³. Thus the floor finish load = $20 * 0.075 = 1.5$ kN/m².
 - Weight of water proofing on roof = 4.0 kN/m²

- Weight of masonry walls: The unit weight of masonry was considered as 20 kN/m^3 . The mass of the wall is lumped on the beam levels distributing equally between the storey just above and below the wall (IS 1893:2002, cl. 7.4.1).

15.2.2 Live loads

The building serves its purpose as a residential building. Accordingly the live load on all the floors (except roof) is considered as 2.0 kN/m^2 (IS 875:1987 part 2).

15.2.3 Seismic loads

For seismic assessment, the seismic loads recommended by IS 1893:2002 are used with the following details:

- Zone factor, Z : 0.24 (Seismic zone IV)
- Soil type: II (Medium soil)
- Elastic damping: 5%
- Shape of response spectrum: Is 1893:2002 recommends using the shape of response spectrum as shown in Figure 15.4. The spectrum shown in Figure 4.1 is normalized to peak ground acceleration (PGA) of $1.0g$. To obtain the design basis response spectrum, the ordinate values of the spectrum need to be multiplied by $PGA (= 0.24 \text{ for this case})$.

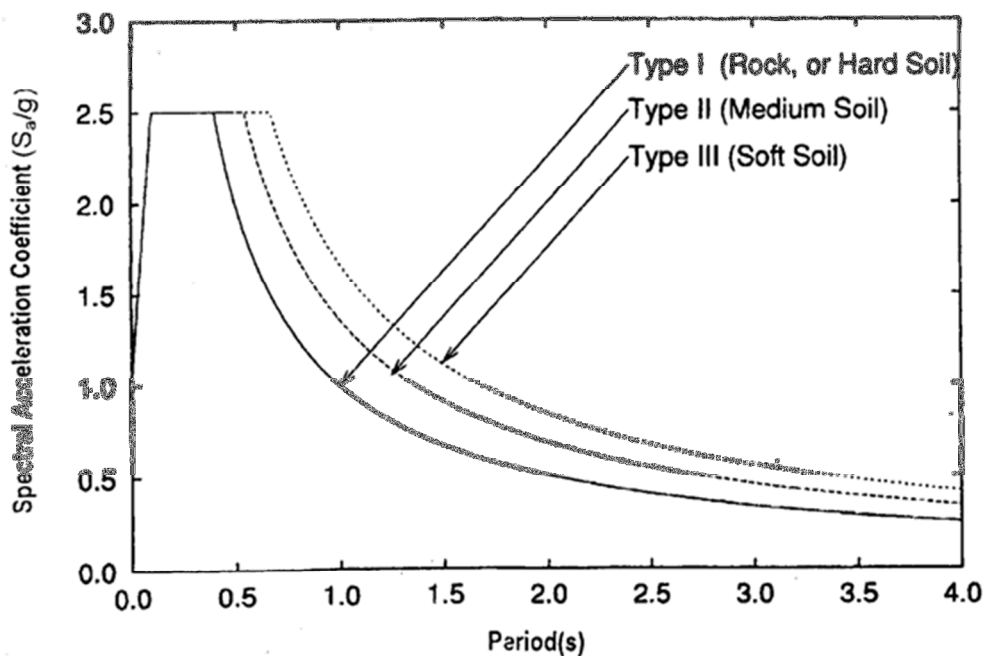


Figure 15.5 Response spectrum shape suggested by IS 1893:2002

Since the philosophy used in this work is based on the nonlinear dynamic analysis of the structure, time history compatible to the spectral shape was needed. The same is presented in Figure 15.6 and was used as input ground motion at the base of the structure.

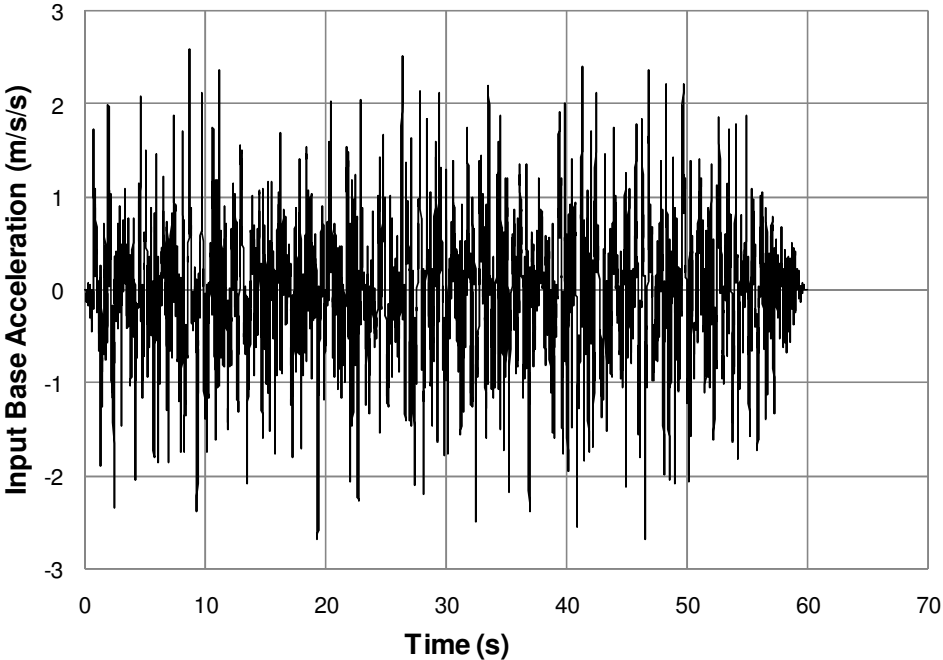


Figure 15.6 Input time history used for the analysis of the structure

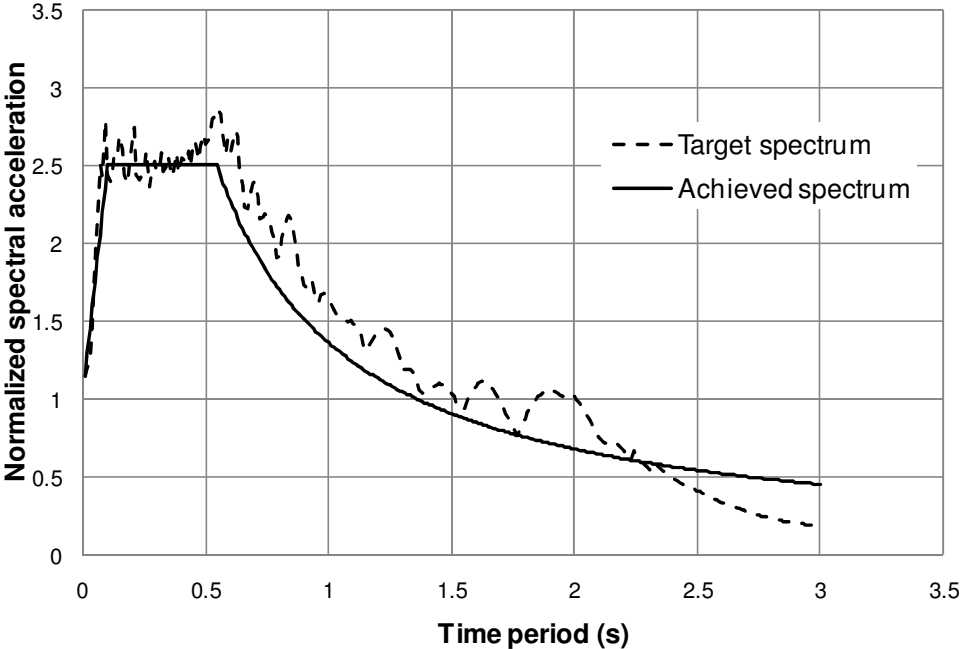


Figure 15.7 Comparison of target and achieved spectral shape using time history

Figure 15.7 shows the comparison of target response spectrum and achieved response spectrum with the time history shown in Figure 15.6. The close comparison of the target and

achieved spectral shape justify the use of the time history for seismic assessment of the structure.

15.3 Results of seismic assessment of as-built structure

The structural model, with various nonlinearities, was subjected to gravity loads followed by seismic loads as per the time history depicted in Figure 15.6. The results of analysis performed for seismic loads along X-direction and Y-direction are presented below:

15.3.1 Results of seismic assessment of as-built structure along X-direction

Figure 15.8 presents the acceleration-time history obtained at the roof of the as-built structure subjected to seismic motion along X-direction. The peak roof acceleration was obtained as 4.85 m/s^2 . On comparing the input base excitation ($\text{PGA} = 0.24g = 2.35 \text{ m/s}^2$), it can be seen that the acceleration is approximately amplified by a factor of 2.

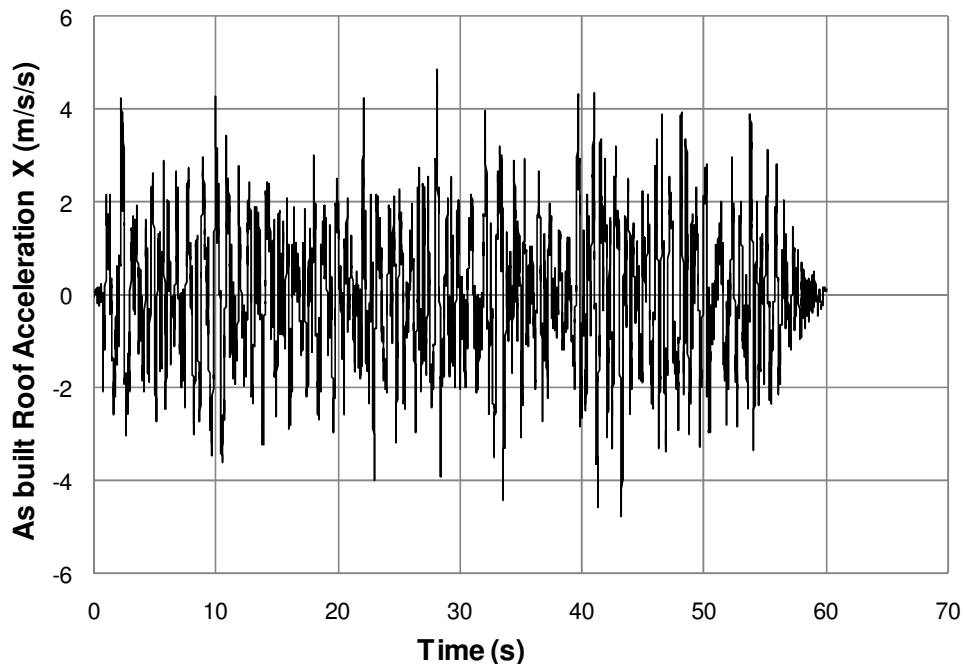


Figure 15.8 Response acceleration-time history obtained for the roof of the structure subjected to ground motion along X-direction

From the analysis, the complete time history of the forces and corresponding deformations at all critical locations (member ends and joints) were obtained. As explained in chapter 4, the joint was modelled using moment and shear springs, with hysteretic characteristics parameters derived as per the recommendations given in chapter 5. The hysteretic response of the various nonlinear springs was studied in detail after the completion of the analysis, from which the degree of damage suffered at various locations of the structure was estimated and the critical locations for retrofitting were determined. Here, typical results are presented.

Let us consider the sub-assembly of the beam-column and joint core at the first floor of column C5 at intersection of grid C and grid 2 (Figure 15.4). Figure 15.9 presents the hysteretic response obtained on the moment spring used to model the joint inelastic behaviour for joint core of the sub-assembly. The hysteretic response of the joint spring clearly displays that the joint has suffered significant inelastic excursion due to the seismic loads, i.e., it has failed under seismic excitation.

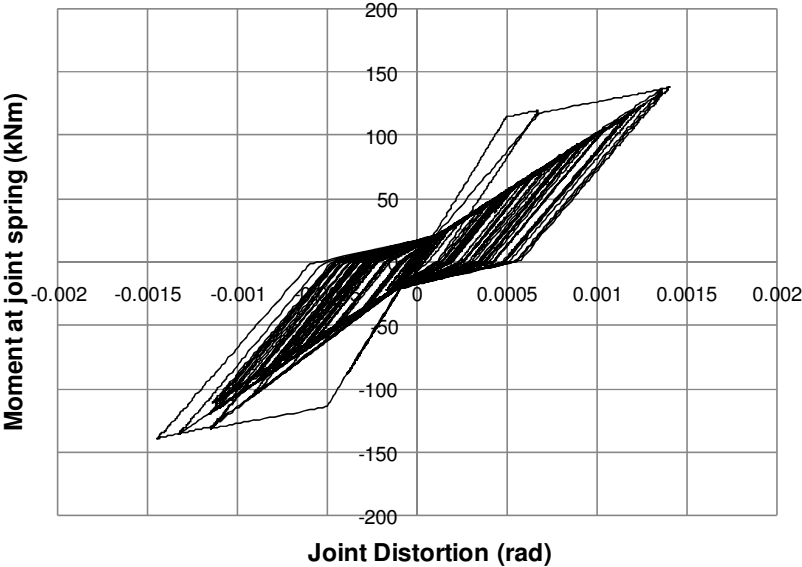


Figure 15.9 Hysteretic response for the joint at 1st floor of column C5 (grid C-2)

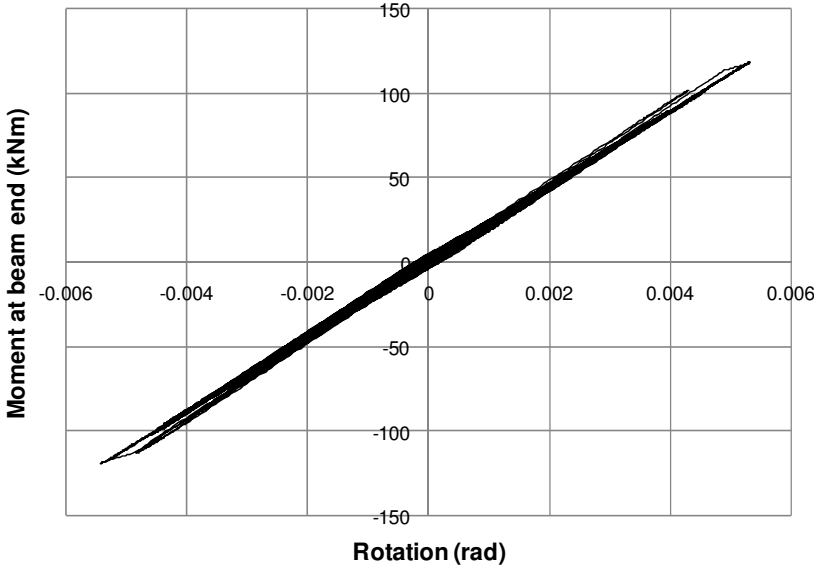


Figure 15.10 Hysteretic flexural response for the beam B2 adjacent to the joint at 1st floor of column C5 (grid C-2)

Figure 15.10 displays the hysteretic flexural response obtained for the beam B2 adjacent to the joint at the first floor of column C5 at intersection of grid C and grid 2 (Figure 15.4). The

hysteretic behaviour of the beam shows almost linear hysteretic response suggesting only minor cracking in the beam due to the seismic loads.

Figure 15.12 presents the hysteretic flexural response of the column C5 adjacent to the joint of first floor at the intersection of grid C and grid 2 (Figure 15.4). Again, the hysteretic behaviour of the column displays almost linear hysteretic response suggesting only minor cracking in the column due to the seismic loads.

This kind of behaviour, where the damage in the joint core is more severe than that in the adjacent beam or column is typical for the structures designed without considering seismic provisions. Similar behaviour was obtained in the experiments on beam-column joint sub-assemblies (chapter 7) and as-built 2D frame structure (chapter 10).

Any seismic analysis, in which the joint inelasticity is ignored may either lead to qualification of the structure or would suggest incorrect locations of expected damage. Thus, considering joint inelastic behaviour is essential for correct seismic assessment of such structures.

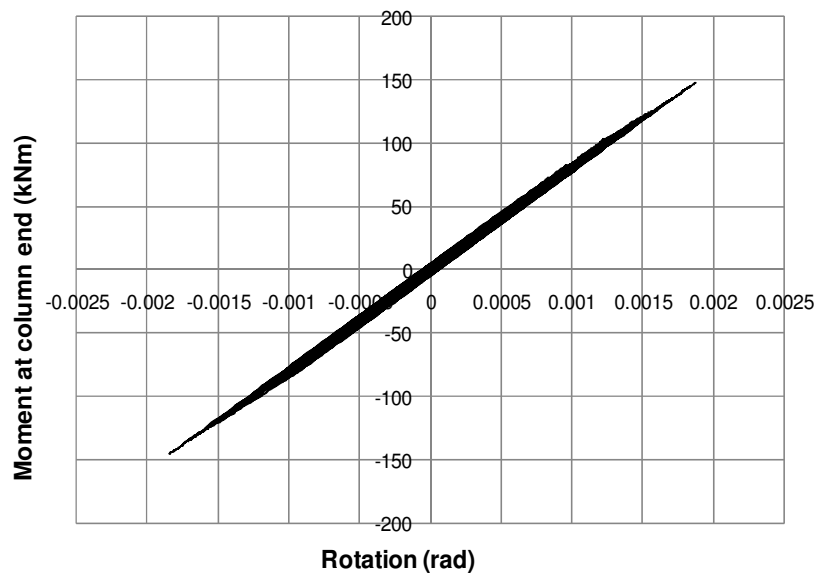


Figure 15.12 Hysteretic flexural response for the column C5 adjacent to the joint at 1st floor of the intersection of grid C-2

Additionally, it is highly important to verify the hysteretic shear behaviour of the members, especially since haunch retrofit is expected to increase the shear forces in the adjoining members. Figure 15.13 displays the hysteretic shear force-shear deformation response obtained for the beam B2 adjacent to the joint at the first floor of column C5 at intersection of grid C and grid 2 (Figure 15.4). The hysteretic behaviour of the beam shows fully linear hysteretic response suggesting no shear damage in the beam due to the seismic loads. Similarly the completely linear response obtained for the column as shown in Figure 15.14 suggests no shear damage in the column as well. It must be noted that such a linear shear

response of the members of as-built structure is one of the major requirements, if haunch retrofit solution is to be used for retrofitting of the structure.

Similarly, all joint sub-assemblies were studied in detail to assess the location and amount of damage suffered by the structure due to seismic loads. Figure 15.15 displays the pictorial representation of the damage inflicted in the various members and joints at grid C. In Figure 15.15, blue dots signify minor to moderate damage, while red dots signify complete damage/collapse.

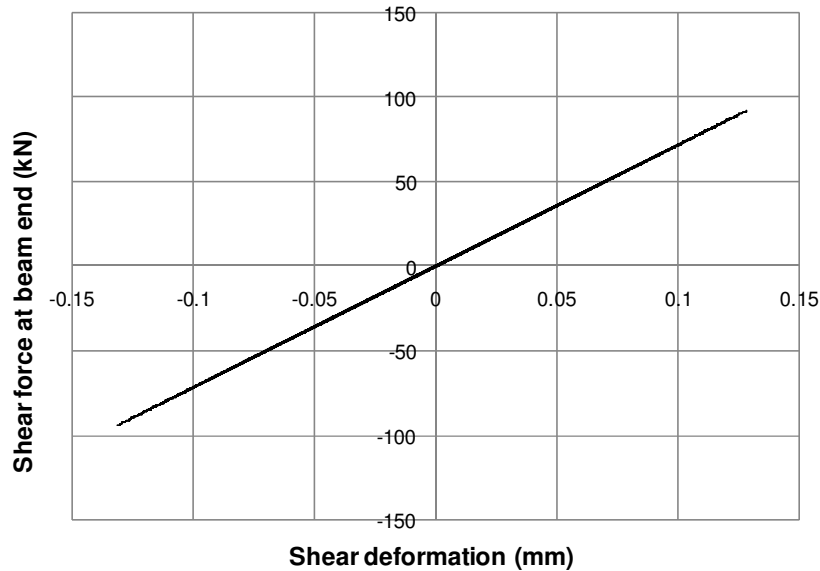


Figure 15.13 Hysteretic shear response for the beam B2 adjacent to the joint at 1st floor of column C5 (grid C-2)

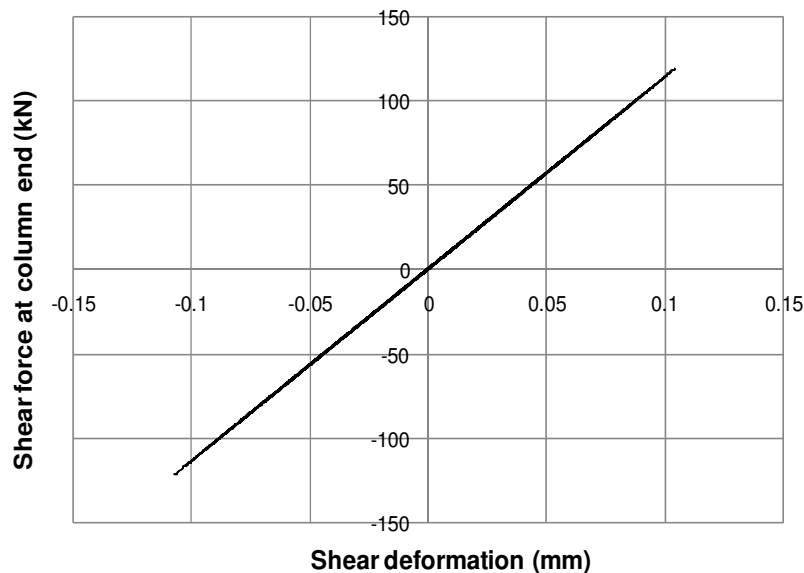


Figure 15.14 Hysteretic shear response for the column C5 adjacent to the joint at 1st floor of the intersection of grid C-2

It is clear from Figure 15.15 that the joints at the 1st and 2nd floors of grid C-2 and C-2* plus the joint at the 1st floor of grid C-3 and C-3* suffered very severe damage. Also, the joints at 1st and 2nd floors of grid C-1 and C-1* plus the joint at 2nd floor of grid C-3 and C-3* also suffered certain damage.

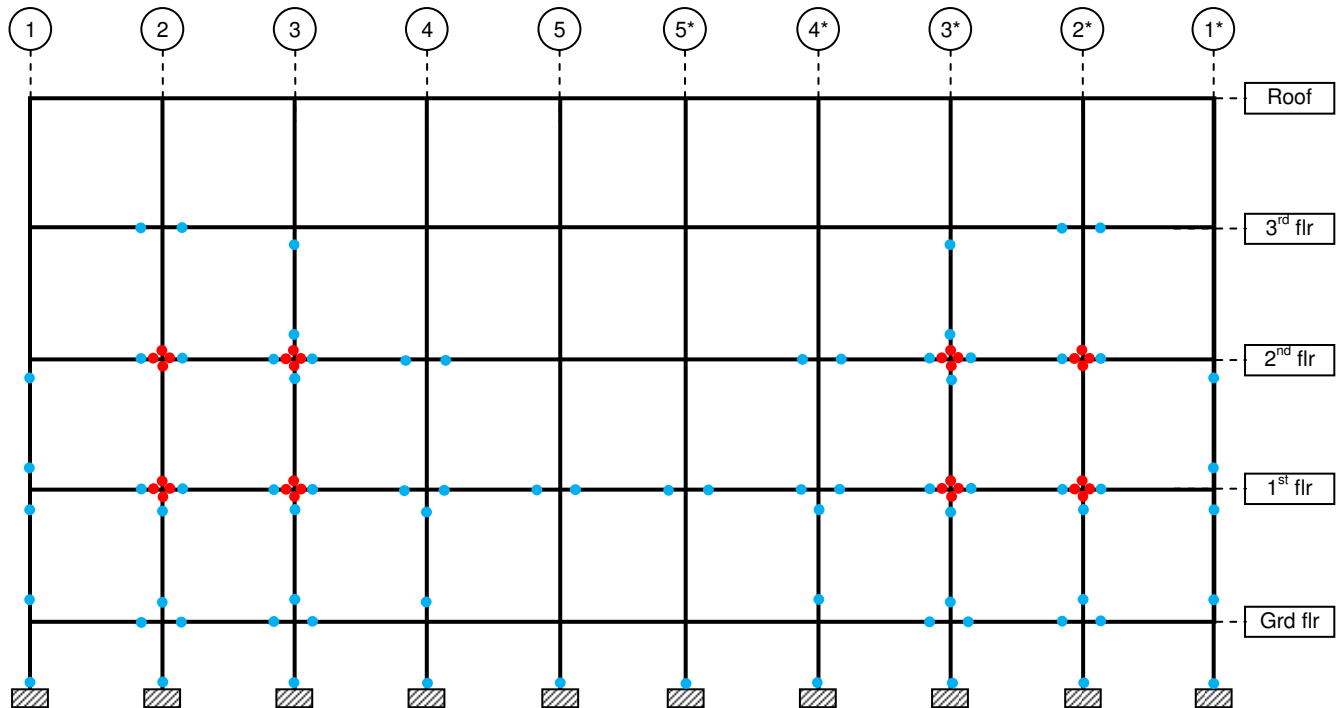


Figure 15.15 Representation of location and degree of damage suffered by Grid C of the structure due to design seismic loads along X-direction

Similar evaluation of analysis results resulted in adjudging the following joints as the major failure locations in the structure:

- Grid A: 1st and 2nd floor joints of grid 4 and 4*
- Grid B: 1st and 2nd floor joints of grid 1, 2, 3 and 1*, 2*, 3*
- Grid C: 1st and 2nd floor joints of grid 1, 2, 3 and 1*, 2*, 3*

15.3.2 Results of seismic assessment of as-built structure along Y-direction

Figure 15.16 presents the acceleration-time history obtained at the roof of the as-built structure subjected to seismic motion along Y-direction. The peak acceleration for the roof was obtained as 4.97m/s² against the PGA of 0.24g (2.35m/s²) indicating that the acceleration is approximately amplified again by a factor of 2.1.

Let us consider the sub-assembly of the beam-column and joint core at the second floor of column C4 at intersection of grid B and grid 2 (Figure 15.4). Figure 15.17 presents the hysteretic response obtained on the moment spring used to model the joint inelastic

behaviour for joint core of the sub-assembly. The hysteretic response of the joint spring clearly displays that the joint has suffered significant damage due to the seismic loads. Figure 15.18 displays the hysteretic flexural response obtained for the beam B1 adjacent to the joint at the second floor of column C4 at intersection of grid B and grid 2 (Figure 15.4). The hysteretic behaviour of the beam shows almost linear hysteretic response suggesting only minor cracking in the beam due to the seismic loads.

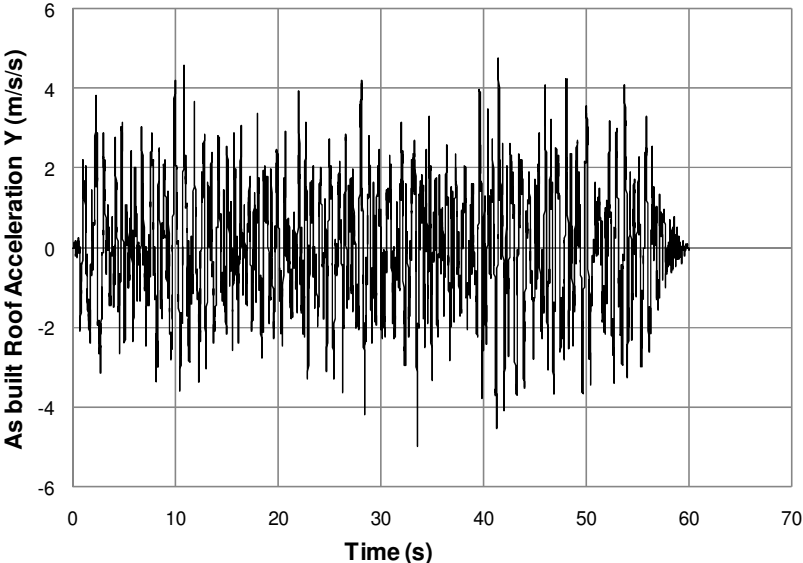


Figure 15.16 Response acceleration-time history obtained for the roof of the structure subjected to ground motion along Y-direction

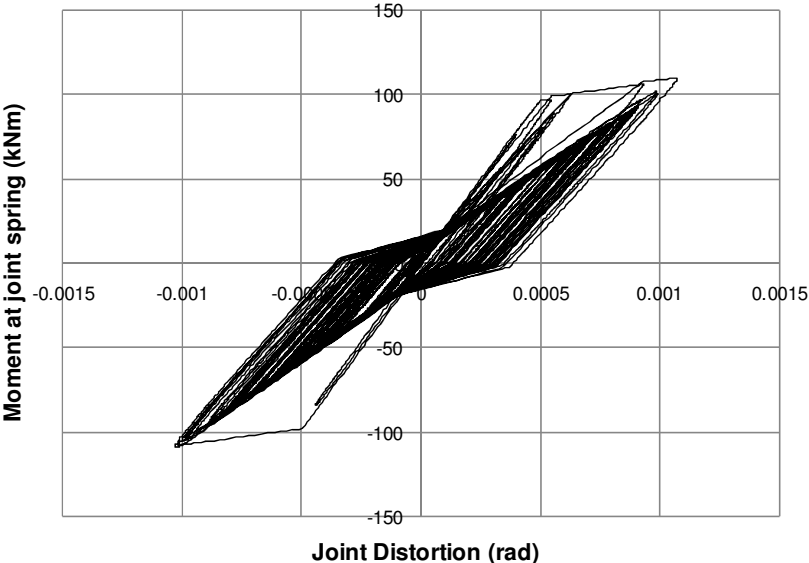


Figure 15.17 Hysteretic response for the joint at 2nd floor of column C4 (grid B-2)

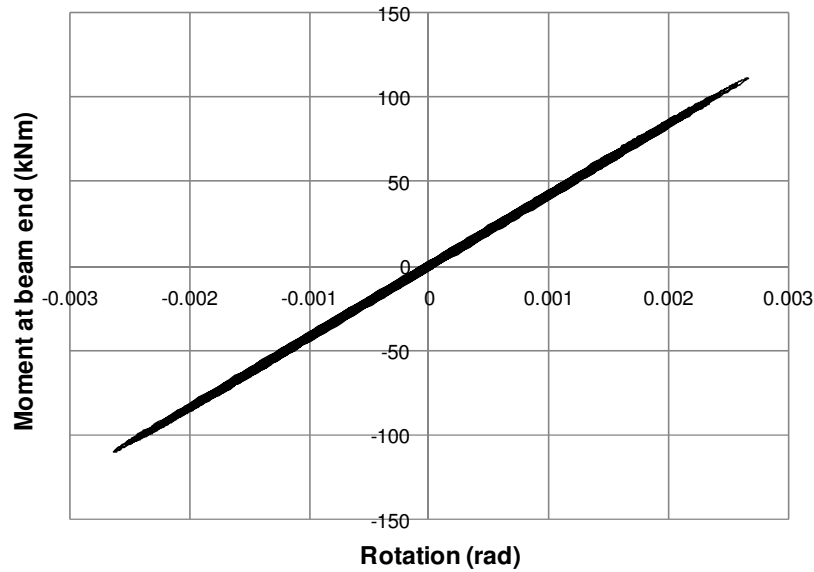


Figure 15.18 Hysteretic flexural response for the beam B2 adjacent to the joint at 1st floor of column C5 (grid C-2)

Figure 15.19 presents the hysteretic flexural response of the column C4 adjacent to the joint of second floor at the intersection of grid B and grid 2 (Figure 15.4). Again, the hysteretic behaviour of the column displays almost linear hysteretic response suggesting only minor cracking in the column due to the seismic loads. Thus, again typical gravity load designed structural behaviour with limited damage in members and severe damage in the joint core is observed for Y-direction also.

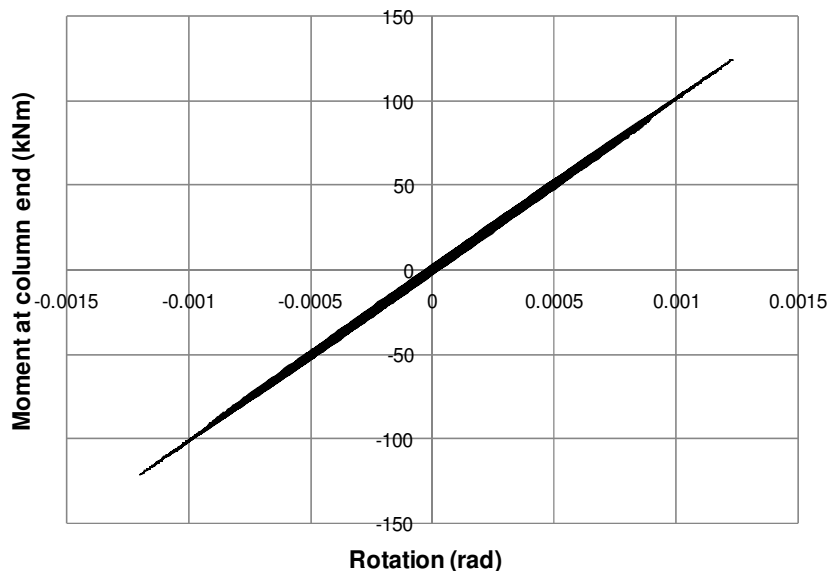


Figure 15.19 Hysteretic flexural response for the column C4 adjacent to the joint at 2nd floor of the intersection of grid B-2

The shear behaviour of the beam and the column framing into the joint was again found to be essentially linear, suggesting that haunch retrofit solution may be suitable to improve the seismic performance of the structure.

Similarly, all joint sub-assemblies were studied in detail to assess the location and amount of damage suffered by the structure due to seismic loads. Figure 15.20 displays the pictorial representation of the damage inflicted in the various members and joints at grid 2.

It is clear from Figure 15.20 that the joints at the 1st and 2nd floors of grid A-2, B-2 and C-2 need retrofitting. Similar evaluation of analysis results resulted in adjudging the following joints as the major failure locations in the structure:

- Grid 1 and 1*: 1st and 2nd floor joints of grids A, B and C
- Grid 2 and 2*: 1st and 2nd floor joints of grids A, B and C
- Grid 3 and 3*: 1st and 2nd floor joints of grids A and C
- Grid 4 and 4*: 1st and 2nd floor joints of grids A, B and C
- Grid 5 and 5*: 1st and 2nd floor joints of grids A, B and C

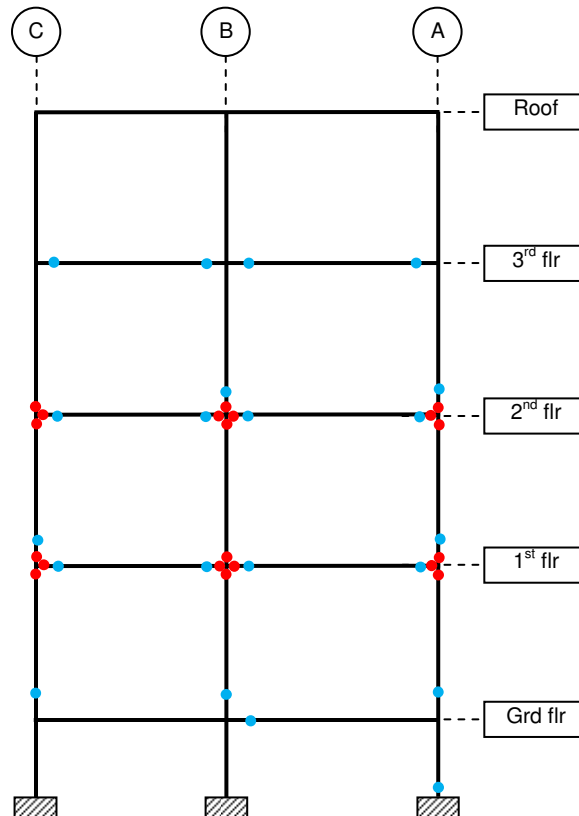


Figure 15.20 Representation of location and degree of damage suffered by Grid 2 of the structure due to design seismic loads along Y-direction

15.4 Design of retrofitting

As seen in previous section, the major failure in the structure was concentrated at the beam-column joints while the members (beams and columns) suffer limited or no damage. Also it was seen that the members were essentially in the linear range when the shear force-deformation behaviour is concerned. Both these points make the fully fastened haunch retrofit solution (FFHRS) ideally suited for the retrofitting of the structure. Only the joints listed in previous section, which failed under seismic loads were strengthened using FFHRS.

15.4.1 Design of FFHRS

The design of FFHRS can be performed following the procedure recommended by Genesio (2012), which is basically an extension of the design recommendations by Pampanin et al (2006) to consider the stiffness of anchors in design calculations. However, this procedure calls for lengthy calculations to be performed to consider the effect of deformations of beams and columns (Pampanin et al, 2006). These effects of member deformations are automatically taken into account when the matrix analysis is performed in software such as SAP2000. Therefore, in this work, a simplified approach towards the design of haunch retrofit solution is followed:

1. At first, based on the experience from the tests on beam-column joints and 2-D structure, preliminary dimensions for the haunch were selected.
2. The haunch was connected perfectly to the structural members framing into the joint at the required location.
3. The forces in the haunch were evaluated considering perfect connectivity of the haunch elements to the structure.
4. The anchorage system was designed using CC method to cater for those forces.
5. If the anchorage system was unable to be designed for the 100% of axial forces arising from the analysis, the same was designed for 80% of the load, since beyond 80% of peak load, the reduced stiffness of the anchorage system results in lesser axial forces in the haunch than obtained considering perfect connectivity (chapter 6).

15.4.2 Sample calculation for design of FFHRS

Let us consider the sub-assembly of the beam-column and joint core at the second floor of column C4 at intersection of grid B and grid 2 (Figure 15.4). Figures 15.17 through 15.19 show that the joint shear failure is the major failure mode for this sub-assembly. The joint is formed by the intersection of column C4 at 2nd floor, which has a section of 300mm x 600mm and beam B1, which has a section of 300mm x 400mm. A haunch element with the dimensions as shown in 15.21 was selected as a trial section for the FFHRS for the joint. The first trial run was performed considering perfect connectivity of this haunch element with the frame members. The axial force-time history in the haunch is displayed in Figure 15.22. The

peak axial load in the haunch element was obtained as 90.59kN. Since the haunch element makes an angle of 45 degrees with horizontal, the peak tension load exerted on the anchor group due to the force in the haunch will be $90.59/1.414 = 64.06\text{kN}$.

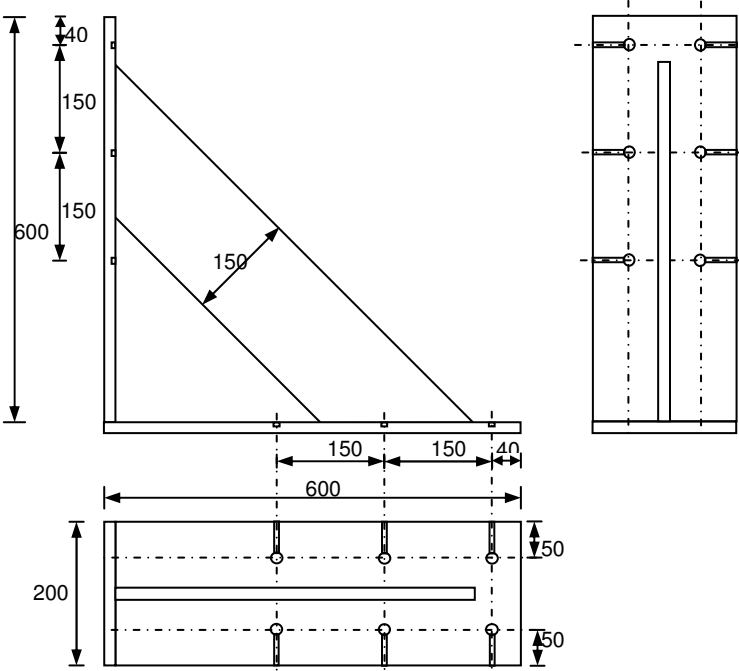


Figure 15.21 Trial haunch element for retrofitting of joint at 2nd floor grid B-2

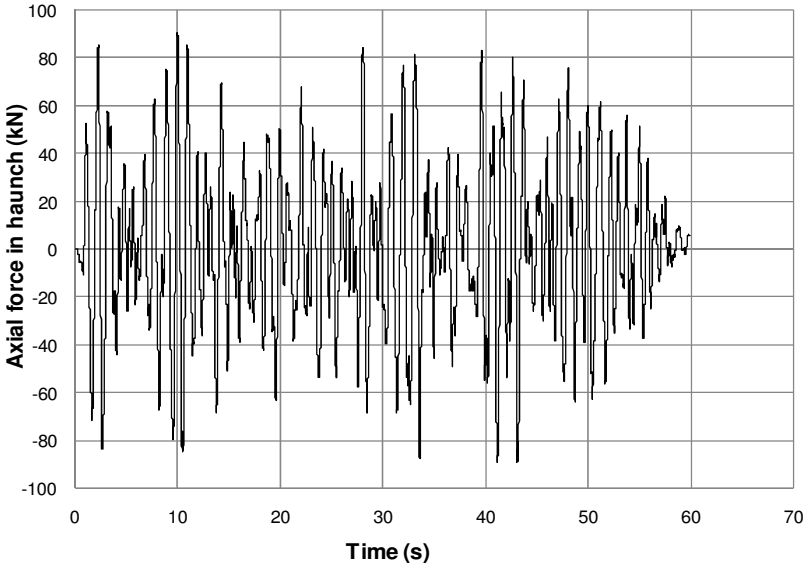


Figure 15.22 Axial force-time response in the haunch element for retrofitting of joint at 2nd floor grid B-2

The anchor system is designed to cater for these forces as explained in chapter 14. Six bonded anchors with an embedment depth of 150mm were found to provide a resisting force

more than that required from the analysis. The same was therefore selected for the FFHRS. In a similar way, the FFHRS was designed for all the joints requiring retrofit. It is important to note that here the design is performed without considering the safety factors suggested by the codes, e.g. ACI 318 (2011). However, it is not important in this case, since the whole philosophy of assessment and retrofit is performance based and the complete nonlinear characteristics are used to model the behavior of the anchors.

15.5 Results of seismic assessment of retrofitted structure

The retrofitted structural model, with various nonlinearities (including anchor springs), was subjected to gravity loads followed by seismic loads as per the time history depicted in Figure 15.6. The results of analysis performed for seismic loads along X-direction and Y-direction are presented below:

15.5.1 Results of seismic assessment of retrofitted structure along X-direction

Figure 15.23 presents the acceleration-time history obtained at the roof of the retrofitted structure subjected to seismic motion along X-direction. The peak roof acceleration was obtained as 5.12 m/s^2 , which was marginally higher than that obtained for as built structure. This signifies that the overall structural forces are not increased significantly, which is an important criteria for good retrofit solution.

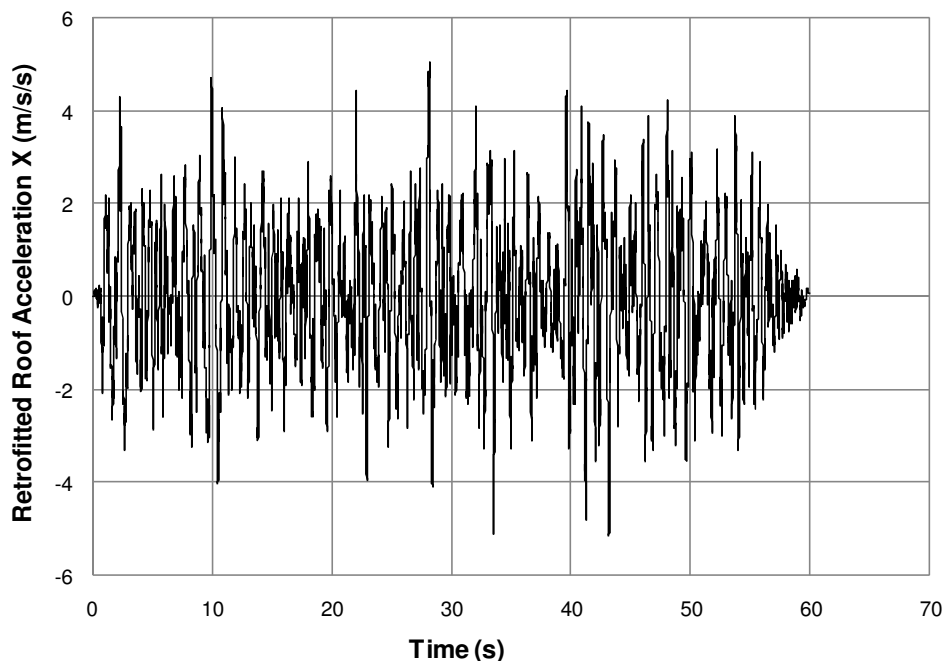


Figure 15.23 Response acceleration-time history obtained for the roof of the retrofitted structure subjected to ground motion along X-direction

From the analysis, the complete time history of the forces and corresponding deformations at all critical locations were obtained. The hysteretic response of the various nonlinear springs was studied in detail after the completion of the analysis, from which the degree of damage suffered at various locations of the structure was estimated. Here, typical results are presented for the location of the joint retrofitted with FFHRS. Figure 15.24 presents the hysteretic response obtained on the moment spring used to model the joint inelastic behaviour for joint core of the sub-assembly formed by the beam-column and joint core at the first floor of column C5 at intersection of grid C and grid 2. The hysteretic response of the joint spring clearly displays that the forces in the joint are significantly reduced due to the introduction of the FFHRS and the joint remains fairly in elastic range.

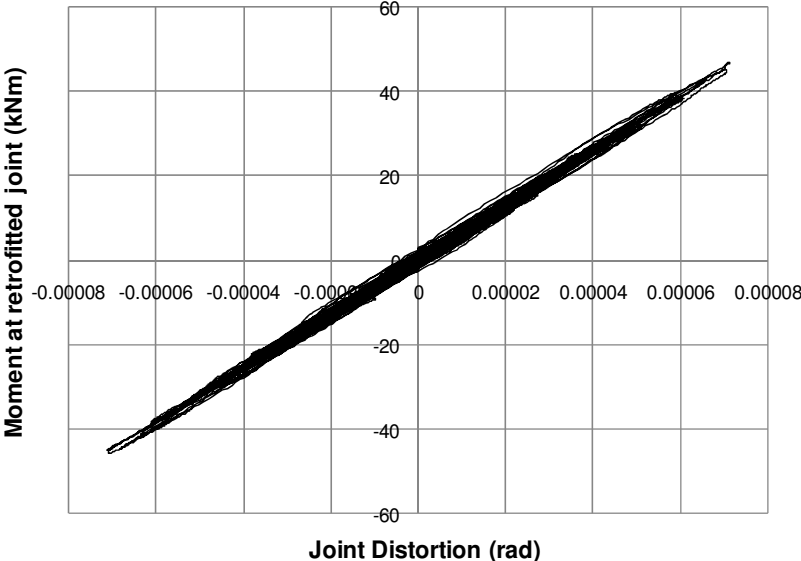


Figure 15.24 Hysteretic response for the retrofitted joint at 1st floor grid C-2

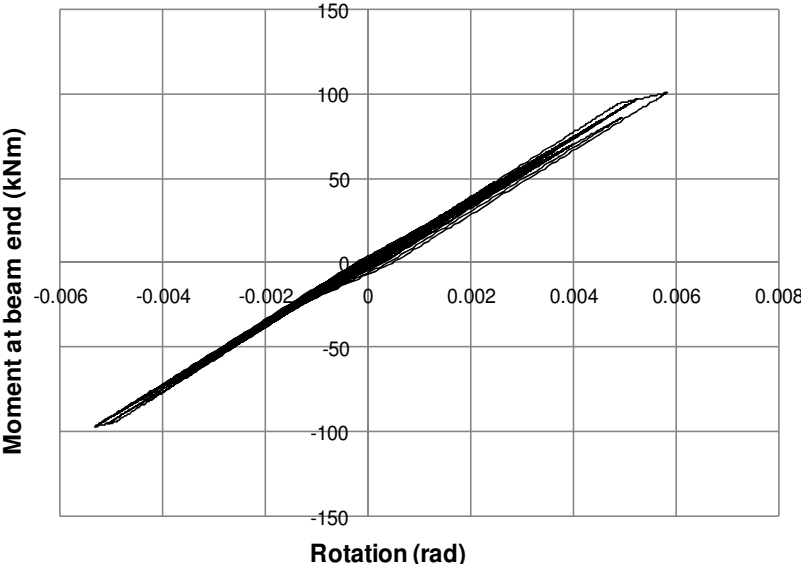


Figure 15.25 Hysteretic flexural response for the critical section of the beam adjacent to the end section of FFHRS

Figure 15.25 displays the hysteretic flexural response obtained for the critical section of the beam adjacent to the end section of FFHRS. It can be seen that at this critical section, the moment in the beam is also reduced compared to the moment at the critical section of the beam in as built structure. This is as expected since the introduction of FFHRS reduces the clear span of the beam, thus reducing the bending moments. The hysteretic behaviour of the beam shows almost linear hysteretic response suggesting only minor cracking in the beam due to the seismic loads.

Figure 15.26 presents the hysteretic flexural response of the column C5 at the critical section. Again the moments in the column at critical section are reduced, which is attributed to the reduction in free height of the column. The influence of reduction in moments is more pronounced in case of column than in the beam. This is understandable since the ratio of unsupported span in case of retrofitted structure to that in case of as built structure is less for column than for the beam.

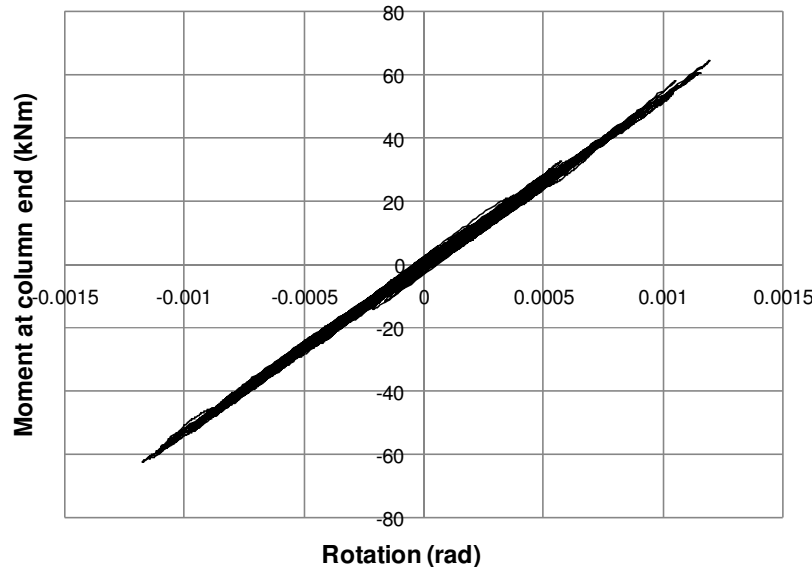


Figure 15.26 Hysteretic flexural response for the column C5 at the intersection of grid C-2, at the critical section adjacent to the end section of the FFHRS

As mentioned earlier, the basic principle of the HRS lies in conversion of the bending moments into axial and shear forces at the critical location. Generally, axial forces are not found to be critical in RC frame structures. However, it is highly important to verify the hysteretic shear behaviour of the members after introduction of FFHRS.

Figure 15.27 displays the hysteretic shear force-shear deformation response obtained for the beam after retrofitting the joint with FFHRS. It shall be noticed that there is almost a 25% increase in the shear forces in the beam due to introduction of the FFHRS. However, the hysteretic behaviour of the beam shows fully linear hysteretic response suggesting no shear damage in the beam due to the seismic loads.

Similarly the hysteretic response obtained for the column as shown in Figure 15.28 gives 10% increase in shear forces in the column but suggests no shear damage in the column. It must be noted that such a linear shear response of the members of retrofitted structure is one of the major requirements, if haunch retrofit solution is to be used for retrofitting of the structure.

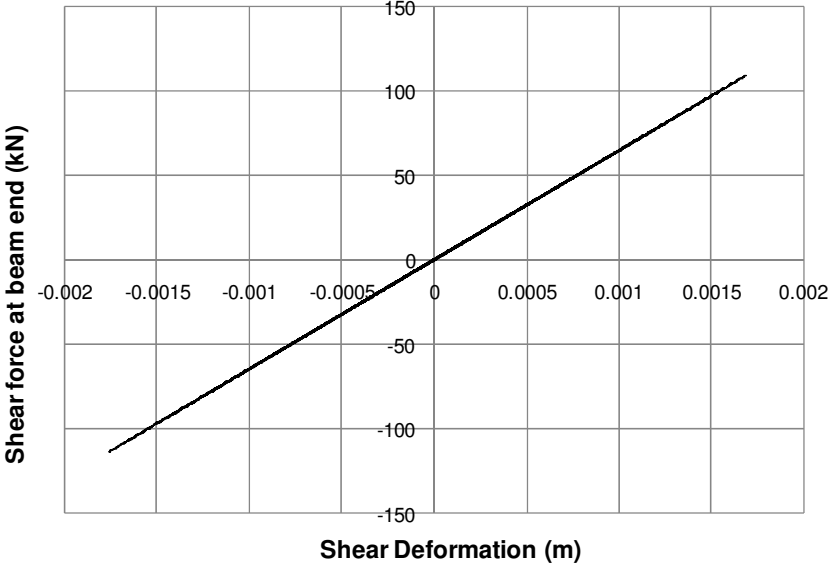


Figure 15.27 Hysteretic shear response for the beam after retrofitting

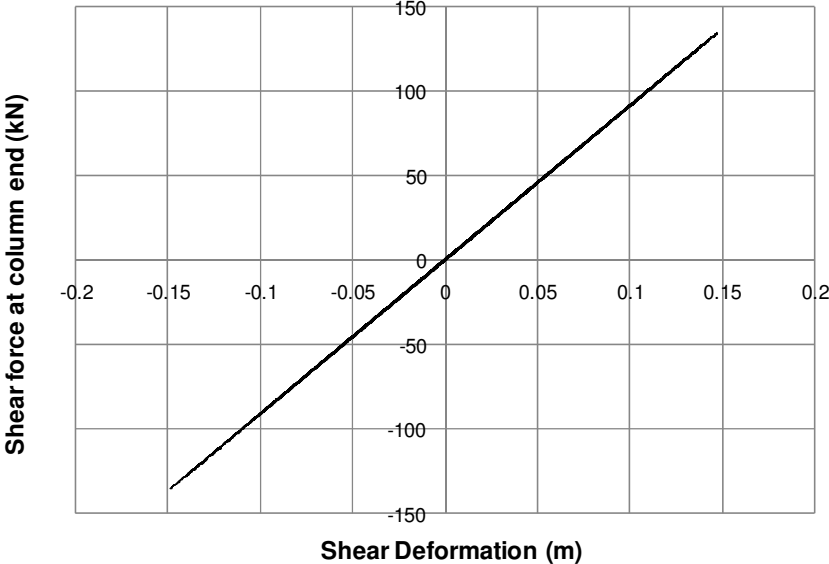


Figure 15.28 Hysteretic shear response for the column after retrofitting

Figure 15.29 displays the estimated damage patterns for grid C of the retrofitted structure. It is clear from Figure 15.29 that the suggested retrofitting using FFHRS only for the joints failing in case of as built structure served its purpose well to upgrade the seismic performance of the structure.

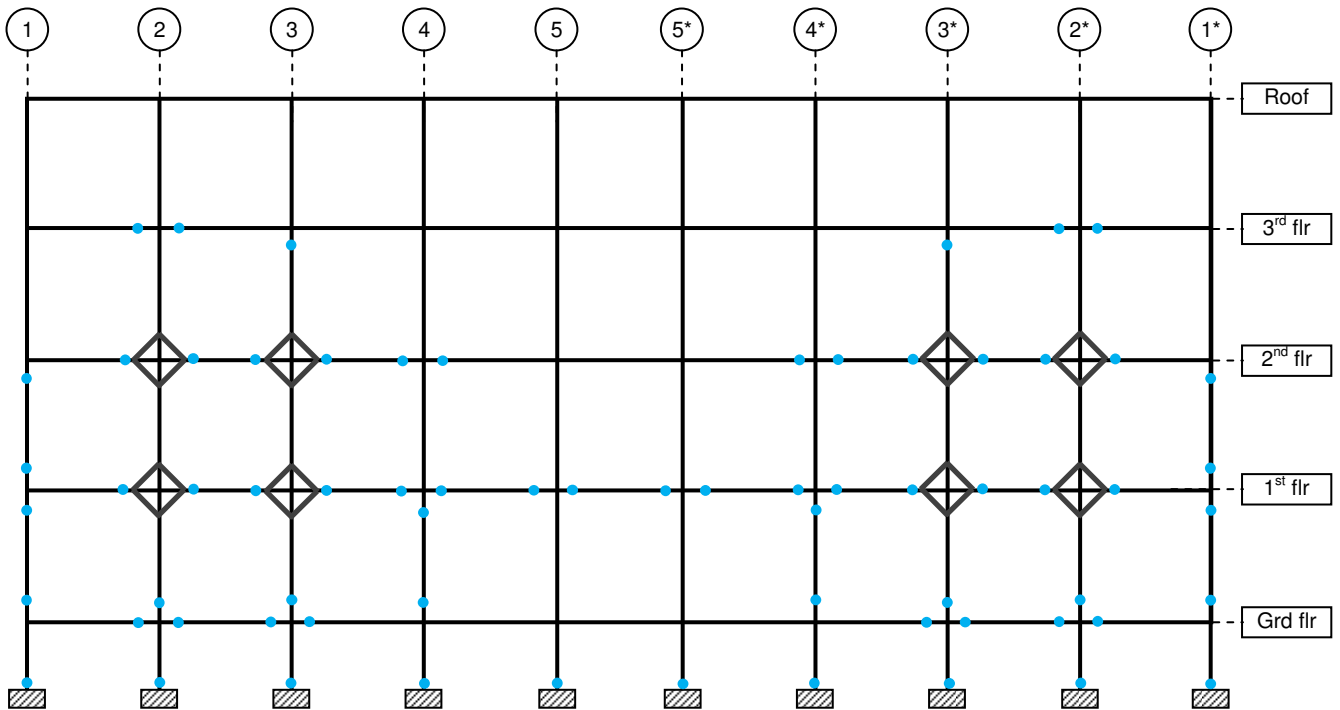


Figure 15.29 Representation of location and degree of damage suffered by Grid C of the retrofitted structure due to design seismic loads along X-direction

15.5.2 Results of seismic assessment of retrofitted structure along Y-direction

Figure 15.30 presents the acceleration-time history obtained at the roof of the retrofitted structure subjected to seismic motion along Y-direction. The peak acceleration for the roof was obtained as 5.38m/s^2 which was again only marginally higher than the peak roof acceleration obtained for the case of as built structure.

Figure 15.31 presents the hysteretic response obtained on the moment spring used to model the joint core of the sub-assembly formed by beam-column and joint core at the second floor of column C4 at intersection of grid B and grid 2. The hysteretic response of the joint spring clearly displays that the forces in the joint are significantly reduced due to the introduction of the FFHRS and the joint remains fairly in elastic range.

Figure 15.32 displays the hysteretic flexural response obtained for the beam adjoining at retrofitted joint at the critical section. Again, a reduction in bending moments compared to that in case of as built structure was observed and the hysteretic behaviour of the beam shows almost linear hysteretic response suggesting only minor cracking in the beam.

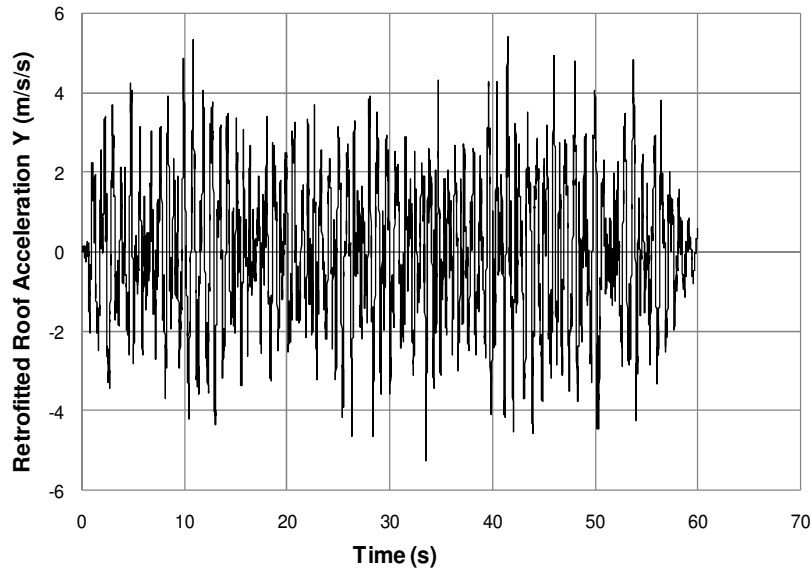


Figure 15.30 Response acceleration-time history obtained for the roof of the retrofitted structure subjected to ground motion along Y-direction

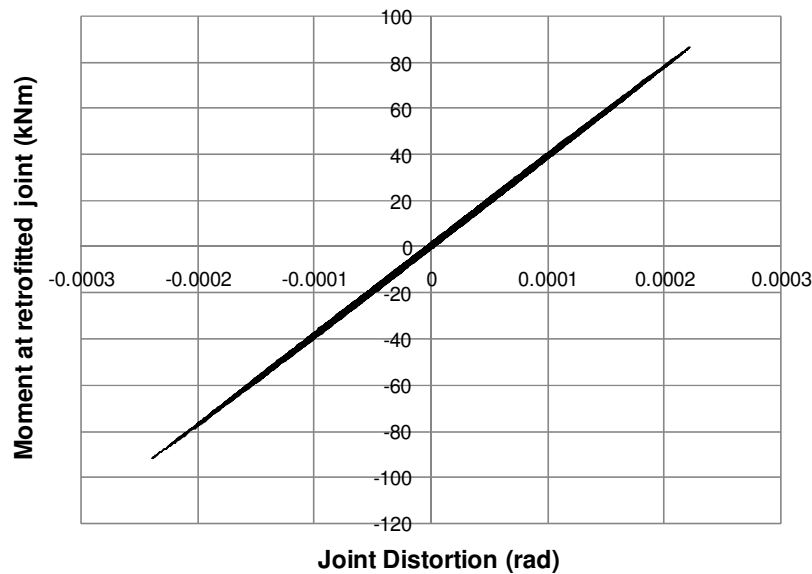


Figure 15.31 Hysteretic response for the retrofitted joint at 2nd floor grid B-2

Figure 15.33 presents the hysteretic flexural response of the column at critical section, which again shows reduced bending moments compared to as built structure and linear response.

The shear behaviour of the beam and the column framing into the joint was again found to be essentially linear, suggesting that haunch retrofit solution is suitable to improve the seismic performance of the structure.

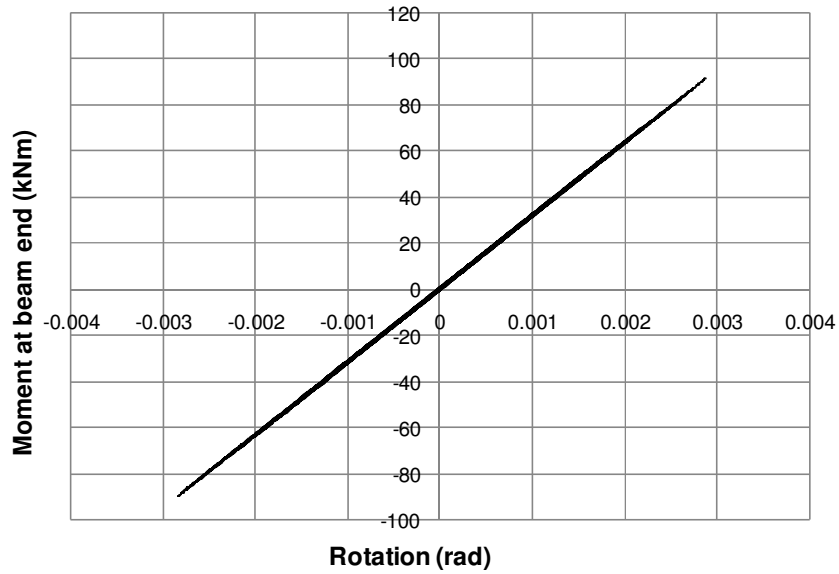


Figure 15.32 Hysteretic flexural response for the beam at critical section for retrofitted structure

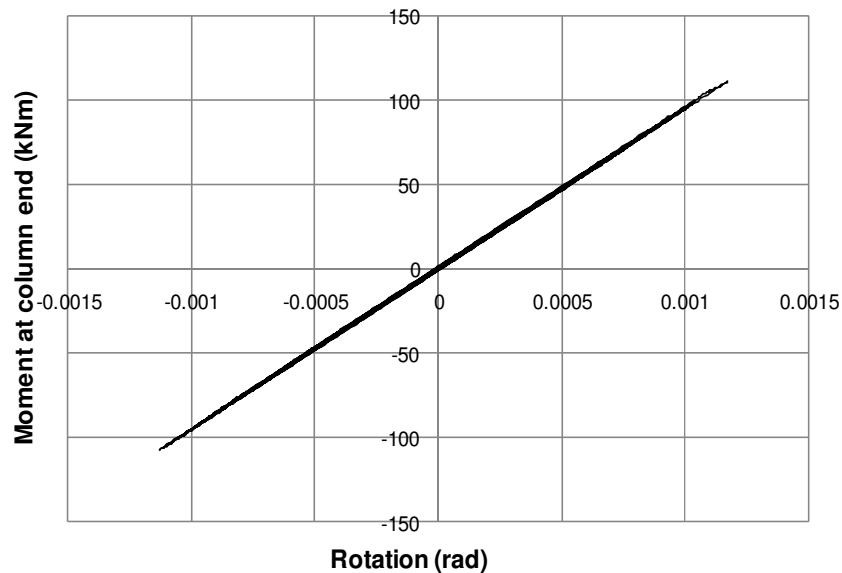


Figure 15.33 Hysteretic flexural response for the column at critical section for retrofitted structure

Figure 15.34 displays the estimated damage patterns for grid 2 of the retrofitted structure. It is clear from Figure 15.34 that the suggested retrofitting using FFHRS only for the joints failing in case of as built structure served its purpose well to upgrade the seismic performance of the structure.

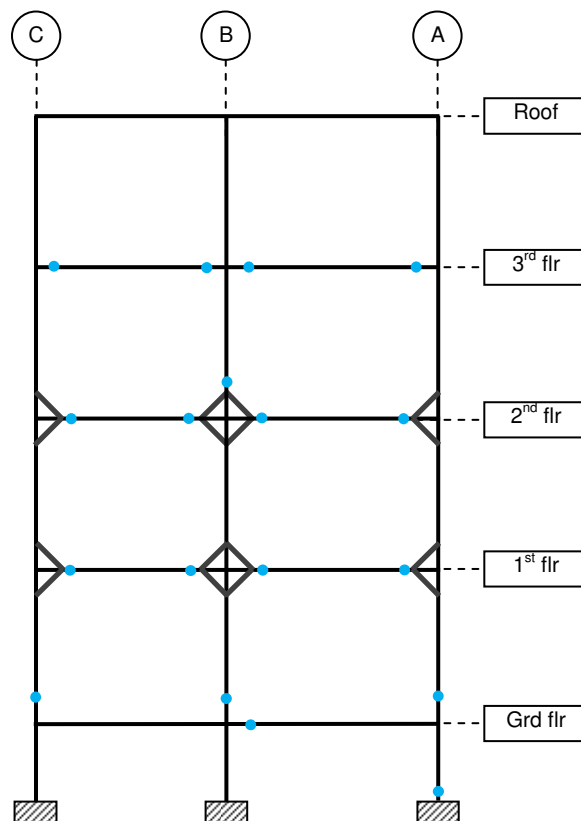


Figure 15.34 Representation of location and degree of damage suffered by Grid 2 of the structure due to design seismic loads along Y-direction

15.6 Analysis under higher level of earthquake

In section 15.3, it was shown that the beam-column joints form the weakest link in case of as built structure and after retrofitting the overall behaviour of the structure significantly improved (section 15.4). Though it is clearly shown that the joints are critical elements and that retrofitting them using FFHRS improves the performance of the structure, it is questionable whether the structure could have survived the earthquake even without retrofitting. This question arises due to the fact that the beams and the columns of the structure were not severely damaged due to the applied earthquake. It is therefore interesting to investigate, how the structure would have behaved if subjected to a higher level of earthquake. As an academic exercise, therefore, in this work, the structure was analyzed under the next level of design earthquake recommended by IS 1893:2002, i.e. the earthquake corresponding to zone V of India's seismological map.

For this exercise, the seismic data was considered the same as given in section 15.2.3 except that the zone factor was considered as 0.36 (zone V) instead of 0.24. The input ground motion as given in Figure 15.6 was scaled up by 1.5 times ($0.36/0.24 = 1.50$) to perform the analysis. Figure 15.35 displays the pictorial representation of the damage inflicted in the various members and joints at grid C due to the beyond design basis earthquake in X-direction. In Figure 15.35, blue dots signify minor to moderate damage,

green dots signify moderate to severe damage, while red dots signify complete damage/collapse. In Figure 15.35, it can be observed that due to higher level of acceleration, severe damage occurs in columns as well as further more joints. A combination of the hinge formation in columns as well as joints is dangerous as it may lead to the formation of mechanism that may lead to collapse of the structure.

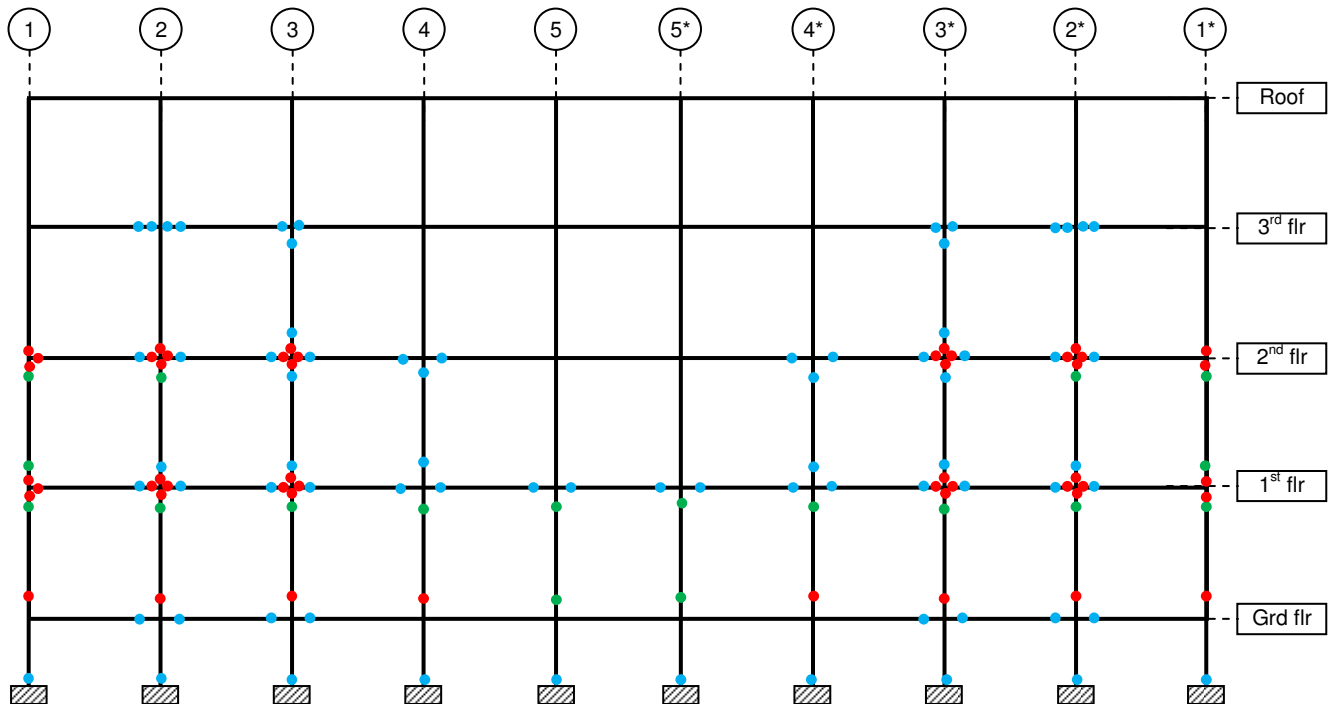


Figure 15.35 Representation of location and degree of damage suffered by Grid C of the structure due to beyond design seismic loads along X-direction

Similar exercise was performed for the structure in Y-direction. The results in the form of hinge formation are presented in Figure 15.36 below. As expected, the already existent severe damage in the joints accompanied with the hinge formation at the base of the columns lead to a mechanism formation.

From figures 15.35 and 15.36 it is clear that the structure would have collapsed under the next higher level of earthquake as per Indian Standard (IS 1893:2002). This exercise further brings out the importance of the beam-column joints modelling in seismic assessment of non-seismically designed structures. It was seen that the severe damage in beam-column joints highly reduces the redundancy in the system and therefore any further hinge formation in columns lead to the formation of mechanism leading to collapse of structure.

To verify the efficacy of FFHRS in improving the seismic behaviour of structure, the retrofitted structure was also subjected to higher level of acceleration. The results of extended analysis on retrofitted structure for X-direction are summarized in Figure 15.37.

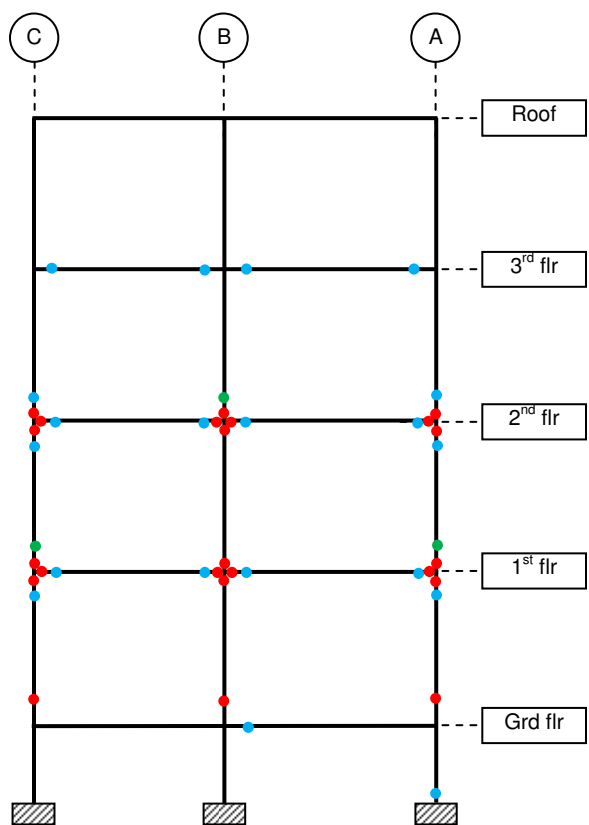


Figure 15.36 Representation of location and degree of damage suffered by Grid C of the structure due to beyond design seismic loads along Y-direction

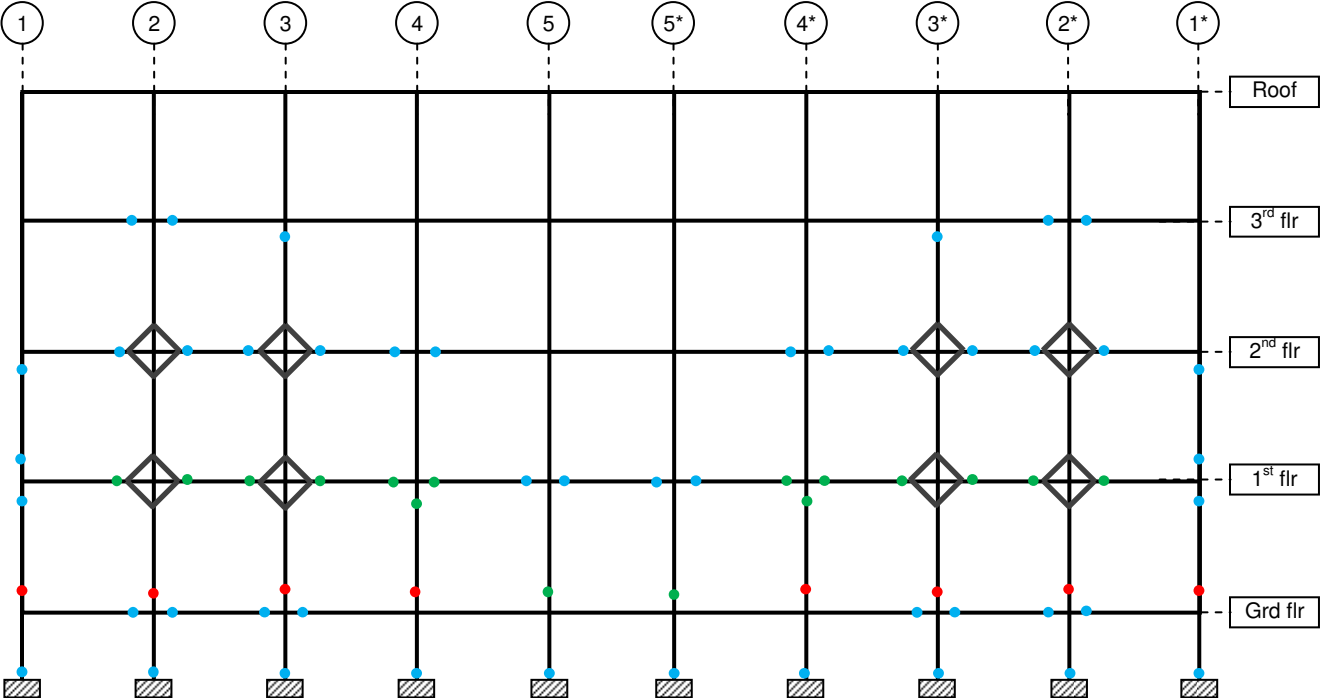


Figure 15.37 Representation of location and degree of damage suffered by Grid C of the retrofitted structure due to beyond design seismic loads along X-direction

From figure 15.37, it is clear that though under higher acceleration levels the columns suffer more severe damage, since the joints remain essentially elastic, the structure does not form a mechanism. This is due to the inbuilt redundancy in the structural system. This clearly displays that by maintaining the beam-column joints in elastic range, FFHRS help in improving the overall seismic behaviour of the non-seismically designed structures.

The exercise was also repeated by subjecting the retrofitted structure in Y-direction to higher levels of earthquake loads. The results of the analysis are summarized in figure 15.38. Again, even though columns suffer severe damage, mechanism formation does not occur since the joints remain essentially elastic.

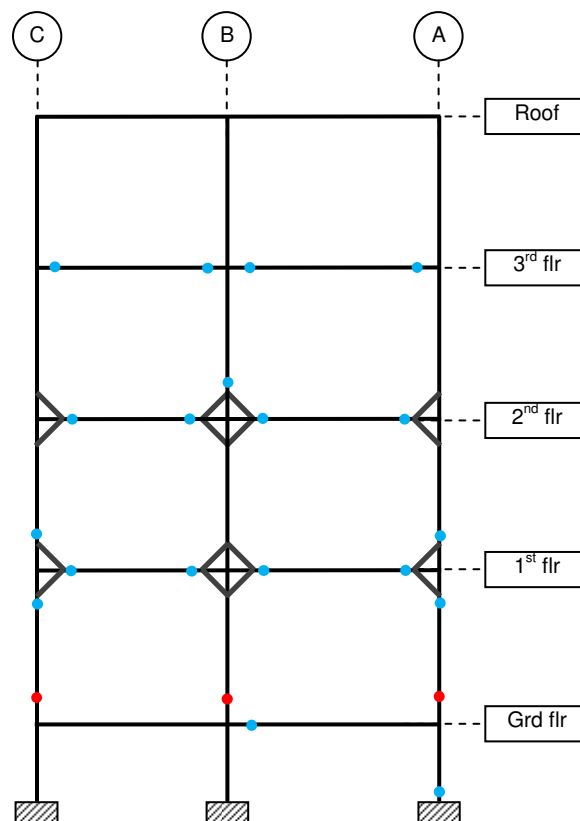


Figure 15.38 Representation of location and degree of damage suffered by Grid C of the retrofitted structure due to beyond design seismic loads along Y-direction

15.7 Summary

In this chapter, the models developed and validated in this work were used to assess the seismic performance of a real life existing RC frame structure under as built condition and based on the results of seismic assessment, a suitable and economical retrofit using FFHRS was designed and the structure was again assessed in retrofitted condition.

The structure selected for this work is an existing residential building in New Delhi, India. The structure was designed in 1982 without giving due considerations to seismic design

philosophy. The structure is a ground + 3 storey structure with the moment resisting beam-column framework as the load resisting system. The structure serves its purpose as a residential building in New Delhi, India, which is classified in seismic zone 4 (severe earthquake intensity) as per Indian Standard, IS 1893 (2002).

It was found that the as built structure displayed shear failure of the beam-column joints typical of such non-seismically designed structures under seismic loads. The retrofit was suggested, which consisted essentially of using FFHRS to retrofit only the joints which displayed joint shear failures. Thus, the retrofitting design was very economical since only the most important locations were first determined and then attended to.

The seismic assessment of the retrofitted structure displayed that with the suggested retrofitting the structure was able to perform much better under seismic loads with no major failure occurring at any location. The case study proved the suitability and applicability of the various models presented in this work for the correct seismic assessment and designing an efficient and economic retrofit.

The structural model was further subjected to beyond design basis earthquake to investigate the performance of the as built and retrofitted structure under higher levels of acceleration. It was found that in case of as built structure a mechanism formation occurred due to higher earthquake level, while the retrofitted structure survives the earthquake with acceptable damage.

16. CONCLUSIONS AND RECOMMENDATIONS

This work has been aimed at understanding and improving the seismic behaviour of poorly detailed RC frame structures, in general, and beam-column joints, in particular. Both experimental and numerical approaches have been employed in order to achieve the same.

In order to understand the seismic behaviour of non-seismically designed and detailed RC beam-column joints, an experimental program was carried out. Five beam-column joints were tested under cyclic loads in the program. The tests clearly confirmed the vulnerability of non-seismically designed joints subjected to seismic loads. The test program provided a great insight into the shear behaviour of poorly detailed beam column joints. In all the tests, joint shear failure was the major failure mode. The influence of type of anchorage of beam reinforcing bars in the joint panel on seismic behaviour of the joints was clearly displayed. The experiments served their purpose as the control specimens for assessing the performance of haunch retrofit solution and also provided data that could be used for validation of the joint model.

Experiments at joint sub-assembly level clearly demonstrated the vulnerability of the joints of non-seismically designed frame structures against seismic forces. However, it is important to understand the behavior of joints when they are an integral part of a whole structure where the joint failure modes also interact with other possible failure modes in the structure. This requires performing experiments at structural level against simulated seismic loads till failure of the structure. In this work, a full scale pushover experiment was conducted on a RC frame which was a replicate of a substructure of an existing office building in India. The structure was constructed with non-seismic detailing and the foundation was constructed with rock anchors to avoid any possible rotation during the experiment. The failure patterns displayed the vulnerability of RC buildings with non-conforming detailing which tend to fail in undesirable failure mechanisms, such as joint shear failures, bond failures, etc.

To understand the real behaviour of beam-column joints in structures under seismic loads, shake table tests were performed on 2D RC frame structures. In order to have a direct comparison with the experiments at sub-assembly level, the basic design of the frames was performed so that the exterior joints of the frames are 2/3rd scale replica of the joints tested earlier. The 2D RC frame structure was subjected to gradually increasing levels of excitation. The crack patterns were marked at the end of each loading wave and it was concluded that joint shear failure was the fundamental mode of failure for the structure.

The experiments carried out on control structural sub-assemblies and structures emphasized on the poor seismic behaviour of the beam-column joints. In order to improve the seismic behaviour of the structures, it is essential to safeguard the beam-column joints by the means of retrofitting. In this work, fully fastened haunch retrofit solution (FFHRS) has been investigated as a viable alternative to retrofit the joints and thereby improve the seismic

performance of the structures. The solution consists of a haunch element, which primarily consists of a diagonal axial element in the form of a machined bar/plate connected to plates at both ends, connected to beam and column. The underlying principle of the HRS is to relocate the plastic hinge away from the vulnerable joint panel/core while enhancing the global response of non-seismically designed RC joint sub-assembly by altering the hierarchy of strength suitably.

The experimental program on retrofitted beam-column joints consisted of performing static-cyclic tests on non-seismically designed full-scale RC exterior joints. Bonded anchors, concrete screws and the bolt type expansion anchors were used to connect the haunch elements to the framing members. In one case, selective weakening of the beam was also employed in addition to the FFHRS. It was concluded that the effectiveness of the FFHRS is directly related to the efficiency of the anchor group used to fasten the haunch elements. In case where the anchor group performed very well (JT1-4), a ductile flexural failure in the beam could be induced, while in case where the anchor group suffered concrete cone failure (JT1-5), joint shear failure occurred. Also, it was observed that the most efficient retrofit solution is achieved when the anchor behaves almost in linear range. As the anchors lose stiffness (e.g. in case of JT1-6), the efficacy of the FFHRS to redistribute the forces reduces.

In order to verify the suitability of the FFHRS for retrofitting of the joints of structures when subjected to dynamic earthquake loading, an exact replica of the frame tested earlier was retrofitted with FFHRS using bonded anchors and tested under dynamic loads. The structure was tested on shake table with the same loading protocol as that of as built structure by subjecting the structure to gradually increasing levels of excitation. The crack patterns were marked at the end of each loading wave. Unlike the test on as built structure, no diagonal shear cracks were observed in the joint panels for the retrofitted structure clearly showing the efficacy of the FFHRS in safeguarding the beam-column joints. The crack patterns were limited to the crack formation in beams and columns, while the joint region was essentially crack free. Also, the cracks formed in beams and columns were only hair line cracks. No spalling was observed in the test. The measured shear deformation suggests no significant distortion of the joint as seen from the crack patterns too. The experiment clearly displayed that the structure retrofitted with the haunch retrofit solution behaved almost in linear fashion till the end of the test and successfully proved the efficacy of retrofit solution.

It was very interesting to note that in case of beam-column joints retrofitted with FFHRS, once a crack appears at the anchor location, it propagates and grows wider with each loading cycle, finally resulting in anchorage failure. Whereas, in case of the structure tested on shake table, even though the crack appeared at the anchor location during the PGA of 0.4g, the crack did not grow wider and the anchor group performed its function very well. It can be attributed to the fact that in case of structure subjected to dynamic loads, the probability of the anchor loaded to its maximum at the same time when the crack width is maximum, is very low (Sharma et al, 2010). Therefore, the performance of the anchors under dynamic loads is

much better than that under cyclic loads. The experiments clearly proved that FFHRS can be used as a practically viable alternative for the seismic retrofitting of poorly detailed beam-column joints.

Even though now it is well-known that the beam-column joints, especially the poorly designed ones, behave highly nonlinearly during the earthquakes, still the analysis approach mainly revolves around considering concentrated plasticity at the member ends and assuming the joint core as rigid. This is attributed to the fact that the models available in literature generally are not simple enough to be used in commercial programs being at the same time able to predict the shear behaviour of the joints nicely. Moreover, the models either require large computational efforts so that they are not practically useful for analyzing the global structural behaviour or they need a special element with various nodes and springs or a special purpose program to implement the joint nonlinearity. This makes it difficult for the designers and analysts to follow the recommended approaches using the commercial programs.

In this work, a new model for predicting the nonlinear shear behaviour of beam-column joints is suggested. The model was implemented in commercial software SAP2000. Special focus was on the shear resisting mechanism and corresponding deformational behaviour of the joint. The model is rational and straightforward in implementation in existing popular commercial programs for design and analysis of RC structures. The model is based on realistic deformational behaviour of the beam-column connections in existing structures and gives due consideration to axial load on column since it considers the principal stress in the joint as the failure criteria. The validation of the model with large number of test results shows excellent agreement between experiment and numerical results. The high risk of not modelling the joint is highlighted. The various advantages of the proposed joint model are:

1. The joint model predictions are very close to the experimentally observed shear behaviour of the beam-column connections.
2. It is shown that the same model is applicable for joints with un-symmetric detailing such as gravity designed and detailed joints with bottom beam bars only partially embedded in the joint and top beam bars bent in, a typical detailing pattern followed throughout the world before the advent of seismic design codes.
3. The joint model is based on realistic deformational behaviour of the joints in structures. This makes the model more appropriate for use in analysis compared to rotational hinge models that use only single rotational spring for modelling the joint.
4. The model considers the principal tensile stress as the parameter for strength of the joint. This has an upper hand over the models that use horizontal joint shear stress as the limiting parameter since they cannot give due consideration to the axial load on the column.
5. Although in this work, only the principal tensile stress and not the principal compressive stress is considered as a limiting criteria, but the same formulations can

be extended to provide an upper limit to maximum principal compressive stress in the joint.

6. The model is easily extendable to cover different kinds of joints namely interior joints, knee joints, corner joints etc. Only the principal stress v/s shear deformation plot has to be defined.
7. The model needs no special software or element for implementation in the existing commercial design and analysis software packages.
8. The extra effort required to model the joint behaviour in the program is minimal and the results give high accuracy.

However, there are certain limitations of the model:

1. The model needs principal stress v/s shear deformation as an input parameter from the user. This can be provided for different kinds of joints and detailing but needs good calibration in the beginning phase.
2. Currently the model uses an indirect and inadequate approach for modelling the bond failure just by reducing the principal stress and shear deformations. This needs an improvement.

The scope of further improvement of the model can be summarized as:

1. The model can be further investigated and validated for different types of joints.
2. Principal stress v/s shear deformation plot that is the core input parameter for the model is currently available for limited cases. A research work is needed to generate such plots for various kinds of joints and detailing so that they can be incorporated in the model.
3. The bond is currently only indirectly incorporated in the model. However, it can be more explicitly incorporated in a way that can consider the effect of bond deterioration on the characteristics of the joint. The approach recommended by Fillipou (1983, 1988), for example, may be used for the same.

In order to realistically simulate the seismic behaviour of non-seismically designed and detailed RC structures, it is essential to model the hysteretic behaviour of the frame members as well as beam-column joint panel region. In this work, new parameters to be used with an existing, simple and practical, pivot hysteretic model (Dowell et al, 1998) are proposed. The main parameters controlling the hysteretic model were first developed for rectangular columns with various levels of axial loads, different kinds of loading cycles, having different reinforcing details etc.

The new parameters for the pivot hysteretic model, improve the two aspects of the originally proposed pivot hysteretic model for circular RC columns (Dowell et al, 1998): (i) covering complete range of axial loads and (ii) considering the effect of transverse reinforcement in

controlling the pinching behaviour of rectangular RC columns. The model parameters were also proposed to model the hysteretic behaviour of poorly detailed RC joints. The hysteretic models for the columns and joints were first validated at the member and sub-assembly level and the same were then implemented and validated at the structural level under quasi-static-cyclic loads. It was shown that the model to consider the inelastic joint distortion along with the hysteretic parameters at the member and joint level could realize the experimental behaviour of the columns, joints and structures quite well. The conclusions on the extended pivot hysteretic model parameters can be summarized as under:

1. The parameters, within the framework of pivot model are able to nicely simulate the hysteretic behaviour of rectangular RC columns, beam-column joints and structures under seismic loads.
2. The model is capable of simulating the behaviour of members having un-symmetric sections, different reinforcing details, various levels of axial loads etc.
3. By modifying the way of defining parameters in the pivot model, the due consideration can be given to full range of axial loads as well as transverse reinforcement of members.
4. The hysteretic parameters proposed for the joints, when coupled with the joint model led to good predictions at the sub-assembly level. The hysteretic loops for the joints and therefore energy dissipation could be simulated quite well.
5. The hysteretic models for the members and joints combined with the inelastic springs modelled at structural level showed good resemblance with the experimental results for structure tested under seismic loads.

Although the model has several advantages as enlisted above, one major limitation of the model is that the hysteretic parameters require calibration. To define these parameters for the members is relatively easy as shown in this work and the equations proposed seem to cover the wide range of columns, the same is not the case for the joints. The data used for proposing the hysteretic parameters for the joints is limited. Moreover, for different types of detailing in the joint, these parameters will vary and therefore a calibration is required for different types of joints as well.

Using the above-mentioned models, the seismic behaviour of a non-seismically detailed structure can be assessed with high reliability and the exact locations requiring retrofitting can be known. A retrofitting using FFHRS can provide good solution to the retrofitting requirement in case where beam-column joints are critical, provided that the framing members have sufficient shear capacity to safely withstand the additional shear to come due to the retrofit. To verify the performance of the joints and thereby structure after retrofitting using FFHRS, an assessment model was presented in this work. The numerical analysis was performed using commercial software SAP2000.

In the tests, it was found that the efficiency of the retrofit solution depends highly on the performance of the anchorage system. It was clearly shown that if the anchorage system performs well, then a high efficiency of the haunch retrofit solution can be expected. Therefore, considering perfect connection of haunch element with frame members, ignoring nonlinear anchor behaviour can be quite unconservative. To include the behaviour of the FFHRS in the joint model, the modelling of stiffness and deformations in the anchor group were incorporated over the complete linear-nonlinear range. The model was validated against a number of experiments at sub-assembly level and also against shake table tests at structural level. It was concluded that the model can successfully simulate the inelastic seismic behaviour of joints and structures retrofitted with FFHRS.

In the end, the models developed and validated in this work were used to assess the seismic performance of a real life existing RC frame structure under as built condition. Based on the results of seismic assessment, a suitable and economical retrofit design was made and the structure was again assessed in retrofitted condition. The structure selected for was an existing residential building in New Delhi, India. It was found that the as built structure displayed shear failure of the beam-column joints typical of such non-seismically designed structures under seismic loads. The retrofit was suggested, which consisted essentially of using FFHRS to retrofit only the joints which displayed joint shear failures. Thus, the retrofitting design was very economical since only the most important locations were first determined and then attended to. The seismic assessment of the retrofitted structure displayed that with the suggested retrofitting the structure was able to perform much better under seismic loads with no major failure occurring at any location. The case study proved the suitability and applicability of the various models presented in this work for the correct seismic assessment and designing an efficient and economic retrofit.

Zusammenfassung (German Summary)

Seismisches Verhalten und Ertüchtigung von Stahlbetonrahmenkonstruktionen unter besonderer Berücksichtigung von Rahmenknoten - Experimente und numerische Modellierung

Kapitel 1: Einleitung

Das Kapitel stellt die Problemstellung und die Zielsetzung der Arbeit dar. Es stellt die Arbeit in den Kontext der aktuellen Forschung und gibt einen Überblick über den Aufbau der Arbeit.

Kapitel 2: Seismisches Verhalten von Rahmenknoten in Stahlbeton-Rahmenkonstruktionen

Das Seismische Verhalten von Rahmenknoten wird erläutert und die verschiedenen Verbindungen nach geometrischer Auslegung, Tragverhalten, Bewehrung und mechanischem Verhalten klassifiziert. Ein Schwerpunkt liegt dabei auf dem Verbund zwischen Bewehrungsstäben und Beton.

Kapitel 3: Literaturlauswertung

Um den aktuellen Stand der Technik darzustellen, wurde eine gründliche Literaturlauswertung durchgeführt. Der Focus der Analyse lag dabei auf den vorhandenen Vorhersagemodellen für die Schubfestigkeit der Knoten und der Simulation des Verhaltens von Stahlbetonrahmenknoten. Bei der Abwägung zwischen Genauigkeit und Anwendungsmöglichkeit in der Praxis, stellt der „average plane stress / plane strain“ Ansatz vorgeschlagen von Priestley (1997) einen praxisnahen und relativ genauen Ansatz dar. Da die Knoten-Element-Modelle, die auf praktische Versuche basieren, nicht aussagekräftig genug sind und die Federmodelle schwierig in der Anwendung und vor allem meistens nicht geeignet für die Anwendung von Knoten in nicht-seismisch ausgelegten Stahlbetonrahmen sind, ist es deshalb erforderlich ein realistisches Modell zu entwickeln, das nicht nur das Verhalten von unzureichend ausgelegten Knoten vorhersagen kann, sondern auch mit allgemeinen nichtlinearen Anwendungsprogrammen verwendet werden kann.

Kapitel 4: Das vorgeschlagene Knotenmodell

Ein neu entwickeltes Modell zur Vorhersage von nichtlinearen Schubverhalten von Rahmenknoten wird vorgestellt. Es ermöglicht eine vernünftige Beschreibung des Schubverhaltens der Knoten und kann mit im Handel erhältlichen Softwareprogrammen verwendet werden. Das Modell basiert auf dem Verformungsverhalten des Knotensystems im Tragwerk und den wichtigsten Bruchlastkriterien, so dass die zentrische Last in der Stütze untersucht werden kann.

Kapitel 5: Pivot-Hysterese-Modellparameter für Stäbe und Knoten

Um das seismische Verhalten von nicht seismisch bemessenen und ausgelegten Stahlbetonkonstruktionen realistisch zu simulieren, ist es notwendig das hysteretische Verhalten der Rahmenstäbe sowie des Rahmenknotenbereichs zu modellieren. Es werden hier Parameter für das Pivot-Hysterese-Modell vorgestellt um eine Anwendung für eine nichtlineare, dynamische Analyse von Stahlbetonrahmenkonstruktionen zu ermöglichen. Vorgeschlagen werden sowohl Parameter für die Analyse von rechtwinkligen Stahlbetonstäben, die die ganze zentrische Last abdecken, und der Querbewehrung, als auch Parameter um das hysteretische Verhalten von nicht-seismisch bemessenen Stahlbetonrahmenknoten zu beschreiben.

Kapitel 6: Bewertungsmodell für eine Ertüchtigung mit nachträglich befestigten Stahldiagonalen (Fully fastened haunch retrofit solution (FFHRS))

Ein numerisches Modell, um das nichtelastische, seismische Verhalten von FFHRS-ertüchtigten Knoten zu beschreiben wird vorgestellt. Das Modell beschreibt das nichtelastische Verhalten von nachträglich montierten Befestigungen, die zur Befestigung der Diagonalelemente mit den Stäben (Balken und Stützen) verwendet werden. Die Hypothesen und Parameter für dieses Modell werden ausführlich diskutiert.

Kapitel 7: Experimentelle Untersuchungen von Rahmenknoten

In diesem Kapitel werden die experimentellen Untersuchungen an nicht seismisch bemessenen Stahlbetonrahmenknoten beschrieben. Die durchgeführten Versuche an 5 Knoten stellen das Schubverhalten der Rahmenknoten dar. In allen Versuchen fand ein Knotenquerkraftversagen statt. Es zeigte sich deutlich ein Einfluss der unterschiedlichen Befestigungen der Bewehrungsstäbe im Knotenbereich auf das seismische Verhalten der Rahmenknoten. Die Untersuchungsergebnisse dienen auch als Referenzwerte zur Modellierung des Knotenmodells und des Bewertungsmodells für FFHRS.

Kapitel 8: Experimentelle Untersuchungen zum nichtelastischem Verhalten von Stahlbetonrahmenkonstruktionen

Im Rahmen dieser Arbeit wurde ein „Pushover“-Test an einem maßstabsgetreuen Stahlbetonnachbau eines Teils eines indischen Bürogebäudes durchgeführt. Die Versagensmuster zeigten die Anfälligkeit von Stahlbetonkonstruktionen mit nicht erdbebengerechter baulicher Durchbildung für Knotenquerkraftversagen, Verbundversagen etc. Die Einzelheiten des Versuchs werden im Kapitel erklärt.

Kapitel 9: Experimentelle Untersuchungen von Stahlbetonrahmen unter dynamischer Belastung (Shake Table Test)

Es werden Rütteltischversuche (Shake Table Tests) mit 2D Stahlbetonrahmen beschrieben. Um einen direkten Vergleich mit den Rahmenknotenversuchen (Kapitel 7) zu haben, wurden die Rahmen so gestaltet, dass die äußeren Knoten eine 2/3 Nachbildung der früher getesteten Rahmenknoten bildeten. Das Bauteil wurde auf dem Rütteltisch geprüft und mit

ansteigender Amplitude belastet. Risse waren am Ende jeder Belastungswelle sichtbar, woraus zu schließen ist, dass Knotenquerkraftversagen die vorherrschende Versagensart darstellte. Am Ende der Versuchsreihe traten offene Diagonalarisse in den Knoten auf. Das Versuchsprogramm zeigte deutlich die Anfälligkeit von nicht seismisch bemessenen Rahmenkonstruktionen bei Erdbebenbeanspruchung auf und konnte als Referenzbauteil herangezogen werden.

Kapitel 10: Experimentelle Untersuchungen zu mit nachträglich befestigten Stahldiagonalen ertüchtigten Rahmenknoten

In diesem Kapitel werden experimentelle Untersuchungen von Rahmenknoten beschrieben, die mit nachträglich befestigten Stahldiagonalen (FFHRS) ertüchtigt wurden. In allen Fällen wurden Rippenstäbe verwendet, die Rahmenendknoten in den Knotenkern gebogen. Es zeigte sich, dass die Effektivität des FFHRS im direkten Zusammenhang mit dem Tragverhalten der Ankergruppe steht, die die Diagonalelemente befestigt. In den Fällen, in denen die Ankergruppe ein gutes Tragverhalten aufwies, konnte ein duktiler Biegeversagen im Balken herbeigeführt werden, wogegen in den Fällen in denen die Ankergruppe mit Betonausbruch versagte, ein Knotenquerkraftversagen auftrat. Der größte Ertüchtigungseffekt konnte bei einem linearen Anstieg der Last auf die Ankergruppe beobachtet werden.

Kapitel 11: Experimentelle Versuche von Stahlbetonrahmen mit nachträglich befestigten Stahldiagonalen unter dynamischer Belastung

Wie in Kapitel 9 wurde der baugleiche Rahmen auf einem Rütteltisch mit der gleichen dynamischen Belastung getestet. Im Gegensatz zum nicht ertüchtigten Rahmen in Kapitel 9 traten hier keine Diagonalarisse auf, was sehr deutlich die Wirksamkeit von FFHRS zeigt. Die Rissmuster beschränkten sich auf Haarrisse in Balken und Stützen, die Rahmenknoten jedoch blieb überwiegend rissfrei. Es trat kein Spalten im Test auf.

Kapitel 12: Vergleich des vorgeschlagenen Knotenmodells mit den Versuchsergebnissen

Es wurde eine Analyse des vorgeschlagenen Knotenmodells (Kapitel 4) durchgeführt und den Versuchsergebnissen gegenübergestellt. Die Anwendbarkeit und die Effektivität des Modells mit Knotenfedern zur Simulation von nichtelastischem Knotenverhalten wurden deutlich, jedoch zeigte sich, dass das Modell ohne Knotenfedern auch Ergebnisse auf der höchst unsicheren Seite ergeben kann. Das Modell wurde sowohl auf der Bauteilebene als auch auf der konstruktiven Ebene angewendet.

Kapitel 13: Vergleich des Pivot-Hysterese Modells für Stäbe und Knoten mit den Versuchsergebnissen

Die Aussagekräftigkeit des Pivot-Hysterese Modells um das hysteretische Verhalten von Stäben, Knoten und Konstruktionen zu beschreiben, wird gezeigt. Die Modellparameter wurden mit den Versuchsergebnissen auf der Stabebene, Knotenebene und konstruktiven

Ebene verglichen. Beim Vergleich mit einer Vielzahl von eigenen und experimentellen und numerischen Ergebnissen aus der Literatur konnte eine gute Übereinstimmung erzielt werden. Es zeigte sich deshalb, dass sich das in dieser Arbeit verwendete numerische Modell gut für eine Simulation von seismischen Verhalten von nicht-seismisch bemessenen Konstruktionen eignet.

Kapitel 14: Vergleich des Bewertungsmodell für eine Ertüchtigung mit FFHRS mit den Versuchsergebnissen

Es wird nachgewiesen, dass das Modell für mit FFHRS ertüchtigte Knoten geeignet ist. Da keine anderen Versuchsergebnisse aus der Literatur verfügbar waren, wurde das Modell mit den Ergebnissen aus Kapitel 10 und 11 verglichen. Das Modell zeigt eine gute Übereinstimmung mit den Versuchsergebnissen. Die Anwendbarkeit des Modells zur Simulation von nichtlinearem Verhalten von mit FFHRS ertüchtigten Rahmenknoten wird somit deutlich.

Kapitel 15: Seismische Beurteilung und Ertüchtigung von bestehenden Stahlbetonrahmenkonstruktionen

Die in dieser Arbeit vorgestellten Modelle wurden bei einer seismischen Beurteilung einer bestehenden Stahlbetonrahmenkonstruktion angewendet. Basierend auf der seismischen Beurteilung wurde eine geeignete, ökonomisch sinnvolle Ertüchtigungslösung mit FFHRS entwickelt und das Bauwerk in ertüchtigten Zustand nochmals bewertet. Als Bauwerk für diese Beurteilung wurde ein Wohnhaus in Neu-Delhi ausgewählt, das nicht für eine seismische Beanspruchung ausgelegt wurde. Es zeigte sich, wie für nicht-seismisch bemessene Konstruktionen üblich, ein Schubversagen der Rahmenknoten. Diese versagenden Rahmenknoten wurden daraufhin mit FFHRS ertüchtigt, um so eine effiziente und ökonomisch sinnvolle Ertüchtigung durchzuführen. Die seismische Beurteilung des ertüchtigten Bauwerks zeigte kein größeres Versagen. Die Fallstudie macht deutlich, dass durch die in dieser Arbeit vorgestellten Modelle eine wirksame und ökonomisch sinnvolle Ertüchtigung ermöglicht wird.

Kapitel 16: Schlussfolgerungen und Ausblick

Das Kapitel fasst die wichtigsten Ergebnisse dieser Arbeit zusammen und gibt einen Überblick über offene Fragen und mögliche zukünftige Forschungsthemen.

REFERENCES

- ACI 318M-11, "Building Code Requirements for Reinforced Concrete", American Concrete Institute, Detroit, Michigan, 2011
- ACI 352R-02, "Recommendations for design of beam-column-joints in monolithic reinforced concrete structures", American Concrete Institute, ACI/ASCE, Committee 352, Detroit, 2002
- Alath, S. and Kunnath, S. K., "Modeling inelastic shear deformations in RC beam-column joints," Engineering Mechanics Proceedings of 10th Conference, May 21–24, University of Colorado at Boulder, Boulder, Colorado, ASCE, New York, 2, 822–825, 1995
- Altoontash, A., "Simulation and damage models for performance assessment of reinforced concrete beam-column joints," PhD Dissertation, Department of Civil and Environment Engineering, Stanford University, Stanford, California, 2004
- Anderson, J.C. and Townsend, W.H., "Models for RC frames with degrading stiffness", ASCE V.103, ST12, Dec 1977, pp 2361-2376
- Anderson, M., Lehman, D., and Stanton, J., "A cyclic shear stress–strain model for joints without transverse reinforcement", Engineering Structures 30 (2008) 941–954
- Appa Rao, G. Milinda A., Mahajan and Rolf Eligehausen, "Efficiency of seismic retrofit of RC beam-column joints", proceedings of Structural Engineering Convention (SEC-2005), 14-16 Dec, 2005, IISc Bangalore, India
- ATC-40, "Seismic Evaluation and Retrofit of Concrete Buildings", Report No. SSC 96-01, Applied Technology Council, California Seismic Safety Commission, California November 1996.
- Baker, A.L.L., and Amarakone, A.M.N., "Inelastic Hyperstatic Frames Analysis", Proceedings of the International Symposium on the Flexural Mechanics of Reinforced Concrete, ASCE-ACI, Miami, November 1964, pp. 85-142.
- Baker, A.L.L., "Ultimate load theory applied to the design of reinforced and prestressed concrete frames", Concrete publications ltd, London, 1956, 91 pp.
- Bakir, P. G., and Bodurođlu, H. M., "A New Design Equation for Predicting the Joint Shear Strength of Monotonically Loaded Exterior Beam-Column Joints," Engineering Structures, V. 24, 2002, pp. 1105-1117

Banon, H., Biggs, J., and Irvine, M., "Seismic damage in reinforced concrete frames", Journal of structural engineering, ASCE, 107 (ST9), 1981, 1713-1729

Belarbi, A., Hsu, T.T.C., "Constitutive Laws of Softened Concrete in Biaxial Tension-Compression", ACI Structural Journal, V. 92, No. 5, Sep.-Oct. 1995, pp. 562-573

Bertero, V.V., and Felippa, C., Discussion of "Ductility of Concrete" by H.E.H. Roy and M.A. Sozen, Proceedings of the international symposium on flexural mechanics of reinforced concrete, ASCE-ACI, Miami, November 1964, pp. 227-234.

Biddah, A. and Ghobarah, A. "Modelling of shear deformation and bond slip in reinforced concrete joints," Structural Engineering and Mechanics 7(4), 413-432 (1999)

Calvi, G.M., Magenes, G. and Pampanin, S. "Experimental Test on a Three Storey R.C. Frame Designed for Gravity Only", 12th European Conference on Earthquake Engineering, London, paper n. 727, 2002

Celik, O.C. and Ellingwood, E.R., "Modelling beam-column joints in fragility assessment of gravity load designed reinforced concrete frames" Journal of Earthquake Engineering, 12:357-381, 2008

CEN Technical Committee 250/SC8. Eurocode 8: Earthquake resistant design of structures – part 1: General rules and rules for buildings (ENV 1998-1-1/2/3), CEN, Berlin, Germany

Chan W.L., "The ultimate strength and deformation of plastic hinges in reinforced concrete frameworks," Magazine of Concrete research, Vol.7, No.21, Nov., 1955, pp. 121-132

Chopra, A.K., "Dynamics of Structures, Theory and Applications to Earthquake Engineering", Prentice Hall of India Pvt. Ltd., New Delhi, 2001

Clyde, C., Pantelides, C.P. and Reaveley, L.D., "Performance-based evaluation of exterior reinforced concrete building joints for seismic excitation" Report No. PEER 2000/05, Pacific Earthquake Engineering Research Center, July 2000

Comité Euro-International du Béton, "Bulletin d'Information No. 213/214 CEB-FIP Model Code 1990," London: Thomas Telford, 1993

Corley, W.G., "Rotational capacity of reinforced concrete beams, " Journal of structural division, ASCE, Vol. 92, ST5, October 1966, pp.121-146.

Costa, JLD, "Reinforced Concrete under Large Seismic Action", Report BYG-DTUR-076, 2003, ISSN 1601-2917, ISBN 87-7877-139-0, Danmarks Tekniske Universitet.

Dhakal, R.P., Pan, T.C., Irawan, P., Tsai, K.C., Lin, K.C., Chen, C.H., “Experimental study on the dynamic response of gravity-designed reinforced concrete connections” *Engineering Structures* 27 (2005) 75–87.

Dowell, R. K., Seible, F., and Wilson, E. L., “Pivot Hysteresis Model for Reinforced Concrete Members”, *ACI Structural Journal*, V. 95, No. 5, 1998, pp. 607-617.

El-Amoury, T., and Ghobarah, A., “Seismic rehabilitation of beam-column joint using GFRP sheets”, *Engineering Structures*, V. 24, 2002, pp. 1397-1407

Eligehausen, R., Mallée, R., and Silva, J., “Anchorage in Concrete Construction”, Wilhelm Ernst & Sohn, Berlin, 2006

Eligehausen, R., Ožbolt, J., Genesio, G., Hoehler, M. S and Pampanin, S. "Three-Dimensional Modelling of Poorly Detailed RC Frame Joints". Proceedings of the Annual NZSEE Conference, Napier, March 2006.

Eligehausen, R., Popov, E.P. and Bertero, V.V., Local Bond Stress-slip Relationships of Deformed Bars under Generalized Excitations, *Report UCB/EERC-83/19, Earthquake Engineering Research Center*, University of California, Berkeley, 1983, 178p.

Eligehausen, R., and Sharma, A., “Seismic Safety of Anchorages in Concrete Structures of Nuclear Power Plants” Proceedings, Post-SMiRT Conference Seminar on Advances in Seismic Design of Structures, Systems and Components of Nuclear Facilities, 2011, Mumbai

Elmorsi, M., Kianoush, M.R., and Tso, W.K., "Modeling bond-slip deformations in reinforced concrete beam-column joints", *Canadian Journal of Civil Engineering*, 27: 490-505, 2000

El-Metwally, S.E., and Chen, W.F., “Moment-Rotation Modeling of Reinforced Concrete Beam-Column Connections” *ACI Structural Journal* 85 (4), 1988, 384-394

ETAG 001 (1997), “Guideline for European Technical Approval of Metal Anchors for Use in Concrete (+Amendments)” Brussels: European Organisation for Technical Approvals (EOTA), 1997

EuroCode 2: “Design of concrete structures – Part1: General rules and rules for buildings”, DD ENV 1992.

Filippou, F.C., D'Ambrisi, A., and Issa, A., “Nonlinear static and dynamic analysis of reinforced concrete subassemblages” Report No. UCB/EERC–92/08, Earthquake Engineering Research Center, August 1992

Filippou, F.C., Issa, A., "Nonlinear analysis of reinforced concrete frames under cyclic load reversals" EERC Report No. UCB/EERC-88/12, September 1988.

Filippou, F.C., Popov, E.P. and Bertero, V.V., "Effects of bond deterioration on hysteretic behaviour of reinforced concrete joints" EERC Report No. UCB/EERC-83/19, August 1983.

Fuchs, W., Eligehausen, R., and Breen, J. E., "Concrete Capacity Design (CCD) approach for fastening to concrete" ACI Structural Journal 92 (1995), No. 1, pp. 73-94

Genesio (2012), "Seismic Assessment of RC Exterior Beam- Column Joints and Retrofit with Haunches Using Post-Installed Anchors", PhD Thesis, IWB, University of Stuttgart

Genesio, G., and Akgüzel, U., "Seismic retrofit for reinforced concrete exterior beam column joints using a fully fastened metallic haunch solution, Part 1: Feasibility study" Stuttgart: IWB, University of Stuttgart, 2009. Test Report No. WS 212/23 - 09/02

Genesio, G., and Sharma, A., „Seismic retrofit solution for reinforced concrete exterior beam-column joints using a fully fastened haunch - Part 2-1: As-built joints" Test Report No. WS 221/07 - 10/01, IWB, University of Stuttgart 2010

Genesio, G., and Sharma, A., "Seismic retrofit solution for reinforced concrete exterior beam-column joints using a fully fastened haunch - Part 2-2: Retrofitted joints" *Test report* No. WS 221/08 - 10/02, IWB, University of Stuttgart 2010

Ghobarah, A. and Biddah, A., "Dynamic analysis of reinforced concrete frames including joint shear deformation" Engineering Structures 21 (1999) 971–987

Ghobarah, A. and Said, A. "Shear strengthening of beam-column joints", Engineering Structures, 24 (2002), pp 881-888

Gill, W.D., Park, R. and Priestley, M.J.N., "Ductility of Rectangular Reinforced Concrete Columns with Axial Load," Department of Civil Engineering, Report 79-1, University of Canterbury, Christchurch, New Zealand, February 1979, 136 pp

Hakuto S, Park R, Tanaka H. Seismic load tests on interior and exterior beam-column joints with substandard reinforcing details. ACI Structural journal 2000; 97(1): 11-25.

Hegger, J., Sherif, A., and Roeser, W., "Non-seismic Design of Beam-Column Joints," ACI Structural Journal, V. 100, No. 5, Sept.-Oct. 2003, pp. 654-664

Hertanto, E., "Seismic assessment of pre-1970s reinforced concrete structure" Mater of engineering thesis, University of Canterbury, Christchurch, New Zealand, 2005

Hognestad, E., "A study of combined bending and axial load in reinforced concrete members," University of Illinois Engineering Experimental Station, Bulletin No.399, 1951, p.128.

Hwang SJ, Lee HJ. Analytical Model for Predicting Shear Strength of Exterior RC Beam-Column Joints for Seismic Resistance. *ACI Structural Journal*, V. 96, No. 5, Sept.-Oct. 1999, pp. 846-857

Hwang, S.J., Lee, H.J., Liao, T.F., Wang, K.C., Tsai, H.H., "Role of Hoops on Shear Strength of Reinforced Concrete Beam-Column Joints" *ACI Structural Journal*, V. 102, No. 3, May-June 2005, pp. 445-453

Hsu, T.T.C., "Softened truss model theory for shear and torsion," *ACI Structural Journal*, V. 85, No. 6, Nov.-Dec.1988, pp. 624-634

ICE Research Committee, "Ultimate load design of concrete structures", Proceedings of the Institution of Civil Engineers, Vol.21, February 1962, pp. 399-442

Ichinose, T., Interaction between Bond at Beam Bars and Shear Reinforcement in RC Interior Joints, Design of Beam-Column Joints for Seismic Resistance, SP-123, American Concrete Institute, Farmington Hills, Mich., 1991, pp. 379-400.

IS 456:2000, "Indian Standard plain and reinforced concrete - Code of Practice (Fourth Revision)", Bureau of Indian Standards, New Delhi, July 2000.

IS 456:1964, "Indian Standard plain and reinforced concrete - Code of Practice (Second Revision)", Bureau of Indian Standards, New Delhi, 1964.

IS 5525:1969, "Indian Standard recommendations for detailing of reinforcement in reinforced concrete works", Bureau of Indian Standards, New Delhi, September 1970.

IS 4326:1976, "Indian Standard earthquake resistant design and construction of buildings — code of practice", Bureau of Indian Standards, New Delhi, 1976.

IS 1893:1984, "Indian Standard criteria for earthquake resistant design of structures (Fourth Revision)", Bureau of Indian Standards, New Delhi, July 1986.

IS 4326:1993, Edition 3.2 (2002-2004) “Indian Standard earthquake resistant design and construction of buildings — code of practice (Second Revision)”, Bureau of Indian Standards, New Delhi, 2002.

IS 1893 (part1): 2002, “Indian Standard criteria for earthquake resistant design of structures, part 1 general provisions and buildings (Fifth Revision)”, Bureau of Indian Standards, New Delhi, June 2002.

IS 13920:1993, Edition 1.2 (2002-2003) “Indian Standard ductile detailing of reinforced concrete structures subjected to seismic forces — Code of Practice”, Bureau of Indian Standards, New Delhi, 2002.

IWB and Ožbolt, J., 2008, “MASA+ (Microplane Analysis Program), Finite Element Program for 3D Nonlinear Analysis of Concrete and Reinforced Concrete Structures”.

Joint ACI-ASCE Committee 352. Recommendations for design of beam-column joints in monolithic reinforced concrete structures. ACI Journal 1985; 82(3): 266-283.

Kent, D.C., and Park, R., “Flexural Mechanics with Confined Concrete”, Journal of the Structural Division, ASCE, Vol. 97, ST7, July 1971, pp. 1969-1990.

Kishimoto, I., Ohno, Y., Nishina, S., Nakagawa T., Iguchi T., Yamaguchi Y., “Flexural characteristics of RC columns with plastic hinges localized by much transverse reinforcement” 13th World Conference on Earthquake Engineering, 2004, Paper No. 1270

Kunnath, S.K., Reinhorn, A.M., and Park, Y.J., “Analytical Modeling of Inelastic Seismic Response of RC Structures,” Journal of Structural Engineering Division, ASCE, V. 116, No. 4, 1990, pp. 996-1017

Kunnath, S. K., Hoffmann, G., Reinhorn, A. M., and Mander, J. B. [1995a] “Gravity-load-designed reinforced concrete buildings — Part I: Seismic evaluation of existing construction,” ACI Structural Journal 92(3), 343–354.

Kunnath, S. K., Hoffmann, G., Reinhorn, A. M., and Mander, J. B. [1995b] “Gravity load-designed reinforced concrete buildings — Part II: Evaluation of detailing enhancements,” ACI Structural Journal 92(4), 470–478.

Kupfer, H., and Bulicek, H., “A consistent model for the design of shear reinforcement in slender beams with I- or Box-shaped cross section”, International workshop on concrete shear in earthquake, Houston, Tex., 1991, pp.256-265

Kupfer, H.B., and Gerstle, K.H., "Behaviour of concrete under biaxial stresses", Journal of the Engineering Mechanics Division, ASCE, 1973, pp. 853-866

Kurose, Y., "Recent studies on reinforced concrete beam-column joints in Japan" Austin, TX, University of Texas, 1987. PMFSEL Report No. 87-8

LaFave, J. M. and Shin, M. (2005) "Discussion of 'Modeling reinforced-concrete beam-column joints subjected to cyclic loading,' by Lowes, L. N. and Altoontash, A.," ASCE Journal of Structural Engineering **131**(6), 992–993

Leon, R. T. "Shear strength and hysteretic behavior of interior beam-column joints," ACI Structural Journal 87(1), 3–11, 1990.

Lettow, S., 2007, "Ein Verbundelement für nichtlineare Finite Elemente Analysen – Anwendung auf Übergreifungsstöße" *Dissertation, IWB Universität Stuttgart, Germany* (in German)

Li, B., Maekawa, K., and Okamura, H., "Modeling of shear transfer in concrete using contact density function", International workshop on concrete shear in earthquake, Houston, Tex., 1991, pp.226-235.

Liu, C., Pampanin, S., Dhakal, R., "Seismic Behaviour of Beam-Column Joint Subassemblies Reinforced With Steel Fibers" Master of Engineering Thesis, University of Canterbury, Christchurch, New Zealand, January, 2006

Lowes, L.N. and Altoontash, A. "Modeling Reinforced-Concrete Beam-Column Joints Subjected to Cyclic Loading", Journal of Structural Engineering, ASCE, pp. 1686 – 1697, December 2003

Lowes, L.N., Mitra, N. and Altoontash, A., "A beam-column joint model for simulating the earthquake response of reinforced concrete frames" Pacific Earthquake Engineering Research Center Report No. PEER 2003/10 Feb 2004

Mahajan, M. A., "Evaluation of shear strength and effective width of reinforced concrete exterior beam–column joints" PhD Thesis, IIT Madras 2009

Mahajan, M. A., Genesio, G., Eligehausen, R. "Numerical study on Interaction of Failure modes of Substandard Exterior RC Beam-Column Joints" Stuttgart: IWB, Universität Stuttgart, 2010. Research Report No. E10/15-BFT/15

Mahrenholtz, C., Eligehausen, R., and Sharma, A., "Behavior of post-installed concrete undercut anchors subjected to high loading rate and crack cycling frequency" 9th US National

and 10th Canadian Conference on earthquake engineering: Reaching beyond borders, session T14, 1589, 25th – 29th July 2010

Mahrenholtz, P., "Anchor Ductility – Development of Ductility Parameters and Evaluation of Data Base" Institut für Werkstoffe im Bauwesen, Universität Stuttgart, 2011

Mander, J.B., Priestley, M.J.N., and Park, R. (1988), *Theoretical stress-strain behavior of confined concrete*, Journal of Structural Engineering, Vol.114, No.8, pp 1804-1826.

Mattock, A.H., Discussion of "Rotational capacity of reinforced concrete beams" by W.G. Corley, Journal of structural division, ASCE, Vol. 93, ST2, April 1967, pp.519-522.

Mitra, N., and Lowes, L.N., "Evaluation, Calibration, and Verification of a Reinforced Concrete Beam-Column Joint Model," ACSE Journal of Structural Engineering, V. 133, No. 1, January 2007, pp. 105-120

Murty, CVR, Rai, D, Bajpai, KK, Jain, SK, "Effectiveness of reinforcement details in exterior reinforced concrete beam-column joints for earthquake resistance", ACI Structural journal 2003; 100(2): 149-156

Ohno, T., and Nishioka, T., "An Experimental Study on Energy Absorption Capacity of columns in Reinforced Concrete Structures," Proceedings of the JSCE, Structural Engineering/Earthquake Engineering, V. 1, No 2., 1984, pp. 137-147

Ortiz, I. R., "Strut-and-Tie Modeling of Reinforce Concrete Short Beams and Beam-Column Joints," PhD thesis, University of Westminster, 1993

Otani, S., "Inelastic analysis of RC frame structures" ASCE Journal of structural division, 1974, Vol. 100, No. ST 7 pp 1433-1449

Ožbolt, J. and Bažant, Z. P. (1992) "Microplane model for cyclic triaxial behavior of concrete" *Journal of Engineering Mechanics, ASCE*, 118, (7), 1365-1386.

Ožbolt, J., Li, Y.J., and Kožar, I., "Microplane Model for Concrete with Relaxed Kinematic Constraint", *International Journal of Solids and Structures* 38(2001), pp 2683-2711

Pampanin, S., Christopoulos, C., and Chen, T.H., "Development and validation of a metallic haunch seismic retrofit system for existing under-designed RC frame buildings" *Earthquake Engineering and Structural Dynamics*, 35, 2006, pp. 1739-1766.

Pampanin S, Magenes G, Carr A. Modelling of shear hinge mechanism in poorly detailed RC beam-column joints. Proceedings of the FIB 2003 Symposium, May 6-8, 2003 Athens, Greece

Pampanin, S., and Christopoulos, C., "Non-invasive retrofit of existing RC frames designed for gravity loads only", FIB Symposium on Earthquake Resistant Structures, 6-8 May, 2003, Athens, Greece

Pampanin, S., Moratti, M. and Calvi, G.M. "Seismic Behaviour of R.C. Beam-Column Joints Designed for Gravity Loads", 12th European Conference on Earthquake Engineering, London, paper n. 726, 2002

Pantelides, C.P., Hansen, J., Nadauld, J., and Reaveley, L.D., "Assessment of Reinforced Concrete Building Exterior Joints with Substandard Details" Report No. PEER 2002/18, Pacific Earthquake Engineering Research Center, May 2002

Pantazopoulou, S., and Bonacci, J., "Consideration of Questions about beam-column joints," ACI Structural Journal, V. 89, No. 1, Jan.-Feb. 1992, pp. 27-37

Park, R. and Paulay, T., "*Reinforced Concrete Structures*", John Wiley & Sons, New York, 1975.

Park, R., Priestley, M.J.N., and Gill, W.D., "Ductility of square-confined concrete columns," Journal of Structural Engineering, ASCE, Vol. 108, ST4, April 1982, pp 929-950

Park S, Mosalam KM. Shear Strength Models of Exterior Beam-Column Joints without Transverse Reinforcement. *PEER Report 2009/106*. Pacific Earthquake Engineering Research Center. University of California, Berkeley, November 2009

Parker, D. E. and Bullman, P. J. M., "Shear Strength within RC Beam-Column Joints," The Structural Engineer, V. 75, No. 4, Feb. 1997, pp. 53-57

Paulay, T. and Priestley, M.J.N., "Seismic Design of Reinforced Concrete and Masonry Buildings", John Wiley and Sons, New York, 1992.

Paulay T, Park R. Joints of reinforced concrete frames designed for earthquake resistance. Research report 84-9, department of civil engineering, University of Caterbury, Christchurch, 1984.

Paulay T, Park R, Priestley MJN. Reinforced concrete beam-column joints under seismic actions. ACI Journal 1978; 75-60: 585-593.

Popovics, S., "A review of Stress-Strain relationships for concrete," Journal of the American Concrete Institute, Proceedings, Vol.67, No.3, March, 1970, pp.243–248.

Popovics, S., "A numerical approach to the complete stress-strain curves for concrete," Cement and Concrete Research, Vol.3, No.5, September 1973, pp. 583-599.

Priestley MJN. Displacement based seismic assessment of reinforced concrete buildings. Journal of earthquake engineering 1997; 1(1): 157-192

Rangan, B. V., "Diagonal cracking strengths in shear of reinforced concrete beams", Civil Engineering Transactions, Institution of Engineers, Australia, Vol. CE 14, No. 1, 1972.

Rehm, G., and Eligehausen, R., "Einfluss einer nicht ruhenden belastung auf das Verbundverhalten von Rippenstaeben (Influence of repeated loads on the bond behavior of deformed bars)," Betonwerk-Fertigteile-Technik, Heft 6, 1977 (In German).

Russo, G and Somma, G., "A design formula for predicting the shear strength of exterior beam column joints under seismic loading" 13th World Conference on Earthquake Engineering, August 1-6, 2004, Paper No. 1282

Roy, H.E.H. and Sozen, M.A., "Ductility of Concrete", Proceedings of the International Symposium on the Flexural Mechanics of Reinforced Concrete, ASCE-ACI, Miami, November 1964, pp. 213-224.

Saatcioglu, M., Ghobarah, A. and Nistor, I., "Reconnaissance Report on the December 26, 2004 Sumatra Earthquake and Tsunami, CAEE ACGP.

Sargin, M., Ghosh, S.K. and Handa, V.K., "Effects of Lateral Reinforcement upon the Strength and Deformation Properties of Concrete", Magazine of Concrete research, Vol. 23, No. 75-76, June-September, 1971, pp. 99-110.

Sarsam, K.F. and Phipps, M.E., "The Shear Design of In-situ Reinforced Beam-Column Joints Subjected to Monotonic Loading," Magazine of Concrete Research, V. 37, No. 130, March 1985, pp. 16-28.

Sawyer, H.A., "Design of concrete frames for two failure states", proceedings of the International symposium on the flexural mechanics of reinforced concrete, ASCE-ACI, Miami, November 1964, pp. 405-431.

Scarpas A., "The inelastic behavior of earthquake resistant reinforced concrete exterior beam-column joints", Master of Engg Thesis, University of Canterbury, Christchurch, New Zealand, 1981

Scott, B.D., Park, R., and Priestley, M.J.N, "Stress-Strain Behavior of Concrete Confined by Overlapping Hoops at Low and High Strain Rates," *ACI Journal Proceedings*, V. 79, No. 1, Jan.-Feb. 1982, pp. 13-27

Scott, R.H., Feltham, I., and Whittle, R. T., "Reinforced Beam-Column Connections and BS 8110," *The Structural Engineer*, V. 72, No. 4, Feb. 1994, pp. 55-60

Sharma, A., Reddy, G.R., Vaze, K.K., and Eligehausen, R., "Pushover experiment and analysis of a full scale non-seismically detailed RC structure" *Int Jr Engg Struct*, Vol. 46, 2013, pp. 218-233

Sharma, A., Eligehausen, R. and Reddy, G.R., "A new model to simulate joint shear behavior of poorly detailed beam-column connections in RC structures under seismic loads, part I: exterior joints" *Engineering Structures*, 33, 2011, 1034-1051

Sharma, A., Genesio, G., Reddy, G.R., Eligehausen, R., Pampanin, S. and Vaze, K.K., "Experimental Investigations on Seismic Retrofitting of Reinforced Concrete Beam-Column Joints" *Proc. of 14th Sym on Earthq. Engg.*, IIT Roorkee, 2010, Paper No. A 007

Sharma, A., Genesio, G., Reddy, G.R., Eligehausen, R., "Nonlinear Dynamic Analysis Using Microplane Model For Concrete And Bond Slip Model For Prediction Of Behavior Of Non-Seismically Detailed RCC Beam-Column Joints, *Journal of Structural Engineering*, SERC, Vol. 36, No. 4, October-November 2009

Sharma, A., Reddy, G.R., Vaze, K.K., Ghosh, A.K., Kushwaha, H.S. and Eligehausen, R., "Investigations on Inelastic Behavior of Non-Seismically Detailed Reinforced Concrete Beam-Column Joints Under Cyclic Excitations", *BARC External Report No. BARC/2008/E/017*, October 2008

Sheikh, S.A., and Uzumeri, S.M., "Properties of concrete confined by rectangular ties," *AICAP-CEB Symposium on structural concrete under seismic actions*, Rome, May, 1979

Shin, M. and LaFave, J. M. "Testing and modelling for cyclic joint shear deformations in RC beam-column connections," *Proceedings of the Thirteenth World Conference on Earthquake Engineering*, August 1-6, 2004, Vancouver, B.C., Canada, Paper No. 0301

Shiohara, H. Quadruple flexural resistance in RC beam-column joints. *13th World Conference on Earthquake Engineering*, Canada, August 1-6, 2004, Paper No. 491

Sinha, B.P., Gerstle, K.H., and Tulin, L.G., "Stress-strain behaviour for concrete under cyclic loading," *Journal ACI*, Vol.61, No.2, February 1964, pp. 195-211.

Soleimani, D., Popov, E.p. and Bertero, V.V., "Nnlinear beam model for RC frame analysis", 7th ASCE conference on electronic computation, St Louis, August 1979

Soliman, M.T.M. and Yu, C.W., "The Flexural Stress-Strain Relationship of Concrete Confined by Rectangular Transverse Reinforcement", Magazine of Concrete research, Vol. 19, No. 61, December, 1967, pp. 223–238.

SP34: 1987, "Handbook on concrete reinforcement and detailing", Bureau of Indian Standards, New Delhi, August 1987.

Stevens NJ, Uzumeri SM and Collins MP. Reinforced concrete subjected to reversed cyclic shear-Experiments and constitutive model. ACI Structural journal 1991; 88(2): 135-146.

Takeda, T., Sozen, M. A. and Nielsen, N. N., "Reinforced concrete response to simulated earthquakes," J. Structural Engineering Division, ASCE, 1970, Vol. 96, No. 12, pp. 2257–2273

Taylor, H.P.J., "The Behavior of In-situ Concrete Beam-Column Joints," Technical Report 42.492, Cement and Concrete Association, Wexham Springs, UK, 1974

Townsend, W.H., and Hanson, R.D., "Hysteresis loops for reinforced concrete beam-column connections", Proceedings of 5th World conference on earthquake engineering, Rome, 1973, V.1, pp 1131-1134

Tsonos, A.G., "Cyclic load behaviour of reinforced concrete beam-column subassemblages of modern structures", ACI Structural journal 2007; 104(4): 468-478

Uma, S.R., Meher Prasad, A., "Seismic Behavior of Beam Column Joints in Reinforced Concrete Moment Resisting Frames", Document No.IITK-GSDMA-EQ31-V1.0, Department of civil engineering, IIT Kanpur, India

Vecchio, F. J. and Collins, M. P., "The modified-compression field theory for reinforced-concrete elements subjected to shear," Journal of the American Concrete Institute 83(2), 219–231, 1986

Vollum, R.L., "Design and Analysis of Exterior Beam Column Connections," *PhD thesis*, Imperial College of Science Technology and Medicine-University of London, 1998

Watanabe, F., and Lee, J.Y., "Theoretical prediction of shear strength and failure mode of reinforced concrete beams", ACI Structural Journal, V.95, No.6, November-December 1998, pp. 749-757.

Wong, H.F., "Shear Strength and Seismic Performance of Non-Seismically Designed RC Beam-Column Joints," PhD thesis, Hong Kong University of Science and Technology, 2005

Wong, H. F., Kuang, J. S., "Effects of beam-column depth ratio on joint seismic behavior" Structures and Buildings 161 (2008); No. 2, pp. 91-101

Youssef M. and Ghobarah A. "Modelling of RC beam column-joints and structural walls", Journal of Earthquake Engineering, Vol. 5, No.1 (2001) 93-111

Zhao, B., Taucer, F., and Rossetto, T., "Field investigation on the performance of building structures during the 12 May 2008 Wenchuan earthquake in China" Engineering Structures 31 (2009) 1707-1723

APPENDIX-A: GENERATION OF HINGE PROPERTIES FOR FRAME MEMBERS

A.1 Determination of Moment-Rotation Characteristics

Theoretical determination of moment-curvature characteristics for reinforced concrete sections with flexure and axial load is based on the following assumptions.

1. Plane sections before bending remain plane after bending.
2. Stress-strain curves for both concrete and steel are known.
3. Tension carrying capacity of concrete is neglected.

The curvatures associated with a range of bending moments and axial loads may be determined using these assumptions and from the requirements of strain compatibility and equilibrium of forces.

A.1.1 Stress Equilibrium and Strain Compatibility

Consider a reinforced concrete section as shown in Figure A.1 (a). Let the section be acted upon by an axial force ' P '. To determine its moment-curvature relationship, the first step is to assume a strain profile as shown in Figure A.1 (b). The strain profile can be fixed by assuming the strain at the extreme compression fiber ' ϵ_{cm} ' and the neutral axis depth ' kd '. Corresponding to the assumed strain profile, the distribution of concrete stress over the compressed part of the section is determined using the stress-strain curve for concrete (Figure A.1(c)). The strains in reinforcement at different levels can be determined from similar triangles of strain profile. For reinforcement bar ' i ' at a depth ' d_i ', the strain ' ϵ_{si} ' is given by

$$\epsilon_{si} = \epsilon_{cm} \frac{kd - d_i}{kd} \quad (\text{A.1})$$

The stresses $f_{s1}, f_{s2}, f_{s3} \dots$ corresponding to strains $\epsilon_{s1}, \epsilon_{s2}, \epsilon_{s3} \dots$ may then be found from stress-strain curve for reinforcing steel. The steel compressive forces, C_s or tensile forces, T_s may be found by multiplying steel stresses and the areas of steel.

$$C_{si} \text{ or } T_{si} = f_{si} A_{si} \quad (\text{A.2})$$

To determine the concrete compressive force, C_{con} and its position from extreme compression fiber, γkd the stress block of concrete is converted to an equivalent rectangular stress block having width equal to mean stress, $\alpha f_c'$ and depth kd .

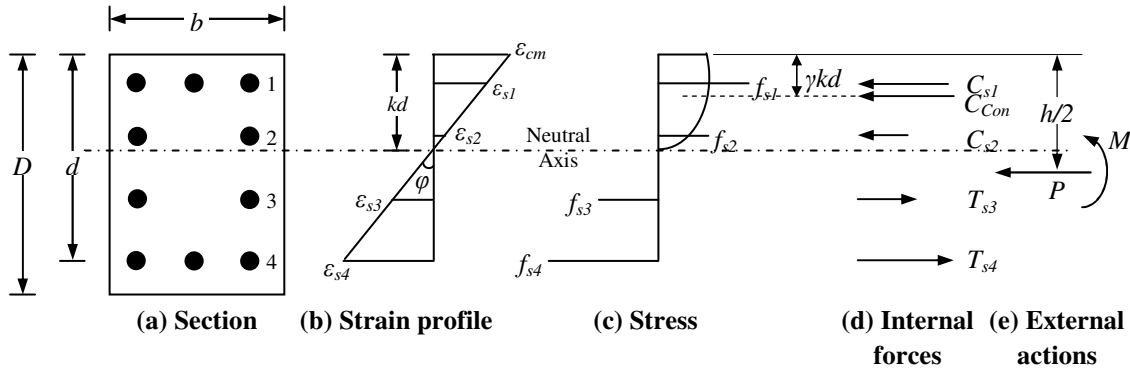


Figure A.1 Theoretical moment-curvature determination

The stress block parameters α and γ are calculated so that the total compressive force C_{con} and its point of application from extreme compression fiber, γkd are same for both the actual stress block and equivalent rectangular stress block. The mean stress factor, α and the centroid factor, γ for any strain ϵ_{cm} at the extreme compression fiber can be determined for rectangular sections from the stress-strain relationship as follows

$$\text{Area under stress-strain curve} = \int_0^{\epsilon_{cm}} f_c d\epsilon_c = \alpha f'_c \epsilon_{cm}$$

$$\therefore \alpha = \frac{\int_0^{\epsilon_{cm}} f_c d\epsilon_c}{f'_c \epsilon_{cm}} \quad (\text{A.3})$$

First moment of area about origin of area under stress-strain curve

$$= \int_0^{\epsilon_{cm}} f_c \epsilon_c d\epsilon_c = (1 - \gamma) \epsilon_{cm} \int_0^{\epsilon_{cm}} f_c d\epsilon_c$$

$$\therefore \gamma = 1 - \frac{\int_0^{\epsilon_{cm}} \epsilon_c f_c d\epsilon_c}{\epsilon_{cm} \int_0^{\epsilon_{cm}} f_c d\epsilon_c} \quad (\text{A.4})$$

The compressive force in concrete is given by

$$C_{con} = \alpha f'_c bkd \quad (\text{A.5})$$

acting at a distance of γkd from the extreme compression fiber.

The force equilibrium equations can be written as

$$P = \alpha f_c' bkd + \sum_{i=1}^n f_{si} A_{si} \quad (\text{A.6})$$

and

$$M = \alpha f_c' bkd \left(\frac{D}{2} - \gamma kd \right) + \sum_{i=1}^n f_{si} A_{si} \left(\frac{D}{2} - d_i \right) \quad (\text{A.7})$$

Where,

n = Number of reinforcement bars

f_{si} = Stress in the i^{th} bar

A_{si} = Area of i^{th} bar

D = Total depth of section

d = Effective depth of the section

d_i = depth of i^{th} bar from extreme compression fiber

The corresponding curvature is given by

$$\varphi = \frac{\varepsilon_{cm}}{kd} \quad (\text{A.8})$$

The theoretical moment-curvature relationship for a given axial load level may be determined by incrementing the concrete strain at the extreme compression fiber, ε_{cm} . For each value of ε_{cm} the neutral axis depth kd that satisfies the force equilibrium is found by adjusting kd until equation (A.6) is satisfied. For the flexure only case, $P = 0$. The moment M corresponding to the assumed ε_{cm} is then calculated using equation (A.7). The corresponding curvature is given by equation (A.8). By carrying out the calculation for a range of ε_{cm} values, the moment-curvature characteristics can be plotted.

A.1.2 Constitutive laws

The equivalent stress block parameters are calculated using equation (A.3) and (A.4) for different values of ε_{cm} depending on which stress-strain model for concrete do we consider. Various stress-strain models for concrete that can be followed are enlisted below for convenience. The models are subdivided as models for unconfined concrete and models for confined concrete.

A.1.2.1 Stress-Strain models for unconfined concrete

Many models for the stress-strain curve of concrete under uniaxial compression have been proposed in past years. Probably the most popular accepted curve is that proposed by Hognestad (1951) (Figure A.2), which consists of a second order parabola up to the

maximum stress f_c'' at a strain ε_0 and then a linear falling branch. The extent of falling branch behavior adopted depends on useful concrete strain assumed as 0.0038.

The corresponding stress was proposed to be $0.85f_c''$. Hognestad's curve was obtained from tests on short eccentrically loaded columns and for these specimens he found that $f_c''=0.85f_c'$. Other proposed stress-strain models for unconfined concrete are summarized elsewhere (Popovics1970). Indian Standard (IS 456:2000) recommends a stress-strain curve very similar to the Hognestad's curve (Figure A.3)).

In IS recommended curve (Fig 5.3), the maximum stress, f_c'' of concrete is assumed as 0.67 times the characteristic cube strength of concrete (f_{ck}). Assuming that cylinder strength is 0.8 times the characteristic cube strength, i.e. $f_c' = 0.8f_{ck}$, this becomes same as Hognestad's value of f_c'' . The ascending curve is exactly similar to that of Hognestad's model assuming $\varepsilon_0=0.002$. The major difference between the two curves is in the post peak behavior. IS456 (2000) recommends no degradation and hence no falling branch in the stress after a strain of 0.002. The ultimate strain is also limited to 0.0035 instead of 0.0038 as recommended by Hognestad (1951).

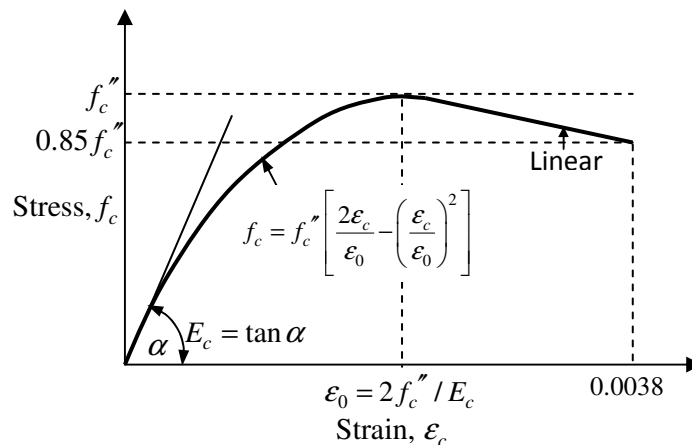


Figure A.2 Hognestad stress-strain model for concrete

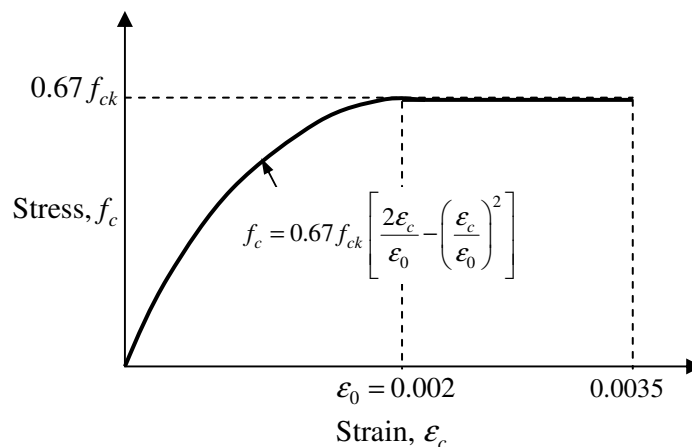


Figure A.3 IS456:2000 recommended stress-strain model for concrete

A.1.2.2 Stress-Strain models for concrete confined by rectangular hoops

In practice, the concrete in structures is always confined by transverse reinforcement commonly in the form of closely spaced steel spirals or rectangular hoops. In this case, at low levels of stress in concrete, the transverse reinforcement is hardly stressed; hence the concrete is unconfined. The concrete becomes confined when at stresses approaching the uniaxial strength, the transverse strains become very high because of progressive internal cracking and the concrete bears out against the transverse reinforcement, which then applies a confining reaction to the concrete. Thus the transverse reinforcement provides passive confinement (Park and Pauley 1975).

Although circular spirals confine concrete much more effectively than rectangular or square hoops, they are rarely used, mainly due to the fact that rectangular sections are more popular in reinforced concrete structural members. Nevertheless, square-confining steel does produce a significant increase in ductility, however, some investigators have observed enhancement of strength whereas some have not.

The confinement by transverse reinforcement has little effect on the stress-strain curve until the concrete reaches its maximum stress. The shape of the stress-strain curve at high strains is a function of many variables, the major ones being the following:

1. The ratio of the volume of transverse steel to the volume of concrete core, because a high transverse steel content will mean a high transverse confining pressure.
2. The yield strength of the confining steel, because this gives an upper limit to the confining pressure.
3. The ratio of the spacing of the transverse steel to the dimensions of the concrete core, because a smaller spacing leads to more effective confinement.
4. The ratio of the diameter of the transverse bars to the unsupported length of the transverse bar, because a large bar diameter leads to more effective confinement. If the flexural stiffness of the hoop bar is small (small diameter compared to unsupported length), the hoops bow outward rather than effectively confining the concrete.
5. The content and size of longitudinal reinforcement, because this steel will also confine the concrete.
6. The strength of the concrete, because low-strength concrete is more ductile than high-strength concrete.

Some of the proposed stress-strain curves for concrete confined by rectangular hoops are shown in Figure A.4.

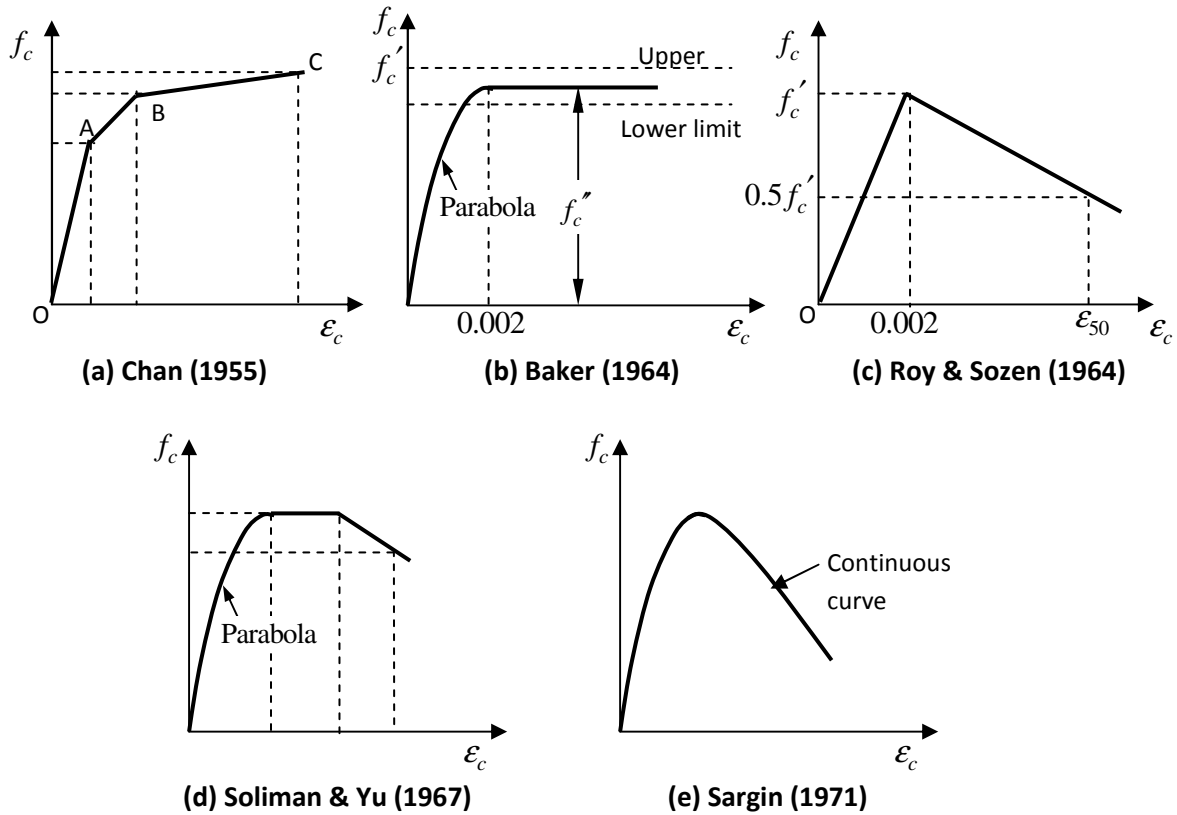


Figure A.4 Stress-strain curves for concrete confined by rectangular hoops

In Chan's (1955) trilinear curve (Figure A.4 (a)) OAB approximated the curve for unconfined concrete and the shape of BC depended on the transverse reinforcement. Baker (Baker and Amarakone 1964) recommended a parabola up to a maximum stress (Figure A.4 (b)), then a horizontal branch to a maximum strain. The maximum stress is dependent on the strain gradient across the section, and the maximum strain is dependent on the strain gradient as well as the transverse steel content.

Roy and Sozen (1964) conducted tests on axially loaded prisms and suggested replacing the falling branch with a straight line having a strain at $0.5f'_c$, which was linearly related to the transverse steel content (Figure A.4 (c)). It is also of interest to note that the tests of Roy and Sozen (1964) indicated that confinement by rectangular hoops did not increase the concrete strength. The curve of Soliman and Yu (1967) consists of a parabola and two straight lines (Figure A.4 (d)). The stresses and strains at the critical points are related to transverse steel content and spacing and the confined area. Sargin et al (1971) have proposed a general equation that gives a continuous stress-strain curve (Figure A.4 (e)) related to the content, spacing and yield strength of the transverse steel, the strain gradient across the section and concrete strength. All of these models do consider the effect of confinement, but they all are having some inherent limitations, mainly because of the simplicity associated with these models. These models will not be discussed further.

A.1.2.3 Kent and Park Model

In 1971, Kent and Park (1971) proposed a stress-strain curve for concrete confined by rectangular hoops (Figure A.5). The suggested relationship combines many of the features of previously proposed curves. A second-degree parabola represents the ascending part of curve and assumes that the confining steel has no effect on the shape of this part of curve or the strain at maximum stress. This essentially means that the ascending curve is exactly the same for both confined and unconfined concrete.

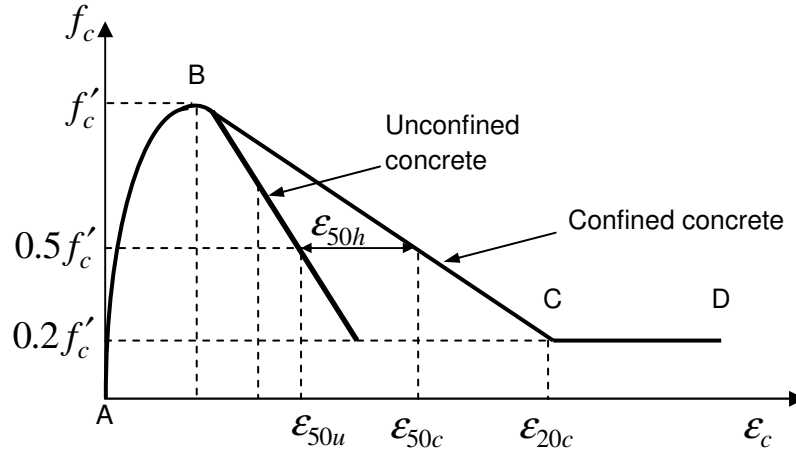


Figure A.5 Kent and Park (1971) model for Stress-strain curve for confined concrete

It is also assumed that the maximum stress reached by confined concrete is equal to the cylinder strength f'_c that is reached at a strain of 0.002. The relationship for the ascending parabola is given as

Region AB, $\varepsilon_c \leq 0.002$

$$f_c = f'_c \left[\frac{2\varepsilon_c}{0.002} - \left(\frac{\varepsilon_c}{0.002} \right)^2 \right] \quad (\text{A.9})$$

The descending part of the confined concrete is modeled as per following formulations.

Region BC, $0.002 \leq \varepsilon_c \leq \varepsilon_{20,c}$

$$f_c = f'_c [1 - Z(\varepsilon_c - 0.002)] \quad (\text{A.10})$$

Where,

$$Z = \frac{0.5}{\varepsilon_{50u} + \varepsilon_{50h} - 0.002} \quad (\text{A.11})$$

$$\epsilon_{50u} = \frac{3 + 0.002 f'_c}{f'_c - 1000} \quad (\text{A.12})$$

$$\epsilon_{50h} = \frac{3}{4} \rho_s \sqrt{\frac{b''}{s_h}} \quad (\text{A.13})$$

f'_c = Concrete cylinder strength in psi.

ρ_s = Ratio of volume of transverse reinforcement to volume of concrete core measured to outside of hoops, i.e.

$$\rho_s = \frac{2(b'' + d'')A_s}{b''d''s_h} \quad (\text{A.14})$$

A_s = Cross-sectional area of the stirrup reinforcement

b'' = Width of confined core measured to outside of hoops

d'' = Depth of confined core measured to outside of hoops

s_h = Spacing of hoops

Figure A.6 shows the various parameters and symbols.

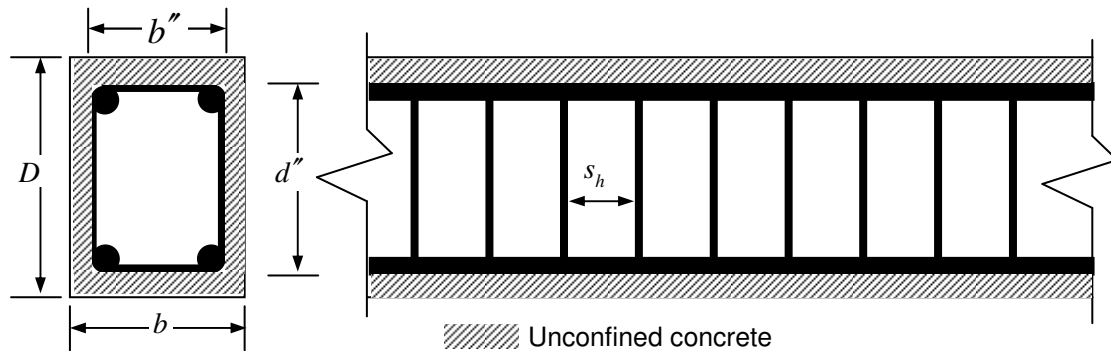


Figure A.6 Transverse confining steel in members

The parameter Z defines the slope of the assumed linear falling branch. ϵ_{50u} is the value of the strain when the stress has fallen to $0.5f'_c$ (50% of the strength is lost) for the case of unconfined concrete. The corresponding value of strain for confined concrete is ϵ_{50c} . ϵ_{50h} is the additional ductility due to transverse reinforcement ($\epsilon_{50c} = \epsilon_{50u} + \epsilon_{50h}$). It is assumed that the cover concrete has spalled off by the time the stress had fallen to $0.5f'_c$.

Region CD, $\epsilon_c \geq \epsilon_{20,c}$

$$f_c = 0.2 f'_c \quad (\text{A.15})$$

This equation accounts for the ability of concrete to sustain some stresses at very large strains.

A.1.2.4 Modified Kent and Park Model

In 1982, a modified form of Kent and Park model was proposed (Park et al, 1982). This model makes an allowance for the enhancement in the concrete strength due to confinement. Figure A.7 shows the modified Kent and Park model.

The maximum stress (at point B) is assumed to be Kf'_c at a strain of $\epsilon_0 = 0.002K$, where,

$$K = 1 + \frac{\rho_s f_{yh}}{f'_c} \quad (\text{A.16})$$

f_{yh} = yield strength of steel hoops.

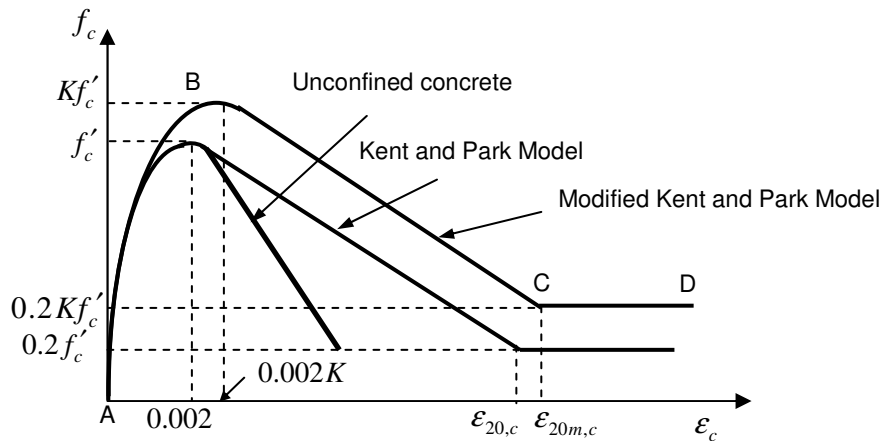


Figure A.7 Modified Kent and Park model for stress-strain curve for confined concrete

The modified Kent and Park stress-strain curve can be defined as

Region AB, $\epsilon_c \leq 0.002K$

$$f_c = Kf'_c \left[\frac{2\epsilon_c}{0.002K} - \left(\frac{\epsilon_c}{0.002K} \right)^2 \right] \quad (\text{A.17})$$

Region BC, $0.002K < \epsilon_c < \epsilon_{20m,c}$

$$f_c = Kf'_c [1 - Z_m (\epsilon_c - 0.002K)] \geq 0.2Kf'_c \quad (\text{A.18})$$

Where

$$Z_m = \frac{0.5}{\frac{3 + 0.29f'_c}{145f'_c - 1000} + \frac{3}{4}\rho_s\sqrt{\frac{b''}{s_h}} - 0.002K} \quad (\text{A.19})$$

f'_c = Concrete cylinder strength in N/mm²

Region CD,

$$f_c = 0.2Kf'_c \quad (\text{A.20})$$

This equation accounts for the ability of concrete to sustain some stresses at very large strains.

A.1.3 Evaluation of stress block parameters

The stress block parameters depend on whether ϵ_{cm} lies in zone AB, BC or CD of Kent and Park model or modified Kent and Park model (considered in this case). For different levels of extreme compression fiber strain, ϵ_{cm} the stress blocks are shown in Figure A.8 (b). The equivalent rectangular stress block is shown in Figure A.8 (c). The values of α and γ is different for different levels of ϵ_{cm} .

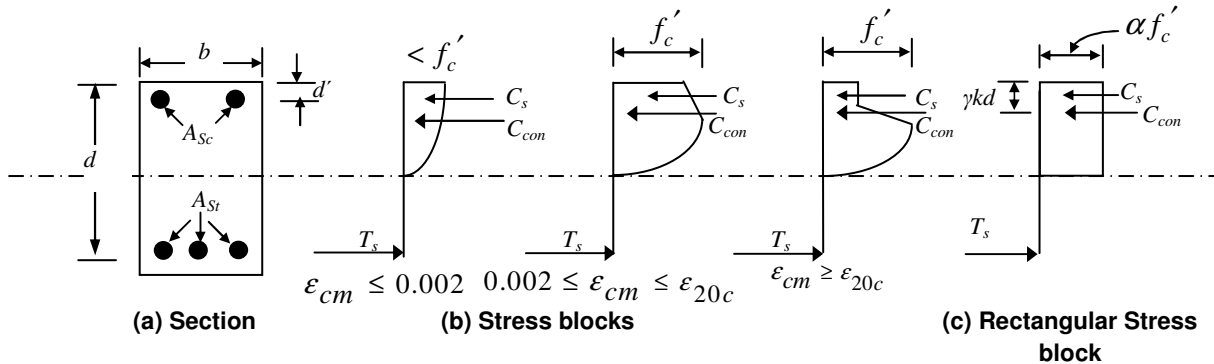


Figure A.8 Stress blocks at different extreme compression fiber strain

1. Stress block parameters for **Kent and Park** model

Region 'AB': $\epsilon_{cm} \leq 0.002$

$$\alpha = \frac{\epsilon_{cm}}{0.002} \left[1 - \frac{\epsilon_{cm}}{0.006} \right] \quad (\text{A.21})$$

$$\gamma = 1 - \frac{\left[\frac{2}{3} - \left(\frac{\varepsilon_{cm}}{0.008} \right) \right]}{\left[1 - \left(\frac{\varepsilon_{cm}}{0.006} \right) \right]} \quad (\text{A.22})$$

Region 'BC': $0.002 \leq \varepsilon_{cm} \leq \varepsilon_{20,c}$

$$\alpha = \frac{1}{\varepsilon_{cm}} \left[\frac{0.004}{3} + (\varepsilon_{cm} - 0.002) - \frac{Z}{2} (\varepsilon_{cm} - 0.002)^2 \right] \quad (\text{A.23})$$

$$\gamma = 1 - \frac{1}{\varepsilon_{cm}} \left[\frac{\left[\left(\frac{\varepsilon_{cm}^2}{2} - \frac{(0.002)^2}{12} \right) - Z \left(\frac{\varepsilon_{cm}^3}{3} - 0.001\varepsilon_{cm}^2 + \frac{(0.002)^3}{6} \right) \right]}{\left[\left(\varepsilon_{cm} - \frac{0.002}{3} \right) - Z \left(\frac{\varepsilon_{cm}^2}{2} - 0.002\varepsilon_{cm} + \frac{(0.002)^2}{2} \right) \right]} \right] \quad (\text{A.24})$$

Region 'CD': $\varepsilon_{cm} > \varepsilon_{20,c}$

$$\alpha = \frac{1}{\varepsilon_{cm}} \left[\frac{0.004}{3} + \frac{0.32}{Z} + 0.2\varepsilon_{cm} - 0.0004 \right] \quad (\text{A.25})$$

$$\gamma = 1 - \frac{1}{\varepsilon_{cm}} \left[\frac{1.2667 \times 10^{-6} + \frac{0.00064}{Z} + \frac{0.8^3}{6Z^2} + 0.1\varepsilon_{cm}^2}{\frac{0.004}{3} - \frac{0.32}{Z} + 0.2\varepsilon_{cm} - 0.0004} \right] \quad (\text{A.26})$$

2. Stress block parameters for **Modified Kent and Park** model

Region 'AB': $\varepsilon_{cm} \leq 0.002K$

$$\alpha = \frac{\varepsilon_{cm}}{0.002K} \left[1 - \frac{\varepsilon_{cm}}{0.006K} \right] \quad (\text{A.27})$$

$$\gamma = 1 - \frac{\left[\frac{2}{3} - \left(\frac{\varepsilon_{cm}}{0.008K} \right) \right]}{\left[1 - \left(\frac{\varepsilon_{cm}}{0.006K} \right) \right]} \quad (\text{A.28})$$

Region 'BC': $0.002K \leq \varepsilon_{cm} \leq \varepsilon_{20m,c}$

$$\alpha = \frac{1}{\varepsilon_{cm}} \left[\frac{0.004K}{3} + (\varepsilon_{cm} - 0.002K) - \frac{Z_m}{2} (\varepsilon_{cm} - 0.002K)^2 \right] \quad (\text{A.29})$$

$$\gamma = 1 - \frac{1}{\varepsilon_{cm}} \left[\frac{\left[\left(\frac{\varepsilon_{cm}^2}{2} - \frac{(0.002K)^2}{12} \right) - Z_m \left(\frac{\varepsilon_{cm}^3}{3} - 0.001K\varepsilon_{cm}^2 + \frac{(0.002K)^3}{6} \right) \right]}{\left[\left(\varepsilon_{cm} - \frac{0.002K}{3} \right) - Z_m \left(\frac{\varepsilon_{cm}^2}{2} - 0.002K\varepsilon_{cm} + \frac{(0.002K)^2}{2} \right) \right]} \right] \quad (\text{A.30})$$

Region 'CD': $\varepsilon_{cm} > \varepsilon_{20m,c}$

$$\alpha = \frac{1}{\varepsilon_{cm}} \left[\frac{0.004K}{3} + \frac{0.32}{Z_m} + 0.2K\varepsilon_{cm} - 0.0004K \right] \quad (\text{A.31})$$

$$\gamma = 1 - \frac{1}{\varepsilon_{cm}} \left[\frac{1.2667 \times 10^{-6} K^2 + \frac{0.00064K}{Z_m} + \frac{0.8^3}{6Z_m^2} + 0.1\varepsilon_{cm}^2}{\frac{0.004K}{3} - \frac{0.32}{Z_m} + 0.2K\varepsilon_{cm} - 0.0004K} \right] \quad (\text{A.32})$$

A.1.4 Algorithm for moment-curvature determination

The following steps shall be carried out to determine moment-curvature characteristics for a given section and axial load.

1. Assume a value of concrete strain at the extreme compression fiber, ε_{cm} .
2. Assume a value of neutral axis depth, kd .
3. Calculate stress block parameters α and γ for assumed value of ε_{cm} using appropriate equation based on the region in which ε_{cm} lies and assumed stress-strain model.
4. Calculate total compressive force in concrete, C_{con} .
5. Calculate strains at different levels of steel and find the corresponding stresses in reinforcement bars using the stress-strain curve for steel.
6. Calculate the compressive (C_{si}) and tensile (T_{si}) forces in reinforcement bars.

7. Check whether the force equilibrium condition is satisfied.
8. If equilibrium is satisfied then the assumed value of kd is correct. Else assume a new value of kd and Go To step 4.
9. Calculate the moment of resistance, M , and the corresponding curvature, φ .
10. Repeat steps 1 to 9 for a range of ε_{cm} .
11. Plot M - φ curve.

A.1.5 Determination of moment-rotation from moment-curvature characteristics

Curvature is defined as rotation per unit length of the member. Therefore, the rotation of a member may be calculated by integrating the curvatures along the length of the member. The rotation between any two points A and B of the member is given by

$$\theta_{AB} = \int_A^B \varphi dx \quad (\text{A.33})$$

where dx is an element of length of the member.

Since $\varphi = M/EI$, we have,

$$\theta_{AB} = \int_A^B \frac{M}{EI} dx \quad (\text{A.34})$$

This is a generalization of first moment-area theorem and it applies to both elastic and plastic curvatures. These equations can be used to calculate rotation of a member if we know the moment-curvature characteristics and the distribution of bending moment.

A.1.5.1 Relationship between curvature and rotation

Consider a cantilever beam subjected to a concentrated load at its free end as shown in Figure A.9 (a). The bending moment diagram and the curvature distribution within elastic range are shown in Figure A.9 (b) and (c) respectively.

From equation (A.34), we get,

$$\theta_{AB} = \int_0^L \frac{M_x}{EI} dx = \int_0^L \frac{Px}{EI} dx \quad (\text{A.35})$$

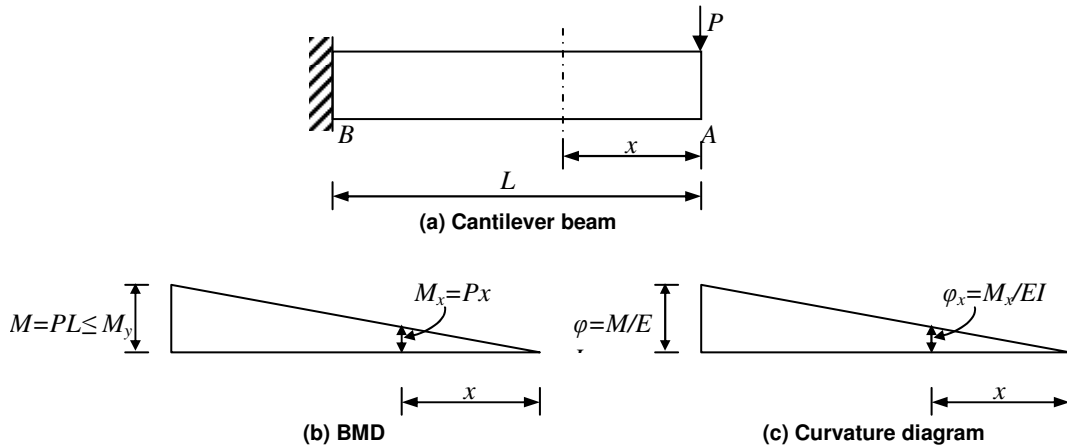


Figure A.9 Cantilever beam and its curvature distribution within elastic range

Since P and EI are constant (within elastic range), we get,

$$\theta_{AB} = \frac{PL^2}{2EI} = \frac{ML}{2EI} = \frac{\phi L}{2} \quad (\text{A.36})$$

Equation (A.36) is valid till the beam is within elastic range, i.e., up to yield point. Therefore we have, yield rotation,

$$\theta_y = \frac{\phi_y L}{2} \quad (\text{A.37})$$

For the reinforced concrete member that has reached the ultimate curvature and bending moment at critical section, the curvature distribution is no more linear, owing to the cracking in the member. Figures A.10 (a), (b) and (c) show a cantilever beam, its bending moment diagram and curvature distribution respectively at ultimate moment.

As can be seen, the region of inelastic curvature is spread over a length of the beam. This region is that, where the bending moment exceeds the yield moment of the section. The curvature fluctuates because of the increased rigidity of the member between the cracks. The rotation of the member at the ultimate condition can be obtained from the actual curvature distribution using equation (A.33). Since the curvature distribution along the length of the member is complex, it is very difficult to use equation (A.33) to calculate the rotation. Therefore, the curvature diagram is idealized as shown by dotted line in Figure A.10 (c).

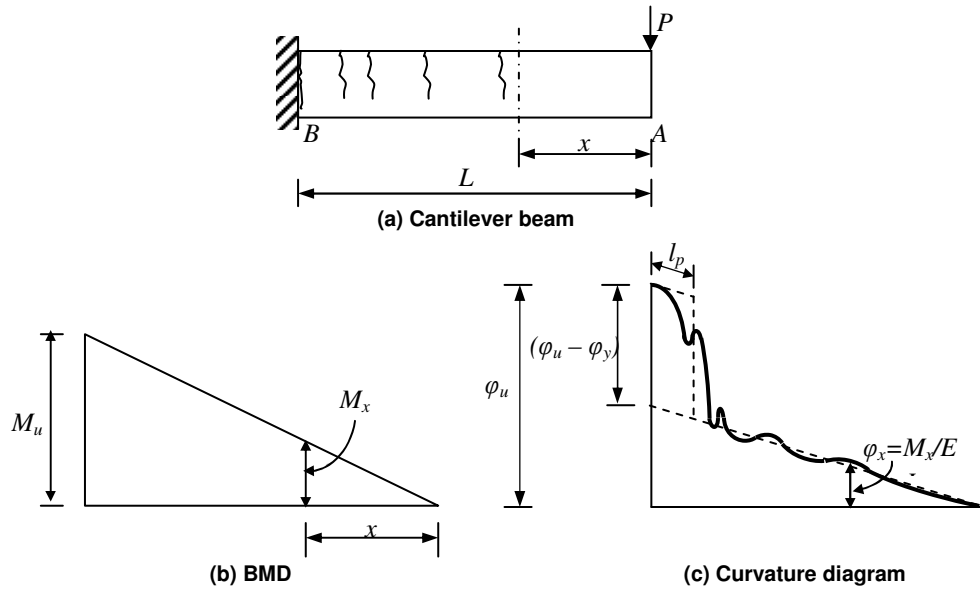


Figure A.10 Cantilever beam and its curvature distribution at ultimate moment

The inelastic area at the ultimate stage can be replaced by an equivalent rectangle having height equal to $(\varphi_u - \varphi_y)$ and width equal to the plastic hinge length, l_p . The plastic hinge length, l_p is the equivalent length of the plastic hinge over which the plastic curvature is assumed to be constant. The width l_p is so chosen that the area of the assumed rectangle is equal to that of the actual inelastic curvature distribution. Therefore, the plastic rotation is given as

$$\theta_p = (\varphi_u - \varphi_y) l_p \quad (\text{A.38})$$

The total rotation at the ultimate moment is given as

$$\theta_u = \theta_y + \theta_p \quad (\text{A.39})$$

Therefore, for a cantilever beam as shown,

$$\theta_u = \varphi_y \frac{L}{2} + (\varphi_u - \varphi_y) l_p \quad (\text{A.40})$$

As seen by above equations, if the moment-curvature characteristics and the geometry of the member are known, the only unknown to determine the moment-rotation characteristics is the plastic hinge length, l_p .

A.1.5.2 Plastic hinge length formulations

Various empirical expressions have been proposed by investigators for the equivalent length of plastic hinge l_p .

1. Baker's formula for members with unconfined concrete (Park and Pauley 1975, Baker 1956, Baker and Amarakone 1964)

$$l_p = k_1 k_2 k_3 \left(\frac{z}{d} \right)^{1/4} d \quad (\text{A.41})$$

where,

- k_1 = 0.7 for mild steel and 0.9 for cold worked steel
- k_2 = $1 + 0.5P_u/P_0$, where P_u = axial compressive force in the member and P_0 = axial compressive strength of member without bending moment.
- k_3 = 0.6 when $f'_c = 35.2 \text{ N/mm}^2$ or 0.9 when $f'_c = 11.7 \text{ N/mm}^2$, assuming $f'_c = 0.85 \times f_{ck}$
- z = Distance of critical section from point of contra-flexure
- d = effective depth of the member.

2. Baker's formula for members confined by transverse steel (Park and Pauley 1975, Baker and Amarakone 1964)

$$l_p = 0.8k_1k_3 \left(\frac{z}{d} \right) c \quad (\text{A.42})$$

where, c is the neutral axis depth at the ultimate moment and the other symbols have the previous meaning.

3. Corley's formula (Park and Pauley 1975, Corley 1966)

$$l_p = 0.5d + 0.2\sqrt{d} \left(\frac{z}{d} \right) \quad (\text{A.43})$$

where symbols have the same meaning as given above.

4. Mattock's formula (Park and Pauley 1975, Mattock 1967)

$$l_p = 0.5d + 0.05z \quad (\text{A.44})$$

5. Sawyer's formula (Park and Pauley 1975, Sawyer 1964)

$$l_p = 0.25d + 0.075z \quad (\text{A.45})$$

6. Pauley-Priestley formula (Pauley and Priestley 1992)

$$l_p = 0.08z + 0.022d_b f_y \quad (\text{MPa}) \quad (\text{A.46})$$

where,

d_b = diameter of main reinforcing bars

f_y = yield strength of reinforcement bars, in MPa

In addition to above formula, Pauley and Priestley (1992) also recommend using an approximation of $l_p = 0.5d$

A.2 Determination of Shear Force-Deformation Characteristics

It is possible that a reinforced concrete member may fail in shear instead of flexure. The behavior of reinforced concrete member at failure in shear is distinctly different from its behavior in flexure. In shear, the beam fails abruptly without sufficient advanced cracking. Therefore, it is necessary that shear force-deformation characteristics shall be determined in addition to the moment-rotation characteristics to get the true picture of the failure.

A.2.1 Formulations for prediction of shear force-deformation characteristics

There are several models available in literature to calculate the shear strength of the members. However, most of them do not give the corresponding shear deformation. To predict the shear force-deformation characteristics, an incremental analytical approach (Watanabe and Lee 1998) was followed in this work. The model is based on the truss mechanism. In the analysis, the stirrup strain is gradually increased with a small increment and the resisting shear at each step is calculated.

Figure A.11 shows (a) truss model, (b) moment diagram and (c) axial strain distributions of diagonally cracked concrete member sections where the member has an anti-symmetric moment distribution along member axis. The section A-A is the assumed critical section for shear, at a distance of j_t from the maximum moment section.

Figure A.11 (d) shows the stress state of a concrete element at the centroidal axis of the assumed critical shear failure section. The stress state is characterized by a biaxial stress

field in the concrete and a uniaxial tension field in the shear reinforcement. Kupfer and Bulicek (1991) gave the equilibrium condition of stresses and compatibility condition of strains for the concrete element shown.

In Figure A.11,

- j_t = Distance between upper and lower stringers
- l = Clear span length

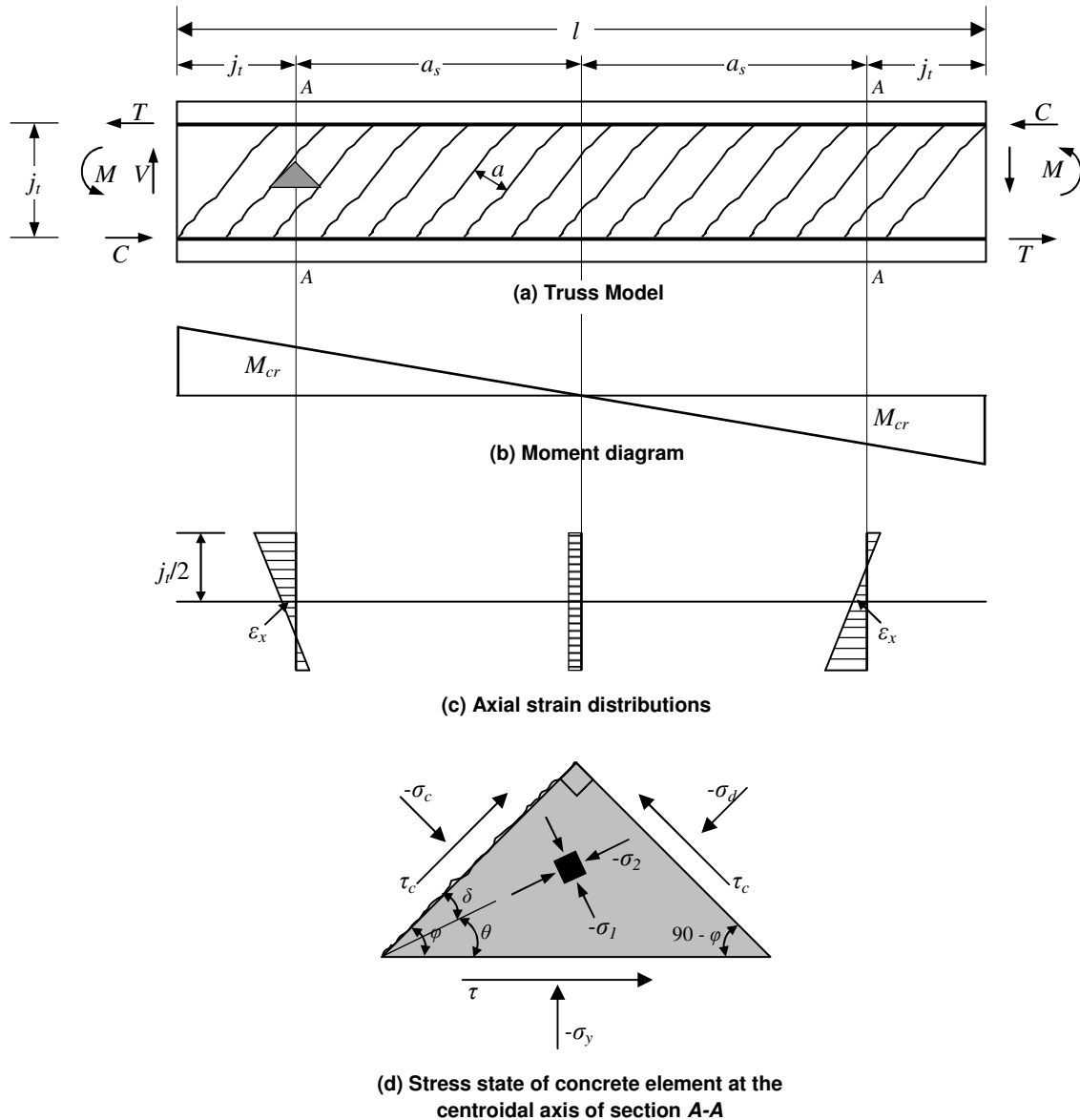


Figure A.11 Modeling of members and stress state of concrete element

- a_s = Shear span
- M = Bending moment
- V = Shear force

M_{cr}	=	Moment at the critical section for shear
C	=	Flexural compressive force at the beam end sections
T	=	Flexural tensile force at the beam end sections
τ	=	Horizontal shear stress in concrete due to external shear
τ_c	=	Shear stress at cracked surface due to aggregate interlock
σ_c	=	Normal stress at cracked surface due to aggregate interlock
σ_d	=	Normal stress in concrete parallel to crack inclination
σ_1, σ_2	=	Principal stresses in the concrete element
σ_y	=	Vertical compressive stress of the concrete element induced from shear reinforcement.
φ	=	Diagonal crack inclination
θ	=	Inclination of principal compressive stress
δ	=	Angle between φ and θ
a	=	Average spacing of diagonal cracks measured perpendicular to the cracks.

A.2.2 Equilibrium condition of stresses (Watanabe and Lee, 1998)

The equilibrium condition of stresses is defined by following equations

$$\sigma_d = -\frac{2\tau}{\sin 2\varphi} - 2\tau_c \cot 2\varphi + \sigma_c \quad (\text{A.47})$$

$$\tau = \tau_c + (\sigma_c - \sigma_y) \cot \varphi \quad (\text{A.48})$$

$$\sigma_y = -\rho_w f_{ws} \quad (\text{A.49})$$

Here, ρ_w is the ratio of shear reinforcement and f_{ws} is the stress of shear reinforcement at each loading step in the incremental analysis, which is obtained from the stress-strain curve for the shear reinforcement.

The principal stresses of concrete, σ_1 and σ_2 are given by

$$\sigma_{1,2} = \frac{1}{2} \left(\sigma_d + \sigma_c \pm \sqrt{(\sigma_d - \sigma_c)^2 + 4\tau_c^2} \right) \quad (\text{A.50})$$

The crack inclination, φ is given by is given by

$$\cot \varphi = -\frac{n}{2} + \sqrt{1 + \left(\frac{n}{2}\right)^2} \quad (\text{A.51})$$

$$n = \frac{\sigma_{xf}}{\tau_f} \quad (\text{A.52})$$

σ_{xf} is the axial stress and τ_f is the shear stress at the centroidal axis due to load effect just before diagonal cracking. For beams since, $\sigma_{xf} = 0$, therefore $\varphi = 45$ degrees.

The angle, δ between φ and θ is calculated by

$$\tan 2\delta = \frac{2\tau_c}{-\sigma_d + \sigma_c} \quad (\text{A.53})$$

Therefore, the inclination of the principal compressive stress, θ is given as

$$\theta = \varphi - \delta \quad (\text{A.54})$$

A.2.3 Compatibility condition of strains

Figure A.12 shows the strain state of diagonally cracked concrete at the centroidal axis of section A-A of Figure A.11 (a). In Figure A.12, ε_x and ε_y are the smeared strains of cracked concrete in x and y directions respectively, and ε_{10} and ε_{20} are the tensile and compressive principal strains of the concrete itself respectively.

In any considered direction, the smeared strain of cracked concrete ε results from the strain of concrete ε_0 and the smeared strains ε_w and ε_v due to crack opening w and crack shear displacement v , respectively. That is

$$\varepsilon = \varepsilon_0 + \varepsilon_w + \varepsilon_v \quad (\text{A.55})$$

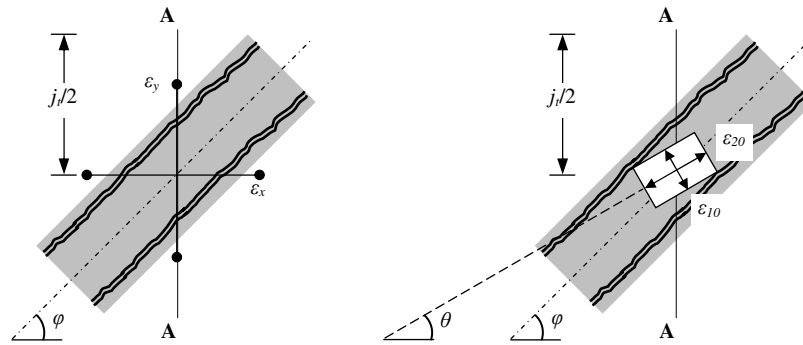


Figure A.12 Strain state of cracked concrete at the centroidal axis of section A-A

Then the smeared strains ε_x and ε_y in x and y directions can be expressed as

$$\varepsilon_x = \varepsilon_{x0} + \varepsilon_{xw} + \varepsilon_{xv} \quad (\text{A.56})$$

$$\varepsilon_y = \varepsilon_{y0} + \varepsilon_{yw} + \varepsilon_{yv} \quad (\text{A.57})$$

The concrete strains ε_{x0} and ε_{y0} in x and y directions can be derived from the principal strains ε_{10} and ε_{20} of the concrete as

$$\varepsilon_{x0} = \varepsilon_{10} \sin^2 \theta + \varepsilon_{20} \cos^2 \theta \quad (\text{A.58})$$

$$\varepsilon_{y0} = \varepsilon_{10} \cos^2 \theta + \varepsilon_{20} \sin^2 \theta \quad (\text{A.59})$$

The smeared uniaxial strains ε_{xw} and ε_{yw} and shear strains ε_{xv} and ε_{yv} of cracked concrete in both x and y directions are expressed as

$$\varepsilon_{xw} = \sin^2 \varphi \times \frac{w}{a} \quad (\text{A.60})$$

$$\varepsilon_{yw} = \cos^2 \varphi \times \frac{w}{a} \quad (\text{A.61})$$

$$\varepsilon_{xv} = -\sin \varphi \cos \varphi \times \frac{v}{a} \quad (\text{A.62})$$

$$\varepsilon_{yv} = \sin \varphi \cos \varphi \times \frac{v}{a} \quad (\text{A.63})$$

Using equations (A.55) through (A.63), we get the expressions for the smeared strains, w/a and v/a , due to diagonal cracks as

$$\frac{w}{a} = \varepsilon_x + \varepsilon_y - \varepsilon_{10} - \varepsilon_{20} \quad (\text{A.64})$$

$$\frac{v}{a} = \varepsilon_y \tan \varphi - \varepsilon_x \cot \varphi - \varepsilon_{10} \frac{\sin^2 \varphi - \sin^2 \theta}{\sin \varphi \cos \varphi} + \varepsilon_{20} \frac{\cos^2 \varphi - \sin^2 \theta}{\sin \varphi \cos \varphi} \quad (\text{A.65})$$

A.2.4 Constitutive laws

Constitutive laws proposed by Kupfer and Gerstle (1973) are used to calculate the principal concrete strains ε_{10} and ε_{20} , corresponding to the stresses σ_1 and σ_2 are obtained as.

$$\varepsilon_{10} = \frac{\sigma_1 + \sigma_2}{9K_s} + \frac{2\sigma_1 - \sigma_2}{6G_s} \quad (\text{A.66})$$

$$\varepsilon_{20} = \frac{\sigma_1 + \sigma_2}{9K_s} + \frac{2\sigma_2 - \sigma_1}{6G_s} \quad (\text{A.67})$$

K_s and G_s are the secant compressive and shear modulus, respectively and are expressed as follows

$$K_s = 17000 \left(1 - 1.6 \left(\frac{\tau_0}{\nu f'_c} \right)^{1.8} \right) \quad (\text{MPa}) \quad (\text{A.68})$$

$$G_s = 13000 \left(1 - 3.5 \left(\frac{\tau_0}{\nu f'_c} \right)^{2.5} \right) \quad (\text{MPa}) \quad (\text{A.69})$$

where τ_0 is the octahedral stress given by

$$\tau_0 = \frac{\sqrt{2}}{3} \cdot \sqrt{\sigma_1^2 + \sigma_2^2 - \sigma_1 \sigma_2} \quad (\text{A.70})$$

and $\nu f'_c$ is the reduced uniaxial compressive strength of concrete (defined as effective compressive strength of concrete). For the failure criteria of concrete, it is assumed that the compressive failure of concrete occurs when the principal compressive stress σ_2 in the cracked concrete attains the effective compressive strength $\nu f'_c$. The effect of principal stress σ_1 on the failure criteria is ignored because its value is very small. The value of $\nu f'_c$ is given by

$$\nu f'_c = \frac{f'_c}{1.0 + \frac{350w/a}{f_c'^{0.1}}} \quad (\text{MPa}) \quad \text{for } f'_c \leq 70 \text{MPa} \quad (\text{A.71})$$

$$v f_c' = \frac{70}{(1.0 + 230w/a)} + \frac{(f_c' - 70)}{\left(1.0 + 170(w/a)\sqrt{70/f_c'}\right)} \text{ (MPa) for } f_c' > 70 \text{ MPa} \quad (\text{A.72})$$

The shear stress, τ_c and normal stress, σ_c due to aggregate interlock at cracked surface are obtained using Lee et al (1991) model and are given by

$$\tau_c = 3.83 f_c'^{1/3} \frac{v^2}{w^2 + v^2} \text{ (MPa)} \quad (\text{A.73})$$

$$\sigma_c = -3.83 f_c'^{1/3} \left(0.5\pi - \tan^{-1} \left(\frac{w}{v} \right) - \frac{wv}{w^2 + v^2} \right) \text{ (MPa)} \quad (\text{A.74})$$

The average spacing of shear cracks, a is given by

$$\frac{1}{a} = 5 \frac{\rho_w}{d_s} + \frac{2}{j_t} \quad (\text{A.75})$$

where d_s is the diameter of shear reinforcement.

The stress and strain of the shear reinforcement, f_{dc} and ε_{dc} corresponding to the diagonal cracking are given by

$$f_{dc} = \frac{Q_s}{\rho_w \cdot b \cdot j_t \cdot \cot \phi} \quad (\text{A.76})$$

$$\varepsilon_{dc} = \frac{f_{dc} A_{sw}}{E_c \cdot b \cdot s + E_s \cdot A_{sw}} \quad (\text{A.77})$$

where Q_s is the shear force at diagonal cracking given by

$$Q_s = v_c \cdot b \cdot d \quad (\text{A.78})$$

where,

E_c is the elastic modulus of concrete,

E_s is the elastic modulus of shear reinforcement, and

v_c is the shear strength of the concrete without shear reinforcement

The value of v_c as recommended by Indian Standard (IS 456:2000, Rangan 1972) is given by

$$v_c = \frac{\sqrt{0.8f_{ck}} (\sqrt{1+5\beta} - 1)}{6\beta} \text{ (MPa)} \quad (\text{A.79})$$

where,

$$\beta = \frac{0.116f_{ck}bd}{100A_{st}} \geq 1.0 \quad (\text{A.80})$$

The value of v_c as recommended by ACI (ACI 318-11) is given by

(a) For members subjected to shear and flexure only

$$v_c = \frac{\sqrt{f'_c}}{6} \text{ (psi)} \quad (\text{A.81})$$

(b) For members subjected to axial compression in addition to shear and flexure

$$v_c = \left(1 + \frac{P}{14A_g}\right) \frac{\sqrt{f'_c}}{6} \text{ (psi)} \quad (\text{A.82})$$

where, P is the axial force (in N), and A_g is the gross area of the section (in mm^2).

A.2.5 Algorithm for prediction of shear characteristics

The following steps shall be carried out to determine the shear characteristics for a given section and axial load.

1. Set $w = 0$, $v = 0$.
2. Calculate ϕ and a using equations (A.51) and (A.75) respectively.
3. Calculate v_c and hence Q_s .
4. Calculate f_{dc} and ε_{dc} using equations (A.76) and (A.77) respectively.
5. Set $\varepsilon_y = \varepsilon_{dc}$.
6. Increment ε_y . $\varepsilon_y = \varepsilon_y + \Delta\varepsilon_y$

7. Calculate f_{ws} as a function of ε_y from stress-strain curve.
8. Assume a value of Δw and Δv . Increment w and v . $w = w + \Delta w$, $v = v + \Delta v$.
9. Calculate $v f'_c$ using equation (A.71) or (A.72).
10. Calculate $\Delta\tau_c$, $\Delta\sigma_c$, $\Delta\tau$, $\Delta\sigma_d$, $\Delta\sigma_1$, and $\Delta\sigma_2$ to satisfy stress equilibrium using equations (A.73), (A.74), (A.48), (A.49), (A.50) respectively.

$$\Delta f = f(w + \Delta w, v + \Delta v) - f(w, v)$$
11. Calculate $\Delta\theta$, ΔK_s and ΔG_s using equations (A.53), (A.68) and (A.69).
12. Calculate $\Delta\varepsilon_{10}$ and $\Delta\varepsilon_{20}$ to satisfy strain compatibility using equations (A.66) and (A.67) respectively.
13. Calculate Δw and Δv using equations (A.64) and (A.65).
14. If the calculated value of Δw and Δv are same as the values assumed in step 8, then the new value of w and v are given by $w = w + \Delta w$, $v = v + \Delta v$. Else assume a new value of Δw and Δv and go to step 8.
15. Calculate $\Delta V = (\Delta\tau)bd$. $V = V + \Delta V$.
16. If current V is smaller than previous V , then stop else go to step 6.

A.3 Determination of Torsional Moment-Rotation Characteristics

The torsional hinge characteristics of the section can be determined on the basis of Space Truss analogy (Park and Paulay, 1975). The cracking torsion, T_{cr} is calculated as

$$T_{cr} = 0.33\sqrt{f'_c}(A_c^2/P_c) \quad (\text{A.83})$$

Where,

f'_c = Standard Cylinder compressive strength of concrete, considered as 0.8 times the standard cube strength of concrete

A_c = Gross Area of concrete section in mm^2

P_c = Perimeter of concrete section in mm

The ultimate torsional resistance, T_u of the section is calculated as

$$T_u = 2A_o A_{sv} f_{sv} \cot\theta / s_v \quad (\text{A.84})$$

Where,

A_o = gross area enclosed by shear flow path, considered as 0.85 times the area enclosed by centerline of the outermost closed transverse reinforcement

A_{sv} = Area of one leg of transverse reinforcement

f_{sv} = Yield/Ultimate stress of transverse reinforcement

s_v = centre to centre spacing of transverse reinforcement

The cracked stiffness of the section, $K_{t,cr}$ is considered as (Park and Pauley, 1975)

$$K_{t,cr} = E_s (B_o D_o) 2 A_{sv} \sqrt{m_t} / \{(B_o + D_o) s_v\} \quad (\text{A.85})$$

Where,

B_o = Shorter dimension of transverse reinforcement

D_o = Longer dimension of transverse reinforcement

E_s = Modulus of elasticity of transverse reinforcing steel

M_t = Ratio of yield stress of transverse reinforcement to that of longitudinal reinforcement

Though, the formulations are quite simplified, they are found to generally suffice for modeling the torsional behavior of the members.

APPENDIX-B PROCEDURE TO PERFORM INELASTIC STATIC ANALYSIS

B.1 General Procedure

The inelastic analysis of the joint-subassemblies as well as the structure was performed following the pushover analysis procedure. Pushover analysis is a tool to obtain the load-displacement plot for a structure, sub-assembly or a member. It involves applying loads to the model of the structure incrementally, i.e., pushing the structure, and plotting the total applied force and the associated displacement at each increment. With the increase in the magnitude of loading, the weak links and failure modes of the structure are found. The overall capacity of the structure depends on the strength and deformation capacities of the individual components of the structure. Therefore, the analysis requires the geometry of structure, loading pattern, hinge locations and hinge properties in terms of moment-rotation characteristics, shear force-deformation characteristics etc for each and every member to be given as input.

In pushover analysis, the load is first applied to the model of the structure and is increased linearly until certain members yield. At this point, the hinge formation takes place at the yielding locations. The load and corresponding displacement is recorded at this point. The structural model is now modified to take into account the hinge formation. The load is again increased linearly until some other members yield. The procedure is repeated till failure and the load-displacement curve is plotted.

Structural capacity is represented by a pushover curve. The most convenient way to plot the force – displacement curve is by tracking the base shear and the roof displacement. The following procedure can be used to construct a pushover curve (ATC-40, 1996):

1. Create the computer model of the structure.
2. Apply the lateral forces to the structure in proportion to the product of the mass and fundamental mode shape. The analysis should also include gravity loads. In this thesis, since the load pattern was known beforehand, the same was applied to the structure. Otherwise, the load can be applied in any of the following height wise patterns.
 - i) Apply lateral forces to each storey in proportion to the standard code procedure. This distribution is a triangular distribution on the structure. One can also apply parabolic distribution of loads depending on the fundamental mode.
 - ii) Apply lateral load in proportion to the product of storey masses and first mode shape of the elastic model of the structure (i.e., the capacity curve is generally constructed to represent the first mode response of the structure based on the assumption that the

fundamental mode of the vibration is the predominant response of the structure). This is generally valid for the buildings with the fundamental periods of vibration up to about one second.

iii) The load is applied until first yielding takes place. For each increment beyond yielding, adjust the forces to be consistent with the changing deflected shape.

3. Calculate member forces for required combinations of vertical and lateral load.
4. Adjust lateral force level so that certain element/elements reach their yield strength.
5. Record the base shear and the roof displacement.
6. Revise the model using post-yield stiffness for the yielding elements.
7. Apply the new increment of lateral load to the revised structure such that another element (or a group of elements) yields.
8. Add the increment of lateral load and the corresponding increment of roof displacement to the previous totals to give the accumulated values of the base shear and roof displacement.
9. Repeat the above steps until the structure reaches an ultimate limit, such as instability from P- Δ effects: distortions considerably beyond the desired the performance level, etc.

B.2 Nonlinear static pushover analysis of a portal frame (Example)

Consider a single bay single storey portal frame structure subjected to a concentrated lateral load P as shown in Figure B.1. Let the cross-section for both beam and column be 200mm X 200mm.

The dimensions and properties are enlisted below

$$\begin{aligned}L &= 4\text{m} \\E &= 2.5 \times 10^{10} \text{ N/m}^2 \\B &= 0.2\text{m} \\D &= 0.2\text{m}\end{aligned}$$

Thus,

$$I = 1.333 \times 10^{-4} \text{ m}^4$$

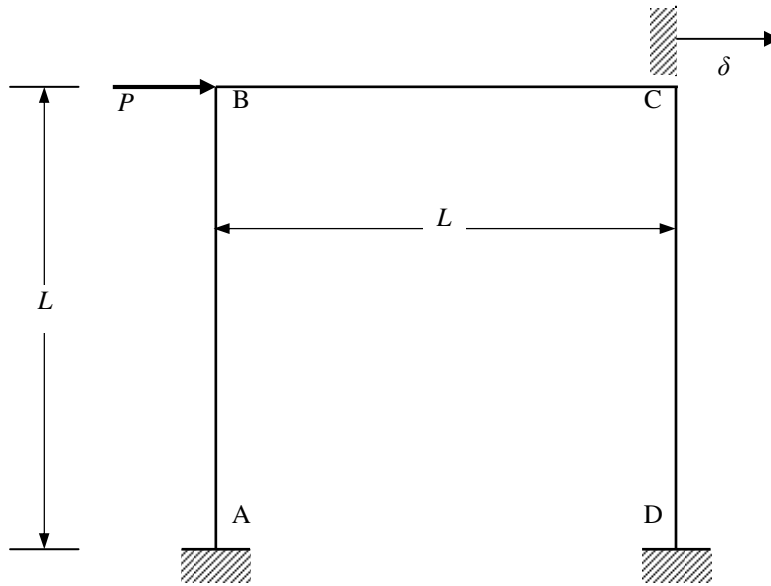


Figure B.1 Portal frame structure for pushover analysis

Let us assume elastic-perfectly plastic moment-rotation characteristics for the section as shown in Figure B.2. The yield moment is assumed to be 100kN-m and the ultimate rotation is assumed as 0.05rad. The elastic rotation is not needed since, that depends on the elastic stiffness of the structure and is equal to the elastic rotation corresponding to the yield moment.

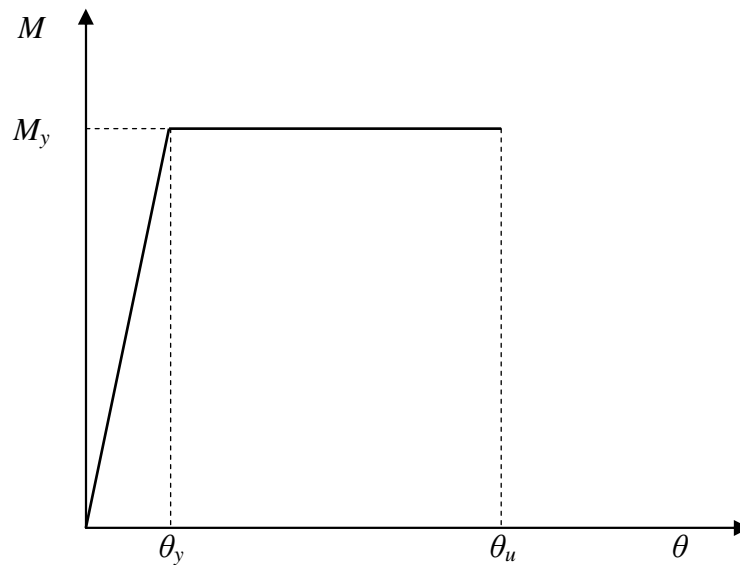


Figure B.2 Assumed moment-rotation characteristics for the members of frame

The salient points of the M - θ curve are

$$M_y = 100 \text{ kN-m}$$

θ_y = Rotation corresponding to the yield moment (depends on the elastic stiffness of the structure)

$$\theta_u = 0.05 \text{ rad}$$

The elastic bending moment diagram for the frame is shown in Figure B.3. By elastic analysis, we get,

$$\text{Base moments, } M_{AB} = M_{DC} = \frac{4}{14} PL \quad (\text{B.1})$$

$$\text{End moments, } M_{BA} = M_{BC} = M_{CB} = M_{CD} = \frac{3}{14} PL \quad (\text{B.2})$$

$$\text{Base rotations, } \theta_A = \theta_D = 0 \text{ (Fixed base)} \quad (\text{B.3})$$

$$\text{Joint rotations, } \theta_B = \theta_C = \frac{0.0714 PL^2}{2EI} \quad (\text{B.4})$$

$$\text{Lateral displacement, } \delta = \frac{0.1190 PL^3}{2EI} \quad (\text{B.5})$$

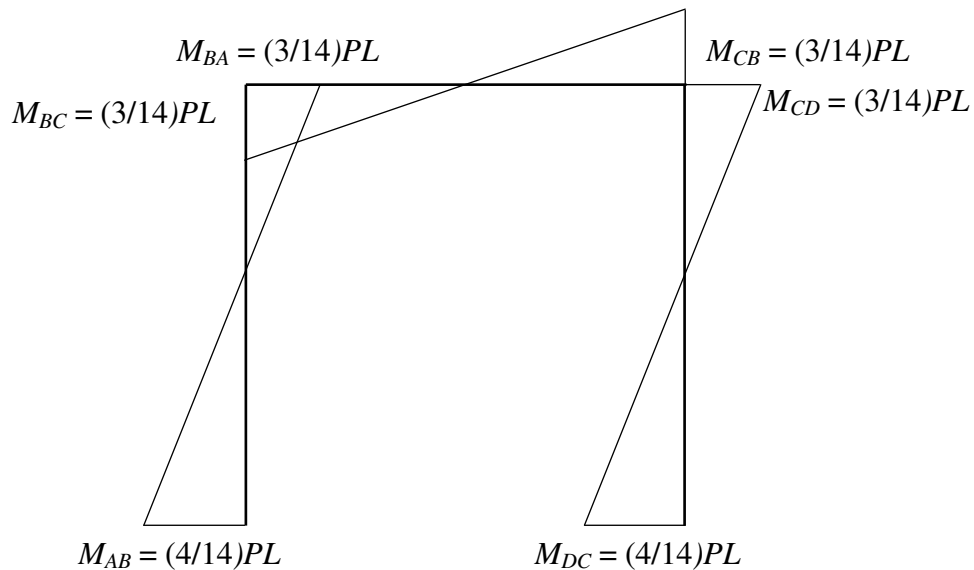


Figure B.3 Initial elastic bending moment diagram of the frame

Since the maximum bending moment occurs at the base of the structure, the hinges will be formed first at the end of the columns i.e. at ends A and D. These hinges will be formed at a load P which will correspond to a moment M_y at these locations. Therefore, the load corresponding to first hinge formation P_l can be obtained by equating the moment due to this load at the ends A and D to the yield moment M_y .

$$\frac{4}{14} P_1 L = M_y \quad (\text{B.6})$$

In our case, $L = 4\text{m}$ and $M_y = 100\text{kN-m}$.

Putting these values in Eq. (B.6), we get,

$$P_1 = \frac{14}{4} \frac{M_y}{L} = \frac{14}{4} \times \frac{100}{4} = 87.5\text{kN}$$

The corresponding joint rotation and lateral displacement can be obtained by putting the value of P_1 in equations (B.4) and (B.5) respectively. Therefore,

$$\theta_{B1} = \theta_{C1} = \frac{0.0714 P_1 L^2}{2EI} = \frac{0.0714 \times 87.5 \times 1000 \times 4^2}{2 \times 2.5 \times 10^{10} \times 1.333 \times 10^{-4}} = 0.015\text{rad}$$

$$\delta_1 = \frac{0.1190 P_1 L^3}{2EI} = \frac{0.1190 \times 87.5 \times 1000 \times 4^3}{2 \times 2.5 \times 10^{10} \times 1.333 \times 10^{-4}} = 0.1\text{m}$$

$$\text{End moments, } M_{AB} = M_{DC} = \frac{4}{14} \times 87.5 \times 4 = 100\text{kN-m}$$

$$\text{Joint moments, } M_{BA} = M_{BC} = M_{CB} = M_{CD} = \frac{3}{14} \times 87.5 \times 4 = 75\text{kN-m}$$

At this step, corresponding to $P = 87.5\text{kN}$, the moment at ends A and D reach the yield value and therefore, a plastic hinge formation takes place at these locations. The structure will now act as a hinged base portal frame and therefore, a new modified model of the structure is required. The modified model is shown in Figure B.4.

For this structure, again from elastic analysis we get,

$$\text{Base moments, } M_{AB} = M_{DC} = 0 \quad (\text{Hinged base}) \quad (\text{B.7})$$

$$\text{End moments, } M_{BA} = M_{BC} = M_{CB} = M_{CD} = \frac{PL}{2} \quad (\text{B.8})$$

$$\text{Base rotations, } \theta_A = \theta_D = \frac{PL^2}{3EI} \quad (\text{B.9})$$

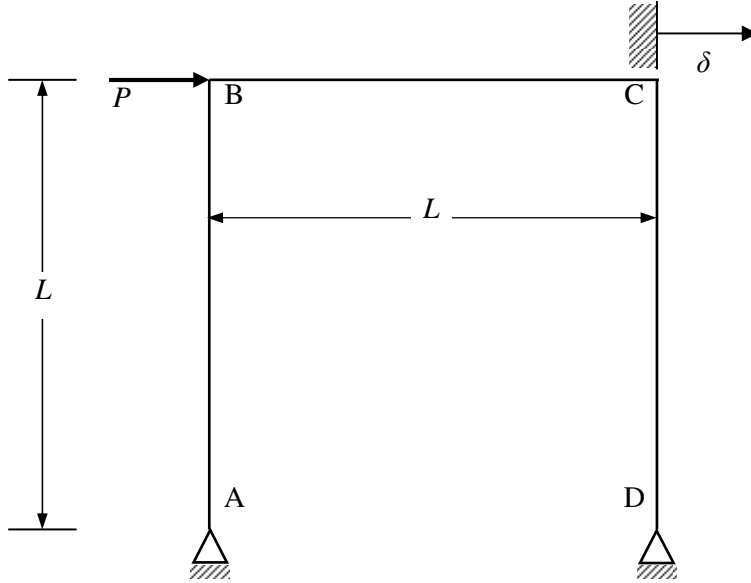


Figure B.4 Modified model of Portal frame structure after hinge formation at base

$$\text{Joint rotations, } \theta_B = \theta_C = \frac{PL^2}{12EI} \quad (\text{B.10})$$

$$\text{Lateral displacement, } \delta = \frac{PL^3}{4EI} \quad (\text{B.11})$$

Ends B and C have already received a moment of 75kN-m due to P_1 . The moment carrying capacity of members is 100kN-m. Therefore, additional moment that the members can take before formation of hinges is equal to $100 - 75 = 25\text{kN-m}$. The additional load P_{2add} corresponding to the second hinge formation can be obtained by equating the expression for end moments (Eq. (B.8)) to 25kN-m. That is,

$$\frac{P_{2add} \times 4}{2} = 25\text{kN-m} \Rightarrow P_{2add} = 12.5\text{kN}$$

Therefore the total load on the structure corresponding to second hinge formation is given by $P_2 = P_1 + P_{2add} = 87.5 + 12.5 = 100\text{kN}$

The additional base rotations due to P_{2add} are obtained as (Eq. (B.9))

$$\theta_{A2add} = \theta_{D2add} = \frac{12.5 \times 10^3 \times 4^2}{3 \times 2.5 \times 10^{10} \times 1.333 \times 10^{-4}} = 0.02\text{rad}$$

Similarly, the additional joint rotations due to P_{2add} are obtained as (Eq. (B.10))

$$\theta_{B2add} = \theta_{C2add} = \frac{12.5 \times 10^3 \times 4^2}{12 \times 2.5 \times 10^{10} \times 1.333 \times 10^{-4}} = 0.005 \text{rad}$$

Adding these rotations to the rotations in the first step, we get the total base and joint rotations at this step as

$$\theta_{A2} = \theta_{D2} = \theta_{A1} + \theta_{A2add} = \theta_{D1} + \theta_{D2add} = 0 + 0.02 = 0.02 \text{rad}, \text{ and}$$

$$\theta_{B2} = \theta_{C2} = \theta_{B1} + \theta_{B2add} = \theta_{C1} + \theta_{C2add} = 0.015 + 0.005 = 0.02 \text{rad}.$$

The additional roof displacement, due to P_{2add} is obtained as (Eq. (B.11))

$$\delta_{2add} = \frac{12.5 \times 10^3 \times 4^3}{4 \times 2.5 \times 10^{10} \times 1.333 \times 10^{-4}} = 0.06 \text{m}$$

Adding this displacement to the displacement in the first step, we get the total roof displacement at this step as

$$\delta_2 = \delta_1 + \delta_{2add} = 0.1 + 0.06 = 0.16 \text{m}$$

At this step, corresponding to $P = 100 \text{kN}$, the moment at ends B and C also reach the yield value and therefore, a plastic hinge formation takes place at these locations also in addition to ends A and D. The structure will now form a mechanism and will not be able to resist any further loads and will only undergo displacement. The modified model of the structure and the mechanism formed is shown in Figure B.5.

At this step, the mechanism has been formed and from geometry of the structure it is clear that, $\theta_A = \theta_B = \theta_C = \theta_D = \theta$.

Also, we have,

$$\delta = \theta \times L \tag{B.12}$$

At the end of second step, the member end rotations were 0.02rad. The total rotational capacity of the members is 0.05rad (Figure B.2). Therefore the additional rotational capacity of the members left is $\theta_{3add} = 0.05 - 0.02 = 0.03 \text{rad}$.

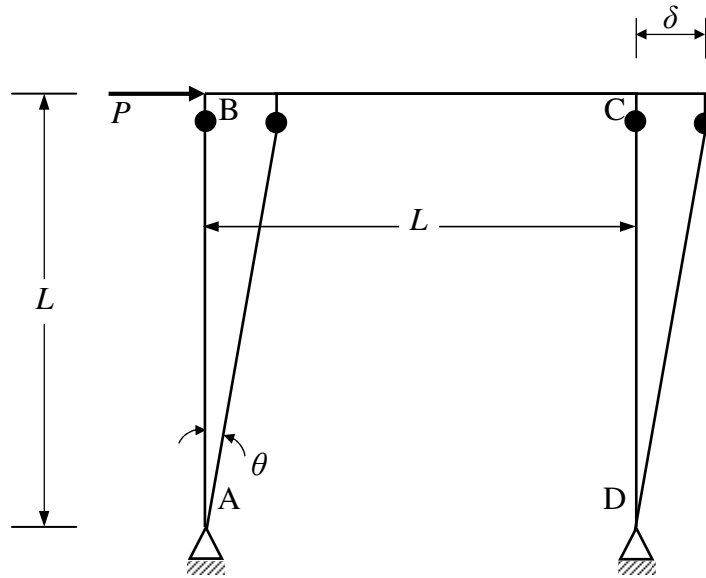


Figure B.5 Mechanism formed by Portal frame structure

The additional displacement that the structure can undergo is obtained as (Eq. (B.12))

$$\delta_{3add} = \theta_{3add} \times L = 0.03 \times 4 = 0.12\text{m}$$

The total roof displacement at the end of this step is given by

$$\delta_3 = \delta_2 + \delta_{3add} = 0.16 + 0.12 = 0.28\text{m}$$

The results of the pushover analysis for the above structure are summarized in Table B.1.

Table B.1 Results of pushover analysis for portal frame

Step, I	Load P_i (kN)	θ_A, θ_D (rad)	θ_B, θ_C (rad)	Deflection, δ (m)	Remarks
0	0	0	0	0	Initialization
1	87.5	0	0.015	0.1	First yield
2	100	0.02	0.02	0.16	Mechanism
3	100	0.05	0.05	0.28	Ultimate

Plotting the values given in Table B.1, we get the load-displacement curve or the capacity curve for the structure. The capacity curve for the above-analyzed structure is shown in Figure B.6.

As seen above, the pushover analysis is essentially a sequential elastic analysis in which we modify the structure at each step to take into account the non-linear characteristics of the

members. The curve becomes smoother if the number of elements in the structure is large or if the input moment-rotation characteristics given are curvilinear.

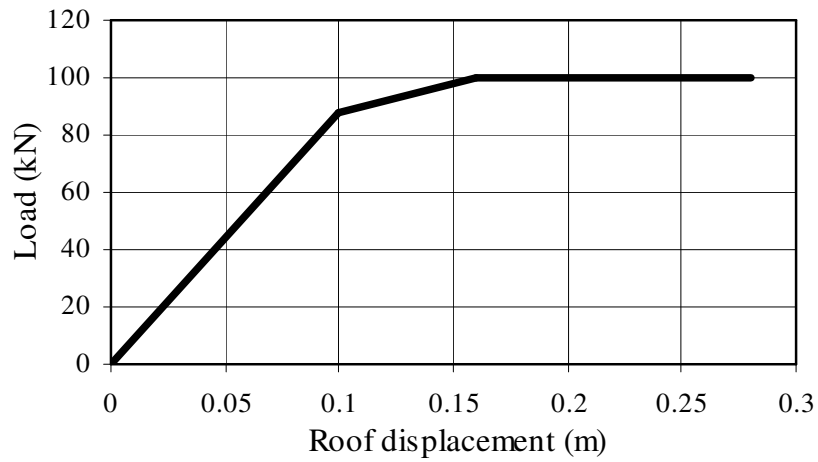


Figure B.6 Load-displacement plot for the portal frame structure

Using the procedure explained in this section, the joints and structures were analyzed to obtain the load-displacement (Pushover) curves as shown in chapter 12.

APPENDIX-C 3D FE ANALYSIS OF BEAM-COLUMN JOINTS UNDER CYCLIC LOADS

In chapter 6, it was mentioned that due to the unavailability of sufficient database of the beam-column joint tests with results on joint shear force and deformation, 3D FE numerical analysis was performed on few beam-column joints. The analyses were performed using the general purpose finite element Code MASA, developed at the Universität Stuttgart (IWB and Ožbolt, 2008). The program is capable of performing 3D nonlinear analysis of structural elements made of quasi-brittle materials, like concrete, based on a microplane material model with relaxed kinematic constraint (Ožbolt et. al, 2001). The philosophy and methodology to perform 3D FE numerical analysis is presented in this chapter. The same philosophy was also employed by Mahajan (2009) and Genesio (2012). The results of their parametric studies were also utilized to propose the parameters for pivot hysteresis rule for the beam-column joints.

C.1 Microplane model with relaxed kinematic constraint (Ožbolt et. al, 2001)

The constitutive law employed for concrete in this work is Microplane model with relaxed kinematic constraint (Ožbolt et. al, 2001). The model utilizes the strength of both macroscopic and microscopic models and therefore is known to provide results in very good agreement with the experiments. The model is able to reasonably correctly describe micro-structural phenomena such as cohesion, friction and aggregate interlock etc.

Contrary to classical macroscopic kind of constitutive laws, which are based on tensorial invariants of stresses and strains, in the microplane model the material response is calculated based on the monitoring of stresses and strains in a different predefined directions. Integrating microplane stresses in a thermodynamically consistent way, from a known macroscopic strain tensor it is possible to calculate macroscopic stress tensor. The constitutive framework is similar to discrete type of the models (e.g. random particle model) with the difference that the model is formulated in the framework of continuum. The physical concept behind the microplane model was already discussed at the beginning of last century by Mohr (1900) and Taylor (1938). The microplanes may be imagined to represent damage planes or weak planes in the microstructure, such as those that exist at the contact between aggregate and the cement matrix or slip planes in the theory of plasticity as shown in FigureC.1 (Ožbolt et al 2001).

Generally, in macroscopic models, the macroscopic strain tensor is related to a macroscopic stress tensor through a constitutive relationship valid at macro level. In microplane model, there are a few more steps involved. Basically, in the microplane model the macroscopic strain tensor is projected at the integration point and is then is decomposed into components

on a certain number of microplanes (directions) that are used to characterize a material element.

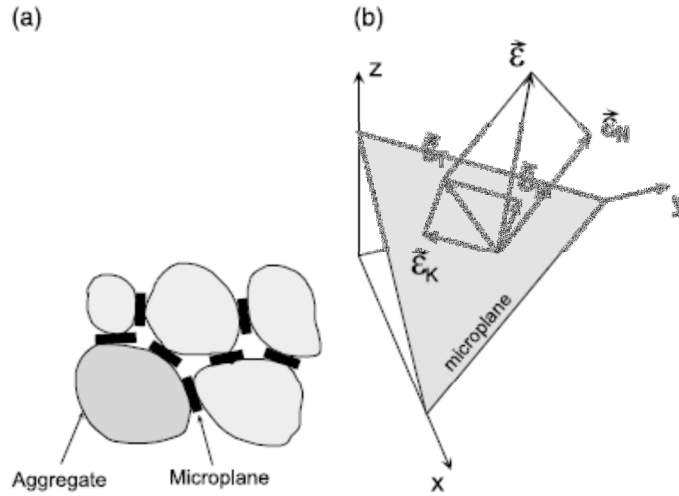


Figure C.1 Microplane model: (a) Idealized contact planes and (b) decomposition of the total macroscopic strain tensor on the microplane (Ožbolt et al 2001)

In the model each microplane is defined by its unit normal vector components n_i . Microplane strains are assumed to be the projections of macroscopic strain tensor ϵ_{ij} (kinematic constraint). On the microplane are considered normal (σ_N, ϵ_N) and two shear stress-strain components ($\sigma_K, \sigma_M; \epsilon_K, \epsilon_M$). To realistically model concrete, the normal microplane stress and strain components have to be decomposed into volumetric and deviatoric parts ($\sigma_N = \sigma_V + \sigma_D$, $\epsilon_N = \epsilon_V + \epsilon_D$). Unlike to most microplane formulations for concrete, which are based on the kinematic constrain approach, to prevent unrealistic model response for dominant tensile load, in this model kinematic constrain is relaxed (Ožbolt et al. 2001). Based on the micro-macro work conjugancy of volumetric-deviatoric split and using in advance defined microplane stress-strain constitutive laws, the macroscopic stress tensor is calculated as an integral over all possible, in advance defined, microplane orientations:

$$\sigma_{ij} = \sigma_V \delta_{ij} + \frac{3}{2\pi} \int_S \left[\sigma_D \left(n_i n_j - \frac{\delta_{ij}}{3} \right) + \frac{\sigma_K}{2} (k_i n_j + k_j n_i) + \frac{\sigma_M}{2} (m_i n_j + m_j n_i) \right] dS \quad (C.1)$$

Where S denotes the surface of the unit radius sphere and δ_{ij} denotes Kronecker delta and k_i and m_i are directions of shear microplane components.

Figure C.2 shows the implementation of the same in the 3D FE level (Ožbolt, 2009). As shown, for a 3D solid finite element having eight integration points, the macroscopic strain tensor is first projected to each integration point and then it is decomposed along different orientations. This can easily be done if we know the direction cosines for each orientation (microplane). These projected strains are then decomposed further in normal and shear

components. Stress-strain relations on each microplane are then employed to determine the respective micro-stress components. Finally, using the principle of virtual work, a numerical integration over the total number of microplanes representing the material point is performed to determine the macroscopic stress components.

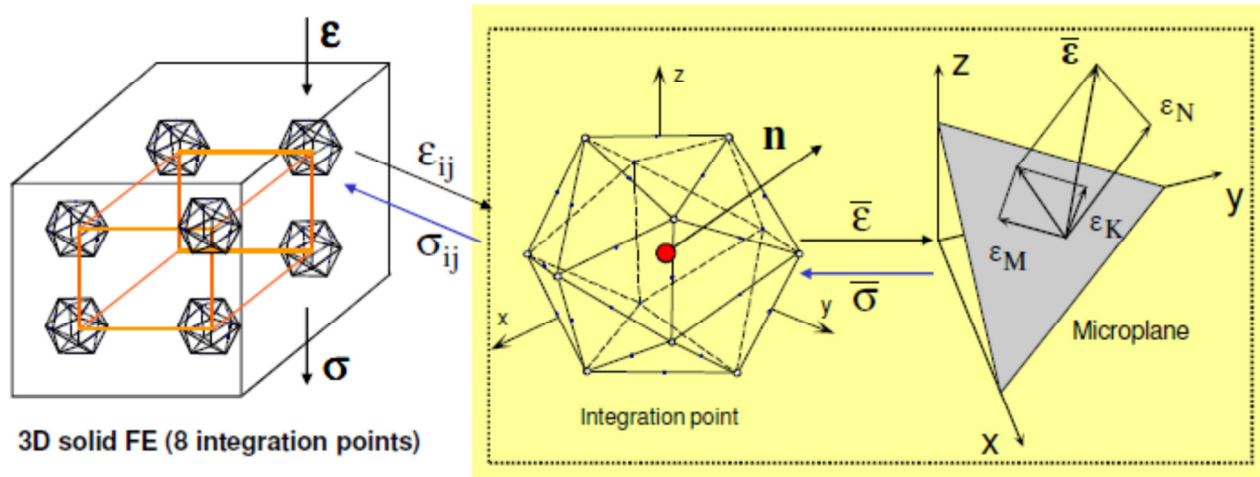


Figure C.2 Concept of microplane model (Ožbolt, 2009)

At an integration point, the number of microplanes considered can have any natural number as a value. Obviously, larger number of microplanes will produce more accurate results but at the same time will need much higher computational effort. A good balance between the computational time and accuracy can be obtained by considering 21 microplanes as shown in Figure C.2. A major advantage of the model is that since microplanes with different spatial orientations have been considered, the tensorial invariant restrictions are automatically fulfilled and they need not be directly enforced.

To account for large strains and large displacements, Green-Lagrange finite strain tensor is used. Furthermore, to account for the loading history of concrete, the co-rotational stress tensor is employed. Detailed discussion of the features and various aspects related to the finite strain formulation of the microplane model are beyond the scope of the present paper. For more detail refer to Bažant et al. (2000) and Ožbolt et al. (2001).

C.2 Overview of MASA

MASA, a Finite Element Program for 3D Nonlinear Analysis of Concrete and Reinforced Concrete Structures, has been developed at the Institut für Werkstoffe im Bauwesen, Universität Stuttgart. The code follows the microplane material model for concrete as described in previous section. Program MASA is aimed to be used for nonlinear three-dimensional (3D) smeared fracture finite element analysis of structures made of quasi-brittle materials. Although different kind of materials can be employed, the program is mainly written to be used for nonlinear analysis of concrete and reinforced concrete (RC) structures in the

framework of the local or nonlocal continuum theory, i.e. damage and fracture phenomena are treated in a smeared way (smeared crack approach).

Quasi-brittle material (concrete) is in the program discretized by the eight node (hexa) or four node (tetra) solid finite elements. The discretization of the reinforced bars is performed by two-node truss elements or alternatively by beam elements. As the global solution strategy, three possibilities can be used: (1) Constant stiffness method (CSM), (2) tangent stiffness method (TSM) and (3) secant stiffness method (SSM). The analysis is incremental and therefore the total applied load has to be divided into a number of load or displacement increments.

To prepare input data as well as to analyze the results of the finite element analysis, commercial pre- and post-processing package FEMAP[®] is used. The program generates nodes, nodal connectivity, boundary conditions, material data and loads which are required for the finite element code of MASA. The link between FEMAP[®] and MASA is realized through an input interface program which from FEMAP[®] output data (neutral file) generates input data of the FE code. To generate post-processing output results from the numerical results of the FE code, an output interface program can be used. The post-processing output results can be read and graphically interpreted by FEMAP[®].

To assure mesh independent result, simple crack band method (Bažant and Oh, 1983) is followed. The main assumption of the crack band method is that damage (crack) is localized in a row of finite elements. To assure a constant and mesh independent energy consumption capacity of concrete (concrete fracture energy G_F) the constitutive law needs to be modified such that:

$$G_F = A_f h = \text{Constant} \quad (\text{C.2})$$

Where,

A_f = the area under the uniaxial tensile stress-strain curve and

h = average element size (width of the crack band).

C.3 Constitutive law for reinforcement steel

The constitutive law for steel is defined by uniaxial stress-strain law. Presently the three-linear stress-strain curve can be used. The curve is defined by following four parameters:

- (1) Initial Young's modulus E_0
- (2) Hardening modulus E_h
- (3) Yield stress f_y
- (4) Tensile (Compressive) strength f_s

Figure C.3a shows the basic input parameters needed for reinforcement steel. The loading-unloading rules for monotonic and cyclic version of the program are plotted in Figure C.3b.

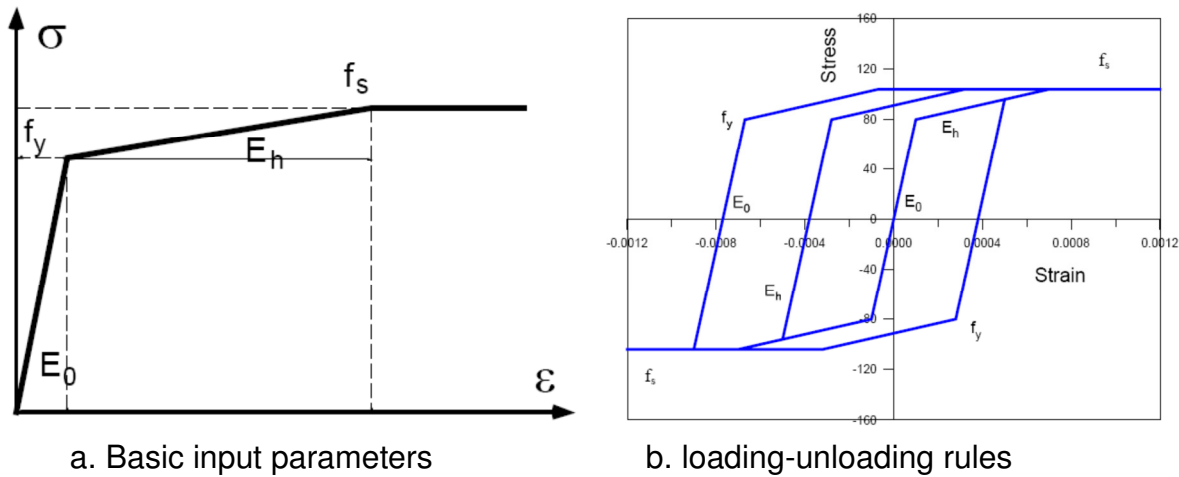


Figure C.3 Uniaxial constitutive stress-strain relationship for reinforcement steel

C.4 Discrete Bond Model

MASA uses a discrete bond model for reinforcement which essentially consists of one-dimensional nonlinear springs (Figure C.4) with a bond-slip relationship (Lettow 2007). This model is an extension of the bond model proposed by Eligehausen et al (1983). The bond element serves as a means of connecting the reinforcement bar element to the surrounding 3-dimensional concrete elements. Only the degrees of freedom in the direction of the slip, i.e. the longitudinal axis of the bars are considered and the connection in the other directions is assumed as perfect. Thus, the bond element is essentially a two-node finite element. The element displacement field is a slip which is defined as a relative movement between the reinforcement bar and concrete in the direction parallel to the axis of the bar.

The unknowns are the slips s_i and s_j at the two ends of the element (Figure C.4). The displacement field $s(x)$ is assumed to be linear along the elemental axis with the following relations applicable

$$\{s(x)\} = [B(x)]\{s\} \quad (C.3)$$

$$[B(x)] = [1-x/l \quad x/l] \quad (C.4)$$

$$\{s\} = \{s_i \quad s_j\}^T \quad (C.5)$$

Matrix, $[B]$ relates the nodal displacement vector $\{s\}$ with the displacement field $\{s(x)\}$, l is the element length.

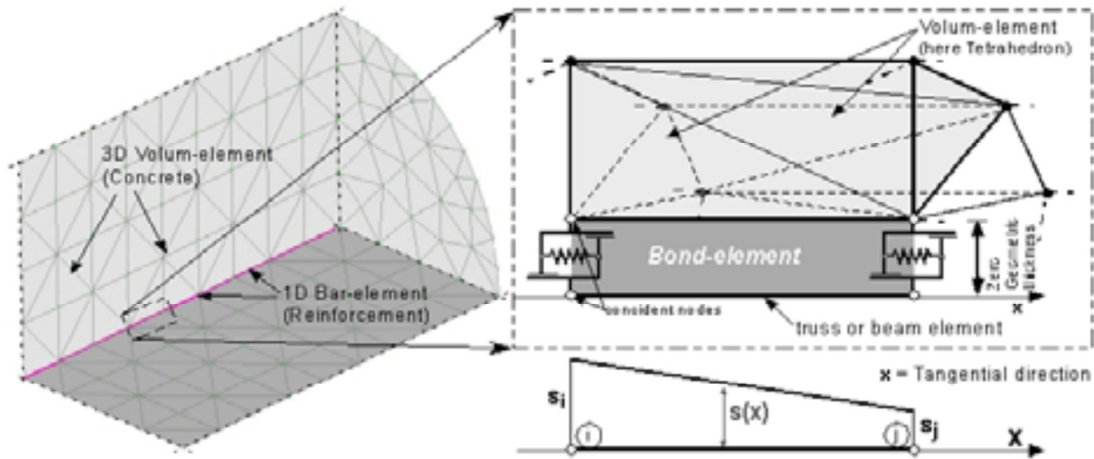


Figure C.4 Bond model implemented in MASA (Lettow 2007)

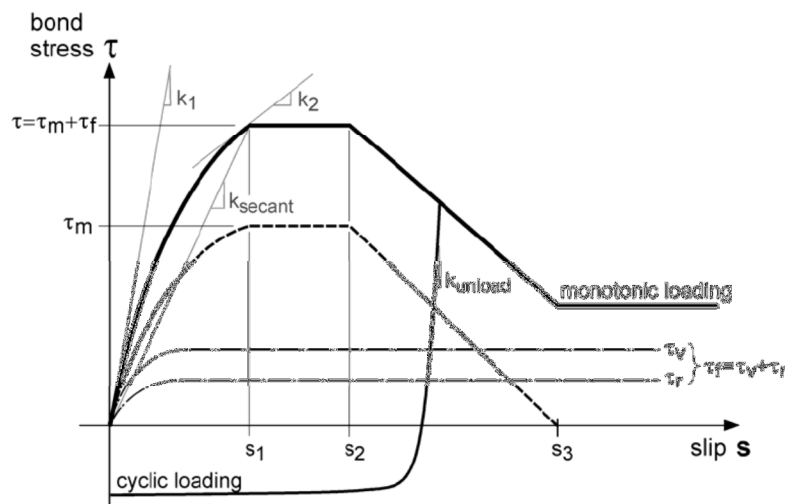


Figure C.5 Bond-slip monotonic relationship for deformed bars (Lettow 2007)

The bond resistance is divided into two components namely, a mechanical interaction component, τ_m and a frictional component, τ_f (Yankelevsky et al 1987). The bond stress-slip relationship depends on the state of stresses and strains in concrete and reinforcement, on type of loading and on geometry (Figure C.5) (Lettow 2007). The bond stress-slip relationship is defined as follows (Lettow, 2007).

For $s \leq s_1$

$$\tau(s) = \tau_0 \cdot \left(\frac{s}{s_0} \right) \cdot \left[\left(\frac{k_2}{k_1} \right) + \left(1 - \left(\frac{k_2}{k_1} \right) \right) \cdot \left(\frac{1}{1 + \left(\frac{s}{s_0} \right)^R} \right)^{1/R} \right] \quad (C.6)$$

For, $s_1 < s \leq s_2$

$$\tau(s) = \tau_m + \tau_f \quad (C.7)$$

For, $s_2 < s \leq s_3$

$$\tau(s) = \tau_m \cdot \left(\frac{s_3 - s}{s_3 - s_2} \right) + \tau_f \quad (C.8)$$

For, $s_3 < s$

$$\tau(s) = \tau_f \quad (C.9)$$

Where,

$$s_0 = s_1 \cdot \left(\frac{k_{secant} - k_2}{k_1 - k_2} \right) \quad (C.10)$$

and

$$\tau_0 = s_0 k_1 \quad (C.11)$$

Lettow (2007) has performed various tests on different size of bars and different grades of concrete and has provided the parameters required for different size of bar and different concrete strengths.

In Figure C.6, the assumption for the bond-slip cyclic relationship for deformed bars as implemented in MASA is shown. Bond degradation is assumed to occur after a certain slip due to the mechanical damage of the concrete-steel interface produced by the ribs of the reinforcement bars. More details can be found in Eligehausen et al. (1983).

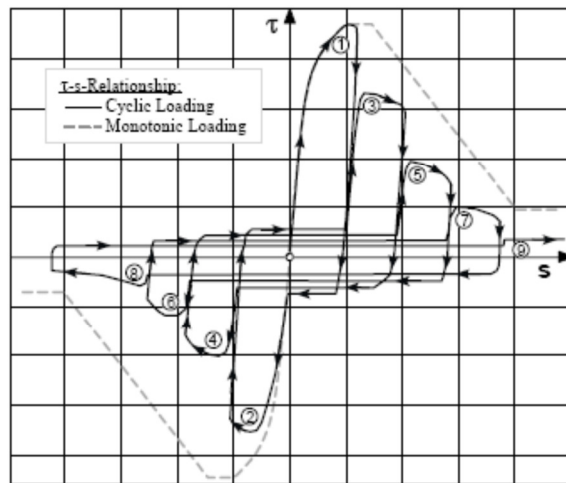


Figure C.6 Bond-slip cyclic relationship for deformed bars used in MASA (Eligehausen et al. 1983)

C.5 Numerical modeling of beam-column joints in MASA

Figure C.7 shows the typical 3-D Finite Element (FE) models of an exterior joint analyzed using MASA. The elements for load application and providing restraints are modeled as linear elastic elements to avoid local crushing behavior of those elements. The FE discretization of the models was performed using eight node hexahedral elements with linear strain field.

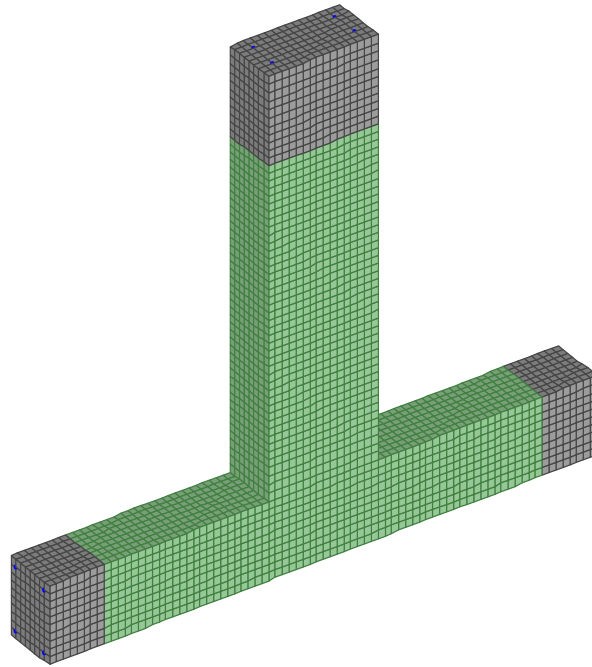


Figure C.7 3D FE Model of a typical exterior joint

Figure C.8 shows the corresponding reinforcement cage for the model. 1-D bond elements were modeled as explained in Figure C.4, with the characteristics as shown in Figures C.5 and C.6 for monotonic and cyclic behavior respectively. The analysis considering perfect bond assumption was also carried out and it was found that it does not yield sufficiently accurate results (Sharma et al, 2009). Further details can be obtained from Sharma et al (2009).

C.6 Results of numerical analyses

Figure C.9 shows the cyclic analysis results superimposed on the experimental cyclic loops. The analytical cyclic loops can be seen to follow the experimental loops very closely and can be used for estimating the values of parameters to be used with pivot hysteresis model. It is seen that by using the modeling approach as described here, the pinching effects are also very well simulated numerically.

Figure C.10 displays the failure mode and crack pattern obtained from numerical analysis. In the experiment, it was found that most of the damage was confined to the joint core while beam and column stub suffered little damage (Jain and Murty 1999). Therefore, it can be concluded that the numerical analysis procedure can predict the overall behavior and the joint deformations well. Therefore, the same can be used as a replacement of the experiment to fill for the missing information from the test data.

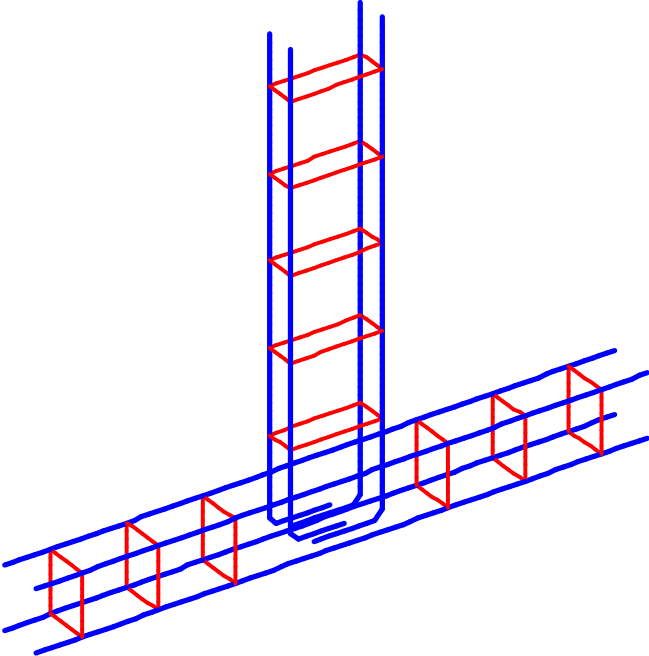


Figure C.8 Reinforcement cage for the exterior joint

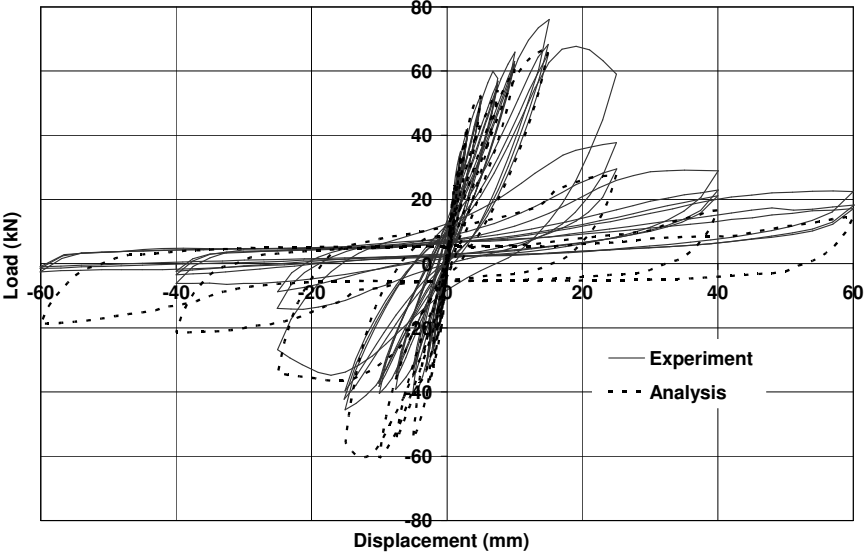


Figure C.9 Comparison of experimental and numerical hysteretic loops for the exterior joint

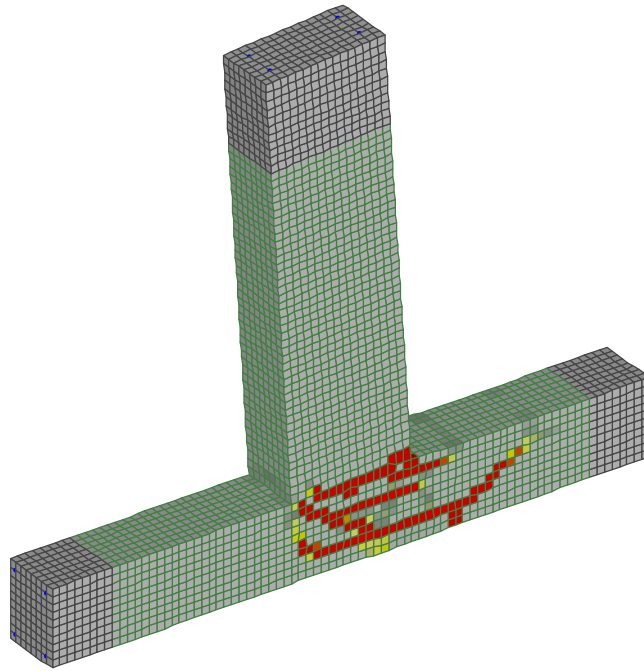


Figure C.10 Failure mode obtained from numerical analysis

Curriculum Vitae

Personal Data

Akanshu Sharma
Born on the 23rd of September, 1978
in New Delhi, India

Education

1983 – 1989 Primary School, New Delhi, India
1989 – 1994 Secondary School, New Delhi, India
1994 – 1996 Higher Secondary School, New Delhi, India
1997 – 2001 Regional Engineering College Silchar, India
2001 Bachelor of Engineering (Hons.) in Civil Engineering
2002 – 2004 Indian Institute of Technology Delhi, New Delhi, India
2004 Master of Technology (Hons.) in Structural Engineering
2009 – 2013 University of Stuttgart, Germany (as visiting researcher)
2013 Doktor-Ingenieur (Ph. D.)

Experience

2004 – 2006 Bhabha Atomic Research Centre, Mumbai, India
Scientific Officer, C
2006 – 2009 Bhabha Atomic Research Centre, Mumbai, India
Scientific Officer, D
2009 – 2013 Bhabha Atomic Research Centre, Mumbai, India
Scientific Officer, E
2008 – 2013 University of Stuttgart, Germany
Visiting researcher

List of publications

Peer Reviewed Journals

1. **Akanshu Sharma**, R. Eligehausen, J. Hofmann, "Numerical modeling of joints retrofitted with haunch retrofit solution" accepted for publication in *ACI Structural Journal* (2013)

2. **Akanshu Sharma**, Reddy, G.R., Eligehausen, R., Genesio, G., and Pampanin, S., "Seismic response of RC frames with haunch retrofit solution" accepted for publication in *ACI Structural Journal* (2013)
3. **Akanshu Sharma**, G.R. Reddy, K.K. Vaze, R. Eligehausen, "Seismic Assessment of Full Scale Non-Seismically Detailed RC Structure By Pushover Method – Experiment And Analysis" *Engineering Structures* 46 (2013) 218–233
4. **Akanshu Sharma**, R. Eligehausen, G.R. Reddy, "Pivot hysteresis model parameters for RC columns, joints & structures", *ACI Structural Journal*, V. 110, No. 2, March-April 2013, pp 217-227.
5. Vinay Mahadik, **Akanshu Sharma**, J. Ožbolt, Y.M. Parulekar, G.R. Reddy and K.K. Vaze, "Simulation of flexural behavior of a simply supported beam subjected to corrosion" *J. Struct. Engg. SERC*, Vol. 40, No.1, April-May-2013, pp.80-84.
6. Joško Ožbolt, Josipa Bošnjak, Goran Periškić, **Akanshu Sharma**, "3D Numerical analysis of reinforced concrete beams exposed to elevated temperature" *Engineering Structures*, 2013
7. Rahim A, Sharma UK, Murugesan K, **Akanshu Sharma** and Arora P "Multi-response optimization of post fire residual compressive strength of high performance concrete" *Construction and Building Materials* 38 (2013) pp 265–273
8. Joško Ožbolt, **Akanshu Sharma**, "Numerical simulation of dynamic fracture of concrete through uniaxial tension and L-specimen", *Engg. Fracture Mechanics*, 85 (2012) 88–102
9. Rahim A, Sharma UK, Murugesan K, **Akanshu Sharma** and Arora P, "Optimization of post-fire residual compressive strength of concrete by Taguchi method", *Journal of Structural Fire Engineering*, Vol 3, No. 2, June 2012, 169-180
10. **Akanshu Sharma**, G.R. Reddy, K.K. Vaze, "Shake table tests on a Non-Seismically Detailed RC frame structure" *Int Jr of Struct Engg and Mechanics*, Vol. 41, No. 1, January 10, 2012, pp 1-24.
11. Joško Ožbolt, **Akanshu Sharma**, "Numerical simulation of reinforced concrete beams with different shear reinforcements under dynamic impact loads", *International Journal of Impact Engineering* 2011; 38: 940-950
12. Joško Ožbolt, **Akanshu Sharma**, H. W. Reinhardt, "Dynamic Fracture of Concrete – 3D Numerical Study of Compact Tension Specimen" *Applied Mechanics and Materials* Vol. 82 (2011) pp 39-44
13. **Akanshu Sharma**, G.R. Reddy, R. Eligehausen, K.K. Vaze, "Experimental and analytical investigations on seismic behavior of reinforced concrete framed structure by pushover method" *Int Jr Struct Engg and Mech*, V. 39, No. 1, 2011
14. Peter A, Mamidi G, Murugesan K, Sharma UK, **Akanshu Sharma** and Arora P, "Effect of boundary conditions on thermo-hydraulic behavior of clay buffer used in nuclear waste repository", *Energy Procedia* 2011, vol. 7 , pp 495–501.
15. **Akanshu Sharma**, G.R. Reddy, R. Eligehausen, K.K. Vaze, "Strength and Ductility of RC Beam-Column Joints of Non-Safety Related Structures and Recommendations by National Standards", *Int. Jr of Nuclear Engg and Design*, Vol. 241, Issue 5, 2011

16. J. Ožbolt, **Akanshu Sharma**, H. W. Reinhardt, "Dynamic fracture of concrete - Compact tension specimen" *Int Jr Solids and Structures*, Vol. 48, Issue 10, May 2011
17. **Akanshu Sharma**, R. Eligehausen, G.R. Reddy, "A new model to simulate joint shear behavior of poorly detailed beam-column connections in RC structures under seismic loads, part I: exterior joints" *Int Jr Engineering Structures*, Vol. 33, Issue 3, March 2011, 1034-1051
18. S.C. Yaragal, K.S.B. Narayan, K. Venkataramana, K.S. Kulkarni, H.C.C Gowda, G.R. Reddy, **Akanshu Sharma**, "Studies on Normal Strength Concrete Cubes Subjected to Elevated Temperatures", *International Journal of Structural Fire Engineering*, Vol. 1, No. 4, Dec 2010
19. **Akanshu Sharma**, C. Mahrenholtz, R. Eligehausen, G.R. Reddy, K.K. Vaze, A.K. Ghosh, H.S. Kushwaha, "Probabilistic evaluation of load on anchor for concrete structures corresponding to maximum crack width", *Int. J. Earth Sc. Engg.*, V.3, N.4, 2010, 798-811.
20. **Akanshu Sharma**, J. Ožbolt, G.R. Reddy, K.K. Vaze, A.K. Ghosh, H.S. Kushwaha, "Effect of loading rate on load-deflection behavior and failure mode of plain concrete slabs – 3D finite element analysis approach" *Int. J. Earth Sc. Engg.*, V.3, N.4, 2010, 812-822.
21. Thapa, M., Babunarayan, K.S., Halemane, K.P., Venkataramana, K., Yaragal, S.C., Ramesh Babu, R., **Akanshu Sharma**, Reddy, G.R., "Significance of modeling techniques in pushover analysis of RC buildings", *Int. J. Earth Sc. Engg.*, V.3, N.4, 2010, 699-709.
22. Babu Narayan K.S., Anil Kumar G, Chandrakala C, Shashikumar H.M., Venkataramana K., Yaragal S.C., Gowda H.C.C., Reddy G.R. and **Akanshu Sharma**, "Studies on Concrete Cylinders Subjected to elevated Temperatures", *Int. J. Earth Sc. Engg.*, V.3, N.4, 2010, 691-698.
23. Yaragal S.C., Clarke K.S., Babu K.M., Ashokumar S, Venkataramana K., Babu Narayan K.S., Gowda H.C.C., Reddy G.R., and **Akanshu Sharma**, "Strength Retention Characteristics of Concrete Cubes Subjected to Elevated Temperatures", *Int. J. Earth Sc. Engg.*, V.3, N.4, 2010, 789-797.
24. Chethan K., R.R. Babu, K. Venkataramana, **Akanshu Sharma**, "Influence of Masonry Infill on Fundamental Natural Frequency Of 2D RC Frames", *J. Struct. Engg.*, SERC, Vol. 37, No. 2 , 2010
25. **Akanshu Sharma**, G.R. Reddy, Rolf Eligehausen, K.K. Vaze, A.K. Ghosh, H.S. Kushwaha, "Experiments on reinforced concrete beam-column joints under cyclic loads and evaluating their response by nonlinear static pushover analysis", *Int. Jr of Struct Engg and Mechanics*, Vol. 35, No. 1, May 2010
26. **Akanshu Sharma**, G. Genesisio, G.R. Reddy, R. Eligehausen, "Nonlinear Dynamic Analysis Using Microplane Model For Concrete And Bond Slip Model For Prediction Of Behavior Of Non-Seismically Detailed RCC Beam-Column Joints, *J. Struct. Engg.*, SERC, Vol. 36, No. 4, 2009
27. Chethan K, RR Babu, K Venkataramana and **Akanshu Sharma**, "Study on Dynamic Characteristics of 3D Reinforced Concrete Frame with Masonry Infill", *Journal of CPRI*, V. 5, N.2, 2009

28. **Akanshu Sharma**, G.R. Reddy, L. Varshney, H.B. Kumar, K.K. Vaze, A.K. Ghosh, H.S. Kushwaha, T.S. Krishnamoorthy “Experimental Investigations on Mechanical and Radiation Shielding Properties of Hybrid Lead-Steel Fiber Reinforced Concrete”, Int. Jr of Nuclear Engg and Design Vol. 239, 2009.

Conferences and Workshops

1. **Akanshu Sharma**, Rolf Eligehausen, Jan Hofmann, “Seismic Assessment and Retrofitting of Reinforced Concrete Frame Structures” 1st Int. Conf. on Tech. Innovation in Nuclear Civil Engg: Construction and Strengthening of Nuclear Buildings, Paris, 2013
2. Rolf Eligehausen, **Akanshu Sharma**, Jan Hofmann, “On Seismic Safety Issues of Post-Installed Anchors in Nuclear Power Plants” 1st Int. Conf. on Tech. Innovation in Nuclear Civil Engg: Construction and Strengthening of Nuclear Buildings, Paris, 2013
3. J. Ožbolt, **Akanshu Sharma**, “Dynamic Fracture of Quasi Brittle Materials: Failure Mode and Crack Branching”, 3rd Int. Conf. on Comp. Modeling of Fract and Failure of Mats and Structs, CFRAC, Prague, 2013
4. J. Ožbolt, B. Irhan, **Akanshu Sharma**, “Modelling Concrete under High Loading Rates and Impact”, 3rd Int. Conf. on Comp. Modeling of Fract and Failure of Mats and Structs, CFRAC, Prague, 2013
5. J. Ožbolt, J. Weerheijm and **Akanshu Sharma**, “Dynamic tensile resistance of concrete – split hopkinson bar test” VIII Int. Conf. on Fract. Mech. of Conc. and Conc. Structs., FraMCoS-8, 2013, paper no. 361
6. J. Bošnjak, J. Ožbolt, **Akanshu Sharma**, Goran Periškić, “Permeability of concrete at high temperatures and modelling of explosive spalling” VIII Int. Conf. on Fract. Mech. of Conc. and Conc. Structs., FraMCoS-8, 2013, paper no 363
7. **Akanshu Sharma**, J. Ožbolt, G.R. Reddy, K.K. Vaze, “Dynamic Fracture of Concrete and Reinforced Concrete specimens and structural elements – numerical simulation”, Structural Engineering Convention (SEC), 2012
8. **Akanshu Sharma**, G.R. Reddy. R. Eligehausen, K.K. Vaze, “Modelling Beam-column joints in performance analysis of Reinforced Concrete Frame Structures” Structural Engineering Convention (SEC), 2012
9. V.K. Mahadik, **Akanshu Sharma**, Y.M. Parulekar, G.R. Reddy, K.K. Vaze, “Modelling Effect of Reinforcement Corrosion on Structural Behaviour of Beams” Structural Engineering Convention, (SEC) 2012
10. V.K. Mahadik, **Akanshu Sharma**, G.R. Reddy, K.K. Vaze, “Performance based design of real life RC frame structure—A Case Study”, Structural Engineering Convention, SEC 2012
11. **Akanshu Sharma**, G.R. Reddy, Joško Ožbolt, K.K. Vaze, “Dynamic fracture of concrete – Rate sensitivity and inertia” Int. Congress on Comp. Mech. and Sim. (ICCMS), 2012
12. T. Singh, **Akanshu Sharma**, J.Ožbolt and G.R. Reddy, “Numerical Simulation of Reinforced Concrete Slab under Impact Loading” Int. Congress on Comp. Mech. and Sim. (ICCMS), 2012

13. V.K. Mahadik, **Akanshu Sharma**, J. Ožbolt, Y.M. Parulekar, G.R. Reddy and K.K. Vaze, "Simulation of flexural behavior of a simply supported beam subjected to corrosion" Int. Congress on Comp. Mech. and Sim. (ICCMS), 2012
14. Mahadik V.K., **Akanshu Sharma**, Y.M. Parulekar, G.R. Reddy and K.K. Vaze, "Behavior of Corroded Reinforced Concrete Beams under Flexure-Numerical Simulation" 28th NCCE & National Seminar on Role of Infrastructure for Sustainable Development, The Institution of Engineers (India), 2012
15. Genesio G, Eligehausen R, **Akanshu Sharma**, Pampanin S, "Application of Post-Installed Anchors for Seismic Retrofit of RC Beam-Column Joints: Design and Validation", 3rd Int. Conf. on Conc. Repair, Rehab. and Retrofit, Cape Town, 2012
16. **Akanshu Sharma**, "Inelastic Seismic Analysis of As-Built and Retrofitted RC Frame Structures Considering Joint Distortion" 9th fib International PhD Symposium in Civil Engineering, 2012, Karlsruhe, Germany.
17. **Akanshu Sharma**, J. Ožbolt, G.R. Reddy, J. Hofmann, K.K. Vaze, "Numerical Simulation of Concrete and Reinforced Concrete under High Rate Loading" Struct Mech in Reactor Technology, SMiRT 21, 2011, New Delhi: Paper ID#95
18. **Akanshu Sharma**, R. Eligehausen, G.R. Reddy, J. Hofmann, K.K. Vaze, "Inelastic Seismic Analysis of RC Framed Structures Considering Joint Distortion" Struct Mech in Reactor Technology, SMiRT 21, 2011, New Delhi: Paper ID#195
19. **Akanshu Sharma**, G.R. Reddy, R.R. Babu, D. Revanna, K.K. Vaze, "Experimental Seismic Assessment of Full Scale Non-seismically Detailed RC Structure by Pushover Method" Struct Mech in Reactor Technology, SMiRT 21, 2011, New Delhi: Paper ID#316
20. **Akanshu Sharma**, G.R. Reddy, R.R. Babu, K.K. Vaze, "Seismic Shake Table Tests on a Gravity Load Designed Frame Structure – Linear to Nonlinear Testing" Struct Mech in Reactor Technology, SMiRT 21, 2011, New Delhi: Paper ID#317
21. Babita Sah, **Akanshu Sharma**, Y Singh, P Bhargava, GR Reddy, KK Vaze, "Nonlinear seismic evaluation of rc framed structures subjected to elevated temperatures" Struct Mech in Reactor Technology, SMiRT 21, 2011, New Delhi: Paper ID#584
22. J.Ožbolt, G.Periškić, **Akanshu Sharma**, J.Bošnjak, V.Travaš, H.W. Reinhardt, "Modeling of Concrete Exposed to Severe Loading Conditions – Impact and Fire", Post-SMiRT Conf. Seminar on Advances in Seismic Design of Structures, Systems and Components of Nuclear Facilities, 2011, Mumbai
23. Rolf Eligehausen, **Akanshu Sharma**, "Seismic Safety of Anchorages in Concrete Structures of Nuclear Power Plants" Post-SMiRT Conf. Seminar on Advances in Seismic Design of Structures, Systems and Components of Nuclear Facilities, 2011, Mumbai
24. J. Ožbolt, **Akanshu Sharma**, H.W. Reinhardt, "Dynamic Fracture of Concrete – 3D Numerical Study of Compact Tension Specimen" 3rd Int Workshop on Performance, Protection & under Extreme Loading, (Protect), 2011, Milano
25. J. Ožbolt, **Akanshu Sharma**, H.W. Reinhardt, "Numerical Analysis of Dynamic Fracture of Concrete – Failure Mode & Velocity of Crack Propagation" 2nd Int. Conf. on Comp. Modeling of Fract and Failure of Mats and Structs (CFRAC),

26. **Akanshu Sharma**, G.R. Reddy, K.K. Vaze, J. Ožbolt, J. Hofmann, “Assessing the Performance of Reinforced Concrete Structures under Impact Loads” 4th Nat. Conf. on Nuclear Reactor Technology (NRT-4), Mumbai, 2011, paper no. ST-04
27. **Akanshu Sharma**, G.R. Reddy, K.K. Vaze, R. Eligehausen, J. Hofmann, “Importance of Modeling Beam-Column Joints for Seismic Safety of Reinforced Concrete Structures” 4th Nat. Conf. on Nuclear Reactor Technology (NRT-4), Mumbai, 2011, paper no. ST-05
28. **Akanshu Sharma**, G.R. Reddy, K.K. Vaze, R. Eligehausen, J. Hofmann, “Safety Related Issues in Anchorage in Concrete Structures” 4th Nat. Conf. on Nuclear Reactor Technology (NRT-4), Mumbai, 2011, paper no. ST-13
29. Peter AA, Mamidi G, Murugesan K, Sharma UK, **Akanshu Sharma**, Arora P, “Effect of Boundary Conditions on Thermo-hydraulic Behaviour of Clay Buffer used in Nuclear Waste Repository”, Asian Nuclear Prospects 2010
30. **Akanshu Sharma**, Genesio G, Reddy GR, Eligehausen R, Pampanin S, Vaze KK, “Experimental Investigations on Seismic Retrofitting of Reinforced Concrete Beam-Column Joints”, Paper No A 007, 14th Sym on Earthquake Engg, IIT Roorkee, 2010
31. Genesio G, **Akanshu Sharma**, Eligehausen R, Pampanin S, Reddy GR, “Development of Seismic Retrofit Technique of RC Frame Using Fully Fastened Haunch Elements: Static to Dynamic Testing”, Paper No A 0017, 14th Sym on Earthquake Engg, IIT Roorkee, 2010.
32. S.C. Yaragal, K.S.B. Narayan, K. Venkataramana, K.S. Kulkarni, **Akanshu Sharma**, G.R. Reddy, “Relationship between Compressive and Splitting Tensile Strength of Concrete Subjected To Elevated Temperatures” Int Conf on Innovative World of Struct Engg, 2010, India
33. C. Mahrenholtz, R. Eligehausen, **Akanshu Sharma**, “Behavior of post-installed concrete undercut anchors subjected to high loading rate and crack cycling frequency” 9th US National and 10th Canadian Conf on earthq engg: Reaching beyond borders, session T14, 1589, 2010
34. G. Genesio , R. Eligehausen, **Akanshu Sharma** and S. Pampanin, “Experimental and numerical study towards a deformation-based seismic assessment of substandard exterior RC beam-column joints” Int Conf on fract mechanics of conc and conc structs, 2010, Jeju Island Korea.
35. S.C Yaragal., K.S.B. Narayan, K. Venkataramana, K.S. Kulkarni, H.C.C. Gowda, **Akanshu Sharma**, and G.R. Reddy, “Prediction equations for residual strength assessment of normal strength concrete cubes subjected to elevated temperatures”, NITK-Kagoshima University Japan Joint Int. Seminar 2010, Paper No. 4
36. **Akanshu Sharma**, Mahrenholtz C, Eligehausen R, Reddy G R, Vaze K K, Ghosh A K and Kushwaha H S (2010), “Probabilistic evaluation of load on anchor for concrete structures corresponding to maximum crack width”, Int Conf on Emerging Trends in Engineering, 2010, Civil Engineering Section, pp.280-292.
37. **Akanshu Sharma**, Ozbolt J, Reddy G R, Vaze K K, Ghosh A K and Kushwaha H S (2010), “Effect of loading rate on load-deflection behavior and failure mode of plain concrete slabs – 3D finite element analysis approach”, Int Conf on Emerging Trends in Engineering, 2010, Civil Engineering Section, pp.293-302.

38. Babu Narayan K S, Yaragal S C, Shrilaxmi, Kulkarni K S, Anil Kumar G, Venkataramana K, Reddy G R and **Akanshu Sharma** (2010), "Flexural strength retention characteristics of concrete subjected to elevated temperatures", Int Conf on Emerging Trends in Engg, 2010, pp.15-20.
39. Yaragal S.C., Babu Narayan K.S., Venkataramana K., Kulkarni K.S., Gowda H C.C., **Akanshu Sharma**, and Reddy G.R., "Studies on characteristics of concrete cubes subjected to elevated temperatures", Int Conf on Materials, Mechanics and Management, 2010, India.
40. Yaragal S.C., Clarke K.S., Babu K.M., Ashokumar S, Venkataramana K., Babu Narayan K.S., Gowda H.C.C., Reddy G.R., and **Akanshu Sharma**, "Strength Retention Characteristics of Concrete Cubes Subjected to Elevated Temperatures", Int conf on Advances in Conc, Struct and Geotech Engg, 2009.
41. Babu Narayan K.S., Anil Kumar G, Chandrakala C, Shashikumar H.M., Venkataramana K., Yaragal S.C., Gowda H.C.C., Reddy G.R. and Akanshu Sharma "Studies on Concrete Cylinders Subjected to Elevated Temperatures" Int conf on Advances in Conc, Struct and Geotech Engg, 2009.
42. Reddy GR, **Akanshu Sharma**, Dubey PN and Parulekar Y, "Seismic retrofitting of lifeline structures and systems" Workshop on Rehabilitation and Retrofitting of Structures, IIT Bombay, August 28-30, 2009.
43. **Akanshu Sharma**, R Eligehausen, G.R. Reddy, K.K. Vaze, A.K. Ghosh, H.S. Kushwaha "Simplistic nonlinear modeling of RC beam-column joints strengthened with FRP based on pushover analysis" Theme Meeting on Retrofit & Rehab of Structs and Int Seminar on Struct Rehab, India, 2009, pp. 58-67.
44. Monika Thapa, Babu Narayan K.S., Halemane K.P., Venkataramana K., Yaragal S.C., **Akanshu Sharma** "Sensitivity Analysis of Pushover method in Nonlinear Analysis of RC Structures", Theme Meeting on Retrofit & Rehab of Structs and Int Seminar on Struct Rehab, India, 2009, pp. 31-38.
45. **Akanshu Sharma**, Ramnik Singh, G.R. Reddy, K.K. Vaze, A.K. Ghosh, H.S. Kushwaha, "Tuned Water and Gel Dampers for Response Control of Structures", 6th Struct Engg Convention (SEC), 2008, pp. 885-892.
46. Chethan. K, R. R. Babu, K. Venkataramanna, **Akanshu Sharma**, "Seismic Behavior of RC Frame with Un-Reinforced Masonry (URM) Infill Panels" Theme 8, Earthquake Resistant Concrete Structures, ICI-IWC 2008, 11-13 Dec, 2008
47. **Akanshu Sharma**, G.R. Reddy, "Advanced Mathematical Modeling of Structural Concrete", *Theme Workshop on Concrete for Coastal Environment*, October 7-8, 2008, National Institute of Technology Surathkal, Mangalore, India.
48. Bharatkumar, B.H., Udhayakumar, V., Balasubramanian, K., Krishnamoorthy, T.S., Lakshmanan, N., **Akanshu Sharma** and Reddy, G.R., "Investigations on the lead-steel Hybrid fibre Reinforced concrete", 7th Int RILEM Sym. on Fibre Reinf Conc: Design and Applications, BEFIB, 2008, pp. 1089-1097
49. G.R. Reddy, **Akanshu Sharma**, Y.M. Parulekar, P.N. Dubey, "Research Activities on Earthquake Engineering and Structural Dynamics at Bhabha Atomic Research Centre",

Indo-Japan Theme Meet & Workshop on Disaster Risk Reduction-Earthq, Landslides and Tsunami, 2008, India, paper no. III-2

50. G.R. Reddy, **Akanshu Sharma**, "Seismic Strengthening and retrofit of structures", Tutorial on Design, Testing and Retrofitting of Structures for Earthquake Loading, 2008, Central Power Research Institute, Bangalore, pp. 45-58.
51. G.R. Reddy, Y.M. Parulekar, **Akanshu Sharma**, P.N. Dubey, K.N. Vaity, M.R. Kukreja, K.K. Vaze, A.K. Ghosh, H.S. Kushwaha, "Earthquake Engineering and Structural Dynamics Studies at Bhabha Atomic Research Centre", 3rd Indo-German Workshop and Theme Meet on Seismic Safety of Struct, Risk Assessment and Disaster Mitigation, 2007, Mumbai, pp. 175-189
52. **Akanshu Sharma**, G.R. Reddy, K.N. Vaity, K.K. Vaze, A.K. Ghosh, H.S. Kushwaha, "On Ductility of Reinforced Concrete Beam-Column Joints and Seismic Response Reduction Factors", 13th Sym on Earthq Engg, 2006, IIT Roorkee, 865-877.
53. G.R. Reddy, K.N. Rao, R. Narasimhan, K. Srinivas, K.S. Kumar, Y.M. Parulekar, S.M. Basha, V.S. Thomas and **Akanshu Sharma**, "Seismic Retrofitting of Apsara Reactor Building", Nat. Conf. on Operating Experience of Nuclear Reactors and Power Plants (OPENUPP-2006), 2006, Mumbai, 962-967.
54. **Akanshu Sharma**, K.N. Vaity, G.R. Reddy, K.K. Vaze and A.K. Ghosh, "Nonlinear Seismic Analysis and Methods of Retrofitting – A Case Study", Structural Engineering Convention (SEC), , 2005, IISc, Bangalore
55. G.R. Reddy, **Akanshu Sharma**, Y.M. Parulekar, K.K. Vaze, A.K. Ghosh, H.S. Kushwaha, "Seismic Retrofitting of Existing Concrete Structures using Energy Absorbers", 2nd Nat. Conf. on Advances in Mat and Mech of Conc Structs (NCAMMCS), 2005, IIT Madras
56. **Akanshu Sharma**, K.N. Vaity, G.R. Reddy, "Upgradation of Concrete Structures with Fiber Reinforced Composites", 8th Technical Programme Discussion Meeting of BRNS Projects, 2006, Mumbai.

Technical Reports

1. **Akanshu Sharma**, Reddy GR, Vaze KK, "Experimental and Numerical Investigations on As-Built and Retrofitted RC Frames under Dynamic Earthquake Loading" BARC External Report No. BARC/2013/E/008, 2013
2. **Akanshu Sharma**, Reddy GR, Vaze KK, "Experimental and Analytical Investigations on Seismic Behavior of Reinforced Concrete Exterior Beam-Column Joints without and with Retrofitting" BARC External Report No. BARC/2013/E/009, 2013
3. **Akanshu Sharma**, Reddy GR, Vaze KK, "Pushover Experiment and Analysis of Four Storey Full Scale Reinforced Concrete Structure before and after Retrofitting", BARC External Report No. BARC/2013/E/007, 2013
4. **Akanshu Sharma**, Reddy GR, Vaze KK, Eligehausen R, Hofmann J, "Nonlinear seismic analysis of reinforced concrete framed structures considering joint distortion" BARC external report No. BARC/2011/E/026, January 2012.
5. **Akanshu Sharma**, Reddy GR, Vaze KK, Ožbolt J, Hofmann J, "Behaviour of Plain and

- Reinforced Concrete under High Rate Loading” BARC external report No. BARC/2010/E/014, December 2010.
6. **Akanshu Sharma**, Eligehausen R, Hofmann J, Reddy GR and Vaze KK, “Nonlinear Static, Cyclic and Dynamic Earthquake Analysis of Reinforced Concrete Framed Structures Considering Joint Distortion” Report No. E10/16-BARC/04, Institute for construction materials, University of Stuttgart, Germany, September 2010
 7. **Akanshu Sharma**, Ozbolt J, Hofmann J, Reddy GR and Vaze KK, “Numerical Simulation of Plain and Reinforced Concrete under High Rate Loading” Report No. E10/17-BARC/05, Institute for construction materials, University of Stuttgart, Germany, September 2010
 8. Genesio G, **Akanshu Sharma**, “Seismic retrofit solution for reinforced concrete exterior beam-column joints using a fully fastened haunch, Part 2-1: As-built joints - Test report” Report No. WS 221/07 - 10/01, Institute for construction materials, University of Stuttgart, Germany, June 2010.
 9. Genesio G, **Akanshu Sharma**, “Seismic retrofit solution for reinforced concrete exterior beam-column joints using a fully fastened haunch, Part 2-2: Retrofitted joints - Test report” Report No. WS 221/08 - 10/02, Institute for construction materials, University of Stuttgart, Germany, June 2010.
 10. **Akanshu Sharma**, G.R. Reddy, K.K. Vaze, A.K. Ghosh, H.S. Kushwaha, Rolf Eligehausen, “Joint model to simulate inelastic shear behavior of poorly detailed exterior and interior beam-column connections reinforced with deformed bars under seismic excitations”, BARC External Report No. BARC/2009/E/026, December 2009
 11. **Akanshu Sharma**, R. Eligehausen, G.R. Reddy, K.K. Vaze, A.K. Ghosh, H.S. Kushwaha, “Modelling of Shear Behavior of Exterior Beam-Column Connections for Nonlinear Static Pushover Analysis of Reinforced Concrete Framed Structures under Seismic Excitations” Report No. E 09/02-BARC/03, Institute for construction materials, University of Stuttgart, Germany, August 2009
 12. **Akanshu Sharma**, C. Mahrenholtz, R. Eligehausen, G.R. Reddy, K.K. Vaze, A.K. Ghosh, H.S. Kushwaha, “Evaluation of Load on Anchor Corresponding to Maximum Crack Width – A Probabilistic Approach” Report No. E 09/01-BARC/02, Institute for construction materials, University of Stuttgart, Germany, August 2009
 13. C. Mahrenholtz, **Akanshu Sharma**, “Influence of High Rate - Hilti HDA” Report No. AF09/03-RWE07/03 Institute for construction materials, University of Stuttgart, Germany, July 2009
 14. **Akanshu Sharma**, G.R. Reddy, K.K. Vaze, A.K. Ghosh, H.S. Kushwaha, “Experimental and Analytical Evaluation of Strength and Deflections of Reinforced Concrete Beam-Column Joints Using Nonlinear Static Analysis”, BARC External report No. BARC/2009/E/012, July 2009
 15. **Akanshu Sharma**, G.R. Reddy, K.K. Vaze, A.K. Ghosh, H.S. Kushwaha, Rolf Eligehausen, “Investigations on Inelastic Behavior of Non-Seismically Detailed Reinforced Concrete Beam-Column Joints Under Cyclic Excitations”, *BARC External Report* No. BARC/2008/E/017, October 2008
 16. **Akanshu Sharma**, G.R. Reddy, K.K. Vaze, A.K. Ghosh, H.S. Kushwaha, Rolf

Eligehausen, "Experimental and Analytical Investigation on Behavior of Scaled Down Reinforced Concrete Framed Structure Under Monotonic Pushover Loads", *BARC External Report No. BARC/2008/E/018*, October 2008

17. **Akanshu Sharma**, K.N. Vaity, G.R. Reddy, K.K. Vaze and A.K. Ghosh, "Seismic Requalification of RLG Building", BARC Internal Technical Report, BARC/2005/015, December 2005.
18. **Akanshu Sharma**, "Nonlinear Analysis of Structures Subjected to Seismic Excitation" Master Thesis, Indian Institute of Technology Delhi, 2004.

Newsletters

1. **Akanshu Sharma**, C. Mahrenholtz, P.N. Dubey, C.C. Gupta, S.K. Mishra, G.R. Reddy, R. Eligehausen, S. Guha, T.V.S. Murthy, R.L. Suthar, K. Srinivas, J.K. Chakravarty, K.K. Vaze, "Experiments on Reinforced Concrete Structures; sub-assemblages and components for seismic safety – Post installed anchors", *BARC Newsletter*, March-April 2011.
2. G. R. Reddy, **Akanshu Sharma**, P. N. Dubey and Y. M. Parulekar, "Investigations on Reinforced Concrete Structures" Feature article, *BARC Newsletter*, Issue No. 312, Jan-Feb 2010.
3. Ramesh Babu R., Murthy S., Selvam P., Shashidhar, Bharath Kumar S., Chethan K., Venkataramana K., Babu Narayan K.S., **Akanshu Sharma** and Reddy G.R. "Earthquake Response Characteristics of 2D RC Frames with masonry Infill panels", *NITK Research Bulletin*, Vol. 18, Number 1, 2009
4. G.R. Reddy, Y.M. Parulekar, **Akanshu Sharma**, P.N. Dubey, K.N. Vaity, A. Ravi Kiran, M.K. Agrawal, K.K. Vaze, A.K. Ghosh, H.S. Kushwaha, "Studies on Response of Structures, Equipment and Piping Systems to Earthquake and its Mitigation", *BARC Newsletter*, Issue No. 290, March 2008, pp. 15-30.
5. G.R. Reddy, **Akanshu Sharma**, P.N. Dubey, Y.M. Parulekar, K.K. Vaze, A.K. Ghosh, H.S. Kushwaha, "Some Advanced Methods for Safe and Economical Seismic Design, Requalification and Retrofitting of Structural Systems", *Indian Nuclear Society Newsletter*, Vol. 4, No. 1, Jan-Mar 2008.

Hiermit versichere ich, die vorliegende Dissertation ohne Hilfe Dritter nur mit den angegebenen Quellen und Hilfsmitteln angefertigt zu haben. Alle Stellen, die aus den Quellen entnommen wurden, sind als solche kenntlich gemacht worden. Diese Arbeit hat in gleicher oder ähnlicher Form noch keiner Prüfungsbehörde vorgelegen.

Akanshu Sharma